

Synthesis of Polymer-DNA Origami Hybrid Nanostructures

Dissertation

zur Erlangung des Grades “Doktorin der Naturwissenschaften”
im Promotionsfach Chemie

am Fachbereich Chemie, Pharmazie, Geographie und Geowissenschaften
der Johannes Gutenberg-Universität Mainz

Pia Winterwerber

Mainz 2023



MAX-PLANCK-INSTITUT
FÜR POLYMERFORSCHUNG



JOHANNES GUTENBERG
UNIVERSITÄT MAINZ

Dekan

[REDACTED]

1. Berichterstatter

[REDACTED]

2. Berichterstatter

[REDACTED]

Datum der mündlichen Prüfung:

24.07.23

D77 – Mainzer Dissertation

Die vorliegende Arbeit wurde in der Zeit von Juni 2018 bis Juni 2022 am Max-Planck-Institut für Polymerforschung [REDACTED] angefertigt.

Hiermit versichere ich, Pia Winterwerber, gemäß § 10 Abs. 3d der Promotionsordnung vom 24.07.2007:

Ich habe die jetzt als Dissertation vorgelegte Arbeit selbstständig angefertigt und alle benutzten Hilfsmittel (Literatur, Apparaturen, Material) in der Arbeit angegeben. Ich habe die Dissertation nicht als Prüfungsarbeit für eine andere Prüfung eingereicht. Ich habe weder die jetzt als Dissertation vorgelegte Arbeit noch Teile der Abhandlung als Dissertation bei einer anderen Fakultät oder einem anderen Fachbereich eingereicht.

Mainz, Juni 2023

Pia Winterwerber

Danksagung

[REDACTED]

[REDACTED]

[REDACTED]

[REDACTED]

[REDACTED]

[REDACTED]

[REDACTED]

[REDACTED]

[REDACTED]

[REDACTED]

[REDACTED]

[REDACTED]

[REDACTED]

[REDACTED]

[REDACTED]

[REDACTED]

[REDACTED]

[REDACTED]

[REDACTED]

[REDACTED]

Publications

Over the course of my PhD project, I was working on the publications presented below. The publications are listed according to their appearance in this thesis.

Publication list

1. „Functional DNA-Polymer Conjugates”

Whitfield, C. J. ‡, Zhang, M. ‡, **Winterwerber, P.**, Wu, Y. Z., Ng, D. Y. W., Weil, T. *Chemical Reviews* **2021** *121* (18), 11030–11084.

doi.org/10.1021/acs.chemrev.0c01074

2. “DNA Origami meets polymers: A powerful tool for defined nanostructure design”

Hannewald, N. ‡, **Winterwerber, P.** ‡, Zechel, S., Ng, D. Y. W. Hager, M. D., Weil, T., Schubert, U. S. *Angew. Chem. Int. Ed.* **2021** *60* (12) 6218–6229.

doi.org/10.1002/anie.202005907

3. “Photocontrolled Dopamine Polymerization on DNA Origami with Nanometer Resolution”

Winterwerber, P., Harvey, S., Ng, D. Y. W., Weil, T. *Angew. Chem. Int. Ed.* **2020**, 59, 6144.

doi.org/10.1002/anie.201911249

4. “Multiple Wavelength Photopolymerization of Stable Poly(Catecholamines)-DNA Origami Nanostructures”

Winterwerber, P., Whitfield, C. J., Ng, D. Y. W., Weil, T. *Angew. Chem. Int. Ed.* **2022**, accepted article

doi.org/10.1002/anie.202111226

5. “Squaric Ester-Based, pH-Degradable Nanogels: Modular Nanocarriers for Safe, Systemic Administration of Toll-like Receptor 7/8 Agonistic Immune Modulators”

Huppertsberg, A., Kaps, L., Zhong, Z., Schmitt, S., Stickdorn, J., Deswarte, K., Combes, F., Czysch, C., De Vrieze, J., Kasmi, S., Choteschovsky, N., Klefenz, A., Medina-Montano, C., **Winterwerber, P.**, Chen, C., Bros, M., Lienenklaus, S., Sanders, N. N., Koynov, K., Schuppan, D., Lambrecht, B. N., David, S., De Geest, B. G., Nuhn, L. *JACS* **2021**, 143 (26) 9872.

doi.org/10.1021/jacs.1c03772

6. „Fluorescent Nanodiamond– Nanogels for Nanoscale Sensing and Photodynamic Applications“

Wu, Y., Alam, M. N. A., Balasubramanian, P., Winterwerber, P., Ermakova, A., Müller, M., Wagner, M., Jelezko, F., Raabe, M., Weil, T. **2021** *Advanced NanoBiomed Research*, 1(7), 2000101.

doi.org/10.1002/anbr.202000101

7. “Supramolecular Toxin Complexes for Targeted Pharmacological Modulation of Polymorphonuclear Leukocyte Functions”

Heck, A. J., Ostertag, T., Schnell, L., Fischer, S., Agrawalla, B. K., Winterwerber, P., Wirsching, E., Fauler, M., Frick, M., Kuan, S. L., Weil, T., Barth, H. *Adv. Healthc. Mater.* **2019**, 8, 1900665.

doi.org/10.1002/adhm.201900665

‡ These authors contributed equally to this work.

Publication context

The fusion of biomolecules and synthetic polymers has paved the way to a novel class of hybrid materials that combine the advanced features of both building blocks in a synergistic fashion. In particular, DNA nanostructures can benefit from various functional groups and responsive properties that can be imparted by polymers, whereas the unique programmability and supramolecular recognition of DNA can assist in constructing higher ordered architectures.

Within this PhD project, the current state of the art in the field of DNA-polymer conjugates was surveyed and discussed. Herein, the manifold approaches towards DNA-polymer conjugates, their supramolecular assemblies, and the functions and applications thereof are described. With respect to the outline of this thesis, chapter 3.2 of our review (1) on “Noncovalent DNA – Polymer Conjugates” is of great relevance for the research presented later on and thus, included into the introduction. Likewise important for the introduction of this thesis is publication 2 on “DNA Origami Meets Polymers”, which can be regarded as a follow-up, narrowing the focus to conjugates involving DNA origami platforms. Explicitly, bottom up and top down methodologies together with their characteristics and prospects are compared, leading over to the results and discussion part.

Here, two research papers describe the bottom up fabrication of defined poly(catecholamines)–DNA origami nanostructures. In 3, we established a photopolymerization system on DNA origami tubes with spatiotemporal control at nanometer resolution. The preinstalled photosensitizer protoporphyrin IX responds to white light and triggers formation of polydopamine at designated areas, yielding polymer-ring DNA tubes. In a subsequent study (4), we could further develop the technique towards multi-wavelength polymerization of various catecholamines via facile sequential processes. By imprinting

polymeric layers at these designated areas, we modulate the surface chemistry of the DNA objects, subsequently promoting cellular uptake.

In addition to DNA-polymer nanoobjects, there is a vast range of nanocarriers built from different platforms that emerged prominently in the area of biomedical applications. Supramolecular interactions allow for the formation of polymeric nanogels (5), coating of fluorescent nanodiamonds (6), and the assembly of protein complexes (7), among others. For thorough analysis of these nanoparticles, imaging techniques are essential to deepen the understanding of size distribution and homogeneity, as well as morphology. Here, I could provide further insights into the investigated systems by atomic force microscopy studies.

In summary, the first presented reviews set the framework for our investigations on the photopolymerization of catecholamines on DNA origami templates. The obtained polymer–DNA hybrids benefit from the precisely defined DNA playground and the advanced features of the formed poly(catecholamines), *e.g.*, in a biological context. Further nanocarriers systems are introduced to cover the current research in the field broadly.

Abstract

While seminal advances have extensively refined polymer chemistry, the absolute control over sequence, monomer addition and directionality remain elusive. Among Nature's macromolecular systems, the simplicity of DNA interactions has inspired and paved the way toward DNA nanotechnology and engineering. Herein, the complementary base pairing responsible for the famous double helix structure provides unique programmability, granting the capability to create complex geometric objects as DNA origami. As an engineering material with pinpoint accuracy in the range of nanometers, DNA origami can reliably assist in the molecular and functional organization of other molecules. Polymer chemistry, on the other hand, has seen large advances in directing polymerization processes, rheological features and phase separation. By merging the fields of DNA origami and polymer chemistry, their respective potential can be integrated into hybrid objects of advanced properties, to achieve complementarity and to break traditional boundaries that have limited their use.

In the context of this thesis, representative DNA origami structures are combined with the formation of bioinspired polymers. By equipping the DNA origami within a photopolymerization system to direct polymer growth, we show that complex nano-objects can be synthesized with full 3-D customization of the surface contour and polymer patterning. Conventionally, densely packed DNA origami structures can only exist in the presence of divalent cations and are degraded through nucleases in biological settings. On the other hand, the formation of polydopamine, a prominent representative of poly(catecholamines), is typically a straightforward yet rather uncontrolled process used for coating of substrates. Within this work, DNA origami tubes in the 100 nm regime are built from the bottom-up so that reaction centers can be introduced at the designated positions. These reaction centers are composed of a specific DNA sequence that builds tertiary G-quadruplex structures to host catalytic macrocycles. Here, photosensitizers were chosen to be embedded that generate reactive oxygen species when exposed to light of a specific wavelength. In this oxidative environment, the multistep polymerization of the monomers, dopamine and norepinephrine, is triggered and due to their adhesiveness, polymeric layers are imprinted alongside the reaction centers. This process offers exclusive spatial-temporal control enabled through the synergy of DNA and polymer technologies: On/off switching of the light source directly starts/stops polymerization and in turn polymer layer dimensions, whereas nanopatterning is achieved through the positioning of reaction centers across the origami pegboard. Furthermore, by applying photosensitizers with different absorption profiles, multiwavelength responsiveness can be installed, and the versatility of DNA complementary binding allows for multistep reaction processes as well as post modifications. Importantly, polymer-decorated DNA origami tubes exhibit enhanced stability in challenging chemical environments like ion-depleted media. From a biological perspective, polymer modification could impact the DNA origami fate *in vitro* with polynorepinephrine coating in enabling and enhancing cellular uptake.

Collectively, the presented approaches herein illustrate how the combination of DNA nanotechnology and polymer chemistry can not only alleviate intrinsic limitations but also complement each other. This paves the way for future endeavors 1) to create soft polymeric objects with full geometric versatility, 2) in rebuilding reaction vessels in cells similar to Nature's compartmentalization strategy and 3) exploiting the DNA origami's modularity to mimic and study viruses.

Zusammenfassung

Das Feld der Polymerchemie ist geprägt durch kontinuierlichen Fortschritt und Weiterentwicklungen, doch die absolute Kontrolle über Sequenz, Monomerzugabe und Richtungsabhängigkeit bleibt schwer zu erreichen. Unter den biomakromolekularen Systemen der Natur haben die Einfachheit der DNA-Wechselwirkungen den Weg zur DNA-Nanotechnologie inspiriert und geebnet. Die komplementäre Basenpaarung, die zur berühmten Doppelhelixstruktur führt, bietet eine einzigartige Programmierbarkeit und ermöglicht die Herstellung komplexer geometrischer Objekte wie DNA-Origami. Als Baumaterial mit punktgenauer Adressierbarkeit im Nanometerbereich kann DNA-Origami zuverlässig die molekulare und funktionelle Organisation anderer Moleküle ermöglichen. Die Polymerchemie wiederum hat große Fortschritte bei der Steuerung von Polymerisationsprozessen und resultierender Polymere gemacht. Durch die Fusion der Bereiche DNA Origami und Polymerchemie kann ihr jeweiliges Potenzial in hybriden Objekten mit fortschrittlichen Eigenschaften integriert werden, die von einer Disziplin allein kaum erreicht werden. Im Rahmen dieser Arbeit werden repräsentative DNA-Origami-Strukturen mit der Bildung von bioinspirierten Polymeren kombiniert. Indem die DNA-Objekte mit einem Photopolymerisationssystem zur Steuern der Polymerbildung ausgestattet werden, soll das Verständnis der DNA-Polymer-Kombination vertieft werden. Üblicherweise erfordern die dicht gepackte DNA-Origami-Strukturen die Gegenwart zweiwertiger Kationen und werden in biologischen Umgebungen durch Nukleasen abgebaut. Andererseits ist die Bildung von Polydopamin, einem prominenten Vertreter der Poly(catecholamine), typischerweise ein unkomplizierter, jedoch eher unkontrollierter Prozess, der zur Beschichtung von Substraten verwendet wird. Im Rahmen dieser Arbeit werden DNA-Origami-Röhrchen mit einer Größe von etwa 100 nm aufgebaut und Reaktionszentren an gewünschten Positionen eingeführt. Diese Reaktionszentren bestehen aus einer spezifischen DNA-Sequenz, die tertiäre G-Quadruplex-Strukturen bildet. Hier können Photosensibilisatoren eingebettet werden, die reaktive Sauerstoffspezies erzeugen, wenn sie mit Licht einer bestimmten Wellenlänge bestrahlt werden. Die oxidative Umgebung leitet die mehrstufige Polymerisation der Monomere Dopamin und Noradrenalin ein, und aufgrund ihres Haftvermögens werden polymere Schichten entlang der Reaktionszentren abgelagert. Dieser Prozess bietet eine exklusive räumliche und zeitliche Kontrolle, ermöglicht durch die Synergie von DNA- und Polymertechnologien: Durch das Ein- und Ausschalten der Lichtquelle wird die Polymerbildung und damit die Höhe der Polymerschicht direkt ausgelöst bzw. gestoppt, während die Nanostrukturierung durch die Positionierung der Reaktionszentren auf dem Origami-Vorlage sichergestellt wird. Durch die Verwendung von Photosensibilisatoren mit unterschiedlichen Absorptionsprofilen kann außerdem eine Multiwellenlängenempfindlichkeit eingebaut werden, während die komplementäre DNA-Hybridisierung mehrstufige Reaktionsprozesse sowie nachfolgende Modifikationen ermöglicht. Es ist hervorzuheben, dass die mit Polymeren dekorierten DNA-Origami-Röhrchen eine verbesserte Stabilität in herausfordernden chemischen Umgebungen wie etwa fehlende Ionenstärke, aufweisen. Aus biologischer Sicht zeigt sich, dass die Polymermodifikation das Schicksal der DNA-Origami *in vitro* beeinflusst, wobei die Polynorepinephrin-Beschichtung vielversprechend die Aufnahme in die Zellen ermöglicht beziehungsweise verbessert.

Zusammenfassend zeigen die hier vorgestellten Methoden wie die Kombination von DNA-Nanotechnologie und Polymerchemie nicht nur den jeweiligen Limitierungen entgegenwirkt, sondern zusätzliche Vorteile

schaffen kann. Dies bildet die Grundlage für künftige Bestrebungen, 1) polymere Objekte von geometrischer Vielseitigkeit zu schaffen, 2) nanoskalige Reaktionsräume nach dem Vorbild von Zellkompartimenten nachzubauen und 3) die Modularität der DNA-Origami zur Nachahmung und Untersuchung von Viren zu nutzen.

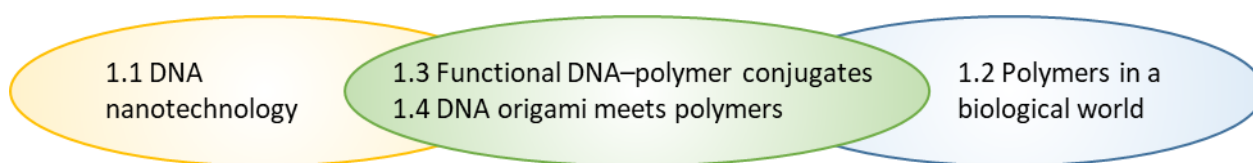
Table of Contents

Danksagung	4
Publications	5
Abstract.....	8
Zusammenfassung	9
Table of Contents.....	11
1. Introduction	13
1.1 DNA nanotechnology	13
1.1.1 DNA as a building material	13
1.1.2 DNA origami.....	16
1.2 Polymers in a biological world.....	23
1.2.1 Poly(catecholamines)	23
1.2.2 Photodynamic Therapy, Photosensitizer, and Photopolymerization.....	29
1.3 Functional DNA–polymer conjugates: Noncovalent DNA–polymer interactions	33
1.4 DNA origami meets polymers: A powerful tool for defined nanostructure design	45
2. Motivation	59
3. Results and Discussion	63
3.1 Photocontrolled dopamine polymerization on DNA origami with nanometer resolution	63
3.2 Multiple wavelength photopolymerization of stable poly(catecholamines)-DNA origami nanostructures	71
3.3 Excursus: Further nanoparticulate systems based on supramolecular assemblies.....	82
4. Conclusion and Outlook	85
5. References.....	89
6. Appendix	97
6.1 Supporting information for publication „Photocontrolled Dopamine Polymerization on DNA Origami with Nanometer Resolution“	97
6.2 Supporting information for publication „Multiple Wavelength Photopolymerization of Stable Poly(Catecholamines)-DNA Origami Nanostructures“	112
6.3 Comprehensive overview of review “Functional DNA – Polymer Conjugates”	135

6.4	Publication „Squaric Ester-Based, pH-Degradable Nanogels: Modular Nanocarriers for Safe, Systemic Administration of Toll-like Receptor 7/8 Agonistic Immune Modulators“	190
6.5	Publication „Fluorescent Nanodiamond–Nanogels for Nanoscale Sensing and Photodynamic Applications	202
6.6	Publication „Supramolecular Toxin Complexes for Targeted Pharmacological Modulation of Polymorphonuclear Leukocyte Functions“	211

1. Introduction

The programmability of DNA and its structural fidelity render it the molecule of choice for the self-assembly of exceptionally precise structures on the nanoscale. Polymer chemistry, on the other hand, provides synthetic as well as bioinspired or biomimetic macromolecules of broad chemical diversity and responsiveness. The merging of these fields leads to a novel class of hybrid materials that could advance our understanding of soft material engineering and chemistry at interfaces. In this respect, functional DNA-polymer conjugates, particularly DNA origami-polymers are highlighted.



1.1 DNA nanotechnology

1.1.1 DNA as a building material

DNA is a precision polymer that functions as the main avenue of information storage in biology, coding the entire spectrum of components that represents life in the smallest unit.. DNA stores information within its sequence and thanks to next-generation sequencing techniques, it currently takes only mere hours to screen undiagnosed patients and provide analytical data on a genetic level.¹ However, it was tumultuous times when Watson and Crick postulated a molecular structure for deoxyribonucleic acid in 1953.^{3,4} An X-ray based fiber diffraction image taken by Rosalind Franklin's student provided critical evidence in identifying the structure of DNA.⁵ Namely, DNA consists of two chains that wound helically round a common axis whilst running in opposite directions (Figure 1). The chains are built from only four monomers – nucleotides – that are in turn composed of nitrogen-containing nucleobases cytosine (C), guanine (G), adenine (A) or thymine (T) together with a deoxyribose unit and a phosphate group. Two DNA chains coil around each other according to base pairing rules. Pyrimidines T and C pair with purines A and G through two or three hydrogen bonds, respectively. Remarkably, the double helical structure of DNA will always form as long as the chains are complementary in sequence. The hydrophobic bases point inward while the alternating sugar-phosphate backbones form a negatively charged exterior.⁶ However, there are examples of extraordinary nucleotide sequences that lead to DNA superstructures different from the double helix.⁷ Notably, base recognition and the formation of hydrogen bonds results in perfect binding of two complementary DNA strands but base-stacking interactions predominantly contribute to duplex stability in aqueous environment.⁸ Furthermore, double-stranded DNA (dsDNA) is considered as rather

stiff over a range of tens of nanometers, single-stranded DNA (ssDNA) in contrast acts like a flexible and elastic polymer adapting a coiled conformation.⁹

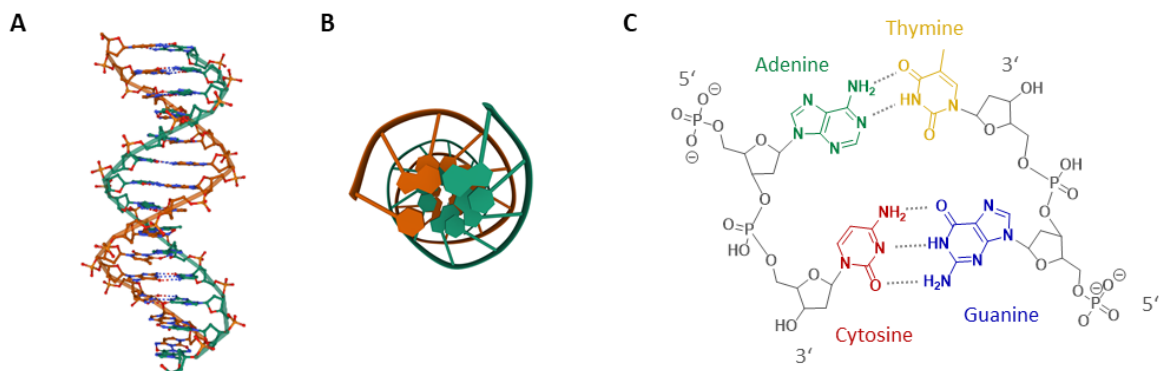


Figure 1 Deoxyribonucleic acid (DNA) consists of two chains that wound helically around a common axis whilst running in opposite directions. (A) Double helix structure of two complementary nucleotide strands (orange and green) in solution. (B) Duplex stability is mainly driven by base pair stacking, as shown in top view. dsDNA images were created from PDB: 2M2C.¹⁰ (C) Hydrogen bonding between base pairs adenine-thymine and cytosine-guanine further stabilizes the structure and ensures complementary recognition.

Two remarkable features of DNA are accounted for its extraordinary impact on biology: its digital nature and its complementarity.¹¹ Firstly, digital information is encompassed in genes that encode proteins as well as the gene regulatory network controlling the behavior of genes. Secondly, the complementarity of DNA is not only recognized as the basis of replication in living systems, but also gives rise for the field of DNA nanotechnology. Here, DNA is taken out of the biological context and is utilized as a non-biological engineering material for the manufacturing of 2D and 3D DNA structures of nanoscale dimensions.¹² The predictable nature of DNA interactions enables the rational design and self-assembly of nanostructures and has truly transformed nanoscience.¹³ In this regard, what is it that makes nanoscale objects a cutting edge research area? For over a century, synthetic chemists have manipulated countless molecules on the angstrom level, which is an order of magnitude smaller than the scale exploited in nanoscience.¹⁴ However, as the length scale increases to the nanometer regime, the energy landscape become more complex as molecules need to overcome entropic effects where both molecular and long-range order becomes critical. Here, Nature sets superlative standards when it comes to matters like bottom-up synthesis and self-assembly processes. Self-assembly describes the autonomous and spontaneous organization of individual components into patterns or structures without external instruction.^{15, 16} Nature masters the design of chemically complementary and structurally compatible constituents to organize nonliving components into living, biological systems. The dynamic cell membrane is an exquisite example for the assembly of different molecules into a complex asymmetric pattern.^{17, 18} In order to guide the subsequent self-assembly of the molecules, they have to be coded with intrinsic information such as shape, surface properties, charge, polarizability, magnetic dipole, mass, among others.¹⁵ Molecular self-assembly relies on the

formation of numerous non-covalent or weak covalent bonds including hydrogen and coordination bonds as well as van der Waals, electrostatic, and hydrophobic interactions. While each of the bonds is rather weak on an individual level, collective interactions can result in a directionality that determines bulk behavior such as attraction and repulsion.¹⁶ While this programmed self-assembly process represents a bottom-up approach in creating functional structures, top-down techniques begin with larger structures and decrease their dimensions by means of external assembly tools. Yet, building from the bottom up enables larger chemical diversity and closer proximity between entities.¹⁴

Four decades ago, Nadrian Seeman recognized the potential of self-assembling DNA for controlled bottom-up nanofabrication.¹⁹ He pursued the idea of arranging biomacromolecules such as proteins into well-ordered lattices for crystallography through DNA-based scaffolds, thus, laying the foundation for DNA nanotechnology. Structural DNA nanotechnology is based on several pillars of which the aforementioned hybridization is probably the most apparent. However, little biology would happen if DNA was permanently locked in its double helical structure.²⁰ It is the branched manifestations that occur during semiconservative replication (triply branched replication forks⁴) and genetic recombination (four-arm branched Holliday junctions²¹) that significantly give biological meaning to DNA (Figure 2). With respect to controlled self-assembly of artificial DNA nanostructures, however, these branched junctions have two limitations: their geometric flexibility and instability resulting from branch migration due to sequence symmetry. By making DNA arms with unique sequences, Holliday junctions can be rendered immobile which marks the turning point in creating DNA nanostructures. Furthermore, predesigned ssDNA overhangs – so-called sticky ends – can be introduced to the DNA arms to potentially extend the structure into an infinite lattice. The symmetry-lacking sequences required here cannot be readily obtained from natural sources, emphasizing the need for the synthesis of DNA strands of arbitrary sequences. This demand could be met through the advent of phosphoramidite chemistry and adaptation of solid-phase oligonucleotide synthesis.^{22, 23} The availability of immobile junctions then led to the first 3D DNA nanoobject, a DNA cube, where the vertices are built from the branched junction points and the edges are formed by rigid dsDNA domains, resulting from hybridization of the sticky ends.²⁴ Another milestone in the field was the introduction of a double-crossover molecule (DX) where two DNA double helices are linked together via two strand exchanges.^{25, 26} In detail, a strand exchange occurs when a DNA strand starts on one helix and switches to the next helix. In contrast to Holliday junctions, a DX motif cannot rotate freely and offers sufficient stability necessary for the formation of rigid periodic structures. This strategy was then employed to assemble the first crystalline 2D DNA array which was imaged by atomic force microscopy.²⁷ Later on, triple crossover molecules (TX) were designed and besides these diverse lattice geometries, structural DNA nanotechnology has produced polyhedrons, nanotubes, nanowires, and walking devices, among others.²⁸⁻³²

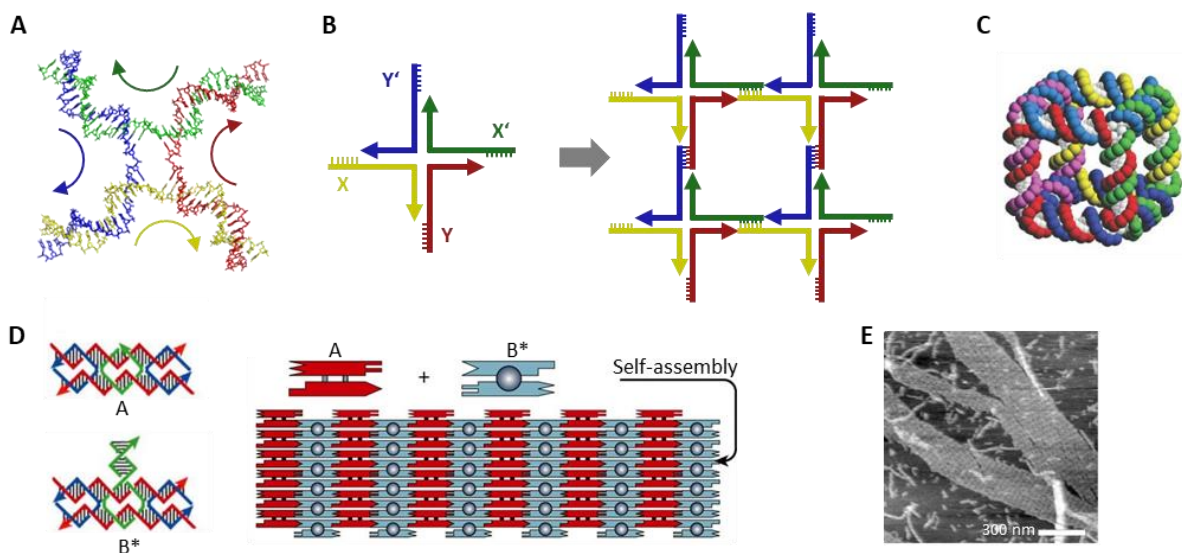


Figure 2 (A) A Holliday junction contains four double-stranded arms. In case of symmetrical sequences, the branchpoint is mobile and can migrate. (B) Employing unique sequences, however, renders these junctions immobile and incorporation of single-stranded overhangs further enables creation of infinite lattices. (C) A three-dimensional cube-like structure can be created by formation of interconnected rings from ligated DNA strands. (D) Double-crossover molecules can be programmed by controlling their sticks ends in such a way that they produce two-dimensional arrays. (E) Atomic force spectroscopy image of a crystalline 2D DNA array made from DX motifs. Reprinted and adapted with permission from ^{33, 34, 27}.

In brief, the success of DNA as the molecule of choice in nanotechnology attributes to the programmability of Watson–Crick base pairing, the predictability of the DNA double helix together with stably branched DNA motifs, automated synthesis of configurable oligonucleotides as well as the chemical stability and inertness of DNA that leaves little space for secondary interactions.

1.1.2 DNA origami

While DNA nanotechnology was continuously gaining attention in the late 1990s, the field experienced an impressively fast expansion starting in 2006. This development is to be credited to the emergence of a new technique called “DNA origami” by Paul Rothemund.³⁵ Similar to the Japanese art of folding a flat sheet of paper into arbitrarily formed objects, a long ssDNA strand can be folded into predefined shapes and patterns. The DNA origami methodology circumvents certain obstacles that previous strategies were facing and significantly increases the complexity and size of the assembled structures. Formerly described techniques rely on short DNA oligonucleotides only and are therefore sensitive to stoichiometric ratios. Furthermore, purification of individual strands is necessary to obtain reasonable yields and infinite periodic arrays only provide limited individual addressability.^{36, 37} In DNA origami, however, a long ssDNA (scaffold DNA) can be folded into a desired and fully predefined shape assisted by hundreds of short synthetic oligonucleotides. They are designed to bind to distinct positions along the scaffold DNA in crossover motifs, thus, bringing formerly distant parts into close proximity and

locking the scaffold in place (Figure 3). In accordance to their literal function, these oligonucleotides are referred to as staple strands.

The most prominent scaffold strand in the field is a circular 7-kilobase phage genome whose folding creates a surface area of roughly 8000–10000 nm² and an overall mass of approximately 5 mega Daltons.¹³ Likewise, the size of the corresponding origami structure depends on the length of the scaffold DNA and researchers have examined various ways to generate tailored scaffolds.^{37, 38} The fact that the sequence and consequential position of each staple strand is predefined and precisely known renders origami structures being portrayed as a programmable pegboard with a resolution of 4–6 nm. As a further benefit of the scaffold-based approach, stoichiometry considerations are negligible since staple strands can be applied in excess without the need for preceding purification steps. Noteworthy, each nanostructure demands for a unique set of several hundred ssDNA strands but the continuously decreasing costs of oligonucleotide synthesis have eased this concern.^{39, 40} In line with the original rectangle proposed by Rothemund, two-dimensional origami structures entail a single layer of helices that have interhelical crossovers every 180°, leading to a planar sheet. In order to generate three-dimensional structures, multiple 2D-sheets can be assembled into higher-ordered objects by additional crossovers at the edges.⁴¹ The resulting 3D structures then encompass an internal cavity as demonstrated by Andersen and Coworkers in 2009. Their famous DNA box even exhibits a flexible lid, making the DNA object changing its topology in response to the addition of complementary DNA-keys.⁴²

Multilayered 3D origami is an expedient extension since single-layer structures tend to deform and fluctuate in solution. To increase the resistance to mechanical stress, DNA helices are densely packed through a defined arrangement of crossovers at, for instance, every 270°.⁴³ While the connection of one helix to three adjacent helices results in an hexagonal cross-section, rectangular structures with higher density can be made from layers of helices packed on a square lattice geometry.⁴⁴ However, lattice-based designs are not suitable for the formation of material-efficient, hollow, or porous DNA nanoobjects. In contrast to multi-layered structures, wireframe approaches, *i.e.* DNA designs based on 3D meshing, require less material per volume and produce DNA-economical constructs.⁴⁵ Here, macroscopic engineering methods are applied to the nanoscale: In a top-down manner, the object of interest is transcribed into a mesh (vertices, edges, and faces), followed by rendering a wireframe model with a scaffold strand routing through the mesh and the generation of respective stapling sequences.⁴⁶ This way, highly curved and complex 2D- and 3D-structures such as spheres, screws, various meshes, even up to bunny-shapes were fabricated.⁴⁷⁻⁴⁹ Further endeavors focus on scaffold-free approaches to omit the need for a long scaffold DNA and the so derived objects are therefore not constrained in size and scale.⁵⁰

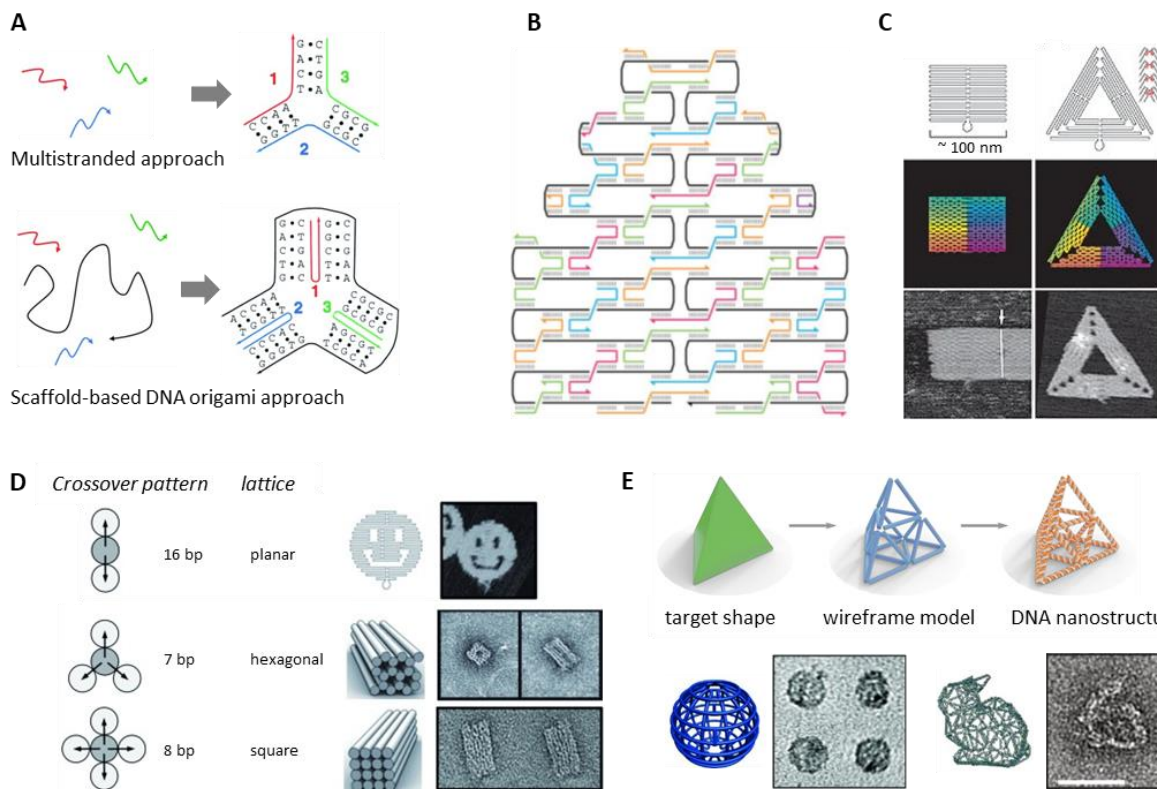


Figure 3 (A) DNA-based architectures can be built in a multistranded (hierarchical assembly of oligonucleotides through cohesion of sticky ends) or scaffold-mediated approach (folding of a single-stranded scaffold by a set of designated oligonucleotides). (B) Mainly 32-mers are spanning three helices, thus, forming the scaffold strand into any desired origami design. (C) Examples of rectangular and triangular origami, imaged by atomic force microscopy. (D) Depending on the design of the crossover patterns, various 2D- and 3D-origami can be constructed. (E) Wireframe approaches, *i.e.* DNA designs based on 3D meshing, require less material per volume and produce DNA-economical constructs. Reprinted and adapted with permission from ^{35, 41, 46-48}.

Functionalization of origami structures

While the chemical inertness of the DNA molecule is essential to impart high stability and high fidelity in DNA nanotechnology, it leaves the mere DNA nanostructures lacking in function. Except for functional DNA structures such as aptamers or DNAzymes, DNA is mainly considered as a molecular scaffold. In order to make functional DNA nanostructures, the integration of other molecules and materials is necessary which often requires chemical modification of the DNA strands. Automated phosphoramidite-based DNA synthesis is performed from the 3'- to the 5'-end and supports modification of oligonucleotides at the 3'-site (modified solid support), internally (either modified nucleobases or non-nucleobase phosphoramidites containing modifications), and at the 5'-site (modified phosphoramidites without the possibility for further chain elongation) (Figure 4).⁵¹ In many cases, required phosphoramidites are not commercially available, synthetically demanding, or that the functional moiety is not compatible with either DNA synthesis or succeeding workup. Here, milder

reactive handles are introduced to the DNA strand synthesis and the desired functionality is coupled to the handle in a post-synthesis fashion. Noteworthy, these conjugation reactions involve unprotected and charged oligonucleotides and are preferably performed in aqueous environments, further narrowing down the possible chemistries. Most prominent chemical handles are amino groups, thiols, and (cyclo-)alkynes that react with activated carboxylates (*e.g.*, NHS esters), maleimides, and azides, respectively. Two basic methods are distinguished for subsequent incorporation of the modified oligonucleotides into DNA nanostructures. The functionalized DNA strands is either (A) directly integrated in the origami structure as a staple strand that contributes to the folding of the scaffold strand or (B) attached after origami annealing by hybridization to staple strand extensions protruding from the surface.¹²

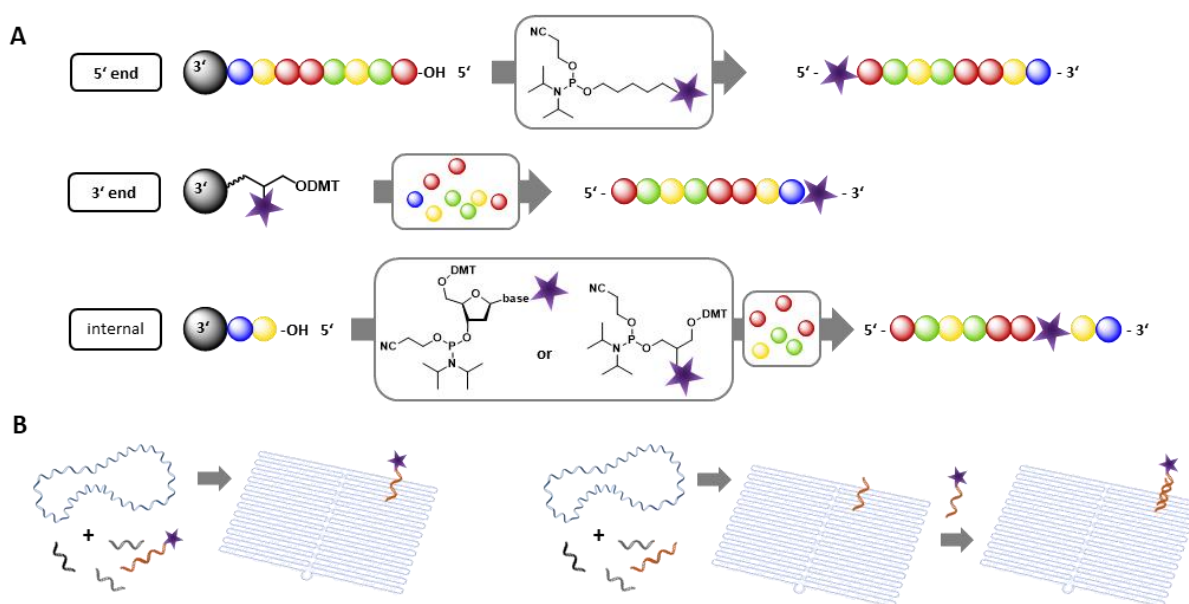


Figure 4 (A) Automated phosphoramidite-based DNA synthesis allows for modification of oligos and is performed from the 3'- to the 5'-end. It supports internal and 5'-modifications through respective phosphoramidites as well as 3'-modifications through modified solid supports. (B) Modified oligos can be used to introduce functional moieties into DNA origami. Either through direct integration in the origami structure as a staple strand or attached after origami annealing by hybridization to staple strand extensions protruding from the surface.

The first method offers high positional control and is facile since it only necessitates one hybridization step (*i.e.* folding of origami structure), however, the desired entity has to withstand high temperatures employed in the denaturation step prior to origami annealing. If several copies of the same modification are to be introduced at multiple position within the DNA framework, a unique DNA strand of the specific sequence is required for each modification site, potentially making it costly. The second method circumvents these drawbacks. Hybridization of the modified oligonucleotide to staple strand extensions occurs at much lower temperature (or even room temperature) and since these staple strand extensions can comprise the same sequence, only one kind of modified oligonucleotide is necessary to decorate several positions. Still, if orthogonal reactions are of interest, sequences of

protruding staple strands and complementary oligonucleotides can be easily adjusted. Although superior in the aspects described above, the second technique might have less position fidelity and lower functionalization density compared to the first approach.

Once integrated into the DNA nanostructure, chemical functionalities can aid in performing chemical reactions with further control over distances, ranging from covalent reactions, polymerizations, cross-linking, and metallization of the template. Furthermore, precise incorporation of macromolecular entities such as proteins or inorganic nanoparticles has received considerable attention. The efficiency of enzyme cascades, for instance, could be increased through controlled spacing between the enzymes.⁵²⁻⁵⁴ The most common modification in DNA nanotechnology, however, involves chromophores in Förster Resonance Energy Transfer (FRET) studies^{55,56} and applying them within the development of sensors,⁵⁷ photonic wires,^{58,59} light-harvesting systems,⁶⁰ among others. Since the decoration on DNA/DNA nanostructures with fluorophores is rather straightforward, Jungmann et al. took super-resolution microscopy on a next level by making use of transient binding events of short oligonucleotides in “DNA-PAINT” (*i.e.* points accumulation for imaging in nanoscale topography).⁶¹⁻⁶³ Here, the dynamic binding and unbinding of dye-labeled ssDNA (imager strands) to complementary targets (docking strands) fixed on DNA origami or cells creates stochastic fluorescence on/off-states necessary for imaging.

DNA origami in a biological context

In a cell-free setting, accompanied by continuous reduction in the cost of DNA synthesis, the increase in complexity of DNA nanostructures become more accessible. However, the full potential offered by DNA objects in terms of small sizes, biocompatibility, and programmability has yet to be exploited at the interface with biology. Prevailing hurdles entail stability of the structures after administration and reaching of target cells, uptake, endosomal escape and subcellular localization which have impeded adequate progress of the field. It is therefore necessary to bridge the gap from experiments in simple, isolated solutions to complex, heterogeneous cellular environments. In order to do so, two major factors that limit the stability of DNA nanostructures have to be taken into account: low level of magnesium ions and the presence of nucleases (Figure 5).⁶⁴ Divalent magnesium ions are typically required to compensate electrostatic repulsion between neighboring helices in DNA origami whereas nucleases are found in virtually all kinds of body fluids and tissues, thus, putting a threat on the nanostructures' integrity.

In order to stepwise elucidate the origamis' performance in a biological context, various approximations of the final target environment can be conducted first. Lysates as mixtures of cellular components after homogenization of cells can be used to evaluate the integrity of DNA nanostructures

in a medium that closely resembles intracellular environment. Serum stability studies can also mimic certain parts of cellular environment due to the lack of stabilizing cations and by exposing the structures to nucleases. In an early study, DNA origami nanostructures were found to be stable in cell lysate for up to 12 hours, whereas long single- and double-stranded nucleic acids could not be recovered after incubation.⁶⁵ In addition, high-speed AFM studies revealed that degradation profiles of 2D shapes are structure-dependent.⁶⁶ To date, numerous reports on enhancing the stability of origami have been published. The envelopment of DNA nanostructures in PEGylated bilayers, for instance, furnished protection against nuclease digestion, mimicking the morphology of enveloped viruses.⁶⁷ Since DNA is negatively charged, electrostatic interactions with positively charged molecules can be exploited for origami coating to enhance stability. In that respect, cationic albumin could be either directly bound to origami structures or indirectly after modification of the native protein with a dendron part acting as a cationic binding domain.^{68,69} Furthermore, decoration of DNA objects with DNA itself, *e.g.*, oligonucleotide strands, also offers promising results: Functionalization of the outer surface with dendritic ssDNA reduces nuclease digestion due to putative steric hindrance.⁷⁰ Through enzymatic polymerization, DNA origami nanostructures can site-specifically be modified with polynucleotide brushes of different heights and compositions, thus, contributing to their stability and also providing a route to smart, cleavable objects by asymmetric decoration.⁷¹ Very recently, minor-groove binders were shown to control DNase-mediated degradation rates of wireframe origami structures in serum under *in vitro* conditions.⁷² As an alternative to the modification of DNA origami with external molecules, the structures themselves can be manipulated intrinsically. Whereas conventionally employed DX motifs connect two adjacent helices, a so-called paranemic crossover (PX) is a four-stranded DNA structure that connects strands of the same polarity at every possible point. Importantly, PX DNA demonstrates significantly enhanced resistance against nucleases that scales with the number of crossovers.⁷³

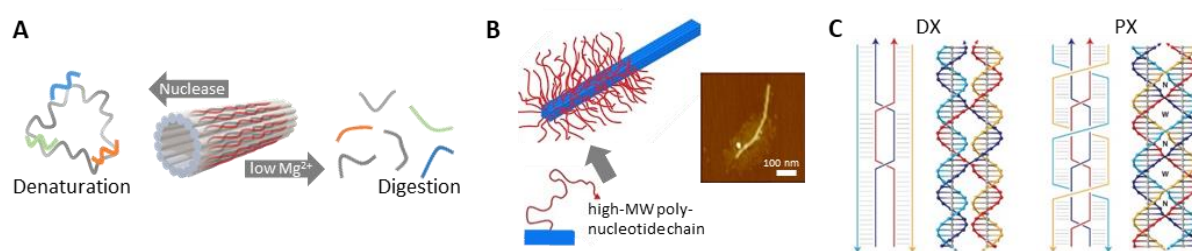


Figure 5 (A) In a biological context, DNA origami structures are susceptible towards the presence of nucleases and a lack of stabilizing ions, leading to denaturation or digestion processes, respectively. (B) Site-specific and enzyme-catalyzed modification of origami tubes with polynucleotide chains increases their nuclease resistance. (C) Contrary to DX motifs, paranemic crossovers connect strands of the same polarity at every possible point, thus, contributing to stability. Printed and adapted with permission from ^{71,73}.

For cell targeting it is crucial that DNA origami structures maintain integrity for a sufficient period of time, *i.e.*, surviving in the blood stream when delivering *in vivo*. Typically, DNA origami are

assembled in buffers with high Mg^{2+} concentrations (~ 10 mM) so that the counterions can stabilize the dense package of negatively charged DNA helices. However, once formed, the structures are able to withstand low levels of Mg^{2+} whilst this effect largely depends on the individual superstructure.⁷⁴ Alternatively, 3D origami can be formed in magnesium-free buffer containing low levels of the DNA-condensing agent spermidine. In contrast to conventionally annealed origami, spermidine-stabilized structures could be delivered into mammalian cells via electroporation.⁷⁵

In addition to these strategies, polymer coating of DNA origami attracts considerable attention and chapters **1.3** and **1.4** highlight respective endeavors in greater detail. However, a prominent example in this regard is the electrostatic coating of DNA nanostructures with polylysine-polyethylene glycol block copolymers which is simple to manufacture yet effective in protecting the structures from nuclease degradation.⁷⁶ Whereas the attained polymer–DNA hybrid structures were found to increase nuclease resistance by approx. 400-fold, glutaraldehyde mediated cross-linking of the polymer coating could extend survival of corresponding DNA origami by another 250-fold even with excess DNase I.⁷⁷

78

Once the stability issues are adequately addressed, one can finally make use of the unprecedented addressability of the platform. In order to target specific cells, ligands can be introduced that specifically recognize and bind to receptors on the relevant cell type. Here, aptamers, *i.e.*, oligonucleotides whose 3D structures provide affinity for a given target and that resemble the selectivity and specificity of antibodies, are broadly explored.⁷⁹⁻⁸² Notably, the size and shape of the pristine DNA origami structure without further modifications already affects the membrane translocation.^{83, 84} Moreover, DNA origami enables investigation of distance-dependent multivalent binding effect by deterministic positioning of multiple-affinity ligands when targeting thrombin molecules.⁷⁹ In comparison to small molecule target binding, protein–aptamer complexes can be visualized in AFM imaging, allowing direct yet fairly labourious analysis. Similarly, DNA rectangles were equipped with 12 aptamers targeting a malaria biomarker in human blood plasma and binding was monitored by AFM.⁸⁵ In a more dynamic approach, a cocaine aptamer-modified DNA nanocage was capable of sensing cocaine concentrations due to binding-induced conformational changes.⁸⁶ Also based on dynamic binding, a DNA nanorobot was constructed to transport payloads specifically to tumors. Herein, a nucleolin-targeting aptamer is positioned on the outer surface which serves not only as a targeting domain but also as an opening mechanism of the nanorobot upon binding where the protease thrombin is loaded into the inner cavity. After intravenous injection in tumor-bearing mouse models, the inner cavity exposes thrombin, thus, inducing intravascular thrombosis and tumor necrosis.⁸⁷ This example illustrates the capability of the DNA origami technology for orthogonal modifications in a highly precise fashion.

1.2 Polymers in a biological world

1.2.1 Poly(catecholamines)

With the advent of modern polymerization technologies, polymer chemists can synthesize a plethora of polymers with an unprecedented degree of homogeneity and tailorable features. The increasing global need for sustainable polymers to address environmental and climate challenges has fueled the community to relook into polymer chemistry and seek inspiration from biopolymers. Synthesized by living organisms, biopolymers perform purposeful tasks such as cellulose being an important component of green plants' cell walls, chitosan stabilizing the outer skeleton of insects, among others.

When human skin is exposed to UV irradiation, for instance, it darkens. This phenomenon is due to the evolution of melanin, a class of natural pigments that are responsible for the coloring of skin, hair, feathers, and eyes of organisms.⁸⁸ Eumelanin, the most common type, is produced in an enzymatic multistage process, starting with the amino acid tyrosine that undergoes oxidation and subsequent polymerization to give brown and black pigments.^{89,90} Melanocytes – melanin synthesizing cells – are found in the basal layer of the epidermis and once produced, melanin is packed into organelles – melanosomes – that are delivered to surrounding cells to protect them against UV radiation (Figure 6).

The first oxidation product of tyrosine in melanin production, the non-proteinogenic amino acid L-DOPA (3,4-dihydroxy-L-phenylalanine), is further found in the marine world as a vital part in the byssal fibers of mussels.⁹¹ Mussels can adhere to virtually all types of inorganic and organic surfaces, a characteristic which is attributed to the special composition of their anchoring threads. Rich in both L-DOPA and amine containing residues (lysine and histidine), mussel foot proteins can form extremely strong covalent and non-covalent interactions with substrates. Moreover, similar to melanin production, oxidation of L-DOPA's catechol moieties in alkaline seawater leads to bulk solidification of the mussel foot proteins, representing a robust glue. Inspired by the adjacent coexistence of catechol and amine units, dopamine was therefore considered as a small molecule representing a powerful building block for spontaneous polymerization processes.⁹² Together with other natural catecholamines such as norepinephrine, L-DOPA and dopamine are known for their role as neurotransmitters, hormones and pigments and are now repurposed in a chemical fashion and exploited for, *e.g.*, the coating of surfaces.^{93, 94} This class of molecules is characterized by the aforementioned catechol group and ethylamine side chain whereas the individual compounds differ in their side chain modification on the carbon atoms of the ethyl side chain.

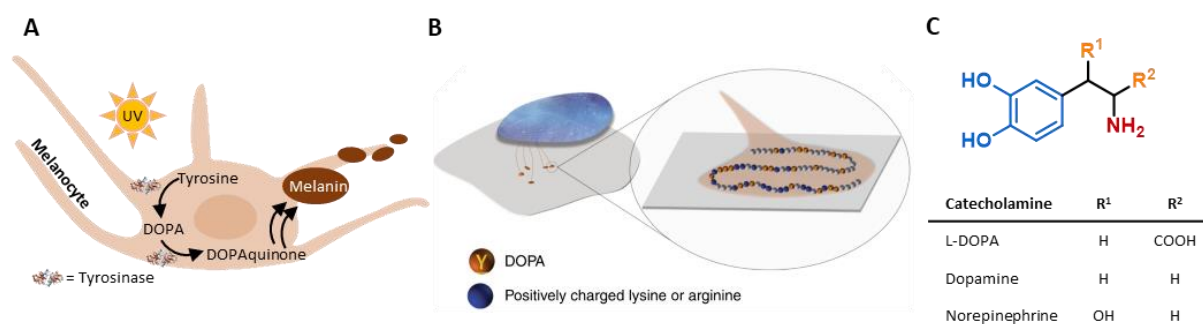


Figure 6 (A) In melanocytes, a multi-step enzymatic process converts the amino acid tyrosine into melanin when exposed to UV-irradiation. (B) The ability of mussels to adhere to virtually any surface is attributed to the predominance of both L-DOPA and amine containing residues in mussel threads. Reprinted and adapted with permission from ⁹⁵. (C) Catecholamines are characterized by a catechol group and ethylamine side chain.

In their seminal work in 2007, Lee and coworkers subjected dopamine to conditions similar to that of mussels in order to mimic and explore the formation of a super glue.⁹² Simple immersion of objects into a solution of dopamine buffered at pH 8.5, *i.e.*, resembling the slightly alkaline marine environment, induced spontaneous deposition of thin polymeric films. Remarkably, this autooxidation of dopamine in the presence of dissolved oxygen demonstrated to be a universal strategy to coat a broad variety of surfaces such as metals, glass, polymers, and even PTFE.⁹⁶⁻⁹⁸ Although the mechanism of pDA formation is similar to melanin biosynthesis and despite huge efforts in the field, the full structure of pDA has yet not been fully elucidated (Figure 7).^{99, 100} As in melanin formation, the polymerization of dopamine starts with oxidation to a quinone molecule. Then, in alkaline environment, the nucleophilic attack of the free amine at the C6 position leads to cyclization and formation of leucodopaminechrome. Additional oxidation and isomerization results in 5,6-dihydroxyindole (DHI) which is further oxidized into 5,6-indolquinon. These two intermediates are important for polymerization as they can undergo comproportionation to two semiquinone radical groups which can then couple covalently. Carbon-carbon bonds between adjacent aromatic nuclei can occur at any free positions on the rings which leads to dimers, trimers, higher order oligomers and their aggregates.^{101, 102} However, these pathways are complex and still remain ambiguous, which also applies for the ultimate chemical structure of pDA. Numerous studies were performed and suggest the presence of supramolecular aggregates based on charge transfer, π - π and cation- π interactions, non-covalently self-assembly of dopamine and intermediates as well as covalent oligomers and polymers.^{92, 99, 100} With respect to the latter category, even high molecular weight polymers up to 200 nm in length were recently found to be existent in pDA films.¹⁰³

In spite of its complex and unclear structure, the simplicity of pDA synthesis and its decent physical and chemical features have granted pDA much acclaim across a multitude of science and engineering disciplines. In a biology related context, pDA coatings could assist in building DNA microarrays and biosensors. In a single-step process, deposition of pDA from dopamine solutions on

thin gold microarray elements can be achieved and reacted with amine-modified ssDNA strands. Subsequent detection of biomolecules by surface plasmon resonance imaging benefits from the pDA layers that interestingly provide good resistance to nonspecific binding events.¹⁰⁴ Likewise, the universal adhesiveness of pDA can be exploited to coat nanoparticles of diverse chemical nature, such that the intermediate polymer layer covalently bounds oligonucleotides via amine or thiol functionalities. The decorated nanoparticles exhibit high loading density of DNA while preserving its biological function which is crucial when aiming for successful cell targeting or subsequent hybridization steps.¹⁰⁵ Evidently, not only oligonucleotides can be bound to pDA-coated NP, also H₂N- and SH-containing BSA, poly-L-lysine, among others, can thereby be attached to modulate pharmacokinetics of the NP without the need for reactive linker chemistry or pH- and concentration-sensitive electrostatic adsorption.¹⁰⁶ In general, the uptake of nanoparticles into cells is a highly regulated mechanism and depends on several factors such as size, shape, net charge, among others. Cationic nanomaterials are conventionally preferred carriers due to their high ability to penetrate the negatively charged cell membrane. Yet, these nanoparticles are known to cause cytotoxicity and immune response, thus, limiting their clinical translation. Abandoning positive surface charges of particles often leads to rather poor cell uptake and numerous counterstrategies have been developed.^{107, 108} Notably, polydopamine coating as a non-cationic biomaterial can abundantly enter various cell types.¹⁰⁹ While there is evidence for dopamine receptor-mediated binding of pDA-coated NP through monomeric DA units¹¹⁰ and also three specific pathways in HeLa cells¹¹¹, other mechanisms involving cell-surface receptors are still under investigation. In an approach to reduce the chemical variety to only the most essential moieties in pDA while achieving similar properties, a random copolymer with catechol and amine side chains and a molecular weight of 160–210 kDa was generated. Incubation with various substrates analogously to classic pDA deposition protocols led to the desired polymer coating. Noteworthy, no further surface treatment was necessary to immobilize DNA, thus, presenting a robust and cost-effective method for microarray fabrication. Compared to conventional pDA coating, this strategy have led to more defined and more homogenous polymer films which can assist biosensor fabrication.¹¹²

In spite of the attractive attributes, the extensive use of pDA coating is facing certain limitations. A lack in synthetic control and resulting surface morphology turned out to be a substantial concern, also prohibiting further translation to applications. During polymerization of DA, formation of nano-/ microparticulate aggregates of pDA and oligoDA is inevitable. These aggregates either form in solution and deposit through π - π and van der Waals forces or grow directly from the surface by polymerization. Surface roughness is therefore significantly higher.¹¹³ However, when a smoother surface is required, DA can be replaced by another catecholamine: norepinephrine.^{114, 115} Polynorepinephrine (pNE) coating show similar simplicity in formation and ability to adhere to various

materials but can provide ultrasmooth surfaces. Although the molecular structure of both monomers, DA and NE, differs solely in the presence of an additional alkyl hydroxyl group, the respective intermediates in the polymerization process drastically impact surface morphology later on.^{116, 117} Under oxidative conditions, NE can be transformed into 3,4-dihydroxymandelic acid, which is followed by an oxidative cleavage of the side chain. The resulting catechol aldehyde (3,4-dihydroxybenzaldehyde, DHBA) subsequently reacts with another monomer's amine moiety in a reversible Schiff-base formation reaction. The so-formed DHBA-NE product is pivotal in preventing intermolecular aggregation of NE intermediates and thus, reducing surface roughness. The role of DHBA is also supported by the observation that simple addition of DHBA to the pDA polymerization process leads to a smoother surface compared to conventional pDA coatings.¹¹³

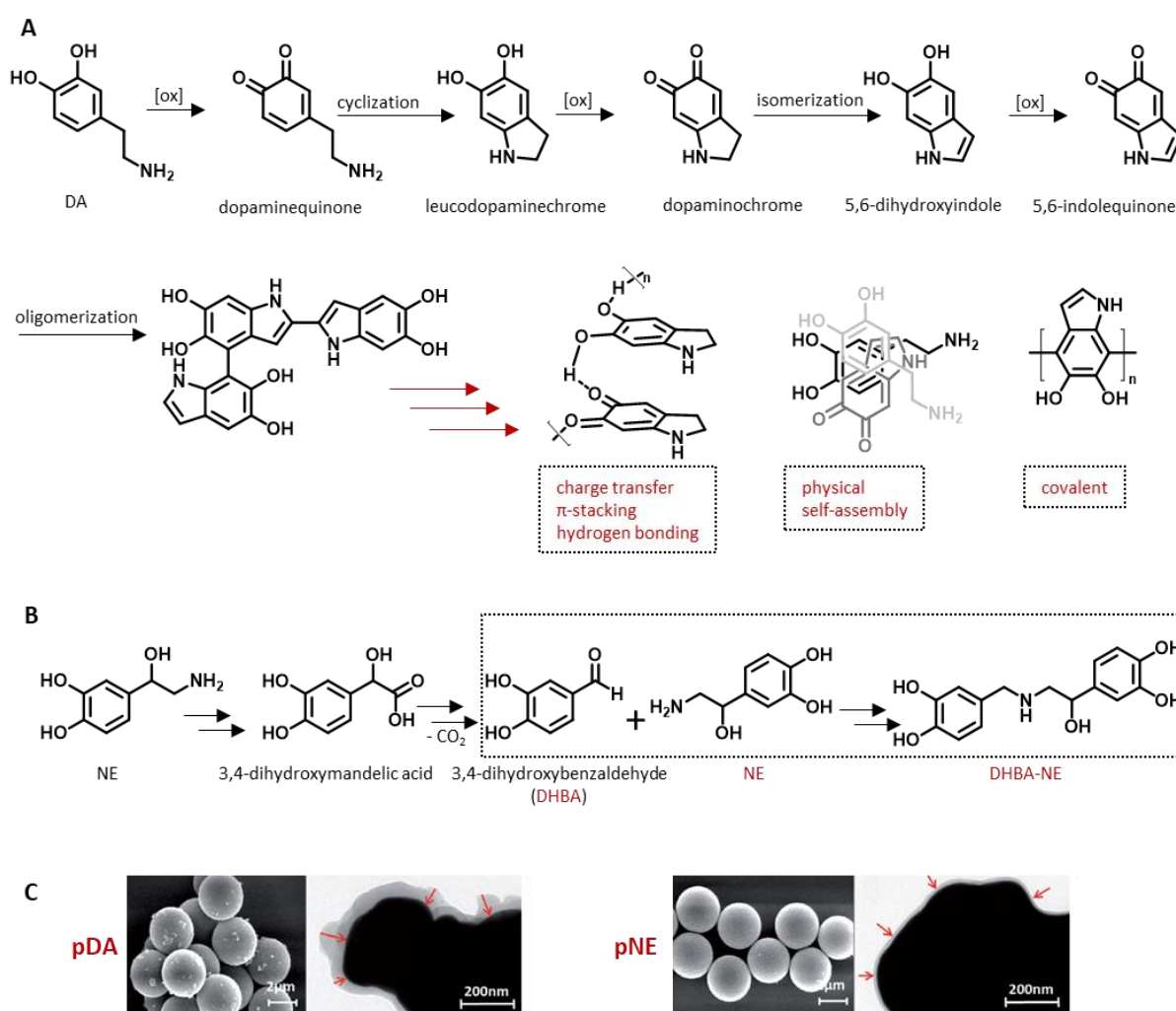


Figure 7 (A) The formation of polydopamine involves many oxidation, cyclization, and isomerization steps. The structure of the polymer is still under elucidation, however, the presence of monomers, oligomers, polymers and supramolecular aggregates are reported. (B) Polynorepinephrine surfaces are described as ultrasmooth, a feature which is mainly attributed to the occurrence of the intermediate 3,4-dihydroxybenzaldehyde. (C) SEM and TEM images show the reduced surface roughness of pNE-coated PS and silver particles compared to pDA-coating. Printed and adapted with permission from¹¹³.

The presence of an aliphatic secondary amine of DBHA-NE can also be exploited for biomedical applications as a nitrite oxide (NO)-loading platform. Physical adsorption of NO-containing compounds as well as stability considerations can thereby be omitted.¹¹³ Furthermore, the additional hydroxyl group in pNE coatings can serve as a handle for post modification by initiating ring opening polymerization of lactone monomers and inducing a hydrophobic film on top of the pNE layer.¹¹⁴ Similar to pDA, the features of pNE such as high biocompatibility and almost substrate-independent coating have been leveraged in biological applications. Although pNE shows equal or even superior performance, research on pDA is more established. One minor reason may be higher costs of the NE monomer. However, there are studies reporting higher suitability of pNE compared to other catecholamines: Especially with regards to the surface modification of cardiovascular materials, pNE coating demonstrated best histocompatibility and less adhesion of platelets.⁹⁴ In another work, pNE nanoparticles were fabricated through autoxidation and loaded with doxorubicin. Here, particle size optimization was achieved by varying solvent and monomer dosage. The NP exhibited higher pharmaceutical cytotoxicity than the free drug and are thus regarded as promising drug delivery vehicles.¹¹⁸ Also when manufacturing nanoparticles from pNE in an oil-in-water process, the polymerization protocol can be adapted to influence the later shape of the particles. The concentration of copper ions, for instance, will impact the diameter of the derived microcapsules and shell thickness.¹¹⁹ Moreover, particles do not have to be built purely from pNE. The adhesiveness of pNE can be utilized to coat, *e.g.*, FeOOH particles and to entrap an anticancer drug. Here, again, the authors favored pNE over pDA because of more uniform and thinner coating properties.¹²⁰

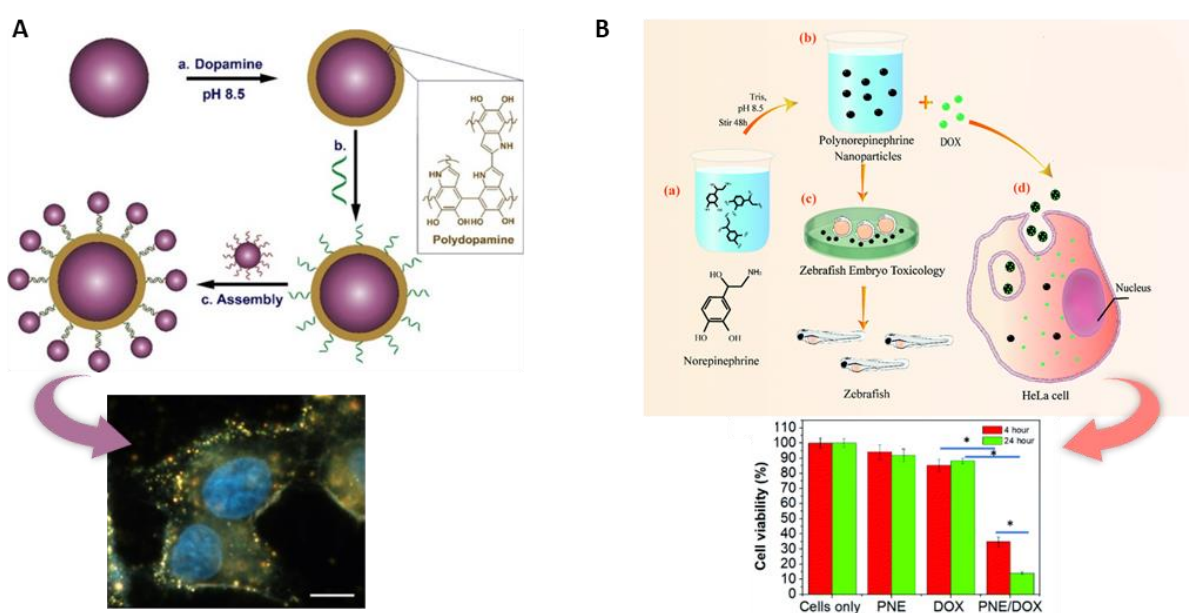


Figure 8 (A) The universal adhesiveness of pDA can be exploited to coat nanoparticles with oligonucleotides via amine or thiol functionalities, directing cancer cell targeting. Overlaid dark field and fluorescent image of aptamer-modified Au-PDA particles, scale bar is 20 μm. (B) Polynorepinephrine particles can be loaded with DOX for delivery into HeLa cells. Quantification of cell viability upon treatment with only pNE particles, free DOX, and DOX-loaded pNE particles illustrates the efficacy of the combined approach. Printed and adapted with permission from ^{105, 118}.

Concluding, whenever a biocompatible and versatile coating in the nm Range is required, catecholamine monomers are promising candidates with almost 15 years of extensive research going on.

1.2.2 Photodynamic Therapy, Photosensitizer, and Photopolymerization

Polymerization of monomers can be triggered by various stimuli such as by chemical, thermal, or electrochemical means to successfully overcome the energy barrier. Compared to these conventional processes, photoinduced polymerization systems can be fairly easily exploited for complex and selective macromolecular synthesis at ambient conditions. Chemically induced reactions, for instance, require the addition of a reactive agent, and – if no quenching reaction is applied – the reaction will continue until these triggers are fully exhausted. Thermal processes are enabled through an increase in heat, limiting in certain cases the use of temperature-sensitive substrates, *e.g.*, biomolecules. The success of photopolymerization, however, is founded upon the rise of light emitting diode (LED) technology on the one hand, and the advent of controlled radical polymerization on the other.¹²¹ Herein, a chromophore is excited through photons from the incident light, promoting an electron to higher energy orbitals and thus, generating more energetic species. The excited state chromophore will eventually undergo one of several processes to transfer the additional energy and thereby fall to an energetically stable state again. A photochemical reaction is only started when energy is transferred to another molecule, instead of deactivation through thermal radiation or luminescence. Photosensitizers (PS) represent a class of molecules that possess these particular features and are therefore exploited in photopolymerization. They absorb energy from light spanning the UV, visible or infrared-spectrum and transfer this energy either directly or by a chemical reaction to nearby molecules.^{122, 123} According to their mode of action, they can be classified as type I or type II PS (Figure 9). Type I PS in their excited triplet state react directly with the substrate, forming the product and releasing the PS in its initial relaxed state. Excited type II PS, however, firstly excite ground state oxygen into the singlet state which in turn reacts with the substrate, leading to product formation.

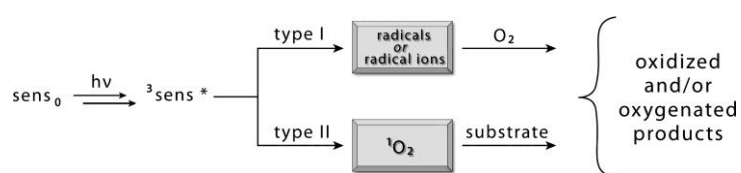


Figure 9 Photosensitized reactions can be classified into two pathways. Activated type I photosensitizer react with the acceptor, in a one-electron transfer reaction, to produce a radical ions and reactive oxygen species. In type II photosensitized reactions, the excited PS reacts with a ground state oxygen molecule into singlet oxygen which then react with the substrate to form product. Reprinted with permission from ¹²².

A prominent example of the application of a PS in a biomedical context can be found in photodynamic therapy (PDT).¹²⁴ PDT is a mainly minimally invasive method for the treatment of tumors or defective tissue and relies on three components: light, a photosensitizer, and tissue oxygen. The PS is either locally or systemically applied, whereas specific tumor characteristics such as excessive cell growth, increased metabolic activity or increased perfusion enforce the accumulation of PS at the required side of action. Strong absorption of the PS in red/near infrared spectrum is preferred as it allows for deeper

tissue penetration, referred to as the therapeutic window.¹²⁵ Once brought into its excited triplet state, the PS can either directly interact with the substrate such as the cell membrane (type I) or forming highly cytotoxic singlet oxygen which in turn reacts with amino acid residues or unsaturated lipids (type II). The half-life of singlet oxygen in biological systems is approximately 40 ns, defining a radius of action in the range of 20 nm so that only proximal cells are directly affected in PDT. The so caused destruction of cellular membranes and deactivation of enzymes eventually lead to cell death, marking therapeutic success.¹²⁶ Cell death can comprise apoptosis, necrosis, and autophagy events and the dominance of each pathway also is significantly influenced by the localization of the photosensitizer (Figure 10). As a consequence, the multifactorial photodamage thus depends on the type of photosensitizing agent, its concentration and localization, light exposure dose as well as oxygen availability.

More than 100 years ago, Eosin Y was used in the first medical photosensitization reaction in which the interplay of the fluorescent compound and light was exploited to treat skin tumors.¹²⁷ This was preceded by the observation that the oral application of Eosin Y provoked dermatitis in sun-exposed areas of the skin. Eosin Y is an anionic xanthene dye derived from fluorescein that exhibit intense absorption bands in the green wavelength range from 480–550 nm and its high singlet oxygen quantum yield is marking Eosin Y primarily as a type II PS.^{128, 129} This capability is for instance reflected in a study where excitation of incorporated Eosin Y causes lipid hydroperoxidation of unsaturated chains in Langmuir monolayers.¹³⁰ Furthermore, by incorporating the PS into smart carrier systems it is even possible to elevate the level of spatiotemporal control in PDT. Conjugation of Eosin Y to pH-responsive block copolymers results in inactive drug micelles in extracellular milieu but upon endosomal uptake, however, micellar breakdown release makes the PS responsive for PDT again.¹³¹ Similar to other medical treatments, PDT also benefits from utilizing pharmacologically inactive prodrugs instead of readily available drug molecules to ensure selective targeting, increased biodistribution and minimize side effects. Aminolevulinic acid (ALA) combines extraordinary benefits for PDT in that respect: Being an endogenous key precursor in the bioformation of heme, its external administration outplays downstream enzyme activity, leading to accumulation of the prodrug in the cell. In particular, ALA, marketed as Levulan, is quickly converted into protoporphyrin IX (PPIX) – being the potent photosensitizer herein – but not further into heme due to insufficient enzyme rates in subsequent synthesis.¹³² PPIX is a planar, tetrapyrrolic molecule that exhibit the typical porphyrin absorption spectrum with a strong Soret band around 400 nm and weaker absorptions between 450–700 nm, so-called Q bands. Several hours after ALA administration, PPIX accumulation enables for excitation at 635 nm and 375–400 nm and subsequent formation of singlet oxygen.¹²⁶ Notably, excitation with artificial light sources can be rather painful, such that topical application on skin and exposure to daylight showed to have similar effects but with far milder symptoms.^{133, 134}

While ALA localizes in mitochondria, another effective PS, methylene blue, is mainly localizing in lysosomes.^{127, 135} This target-specific knowledge could be leveraged to improve PDT: The efficiency of photoinduced cell death showed to primarily depend on the specific location of the generation of reactive species rather than the amount of oxidant species. Due to their relatively short lifetime, they cause damage with the nm-vicinity of the PS and can thereby equip PDT with spatial control. The phenothiazinium dye methylene blue is a promising candidate for PDT also because of its high absorbance in the red spectral region (550–700 nm), *i.e.*, within the therapeutic window and its triplet state exhibits appropriate energies for the sensitization of oxygen.¹²⁸ Once more, the involvement of nanomedicine demonstrated to increase the therapeutic effect. Compared to free MB, MB-modified gold nanoparticles significantly enhance PDT efficiency (2-fold) while reducing the PS's dark toxicity.¹³⁶ Furthermore, simultaneous imaging and PDT could be achieved through the encapsulation of MB into silica nanoparticles, thus, providing *in vivo* image-guidance for site-specific therapy.¹³⁷

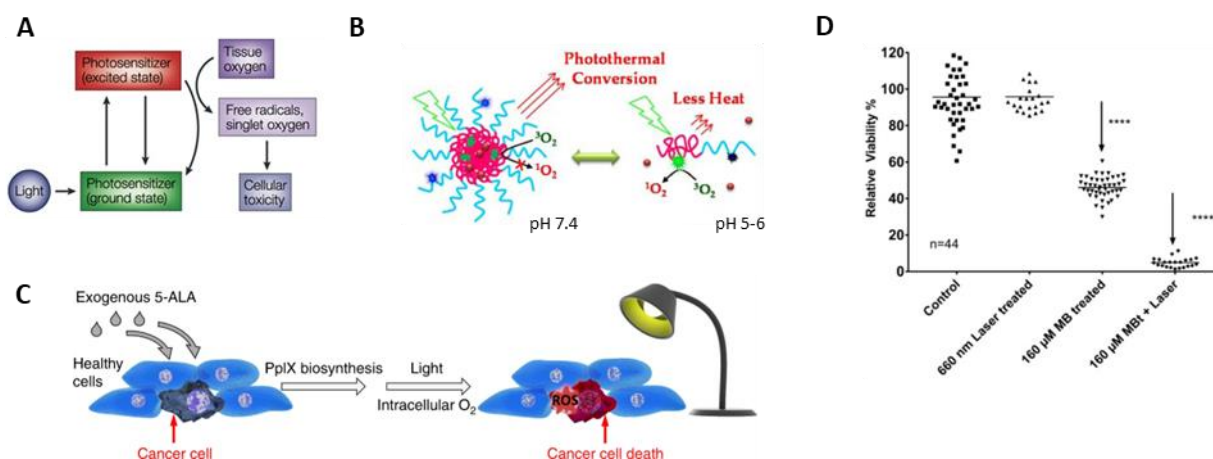


Figure 10 (A) In photodynamic therapy, the interplay of light, photosensitizer and tissue oxygen is critical for therapeutic success. (B) Eosin-conjugated pH-responsive polymeric nanoparticles enable spatiotemporal switching in PDT. At neutral pH in extracellular environment and cytosol, PS is trapped in micelles and only exposed under acidic conditions, restoring its photodynamic effect. (C) Cancer cells show a precedence in converting the prodrug ALA into protoporphyrin IX, a very potent PS whose accumulation in mitochondria enables PDT with reduced side effects. (D) When investigating the photodynamic effect of MB on cancer cells (Detroit 562), best results were achieved by irradiation of MB. Here, up to 95% reduction of the cell viability compared to the control was observed, whereas almost half of this cell loss is attributed to light specific effects. MB treatment alone accounts for only 67% reduction of cell viability and laser treatment alone rarely had an effect at all. Reprinted and adapted with permission from reference ^{126, 131, 138, 139}.

Similar to PDT but in a less biological setting, photo-responsive molecules such as chromophores can also be exploited to implement extrinsic control into polymerization reactions through light (Figure 11). While the chromophore's molecular structure determines its physical and chemical properties such as excited state lifetime or wavelength-responsiveness, the solvent environment and temperature impact quantum yields.¹²¹ Being an externally applied stimulus, both wavelength and intensity can be simply adjusted for any particular reaction, providing high degree of adaptability. The major benefit associated with photopolymerization is the facile temporal control of polymer growth by switching the light source between ON/OFF states. Thereby, the generation of reactive species can

be initiated and stopped on demand and the monomer conversion follows a step-like process. In an ideal scenario, no additional conversion occurs during the dark phase, however, in some reported systems, a minor polymer growth can be observed. *In situ* monitoring by NMR spectroscopy revealed that this particularly impacts Cu-mediated CRP where increased lifetimes of residual Cu(I) catalyst support chain growth after initial photoactivation.¹⁴⁰ Although this observation is not applicable to the broad range of photopolymerization systems, it reveals the necessity to ensure careful investigation of off-cycle measurements in appropriate time periods. In contrast to the vast amount of oxygen tolerating polymerization techniques, advanced temporal control can be achieved through a dual-gated polymerization system based on light and oxygen presence. Here, oxygen is not only tolerated but indispensably integrated into the RAFT process. Only upon illumination and under aerobic conditions, the photocatalyst together with a co-catalyst can activate the RAFT agent. Thus, purging of the reaction with an inert gas even during irradiation results in cessation of polymerization while reapplying oxygen has the reverse effect.¹⁴¹

As an extension of aforementioned temporal control, spatial control can exclusively extend the application of photopolymerization. The precise activation of polymer growth only in certain areas can for instance be implemented through physical barriers, so-called photomasks, or laser technologies.^{142, 143} Comparable to PDT, the creation of polymer brush patterns benefits from the rather short excited life state of the photocatalyst: Since reactive species cannot diffuse over distances greater than 20 nm, structural resolution does not suffer from significant losses. In particular, substrates are modified with a layer of initiators and through application of a photomask, brush growth can be spatially confined whereas non-exposed areas of initiators are still active for subsequent reactions steps.¹⁴⁴

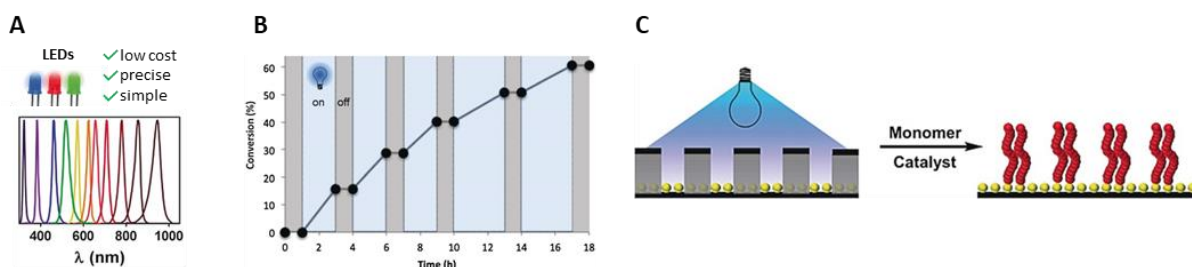


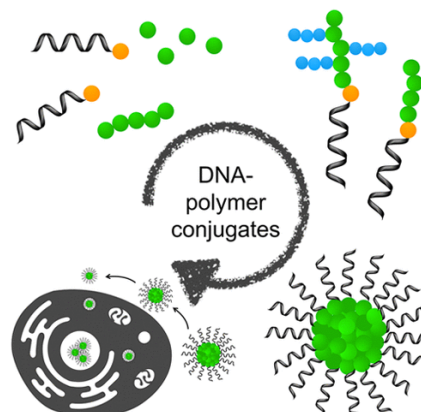
Figure 11 (A) LEDs are a convenient light source for photochemistry thanks to low cost, precise emission wavelength, and simple equipment. (B) Temporal control, *i.e.*, switching between ON and OFF states, is one of the major benefits of photopolymerization. (C) Photomask technologies can further provide spatial control and distinctly localize areas of chain growth. Figures adapted from ¹²¹.

1.3 Functional DNA–polymer conjugates: Noncovalent DNA–polymer interactions

Publication: “**Functional DNA—Polymer Conjugates**”

Colette J. Whitfield, Meizhou Zhang, Pia Winterwerber, Yuzhou Wu, David Y. W. Ng, Tanja Weil *Chem. Rev.* **2021**, 121, 11030-11084.

The publication in this chapter is reprinted under creative commons (CC BY 4.0).



The biological role and impact of DNA is fairly evident, however, its integration into the synthetic world of chemists and material scientists shed a different light. Here, solid phase synthesis paved the way for facile generation of short DNA strands of arbitrary sequences and incorporation of chemical functionalities and handles. Together with the near limitless capacity of polymer chemistry to yield macromolecules with complementary features, novel hybrid materials with unique characteristics can be created. Most prominent are amphiphilic DNA–polymer conjugates that give access to various morphologies such as spherical and rod-like micelles. These nanostructures can further be equipped with stimuli-responsiveness towards physical properties and competitive complementary DNA binding, giving rise to functional and dynamic systems.

The review presented in this chapter discusses the progress of DNA–polymer conjugates, picking up synthetic routes and state-of-the-art applications. Of particular importance for this thesis is the review section on “Noncovalent DNA–polymer interactions” as it combines the two fields of “DNA nanotechnology” and “polymers” described in introduction chapters **1.1** and **1.2** and gives fundamental knowledge into the work discussed in the “Results and discussion” (**3**) part later on in this thesis. The review section “Noncovalent DNA–polymer interactions” also reflects my contribution to the *Chem. Rev.* article as the section’s conceptual structure, literature screening and discussion as well as writing was performed by me. In brief, the chapter reports how the rather inert structure of DNA can be exploited for touch points with polymer chemistry through its nucleobases, the negatively charged phosphate-deoxyribose backbone, the major/minor grooves of the double helix as well as the 5’/3’ termini.

Functional DNA–Polymer Conjugates

Colette J. Whitfield,[§] Meizhou Zhang,[§] Pia Winterwerber, Yuzhou Wu,^{*} David Y. W. Ng,^{*} and Tanja Weil^{*}

Cite This: *Chem. Rev.* 2021, 121, 11030–11084

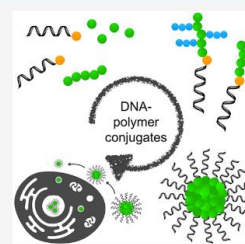
Read Online

ACCESS |

Metrics & More

Article Recommendations

ABSTRACT: DNA nanotechnology has seen large developments over the last 30 years through the combination of solid phase synthesis and the discovery of DNA nanostructures. Solid phase synthesis has facilitated the availability of short DNA sequences and the expansion of the DNA toolbox to increase the chemical functionalities afforded on DNA, which in turn enabled the conception and synthesis of sophisticated and complex 2D and 3D nanostructures. In parallel, polymer science has developed several polymerization approaches to build di- and triblock copolymers bearing hydrophilic, hydrophobic, and amphiphilic properties. By bringing together these two emerging technologies, complementary properties of both materials have been explored; for example, the synthesis of amphiphilic DNA–polymer conjugates has enabled the production of several nanostructures, such as spherical and rod-like micelles. Through both the DNA and polymer parts, stimuli-responsiveness can be instilled. Nanostructures have consequently been developed with responsive structural changes to physical properties, such as pH and temperature, as well as short DNA through competitive complementary binding. These responsive changes have enabled the application of DNA–polymer conjugates in biomedical applications including drug delivery. This review discusses the progress of DNA–polymer conjugates, exploring the synthetic routes and state-of-the-art applications afforded through the combination of nucleic acids and synthetic polymers.



CONTENTS

1. Introduction	11031	4.1. Static Nanostructures	11059
2. Chemistries on DNA	11031	4.1.1. Assemblies Induced by Hydrophobic Interactions through the Polymer Segment	11059
2.1. Solid Phase Synthesis	11031	4.1.2. Assemblies Induced by Sequence Hybridization of the DNA Segments	11061
2.2. In Solution	11033	4.1.3. Nanostructures Involving DNA and Polymer Induced Assembly	11063
2.3. Complexation	11034	4.2. Dynamic Nanostructures	11065
3. DNA–Polymer Synthesis	11037	4.2.1. DNA Programmable Dynamic Nanostructures	11065
3.1. Covalent DNA–Polymer Conjugates	11038	4.2.2. Temperature-Responsive Dynamic Nanostructures	11066
3.1.1. Polymerization Methods	11038	4.2.3. pH-Responsive Dynamic Nanostructures	11069
3.1.2. DNA–Polymer Conjugate Synthesis Limitations	11039	4.2.4. Light-Responsive Dynamic Nanostructures	11069
3.1.3. Solution-Based ODN–Polymer Synthesis	11042	5. Functionality of DNA–Polymer Conjugates	11070
3.1.4. 1D DNA–Polymer Synthesis	11045	5.1. Functionality from the Polymer	11070
3.1.5. 2D and 3D Polymerization Platforms	11046	5.2. Functionality Based on DNA	11072
3.2. Noncovalent DNA–Polymer Interactions	11048		
3.2.1. Templating of Polymers by Single and Double Stranded DNA	11049		
3.2.2. Polymer Decoration of DNA Nanostructures	11053		
3.3. Chemistry of DNA–Polymer Conjugates Postcoupling	11056		
3.3.1. Chemistries on the Polymer	11056		
3.3.2. Chemistries on the DNA	11056		
3.4. Characterization of DNA–Polymer Conjugates	11056		
4. Supramolecular DNA–Polymer Complexes	11058		

Special Issue: Polymeric Biomaterials

Received: October 2, 2020

Published: March 19, 2021



For reasons of clarity, only review chapter 3.2 on “Noncovalent DNA–Polymer Interactions” is displayed here. Pages before (11031–11047) and afterwards (11057–end) are listed comprehensively as part of the full article in the Appendix at the end of this thesis.

addition of defined monomers via stepwise coupling and washing was realized. In this instance, two phosphoramidite oligomers consisting of either a hexaethylene glycol or hexaethylene (HE) unit were adopted as hydrophilic and hydrophobic monomers and ordered in a controlled manner (Figure 10B). In their first work, polymer lengths of up to 12 units were explored and shown to have high control over the sequence. They next explored polymer lengths up to 24 units with varying content demonstrating the ability to increase polymer length through this approach.⁷⁹ This method highlighted the potential for DNA–polymer conjugation where both the DNA and polymer content are sequence defined, although polymer length is still limited and may require further exploration to improve the solid phase monomer conjugation scope.

The examples so far have produced a conjugate containing DNA as a polymer block; however, they have not exploited the capabilities of DNA to guide the polymerization to precise assemblies through its sequence-specific interactions. DNA sequences can be programmed through their specific base pairing to form folded nanostructures. DNA nanostructures were first envisaged by Seeman in 1980, beginning as lattice structures up to more recent examples of sophisticated DNA origami structures as reviewed previously.¹³² DNA origami was proposed by Rothemund¹³³ and has provided a powerful approach to engineer nanoscale functional structures.^{134,135} Structural DNA nanotechnology was first employed in covalent conjugation with polymers by O'Reilly's group, demonstrating the use of a DNA tetrahedron as a structural anchor for polymer attachment.⁹⁹ The polymer-decorated DNA nanostructure was realized through Cu-catalyzed click chemistry between the alkyne bearing DNA tetrahedron and azido-functionalized pNIPAM (Figure 11A). A 100-fold decrease in reagent concentrations was stipulated in comparison to their ODN equivalent solution-based click reactions. Additionally, CuSO₄/tris(hydroxypropyltriazolylmethyl)amine (THPTA) was adopted rather than CuI·P(OEt)₃. However, as with the attempts using polymer brushes, steric effects are deterministic on the efficiency and can result in low coupling yields. By *grafting from* the nanostructure, steric restraints are reduced for the monomer polymerization processes. The added advantage of employing a 3D DNA nanostructure backbone afforded polymer patterning through the site specific attachment.

In the previous example, the functionalized DNA strand was part of the folded nanostructure. However, in another instance, site specific control was employed through complementary base pairing an ODN bearing the radical initiators.⁵⁷ The origami was designed to exhibit "sticky" ssDNA at precise locations to guide the initiator-ODN to the pre-designated sites (Figure 11B). To perform the polymerizations from DNA origami, ATRP was employed to achieve reactions in aqueous conditions and at room temperature—a requirement when handling DNA origami. Due to the low concentrations of DNA origami available, sacrificial ATRP initiators were required in solution to maintain the radical equilibrium. Under these conditions, polymerization of PEGMA successfully generated a polymer brush. By adopting copolymerization with the cross-linker PEG dimethacrylate (PEGDMA), a dense polymer network can also be created. The DNA origami tile structure can also fold to form a tube shape, converting the 2D patterned surface to a 3D dual-surface containing specific internal and external contours (Figure 11C).⁵⁶ Here, ATRP initiators were

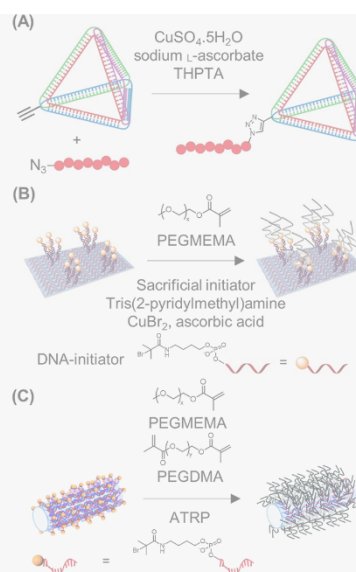


Figure 11. 2D and 3D DNA polymer conjugates on “solid” DNA nanostructures. (A) *Grafting to* DNA tetrahedron through click chemistry of pNIPAM to the alkyne-DNA nanostructure.⁹⁹ Adapted with permission from ref 99. Copyright 2013 American Chemical Society. (B) *Grafting from* DNA origami tiles through Cu-catalyzed ATRP. Initiators are initially bound to the origami structure through complementary sticky sequences followed by the ATRP reaction.⁵⁷ Adapted with permission from ref 57. Copyright 2016 John Wiley and Sons. (C) *Grafting from* a DNA origami tube through ODN bound initiators.⁵⁶ Adapted with permission from ref 56. Copyright 2018 the Royal Society of Chemistry.

similarly placed in precise patterns to decorate the outer surface of the tube. The polymerization conditions remained unchanged between the tile and tube configuration, therefore demonstrating the versatility of ATRP on DNA origami for nanoscale precision of DNA–polymer hybrid nanostructures.

3.2. Noncovalent DNA–Polymer Interactions

Apart from the covalent DNA–polymer conjugates reviewed above, there is also the emerging class of supramolecular assemblies of DNA and polymers which is driven by noncovalent interactions. Here, intermolecular communication is enabled through the close proximity and attraction of both materials, which lead to systems of dynamic nature. While covalent conjugation requires chemical manipulation of the DNA strands to equip them with reactive handles, noncovalent approaches do not face these constraints and can typically be realized with nonmodified and readily available nucleic acids. The highly programmable primary structure of DNA as well as the ability to shape secondary and tertiary structures can be exploited to control the sequence of polymers that are structurally unrelated to nucleic acids. This strategy takes inspiration from one of the essential processes found in living nature, where the DNA-encoded information on life is replicated, transcribed, and translated through RNA into proteins. Noncovalent assemblies can be classified by their mode of interaction as well as by the designated purpose. DNA provides multifaceted interaction modes that arise from its unique structure in all three dimensions as discussed in section

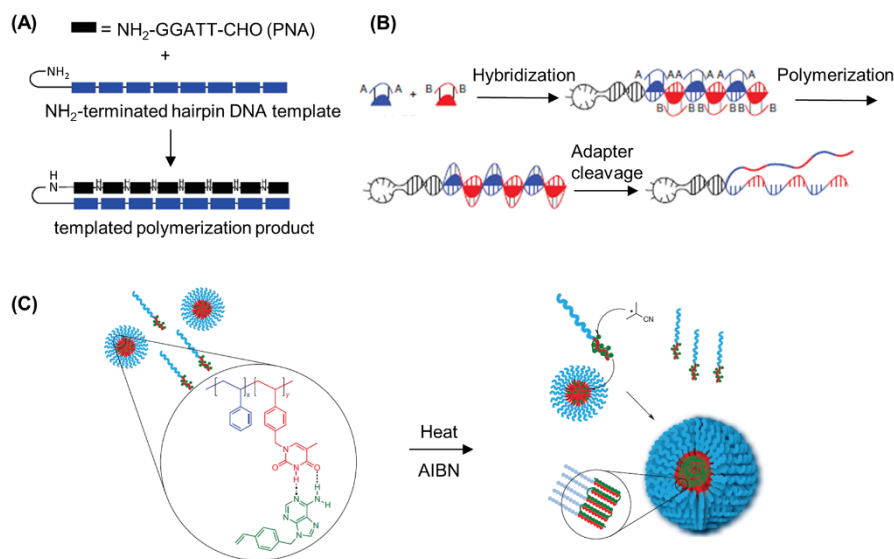


Figure 12. Various strategies to sequence-controlled polymer growth with ssDNA. (A) DNA-templated polymerization of PNA pentamer aldehydes on an amine-terminated hairpin DNA template.⁷⁸ Reproduced with permission from ref 78. Copyright 2008 American Chemical Society. (B) Codon-mediated linkage of AA/BB-substrates yields polymers that can be released from the templating DNA by cleavage of the disulfide linkers.⁵⁹ Reproduced with permission from ref 59. Copyright 2013 Springer Nature. (C) The combination of segregation and templating techniques ensures confined chain growth along a template in discrete micelle cores that affords polymers of high molecular weights.¹³⁸ Reproduced with permission from ref 138. Copyright 2012 Springer Nature.

2. ssDNA is accessible via Watson–Crick base pairing whereas the negatively charged phosphate backbone is prone to electrostatic interaction with polycations. dsDNA expands the toolkit by enabling hydrophobic groove binding and intercalation of planar molecules into the stacking bases along the DNA backbone. In comparison to covalent conjugation strategies, the herein described noncovalent interactions are *per se* not specific, yet several studies aim to circumvent these intrinsic restrictions and seek for spatially controlled attachments. Since DNA is a multifaceted platform, one can utilize its exceptional customizability to design tailor-made polymers by either templating or patterning approaches. On the one hand, ssDNA and dsDNA allow sequence transfer onto growing polymers and the templating of supramolecular 1D and 2D structures, respectively. On the other hand, DNA can be arranged in complex nanostructures which can be covered with polymers, rendering new features to the synthetic building block and yielding three-dimensional constructs. Furthermore, the extraordinary fidelity of certain DNA arrays, e.g., DNA origami, permits the patterning of polymers in distinct shapes and with a precision that outcompetes other techniques, such as lithography or conventional self-assembly. However, independent of the applied technique, the DNA template can be either removed after polymer synthesis or become part of the reaction product. In line with the focus of this review, we survey promising strategies to develop DNA–polymer conjugates via noncovalent interactions.

3.2.1. Templating of Polymers by Single and Double Stranded DNA. One of the greatest advantages of DNA over synthetic polymers is the unprecedented level of sequence-control as well as the consequential precision in molecular weight and distribution. It therefore is attractive to exploit this unique characteristic and potentially transfer the molecular

information onto polymers. In this way, ODNs can function as molecular matrices that recognize and interact with guest molecules and, thus, organize them according to their sequence and guide subsequent polymerization. An early example of how the sequence of nucleic acids might be harnessed was demonstrated by Liu and co-workers¹³⁶ wherein short PNA sequences were arranged in a sequence-specific fashion along an amine-end-modified ODN template via complementary base pairing. Aldehyde moieties on the tetrameric PNA monomers allowed for distance-dependent reductive amination coupling, ligating the monomeric units, which consequently generated polymers with molecular weights of 10 kDa. Introduction of mismatches afforded no or only truncated polymers, depending on the position at which the error was placed. Furthermore, the presence of additional building blocks with closely related sequences did not disturb the formation of the desired product. Thus, efficient and sequence-specific conjugation of nucleic acid templates and non-natural polymers steered by hydrogen bonding of base pairs could be established. In a follow-up study, the group expanded their monomer scope through a side-chain-functionalized PNA tetramer and pentamer aldehydes⁷⁸ (Figure 12A). Thereby, they could fabricate densely functionalized polymers, involving a PNA 40-mer with more than half the nucleotides bearing side chains. Interestingly, the polymerization efficiency mainly depended on the position and stereochemistry of the side chains rather than on size, hydrophobicity, or charge. As briefly mentioned above, Nature has the capability to translate the genetic information stored in nucleic acids into amino acid-based peptides and proteins. Based on their previous work, Liu's group aimed to mimic the last step of Nature's protein machinery where the sequence of a nucleic acid template allows a codon-mediated conversion into an amino acid

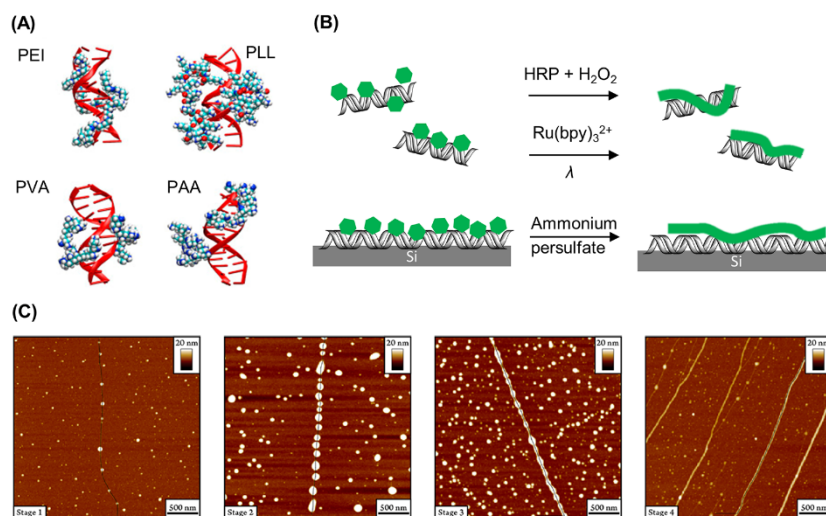


Figure 13. Electrostatic interactions allow the alignment of positively charged monomers and polymers along the DNA backbone. (A) Complexes of DNA with two polycation chains for DNA–PEI, DNA–PLL, DNA–PVA, and DNA–PAA systems.¹⁴¹ Reproduced with permission from ref 141. Copyright 2018 Elsevier Ltd. (B) The electrostatic alignment of aline monomers on DNA, either in solution or on Si substrates, and subsequent oxidation leads to the formation of poly(aniline) structures along the DNA template. Oxidation can be induced enzymatically (HRP), via photo-oxidation of Ru complexes or by using oxidants (APS). (C) AFM images of the polymerization process could reveal four distinct stages in the formation and growth of poly(pyrrole).¹⁴⁹ Reproduced with permission from ref 149. Copyright 2014 American Chemical Society.

sequence and, in the end, a protein is released (Figure 12B).⁵⁹ These codons bear a template recognition site as well as the corresponding amino acid. In order to exploit this strategy and likewise introduce sequence-specificity to non-natural polymers, the group designed a codon comprising a PNA pentamer for template recognition and a synthetic polymer building block. Through the employment of PEG as the initial polymer model and by achieving molecular weights of up to 10 kDa, they could further incorporate α -D- and β -peptide backbones with various side-chain functionalities to accomplish longer and structurally more diverse polymers (26 kDa). Among several investigated conjugation strategies, copper-catalyzed alkyne–azide cycloaddition of AA-/BB-substrates proved to be most efficient. Moreover, by equipping the codon with a disulfide bridge between the polymer building block and the PNA adapter as a cleavable linker, the polymeric product could be liberated afterward. Though the approach described here utilizes Watson–Crick base pairing to produce sequence-controlled polymers without the need for Nature’s enzymatic toolbox, the structural diversity of the substrates is still limited to macrocycles for entropic reasons. However, the codon design theoretically supports the incorporation of several building blocks without the need to readjust the template recognition site.

Another seminal approach to adopt from Nature’s capability to make exact copies of nucleic acid strands was investigated by the Sleiman group.¹³⁷ Step-growth polymerization techniques typically suffer from poor control over molecular weight which inevitably leads to broad molecular weight distributions. They therefore employed nucleobase recognition to surpass these barriers and to synthesize conducting polymers of low dispersities. Instead of using pure ODNs as a template, a thymine-decorated polymer was manufactured via living ring-opening metathesis polymerization (ROMP). Alignment of

adenine-containing monomers by complementary base pairing along the template strand and subsequent Sonogashira coupling afforded well-defined daughter strands of conducting polymers. Whereas nontemplated polymerization or polymerization with an incorrect template only produced low polymerization degrees and high dispersities ($PDI > 2$), the presence of the correct template significantly narrowed the molecular weight distribution ($PDI = 1.2$) and yielded similar polymerization degrees compared to the parent strands. Thus, the all-synthetic strategy proved to be capable of programming the structure, length, and dispersity of commonly poorly-defined polymers by hydrogen bonding interactions. Following this, O’Reilly and co-workers furthered nucleobase-promoted polymer templating by combining the methodology with a segregation strategy that makes use of block copolymer self-assembly (Figure 12C).¹³⁸ Their bioinspired dual templating/segregation approach relies on the isolation of propagating radicals in discrete micelle cores, thus enabling confined chain growth along a template. Briefly, a block copolymer of styrene (St) and the thymine analogue 1-(vinylbenzyl)thymine (VBT), PSt₁₁₅-*b*-PVBT₁₈, was synthesized that forms stable micelles in chloroform. The hydrogen bond interaction of the thymine template with a vinyl derivative of adenine (VBA) ensured the solubility of the adenine monomer in the solvent. Furthermore, the addition of the complementary adenine monomer led to a dynamic exchange of adenine-loaded templates into the micelle where the ensuing polymerization was taking place. A so-called “hopping” mechanism of propagating radicals along adjacent templates in the micelle core can theoretically explain the remarkably high molecular weights of the daughter polymers of up to 400 kDa, even though the template only counts 18 thymine residues. Hence, nucleobase templating enriched the free radical polymerization to yield narrowly distributed

daughter strands ($PDI \leq 1.08$) by suppressing bimolecular termination in a confined environment.

The examples discussed so far mainly report on nucleobase-modified polymers or closely related structures such as peptide nucleic acids. To further develop the field, Zhou et al. studied the triplex hybridization of a polymer with a full carbon backbone alongside DNA and RNA ODNs to produce conjugates that might be suitable for DNA loading onto nanoparticles or delivery of siRNA in biomedical applications.¹³⁹ Here, RAFT polymerization of various acrylates yielded polyacrylates with tunable side chains. As a key step, these copolymers were equipped with triaminotriazine (so-called melamine) handles by amidation of NHS moieties along the backbone. Melamine can recognize thymine and uracil hydrogen bonding patterns in various media and, therefore, ensured the hybridization with ODNs comprising two blocks of the respective amino acid that are bridged by a cytosine linker ($dT_{10}C_{10}T_{10}$). Notably, the RAFT copolymers are intrinsically characterized by stereoregio backbone heterogeneity and still engage T/U rich ODNs with nanomolar affinity upon mixing in a 1:1 ratio. The supposed triplex hairpin binding model of the compounds was further affirmed by FRET studies.

The work described here represents a rare example of DNA–polymer conjugates that are solely based on hydrogen bonding between a fully synthetic polymer and complementary nucleic acids without the support of electrostatic interaction. However, substantially more studies address the negatively charged phosphate backbone of DNA with respective polyplexes due to the convenient and spontaneous mode of interaction. For instance, electrostatic complexation can be exploited to condense siRNA onto a positively charged supramolecular polymer for drug delivery purposes.¹⁴⁰ The cationic polymer can enter cellular membranes via charged-mediated endocytosis and successfully deliver its cargo, thus inducing gene silencing. Supramolecular complexes of nucleic acids with cationic polymers have emerged prominently in the area of gene delivery in order to circumvent viral delivery vectors. In this respect, several positively charged polymers such as polyethylenimine (PEI), poly L-lysine (PLL), polyvinylamine (PVA), and polyallylamine (PAA) are subjects of current research (Figure 13A).¹⁴¹

Electrostatic interactions also play a key role in the studies of the Herrmann group where they fabricated light harvesting DNA complexes and described the salt-free hybridization of PEGylated ODNs in water.^{142,143} In a two-step process, a water-soluble surfactant is employed to transfer the DNA into an organic phase where it is substituted by an amine-containing molecule, for instance, amine-PEG. Hereby, ODNs can be noncovalently encapsulated with a PEG shell that allows for the formation of metal-free dsDNA with remarkably high thermostability.

Likewise, electrostatic interactions can be further utilized to template polymerization along DNA, enabling these interactions to dictate bond formation processes. There are a high number of studies demonstrating the use of DNA templates to exert control over the respective sequence and structure as an appealing strategy in the field of conducting nanowires. In particular, polyaniline, polypyrrole, and polythiophene are well investigated.¹⁴⁴ Polyaniline (PANI) is commonly synthesized in a strongly acidic environment through chemically or electrochemically induced oxidation of aniline monomers. However, these harsh conditions prevent the use of biological

templates as they are highly sensitive materials. Oxidative polymerization of aniline therefore necessitates the adjustment of reaction conditions toward mild pH ranges and tolerable oxidation agents (Figure 13B). In an initial attempt, Simmel and co-workers employed three different stimuli to trigger the polymerization of aniline along a λ -DNA template in solution as well as on a chip surface.¹⁴⁵ Prior to polymerization, DNA and monomers were simply incubated in phosphate buffer at pH 4.3, without the need for any chemical modification. Positively charged anilinium ions act as counterions for the negatively charged phosphate backbone and are organized accordingly. Enzyme-mediated oxidation through horseradish peroxidase (HRP) and hydrogen peroxide, photo-oxidation using a ruthenium complex, and ammonium persulfate as an oxidant all proved to be capable of yielding PANI-decorated DNA conjugates. In a similar approach, the group of He aimed to fabricate conducting polyaniline nanowires along pre-oriented DNA templates which were aligned on a Si substrate.¹⁴⁶ Oxidation of aniline was also induced enzymatically by HRP and hydrogen peroxide. Adjusting the pH value to pH 4.0 turned out to be crucial with regard to wire quality: at a pH of 5, the continuous formation of wires was interrupted by polyaniline particles; however, lowering the pH to 3.2 yielded only incomplete polymerization. Thus, the optimal pH range to ensure continuous and regular polymerization was on the one hand determined by the optimized electrostatic alignment of aniline monomers along the template and on the other hand helped to retain sufficient enzyme activity. By incorporating AuNPs into polyaniline nanowires derived from DNA templates, Wang et al. showed the novel construction of hybrid nanowires with expanded electrical properties.¹⁴⁷ Therefore, a sequential assembly process was applied: positively charged AuNPs were aligned on surface-immobilized DNA templates, affording narrow AuNP chains. The gaps between neighboring particles were then bridged by Ru-mediated photopolymerization of aniline derivatives in acidic media. The alternating AuNP–polyaniline hybrid nanowire could then be visualized by atomic force microscopy (AFM).

As with many other aromatic heterocycles, pyrrole can also be polymerized in oxidative environments. Thus, double helical DNA permits the construction of 1D nanostructures through the organization of the pyrrole precursors and subsequent oxidation and polymerization. In order to generate pure polypyrrole–DNA conjugates with alkynyl side groups, Horrocks and co-workers implemented chemical modifications into a thienyl-pyrrole monomer (TP).¹⁴⁸ It could be shown that monomer functionalization had no negative impact on the oxidative polymerization that was mediated through ferric chloride ($FeCl_3$). Treatment of the conjugates with Tollen's reagent led to the binding of silver cations to alkynyl residues which facilitated nucleation and growth of Ag clusters along the backbone. Compared to unmodified poly(thienyl-pyrrole), many small nanocrystals are formed closely to each other, attaining uniform distribution and enhanced conductive properties. In an ensuing study by Hannant et al., the same monomer was employed to further investigate click chemistry for postmodifications which might be of interest for sensing applications.¹⁵⁰ Importantly, the pentynyl-substituted pyrrole derived nanowires retained structural integrity and remained active, i.e., conductive, after addition of azido molecules via the succeeding click reaction. To broaden the monomer scope and to demonstrate the generality of the electrostatically driven templating approach, Houlton and co-workers polymerized

dithienyl pyrrole monomers (TPT) along DNA templates.¹⁵¹ Though this monomer only comprises 1/3 of the number of hydrogen donor sites compared to pyrrole and therefore reduced bonding capabilities, successful DNA recognition and interaction was still possible. The higher structural regularity of the polymer justifies the use of a less active monomer, since simply mixing thiophene and pyrrole monomers only yields randomly alternating sequences.

Investigation of the growth mechanism of pyrrole monomers along DNA templates by AFM imaging unveiled a stepwise polymerization process. First, low densities of conducting polymer bind to DNA as apparently spherical particles, followed by denser particle packing in a beads-on-a-string fashion, which then resulted in subsequent dynamic reconfiguration, finally elongating and merging the particles in highly regular nanowires with smooth morphology (Figure 13C).¹⁴⁹

The controllable interplay of not only electrostatic but also hydrophobic interactions between DNA and polymers opens up a completely different possibility to define the morphology of resulting conjugates. Once more, nature was used as a role model with respect to its outstanding ability to store genomic DNA with the help of histones. Chen and co-workers tread new pathways for the noncovalent interaction of block copolymers and DNA by establishing a two-step self-assembly process.¹⁵² Notably, the micelle formation of amphiphiles is not only determined by their concentration (critical micelle concentration, CMC) but also significantly relies on the ratio of water phase to organic phase, which is known as the critical water content (CWC). Based on the latter phenomenon, the group designed a self-assembling system of polymers and DNA which is first guided by weak electrostatic interactions that are subsequently caught up by hydrophobic driving forces. They therefore utilized a copolymer that comprises two blocks, a hydrophilic PEG and a hydrophobic poly(4-vinylpyridine) (P4VP). Below the CWC for micellization, the positively charged P4VP interacts with DNA, forming linear complexes in which the DNA is encapsulated by the polymer. Gradual increase of the water content allows for hydrophobic aggregation of the P4VP blocks between polymer chains in solution and polymer chains on the DNA. The hydrophobic interaction then forces rearrangement of the complex and finally leads to core-shell nanofibers in which DNA wraps around the hydrophobic polymer aggregate. When employing monodisperse and relatively short DNA templates, these properties were transferred into the DNA-polymer conjugates which are monodisperse in both length and width. The necessity of the DNA template is clearly evident since the copolymer alone only accumulated in spherical micelles under identical conditions.

Besides the binding modes discussed here, the Watson-Crick base pairing and resultant double helix structure further render DNA attractive for the intercalation of planar molecules. In duplex DNA, the environment of nucleobases leads to π - π -stacking of adjacent aromatic systems, a structural motif that has a greater impact on helix stability than hydrogen bonds of complementary bases. Compounds that recognize DNA via interaction within the stacking bases are therefore potential handles for attaching or growing polymers along the DNA template. Hence, respective initiators, monomers, or the *a priori* synthesized polymer have to be equipped with suitable intercalators. Although ethidium bromide is a very strong DNA binder, utilization of weaker intercalating molecules such as acridine can add the potential for reversibility to the complex.

O'Reilly and co-workers employed RAFT polymerization to synthesize a series of acridine end-terminated polymers, including pNIPAM and pDMAM and investigated the effect of polymer structure on the nature and strength of the interaction with DNA.⁴⁰ Indeed, differences in complexation behavior were observed, which were potentially caused by the relative tendencies of the different polymers to self-assemble when brought into close proximity. For instance, a high load of pNIPAM onto calf thymus DNA and full occupancy of intercalation sites induced irreversible aggregation. The DNA-guided vicinity of polymer chains quasi-imitates the process when hydrogen bonds between the amide groups of pNIPAM are formed, normally giving rise to its temperature-responsive character. On the other hand, the compact structure of pDMAM tolerated higher densities of polymer intercalation without aggregation occurring. Thus, the combination of pDMAM and a significantly shorter and well-defined DNA sequence (63 base pairs) yielded discrete and possibly brush-like nanoparticles with sizes of 10 nm. Importantly, DNA or polymer alone as well as acridine-lacking polymer does not form comparable assemblies. In a different approach, Pike and co-workers instead used monomers with π -stacking anchoring groups to arrange the monomers within the DNA helix and conducted polymerization after intercalation.⁵¹ Based on the intercalation of diazido derivatives of proflavine into the double helix, the azido groups exposed themselves into the major grooves of the DNA. Here, copper-catalyzed click reaction with thienyl-pyrrole monomers was performed. Crucially, proflavine intercalation was not hampered by the ensuing click reaction of the functional groups nor was intercalation of a presynthesized unit of intercalator and monomer successful, due to hydrophobic and steric impediments. Polymerization of the spatially organized pyrrole units was initiated by residual oxygen species in the solvent, without the need for a chemical oxidant.

While this strategy relies both on intercalation within the stacking nucleobases and on chemical reactions taking place in the major groove of DNA, DNA grooves alone also provide the opportunity for noncovalent attachment of polymers. Furthermore, the impact of adjacent base pairs on the groove environment adds a certain level of sequence-specificity to the system which is less prominent among intercalators. To ensure an ideal interaction, groove binding compounds typically comprise at least two aromatic rings while still being flexible in contrast to rigid polycyclic planar molecules that are suitable for intercalation. Deiana et al. investigated the binding mode of an anthracenyl polymer with dsDNA as well as the binding strength and mechanism.¹⁵³ The polymer was synthesized by ATRP from an anthracene macroinitiator with 4 initiator sites, and DNA interaction was induced by simple mixing of the compounds. Association constants in the 10^5 M⁻¹ range are higher than those found for intercalating molecules or electrostatic interactions, thus indicating successful groove binding. Furthermore, the association stoichiometry was ascertained to be 1 polymer-adduct for every 5 base pairs, showing that most sites of DNA participate in the association process. Although groove binding is mainly attributed to hydrophobic forces, van der Waals forces and hydrogen bonding may also be involved in the process, promoted by the hydrophilic polymeric arms.

As already emphasized in the previous section (3.1), the synthesis of covalent amphiphilic conjugates of ODNs and polymers is problematic, especially due to solvent incompat-

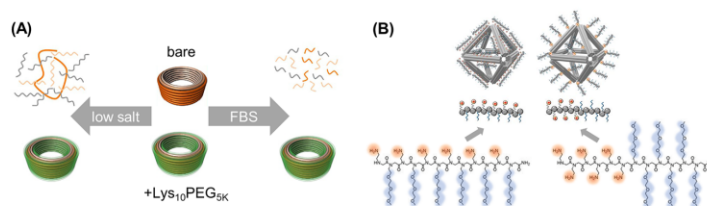


Figure 14. Intrinsic instability of DNA nanostructures under low salt conditions or in the presence of nucleases and fetal bovine serum (FBS) is addressed by many groups. (A) Shih and co-workers could increase the stability of DNA origami by electrostatic coating with PEG–polylysine copolymers.⁶¹ Reproduced with permission from ref 61. Copyright 2017 Springer Nature. (B) Block- and brush-type copolymers of PEG and peptide mimetics (so-called peptoids) were found to also reduce the susceptibility of DNA nanostructures.¹⁶¹ Reproduced with permission from ref 161. Copyright 2020 National Academy of Sciences.

ibility, low conjugation yields, and phase-separation. Host–guest interactions can potentially alleviate some of these concerns by constructing a special hydrophobic molecular environment to compensate for the difference between hydrophilic and hydrophobic components in solution. This environment exists as hydrophobic cavities within a general hydrophilic exterior thus allowing the encapsulation of molecules that would otherwise phase-separate. Varghese and co-workers exploited this interaction mode by equipping DNA with a prominent host molecule (β -cyclodextrin) which can trap adamantine-modified hydrophobic guests.¹⁵⁴ Supramolecular chemistry widely explores this class of host–guests due to their efficient and highly specific molecular recognition, low price, and simplistic modification. The spontaneously formed self-assemblies from the generated DNA-amphiphiles were found to be thermally stable which is attributed to extremely strong hydrophobic interactions. However, this technique is predominantly exploited to attach small molecules or oligomers rather than polymers.¹⁵⁵ At this point it is important to note that this observation applies to almost all approaches relying on noncovalent interactions. A rare example for a polymer-based strategy is reported by Thelu et al. in a follow-up study to their work described above.¹⁵⁶ Herein, adamantyl-terminated 8-arm PEG polymer is encapsulated by X- or Y-shaped DNA carrying β -cyclodextrin at the end of all ODN arms. The combination of a multivalent host with a star-like guest led to nanogel formation, and the gelation was concentration dependent. Moreover, the applicability of these nanoparticles in a biomedical context was accomplished by demonstrating successful drug loading, good cell permeability, and delivery into cells. Thus, due to the universal and modular nature of the host–guest interaction, the approach holds the potential to be further developed.

3.2.2. Polymer Decoration of DNA Nanostructures.

While ss- and dsDNA are extensively leveraged to tailor the polymer sequence and nanostructure and to provide integrative functions, polymers themselves can also benefit DNA in several ways. Higher ordered DNA arrays such as DNA origami are exceedingly versatile building platforms, but they face intrinsic stability drawbacks. Due to their nature, DNA objects are prone to enzymatic degradation through nucleases when encountering physiological environments, thus limiting their progress in biomedicine. Even though degradation might be delayed by packing DNA structures of high density or by having multiple interstrand crossings, it cannot be completely impeded.^{157,158} In addition, DNA origami's integrity is highly dependent on sufficient levels of divalent cations that allow close proximity of DNA strands by

compensating charge repulsion of the phosphate backbones. Hence, several studies seek to diminish DNA susceptibility through polymer-based approaches. Despite the drastically reduced accessibility of 2D and 3D DNA objects in contrast to nonfolded DNA sequences, electrostatic interaction can still be exploited in order to achieve an efficient polymer coating. Divalent cations are hereby substituted by polymeric polycations, either naturally derived or of artificial origin. However, without the possibility of confining the electrostatic interactions in a designated area, coverage will occur nonspecifically which might hamper additional postmodifications.

Various polymers were investigated to determine their structure-binding relationship and their impact on origami stability. For instance, ATRP-generated block copolymers of PEG (to improve biocompatibility and protection efficiency) and methacrylate derivatives (to serve as cationic blocks) were attached to a 60-helix bundled DNA structure.⁶⁰ Notably, for successful binding, the ratio of amines within the polymer to phosphate groups within the DNA backbone (N/P ratio) was found to be pivotal. The number of cationic blocks of the copolymer; however, only had a minor impact on binding affinities. Ahmadi et al. followed suit and studied the effect of polymerization degree, charge density, and N/P ratio of linear PEI and chitosan on coating efficiency.¹⁵⁹ In line with other studies, the N/P ratio significantly determines the extent of interaction with DNA. However, LPEI performed better than chitosan in protecting DNA from salt-depletion and nucleases, even at lower ratios which the authors attributed to its higher charge density. Moreover, the study reveals how challenging the characterization of polymer-decorated DNA nanostructures might be. While bare origamis could be imaged by negative stain TEM, LPEI-coated origamis were only visible after removing the polymer shell. The indirect proof of polymer coverage described here is often the only way to analyze the conjugate (more examples to follow within this section). In 2017, electrostatic coating of DNA origami structures by copolymers from PEG- and polylysine-building blocks were reported by two different groups.^{61,160} The polylysine block interacts with DNA while the corresponding PEG block builds a protective layer and shields the sensitive DNA backbone. The Schmidt lab synthesized PEG_{12 kDa}PLys₁₈ by ring-opening polymerization induced by an amino-terminated PEG macroinitiator while the Shih group utilized commercially available PEG_{5 kDa}PLys₁₀ polymers (Figure 14A). Both coatings proved to enable DNA nanostructures to withstand low salt and high nuclease conditions. However, it is important to note that the coating produced with the in-

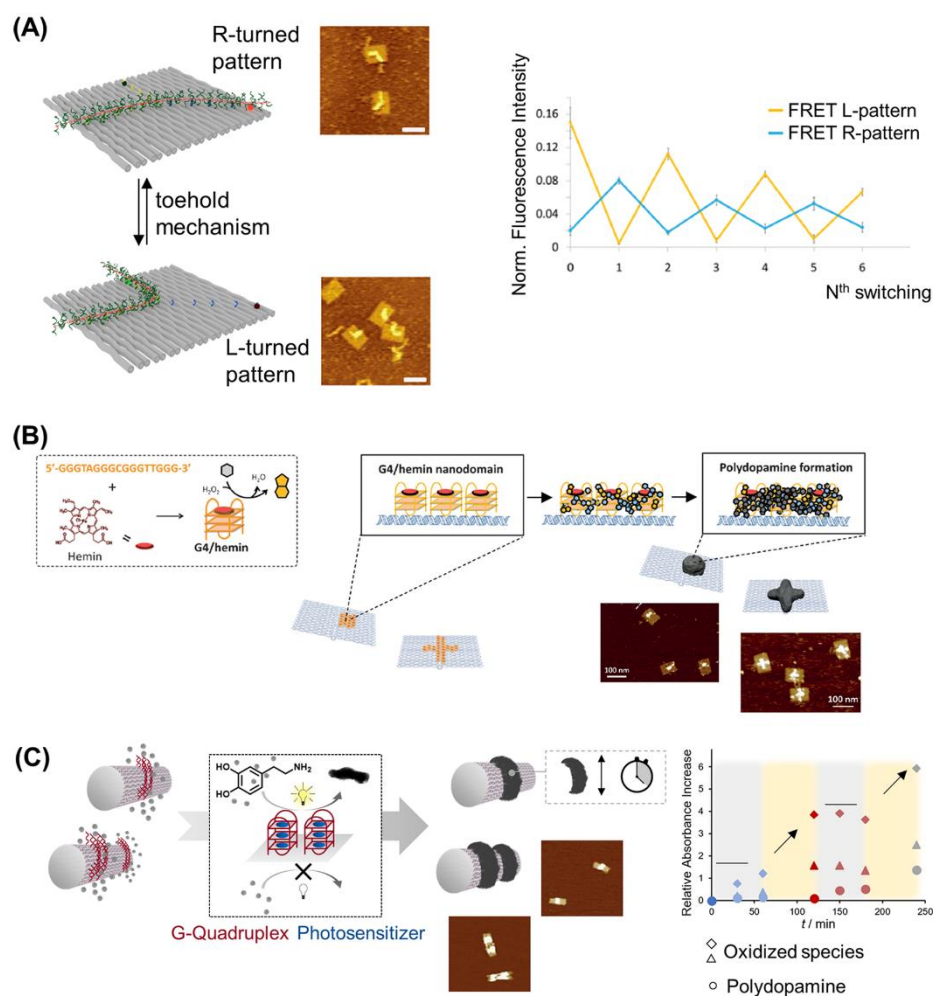


Figure 15. By exploiting the unique addressability of DNA origami, polymer patterning on the nanoscale can be realized. (A) The Gothelf lab developed various strategies to synthesize sophisticated polymers that can be routed on DNA origami platforms on a single-chain level. Furthermore, repetitive switching of the polymer chains was achieved. Switching of the polymer conformation could be monitored by FRET pairs.⁵⁴ Reproduced with permission from ref 54. Copyright 2016 American Chemical Society. (B) The spatially controlled formation of polydopamine in designated patterns was demonstrated by the Weil group by installing enzyme mimicking reaction centers on DNA origami that guided the polymer growth.⁶² Reproduced with permission from ref 62. Copyright 2018 John Wiley and Sons. (C) Further temporal control over polymer formation was implemented by trapping a photosensitizer at distinct positions on 3D origami tubes.⁶⁴ Reproduced with permission from ref 64. Copyright 2020 John Wiley and Sons.

house synthesized copolymer did not allow for further surface functionalization due to the shielding effect by the polymers. Schmidt and co-workers circumvented these restrictions by applying the shorter polymer as it was utilized in the Shih lab, and thus, modifications using AuNP were no longer hampered by the polyplex formation. An important consideration for an electrostatic-based polymer coating is its suitability in a physiological context where charged interactions are subjected to the influences of complex fluids. Interestingly, Shih and co-workers could not only reach a 1000-fold increased stability under cell culture conditions but also confirm the integrity of protected DNA origamis after cell uptake. Remarkably, these

results were achieved with dendritic cells that are known for highly efficient DNA degradation, which therefore represent a challenging scenario for the DNA nanostructures. Recently, Gang and co-workers expanded the polymer scope for electrostatic protection by presenting peptoids as valuable candidates.¹⁶¹ (Figure 14B) Peptoids are peptide mimetics in which side chains are anchored to the nitrogen atom of the backbone instead of the α -carbon, so that secondary structures and proteolysis are suppressed. Positively charged motifs and PEG monomers were used to construct block-type and brush-type copolymers via solid phase synthesis. The latter architectures were advantageous in stabilizing DNA in

biomimetic fluids due to multivalent interactions along the backbone.

In summary, electrostatic polymer coatings provide appealing simplicity when aiming for increased stability of DNA nanostructures. Additionally, polyamines are even more competent in their stabilizing effect than commonly utilized magnesium ions during origami synthesis.¹⁶² Nevertheless, the polymer–DNA conjugates derived are of rather low specificity, which is adequate in only addressing stability issues. For more sophisticated objectives, polymer deposition with spatial and temporal control is more ideal. Additionally, unspecific coating inadvertently wraps reactive handles within the polymer shell thus jeopardizing the key aspect of DNA origami structures. In order to conserve the fidelity of DNA origami, some researchers designed individual strategies to orchestrate polymer alignment. Among the spectrum of suitable non-covalent interactions, complementary base pairing can enable highly precise attachment of polymers, even on a single polymer chain level. Therefore, it is necessary to furnish both DNA origami and polymers prior to conjugation: complementary ODNs have to be mounted on the DNA origami scaffold at designated positions as well as on the polymer chains, guiding the interaction of both building blocks. Gothelf and co-workers developed a method to equip several side groups of a polymer with ODN handles allowing a polymer to interact with a DNA origami template on multiple sites, not only via, e.g., end-group modification. Thus, the alignment of single polymer chains along a predestined path on DNA origami was envisioned.¹⁶³ In detail, solid phase DNA synthesis was employed to graft ODNs from several side chains of a poly(phenylenevinylene) polymer while additional PEG side chains ensured water solubility of the construct which is required for successful DNA conjugation later on. The sophisticated nature of the polymer led to a rather broad size distribution as characterized by GPC (340–3300 kDa) and AFM (length range of 20 to 200 nm), presumably due to partial degradation during purification. However, binding yields of polymers to various DNA origami tiles were still very high according to AFM images. It should be noted that more complex alignments, for instance, a staircase path instead of a U-shape, lower the assembly efficiency. While the visualization of these 2D origami structures was accessible by AFM, the same analysis was highly difficult for 3D objects. 3D characterization was only possible when applying the DNA PAINT technique, again highlighting the challenges in investigating polymer–DNA origami conjugates. In a follow-up study, the Gothelf lab further developed their strategy by installing a programmable switch within the polymer configuration on DNA origami (Figure 15A).⁵⁴ Since complementary base pairing is always of a reversible nature, a so-called toehold mechanism can be applied to trap and release the ODN-modified polymers through different anchors on the DNA origami platform, thus guiding the polymer along various routes. Despite the elaborated efforts, the approach is hampered by synthetic and analytical issues, arising from the very low dimensions on the nanometer scale. Notably, only half of the origami structures exhibited well-aligned polymers, demonstrating challenges during conjugation. Furthermore, repeated switching of the polymer conformation and subsequent AFM imaging was not possible due to very strong background noise resulting from added displacement strands. Subsequently, each cycle of conformation switch was performed in solution, which enabled purification after each

step. Moreover, simultaneous alignment of two different conductive polymers and the ensuing interpolymer energy transfer was not successful, indicating the limits for conjugation of intricate polymers.¹⁶⁴

Despite the rather low number of reports on distinct polymer patterning on DNA origami, there are some studies that do not involve base pairing but electrostatic interactions. In contrast to the studies discussed above, here, electrostatic coating is restricted to only occur within distinct boundaries. This is enabled by pursuing a fundamentally different strategy compared to the aforementioned interactions of polycations with the DNA origami. Here, polymers are grown directly from the DNA surface while simultaneously forming stabilizing electrostatic interactions. As mentioned earlier, the aniline monomer responds to oxidative polymerization as it can be activated by oxidants, photoreactive metal complexes, or enzymes, such as horseradish peroxidase (HRP). Ding and co-workers took inspiration from the latter mechanism and established a HRP-mimicking system to polymerize aniline on DNA.¹⁶⁵ Therefore, they equipped a DNA template with guanine-rich sequences that are known to build so-called G-quadruplexes, representing DNAzymes. Upon incorporation of hemin as a cofactor and the addition of hydrogen peroxide, oxidation of aniline is induced. Due to electrostatic interactions, generated aniline radicals adhere to the negatively charged phosphate backbone in close proximity, thus attaining local polyaniline formation close to the DNAzymes. The group then transferred the regioselective polymer growth to 2D DNA origami triangles.⁶³ They could demonstrate that polyaniline was only fabricated around the catalytic sites whereas DNAzyme-free regions did not form any polymer. However, polymerization directly on DNA origami templates required specific adjustment to the ionic strength of the system to balance reaction kinetics and DNA stability. Weil and co-workers adapted the HRP-mimicking polymerization system for the shape-controlled formation of polydopamine (Figure 15B).⁶² Normally, dopamine tends to self-polymerize in neutral and basic pH, yielding a highly adhesive polymer comprising a multifaceted structure of covalent and non-covalent interactions that is not yet fully understood. By conducting the polymerization in acidic milieu with the help of DNAzymes, the group could implement significant control over dopamine formation. Various polymer patterns on a DNA nanosheet were accomplished, and furthermore, polydopamine acted as a “supramolecular glue”, shaping the origami conformation as the polymerization progressed. It is important to recognize that a slightly acidic pH was crucial for successfully controlling polymer formation as well as the ionic strength of the reaction. High ionic concentration disfavored the electrostatic interaction of dopamine and subsequent reaction intermediates with the DNA template, giving rise to polymerization in solution instead of the origami surface. Nevertheless, DNA stability has to be monitored closely when operating in ion-deficient environments. Recently, the Weil group further developed the method by switching from a chemically induced polymerization to a photo triggered variant allowing the control of the reaction over time (Figure 15C).⁶⁴ G-quadruplexes were employed to trap the photosensitizer protoporphyrin IX at distinct positions on 3D DNA origami tubes, and upon irradiation with visible light, polydopamine formation was induced without the need for further reagents. Not only was the process locally confined, temporal control was dictated by simply switching off and on

the light. Despite the noncovalent nature of the polydopamine–DNA hybrid structure, electrostatic interaction between polydopamine and the DNA survived the total depletion of ions in aqueous medium, confirming its high binding capabilities. Additionally, it was shown that just the presence of one or two polymer rings was sufficient to confer stabilization of the DNA origami in pure water.

In the studies reviewed here, the patterning of polymeric structures on a DNA template via noncovalent interactions remains relatively scarce due to several aforementioned challenges. Complementary base pairing appears to be the most intuitive approach to arrange polymers along several ODN anchors on a DNA template; however, it necessitates a modification of both building blocks. Electrostatic coating leads to nonspecific coverage in general, yet various groups designed DNAzyme-based systems to locally restrict polymer growth from the DNA surface. The nanopatterning achieved using this method has allowed the customization of structures in nanoscale resolutions that are yet unachievable by other technologies.

3.3. Chemistry of DNA–Polymer Conjugates Postcoupling

3.3.1. Chemistries on the Polymer. In the synthetic approaches reviewed above, we describe the conjugation of polymers to DNA where reactions are often compromised by the combined limitations of the polymer and the DNA. However, postfunctionalization of the DNA–polymer conjugate offers further access to manipulate nanostructure behavior and function. To realize these postfunctionalization prospects, functional groups need to be embedded in the polymer backbone or at the antipodal terminus. Depending on the polymer employed, modifications can be implemented at points along the backbone; however, functional groups must be compatible with or protected from the coupling chemistry employed for DNA conjugation. In doing so, there are several avenues for secondary polymer functionalization, such as cross-linking or small molecule attachment. Postconjugation polymer cross-linking of an amphiphilic polymer was demonstrated to create a nanoparticle bearing six ODNs.¹⁶⁶ Here, a DNA nanocage was synthesized bearing 8 ssDNA–amphiphile conjugates at the cube corners. The amphiphiles were found to self-assemble in the hollow cube core, demonstrating the guided self-assembly through DNA structures. The polymer consisted of HE and amino groups (Am) in the sequence 5'-Am-(HE)3-Am-(HE)3-Am-DNA-3' and was cross-linked with sebacic acid bis(*N*-succinimidyl) ester to produce the nanoparticle. Cross-linking the polymer chains provides the opportunity to alter the physical properties as well as structure and function, which will be considered in section 4.2.1.

Small molecular attachment is also possible through secondary coupling reactions. In one example, a PEG chain was functionalized by a NHS group at one terminal and a maleimide at the other.¹⁶⁷ DNA coupling was performed through amine-NHS coupling, leaving the maleimide group available and unchanged. A thiol-modified folic acid could then be coupled through a thiol Michael addition to yield a doubly conjugated polymer chain. Although there are a few examples in the literature, the development of bioorthogonal reactions directly fuels the available prospects of postconjugation functionalization of DNA–polymer conjugates. In doing so, this strategy can potentially enable an increase in functional diversity as well as the capability to program complex solution behavior.

3.3.2. Chemistries on the DNA. Likewise, postconjugation modification can be achieved through the DNA block, offering several additional strategies unique to the DNA such as chain extension with PCR or hybridization of a complementary ssDNA. One drawback of DNA–polymer synthesis with a user-defined DNA sequence is the length limitation of solid phase synthesis. The polymerase chain reaction (PCR) is a well-established technique employed to replicate short (50 bp) to long (30 kb) lengths of DNA using specific primers to amplify the region of interest. In the case of DNA–polymer conjugates, PCR was employed to synthesize di- and triblock copolymer conjugates of defined DNA length and content bearing polymer termini.⁷¹ This PCR method employs presynthesized ODN–polymer conjugates as the primers, where the conjugation was produced via *grafting to*, to amplify a specific length of DNA. The amplification occurs through the binding of each primer to the long ssDNA sequence, followed by extension from the 3'-ODN-end by the DNA polymerase. This results in a long length of DNA bearing a polymer at the 5'-end. Monodispersity of the central block is therefore achieved and yields either a single or double terminal polymer conjugate determined by the primers used. Additionally, as the primers are independent of each other, the conjugated polymer can be varied and therefore can bear two alternative polymers as part of the triblock, for example, PEG–DNA–PPO or NIPAM–DNA–PEG. In this example, amplification was employed to reshape the conjugate structure. Amplification can also pose benefits for downstream binding or signal enhancement. Rolling circle amplification is an alternative DNA replication technique where DNA sequences are copied from circular DNA. In the case of DNA–polymer conjugates, ssDNA penetrating from the conjugate is available to perform primer functions for DNA polymerase extension from the 3-end. Specifically, ssDNA was bound to polymers at the 5'-end and could bind to the circular DNA at designated positions through complementary base pairing.¹⁶⁸ Once bound, the DNA polymerase can perform the extension and displacement for continued amplification resulting in long ssDNA protruding from the polymer conjugate. Through the employment of postmodification, the long DNA chain is not present during the conjugation reaction, thus avoiding steric challenges. Therefore, the use of postcoupling extension to the DNA block through PCR and RCA demonstrates a synthetic approach to long DNA–polymer conjugates. Chemistries could also be envisaged on DNA postcoupling. As with the polymer reactions, the compatibility with the DNA–polymer coupling reaction is required.

3.4. Characterization of DNA–Polymer Conjugates

The characterization of DNA–polymer conjugates requires a range of techniques due to the variety of approaches and products synthesized. In particular, the production scale of DNA–polymer conjugates has been a primary concern, which is often the bottleneck for analytical tools with poor limit of detection. For conventional polymer synthesis, there are two key techniques: gel permeation chromatography (GPC) and dynamic light scattering (DLS), which are the benchmark characterization techniques to determine polymer quality. For both techniques, approximately 10–50 nmoles of conjugate is required to provide an adequate signal for analysis. This often restricts the number of experimental variables one is able to explore due to the limited amount of material available. GPC and DLS analysis can be applied to all conjugates formed

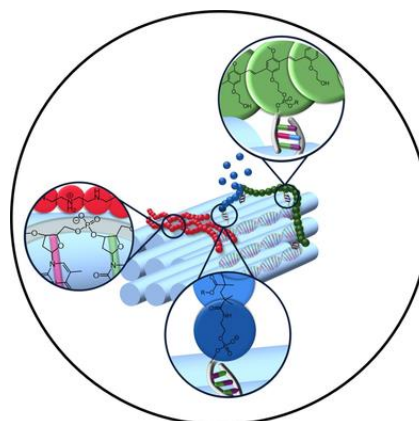
1.4 DNA origami meets polymers: A powerful tool for defined nanostructure design

Publication: “DNA Origami Meets Polymers: A Powerful Tool for the Design of Defined Nanostructures”

Nadine Hannewald[§], Pia Winterwerber[§], Stefan Zechel, David Y. W. Ng, Martin D. Hager, Tanja Weil, Ulrich S. Schubert *Angew. Chem. Int. Ed. Engl.* **2020**, 60, 6218-6229.

[§]The authors contributed equally to this work.

The publication in this chapter is an open access article under the terms of the Creative Commons Attribution License (CC BY 4.0).



DNA origami is an exceptional demonstration of DNA nanotechnology’s versatile toolkit and since its advent in 2006, the field has received great attention and proved to reliably produce highly precise nanostructures. As a natural consequence of its inherent programmability, DNA origami represents the ideal template for the routing and directing the assembly of polymers. It surpasses conventional top-down approaches such as lithography and bottom-up approaches such as self-assembly due to its flexibility and molecular engineering capacities on the nanometer scale. Equally, DNA origami nanostructures benefit from polymer integration in various areas: increased stability, stimuli responsiveness, reversible actuation, among others.

The review presented in this chapter concludes the introduction by focusing on the synergy of DNA origami and polymers in particular and embeds the work in the main part of this thesis. Various techniques to create DNA origami–polymer hybrid structures are exemplified, namely *grafting from* and *grafting to* approaches: The polymer is either grown from the initiator-equipped origami *in situ* or formed and modified prior to origami attachment. In addition, the different modes of interaction forces and anchor points of both building blocks are discussed. The emphasis is on the future perspectives as well as exploring the limitations in synthesis and analysis of the field which delay its progress.

As a shared first author I was involved in the conceptual design of the article, the elaboration of discussion and focal points, and writing of the manuscript. Together, we aimed to give a realistic and rationale point of view on the current state of DNA origami–polymer nanostructure research.

Hybrid Materials

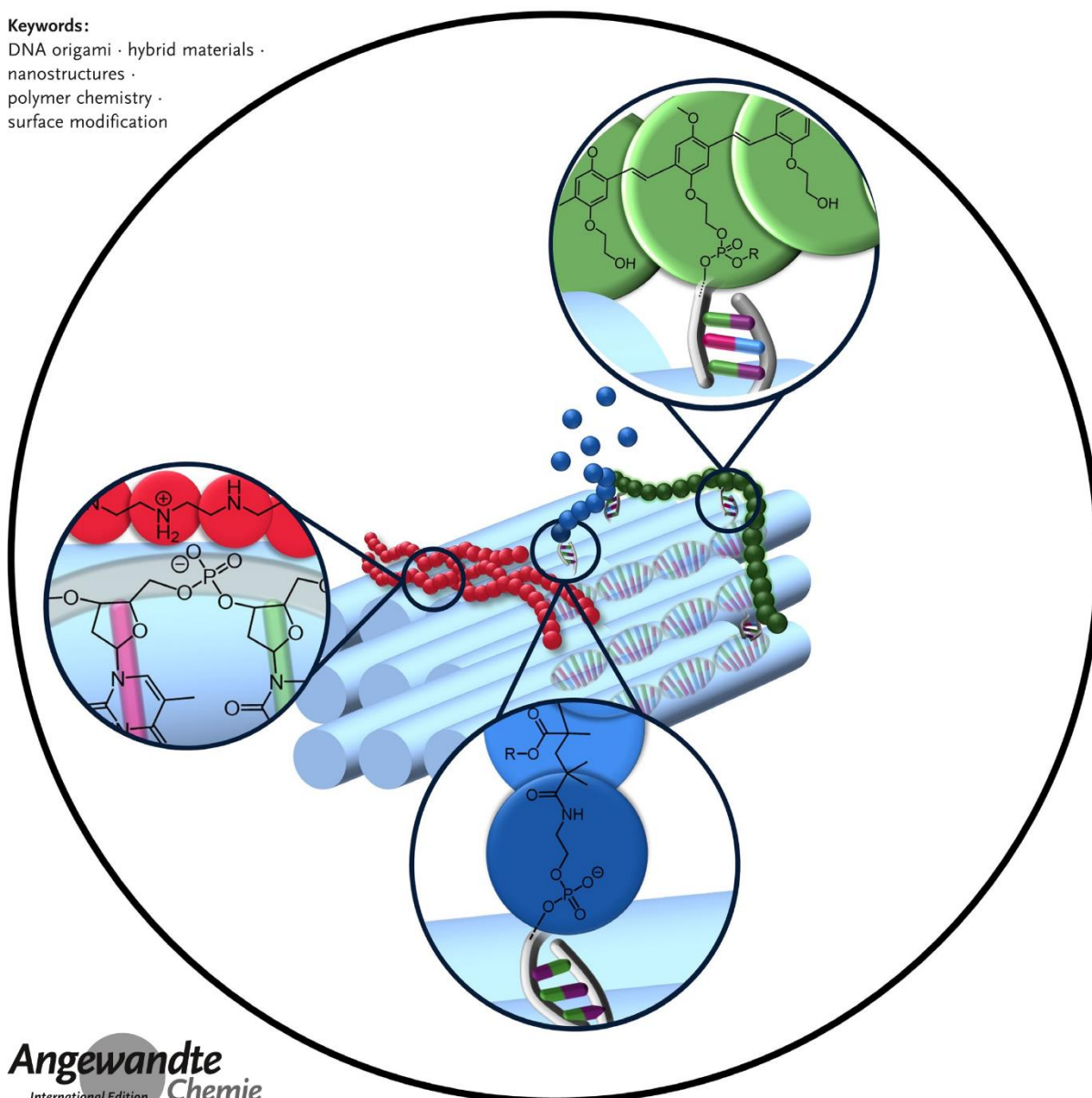
How to cite: *Angew. Chem. Int. Ed.* **2021**, *60*, 6218–6229International Edition: doi.org/10.1002/anie.202005907German Edition: doi.org/10.1002/ange.202005907

DNA Origami Meets Polymers: A Powerful Tool for the Design of Defined Nanostructures

Nadine Hannewald⁺, Pia Winterwerber⁺, Stefan Zechel, David Y. W. Ng,
Martin D. Hager, Tanja Weil, and Ulrich S. Schubert*

Keywords:

DNA origami · hybrid materials ·
nanostructures ·
polymer chemistry ·
surface modification



The combination of DNA origami nanostructures and polymers provides a new possibility to access defined structures in the 100 nm range. In general, DNA origami serves as a versatile template for the highly specific arrangement of polymer chains. Polymer-DNA hybrid nanostructures can either be created by growing the polymer from the DNA template or by attaching preformed polymers to the DNA scaffold. These conjugations can be of a covalent nature or be based on base-pair hybridization between respectively modified polymers and DNA origami. Furthermore, the negatively charged DNA backbone permits interaction with positively charged polyelectrolytes to form stable complexes. The combination of polymers with tuneable characteristics and DNA origami allows the creation of a new class of hybrid materials, which could offer exciting applications for controlled energy transfer, nanoscale organic circuits, or the templated synthesis of nanopatterned polymeric structures.

1. Introduction

The fabrication of functional nanoparticles and defined nanoscale surfaces represents an intensively investigated topic of current research. Besides the synthesis of such materials, the improvement in the fabrication of smaller and more precise geometries as well as the development of precisely addressable surfaces is also of interest. Significant improvements in such fabrication techniques could be of further usage for, for example, reducing the size of data storage, optical devices, or the development of new drug-delivery systems.^[1–3]

Such nanostructures can be fabricated in many ways, but two of the most important methods are lithography and self-assembly. Lithography, as a top-down technique, enables manipulation of larger objects to result in smaller-size geometries with the desired shape.^[4] Nevertheless, it often requires expensive and complicated setups, thus making the fabricated samples expensive and not suitable for the large-scale fabrication of nanostructures.^[5] In contrast, self-assembly, as a bottom-up process, relies on the interactions of the assembling units without any external stimuli, which will be discussed in the following only for small molecules.^[4] Such moieties can be, for example, based on hydrogen bonding,^[6] van der Waals forces,^[7] hydrophobic and hydrophilic^[8–9] interactions, or π - π stacking.^[10] During the self-assembly processes of synthetic molecules, various desired structures could be formed, which makes this process a low cost and fast alternative compared to lithography.^[11] However, not all geometries can be realized in this way.

One prominent example for a versatile self-assembling process in nature is the formation of the DNA double helix, which is based on hydrogen bonding between complementary base pairs. In 1982, Seeman took inspiration from such processes and realized the folding of DNA into designed superstructures.^[12,13] This idea was further expanded by Rothemund in 2006, by establishing the so-called DNA origami technology, which led to a breakthrough in the

construction of DNA objects.^[14] In this approach, a long, circular single-stranded DNA (“scaffold DNA”) is folded into a distinct shape with the help of a set of short “staple strands”. These staple strands are designed to hybridize to complementary sequences within the scaffold DNA. Elongating particular staple strands by short oligonucleotides results in surface-protruding single-stranded DNA (ssDNA), which can subsequently undergo hybridization to additional molecules. (Figure 1) Thus, DNA origami provides a precisely addressable surface and has been shown to be a powerful tool for the distinct positioning of, for example, nanoparticles in a predefined manner.^[12,15]

In this Minireview, we focus on the functionalization of DNA origami nanostructures with synthetic polymers or polymer-oligonucleotide conjugates to afford unique hybrid nanostructures that are very challenging to achieve with other techniques. However, in contrast to previous contributions, the pure self-assembly behavior of polymer-DNA conjugates will not be discussed.^[16–18] However, a range of methods for the attachment of polymers onto DNA nanostructures in a predefined manner is described in detail. Additionally, the advancements as well as the limitations of the functionalization of DNA origami is discussed and compared to lithography and traditional self-assembly methods. Finally, we show that the functionalization of DNA origami can be a powerful tool for the preparation of polymeric nanostructured objects.

[*] N. Hannewald,^[1] Dr. S. Zechel, Dr. M. D. Hager, Prof. Dr. U. S. Schubert
Laboratory of Organic and Macromolecular Chemistry (IOMC)
Friedrich Schiller University Jena
Humboldtstrasse 10, 07743 Jena (Germany)
E-mail: ulrich.schubert@uni-jena.de

N. Hannewald,^[1] Dr. S. Zechel, Dr. M. D. Hager, Prof. Dr. U. S. Schubert
Jena Center for Soft Matter (JCSM)
Friedrich Schiller University Jena
Philosophenweg 7, 07743 Jena (Germany)

P. Winterwerber,^[1] Dr. D. Y. W. Ng, Prof. Dr. T. Weil
Max Planck Institute for Polymer Research
Ackermannweg 10, 55128 Mainz (Germany)

[†] These authors contributed equally to this work.

ORCID The ORCID identification numbers for some of the authors of this article can be found under:

<https://doi.org/10.1002/anie.202005907>.

© 2020 The Authors. Published by Wiley-VCH GmbH. This is an open access article under the terms of the Creative Commons Attribution License, which permits use, distribution and reproduction in any medium, provided the original work is properly cited.

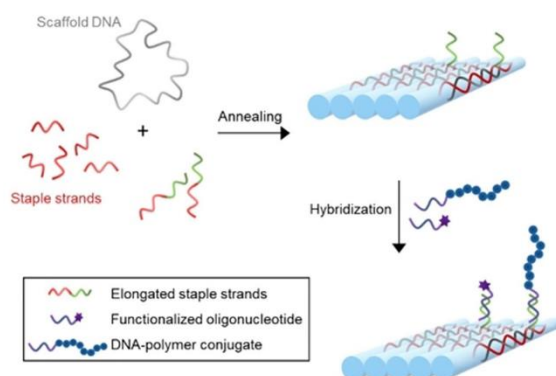


Figure 1. DNA origami structures are created by annealing a scaffold DNA, respectively designed staple strands, and elongated staple strands. The protruding DNA strands can be hybridized to complementary, functionalized oligonucleotides and DNA-polymer conjugates.

2. Polymers and DNA Origami: How to Bridge the Fields

The combination of polymers and DNA origami has the power to merge the fields of synthetic and natural macromolecules, while getting the best of both worlds.^[19,20] On the one hand, the unprecedented addressability of DNA origami may organize polymers on the nanoscale into structures as

polymers are typically known for entanglement and, thereby, pave the way for nanotechnological devices and structure-function investigations. On the other hand, there is a large pool of polymers with a vast range of appealing and adjustable characteristics such as various charges, hydrophobicity or hydrophilicity, as well as stimulus-responsiveness, and they may also stabilize DNA objects. There is a versatile range of ways to guide the process and achieve this fusion (Figure 2). Two fundamental strategies have to be distinguished here: Either the polymer is grown *in situ* on the DNA origami template (see Section 2.1) or the polymer is preformed and modified prior to conjugation to the DNA platform (see Section 2.2).

On the molecular level, the underlying principles for polymer attachment are manifold. The polymer can be electrostatically trapped to the negatively charged DNA backbone by the incorporation of respective positive counter charges or be bound to the DNA origami surface through base-pair hybridization. The oligonucleotides required for this can be introduced by click reactions, by established bioconjugation techniques, or grown from nucleotides. Furthermore, hydrophobic interactions between the implemented polymers can be exploited to arrange polymer-DNA constructs into higher ordered structures (see Section 2.3). However, the rather small number of publications in the field of DNA origami and polymer hybrids gives a first hint of how challenging this topic seems to be. Not only does synthesis suffer from various issues, such as solubility issues or steric



Nadine Hannewald studied chemistry at the Friedrich Schiller University in Jena and graduated in 2018 in the field of organic and macromolecular Chemistry. She is currently working as a PhD student in the group of Prof. Schubert, where she focuses on the synthesis of well-defined polymer architectures for attachment to DNA origami.



Tanja Weil studied chemistry at the TU Braunschweig (Germany) and the University of Bordeaux (France) and completed her PhD at the Max Planck Institute for Polymer Research (MPIP) in Mainz, for which was awarded the Otto-Hahn Medal in 2003. After several years in industry, she returned to academia by accepting an Associate Professor position at the National University of Singapore in 2008. In 2010, she joined the University of Ulm as Director of the Institute of Organic Chemistry III. Since 2017, she has been Director at the MPIP, heading the department "Synthesis of Macromolecules".



Pia Winterwerber studied Biomedical Chemistry at the Johannes Gutenberg University, Mainz (Germany), and received her master's degree in 2018. During her studies she focused on the synthesis of hyper-branched star polymers as well as amphiphilic biomacromolecule conjugates. She joined the group of Prof. Dr. Tanja Weil at the Max Planck Institute for Polymer Research, Mainz, in 2018 as a PhD student, and is now working on the development of DNA origami hybrid nanostructures.



Ulrich S. Schubert studied chemistry in Frankfurt and Bayreuth (both Germany) and at Virginia Commonwealth University, Richmond (USA). After PhD studies at the Universities of Bayreuth and South Florida, and postdoctoral training with J.-M. Lehn, he moved to the TU Munich (Germany), where he obtained his Habilitation in 1999. 1999–2000 he was Professor at the University of Munich and 2000–2007 Full Professor at the TU Eindhoven (The Netherlands). Since 2007, he has been a Full Professor at the Friedrich Schiller University Jena (Germany). He is an elected member of the German National Academy of Science and Engineering (acatech) and external scientific member of the Max-Planck-Gesellschaft (MPI for Colloid & Interfaces, Golm).

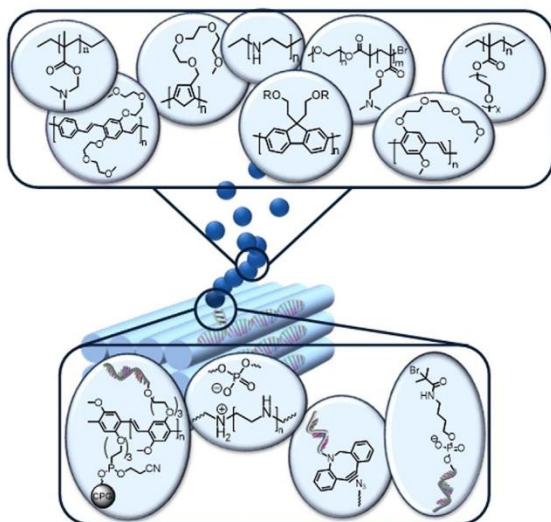


Figure 2. Schematic representation of polymer structures immobilized on DNA origami. The bottom box depicts the attachment mechanisms and moieties involved.

hindrance of both the DNA and polymer reactive sites, but the characterization techniques are also very limited. One of the key drawbacks is the typically extremely low amount of DNA origami structures available, which impedes or even prohibits, for example, freeze-pump-thaw cycles for controlled radical polymerizations, sufficient amounts of attached initiator sites, or conventional polymer analysis by size-exclusion chromatography (SEC), nuclear magnetic resonance (NMR), or dynamic light scattering (DLS).

2.1. Polymer Growth from DNA Origami

The grafting from strategy is a convenient approach towards the synthesis of biomolecule-polymer constructs with tailored properties, which are characterized by facile purification of the conjugate and commonly a high graft density.^[21] Controlled polymerization techniques have emerged as a powerful method to create polymers of controlled molecular weights and well-defined architectures.^[22] Among others, atom transfer radical polymerization (ATRP) provides the possibility to conduct the polymerization under biologically relevant conditions that are suited to the stability of biomolecules, a low concentration of functional groups, or the presence of salts when working with buffers.^[23] However, successful polymerization from the biomolecule surface demands the installation of reactive handles which serve as initiator sites. We employed the highly precise scaffold of DNA origami to anchor ATRP initiators at predefined positions and, thereby, achieve directed polymer growth on the nanoscale (Figure 3).^[24] DNA origami sheets were equipped with different patterns of surface-protruding, short oligonucleotide sequences. Complementary oligonucleotides were modified with ATRP initiators and attached to the DNA

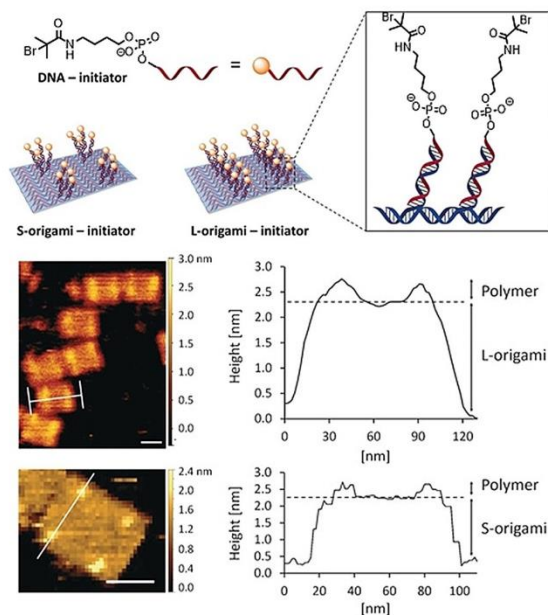


Figure 3. Top: Schematic representation of the DNA origami initiators used in the ATRP of PEGMEMA. Bottom: AFM images and height profiles of the L- and S-origami after polymerization on DNA. Reprinted from Ref. [24] with permission.

origami template by base-pair hybridization. This macro-initiator was then utilized to induce the polymerization of poly(ethylene glycol) methyl ether methacrylate (PEGMEMA). This monomer was chosen because of its biocompatibility as well as its solubility in water, and the rather bulky side chains were considered to facilitate monitoring of the polymerization process by atomic force microscopy (AFM). Furthermore, the presence of sacrificial initiators (excess amount of free initiator DNA not attached to the DNA origami) was found to be crucial for successful polymer growth. Visualization of the origami structures by AFM, in particular recording the height profile, revealed the appearance of new objects where initiator sites were located at defined positions on the DNA nanotile. Furthermore, these objects have different mechanical properties which correspond to features of soft polymeric materials, such as PEGMEMA. Nevertheless, typical characterization of the polymer, such as determination of the chain length or dispersity by size-exclusion chromatography, is not feasible here because of very low quantities. The incorporation of the bifunctional monomer PEG dimethacrylate (PEGDMA) to the polymerization process led to a cross-linked polymer, whose structure could be preserved even after removal of the DNA template.

An essentially different polymerization technique, but also a grafting-from strategy from DNA nanostructures, was introduced by Ding and co-workers.^[25] They decorated a double-stranded DNA template with guanine-rich oligonucleotide sequences, the so-called DNAzymes, which are capable of mimicking the activity of the enzyme horseradish

peroxidase (HRP). Upon incorporation of the cofactor hemin and addition of hydrogen peroxide, the active DNAzyme catalyzes the polymerization of aniline. Thus, 1D polyaniline (PANI) structures were formed by a *para*-coupling reaction, wherein the generated aniline radicals diffuse to the charged DNA surface. The regioselective formation of PANI was then transferred to 2D origami triangles (Figure 4).^[26] However, the use of DNA origami structures was challenging and required optimization of the reaction conditions: Whereas a high ionic strength disfavored the *para*-coupling reaction of PANI, an insufficient Mg^{2+} concentration compromises the stability of the DNA folding. By AFM imaging, the group could show that polymer growth was favored around the DNAzymes and did not grow over the DNAzyme-free regions. Thus, structural information transfer from the origami pattern to PANI was achieved, thereby leading to a polymer of predefined geometry. Furthermore, the reversible redox behavior of polyaniline, which can be triggered by pH changes, renders these conductive hybrid objects promising candidates for the fields of electronics, sensors, and energy storage.

The relatively simple and tolerant polymerization strategy was also applied to the polymerization of dopamine on DNA origami nanostructures.^[27] Polydopamine is a mussel-inspired polymer which has aroused great interest among material scientists because of its excellent capability for surface functionalization.^[28,29] However, the self-polymerization of dopamine and the not yet fully elucidated multifaceted polymer structure hamper its full potential. By employing the same DNAzymes as described above, we could induce and promote polydopamine formation on a 2D DNA nanosheet. It was essential to conduct the polymerization in an acidic milieu to suppress the self-polymerization of dopamine and to gain control over the process. Different polydopamine shapes and sizes were obtained by arranging the catalytic centers in different patterns on the origami scaffold, and the reaction

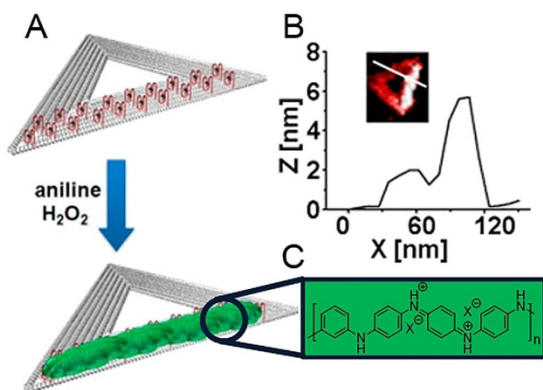


Figure 4. A) DNA-templated synthesis of polyaniline (green) on origami triangles (gray) with DNAzymes (red structures with black dots) in the presence of aniline and H_2O_2 . B) AFM image of a single PANI-coated origami triangle. C) Structure of the emeraldine salt form of PANI. Reprinted from Ref. [26] with permission; Copyright (2020) American Chemical Society.

kinetics could be manipulated by altering the ionic strength and hydrogen peroxide concentration. The fabricated polydopamine nanostructures could serve as a “supramolecular glue”, thus guiding the origami conformation. This is an illustrative example of how the DNA template can affect the polymer formation and vice versa. In a follow-up study, 3D origami structures were decorated with a photosensitizer, which was trapped at distinct positions by guanine-rich oligonucleotides (G-quadruplexes; Figure 5).^[30] Upon irradiation with visible light, dopamine was oxidized and polydopamine was deposited around the reaction centers. As a consequence of the light stimulus, the presence of hydrogen peroxide is no longer needed, which keeps the system simple. In addition, the polymerization process could be temporally controlled by simply switching the light on and off. In this way, photopatterned 3D nanostructures with dimensions far below 100 nm were created, which could not only preserve the DNA template in salt-depleted media but they could also be released from the template under strong acidic conditions.

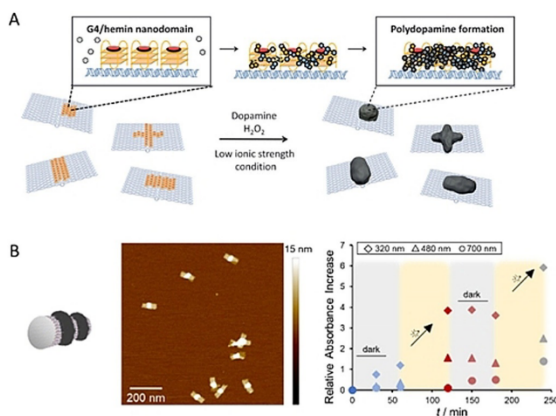


Figure 5. A) Chemically triggered formation of polydopamine on 2D DNA origami by DNAzymes to create highly precise hybrid objects.^[27] B) Photoinduced formation of polydopamine on 3D DNA origami under spatiotemporal control with the help of a locally trapped photosensitizer. Reprinted from Ref. [30] with permission.

2.2. Polymer Attachment to DNA Origami

In all the examples discussed above, the polymer chain was grown from the DNA origami surface in distinct patterns, either covalently attached to the initiators by a controlled polymerization technique or noncovalently deposited next to the initiators on the DNA template. In contrast to this methodology, one can also make use of a preformed polymer, artificially synthesized or biologically derived, with graft-suitable reactive handles and attach it to DNA nanostructures. Besides the rather intuitive idea of trapping a positively charged polymer by electrostatic interactions, it is also appealing to hybridize polymers by base-pair recognition or to exploit the attractive area of click chemistry. However, many of the studies illustrate the boundaries of the bespoke strategies, such as the steric hindrance of polymers, their

solubility, and the stability of DNA, which all impair successful conjugation.

2.2.1. Electrostatic Interactions

The ionic nature of the phosphate backbone of DNA makes it possible to attach polymers through electrostatic interactions to DNA origami. Usually, the DNA origami structures are stabilized by the divalent cation Mg^{2+} , which screens the negatively charged phosphate backbone of the DNA sequence to compensate charge repulsion between closely packed DNA strands. In a multitude of studies, the applied polymers comprise amino moieties in the side chain or backbone that undergo quaternization of the nitrogen atom when applied in acidic media. These polycations can then interact with DNA origami through ionic interactions.

Based on this idea, Kiviahio et al. investigated the electrostatic binding between a 60-helix-bundled DNA nanostructure and cationic block copolymers.^[31] To assess the effect of the polymer structure on the binding affinity, the authors synthesized AB- and ABA-type copolymers by ATRP. For this, they utilized a respective mono- and bifunctional PEG-based macroinitiator to polymerize 2-dimethylaminoethyl methacrylate (PDMAEMA), where the PEG moiety was intended to increase the poor biocompatibility of PDMAEMA. Coating was achieved by simply mixing the compounds under mild acidic conditions to ensure protonation of the amines. It could be demonstrated that all the polymers had a suitable binding efficiency but, interestingly, the block structure only had a minor impact. Instead, the ratio of total number of polymer amines and the total number of phosphates in DNA (referred to as the N/P ratio) was pivotal, irrespective of the arrangement of the nitrogen atoms in the polymer. Moreover, various polymer coatings were suited to control the activity of enzyme-loaded DNA origami nanocontainers, as indicated by the bioluminescence reaction of luciferase enzymes. In a further study, commercially available linear polyethyleneimine (LPEI) and chitosan as a natural polymer were applied to form polyplexes with DNA origami nanostructures (Figure 6).^[32] The authors aimed to investigate several factors that might have an impact on the origami stability under physiological conditions, such as degree of polymerization, charge density, and nitrogen to phosphate ratio. Three different DNA objects were synthesized and applied for this purpose: a nanorod, a nanobottle, and a wireframe origami structure. After simple mixing of the DNA and polymer compounds, successful coating was demonstrated with the PicoGreen assay, which relies on the intercalation of the dye into the DNA double helix while exhibiting strong fluorescence. As a consequence of the polycation coating, PicoGreen was expelled from the polymer-DNA complex, thereby resulting in a decrease in the fluorescence. Although bare origami could be imaged by negative-stain transmission electron microscopy (nsTEM), the staining of the LPEI-modified origami was only possible after removing the polymer coating by treatment with polyanionic dextran sulfate; this revealed intact origami structures and, thus, indirectly indicated successful encapsulation by the polymer. It could be shown that LPEI protects

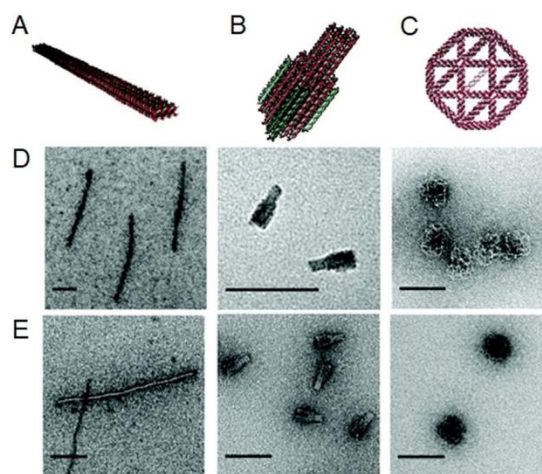


Figure 6. Representation of the different DNA origami structures. A) nanorod, B) nanobottle, and C) wireframe structure. D) TEM images of uncoated DNA origami structures. E) Origami structures stained with uranyl acetate after decomplexation with dextrane sulfate revealed intact origami structures. Reprinted from Ref. [32] with permission.

the structural integrity of the DNA origami more efficiently than chitosan and that this ability strongly depends on the nitrogen to phosphate (N/P) ratio. However, it must be considered that the unique addressability of the DNA origami surface might be masked by the polymer coating.

In 2017, two studies investigated the use of PEG-oligolysine-based copolymers to protect DNA origami structures against low-salt denaturation and nuclease degradation, while the lysine block provides the positive charges to electrostatically interact with the DNA object, and the PEG is envisioned to have a shielding effect.^[33,34] The Schmidt group synthesized poly(ethylene glycol)-*b*-poly(L-lysine) (PEG_{12kDa}-PLYS₁₈) by ring-opening polymerization of *N*-trifluoroacetyl-L-lysine *N*-carboxyanhydride initiated by an amine-terminated 12 kDa PEG macroinitiator. In contrast to bare origami structures, polymer-coated objects resisted the treatment of DNase I, fetal bovine serum (FBS), and low salt levels, and maintained structural integrity. However, the attachment of sterically demanding gold nanoparticles (AuNP) did not survive the process of polyplex formation; detachment could be visualized by transmission scanning electron microscopy (tSEM). The problem could be circumvented by employing shorter PEG chains, which still offer the same protection efficiency. These findings are in agreement with a similar study by Shih and co-workers, who examined the beneficial contribution of the PEG_{5kDa}-PLYS₁₀ polymer coating to the origami stability. They could further prove that surface addressability of the DNA nanostructures was not constrained by the polymer film and immobilized ligands were capable of targeting receptors, thereby leading to cellular uptake of the hybrid objects. Very recently, Gang and co-workers endeavored to also push the limits of the stability of DNA assembly in complex biological fluids (Figure 7).^[35] They put a novel class of polycationic polymers,

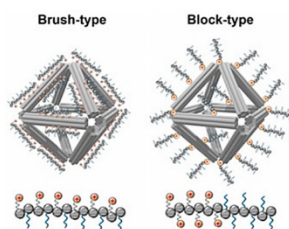


Figure 7. “Brush-” and “block-type” peptoids should lead to different surface coatings on octahedra-shaped DNA origami. Reprinted from Ref. [35] with permission.

namely peptoids, to the test. Peptoids are emerging peptidomimetics, whose side chains are not appended to the α -carbon but to the nitrogen atom of the peptide backbone, thus, preventing secondary structure formation through hydrogen bonding and providing proteolysis resistance. In line with the approaches discussed above, the group explored the effect of peptoid architecture and sequence dependency on the origami stability. For this, they synthesized, by solid-phase peptoid synthesis, brush- and block-like peptoids that were built from positively charged monomers (electrostatic DNA complexation) and neutral oligo(ethyleneoxy) moieties (surface passivation). They could demonstrate that brush-like peptoids were superior in protecting wireframed octahedra-shaped DNA origami. Moreover, the capability of these structures to serve as a drug carrier with controlled release of doxorubicin was shown, which had not been achieved before. All these coating strategies are rather easily achieved by simply mixing the origami nanostructures with an excess of polymer, but they lack the possibility to arrange the polymer in distinct patterns.

2.2.2. Oligonucleotide Hybridization

The attachment of polymers through ionic interactions, which are often just used to stabilize DNA, is very advantageous in terms of synthesis as well as the ease and straightforward fusion of a polymer and DNA origami. Nonetheless, this strategy does not consider the unique addressability provided by the DNA origami scaffold; on the contrary, it might even hinder it. Hence, the linkage of polymers to DNA objects by complementary base-pair recognition allows the highly precise positioning of single polymer chains and overcomes their lack of intrinsic self-assembly properties. To equip polymers with the necessary handles, namely, oligonucleotides that are complementary to ssDNA sequences on the origami surface, one can either functionalize the polymer's end group or the side chains accordingly. It has been proven useful to either “click” the oligonucleotide to the polymer or to grow oligonucleotides directly from the polymer backbone. In both cases, hybridizing the respective polymer to the DNA origami is always reversible and should permit programmed switching.

Gothelf and co-workers see a great prospective in binding conjugated and, therefore, potentially conducting polymers on DNA origami templates to build molecular-scale elec-

tronic or optical wires.^[36] For this purpose, they synthesized a conjugated poly(phenylenevinylene) polymer with alkoxy side chains (APPV) from a dithiocarbamate precursor. Each phenylene unit in the backbone bears a triethylene glycol side chain and with the help of protective group chemistry, a small number of hydroxy groups were employed to attach the polymer to the solid support; the remaining hydroxy groups were used in automated solid-phase DNA synthesis to graft 9-mer oligonucleotides. By this approach, they obtained a fully water-soluble brush polymer with ssDNA extending from the majority of the repeating units. However, the size distribution was rather broad, as characterized by gel-permeation chromatography (GPC; 340–3300 kDa) and AFM (lengths in the range of 20 nm to 200 nm), which the authors explain through partial degradation during purification. By equipping 2D and 3D DNA origami templates with complementary oligonucleotide sequences, they could link single polymer chains to the template in different geometries. Moreover, they could observe Förster resonance energy transfer (FRET) between the attached polymer (donor) and a co-immobilized acceptor dye, thereby proving that absorption and emission of the polymer backbone is not harmed by the applied methods. Further studies that exploit this strategy towards the development of nanocircuits are discussed in Section 3.

In contrast to the rather sophisticated and challenging solid-phase synthesis of oligonucleotides directly from the polymer backbone, one can also furnish the polymer with a suitable end group and “click” it to the respective ssDNA. In this context, copper-catalyzed azide–alkyne reactions (CuAAC)^[37] as well as a copper-free variant involving a strain-promoted azide–alkyne click reaction (spAAC)^[38,39] have been utilized in different studies. For the development of a DNA origami assisted electrooptical modulator, Canary and co-workers equipped two different kinds of organic semiconductors, namely oligomers of poly(phenylene vinylene) (HPV) and oligoaniline (OANI), with ssDNA strands, which allows their attachment to a DNA origami scaffold (Figure 8).^[37]

By this approach, the symmetric oligomers with azide groups at each end were “double-clicked” by CuAAC to oligonucleotide strands containing a propargyl residue. Consequently, the obtained structure consisted of a polymer with oligonucleotide sequences at both ends. By hybridizing the polymer-DNA constructs to a DNA origami frame with four complementary anchor strands, the semiconductors were brought into proximity, thereby forming a cross-like structure. By tuning the oxidation state of polyaniline, the energy transfer from HPV to OANI could be tuned, as visualized by an altered fluorescence signal. However, the hybridization efficiency of only 20% correctly formed polymer-DNA origami structures (determined by AFM) illustrates how challenging the formation of these hybrid objects is, although base-pair hybridization is often assumed to be straightforward. Mertig and co-workers also employed click reactions to conjugate conducting polymers in distinct patterns to an origami surface (Figure 9).^[38] For this, they synthesized well-defined thiophene-based polymers with dispersities between 1.1 to 1.3 by Kumada polycondensation. Oligoethylene glycol bearing side chains ensured water solubility of the polymer

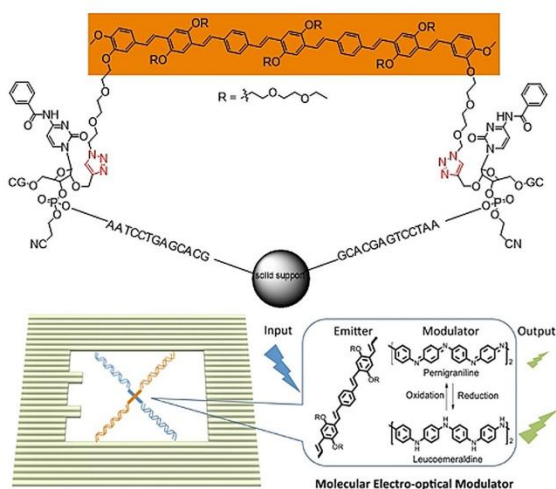


Figure 8. Top: Product of the double-CuAAC reaction between an azide-functionalized oligomer (OPV) and an alkyne-functionalized oligonucleotide sequence, immobilized on a solid support (controlled pore glass). Bottom: Schematic representation of the x-shaped OANI- and OPV-DNA conjugate on the DNA origami frame. OANI (blue) acts as a modulator of the fluorescence intensity of the OPV (orange). Reprinted from Ref. [37] with permission. Copyright (2020) American Chemical Society.

and thereby allowed reaction of the azide-functionalized polymer and dibenzocyclooctyne-end-capped oligonucleotide in aqueous solution. It is noteworthy that the degree of functionalization of the polymers is only in the moderate range of 38–71%. However, unfunctionalized polymer chains are not considered to participate in, or even harm, further transformations. Three different oligonucleotide sequences were conjugated to the polymers and were attached to three different DNA origami pads with patterns of respective handles to study sequence-hybridization effects. Virtually all the pads displayed at least one attached object, but the overall occupation probability per handle was roughly one third. For example, 4 out of 14 handles on one origami pad displayed an attached object. This again indicates that hybridization of polymers to DNA surfaces is difficult and sterically demanding. Applying surfactants to polymer-decorated origami was accompanied by a blue-shifted increase in the fluorescence and, thus, indirectly showed that interchain π - π stacking of polythiophene units occurs. This feature might offer the possibility to fine-tune optical properties on a molecular level.

2.3. Higher Order Structures

In addition to the attachment methods discussed above, one can also make use of the hydrophobic effect to form higher ordered structures built from DNA origami and polymers. By applying hydrophobic polymers to DNA scaffolds, surface properties can be altered significantly and, thus, self-assembly of amphiphilic structures can be induced.

In 2015, Liu and co-workers showed that attaching hydrophobic dendrons to DNA origami rectangles could lead to the formation of surface areas with a high local concentration of hydrophobic molecules, which, as a result of the hydrophobic effect, guided origami folding into various thermodynamically stable products. Poly(aryl ether) dendrons were conjugated to oligonucleotides through solid-phase synthesis, whereas modification with oligo(ethylene glycol) tails should increase the water solubility of the dendrons. Upon traditional origami annealing in the presence of both elongated capture strands (handles on the origami) and oligonucleotide-bearing dendrons (complementary to handles on the origami), sandwich-like structures were created. In a follow-up study, the same group created polymer vesicles on the shell of a DNA origami cube (Figure 10).^[40]

The attachment of the above-mentioned hydrophobic dendrons to origami cubes led to aggregation and precipitation events, most likely because of π - π stacking between several cuboid frames (frame-frame interactions). The addition of a second hydrophobic dendron, the so-called principal amphiphile (PA), to the amphiphilic construct breaks the frame-frame interactions and promotes stronger PA-frame interactions, thereby resulting in the formation of heterovesicles. To demonstrate the applicability of this process to different molecules, the dendrons were substituted by polymers: DNA cuboids were covered with thermoresponsive poly(propylene oxide) (PPO) and upon heating, the polymer became hydrophobic and, thus, guided a second PPO polymer to form heterovesicles.

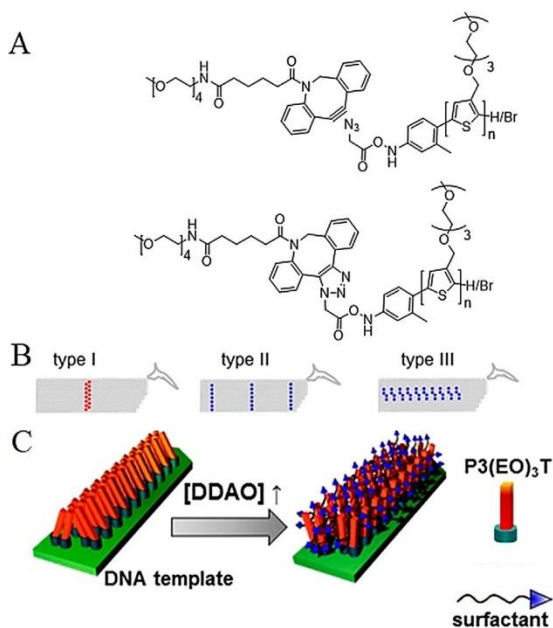


Figure 9. A) spAAC reaction with a cyclooctyne-functionalized oligonucleotide and azide-functionalized polythiophene. B) The three different DNA origami pad types. C) Illustration of aggregated P3(EO)₃T on the DNA origami (left) and the deaggregated structure (right) after the addition of surfactant. Printed from Ref. [38] with permission. Copyright (2020) American Chemical Society.

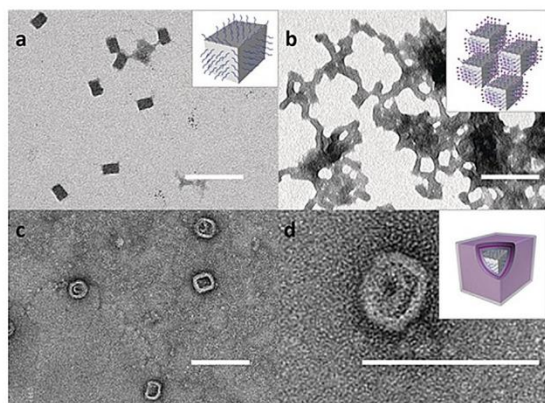


Figure 10. TEM images of the DNA-cube-dendron aggregates. a) Origami cuboid. b) Aggregates formed upon addition of D₇DOEG. c,d) Heterovesicles formed from the aggregate after the addition of G₂Cl 18. Reprinted from Ref. [40] with permission.

This is an impressive example of higher order assemblies based on polymer-decorated DNA origami structures; however, the intricate technique requires a strong background in the field of frame-guided assembly to be successful. The use of hydrophobic interactions between polymers attached to 3D DNA nanostructures was also shown to yield larger DNA micelles.^[41,42] For this purpose, DNA nanostructures of three different forms (trigonal prism, cube, and pentagonal prism) were decorated with oligonucleotides covalently linked to hexaethylene phosphate to yield DNA nanostructures with polymer strands.^[41] It could be revealed that the number of hexaethylene phosphate repeating units is crucial for the micellization: At least six of these repeating units are required to form higher ordered structures, with micellar structures being observed when the number of repeating units is increased to at least eight.^[41] Not only were micelles with cubic DNA structures synthesized, but trigonal and pentagonal prisms were also obtained. TEM, AFM and DLS were utilized to compare the micelles of the different DNA structures, which revealed that they appear to have approximately the same size and that the size is only influenced by the number of repeating units of the hexaethylene phosphate. The group further investigated the influence of a combination of hydrophobic and hydrophilic repeating units in the DNA polymer conjugates attached to the prismatic structures.^[42] The hydrophobic block consisted of 1,12-dodecanediol (HE), and the hydrophilic block was represented by hexaethyloxy glycol (HEG). First experiments combined the cubic DNA structure with four DNA copolymer strands, which consisted of six HE and six HEG units, in different orders. Notably, higher mobility in the gel electrophoresis was observed as the HE block length was increased, which was explained by the folding of the polymer chains into the cage structure.^[42] The nanostructure with the HE₆HEG₆ block copolymer was exceptional, as it formed rings of three to five polymer-decorated DNA cubes in a doughnut-like fashion instead of the expected micellar structures. By increasing the length of the hydrophilic HEG block, the diameter of the ringlike

assemblies could be increased, in contrast to the HE₆HEG₆ block copolymer, which indicates that the HEG block acts as a spacer.^[42] Remarkably, the formation of micelles was not observed when (block) copolymers consisting of hydrophobic and hydrophilic units were used. These can only be observed in the case of hydrophobic polymers.^[42] The previously discussed examples show that not only can DNA origami be utilized to direct polymers into larger structures and desired shapes, but polymer–polymer interactions also allow macromolecular structures to be created with prior-folded DNA origami.

3. Next-Generation Polymeric Hybrid Materials: Fields of Application

In the previous section, we highlighted different techniques for linking polymers and DNA origami as well as the influence on each other. Although there are fewer examples than one might expect regarding the potential provided by these materials, and although there are still some challenges to overcome, several studies report the first steps towards future applications and prospects.

Gothelf and co-workers exploited their system of attaching a conjugated brush-like polymer with oligonucleotide side chains onto DNA origami tiles to contribute to the area of nanophotonic and nanoelectronic devices. They not only attached the polymer to the origami platform, they also precisely forced the polymer to switch its position and conformation (Figure 11 a).^[43] For this, two sets of so-called guiding strands were employed that allow the polymer to follow two different routes on the origami tile, depending on which type of guiding strand is applied. The guiding strands are also equipped with a toehold region—a short sequence of nucleotides which does not take part in polymer hybridization. Hence, the guiding strands can be trapped by a fully complementary remover strand, which leads to the release of the polymer. By subsequently adding the other set of guiding strands, the polymer can be routed along the second track on the origami. These events can be monitored by FRET between the polymer and arranged reporter dyes. It should be noted that approximately only half the origami structures displayed well-aligned polymers (AFM) and that surface contamination after the conformation switch significantly harmed imaging. In an ensuing study, the group aimed to investigate the interaction between two different types of conjugated polymers by making use of the unique addressability of DNA origami (Figure 11 b).^[44] In addition to the above-mentioned APPV-DNA copolymer, they similarly synthesized a polyfluorene-DNA pendant (poly(F-DNA)). However, no interpolymer energy transfer was observed on conjugating either polymer to the origami rectangle. This might be caused by a lack of interpolymer contact in combination with interference from unbound polymers, which demonstrates the limits for the conjugation of intricate polymers. The polymers were directly co-localized by hybridization of the side chains for further investigations.

DNA origami is an emerging platform to direct the motion of various objects on the nanoscale; however, the

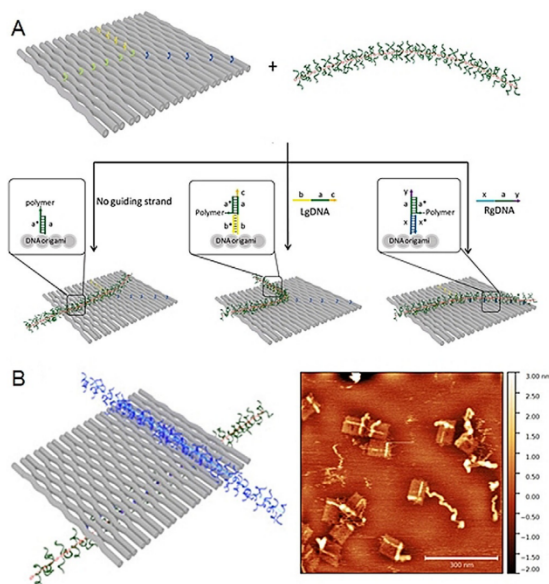


Figure 11. A) Switching of a polymer strand conformation on a DNA origami by adding guiding and remover strands. B) p(F-DNA) (blue) and p(PV-DNA) (green) on a DNA origami tile with the AFM image (right). Reprinted from Refs. [43, 44] with permission. Copyright (2020) American Chemical Society.

movement of the attached objects is often “fuel-based”, that is, employing strand displacement reactions of respectively designed oligonucleotides to break and create old and new bonds. Thus, purification after each step is often necessary. Baumberg and co-workers developed a DNA origami flexor whose actuation is mediated by a thermoresponsive polymer which can be stimulated externally (Figure 12).^[39]

They designed a flexible DNA origami hinge structure, whereby poly(*N*-isopropylacrylamide) (PNIPAM) was attached on either side of the hinge. In this way, a PNIPAM-DNA conjugate was formed by catalyst-free strain-promoted cycloaddition and attached to the complementary capture strands within the hinge region. By fixing a gold nanoparticle and a fluorescent dye at opposite ends, the switch between the

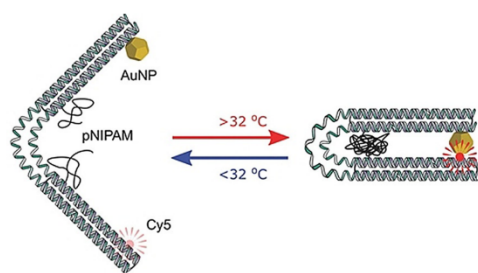


Figure 12. Representation of the DNA origami flexor. Upon heating of the flexor-containing solution, PNIPAM aggregates and leads to a change in the DNA origami shape. Reprinted from Ref. [39] with permission.

opened and closed state of the hinge could be optically monitored. Upon heating above the lower critical solution temperature (LCST) of 32 °C, PNIPAM becomes hydrophobic and forces the hinge to close. This could be conclusively tracked by an increase in fluorescence as well as changes in the size distribution (DLS). However, the AFM images obtained are a vivid example of how difficult direct visualization of conformation-altering DNA origami structures can be.

Tokura et al. further developed their surface-initiated ATRP on a DNA origami tile by transferring the technique to a 3D tube, preliminarily paving the way towards 3D engineering of nanomaterials (Figure 13).^[45] The authors designed a system where orthogonal polymer growth is feasible: After coating of the outer surface with cross-linked PEGMEMA, the inner cavity of the origami tube was equipped with DNAsomes to induce the polymerization of dopamine. Whereas AFM images captured after the first polymerization step could reveal an increase in the height profile and, thus, the presence of polymer, no imaging was possible of the polymer synthesized in the inside. The formation of polydopamine could only be monitored by absorbance spectroscopy, once more emphasizing how complicated the characterization of polymer-DNA hybrid objects is.

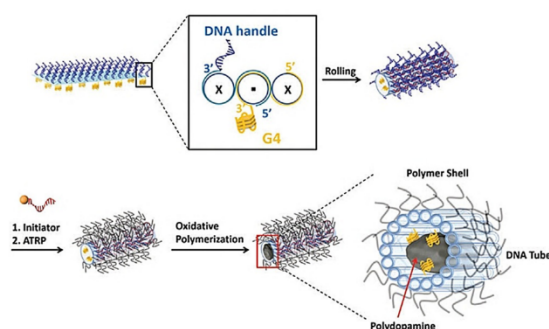


Figure 13. Folding of the DNA origami tube and decoration with oligonucleotide-modified ATRP initiators and the subsequent polymerization of PEGMEMA and PEGDMA. Reprinted from Ref. [45] with permission (published by The Royal Society of Chemistry).

4. Summary and Outlook

The combination of DNA origami and polymers is a strong and emerging tool towards precise surface modification and the creation of elusively defined nanostructures in the low nanometer regime, thus, representing a kind of a “top-up” approach that merges conventional bottom-up and top-down techniques. To date, the arrangement of polymeric objects in a virtually infinite variety of geometries with precision of a few nanometers is not reported by any other methodology. It thereby pushes the limits of established lithography and self-assembly approaches by programming distinct nano-devices. Furthermore, DNA origami allows orthogonal decoration of polymers and other molecules, thereby enabling the investigation of energy-transfer processes, as well as the

installation of suitable reporter systems or targeting groups. In principal, two different strategies lead to the formation of such hybrid structures: either the polymer is grown from the DNA origami template or a preformed polymer is linked to the DNA platform. With regard to the studies discussed herein, it turns out that there are significantly more reports within the latter category. The grafting of polymers from the origami surface is very challenging due to the extremely low concentration of DNA objects and the, therefore, small number of initiator sites as well as the increased sensitivity to oxygen present because of the ultralow reaction volumes. Moreover, it is not possible to determine average molecular weights and distributions of the grown chains. Furthermore, the attachment of polymers to DNA origami faces some hurdles: the solubility of the polymer is preferred to be compatible with DNA, and the entanglement of polymers and the folding of DNA might shield their reactive centers. However, this strategy allows the larger scale synthesis of polymers and their thorough characterization prior to DNA origami fusion.

Whereas the electrostatic coating of DNA nanostructures with polycations may be considered as straightforward, it often only aims to stabilize the inherently susceptible DNA construct in biologically relevant media, but does not exploit the addressability of the platform to achieve molecular patterning. Therefore, hybridization of respectively modified polymers to complementary capture strands on the DNA origami is more expedient, but the conjugation efficiency and the grafting density is often reported as rather low. We regard it as important to once again emphasize the characterization challenges which come along with the synthesis of polymer-DNA origami hybrid structures and which hinder fast progress in the field. The ultrasmall quantities of DNA origami hamper typical polymer analysis methods such as SEC, NMR, or DLS. To monitor the impact of polymers on DNA origami at a qualitative level, agarose gel electrophoresis can be employed. However, the integrity of the structures cannot be confirmed in this way. Therefore, imaging techniques such as AFM and TEM have to be performed to visualize the objects. As a consequence of the small size of DNA origami, such techniques have to be operated in high-resolution modii, and sample preparation, for example, drying effects, has to be taken into account. The most representative image might be captured by performing AFM in a liquid environment, which corresponds to the natural occurrence of DNA origami in aqueous solution. Thus, indirect characterization, for example, FRET, can also be utilized to monitor conformation changes.

In conclusion, the fusion of polymers with DNA origami holds great potential for designing programmable nano-devices with highest structural precision, and there are already pioneering investigations towards the application of this class of new materials.

Acknowledgements

We acknowledge financial support from the German Research Foundation (DFG)—project number 407426226, SFB/

TRR 234 (CatalLight, B01). Open access funding enabled and organized by Projekt DEAL.

Conflict of interest

The authors declare no conflict of interest.

- [1] S. M. Bird, O. El-Zubir, A. E. Rawlings, G. J. Leggett, S. S. Staniland, *J. Mater. Chem. C* **2016**, *4*, 3948–3955.
- [2] M. Scuderi, M. Esposito, F. Todisco, D. Simeone, I. Tarantini, L. De Marco, M. De Giorgi, G. Nicotra, L. Carbone, D. Sanvitto, A. Passaseo, G. Gigli, M. Cuscunà, *J. Phys. Chem. C* **2016**, *120*, 24314–24323.
- [3] B. S. Bolu, R. Sanyal, A. Sanyal, *Molecules* **2018**, *23*, 1570.
- [4] A. Biswas, I. S. Bayer, A. S. Biris, T. Wang, E. Dervishi, F. Faupel, *Adv. Colloid Interface Sci.* **2012**, *170*, 2–27.
- [5] J. E. Poelma, C. J. Hawker, *Nat. Nanotechnol.* **2010**, *5*, 243–244.
- [6] C. C. Robertson, J. S. Wright, E. J. Carrington, R. N. Perutz, C. A. Hunter, L. Brammer, *Chem. Sci.* **2017**, *8*, 5392–5398.
- [7] B. Choi, J. Yu, D. W. Paley, M. T. Trinh, M. V. Paley, J. M. Karch, A. C. Crowther, C.-H. Lee, R. A. Lalancette, X. Zhu, P. Kim, M. L. Steigerwald, C. Nuckolls, X. Roy, *Nano Lett.* **2016**, *16*, 1445–1449.
- [8] J. Zhang, J. Tanaka, P. Gurnani, P. Wilson, M. Hartlieb, S. Perrier, *Polym. Chem.* **2017**, *8*, 4079–4087.
- [9] S. M. Brosnan, H. Schlaad, M. Antonietti, *Angew. Chem. Int. Ed.* **2015**, *54*, 9715–9718; *Angew. Chem.* **2015**, *127*, 9851–9855.
- [10] J. Yang, H. Miao, Y. Wei, W. Li, Y. Zhu, *Appl. Catal. B* **2019**, *240*, 225–233.
- [11] Y. Guo, L. Xu, H. Liu, Y. Li, C. M. Che, Y. Li, *Adv. Mater.* **2015**, *27*, 985–1013.
- [12] B. Saccà, C. M. Niemeyer, *Angew. Chem. Int. Ed.* **2012**, *51*, 58–66; *Angew. Chem.* **2012**, *124*, 60–69.
- [13] N. C. Seeman, *J. Theor. Biol.* **1982**, *99*, 237–247.
- [14] P. W. K. Rothmund, *Nature* **2006**, *440*, 297–302.
- [15] V. V. Thacker, L. O. Herrmann, D. O. Sigle, T. Zhang, T. Liedl, J. J. Baumberg, U. F. Keyser, *Nat. Commun.* **2014**, *5*, 3448.
- [16] F. Jia, H. Li, R. Chen, K. Zhang, *Bioconjugate Chem.* **2019**, *30*, 1880–1888.
- [17] S. I. S. Hendrikse, S. L. Gras, A. V. Ellis, *ACS Nano* **2019**, *13*, 8512–8516.
- [18] H. Sun, L. Yang, M. P. Thompson, S. Schara, W. Cao, W. Choi, Z. Hu, N. Zang, W. Tan, N. C. Gianneschi, *Bioconjugate Chem.* **2019**, *30*, 1889–1904.
- [19] M. Madsen, K. V. Gothelf, *Chem. Rev.* **2019**, *119*, 6384–6458.
- [20] X. Xu, P. Winterwerber, D. Ng, Y. Wu, *Top. Curr. Chem.* **2020**, *378*, 31.
- [21] R. Falatach, C. McGlone, M. S. Al-Abdul-Wahid, S. Averick, R. C. Page, J. A. Berberich, D. Konkolewicz, *Chem. Commun.* **2015**, *51*, 5343–5346.
- [22] M. S. Messina, K. M. M. Messina, A. Bhattacharya, H. R. Montgomery, H. D. Maynard, *Prog. Polym. Sci.* **2020**, *100*, 101186.
- [23] K. Matyjaszewski, *Macromolecules* **2012**, *45*, 4015–4039.
- [24] Y. Tokura, Y. Jiang, A. Welle, M. H. Stenzel, K. M. Krzemien, J. Michaelis, R. Berger, C. Barner-Kowollik, Y. Wu, T. Weil, *Angew. Chem. Int. Ed.* **2016**, *55*, 5692–5697; *Angew. Chem.* **2016**, *128*, 5786–5791.
- [25] Z.-G. Wang, P. Zhan, B. Ding, *ACS Nano* **2013**, *7*, 1591–1598.
- [26] Z.-G. Wang, Q. Liu, B. Ding, *Chem. Mater.* **2014**, *26*, 3364–3367.
- [27] Y. Tokura, S. Harvey, C. Chen, Y. Wu, D. Y. W. Ng, T. Weil, *Angew. Chem. Int. Ed.* **2018**, *57*, 1587–1591; *Angew. Chem.* **2018**, *130*, 1603–1607.

- [28] Y. H. Ding, M. Floren, W. Tan, *Biosurf. Biotribol.* **2016**, *2*, 121–136.
- [29] H. Lee, S. M. Dellatore, W. M. Miller, P. B. Messersmith, *Science* **2007**, *318*, 426–430.
- [30] P. Winterwerber, S. Harvey, D. Y. W. Ng, T. Weil, *Angew. Chem. Int. Ed.* **2020**, *59*, 6144–6149; *Angew. Chem.* **2020**, *132*, 6200–6205.
- [31] J. K. Kiviahio, V. Linko, A. Ora, T. Tiainen, E. Jarvihaavisto, J. Mikkila, H. Tenhu, Nonappa, M. A. Kostiaainen, *Nanoscale* **2016**, *8*, 11674–11680.
- [32] Y. Ahmadi, E. De Llano, I. Barisic, *Nanoscale* **2018**, *10*, 7494–7504.
- [33] N. P. Agarwal, M. Matthies, F. N. Gur, K. Osada, T. L. Schmidt, *Angew. Chem. Int. Ed.* **2017**, *56*, 5460–5464; *Angew. Chem.* **2017**, *129*, 5552–5556.
- [34] N. Ponnuswamy, M. M. C. Bastings, B. Nathwani, J. H. Ryu, L. Y. T. Chou, M. Vinther, W. A. Li, F. M. Anastassacos, D. J. Mooney, W. M. Shih, *Nat. Commun.* **2017**, *8*, 15654.
- [35] S.-T. Wang, M. A. Gray, S. Xuan, Y. Lin, J. Byrnes, A. I. Nguyen, N. Todorova, M. M. Stevens, C. R. Bertozzi, R. N. Zuckermann, O. E. Gang, *Proc. Natl. Acad. Sci. USA* **2020**, *117*, 6339–6348.
- [36] J. B. Knudsen, L. Liu, A. L. Bank Kodal, M. Madsen, Q. Li, J. Song, J. B. Woehrstein, S. F. Wickham, M. T. Strauss, F. Schueder, J. Vinther, A. Krissanaprasit, D. Gudnason, A. A. Smith, R. Ogaki, A. N. Zelikin, F. Besenbacher, V. Birkedal, P. Yin, W. M. Shih, R. Jungmann, M. Dong, K. V. Gothelf, *Nat. Nanotechnol.* **2015**, *10*, 892–898.
- [37] X. Wang, C. Li, D. Niu, R. Sha, N. C. Seeman, J. W. Canary, *Nano Lett.* **2018**, *18*, 2112–2115.
- [38] J. Zessin, F. Fischer, A. Heerwig, A. Kick, S. Boye, M. Stamm, A. Kiri, M. Mertig, *Nano Lett.* **2017**, *17*, 5163–5170.
- [39] V. A. Turek, R. Chikkaraddy, S. Cormier, B. Stockham, T. Ding, U. F. Keyser, J. J. Baumberg, *Adv. Funct. Mater.* **2018**, *28*, 1706410.
- [40] Y. Dong, Y. R. Yang, Y. Zhang, D. Wang, X. Wei, S. Banerjee, Y. Liu, Z. Yang, H. Yan, D. Liu, *Angew. Chem. Int. Ed.* **2017**, *56*, 1586–1589; *Angew. Chem.* **2017**, *129*, 1608–1611.
- [41] C. J. Serpell, T. G. Edwardson, P. Chidchob, K. M. Carneiro, H. F. Sleiman, *J. Am. Chem. Soc.* **2014**, *136*, 15767–15774.
- [42] P. Chidchob, T. G. Edwardson, C. J. Serpell, H. F. Sleiman, *J. Am. Chem. Soc.* **2016**, *138*, 4416–4425.
- [43] A. Krissanaprasit, M. Madsen, J. B. Knudsen, D. Gudnason, W. Surareunghai, V. Birkedal, K. V. Gothelf, *ACS Nano* **2016**, *10*, 2243–2250.
- [44] M. Madsen, R. S. Christensen, A. Krissanaprasit, M. R. Bakke, C. F. Riber, K. S. Nielsen, A. N. Zelikin, K. V. Gothelf, *Chem. Eur. J.* **2017**, *23*, 10511–10515.
- [45] Y. Tokura, S. Harvey, X. Xu, C. Chen, S. Morsbach, K. Wunderlich, G. Fytas, Y. Wu, D. Y. W. Ng, T. Weil, *Chem. Commun.* **2018**, *54*, 2808–2811.

Manuscript received: April 23, 2020
Accepted manuscript online: July 10, 2020
Version of record online: October 28, 2020

2. Motivation

Nature is considered the gold standard when it comes to the construction of precise and highly functional macromolecules such as proteins and DNA. Consequently, scientists feel stimulated to transcribe these into the synthesis of artificial systems with similar advanced properties and the study thereof. In line with that aim, this thesis seeks to contribute to the endeavor by merging the fields of DNA nanotechnology and bioinspired polymers.

Despite continuous advancements in polymer chemistry, the spontaneous self-assembling processes of the polymer chains and the subsequent architectures can only be orchestrated to a limited extent. Thus, the design of highly defined surfaces and soft materials is a bottleneck for patterning on the nanoscale. To overcome these limitations, we envision the DNA origami platform to control polymer growth in a spatiotemporal manner. Herein, we intend to exploit the origami's accuracy not only for precise arrangement of molecules but also for directing reactions *in situ*. This enables us to circumvent typical constraints faced in top-down approaches such as photolithography in which the patterning resolution is limited by the wavelength of light. To spatially direct photoinduced polymer formation only at designated areas, we therefore will build hybrid nanoobjects from the bottom, leveraging the pinpoint addressability of the DNA template. This way we can benefit from the outstanding temporal control of photoreactions while we do not have to compromise on the wavelength dependency of the light source and subsequent nanopatterns.

Our first approach towards a sophisticated DNA-assisted polymerization system is based on tubular DNA origami structures. These can be derived from furling a 70 x 100 nm DNA rectangle alongside the long edges and have proven to be sufficiently robust whilst offering modification sides on both the outer and inner surface. Accordingly, the outer surface will be equipped with a photopolymerization system to guide formation of polydopamine layers. Even though its natural biocompatibility renders polydopamine a promising candidate for application in, *e.g.*, nanomedicine, its fast and rather uncontrolled polymerization kinetics prohibits investigation with defined nanoscale architectures. Conventionally, polydopamine is synthesized by merely bringing dopamine into a slightly alkaline environment and due to its adhesiveness, coating of virtually any kind of substrate can be achieved. In contrast to that, we aim to control polydopamine formation with the combination of DNA origami and photochemistry. A photosensitizer, protoporphyrin IX, is anchored in G-quadruplex sequences in distinct patterns on the DNA surface and thus, reaction should be triggered at these catalytic centers only. Upon white light irradiation, the photosensitizer will locally produce reactive oxygen species which in turn oxidize the dopamine monomer. Dopamine then undergoes a multistep polymerization process and polydopamine will be imprinted alongside the initiation sites. Importantly, this photo-promoted polydopamine formation does not require chemical triggers that could potentially harm biomolecules, and also provides temporal control by simple on-off switching of the light source.

Essentially, not only the dopamine polymerization will benefit from the DNA platform, but also *vice versa*, we aim to implement additional features to the origami such as increased stability. While DNA Origami is typically dependent on cation-supplemented media and the absence of nucleases, we will investigate how polydopamine rings can contribute to this drawback and potentially enable its broader application.

In a follow-up study, we intend to build on the newly introduced approach to control polydopamine formation by means of light and to broaden the scope of photopolymerization. By implementing further photosensitizers, we can design the system responsive to different wavelengths, enabling a sequential order of reactions steps. Multicomponent substructures across 3D space are chemically challenging and we believe that the origami technique together with photopolymerization might be a powerful construction tool in this respect. We therefore introduce a second catecholamine, norepinephrine, that on the one hand possesses similar polymerization attributes as dopamine but on the other hand bears an additional hydroxy group. The additional side group is known to impact resulting surface morphologies and allows for post modification. Collectively, irradiation of protoporphyrin IX, eosin Y and methylene blue at their respective wavelengths will be pursued to induce coating of the DNA origami tubes with rings of polydopamine or polynorepinephrine at distinct positions. Having a pool of various photosensitizers and monomers will ideally allow for 2-step polymerizations that could yield heterogeneous polymer layers or rings of both polymers on one origami structure. Based on the surface modulation of the DNA origami structures, we intend to explore the fate of these nanoobjects at biological interfaces. Typically, the adhesiveness of poly(catecholamines) leads to aggregation and uncontrolled adsorption, preventing their application. Here, we envision to leverage the controlled polymer deposition on a nanometer scale to study interactions of the nanoparticulate hybrid systems with cell membranes and subsequent uptake events. This is facilitated once more through the addressability of the DNA origami platform which can be equipped with single stranded DNA handles to allow orthogonal decoration of distinct fluorophores, enabling colocalization studies within the cells.

By following these concepts, this thesis envisions combining the DNA origami technique and the photopolymerization of catecholamines in a synergistic fashion to enable spatiotemporal control over their polymer formation on the nanoscale that is hardly achieved by conventional techniques. Chemical and biological investigations are designed to contribute to the understanding of how both building blocks can benefit from each other.

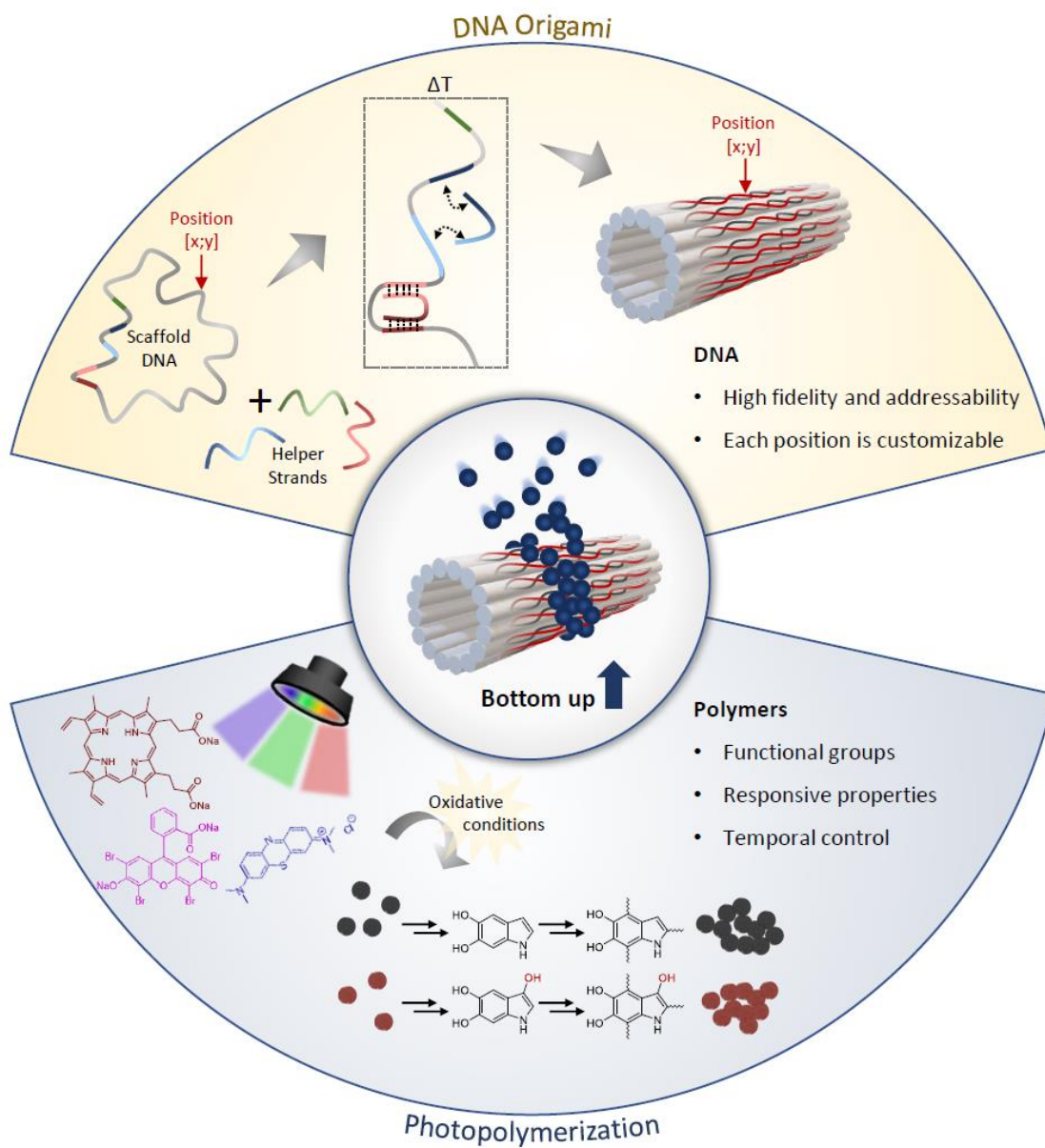
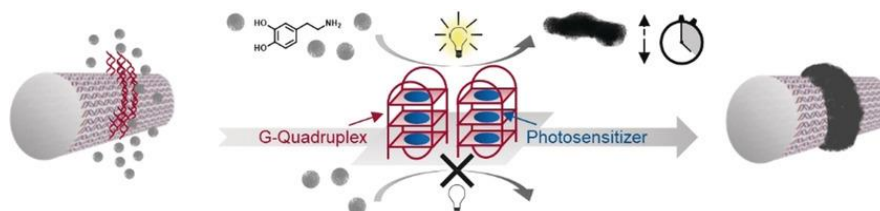


Figure 12 Graphical abstract of the scope of this thesis: Combining the fields of DNA origami and photopolymerization of catecholamines to create advanced hybrid objects from the bottom up.

3. Results and Discussion

3.1 Photocontrolled dopamine polymerization on DNA origami with nanometer resolution

Publication: **“Photocontrolled Dopamine Polymerization on DNA Origami with Nanometer Resolution”**



Pia Winterwerber, Sean Harvey, David Y. W. Ng, Tanja Weil *Angew. Chem. Int. Ed. Engl.* **2020**, 59, 6144-6149.

The publication in this chapter is an open access article under the terms of the Creative Commons Attribution License (CC BY 4.0).

DNA origami inherits the capability to arrange (macro)molecules such as dyes, proteins, nanoparticles, among others within a designated 3-D space. This enables investigation of structure-function relationships or spatial control over distances where required. However, the prospects of DNA origami technology go beyond the simple positioning of objects and can be further exploited for chemical reactions. By equipping DNA origami templates with irradiation-sensitive reaction centers, photopolymerization processes can be spatially and temporally controlled. The nanopatterned polymer-DNA objects exhibit higher stability compared to their bare counterparts. Thus, this chapter aims to emphasize how DNA nanotechnology and polymer chemistry may benefit from each other, resulting in hybrid devices with advanced features.

The herein presented publication is based on DNA origami tubes whose chemically rather inert surface is turned into a patterned template with precisely distributed reaction centers. This is achieved through the incorporation of guanine-rich ssDNA handles at distinct positions that would form so-called G-quadruplexes. These are used for the embedment of a photosensitizer, protoporphyrin IX, which generates active species upon white light irradiation that in turn trigger oxidation and polymerization of dopamine in the vicinity. Polydopamine formation showed to follow the predefined pattern of reaction centers. Thereby, polymer rings can be formed on the origami tubes under spatial-temporal control, following the on/off phases of the light source. Furthermore, this modification significantly alleviates the susceptibility of DNA objects in cation-depleted environment.

As the first author, I conducted all the experiments and analysis, assisted by Sean Harvey on the experimental design. The project was supervised by David Y. W. Ng and Tanja Weil. All authors contributed to writing the manuscript.

Photopolymerization

International Edition: DOI: 10.1002/anie.201911249
German Edition: DOI: 10.1002/ange.201911249

Photocontrolled Dopamine Polymerization on DNA Origami with Nanometer Resolution

Pia Winterwerber, Sean Harvey, David Y. W. Ng,* and Tanja Weil*

Abstract: Temporal and spatial control over polydopamine formation on the nanoscale can be achieved by installing an irradiation-sensitive polymerization system on DNA origami. Precisely distributed G-quadruplex structures on the DNA template serve as anchors for embedding the photosensitizer protoporphyrin IX, which—upon irradiation with visible light—induces the multistep oxidation of dopamine to polydopamine, producing polymeric structures on designated areas within the origami framework. The photochemical polymerization process allows exclusive control over polydopamine layer formation through the simple on/off switching of the light source. The obtained polymer–DNA hybrid material shows significantly enhanced stability, paving the way for biomedical and chemical applications that are typically not possible owing to the sensitivity of DNA.

The creation of functional materials with high control and precision during the synthesis process to provide a shape-customized product is one of the major objectives in the field of nanoscience. Inspired by Nature, bottom-up strategies often exploit the self-assembly capacity of various building blocks to produce ordered structures such as liposomes, polymeric nanoparticles, and viral protein mimics.^[1] Although these structures exhibit a relatively high level of uniformity in terms of size, shape, and functionality, they often lack diverse shapes and the potential for asymmetric and orthogonal molecular modifications.^[2] DNA origami technology, however, provides the opportunity to simultaneously incorporate chemically diverse functional components with controlled stoichiometry to design nanoobjects with ultimate molecular control.^[3]

Rationally designed DNA origami objects originate from the sequence-specific binding properties of DNA: a long, single-stranded DNA scaffold is folded into a distinct archi-

ture guided by a set of short staple strands, which hybridize at programmed positions along this scaffold. Each staple strand can serve as an attachment point for modifications, either directly attached to the staple strand or through a complementary oligonucleotide, furnishing an unprecedented combinatorial platform for designing versatile nanoobjects.^[4] The molecular positioning of, e.g., chromophores, nanoparticles, and drug molecules on the origami surface renders these nanoobjects versatile research tools for various applications in biophysics, medicine, and engineering.^[5] Super-resolution microscopy employs dye-modified origami as a nanoscopic ruler for calibration and applies DNA-PAINT to in vitro applications, making use of transient binding events to monitor target–probe interactions.^[6] Here, fluorescence allows Förster resonance energy transfer (FRET) studies, which are extremely sensitive to slight shifts in the distance between donors and acceptors, thus making it a powerful tool to monitor changes in the conformation of the DNA construct.^[7] In addition, programmable arrays of antenna systems on DNA platforms provide exciting insights into light-harvesting complexes and energy transduction efficacy.^[8] The precise positioning of nanoparticles, e.g., gold nanoparticles and -rods or nanodiamonds on DNA structures opens the possibility to investigate near-field plasmonic coupling with respect to distance, chirality, and orientation.^[9] Furthermore, biological applications benefit from DNA origami's advantages in the study of enzymatic nanoreactors, in which the spatial relationship of reaction cascades of enzymes can be examined.^[10] The clustering behavior of cell-surface receptors can be studied by ligands organized with nanoscale precision on DNA origami.^[11]

However, the prospects of DNA origami methodology go beyond simply positioning objects and may be expanded to perform chemical reactions or even the bottom-up synthesis of macromolecules. In this respect, in situ atom-transfer radical polymerization (ATRP) on DNA origami is suitable for the fabrication of polymers with precisely designed nanopatterns.^[12] By applying initiator sites mimicking horseradish peroxidase activity, it is possible to create template-mediated polyaniline and polydopamine structures of various shapes on the nanoscale.^[13] However, all these reactions are chemically triggered, which does not provide real-time control beyond that of stoichiometry. As such, the use of photochemistry offers an attractive strategy to exert temporal control.^[14] The spatial resolution to create nanopatterns using photochemistry is typically limited by the wavelength of light. Therefore, we envision that these limitations could be overcome by the combination of photochemistry and DNA origami.

[*] P. Winterwerber, S. Harvey, Dr. D. Y. W. Ng, Prof. Dr. T. Weil
Max Planck Institute for Polymer Research
Ackermannweg 10, 55128 Mainz (Germany)
E-mail: david.ng@mpip-mainz.mpg.de
weil@mpip-mainz.mpg.de

S. Harvey, Prof. Dr. T. Weil
Institute of Inorganic Chemistry I, Ulm University
Albert-Einstein-Allee 11, 89081 Ulm (Germany)

Supporting information and the ORCID identification number(s) for the author(s) of this article can be found under:
<https://doi.org/10.1002/anie.201911249>.

© 2019 The Authors. Published by Wiley-VCH Verlag GmbH & Co. KGaA. This is an open access article under the terms of the Creative Commons Attribution License, which permits use, distribution and reproduction in any medium, provided the original work is properly cited.

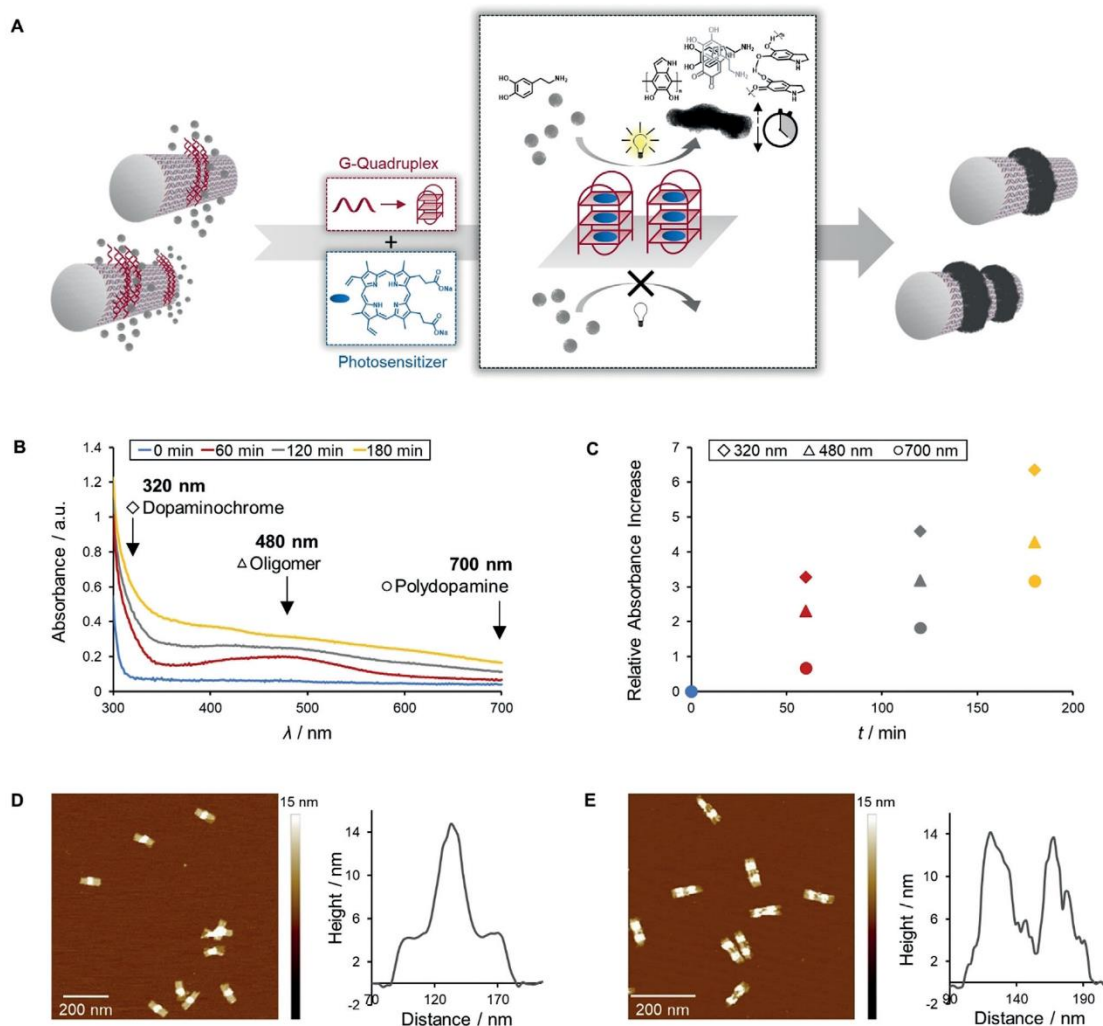


Figure 1. A) Concept of light-triggered polydopamine formation on DNA origami. Upon the irradiation with visible light, the photosensitizer (protoporphyrin IX), which is embedded in G-quadruplex (G4) structures on the DNA template, locally catalyzes the oxidation of dopamine to polydopamine, resulting in well-defined polydopamine–DNA hybrid materials with nanoscale dimensions. B,C) The multistep polymerization of dopamine to polydopamine can be followed by recording the absorbance of the intermediates and final product at 320 nm (dopaminochrome), 480 nm (oligomer), and 700 nm (polydopamine), which steadily increase. D,E) AFM topographic images reveal a significant increase in height where polydopamine is imprinted on top of the G4 pattern.

Herein, we have developed a photopolymerization reaction using a guanine-rich quadruplex (G4) with the embedded photosensitizer protoporphyrin IX (PPIX). The production of reactive oxygen species (ROS) upon irradiation with white light was used to initiate the oxidative polymerization of dopamine with spatiotemporal control (Figure 1A). These G4 sequences, which act as reaction centers for dopamine, were arranged in designated patterns on the DNA origami surface. The array of reaction centers caused dopamine to polymerize and, due to the adhesiveness of the oligomers, allowed the polymer to be imprinted on top of the G4 pattern. With this approach, we have bridged the fields of DNA

origami technology and photoinitiated polymerization to create precisely templated nanostructures far smaller than the wavelength of light.

The DNA origami platforms—tube I and tube II with one and two rings of reaction centers, respectively—were synthesized from scaffold DNA, staples, and G4-extended staple strands in a one-step process, and their integrity was confirmed by atomic force microscopy (AFM), whereby the moderately bulky structure of the G4 sequences appeared as slight dots and lines on the tubes (Figure S2). Steric hindrance due to the curvature guided the folding process towards tubes that present G4 strands on the outside. These extended

structures were then exploited as anchors for retaining the photosensitizer protoporphyrin IX at distinct locations within the DNA framework. Upon binding to the G-quadruplexes, the fluorescence of PPIX significantly increased, indicating successful host–guest binding (Figure S3).^[15] The specificity of this binding event was demonstrated by comparing the employed G4 sequence to an alternately organized guanine-rich oligonucleotide (Figure S4). To induce the polymerization of dopamine, an oxidative environment was required.^[16] The structure of polydopamine is many-faceted and still under discussion: Apart from covalent bonds, also noncovalent interactions such as hydrogen bonding and π – π stacking, among others, are present (Figure S5).^[16,17] Common protocols, i.e., immersing a substrate in an aqueous alkaline solution of dopamine, suffered from poor control over polymerization kinetics and spatial resolution.^[16] To suppress the spontaneous self-polymerization of dopamine, the pH had to be adjusted to the acidic range.^[18] However, in acidic medium, polymerization is inducible only in the presence of strong oxidants such as ammonium persulfate and sodium periodate.^[19] Levkin and co-workers have shown the first example of a light-triggered dopamine polymerization using UV light to generate reactive oxygen species (ROS) in situ that act as oxidants.^[19] However, the use of UV light in DNA origami can induce cross-linking and promote nonlocalized polymerization.^[20] Therefore, we have developed a photosensitizer-mediated system that can be activated by exposure to visible light.

Protoporphyrin IX is utilized in photodynamic therapy^[21] and we examined its capability to trigger ROS formation, in

particular the generation of singlet oxygen (Figure S6). Singlet oxygen generated by irradiation with visible light reacts with imidazole and bleaches *N,N*-dimethyl-4-nitrosoaniline (RNO) through oxidation, while no reaction occurs in the absence of light.^[22] The decrease in RNO absorbance by approximately 20% proved PPIX to be a moderate photosensitizer with rather slow kinetics, facilitating control over the reaction. Furthermore, to control the polydopamine formation, only a narrow pH range proved to permit both initiating and promoting the polymerization process, with pH 6.5 being the most selective (Figure S7). According to our studies, polydopamine formation occurred independently of any external stimulus in neutral and alkaline media. Under acidic conditions, a pH value of 6 allowed the oxidation of dopamine but prohibited subsequent polymerization steps, whereas at pH 5, all reaction was inhibited. At pH 6.5, polydopamine was formed only in the presence of light and photosensitizer, which was crucial for establishing a controlled polymerization process (Figures S8 and S9).

Upon the light-triggered ROS generation by PPIX and subsequent dopamine oxidation, reaction progress was monitored by recording UV/Vis spectra, tracking the increase of oxidized species (dopaminochrome), precursor oligomers, and polydopamine (Figure 1B).^[13b] Initially, oxidation of dopamine to dopaminochrome and ongoing oligomer formation was observed, followed by the emergence of polymeric components. To further prove that polydopamine formation is an ROS-mediated process, we studied the impact of oxygen and imidazole as a singlet oxygen scavenger on the reaction kinetics. Therefore, the reaction was performed according to

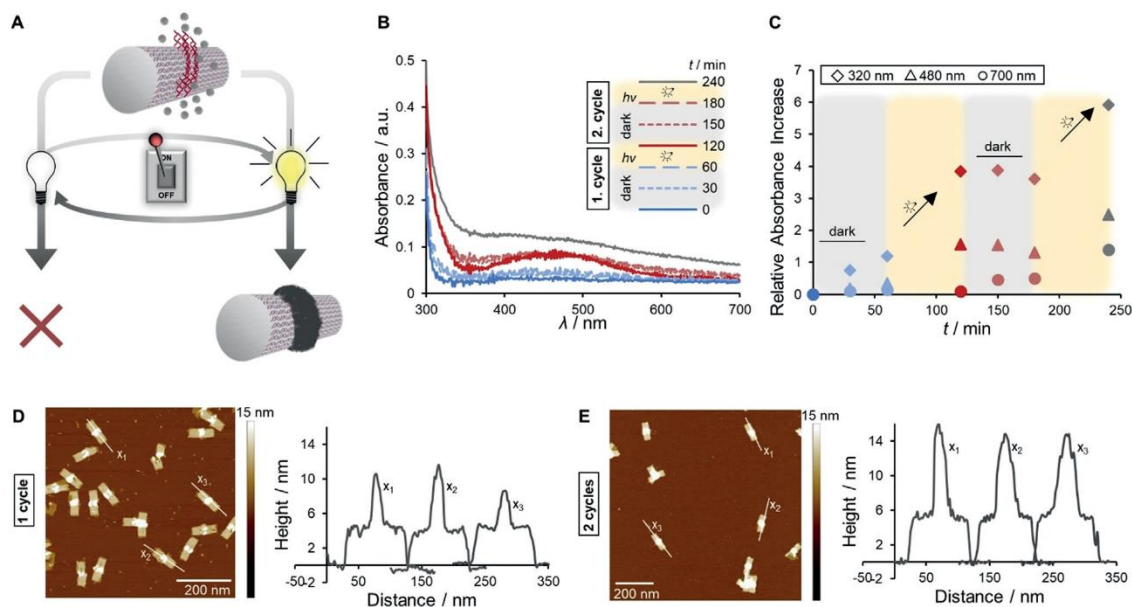


Figure 2. A) Temporal control over the polydopamine formation when the light is switched on and off (1 cycle consists of 1 h dark + 1 h light). B,C) UV/Vis spectroscopy indicates a light-dependent, stepwise polydopamine formation process. D,E) The stepwise polymer growth becomes apparent in AFM topographic images: After 1 cycle, tubes show only a slight increase in height, whereas an approximately 10 nm thick polydopamine layer is present after an additional cycle.

an alternative protocol in which the system is degassed. Both UV/Vis spectroscopy and AFM imaging revealed a suppression of the polymerization when no oxygen was present (Figures S10 and S11). The effect was even stronger in the presence of the scavenger.

As a first indication of successful polymerization, polydopamine-coated structures did not show any migration during agarose gel electrophoresis in contrast to unmodified DNA origami (Figure S12). To directly confirm the presence of the polymer and verify its position, a topographical map of the obtained structures was recorded via AFM measurements (compare Figure S2 and Figure 1D,E). The height profile of both structures exhibited an enhanced peak where G4 sequences were located and reaction was promoted. Thus, the oxidized dopamine species were predominantly generated at the reaction centers and subsequent polymerization preferentially occurred close by, leading to polymer deposition in designated patterns. Due to the intrinsic adhesiveness of the biopolymer, polydopamine-coated areas tend to aggregate and could even form higher-ordered domains (Figure S13). The precise polymer formation with nanometer resolution was further demonstrated by eliminating the DNA template (Figure S14). After treating the mica-deposited sample with hydrochloric acid, the DNA scaffold was degraded through hydrolysis, liberating the polydopamine nanostructures.

In order to achieve not only exact positioning of polydopamine on the DNA platform but also temporal control with light, the reaction mixture containing tube I was alternately exposed to visible light or kept in dark; the absorbance spectra were recorded at distinct time points in order to visualize the polymerization progress (Figure 2A–C). The experiment commenced with a dark period of one hour and the light-dependency of the reaction was revealed: In the absence of light, there was almost no formation of oxidized species and initiation was efficiently suppressed. The dopamine conversion was only triggered after one hour of irradiation, and early intermediates, e.g., dopaminochrome and oligomers, developed. During the ensuing dark period, the absorbance spectra marginally shifted; thus, polymerization was essentially intercepted due to a negligible concentration of radicals. Resuming irradiation caused significantly enhanced overall absorption, indicating that polymerization proceeds. The stepwise progression, as visualized by the relative absorbance increase, substantiates the temporal control through simple switching of the light source on and off (Figure 2C). Furthermore, in addition to qualitative detection, the impact on polymer density and height was investigated via AFM (Figure 2D,E). After one cycle of dark and irradiation phases, there was initial evidence of polydopamine formation. Beside the tubes whose height profile was determined by G4 secondary structures (approximately 3–4 nm in proportion to tube surface), some tubes increased in height due to polydopamine deposition. Extensive polymer coverage occurred upon a successive cycle of dark and irradiation periods, as seen by the dense rings in the center of the tubes, corresponding to an average height increase of up to 10 nm and a total height of 15 nm at these positions (Figure 2E).

DNA origami is emerging as a precise and functional nanomaterial for various biomedical and chemical applications. However, it would be highly desirable to circumvent the intrinsic stability issues and push the limits towards a robust but still versatile nanomaterial in various environments.^[23] Apart from nuclease-mediated digestion, magnesium ions are crucial for DNA origami assembly, but their relatively high concentration (10–20 mM) can interfere with certain applications.^[24] Hence, polydopamine coating was anticipated as a suitable tool to contribute to stability. Repetitive spin filtering was used to transfer bare origami tubes and polydopamine-decorated tube structures from storage buffer into virtually pure water, and these mixtures were incubated for several hours at elevated temperature (Figure 3). Topographical imaging of the nonmodified DNA tubes after treatment revealed a loss of integrity for almost all objects, ranging from small fragments through unfolded segments to intact parts of the original structure. In contrast, tubes bearing a centered

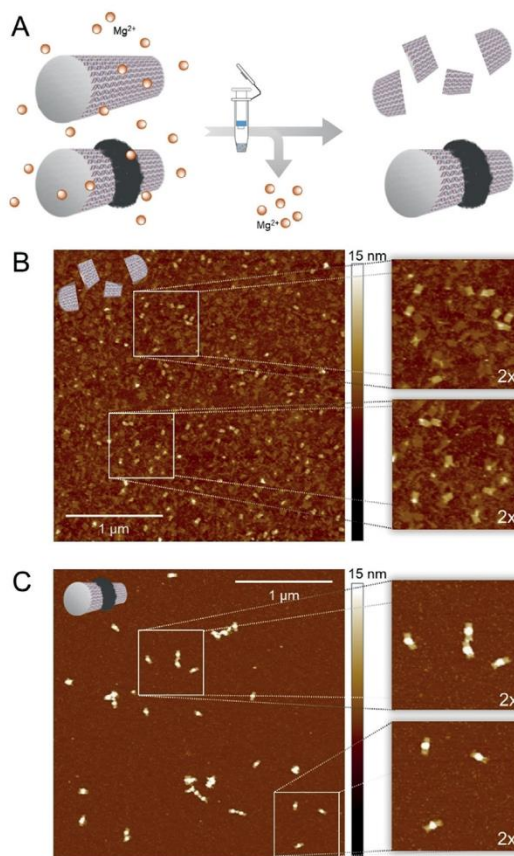


Figure 3. A) Spin-filtering was used to transfer unmodified and polymer-modified origami structures from Mg^{2+} -containing storage buffer into an ion-free environment. Stability assay of unmodified (B) and polydopamine-coated tubes (C) was conducted in pure water at 37°C for 4 h; the structures were subsequently visualized by AFM, showing that polydopamine deposition enhanced the structural integrity.

ring of polydopamine seem to be less susceptible to variations in ionic environment. Apart from clusters of several tubes due to the adhesiveness of polydopamine, individually resolved tubes possess an intact architecture. Hence, when polydopamine is deposited on DNA origami, the structural integrity of DNA is maintained since its inherent susceptibility to lacking ions is reduced.

In conclusion, we have reported the first phototriggered polydopamine polymerization on 3D DNA origami templates to create precise nanostructures. The system benefits from both the unique customization of the DNA origami methodology and the adjustability of utilizing visible light as an external stimulus to achieve unprecedented spatiotemporal control on the nanoscale. Various DNA origami templates were equipped with patterns of G-quadruplex secondary structures, which—along with the embedded photosensitizer protoporphyrin IX—dictated the locally restricted formation of polydopamine. By suppressing the self-polymerization of dopamine at slightly acidic pH and simply switching the light on and off, the characteristics, e.g., density and height of the polymer were tailored. Despite the sophisticated nature of the polydopamine-decorated DNA origami objects, the setup was straightforward, and all materials were biologically derived. The combination of DNA origami technology and polymerizations initiated by visible light allowed the creation of precise photopatterned 3D nanostructures with dimensions far below 100 nm and much smaller than the wavelength of light. Furthermore, the deposition of polydopamine enhanced DNA origami stability, so that it can withstand even pure water conditions, broadening its application scope. Hence, the technique serves as an advanced toolkit for developing DNA-based devices with nanometer resolution, which exhibit customized properties and stability features.

Acknowledgements

T.W. is grateful to the European Union for the ERC Synergy Grant under grant agreement No. 319130 (BioQ). The project was funded by the Deutsche Forschungsgemeinschaft (DFG, German Research Foundation)—Project No. 407426226—TRR 234 CataLight (B01). Open Access charges were covered by the Max Planck Society.

Conflict of interest

The authors declare no conflict of interest.

Keywords: DNA nanotubes · DNA origami · photopolymerization · polydopamine · stability in water

How to cite: *Angew. Chem. Int. Ed.* **2020**, *59*, 6144–6149
Angew. Chem. **2020**, *132*, 6200–6205

- [1] S. Zhang, *Mater. Today* **2003**, *6*, 20–27.
[2] E. C. Wamhoff, J. L. Banal, W. P. Bricker, T. R. Shepherd, M. F. Parsons, R. Veneziano, M. B. Stone, H. Jun, X. Wang, M. Bathe, *Annu. Rev. Biophys.* **2019**, *48*, 395–419.

- [3] a) F. Hong, F. Zhang, Y. Liu, H. Yan, *Chem. Rev.* **2017**, *117*, 12584–12640; b) P. Wang, T. A. Meyer, V. Pan, P. K. Dutta, Y. Ke, *Chem* **2017**, *2*, 359–382; c) T. Tørring, N. V. Voigt, J. Nangreave, H. Yan, K. V. Gothelf, *Chem. Soc. Rev.* **2011**, *40*, 5636–5646.
[4] K. V. Gothelf, *MRS Bull.* **2017**, *42*, 897–903.
[5] a) J. Liu, L. Song, S. Liu, S. Zhao, Q. Jiang, B. Ding, *Angew. Chem. Int. Ed.* **2018**, *57*, 15486–15490; *Angew. Chem.* **2018**, *130*, 15712–15716; b) N. Stephanopoulos, M. Liu, G. J. Tong, Z. Li, Y. Liu, H. Yan, M. B. Francis, *Nano Lett.* **2010**, *10*, 2714–2720; c) J. J. Funke, H. Dietz, *Nat. Nanotechnol.* **2016**, *11*, 47–52.
[6] a) C. Steinhauer, R. Jungmann, T. L. Sobey, F. C. Simmel, P. Tinnefeld, *Angew. Chem. Int. Ed.* **2009**, *48*, 8870–8873; *Angew. Chem.* **2009**, *121*, 9030–9034; b) J. Schnitzbauer, M. T. Strauss, T. Schlichthaerle, F. Schueder, R. Jungmann, *Nat. Protoc.* **2017**, *12*, 1198–1228.
[7] a) E. S. Andersen, M. Dong, M. M. Nielsen, K. Jahn, R. Subramani, W. Mamdouh, M. M. Golas, B. Sander, H. Stark, C. L. Oliveira, J. S. Pedersen, V. Birkedal, F. Besenbacher, K. V. Gothelf, J. Kjems, *Nature* **2009**, *459*, 73–76; b) X. Wei, J. Nangreave, S. Jiang, H. Yan, Y. Liu, *J. Am. Chem. Soc.* **2013**, *135*, 6165–6176.
[8] E. A. Hemmig, C. Creatore, B. Wunsch, L. Hecker, P. Mair, M. A. Parker, S. Emmott, P. Tinnefeld, U. F. Keyser, A. W. Chin, *Nano Lett.* **2016**, *16*, 2369–2374.
[9] a) A. Kuzyk, R. Schreiber, Z. Fan, G. Pardatscher, E. M. Roller, A. Hoge, F. C. Simmel, A. O. Govorov, T. Liedl, *Nature* **2012**, *483*, 311–314; b) W. P. Klein, C. N. Schmidt, B. Rapp, S. Takabayashi, W. B. Knowlton, J. Lee, B. Yurke, W. L. Hughes, E. Graugnard, W. Kuang, *Nano Lett.* **2013**, *13*, 3850–3856; c) C. Rao, Z. G. Wang, N. Li, W. Zhang, X. Xu, B. Ding, *Nanoscale* **2015**, *7*, 9147–9152; d) F. Benn, N. E. C. Haley, A. E. Lucas, E. Silvester, S. Helmi, R. Schreiber, J. Bath, A. J. Turberfield, *Angew. Chem. Int. Ed.* **2018**, *57*, 7687–7690; *Angew. Chem.* **2018**, *130*, 7813–7816; e) T. Zhang, A. Neumann, J. Lindlau, Y. Wu, G. Pramanik, B. Naydenov, F. Jelezko, F. Schuder, S. Huber, M. Huber, F. Stehr, A. Hoge, T. Weil, T. Liedl, *J. Am. Chem. Soc.* **2015**, *137*, 9776–9779.
[10] a) V. Linko, M. Eerikainen, M. A. Kostianen, *Chem. Commun.* **2015**, *51*, 5351–5354; b) Y. Fu, D. Zeng, J. Chao, Y. Jin, Z. Zhang, H. Liu, D. Li, H. Ma, Q. Huang, K. V. Gothelf, C. Fan, *J. Am. Chem. Soc.* **2013**, *135*, 696–702.
[11] W. Hawkes, D. Huang, P. Reynolds, L. Hammond, M. Ward, N. Gadegaard, J. F. Marshall, T. Iskratch, M. Palma, *Faraday Discuss.* **2019**, *219*, 203–219.
[12] a) Y. Tokura, Y. Jiang, A. Welle, M. H. Stenzel, K. M. Krzemien, J. Michaelis, R. Berger, C. Barner-Kowollik, Y. Wu, T. Weil, *Angew. Chem. Int. Ed.* **2016**, *55*, 5692–5697; *Angew. Chem.* **2016**, *128*, 5786–5791; b) Y. Tokura, S. Harvey, X. Xu, C. Chen, S. Morsbach, K. Wunderlich, G. Fytas, Y. Wu, D. Y. W. Ng, T. Weil, *Chem. Commun.* **2018**, *54*, 2808–2811.
[13] a) Z.-G. Wang, Q. Liu, B. Ding, *Chem. Mater.* **2014**, *26*, 3364–3367; b) Y. Tokura, S. Harvey, C. Chen, Y. Wu, D. Y. W. Ng, T. Weil, *Angew. Chem. Int. Ed.* **2018**, *57*, 1587–1591; *Angew. Chem.* **2018**, *130*, 1603–1607.
[14] a) S. Chatani, C. J. Kloxin, C. N. Bowman, *Polym. Chem.* **2014**, *5*, 2187–2201; b) T. Zhang, T. Chen, I. Amin, R. Jordan, *Polym. Chem.* **2014**, *5*, 4790–4796; c) X. Pan, M. A. Tasdelen, J. Laun, T. Junkers, Y. Yagci, K. Matyjaszewski, *Prog. Polym. Sci.* **2016**, *62*, 73–125.
[15] T. Li, E. Wang, S. Dong, *Anal. Chem.* **2010**, *82*, 7576–7580.
[16] H. Lee, S. M. Dellatore, W. M. Miller, P. B. Messersmith, *Science* **2007**, *318*, 426–430.
[17] a) D. R. Dreyer, D. J. Miller, B. D. Freeman, D. R. Paul, C. W. Bielawski, *Langmuir* **2012**, *28*, 6428–6435; b) S. Hong, Y. S. Na, S. Choi, I. T. Song, W. Y. Kim, H. Lee, *Adv. Funct. Mater.* **2012**, *22*, 4711–4717.

- [18] Q. Wei, F. Zhang, J. Li, B. Li, C. Zhao, *Polym. Chem.* **2010**, *1*, 1430–1433.
- [19] X. Du, L. Li, J. Li, C. Yang, N. Frenkel, A. Welle, S. Heissler, A. Nefedov, M. Grunze, P. A. Levkin, *Adv. Mater.* **2014**, *26*, 8029–8033.
- [20] H. Chen, R. Li, S. Li, J. Andreasson, J. H. Choi, *J. Am. Chem. Soc.* **2017**, *139*, 1380–1383.
- [21] J. C. Kennedy, R. H. Pottier, D. C. Pross, *J. Photochem. Photobiol. B* **1990**, *6*, 143–148.
- [22] C. W. Hsieh, C. H. Chu, H. M. Lee, W. Yuan Yang, *Sci. Rep.* **2015**, *5*, 10376.
- [23] H. Bila, E. E. Kurisinkal, M. M. C. Bastings, *Biomater. Sci.* **2019**, *7*, 532–541.
- [24] a) C. Kielar, Y. Xin, B. Shen, M. A. Kostiainen, G. Grundmeier, V. Linko, A. Keller, *Angew. Chem. Int. Ed.* **2018**, *57*, 9470–9474; *Angew. Chem.* **2018**, *130*, 9614–9618; b) V. Linko, B. Shen, K. Tapio, J. J. Toppari, M. A. Kostiainen, S. Tuukkanen, *Sci. Rep.* **2015**, *5*, 15634.

Manuscript received: September 3, 2019

Accepted manuscript online: November 21, 2019

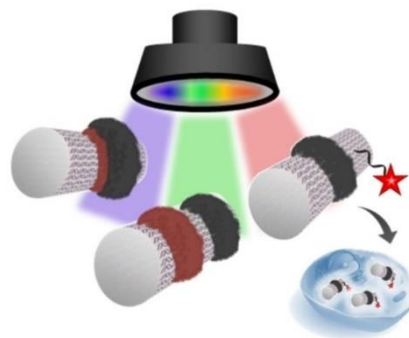
Version of record online: December 27, 2019

3.2 Multiple wavelength photopolymerization of stable poly(catecholamines)-DNA origami nanostructures

Publication: **“Multiple Wavelength Photopolymerization of Stable Poly(Catecholamines)-DNA Origami Nanostructures”**

Pia Winterwerber, Colette J. Whitfield, David Y. W. Ng, Tanja Weil *Angew. Chem. Int. Ed. Engl.* **2021**, 61, e20211122.

The publication in this chapter is an open access article under the terms of the Creative Commons Attribution License (CC BY 4.0).



The generation of multicomponent nanostructures is chemically challenging, and bottom-up routes often build on the self-assembly processes of amphiphilic molecules. Even though assembly can be directed through chemical and physical properties such as the ratio of hydrophilic and hydrophobic parts, control is limited. With the help of DNA nanotechnology, complex polymeric systems are accessible in a highly predictable manner, even on the molecular level, if desired. Building on the knowledge from the previous chapter, the potential from the combination of DNA origami and photopolymerization can be further exploited. Implementing not only one but two photosensitizer of discrete absorption profiles renders the system responsive to different light sources, enabling a stepwise exposure and likewise polymer growth. Together with the expansion of the monomer pool, multicomponent hybrid structures with nanometer resolution can be designed. The advancements originating from polymer decoration of DNA objects become apparent in a biological context where cellular uptake can be fostered.

This chapter is envisioned to highlight the potential of merging DNA origami and multistep photopolymerization for the construction of multicomponent nanostructures. In that respect, eosin y and methylene blue represent photosensitizers that respond to green and red light, respectively. Taking advantage of DNA base pairing, preassembled reaction centers can be introduced to the origami structure to complementary ssDNA overhangs at any time point. This allows distinct patterning of more than one photosensitizer and stepwise polymer growth responding to the applied light source. Norepinephrine is a catecholamine similar to dopamine and could be polymerized likewise through both photosensitizers. Noteworthy, surface roughness of the resulting polymer film is known to be smoother and indeed, poly(norepinephrine) coating induced less aggregation. This is also reflected in biological settings where cellular uptake was most successful for this kind of polymer decoration.

All DNA origami experiments, monitoring and characterization were performed by me. Colette J. Whitfield and David Y. W. Ng conducted cell experiments and analysis. The project was supervised by David Y. W. Ng and Tanja Weil. All authors contributed to writing the manuscript.

Multiple Wavelength Photopolymerization of Stable Poly(Catecholamines)-DNA Origami Nanostructures**

Pia Winterwerber, Colette J. Whitfield, David Y. W. Ng,* and Tanja Weil*

Abstract: The synthesis of multicomponent polymer hybrids with nanometer precision is chemically challenging in the bottom-up synthesis of complex nanostructures. Here, we leverage the fidelity of the DNA origami technique to install a multiple wavelength responsive photopolymerization system with nanometer resolution. By precisely immobilizing various photosensitizers on the origami template, which are only activated at their respective maximum wavelength, we can control sequential polymerization processes. In particular, the triggered photosensitizers generate reactive oxygen species that in turn initiate the polymerization of the catecholamines dopamine and norepinephrine. We imprint polymeric layers at designated positions on DNA origami, which modifies the polyanionic nature of the DNA objects, thus promoting their uptake into living cells while preserving their integrity. Our herein proposed method provides a rapid platform to access complex 3D nanostructures by customizing material and biological interfaces.

Introduction

The spatial control and engineering of objects at nanometer resolution is imperative for the miniaturization of smart materials and devices. In both materials science and biomedicine, the demand for tools to construct multicomponent substructures across 3D space is required to expand the understanding of how surface patterns and object contours modulate interfacial forces. However, the construction of nanostructured surfaces on soft materials that can be freely customized is a bottleneck due to the lack of tools to precisely design them. This problem is further amplified for patterns that are much smaller than the wavelength of light, where top-down approaches, such as lithography, reaches its limits. At this length scale, bottom-up approaches based on self-assembly provide the natural complementarity to top-

down strategies in the fabrication of patterned soft materials.

Unlike the limitations posed by other systems based on synthetic polymers or peptides, DNA nanotechnology is equipped with the precision necessary to program nanostructured surfaces.^[1] Coupled with a DNA origami design,^[2] concepts to investigate epitopes,^[3] protein assemblies,^[4] plasmonic devices,^[5] and biosensing^[6] have recently resulted in critical findings in nanomedicine and biophysics.

In polymer chemistry and patterning, advances in radical and oxidative polymerization as well as the organization of polymer chains have demonstrated that the stringent conditions necessary for DNA origami can be made accessible to largely organic compounds.^[7] Conversely, the combination of DNA nanostructures with charged molecules and polymers has resulted in increased stability under physiological conditions and even in organic solvents, which has been crucial for the rapid expansion of DNA origami platforms in recent years.^[8] However, in comparison to the application-driven counterparts, polymers on DNA origami have yet to show their synthetic potential beyond structured positioning by DNA hybridization on the template.^[9]

In this study, we control a series of photopolymerization reactions using multiple wavelengths to guide independent polymer patterns and fabricate layered structures on the DNA origami (Figure 1). Previously, we have shown that dopamine (DA) can be photopolymerized by protoporphyrin IX (PPIX) that is intercalated into a DNA G-quadruplex (G4), which allows polydopamine to form at designated positions preoccupied by the G4.^[10] Herein, we establish broad wavelength flexibility by using G4s containing eosin Y (EY) and methylene blue (MB), which are activated by green (525 nm) and red (625 nm) light, respectively. Together with blue-light-triggered PPIX (410 nm), these three catalyst centers produce reactive oxygen species (ROS) at their maximum wavelengths to initiate the polymerization of catecholamines. By using both dopamine and norepinephrine (NE), we demonstrate that both monomers can be polymerized sequentially in different configurations, thereby allowing DNA-polymer structures to be customized in the z-direction. The formation of a polymer layer reduces the polyanionic nature of the DNA origami and can thereby facilitate its uptake into living cells, which can be imaged by fluorescence colocalization. Our approach will enable rapid and facile synthesis of multicomponent polymeric patterns with precise shapes and dimensions on DNA origami. Customizing the nano/bio-interphase of DNA objects through surface modulation is crucial for various applications, for example, cellular uptake for therapeutic delivery.

[*] P. Winterwerber, Dr. C. J. Whitfield, Dr. D. Y. W. Ng, Prof. Dr. T. Weil
 Max Planck Institute for Polymer Research
 Ackermannweg 10, 55128 Mainz (Germany)
 E-mail: david.ng@mpip-mainz.mpg.de
 weil@mpip-mainz.mpg.de

[**] A previous version of this manuscript has been deposited on a preprint server (<https://doi.org/10.33774/chemrxiv-2021-dvcpbj>).

© 2021 The Authors. Angewandte Chemie International Edition published by Wiley-VCH GmbH. This is an open access article under the terms of the Creative Commons Attribution License, which permits use, distribution and reproduction in any medium, provided the original work is properly cited.

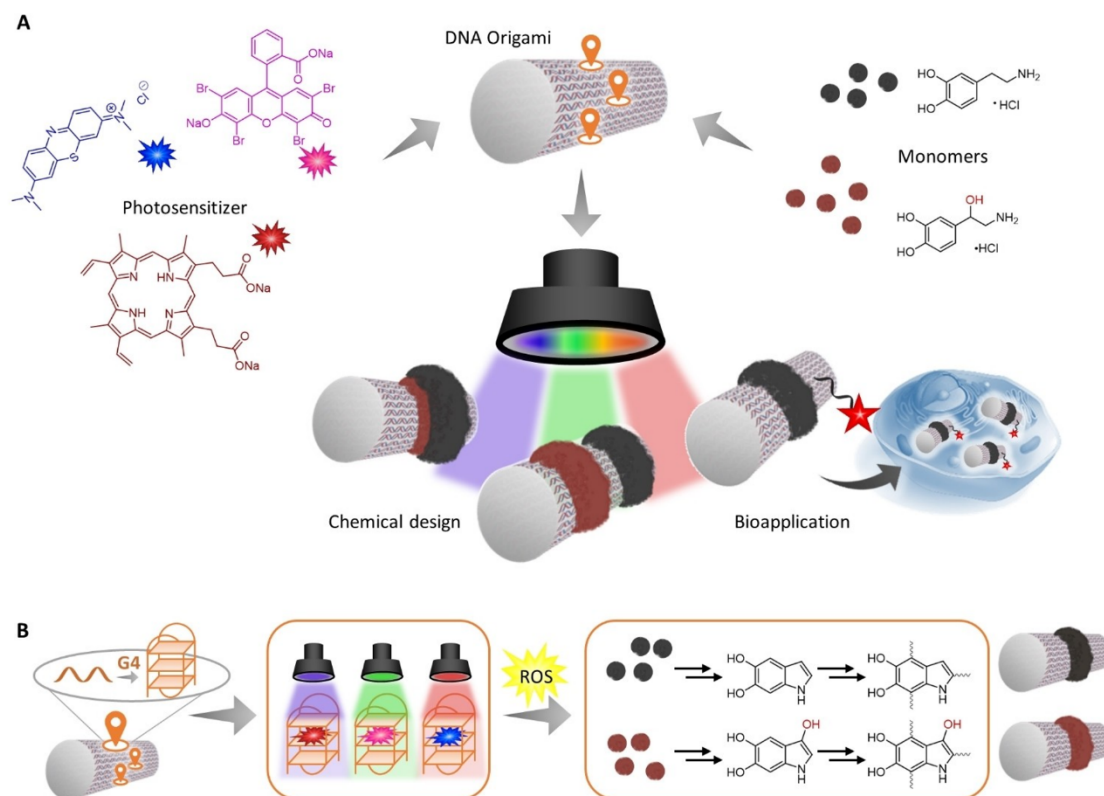


Figure 1. A) Multiple wavelength photopolymerization on DNA origami tubes can be accomplished through the combination of various photosensitizers and two different catecholamine monomers. In this way, polymers can be imprinted at specific sites on the DNA templates under temporal and spatial control. Polymer-DNA hybrid structures can be further leveraged to modulate interactions at the cellular interface. B) The reaction centers, consisting of G-quadruplex (G4) structures and photosensitizers, produce reactive oxygen species (ROS) at their maximum wavelengths to initiate polymerization. The mechanism and structure of both polydopamine^[11] and norepinephrine^[12] are multifaceted and still the object of current elucidation. For reasons of clarity, only a few representative structures are depicted here. Further information on the mechanism, the intermediates, and prevailing interactions is provided in the Supporting Information (Figure S2).

Results and Discussion

To prepare 3D DNA origami tubes for photopolymerization, G-quadruplex structures were arranged on the surface in distinct patterns. These catalytic centers can be tuned for wavelength selectivity by nominating the photosensitizer that will sit within the G-quadruplex (5'-GGG TA GGG C GGG TT GGG-3'). As previously reported, the PPIX-G4 complex produces ROS under irradiation with white light, which in turn trigger the oxidation and polymerization of dopamine. To suppress the well-known self-polymerization of dopamine and to control polymer formation, it is crucial to work in a slightly acidic environment (pH 6.5). Herein, we found that only blue light (410 nm) possesses sufficient energy to initiate the polymerization of dopamine (see Figure S1 in the Supporting Information). Excitation at the Q-bands of PPIX-G4 in the visible spectrum produced insufficient oxidized dopamine species to fuel polymerization. Wavelength specificity in the green and red region was

accomplished by hosting EY^[13] and MB^[14] respectively, within the G4 motif. The propensity of each catalyst to generate singlet oxygen ($^1\text{O}_2$) was analyzed using an assay based on imidazole and *p*-nitrosodimethylaniline (RNO).^[15] Both MB and EY demonstrated higher efficiencies than PPIX in the production of $^1\text{O}_2$, as reflected by the bleaching of RNO being 7 and 11 times faster, respectively (see Figure S3 in the Supporting Information). The initiation of polymerization using EY-G4 and MB-G4 on a tube DNA origami was subsequently attempted at their respective wavelengths (EY: 525 nm, MB: 625 nm). The tube DNA origami scaffold was designed with a central ring containing photosensitizer-loaded G4 sequences. When using 10 mM dopamine in 100 mM buffer (pH 6.5), UV/Vis spectroscopy showed successful polymerization into polydopamine (pDA) after 3 h (see Figure S4A in the Supporting Information). The formation of intermediates including dopaminochrome (320 nm), oxidized oligomers (480 nm), and the eventual pDA (700 nm) could be monitored through their character-

istic absorbances.^[7c] Spatial control over polymerization and the resulting nanostructure were verified by atomic force microscopy (AFM; see Figure S4B in the Supporting Information). A ring of polymers was successfully constructed where the patterned G4 sequences were installed, thus demonstrating that the change of catalytic centers and excitation wavelengths did not affect the control over the polymerization reaction. In comparison, the reaction kinetics of the oxidative polymerization demonstrated that the generation of each intermediate (dopaminochrome, oligomers etc.) including pDA was more efficient for EY (see Figure S4C in the Supporting Information). Despite the differences in kinetics, topological height profile analysis by AFM did not show significant height differences between the different photosensitizers (see Figure S4D in the Supporting Information).

We subsequently investigated different patterns and the impact of the size of clustered G4 centers on the polymerization process. Firstly, we designed an origami tube with a diagonal G4 motif of similar density to the standard ring pattern (see Figure S5 in the Supporting Information). After polymerization, we could detect formation of pDA on the tubes, with varying observation perspective of the designated pattern. The lack of symmetry would mean that the orientation of the origami on the mica surface is subjected to inherent randomness and thus affects the imaging process. Hence, we consider ring patterns as the most reliable to provide robust characterization. In addition, we examined the correlation of polymer formation and the width of the ring system by direct comparison of the structures depicted in Figure 2. AFM images indicate that, when only 22 catalytic centers are incorporated, the oxidative conditions are not sufficient to induce polymerization on each tube. In addition, the thickness of the observable polymer rings is lower compared to the standard origami tube (44 G4). Here, total heights of typically 10–15 nm are attained. When doubling the number of G4 to 88, polymer rings are uniformly grown on almost every origami and the overall heights are similar to the standard 44 G4s. Our findings suggest that there is indeed a minimal number of clustered catalytic centers required to induce polymerization. Regarding the activity of these centers, no upper limit seems to restrict the system. However, full coverage of the tube's surface with G4 sequences would on the one hand restrict further modifications and on the other hand may harm the origami's integrity due to higher tensions in the rolling up process of the tube.

Throughout the experiments it was noted that the polymer-ringed DNA origami tubes tend to aggregate due to the strong adhesiveness of pDA (see Figure S6 in the Supporting Information). Therefore, norepinephrine was introduced as a dopamine analogue to achieve well-dispersible nanoobjects that also remain stable in complex media without aggregate formation. Norepinephrine also belongs to the catecholamine family and poly(norepinephrine) (pNE) reveals material-independent modification capabilities similar to pDA but with an ultrasoft surface morphology.^[12c,16] Chemically, NE possesses an additional hydroxy group and this increase in hydrophilic interactions

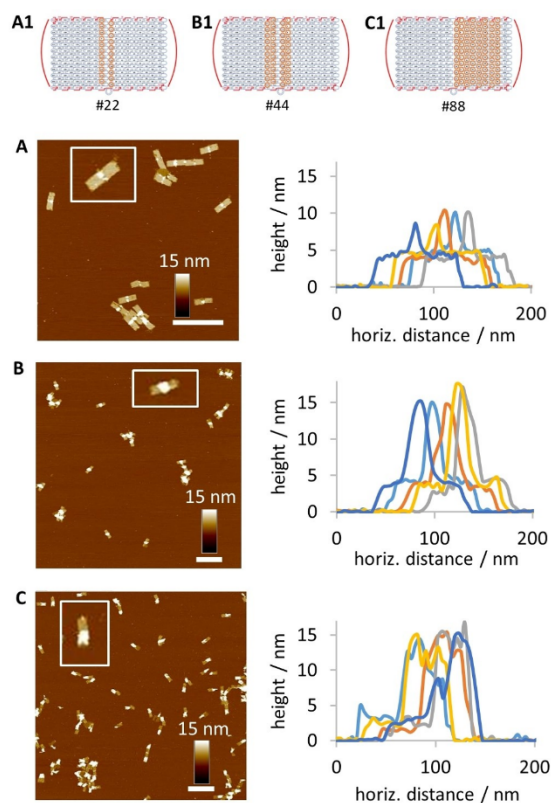


Figure 2. Studies on the correlation of polymer formation and the number of catalytic G4 centers. (A1–C1) DNA origami tubes were designed bearing a ring of 22, 44, or 88 G4 sequences, respectively. Tubes are rolled up by annealing the folding strands (depicted in red). A–C) AFM topographical images of the pDA-ringed origami tubes reveal that a minimal number of 44 catalytic centers is required to reliably induce polymerization.

could potentially prevent aggregation of the formed nanostructures. In contrast to pDA, polymerization to pNE using all three photosensitizers showed a strong preference toward EY and MB (see Figure S7 in the Supporting Information). Observations from UV/Vis spectroscopic analysis suggested that the oxidation of pNE requires a higher performance photosensitizer to fuel the polymerization reaction. Likewise, the eventual formation of pNE on the DNA origami showed that the polymerization was more efficient with EY and MB as the photosensitizer. In dynamic light scattering (DLS) studies, the formation of a pNE ring caused a clear shift of the intensity-based size distribution towards higher hydrodynamic diameters, which can also be seen in the *z*-average values (Figure 3). Moreover, both bare origami and pNE-ringed origami are stable for at least three days and do not show agglomeration (see Figure S8 in the Supporting Information).

Additionally, agarose gel electrophoresis (AGE) supplements the characterization of the origami tubes before and

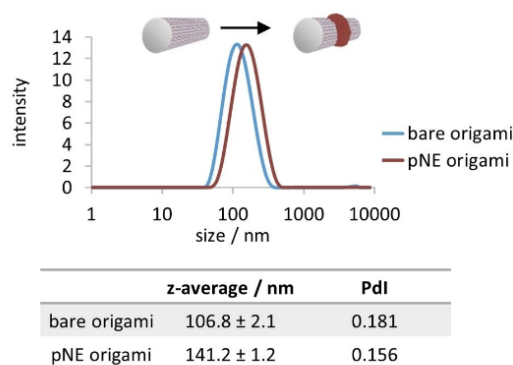


Figure 3. DLS characterization of bare origami tubes and pNE-ringed origami tubes. Polymer growth on the origami causes a significant shift in the intensity-weighted size distribution and z-average values. The numbers should only be considered as a qualitative indication, since DLS operates on the principles of spherical objects, which does not apply that well for these origami structures.

after polymerization of the pDA and pNE polymers (see Figure S9 in the Supporting Information).

Based on the acquired reaction conditions and wavelength selectivities pertaining to DA and NE, sequential polymerization steps were performed to fabricate multi-component nanostructures. The DNA origami tubes were loaded with MB-G4s, and NE and DA were sequentially polymerized at 625 nm for 2 h each (Figure 4A). Successful polymerization was detected for both illumination phases, giving the characteristic profiles for pNE and pDA (see Figure S10 in the Supporting Information). The first irradiation phase resulted in the formation of a pNE layer of $5.2 \text{ nm} \pm 1.5 \text{ nm}$ (Figure 4B). Thereafter, excess NE and oxidized side products were removed by spin filtration and replaced by DA. The second irradiation phase yielded the pDA layer that contributed an additional height increase of $4.3 \text{ nm} \pm 1.8 \text{ nm}$ (total height: $9.5 \text{ nm} \pm 1.8 \text{ nm}$; Figure 4B). The contributed height increase of each component correlates well to their individual single polymerizations. To demonstrate that the second irradiation phase had initiated the polymerization of DA and not the existing pNE (or its adsorbed oligomers), a control experiment was performed without the addition of DA. In this case, no additional polymers were formed (see Figure S11 in the Supporting Information). The upper limit of the layered components is dictated by the access of monomers to the catalytic centers. At a total height of approximately 10–15 nm, the polymer-

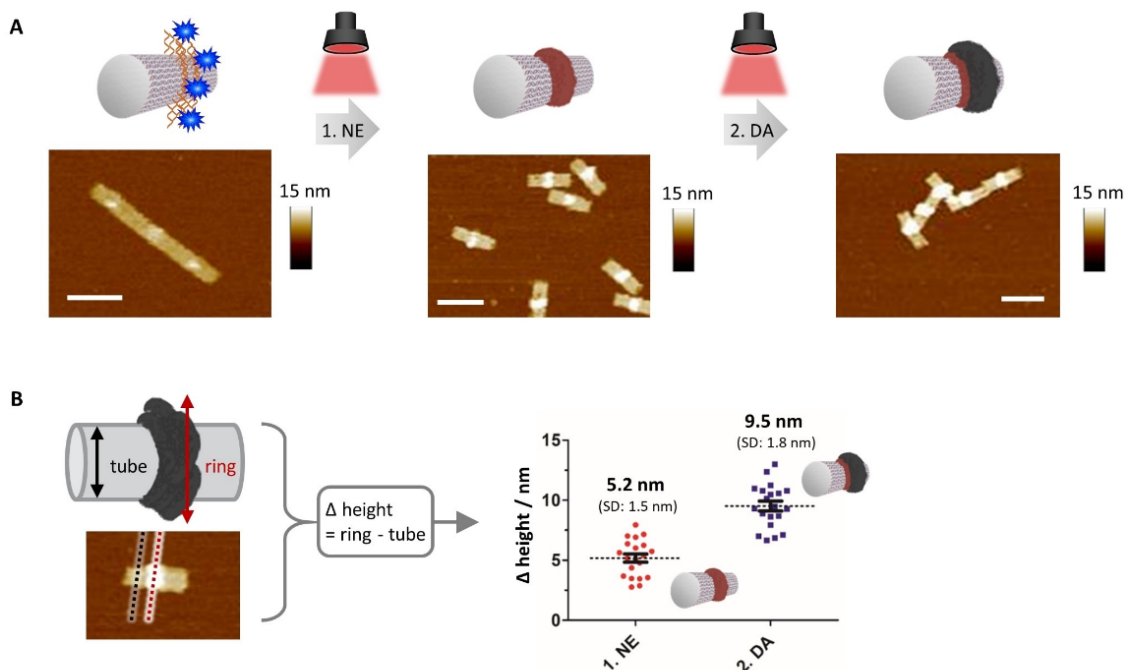


Figure 4. A two-step polymerization process demonstrates the potential of the origami system to induce a layer-by-layer formation of polymers. A) DNA origami tubes are incubated with methylene blue as the photosensitizer and irradiated at 625 nm. In the first illumination phase, norepinephrine (NE) is polymerized, followed by a purification step to remove remaining NE, and dopamine (DA) is added as the second monomer that also polymerizes under irradiation with red light. AFM images show the topographical profile of the DNA origami tubes. The polymer is imprinted on top of the G4 patterns. Scale bars are 100 nm. B) To quantify the thickness of the polymer layers, z-value heights were recorded and calculated as depicted ($n=20$; error bars are SEM).

ization can no longer be guided by the photosensitizer-G4 complex.

Next, we demonstrated wavelength orthogonality for a two-step polymerization to achieve reaction selectivity. The dormancy of MB and EY at opposing wavelengths was first investigated. MB showed no generation of the oxidized species of DA when irradiated at 525 nm, and, likewise, EY was not active at 625 nm (see Figure S12 in the Supporting Information). To ensure that a consecutive activation of each photosensitizer can continuously trigger the polymerization of dopamine, the DNA origami tubes were loaded with ring patterns of EY-G4 and MB-G4 at each tubular end. Polymerization was initiated with DA (10 mM, pH 6.5)

by sequential irradiation at 625 nm and 525 nm for 3 h each. The generation of oxidized intermediates and pDA was verified by UV/Vis spectroscopy (see Figure S13A in the Supporting Information). Control experiments illustrated that the integrity of the DNA origami tube was not damaged by the prolonged irradiation and by the ROS produced by the photosensitizers (see Figure S13B in the Supporting Information).

Subsequently, to broaden the approach, we decoupled the loading of both EY and MB photosensitizers into sequential steps to show that DNA hybridization in a post-polymerization fashion is robust and reliable (Figure 5). The first step involved the attachment of MB onto a DNA

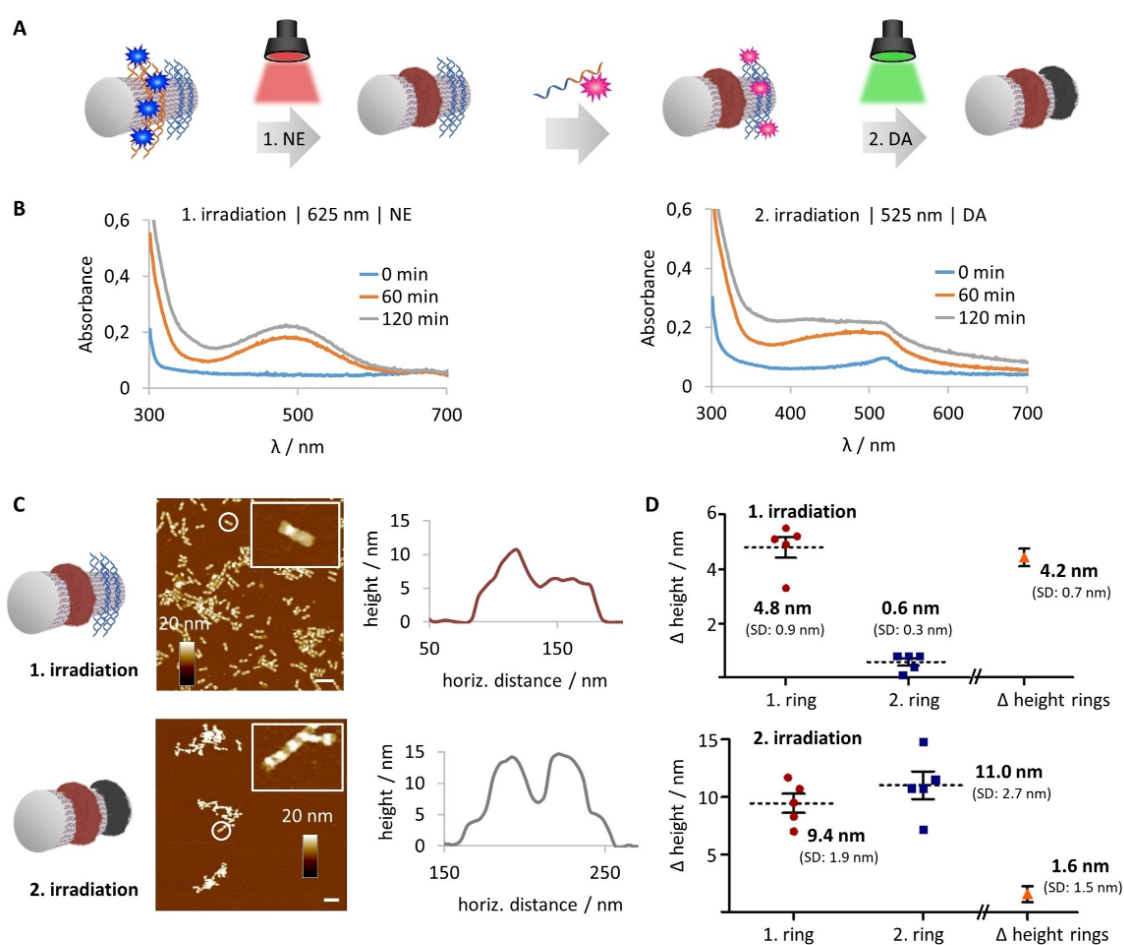


Figure 5. In an advanced two-step polymerization approach, DNA origami tubes were equipped with two different photosensitizers and incubated with two different monomers, which induced polymer formation at distinct rings at different wavelengths. A) DNA origami tubes were endowed with one ring of G4-sequences (orange) and one ring of sticky sequences (blue). MB was loaded onto the G4 sequences, NE was added and incubated at 625 nm. After the first irradiation phase, NE was removed by spin filtration. EY-G4 was annealed on the origami tube, and pDA formation was triggered at 525 nm. B) UV/Vis spectra give the characteristic profiles for pNE and pDA formation, respectively. C) AFM imaging of origami tubes after each step was performed to track and compare the formation of the first and the second polymer ring. Scale bars are 200 nm. Representative height profiles of one ring and two ring structures are depicted. D) Histograms show that only one polymer ring is formed in the first step, whereas a second ring is grown in the second step. Both rings have similar heights ($n=5$; error bars are SEM).

origami tube equipped with a single ring of G4 sequences. Irradiation at 625 nm for 2 h with NE (10 mM, pH 6.5) formed the first polymer ring, which could be visualized by AFM and UV/Vis spectroscopy (Figure 5B,C). Excess NE was removed by spin filtration and the second photosensitizer, EY-G4, was hybridized onto an opposing ring pattern of the same DNA tube using a temperature ramp. The second polymerization step was conducted at 525 nm for 2 h with DA (10 mM, pH 6.5) as the monomer to afford the final nanostructure where pNE and pDA each occupies a single ring. The oxidation profiles of both NE and DA in this dual component system showed consistent polymerization kinetics when compared to the single component system. Furthermore, by comparing the average polymer heights of each irradiation period, sequential ring formation can be tracked (Figure 5D). In the first step, only one position on the origami tube showed polymer formation (4.8 ± 0.9 nm), which is also clearly depicted in the height difference of this polymer ring and the adjacent ring pattern (Δ of 4.2 ± 0.7 nm). In the second step, a second polymer ring was grown at the designated position with a thickness reaching dimensions of the previously grown ring. Interestingly, both polymers exhibit similar heights (Δ of 1.6 ± 1.5 nm).

It is important to note that the existing ring functions as an additional nucleating center, such that activated species from the adjacent ring can diffuse to it, thus resulting in a corresponding increase in height during the activation of the second ring. The presence of all reactive components, namely, monomers, patterned photosensitizers on the DNA origami, and the light source, is essential for the formation of the nanostructure. Control experiments involving only monomer without irradiation, or without embedded photosensitizer did not show polymerization (see Figure S14 in the Supporting Information). In both the coupled and decoupled methods, we demonstrate that sophisticated and multicomponent 3D DNA-polymer hybrids can be accessed easily.

Additionally, the formation of these polymer patterns can be used as a tool to customize the surface chemistry of the DNA origami. Fundamentally, DNA origami structures are highly anionic due to the polyphosphate backbone and thus require divalent cations for stabilization.^[17] Under physiological conditions, DNA origami is prone to degradation through nucleases and the lower concentration of divalent cations in biological fluids.^[18] Furthermore, the DNA superstructure itself also has a major impact on the stability of the objects under these conditions.^[19] 3D assemblies, for example, significantly slow down the nuclease digestion rate when compared to 2D counterparts.^[20]

We therefore subjected our DNA structures, bare and polymer-ringed origami, to cell medium conditions that are encountered when performing cell-uptake studies. Comparatively, naked DNA structures exhibit a higher level of fragmentation than pNE-origami when incubated at 37 °C for 24 h in cell medium (see Figure S15 in the Supporting Information).

Besides stability under physiological conditions, the polyanionic character of DNA prevents its cellular uptake

due to repulsive forces towards the negatively charged cellular membrane. Existing strategies to address this challenge include the attachment of targeting functions (i.e. peptides, proteins, and aptamers) that promote receptor-mediated endocytosis.^[21] In contrast, we hypothesized that the coverage provided by the polymer patterns would reduce the effective charge repulsion and thereby improve transport across the cellular membrane. The respective ring-patterned DNA origami nanostructures with either pNE or pDA were synthesized and annealed with Alexa-647[®] oligonucleotide (see Figure S16 in the Supporting Information). At 10 nM, an efficient cellular uptake into A549 lung adenocarcinoma cells by pNE-origami was observed by confocal laser scanning microscopy after 24 h incubation (see Figure S17 in the Supporting Information). However, significant aggregation was detected for pDA-origami due to the well-known adhesiveness of pDA. In agreement with the literature, Alexa-647[®]-labeled DNA origami alone do not show uptake into cells and neither does the Alexa-647[®] oligonucleotide. To further characterize the stability of the internalized origami samples, another fluorophore, Alexa-488[®], was annealed onto the opposite end of the tube to facilitate co-localization studies (see scheme in Figure 6A). The dual-labeled origami was characterized by AGE followed by gel excision (see Figure S19 in the Supporting Information). By overlaying both channels, colocalization of the two fluorophores indicated that a major proportion of the pNE-origami structures remain intact upon internalization (see Figure S18 in the Supporting Information). Similarly, controls with bare origami showed no cellular uptake, while the aggregation behavior of pDA-origami was apparent. Even though the fluorescence colocalization of pNE-origami samples was positive and the controls excluded the possibility that fragmented components were being taken up, it has to be verified that material is indeed inside the cells. Several reports have shown that the detected fluorescent signal might come from surface-attached or degraded material only.^[21c, 22] We therefore treated origami-incubated cells with DNase I to digest cell membrane artefacts. In the case of pDA-origami, the aggregates were removed with DNase I treatment, thus confirming that the fluorescence signals were largely from membrane-bound material (Figure 6B, see also Figures S18, S20 in the Supporting Information). In the case of pNE-origami, although an observable reduction in fluorescence intensity was also observed,^[21c] z-stack analysis demonstrated that the pNE-origami were successfully internalized (Figure 6B,C). The experiment demonstrated that the adhesive forces of pDA were dominant and that the aggregation behavior prevented the uptake of the conjugates into cells. The collective observations indicate that the existence of the pNE layer mediates the repulsive interactions of DNA origami and facilitated uptake into cells. Through these cell experiments, we demonstrate that polymer patterns on DNA origami could be leveraged to alter and modulate interactions at the cellular interface and to enable the uptake of DNA objects.

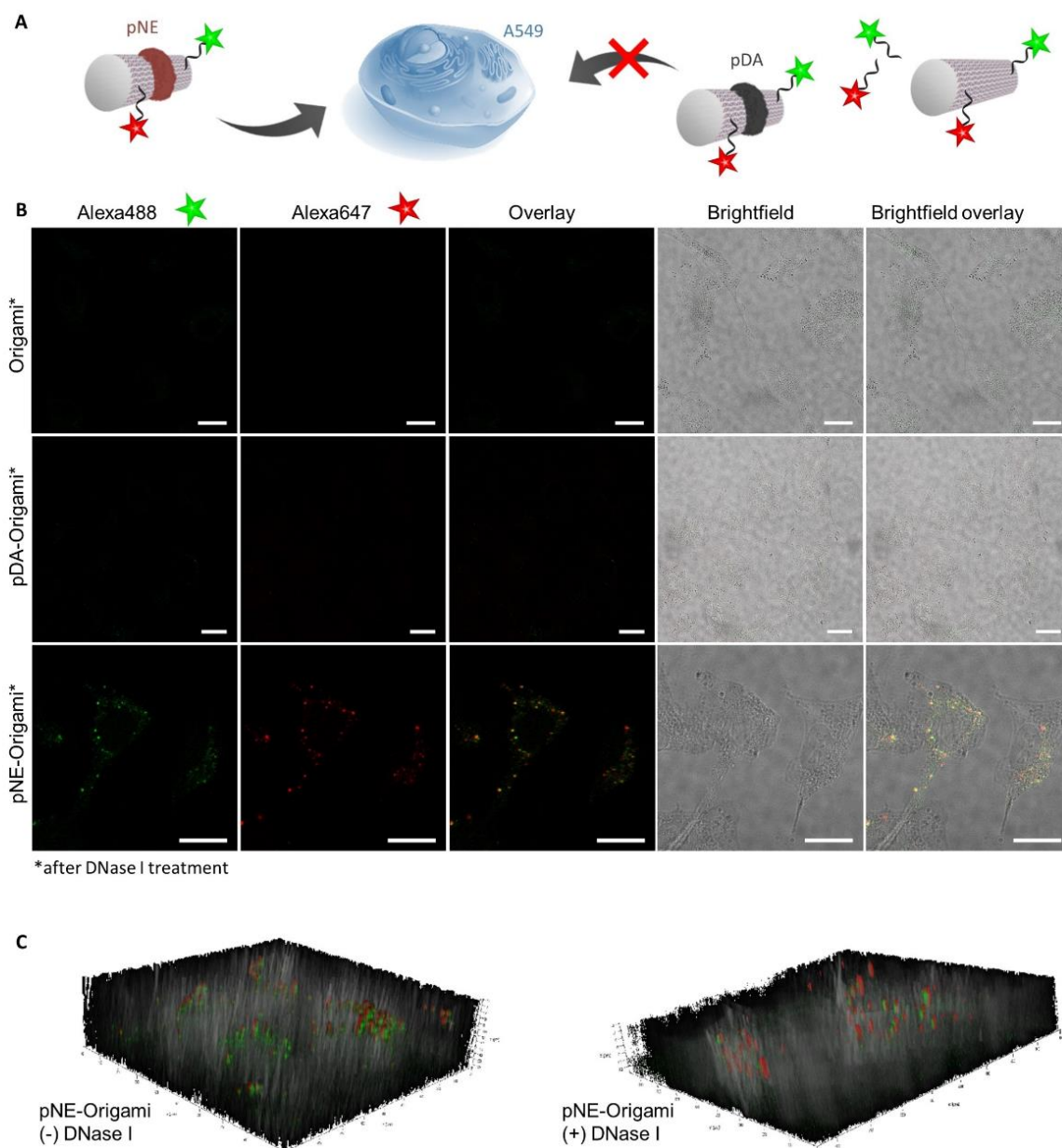


Figure 6. Cellular colocalization of origami nanostructures. A) Schematic representation of the Alexa488- and Alexa647-modification of bare DNA origami tubes as well as pNE- and pDA- ringed tubes. B) Confocal laser scanning micrographs of A549 cells incubated with Alexa488 and Alexa647 double-labeled DNA origami samples for 24 h, recorded after DNase I treatment. Scale bars are 20 μm . C) Z-stacks of pNE-origami incubated cells without and with DNase I treatment prior to imaging. Control images for buffer only and Alexa-oligonucleotides are shown in the Supporting Information (see Figure S18A).

Conclusion

In summary, we have explored the patterned and layered growth of different polymers (pNE and pDA) on DNA origami using multiple wavelengths of light. The concept is

facilitated by manipulating the interaction of G4s with different photosensitizers (PPIX, EY, and MB) such that their position on the DNA origami can be precisely located. As a consequence, the activity of each photocatalyst can be switched from active to dormant states, and vice versa.

Moreover, the fabrication method is flexible so that the sequence of the photopolymerization reaction and/or annealing steps can be changed easily without affecting their efficiencies. The extent of polymer formation can be tracked easily by UV/Vis spectroscopy and AFM imaging, which facilitates structural customization in the z-direction. Furthermore, the polymer patterns altered the intrinsic polyanionic character of the DNA origami while preserving their integrity. By modulating the repulsive forces against the cellular membrane, these hybrid objects could be used for biological applications. In combination, this platform has provided a valuable tool to construct complex polymer-origami architectures that enable the study of customized surface patterns in nanoscience and biomedicine.

Acknowledgements

We acknowledge the financial support by the Deutsche Forschungsgemeinschaft (DFG, German Research Foundation)—Project No. 40742622—TRR 234 CatalLight (B01) and the Max Planck-Bristol Centre for Minimal Biology. Open Access funding enabled and organized by Projekt DEAL.

Conflict of Interest

The authors declare no conflict of interest.

Keywords: Cell Uptake · DNA Origami · Multiwavelength · Photopolymerization · Poly(Catecholamines)

- [1] a) N. C. Seeman, H. F. Sleiman, *Nat. Rev. Mater.* **2018**, *3*, 17068; b) N. C. Seeman, *J. Theor. Biol.* **1982**, *99*, 237–247.
- [2] P. W. Rothemund, *Nature* **2006**, *440*, 297–302.
- [3] a) P. Zhang, X. Liu, P. Liu, F. Wang, H. Ariyama, T. Ando, J. Lin, L. Wang, J. Hu, B. Li, C. Fan, *Nat. Commun.* **2020**, *11*, 3114; b) J. Hellmeier, R. Platzer, A. S. Eklund, T. Schlichthaerle, A. Karner, V. Motsch, M. C. Schneider, E. Kurz, V. Bamich, M. Brameshuber, J. Preiner, R. Jungmann, H. Stockinger, G. J. Schutz, J. B. Huppa, E. Sevcsik, *Proc. Natl. Acad. Sci. USA* **2021**, *118*, e2016857118.
- [4] a) G. Grossi, M. Dalgaard Ebbesen Jepsen, J. Kjems, E. S. Andersen, *Nat. Commun.* **2017**, *8*, 992; b) W. P. Klein, R. P. Thomsen, K. B. Turner, S. A. Walper, J. Vranish, J. Kjems, M. G. Ancona, I. L. Medintz, *ACS Nano* **2019**, *13*, 13677–13689; c) E. Weinhold, B. Chakraborty, *Nanoscale* **2021**, *13*, 2465–2471.
- [5] a) J. Ryssy, A. K. Natarajan, J. Wang, A. J. Lehtonen, M. K. Nguyen, R. Klajn, A. Kuzyk, *Angew. Chem. Int. Ed.* **2021**, *60*, 5859–5863; *Angew. Chem.* **2021**, *133*, 5923–5927; b) L. Nguyen, M. Dass, M. F. Ober, L. V. Besteiro, Z. M. Wang, B. Nickel, A. O. Govorov, T. Liedl, A. Heuer-Jungemann, *ACS Nano* **2020**, *14*, 7454–7461.
- [6] a) E. Silvester, B. Vollmer, V. Prazak, D. Vasishtan, E. A. Machala, C. Whittle, S. Black, J. Bath, A. J. Turberfield, K. Grunewald, L. A. Baker, *Cell* **2021**, *184*, 1110–1121; b) J. Huang, A. Suma, M. Cui, G. Grundmeier, V. Carnevale, Y. Zhang, C. Kielar, A. Keller, *Small Structures* **2020**, *1*, 2000038.
- [7] a) Z.-G. Wang, Q. Liu, B. Ding, *Chem. Mater.* **2014**, *26*, 3364–3367; b) Y. Tokura, Y. Jiang, A. Welle, M. H. Stenzel, K. M. Krzemien, J. Michaelis, R. Berger, C. Barner-Kowollik, Y. Wu, T. Weil, *Angew. Chem. Int. Ed.* **2016**, *55*, 5692–5697; *Angew. Chem.* **2016**, *128*, 5786–5791; c) Y. Tokura, S. Harvey, C. Chen, Y. Wu, D. Y. W. Ng, T. Weil, *Angew. Chem. Int. Ed.* **2018**, *57*, 1587–1591; *Angew. Chem.* **2018**, *130*, 1603–1607; d) J. B. Knudsen, L. Liu, A. L. Bank Kodal, M. Madsen, Q. Li, J. Song, J. B. Woehrstein, S. F. Wickham, M. T. Strauss, F. Schueder, J. Vinther, A. Krissanaprasit, D. Gudnason, A. A. Smith, R. Ogaki, A. N. Zelikin, F. Besenbacher, V. Birkedal, P. Yin, W. M. Shih, R. Jungmann, M. Dong, K. V. Gothelf, *Nat. Nanotechnol.* **2015**, *10*, 892–898; e) A. Krissanaprasit, M. Madsen, J. B. Knudsen, D. Gudnason, W. Surareungchai, V. Birkedal, K. V. Gothelf, *ACS Nano* **2016**, *10*, 2243–2250.
- [8] a) P. Chidchob, T. G. Edwardson, C. J. Serpell, H. F. Sleiman, *J. Am. Chem. Soc.* **2016**, *138*, 4416–4425; b) A. Lacroix, T. G. W. Edwardson, M. A. Hancock, M. D. Dore, H. F. Sleiman, *J. Am. Chem. Soc.* **2017**, *139*, 7355–7362; c) Y. Dong, Y. R. Yang, Y. Zhang, D. Wang, X. Wei, S. Banerjee, Y. Liu, Z. Yang, H. Yan, D. Liu, *Angew. Chem. Int. Ed.* **2017**, *56*, 1586–1589; *Angew. Chem.* **2017**, *129*, 1608–1611; d) J. A. Fan, Y. He, K. Bao, C. Wu, J. Bao, N. B. Schade, V. N. Manoharan, G. Shvets, P. Nordlander, D. R. Liu, F. Capasso, *Nano Lett.* **2011**, *11*, 4859–4864; e) L. Song, Q. Jiang, J. Liu, N. Li, Q. Liu, L. Dai, Y. Gao, W. Liu, D. Liu, B. Ding, *Nanoscale* **2017**, *9*, 7750–7754; f) W. Chen, J. Y. Gerasimov, P. Zhao, K. Liu, A. Herrmann, *J. Am. Chem. Soc.* **2015**, *137*, 12884–12889; g) G. Chakraborty, K. Balinin, G. Portale, M. Loznik, E. Polushkin, T. Weil, A. Herrmann, *Chem. Sci.* **2019**, *10*, 10097–10105; h) H. Li, J. Fan, E. M. Buhl, S. Huo, M. Loznik, R. Gostl, A. Herrmann, *Nanoscale* **2020**, *12*, 21299–21305; i) Y. Yang, Q. Lu, C. M. Huang, H. Qian, Y. Zhang, S. Deshpande, G. Arya, Y. Ke, S. Zauscher, *Angew. Chem. Int. Ed.* **2021**, *60*, 23241–23247; *Angew. Chem.* **2021**, *133*, 23429–23435.
- [9] a) P. Wang, J. H. Huh, H. Park, D. Yang, Y. Zhang, Y. Zhang, J. Lee, S. Lee, Y. Ke, *Nano Lett.* **2020**, *20*, 8926–8932; b) K. Zhou, Y. Zhou, V. Pan, Q. Wang, Y. Ke, *J. Am. Chem. Soc.* **2020**, *142*, 5929–5932.
- [10] P. Winterwerber, S. Harvey, D. Y. W. Ng, T. Weil, *Angew. Chem. Int. Ed.* **2020**, *59*, 6144–6149; *Angew. Chem.* **2020**, *132*, 6200–6205.
- [11] a) S. Hong, Y. S. Na, S. Choi, I. T. Song, W. Y. Kim, H. Lee, *Adv. Funct. Mater.* **2012**, *22*, 4711–4717; b) D. R. Dreyer, D. J. Miller, B. D. Freeman, D. R. Paul, C. W. Bielawski, *Langmuir* **2012**, *28*, 6428–6435; c) H. Lee, S. M. Dellatore, W. M. Miller, P. B. Messersmith, *Science* **2007**, *318*, 426–430.
- [12] a) P. Manini, A. Pezzella, L. Panzella, A. Napolitano, M. d'Ischia, *Tetrahedron* **2005**, *61*, 4075–4080; b) P. Manini, L. Panzella, A. Napolitano, M. d'Ischia, *Chem. Res. Toxicol.* **2007**, *20*, 1549–1555; c) S. Hong, J. Kim, Y. S. Na, J. Park, S. Kim, K. Singha, G. I. Im, D. K. Han, W. J. Kim, H. Lee, *Angew. Chem. Int. Ed.* **2013**, *52*, 9187–9191; *Angew. Chem.* **2013**, *125*, 9357–9361; d) X. Tan, P. Gao, Y. Li, P. Qi, J. Liu, R. Shen, L. Wang, N. Huang, K. Xiong, W. Tian, Q. Tu, *Bioact. Mater.* **2021**, *6*, 285–296.
- [13] a) F. Amat-Guerri, M. M. C. López-González, R. Martínez-Utrilla, R. Sastre, *J. Photochem. Photobiol. A* **1990**, *53*, 199–210; b) D. P. Hari, B. König, *Chem. Commun.* **2014**, *50*, 6688–6699; c) V. Srivastava, P. P. Singh, *RSC Adv.* **2017**, *7*, 31377–31392.
- [14] a) J. P. Tardivo, A. Del Giglio, C. S. de Oliveira, D. S. Gabrielli, H. C. Junqueira, D. B. Tada, D. Severino, R. de Fátima Turchiello, M. S. Baptista, *Photodiagn. Photodyn. Ther.* **2005**, *2*, 175–191; b) P. T. Wu, C. L. Lin, C. W. Lin, N. C. Chang, W. B. Tsai, J. Yu, *Nanomaterials* **2019**, *9*, 14.

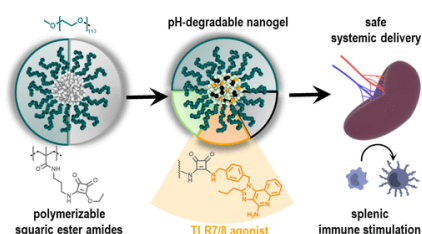
- [15] I. Kraljić, S. E. Mohsni, *Photochem. Photobiol.* **1978**, *28*, 577–581.
- [16] a) S. M. Kang, J. Rho, I. S. Choi, P. B. Messersmith, H. Lee, *J. Am. Chem. Soc.* **2009**, *131*, 13224–13225; b) H. A. Lee, Y. Ma, F. Zhou, S. Hong, H. Lee, *Acc. Chem. Res.* **2019**, *52*, 704–713.
- [17] a) C. Kielar, Y. Xin, B. Shen, M. A. Kostianin, G. Grundmeier, V. Linko, A. Keller, *Angew. Chem. Int. Ed.* **2018**, *57*, 9470–9474; *Angew. Chem.* **2018**, *130*, 9614–9618; b) J. A. L. Roodhuizen, P. Hendriks, P. A. J. Hilbers, T. F. A. de Greef, A. J. Markvoort, *ACS Nano* **2019**, *13*, 10798–10809.
- [18] a) J. Hahn, S. F. Wickham, W. M. Shih, S. D. Perrault, *ACS Nano* **2014**, *8*, 8765–8775; b) H. Bila, E. E. Kurisinkal, M. M. C. Bastings, *Biomater. Sci.* **2019**, *7*, 532–541.
- [19] S. Ramakrishnan, B. Shen, M. A. Kostianin, G. Grundmeier, A. Keller, V. Linko, *ChemBioChem* **2019**, *20*, 2818–2823.
- [20] H. Ijäs, B. Shen, A. Heuer-Jungemann, A. Keller, M. A. Kostianin, T. Liedl, J. A. Ihalainen, V. Linko, *Nucleic Acids Res.* **2021**, *49*, 3048–3062.
- [21] a) S. Ko, H. Liu, Y. Chen, C. Mao, *Biomacromolecules* **2008**, *9*, 3039–3043; b) S. D. Perrault, W. M. Shih, *ACS Nano* **2014**, *8*, 5132–5140; c) M. M. C. Bastings, F. M. Anastassacos, N. Ponnuswamy, F. G. Leifer, G. Cuneo, C. Lin, D. E. Ingber, J. H. Ryu, W. M. Shih, *Nano Lett.* **2018**, *18*, 3557–3564; d) S. Li, Q. Jiang, S. Liu, Y. Zhang, Y. Tian, C. Song, J. Wang, Y. Zou, G. J. Anderson, J. Y. Han, Y. Chang, Y. Liu, C. Zhang, L. Chen, G. Zhou, G. Nie, H. Yan, B. Ding, Y. Zhao, *Nat. Biotechnol.* **2018**, *36*, 258–264; e) J. Liu, L. Song, S. Liu, Q. Jiang, Q. Liu, N. Li, Z. G. Wang, B. Ding, *Nano Lett.* **2018**, *18*, 3328–3334; f) Q. Pan, C. Nie, Y. Hu, J. Yi, C. Liu, J. Zhang, M. He, M. He, T. Chen, X. Chu, *ACS Appl. Mater. Interfaces* **2020**, *12*, 400–409.
- [22] a) A. Lacroix, E. Vengut-Climent, D. de Rochambeau, H. F. Sleiman, *ACS Cent. Sci.* **2019**, *5*, 882–891.

Manuscript received: August 19, 2021
Accepted manuscript online: November 23, 2021
Version of record online: January 3, 2022

3.3 Excursus: Further nanoparticular systems based on supramolecular assemblies

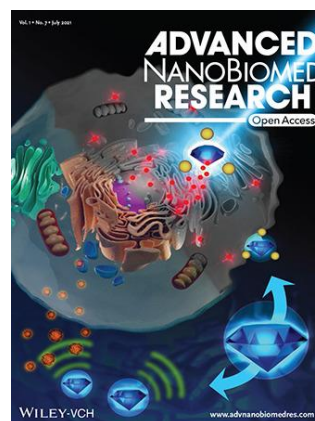
- Publication: **“Squaric Ester-Based, pH-Degradable Nanogels: Modular Nanocarriers for Safe, Systemic Administration of Toll-like Receptor 7/8 Agonistic Immune Modulators”**

Anne Huppertsberg, Leonard Kaps, Zifu Zhong, Sascha Schmitt, Judith Stickdorn, Kim Deswarte, Francis Combes, Christian Czysch, Jana De Vrieze, Sabah Kasmi, Niklas Choteschovsky, Adrian Klefenz, Carolina Medina-Montano, Pia Winterwerber, Chaojian Chen, Matthias Bros, Stefan Lienenklaus, Niek N. Sanders, Kaloian Koynov, Detlef Schuppan, Bart N. Lambrecht, Sunil A. David, Bruno G. De Geest, and Lutz Nuhn *J. Am. Chem. Soc.* **2021**, 143, 9872-9883.



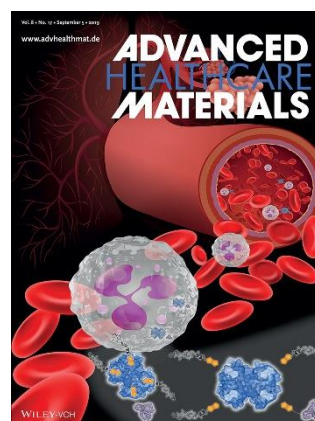
- Publication: **“Fluorescent Nanodiamond–Nanogels for Nanoscale Sensing and Photodynamic Applications”**

Yingke Wu, Md Noor A Alam, Priyadharshini Balasubramanian, Pia Winterwerber, Anna Ermakova, Michael Müller, Manfred Wagner, Fedor Jelezko, Marco Raabe, Tanja Weil *Adv. NanoBiomed. Res.* **2021**, 1, 2000101.



- Publication: **“Supramolecular Toxin Complexes for Targeted Pharmacological Modulation of Polymorphonuclear Leukocyte Functions”**

Astrid Johanna Heck, Theresa Ostertag, Leonie Schnell, Stephan Fischer, Bikram Keshari Agrawalla, Pia Winterwerber, Eva Wirsching, Michael Fauler, Manfred Frick, Seah Ling Kuan, Tanja Weil, Holger Barth *Adv. Healthcare Mater.* **2019**, 8, 1900665.



Steadily progressing as commodities, the advancement of nanomaterials in medicine is essentially based on the factor that their size matches those of most biological molecules and structures. Many endeavors in the field seek to create vehicles in the respective size regime that can be customized towards the designated application whilst gaining thorough understanding thereof.

While DNA origami technology was excessively discussed in previous chapters, this section intends to expand the breadth by exploring other platforms based on supramolecular interactions. In that respect, polymeric nanogels, fluorescent nanodiamonds and enzyme-based approaches are introduced. Though originating from different chemical scaffolds, they are unified in their objective to provide targeted therapy and diagnosis with low side effects.

Drug-functionalized nanogels for immunotherapeutic application represent a class of nanomaterials that exploits the self-assembly tendency of amphiphilic block copolymers. Methacrylamide monomers with squaric ester moieties are polymerized from a PEG-macroinitiator in a controlled RAFT process, forming micelles. Crosslinking of the core with the Toll-like receptor agonist imidazoquinoline and hydrophilization yields pH-responsive nanogels that – contrary to free agonist administration – demonstrated spatially controlled immunostimulatory activity *in vivo*.

Nanodiamonds (ND) present unique magneto-optical properties for nanomedicine and bioimaging due to atomic defects in their lattice, providing non-photobleaching fluorescence. However, colloidal stability of unmodified ND is extremely poor. Making use of noncovalent adsorption and subsequent covalent crosslinking, ND can be coated with polyethyleneimine in the presence of polyvinylpyrrolidone and reactive 4-arm PEG, thus, enabling modification of ND-cell interactions. Postmodification with photoactive Ru-complexes makes the coated ND attractive candidates for photodynamic therapy.

Avidin is a biotin-binding protein of a tetrameric structure, possessing one of the strongest non-covalent interactions between a protein and a ligand found in Nature. By attaching the molecules of interest to biotin one can make use of the four binding pockets of avidin. Stoichiometric-controlled assembly of various molecules is particularly challenging. In a “mix and match” assembly, an enzyme-inhibitor and various targeting peptides could be attached at spatially distinct locations. Cell type-selectivity could be demonstrated *ex vivo*, thus providing a proof-of-concept for therapeutic applications in post-traumatic injury. Here, hyperactivity of the innate immune system can be downregulated through the targeted delivery of the respective enzyme inhibitor.

In all of the nanoparticulate systems discussed above, it is crucial to have narrowly dispersed and homogenous systems as they are envisioned to be administered to the human body for targeted therapy. The sample's size distribution profile can be accessed by spectroscopy techniques such as DLS or FCS. However, AFM can further grant visual insights into the homogeneity and morphology of the

particles as well as their aggregation behavior. Thus, I could deepen the understanding of the nanoparticulate systems presented in this excursus chapter by providing AFM imaging and analysis, helping to gain a solid understanding of the nanoparticle systems.

A comprehensive overview of the full articles is listed in the Appendix of this thesis.

4. Conclusion and Outlook

This thesis strives to contribute to the field of DNA nanotechnology through the implementation of polymer chemistry into DNA origami, ultimately yielding hybrid objects with advanced properties. Briefly, the unique programmability of DNA origami along with a photopolymerization system could be exploited to achieve spatiotemporal control over the formation of two poly(catecholamine)s on 3D DNA templates which can be hardly achieved by conventional techniques. The herein presented concepts not only offer an additional prospect to constrain the polymerization of dopamine and norepinephrine with nanometer resolution but also tackle the intrinsic susceptibility of DNA in certain contexts.

The first project laid the foundation for a novel photoinduced polymerization of dopamine on 3D DNA nanotubes without the need for chemical triggers. Typically, dopamine, a neurotransmitter, undergoes auto-oxidation in alkaline aqueous media leading to spontaneous formation of polydopamine in an uncontrolled fashion. However, its simplicity in formation and ability to adhere to virtually any surface renders it a promising candidate for the modification of DNA objects. Herein, self-polymerization of dopamine was suppressed by keeping the environment slightly acidic (pH 6.5) whereas an irradiation-sensitive polymerization system ensured controlled initiation of dopamine oxidation through visible light. The photosensitizer protoporphyrin IX was embedded in designated patterns on DNA origami tubes and upon white light irradiation, locally produced reactive oxygen species which induced oxidation and eventually, polymerization of dopamine. Polymeric layers of up to 10–15 nm height were imprinted alongside the catalytic centers with lateral dimensions far below 100 nm and thus, much smaller than the wavelength of light. This bottom-up approach can therefore be considered as an attractive alternative to conventional top-down lithographic approaches in creating precise nanopatterns. In the presented studies, photopolymerization further proved to be advantageous in tailoring polymer density and height by simply switching the light source on and off. As anticipated, not only the polymer side could benefit from the DNA technology but also the DNA object itself could profit from polymer decoration. In contrast to bare origami DNA tubes, polymer-ringed tubes demonstrated to withstand pure water conditions. In ion-depleted environment, polymer-DNA hybrid objects could sustain their integrity.

As a continuation of this initial research on the photopolymerization of dopamine, the toolbox of photosensitizers and monomers could be successfully broadened: By embedding eosin Y and methylene blue into the catalytic centers on DNA origami nanotubes, the responsiveness of the polymerization system was shifted towards activation wavelengths of 525 nm and 625 nm, respectively. Similar to dopamine, norepinephrine could be deposited in designated patterns on the origami objects, potentially opening new avenues due to a slightly different surface chemistry arising from the additional hydroxyl group. In each case, polymer-ringed DNA nanotubes of comparable

shapes and dimensions were obtained. Thereby, the adaptability of the platform could be demonstrated as the change of catalytic centers, excitation wavelengths and monomer did not affect the control over the polymerization reaction. All parameters together paved the way for multistep polymerizations on DNA origami towards advanced surface patterning on the nanoscale. This way, a polymer ring spanning around the DNA tube could be produced that comprises layers of polynorepinephrine and polydopamine. It was further possible to stepwise generate DNA objects with two polymer rings whereas the rings were activated through different wavelengths and different monomers. In addition to the chemically driven investigations of the system, the study aimed for a biological impact of the polymer decoration on the interaction of DNA origami with cells. Indeed, the polymer patterns altered the intrinsic polyanionic character of DNA origami while preserving their integrity in A549 uptake studies. Whereas polydopamine mainly led to aggregation, colocalization studies in combination with DNase treatment revealed successful uptake of polynorepinephrine-coated origami tubes.

Throughout the above described projects, the well-known challenges in DNA nanotechnology research were also encountered which, in part, have hindered their progress. Besides the advancements of the DNA origami methodology, the bottom-up synthesis of polymer-DNA origami objects as well as their characterization is limited through various aspects. Typically, the grafting of polymers from the origami surface is difficult due to the extremely low concentration of DNA objects and the consequently small number of initiators. The amount of DNA objects in the picomole range also prevents classical polymer analysis tools such as NMR or SEC. Controlled radical polymerization techniques are further impeded by an increased sensitivity to oxygen because of ultralow reaction volumes. On the other hand, when grafting preformed polymers onto DNA origami, incompatible solubility effects and the shielding of reactive centers result in reduced grafting densities and yields. However, the light-induced and origami-mediated polymerization of poly(catecholamines) – that has parallels to melanin production in the human body – can circumvent some of these drawbacks. The reaction can not only be carried out under ambient conditions even in the smallest volumes but can also be monitored by UV-VIS spectroscopy in real-time. Furthermore, the bulky structure of the formed polymers allows excellent visualization by atomic force microscopy under liquid conditions that resembles the natural occurrence of DNA in aqueous solution. Here, topographic images help in drawing conclusions about location and progress of the polymerization process. Agarose gel electrophoresis can be employed to investigate the impact of polymers as well as their integrity when exposed to, e.g., physiological fluids. To further confirm the presence of polymers on DNA origami, dynamic light scattering additionally provides qualitative information

Since its advent in 2006 and the subsequent progress in fundamental understanding, DNA origami has established a stronghold in the fields of molecular and cellular biophysics, biomimetic systems, energy

transfer photonics as well as diagnostics and therapeutics for human health. We hope that our investigations can especially contribute to the latter topic: In this respect, it could be demonstrated that modification of the origami platform in a post polymerization fashion could boost their stability and interaction with cells. Cells in turn can host a variety of chemical reactions which is largely enabled through compartmentalization and creating demarcated reaction vesicles. Likewise, tubular DNA origami structures could mimic such a confined space making use of both the outer (polymer shielding, active targeting) and inner (enzymatic reactions, drug loading) space. By choosing a suitable photosensitizer that responds to tissue-penetrating wavelengths, even *in situ* oxidative polymerization is conceivable. Not only artificial organelles are of interest but also the vision of creating an artificial virus might be realized through the origami platform. Viruses are naturally evolved nanostructures that form spontaneously by molecular self-assembly of their two main building blocks, namely nucleic acids and proteins. Despite their apparent simplicity, they are Nature's most efficient agents for gene transfer and reveal a well-defined geometry and precise composition. An outstanding feature of viruses is their capability of self-reproducing by hijacking the host cell's replication machinery. Even though the latter challenge seems incredibly grand, the unique addressability of DNA origami together with shielding and cell-penetrating polymers could provide sufficient modularity and tunability to artificially rebuild viruses that could, *e.g.*, carry a genetic code.

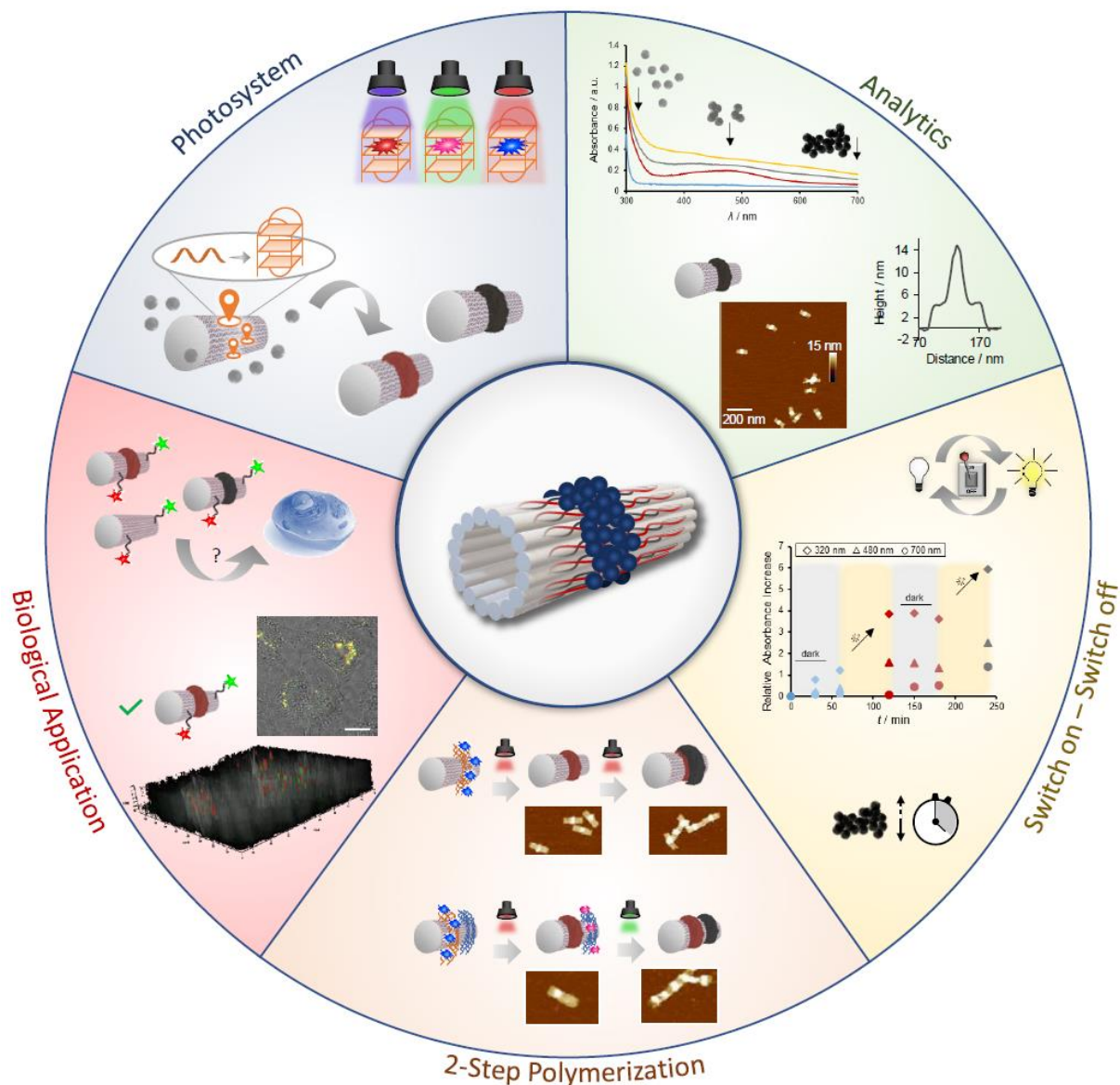


Figure 13 Graphical overview of how photopolymerization on DNA origami can create advanced hybrid objects under spatiotemporal control and how these can be leveraged for paving the way of biological applications.

5. References

1. International Human Genome Sequencing, C., Finishing the euchromatic sequence of the human genome. *Nature* **2004**, *431* (7011), 931-45.
2. Gorzynski, J. E.; Goenka, S. D.; Shafin, K.; Jensen, T. D.; Fisk, D. G.; Grove, M. E.; Spiteri, E.; Pesout, T.; Monlong, J.; Baid, G.; Bernstein, J. A.; Ceresnak, S.; Chang, P. C.; Christle, J. W.; Chubb, H.; Dalton, K. P.; Dunn, K.; Garalde, D. R.; Guillory, J.; Knowles, J. W.; Kolesnikov, A.; Ma, M.; Moscarello, T.; Nattestad, M.; Perez, M.; Ruzhnikov, M. R. Z.; Samadi, M.; Setia, A.; Wright, C.; Wusthoff, C. J.; Xiong, K.; Zhu, T.; Jain, M.; Sedlazeck, F. J.; Carroll, A.; Paten, B.; Ashley, E. A., Ultrarapid Nanopore Genome Sequencing in a Critical Care Setting. *N Engl J Med* **2022**, *386* (7), 700-702.
3. Watson, J. D.; Crick, F. H., Molecular structure of nucleic acids; a structure for deoxyribose nucleic acid. *Nature* **1953**, *171* (4356), 737-8.
4. Watson, J. D.; Crick, F. H., Genetical implications of the structure of deoxyribonucleic acid. *Nature* **1953**, *171* (4361), 964-7.
5. Franklin, R. E.; Gosling, R. G., Molecular configuration in sodium thymonucleate. *Nature* **1953**, *171* (4356), 740-1.
6. Ghosh, A.; Bansal, M., A glossary of DNA structures from A to Z. *Acta Crystallogr D Biol Crystallogr* **2003**, *59* (Pt 4), 620-6.
7. Travers, A.; Muskhelishvili, G., DNA structure and function. *FEBS J* **2015**, *282* (12), 2279-95.
8. Saenger, W., *Principles of Nucleic Acid Structure*. Springer-Verlag: 1984.
9. Simmel, S. S.; Nickels, P. C.; Liedl, T., Wireframe and tensegrity DNA nanostructures. *Acc Chem Res* **2014**, *47* (6), 1691-9.
10. <https://www.rcsb.org/3d-view/2M2C/0>.
11. Hood, L.; Galas, D., The digital code of DNA. *Nature* **2003**, *421* (6921), 444-8.
12. Madsen, M.; Gothelf, K. V., Chemistries for DNA Nanotechnology. *Chem Rev* **2019**, *119* (10), 6384-6458.
13. Seeman, N. C.; Sleiman, H. F., DNA nanotechnology. *Nature Reviews Materials* **2017**, *3* (1).
14. Seeman, N. C.; Belcher, A. M., Emulating biology: building nanostructures from the bottom up. *Proc Natl Acad Sci U S A* **2002**, *99* Suppl 2, 6451-5.
15. Whitesides, G. M.; Grzybowski, B., Self-assembly at all scales. *Science* **2002**, *295* (5564), 2418-21.
16. Zhang, S., Emerging biological materials through molecular self-assembly. *Biotechnology Advances* **2002**, *20* (5-6), 321-339.
17. Devaux, P. F., Static and dynamic lipid asymmetry in cell membranes. *Biochemistry* **1991**, *30* (5), 1163-73.
18. Pohorille, A.; Deamer, D., Self-assembly and function of primitive cell membranes. *Res Microbiol* **2009**, *160* (7), 449-56.
19. Seeman, N. C., Nucleic acid junctions and lattices. *Journal of Theoretical Biology* **1982**, *99* (2), 237-247.
20. Seeman, N. C., Nanomaterials based on DNA. *Annu Rev Biochem* **2010**, *79*, 65-87.
21. Holliday, R., A mechanism for gene conversion in fungi. *Genetical Research* **2009**, *5* (2), 282-304.
22. Beaucage, S. L.; Caruthers, M. H., Deoxynucleoside phosphoramidites—A new class of key intermediates for deoxypolynucleotide synthesis. *Tetrahedron Letters* **1981**, *22* (20), 1859-1862.
23. Caruthers, M. H., Gene synthesis machines: DNA chemistry and its uses. *Science* **1985**, *230* (4723), 281-5.
24. Chen, J. H.; Seeman, N. C., Synthesis from DNA of a molecule with the connectivity of a cube. *Nature* **1991**, *350* (6319), 631-3.
25. Fu, T. J.; Seeman, N. C., DNA double-crossover molecules. *Biochemistry* **1993**, *32* (13), 3211-20.

26. Li, X.; Yang, X.; Qi, J.; Seeman, N. C., Antiparallel DNA Double Crossover Molecules As Components for Nanoconstruction. *Journal of the American Chemical Society* **1996**, *118* (26), 6131-6140.
27. Winfree, E.; Liu, F.; Wenzler, L. A.; Seeman, N. C., Design and self-assembly of two-dimensional DNA crystals. *Nature* **1998**, *394* (6693), 539-44.
28. Yan, H.; Park, S. H.; Finkelstein, G.; Reif, J. H.; LaBean, T. H., DNA-templated self-assembly of protein arrays and highly conductive nanowires. *Science* **2003**, *301* (5641), 1882-4.
29. Liu, D.; Park, S. H.; Reif, J. H.; LaBean, T. H., DNA nanotubes self-assembled from triple-crossover tiles as templates for conductive nanowires. *Proc Natl Acad Sci U S A* **2004**, *101* (3), 717-22.
30. Rothmund, P. W.; Ekani-Nkodo, A.; Papadakis, N.; Kumar, A.; Fygenson, D. K.; Winfree, E., Design and characterization of programmable DNA nanotubes. *J Am Chem Soc* **2004**, *126* (50), 16344-52.
31. Sherman, W. B.; Seeman, N. C., A Precisely Controlled DNA Biped Walking Device. *Nano Letters* **2004**, *4* (7), 1203-1207.
32. He, Y.; Ye, T.; Su, M.; Zhang, C.; Ribbe, A. E.; Jiang, W.; Mao, C., Hierarchical self-assembly of DNA into symmetric supramolecular polyhedra. *Nature* **2008**, *452* (7184), 198-201.
33. "Holliday Junction" by Richard Wheeler is licensed under CC BY-SA 3.0. https://en.wikipedia.org/wiki/Holliday_junction#/media/File:Holliday_junction_coloured.png.
34. Seeman, N. C., DNA in a material world. *Nature* **2003**, *421* (6921), 427-31.
35. Rothmund, P. W., Folding DNA to create nanoscale shapes and patterns. *Nature* **2006**, *440* (7082), 297-302.
36. Topping, T.; Voigt, N. V.; Nangreave, J.; Yan, H.; Gothelf, K. V., DNA origami: a quantum leap for self-assembly of complex structures. *Chem Soc Rev* **2011**, *40* (12), 5636-46.
37. Nummelin, S.; Kommeri, J.; Kostianen, M. A.; Linko, V., Evolution of Structural DNA Nanotechnology. *Adv Mater* **2018**, *30* (24), e1703721.
38. Erkelenz, M.; Bauer, D. M.; Meyer, R.; Gatsogiannis, C.; Raunser, S.; Sacca, B.; Niemeyer, C. M., A facile method for preparation of tailored scaffolds for DNA-origami. *Small* **2014**, *10* (1), 73-7.
39. Schmidt, T. L.; Believeau, B. J.; Uca, Y. O.; Theilmann, M.; Da Cruz, F.; Wu, C. T.; Shih, W. M., Scalable amplification of strand subsets from chip-synthesized oligonucleotide libraries. *Nat Commun* **2015**, *6*, 8634.
40. Marchi, A. N.; Saaem, I.; Tian, J.; LaBean, T. H., One-pot assembly of a hetero-dimeric DNA origami from chip-derived staples and double-stranded scaffold. *ACS Nano* **2013**, *7* (2), 903-10.
41. Sacca, B.; Niemeyer, C. M., DNA origami: the art of folding DNA. *Angew Chem Int Ed Engl* **2012**, *51* (1), 58-66.
42. Andersen, E. S.; Dong, M.; Nielsen, M. M.; Jahn, K.; Subramani, R.; Mamdouh, W.; Golas, M. M.; Sander, B.; Stark, H.; Oliveira, C. L.; Pedersen, J. S.; Birkedal, V.; Besenbacher, F.; Gothelf, K. V.; Kjems, J., Self-assembly of a nanoscale DNA box with a controllable lid. *Nature* **2009**, *459* (7243), 73-6.
43. Douglas, S. M.; Dietz, H.; Liedl, T.; Hogberg, B.; Graf, F.; Shih, W. M., Self-assembly of DNA into nanoscale three-dimensional shapes. *Nature* **2009**, *459* (7245), 414-8.
44. Ke, Y.; Douglas, S. M.; Liu, M.; Sharma, J.; Cheng, A.; Leung, A.; Liu, Y.; Shih, W. M.; Yan, H., Multilayer DNA origami packed on a square lattice. *J Am Chem Soc* **2009**, *131* (43), 15903-8.
45. Zhang, F.; Jiang, S.; Wu, S.; Li, Y.; Mao, C.; Liu, Y.; Yan, H., Complex wireframe DNA origami nanostructures with multi-arm junction vertices. *Nat Nanotechnol* **2015**, *10* (9), 779-84.
46. Piskunen, P.; Nummelin, S.; Shen, B.; Kostianen, M. A.; Linko, V., Increasing Complexity in Wireframe DNA Nanostructures. *Molecules* **2020**, *25* (8).
47. Han, D.; Pal, S.; Yang, Y.; Jiang, S.; Nangreave, J.; Liu, Y.; Yan, H., DNA gridiron nanostructures based on four-arm junctions. *Science* **2013**, *339* (6126), 1412-5.
48. Benson, E.; Mohammed, A.; Gardell, J.; Masich, S.; Czeizler, E.; Orponen, P.; Hogberg, B., DNA rendering of polyhedral meshes at the nanoscale. *Nature* **2015**, *523* (7561), 441-4.
49. Veneziano, R.; Ratanalert, S.; Zhang, K.; Zhang, F.; Yan, H.; Chiu, W.; Bathe, M., Designer nanoscale DNA assemblies programmed from the top down. *Science* **2016**, *352* (6293), 1534.

50. Wang, W.; Chen, S.; An, B.; Huang, K.; Bai, T.; Xu, M.; Bellot, G.; Ke, Y.; Xiang, Y.; Wei, B., Complex wireframe DNA nanostructures from simple building blocks. *Nat Commun* **2019**, *10* (1), 1067.
51. Caruthers, M. H.; Barone, A. D.; Beaucage, S. L.; Dodds, D. R.; Fisher, E. F.; McBride, L. J.; Matteucci, M.; Stabinsky, Z.; Tang, J. Y., Chemical synthesis of deoxyoligonucleotides by the phosphoramidite method. *Methods Enzymol* **1987**, *154*, 287-313.
52. Fu, J.; Liu, M.; Liu, Y.; Woodbury, N. W.; Yan, H., Interenzyme substrate diffusion for an enzyme cascade organized on spatially addressable DNA nanostructures. *J Am Chem Soc* **2012**, *134* (12), 5516-9.
53. Klein, W. P.; Thomsen, R. P.; Turner, K. B.; Walper, S. A.; Vranish, J.; Kjems, J.; Ancona, M. G.; Medintz, I. L., Enhanced Catalysis from Multienzyme Cascades Assembled on a DNA Origami Triangle. *ACS Nano* **2019**, *13* (12), 13677-13689.
54. Kroll, S.; Rabe, K. S.; Niemeyer, C. M., An Orthogonal Covalent Connector System for the Efficient Assembly of Enzyme Cascades on DNA Nanostructures. *Small* **2021**, *17* (51), e2105095.
55. Stein, I. H.; Schuller, V.; Bohm, P.; Tinnefeld, P.; Liedl, T., Single-molecule FRET ruler based on rigid DNA origami blocks. *Chemphyschem* **2011**, *12* (3), 689-95.
56. Funke, J. J.; Dietz, H., Placing molecules with Bohr radius resolution using DNA origami. *Nat Nanotechnol* **2016**, *11* (1), 47-52.
57. Walter, H. K.; Bauer, J.; Steinmeyer, J.; Kuzuya, A.; Niemeyer, C. M.; Wagenknecht, H. A., "DNA Origami Traffic Lights" with a Split Aptamer Sensor for a Bicolor Fluorescence Readout. *Nano Lett* **2017**, *17* (4), 2467-2472.
58. Nicoli, F.; Barth, A.; Bae, W.; Neukirchinger, F.; Crevenna, A. H.; Lamb, D. C.; Liedl, T., Directional Photonic Wire Mediated by Homo-Förster Resonance Energy Transfer on a DNA Origami Platform. *ACS Nano* **2017**, *11* (11), 11264-11272.
59. Madsen, M.; Bakke, M. R.; Gudnason, D. A.; Sandahl, A. F.; Hansen, R. A.; Knudsen, J. B.; Kodal, A. L. B.; Birkedal, V.; Gothelf, K. V., A Single Molecule Polyphenylene-Vinylene Photonic Wire. *ACS Nano* **2021**, *15* (6), 9404-9411.
60. Hemmig, E. A.; Creatore, C.; Wunsch, B.; Hecker, L.; Mair, P.; Parker, M. A.; Emmott, S.; Tinnefeld, P.; Keyser, U. F.; Chin, A. W., Programming Light-Harvesting Efficiency Using DNA Origami. *Nano Lett* **2016**, *16* (4), 2369-74.
61. Jungmann, R.; Steinhauer, C.; Scheible, M.; Kuzyk, A.; Tinnefeld, P.; Simmel, F. C., Single-molecule kinetics and super-resolution microscopy by fluorescence imaging of transient binding on DNA origami. *Nano Lett* **2010**, *10* (11), 4756-61.
62. Jungmann, R.; Avendano, M. S.; Woehrstein, J. B.; Dai, M.; Shih, W. M.; Yin, P., Multiplexed 3D cellular super-resolution imaging with DNA-PAINT and Exchange-PAINT. *Nat Methods* **2014**, *11* (3), 313-8.
63. Schnitzbauer, J.; Strauss, M. T.; Schlichthaerle, T.; Schueder, F.; Jungmann, R., Super-resolution microscopy with DNA-PAINT. *Nat Protoc* **2017**, *12* (6), 1198-1228.
64. Hahn, J.; Wickham, S. F.; Shih, W. M.; Perrault, S. D., Addressing the instability of DNA nanostructures in tissue culture. *ACS Nano* **2014**, *8* (9), 8765-75.
65. Mei, Q.; Wei, X.; Su, F.; Liu, Y.; Youngbull, C.; Johnson, R.; Lindsay, S.; Yan, H.; Meldrum, D., Stability of DNA origami nanoarrays in cell lysate. *Nano Lett* **2011**, *11* (4), 1477-82.
66. Ramakrishnan, S.; Shen, B.; Kostianen, M. A.; Grundmeier, G.; Keller, A.; Linko, V., Real-Time Observation of Superstructure-Dependent DNA Origami Digestion by DNase I Using High-Speed Atomic Force Microscopy. *Chembiochem* **2019**, *20* (22), 2818-2823.
67. Perrault, S. D.; Shih, W. M., Virus-inspired membrane encapsulation of DNA nanostructures to achieve in vivo stability. *ACS Nano* **2014**, *8* (5), 5132-40.
68. Auvinen, H.; Zhang, H.; Nonappa; Kopilow, A.; Niemela, E. H.; Nummelin, S.; Correia, A.; Santos, H. A.; Linko, V.; Kostianen, M. A., Protein Coating of DNA Nanostructures for Enhanced Stability and Immunocompatibility. *Adv Healthc Mater* **2017**, *6* (18).
69. Xu, X.; Fang, S.; Zhuang, Y.; Wu, S.; Pan, Q.; Li, L.; Wang, X.; Sun, X.; Liu, B.; Wu, Y., Cationic Albumin Encapsulated DNA Origami for Enhanced Cellular Transfection and Stability. *Materials (Basel)* **2019**, *12* (6).

70. Kim, Y.; Yin, P., Enhancing Biocompatible Stability of DNA Nanostructures Using Dendritic Oligonucleotides and Brick Motifs. *Angew Chem Int Ed Engl* **2020**, *59* (2), 700-703.
71. Yang, Y.; Lu, Q.; Huang, C. M.; Qian, H.; Zhang, Y.; Deshpande, S.; Arya, G.; Ke, Y.; Zauscher, S., Programmable Site-Specific Functionalization of DNA Origami with Polynucleotide Brushes. *Angew Chem Int Ed Engl* **2021**, *60* (43), 23241-23247.
72. Wamhoff, E. C.; Romanov, A.; Huang, H.; Read, B. J.; Ginsburg, E.; Knappe, G. A.; Kim, H. M.; Farrell, N. P.; Irvine, D. J.; Bathe, M., Controlling Nuclease Degradation of Wireframe DNA Origami with Minor Groove Binders. *ACS Nano* **2022**.
73. Chandrasekaran, A. R.; Vilcapoma, J.; Dey, P.; Wong-Deyrup, S. W.; Dey, B. K.; Halvorsen, K., Exceptional Nuclease Resistance of Paranemic Crossover (PX) DNA and Crossover-Dependent Biostability of DNA Motifs. *J Am Chem Soc* **2020**, *142* (14), 6814-6821.
74. Kielar, C.; Xin, Y.; Shen, B.; Kostianen, M. A.; Grundmeier, G.; Linko, V.; Keller, A., On the Stability of DNA Origami Nanostructures in Low-Magnesium Buffers. *Angew Chem Int Ed Engl* **2018**, *57* (30), 9470-9474.
75. Chopra, A.; Krishnan, S.; Simmel, F. C., Electrotransfection of Polyamine Folded DNA Origami Structures. *Nano Lett* **2016**, *16* (10), 6683-6690.
76. Agarwal, N. P.; Matthies, M.; Gur, F. N.; Osada, K.; Schmidt, T. L., Block Copolymer Micellization as a Protection Strategy for DNA Origami. *Angew Chem Int Ed Engl* **2017**, *56* (20), 5460-5464.
77. Ponnuswamy, N.; Bastings, M. M. C.; Nathwani, B.; Ryu, J. H.; Chou, L. Y. T.; Vinther, M.; Li, W. A.; Anastassacos, F. M.; Mooney, D. J.; Shih, W. M., Oligolysine-based coating protects DNA nanostructures from low-salt denaturation and nuclease degradation. *Nat Commun* **2017**, *8*, 15654.
78. Anastassacos, F. M.; Zhao, Z.; Zeng, Y.; Shih, W. M., Glutaraldehyde Cross-Linking of Oligolysines Coating DNA Origami Greatly Reduces Susceptibility to Nuclease Degradation. *J Am Chem Soc* **2020**, *142* (7), 3311-3315.
79. Rinker, S.; Ke, Y.; Liu, Y.; Chhabra, R.; Yan, H., Self-assembled DNA nanostructures for distance-dependent multivalent ligand-protein binding. *Nat Nanotechnol* **2008**, *3* (7), 418-22.
80. Pan, Q.; Nie, C.; Hu, Y.; Yi, J.; Liu, C.; Zhang, J.; He, M.; He, M.; Chen, T.; Chu, X., Aptamer-Functionalized DNA Origami for Targeted Codelivery of Antisense Oligonucleotides and Doxorubicin to Enhance Therapy in Drug-Resistant Cancer Cells. *ACS Appl Mater Interfaces* **2020**, *12* (1), 400-409.
81. Zhao, S.; Tian, R.; Wu, J.; Liu, S.; Wang, Y.; Wen, M.; Shang, Y.; Liu, Q.; Li, Y.; Guo, Y.; Wang, Z.; Wang, T.; Zhao, Y.; Zhao, H.; Cao, H.; Su, Y.; Sun, J.; Jiang, Q.; Ding, B., A DNA origami-based aptamer nanoarray for potent and reversible anticoagulation in hemodialysis. *Nat Commun* **2021**, *12* (1), 358.
82. Krissanaprasit, A.; Key, C. M.; Pontula, S.; LaBean, T. H., Self-Assembling Nucleic Acid Nanostructures Functionalized with Aptamers. *Chem Rev* **2021**, *121* (22), 13797-13868.
83. Bastings, M. M. C.; Anastassacos, F. M.; Ponnuswamy, N.; Leifer, F. G.; Cuneo, G.; Lin, C.; Ingber, D. E.; Ryu, J. H.; Shih, W. M., Modulation of the Cellular Uptake of DNA Origami through Control over Mass and Shape. *Nano Lett* **2018**, *18* (6), 3557-3564.
84. Rajwar, A.; Shetty, S. R.; Vaswani, P.; Morya, V.; Barai, A.; Sen, S.; Sonawane, M.; Bhatia, D., Geometry of a DNA Nanostructure Influences Its Endocytosis: Cellular Study on 2D, 3D, and in Vivo Systems. *ACS Nano* **2022**.
85. Godonoga, M.; Lin, T. Y.; Oshima, A.; Sumitomo, K.; Tang, M. S. L.; Cheung, Y. W.; Kinghorn, A. B.; Dirkwager, R. M.; Zhou, C.; Kuzuya, A.; Tanner, J. A.; Heddle, J. G., A DNA aptamer recognising a malaria protein biomarker can function as part of a DNA origami assembly. *Sci Rep* **2016**, *6*, 21266.
86. Sheng, Q.; Liu, R.; Zhang, S.; Zheng, J., Ultrasensitive electrochemical cocaine biosensor based on reversible DNA nanostructure. *Biosens Bioelectron* **2014**, *51*, 191-4.
87. Li, S.; Jiang, Q.; Liu, S.; Zhang, Y.; Tian, Y.; Song, C.; Wang, J.; Zou, Y.; Anderson, G. J.; Han, J. Y.; Chang, Y.; Liu, Y.; Zhang, C.; Chen, L.; Zhou, G.; Nie, G.; Yan, H.; Ding, B.; Zhao, Y., A DNA nanorobot functions as a cancer therapeutic in response to a molecular trigger in vivo. *Nat Biotechnol* **2018**, *36* (3), 258-264.

88. Riley, P. A., Melanin. *The International Journal of Biochemistry & Cell Biology* **1997**, *29* (11), 1235-1239.
89. Meredith, P.; Sarna, T., The physical and chemical properties of eumelanin. *Pigment Cell Res* **2006**, *19* (6), 572-94.
90. Meredith, P.; Powell, B. J.; Riesz, J.; Nighswander-Rempel, S. P.; Pederson, M. R.; Moore, E. G., Towards structure-property-function relationships for eumelanin. *Soft Matter* **2006**, *2* (1), 37-44.
91. Waite, J. H.; Tanzer, M. L., The bioadhesive of *Mytilus byssus*: A protein containing L-DOPA. *Biochemical and Biophysical Research Communications* **1980**, *96* (4), 1554-1561.
92. Lee, H.; Dellatore, S. M.; Miller, W. M.; Messersmith, P. B., Mussel-inspired surface chemistry for multifunctional coatings. *Science* **2007**, *318* (5849), 426-30.
93. Nguyen, A.; Azari, S.; Zou, L., Coating zwitterionic amino acid L-DOPA to increase fouling resistance of forward osmosis membrane. *Desalination* **2013**, *312*, 82-87.
94. Tan, X.; Gao, P.; Li, Y.; Qi, P.; Liu, J.; Shen, R.; Wang, L.; Huang, N.; Xiong, K.; Tian, W.; Tu, Q., Poly-dopamine, poly-levodopa, and poly-norepinephrine coatings: Comparison of physico-chemical and biological properties with focus on the application for blood-contacting devices. *Bioact Mater* **2021**, *6* (1), 285-296.
95. Li, Y.; Cheng, J.; Delparastan, P.; Wang, H.; Sigg, S. J.; DeFrates, K. G.; Cao, Y.; Messersmith, P. B., Molecular design principles of Lysine-DOPA wet adhesion. *Nat Commun* **2020**, *11* (1), 3895.
96. Ryu, J. H.; Messersmith, P. B.; Lee, H., Polydopamine Surface Chemistry: A Decade of Discovery. *ACS Appl Mater Interfaces* **2018**, *10* (9), 7523-7540.
97. Beckford, S.; Zou, M., Wear resistant PTFE thin film enabled by a polydopamine adhesive layer. *Applied Surface Science* **2014**, *292*, 350-356.
98. Sileika, T. S.; Kim, H. D.; Maniak, P.; Messersmith, P. B., Antibacterial performance of polydopamine-modified polymer surfaces containing passive and active components. *ACS Appl Mater Interfaces* **2011**, *3* (12), 4602-10.
99. Dreyer, D. R.; Miller, D. J.; Freeman, B. D.; Paul, D. R.; Bielawski, C. W., Elucidating the structure of poly(dopamine). *Langmuir* **2012**, *28* (15), 6428-35.
100. Hong, S.; Na, Y. S.; Choi, S.; Song, I. T.; Kim, W. Y.; Lee, H., Non-Covalent Self-Assembly and Covalent Polymerization Co-Contribute to Polydopamine Formation. *Advanced Functional Materials* **2012**, *22* (22), 4711-4717.
101. Della Vecchia, N. F.; Avolio, R.; Alfè, M.; Errico, M. E.; Napolitano, A.; d'Ischia, M., Building-Block Diversity in Polydopamine Underpins a Multifunctional Eumelanin-Type Platform Tunable Through a Quinone Control Point. *Advanced Functional Materials* **2013**, *23* (10), 1331-1340.
102. Pezzella, A.; Crescenzi, O.; Panzella, L.; Napolitano, A.; Land, E. J.; Barone, V.; d'Ischia, M., Free radical coupling of o-semiquinones uncovered. *J Am Chem Soc* **2013**, *135* (32), 12142-9.
103. Delparastan, P.; Malollari, K. G.; Lee, H.; Messersmith, P. B., Direct Evidence for the Polymeric Nature of Polydopamine. *Angew Chem Int Ed Engl* **2019**, *58* (4), 1077-1082.
104. Wood, J. B.; Szyndler, M. W.; Halpern, A. R.; Cho, K.; Corn, R. M., Fabrication of DNA microarrays on polydopamine-modified gold thin films for SPR imaging measurements. *Langmuir* **2013**, *29* (34), 10868-73.
105. Wang, C.; Zhou, J.; Wang, P.; He, W.; Duan, H., Robust Nanoparticle-DNA Conjugates Based on Mussel-Inspired Polydopamine Coating for Cell Imaging and Tailored Self-Assembly. *Bioconjug Chem* **2016**, *27* (3), 815-23.
106. Liu, J.; Xu, H.; Tang, X.; Xu, J.; Jin, Z.; Li, H.; Wang, S.; Gou, J.; Jin, X., Simple and tunable surface coatings via polydopamine for modulating pharmacokinetics, cell uptake and biodistribution of polymeric nanoparticles. *RSC Advances* **2017**, *7* (26), 15864-15876.
107. Behzadi, S.; Serpooshan, V.; Tao, W.; Hamaly, M. A.; Alkawareek, M. Y.; Dreaden, E. C.; Brown, D.; Alkilany, A. M.; Farokhzad, O. C.; Mahmoudi, M., Cellular uptake of nanoparticles: journey inside the cell. *Chem Soc Rev* **2017**, *46* (14), 4218-4244.
108. McConnell, K. I.; Shamsudeen, S.; Meraz, I. M.; Mahadevan, T. S.; Ziemys, A.; Rees, P.; Summers, H. D.; Serda, R. E., Reduced Cationic Nanoparticle Cytotoxicity Based on Serum Masking of Surface Potential. *J Biomed Nanotechnol* **2016**, *12* (1), 154-64.

109. Ho, L. W. C.; Liu, Y.; Han, R.; Bai, Q.; Choi, C. H. J., Nano-Cell Interactions of Non-Cationic Bionanomaterials. *Acc Chem Res* **2019**, *52* (6), 1519-1530.
110. Liu, Y.; Choi, C. K. K.; Hong, H.; Xiao, Y.; Kwok, M. L.; Liu, H.; Tian, X. Y.; Choi, C. H. J., Dopamine Receptor-Mediated Binding and Cellular Uptake of Polydopamine-Coated Nanoparticles. *ACS Nano* **2021**, *15* (8), 13871-13890.
111. Ding, L.; Zhu, X.; Wang, Y.; Shi, B.; Ling, X.; Chen, H.; Nan, W.; Barrett, A.; Guo, Z.; Tao, W.; Wu, J.; Shi, X., Intracellular Fate of Nanoparticles with Polydopamine Surface Engineering and a Novel Strategy for Exocytosis-Inhibiting, Lysosome Impairment-Based Cancer Therapy. *Nano Lett* **2017**, *17* (11), 6790-6801.
112. Ham, H. O.; Liu, Z.; Lau, K. H.; Lee, H.; Messersmith, P. B., Facile DNA immobilization on surfaces through a catecholamine polymer. *Angew Chem Int Ed Engl* **2011**, *50* (3), 732-6.
113. Hong, S.; Kim, J.; Na, Y. S.; Park, J.; Kim, S.; Singha, K.; Im, G. I.; Han, D. K.; Kim, W. J.; Lee, H., Poly(norepinephrine): ultrasmooth material-independent surface chemistry and nanodepot for nitric oxide. *Angew Chem Int Ed Engl* **2013**, *52* (35), 9187-91.
114. Kang, S. M.; Rho, J.; Choi, I. S.; Messersmith, P. B.; Lee, H., Norepinephrine: material-independent, multifunctional surface modification reagent. *J Am Chem Soc* **2009**, *131* (37), 13224-5.
115. Lee, H. A.; Ma, Y.; Zhou, F.; Hong, S.; Lee, H., Material-Independent Surface Chemistry beyond Polydopamine Coating. *Acc Chem Res* **2019**, *52* (3), 704-713.
116. Manini, P.; Pezzella, A.; Panzella, L.; Napolitano, A.; d'Ischia, M., New insight into the oxidative chemistry of noradrenaline: competitive o-quinone cyclisation and chain fission routes leading to an unusual 4-[bis-(1H-5,6-dihydroxyindol-2-yl)methyl]-1,2-dihydroxybenzene derivative. *Tetrahedron* **2005**, *61* (16), 4075-4080.
117. Manini, P.; Panzella, L.; Napolitano, A.; d'Ischia, M., Oxidation chemistry of norepinephrine: partitioning of the O-quinone between competing cyclization and chain breakdown pathways and their roles in melanin formation. *Chem Res Toxicol* **2007**, *20* (10), 1549-55.
118. Lu, Z.; Douek, A. M.; Rozario, A. M.; Tabor, R. F.; Kaslin, J.; Follink, B.; Teo, B. M., Bioinspired polynorepinephrine nanoparticles as an efficient vehicle for enhanced drug delivery. *J Mater Chem B* **2020**, *8* (5), 961-968.
119. Lu, Z.; Acter, S.; Teo, B. M.; Tabor, R. F., Synthesis and characterisation of polynorepinephrine-shelled microcapsules via an oil-in-water emulsion templating route. *J Mater Chem B* **2021**, *9* (46), 9575-9582.
120. He, Z.; Su, H.; Shen, Y.; Shi, W.; Liu, X.; Liu, Y.; Zhang, F.; Zhang, Y.; Sun, Y.; Ge, D., Poly(norepinephrine)-coated FeOOH nanoparticles as carriers of artemisinin for cancer photothermal-chemical combination therapy. *RSC Adv* **2019**, *9* (18), 9968-9982.
121. Corrigan, N.; Yeow, J.; Judzewitsch, P.; Xu, J.; Boyer, C., Seeing the Light: Advancing Materials Chemistry through Photopolymerization. *Angew Chem Int Ed Engl* **2019**, *58* (16), 5170-5189.
122. Baptista, M. S.; Cadet, J.; Di Mascio, P.; Ghogare, A. A.; Greer, A.; Hamblin, M. R.; Lorente, C.; Nunez, S. C.; Ribeiro, M. S.; Thomas, A. H.; Vignoni, M.; Yoshimura, T. M., Type I and Type II Photosensitized Oxidation Reactions: Guidelines and Mechanistic Pathways. *Photochem Photobiol* **2017**, *93* (4), 912-919.
123. Majumdar, P.; Nomula, R.; Zhao, J., Activatable triplet photosensitizers: magic bullets for targeted photodynamic therapy. *J. Mater. Chem. C* **2014**, *2* (30), 5982-5997.
124. Dougherty, T. J.; Gomer, C. J.; Henderson, B. W.; Jori, G.; Kessel, D.; Korbely, M.; Moan, J.; Peng, Q., Photodynamic therapy. *J Natl Cancer Inst* **1998**, *90* (12), 889-905.
125. Gao, J.; Chen, Z.; Li, X.; Yang, M.; Lv, J.; Li, H.; Yuan, Z., Chemiluminescence in Combination with Organic Photosensitizers: Beyond the Light Penetration Depth Limit of Photodynamic Therapy. *Int J Mol Sci* **2022**, *23* (20).
126. Dolmans, D. E.; Fukumura, D.; Jain, R. K., Photodynamic therapy for cancer. *Nat Rev Cancer* **2003**, *3* (5), 380-7.
127. Ackroyd, R.; Kelty, C.; Brown, N.; Reed, M., The history of photodetection and photodynamic therapy. *Photochem Photobiol* **2001**, *74* (5), 656-69.

128. DeRosa, M., Photosensitized singlet oxygen and its applications. *Coordination Chemistry Reviews* **2002**, 233-234, 351-371.
129. Wilkinson, F.; Helman, W. P.; Ross, A. B., Quantum Yields for the Photosensitized Formation of the Lowest Electronically Excited Singlet State of Molecular Oxygen in Solution. *Journal of Physical and Chemical Reference Data* **1993**, 22 (1), 113-262.
130. Pereira, L. S. A.; Camacho, S. A.; Malfatti-Gasperini, A. A.; Jochelavicius, K.; Nobre, T. M.; Oliveira, O. N., Jr.; Aoki, P. H. B., Evidence of photoinduced lipid hydroperoxidation in Langmuir monolayers containing Eosin Y. *Colloids Surf B Biointerfaces* **2018**, 171, 682-689.
131. Liu, G.; Hu, J.; Zhang, G.; Liu, S., Rationally Engineering Phototherapy Modules of Eosin-Conjugated Responsive Polymeric Nanocarriers via Intracellular Endocytic pH Gradients. *Bioconjug Chem* **2015**, 26 (7), 1328-38.
132. Wachowska, M.; Muchowicz, A.; Firczuk, M.; Gabrysiak, M.; Winiarska, M.; Wańczyk, M.; Bojarczuk, K.; Golab, J., Aminolevulinic Acid (ALA) as a Prodrug in Photodynamic Therapy of Cancer. *Molecules* **2011**, 16 (5), 4140-4164.
133. Beiki, D.; Eggleston, I. M.; Pourzand, C., Daylight-PDT: everything under the sun. *Biochem Soc Trans* **2022**, 50 (2), 975-985.
134. Brancalion, L.; Moseley, H., Laser and non-laser light sources for photodynamic therapy. *Lasers Med Sci* **2002**, 17 (3), 173-86.
135. Martins, W. K.; Santos, N. F.; Rocha, C. S.; Bacellar, I. O. L.; Tsubone, T. M.; Viotto, A. C.; Matsukuma, A. Y.; Abrantes, A. B. P.; Siani, P.; Dias, L. G.; Baptista, M. S., Parallel damage in mitochondria and lysosomes is an efficient way to photoinduce cell death. *Autophagy* **2019**, 15 (2), 259-279.
136. Yu, J.; Hsu, C. H.; Huang, C. C.; Chang, P. Y., Development of therapeutic Au-methylene blue nanoparticles for targeted photodynamic therapy of cervical cancer cells. *ACS Appl Mater Interfaces* **2015**, 7 (1), 432-41.
137. He, X.; Wu, X.; Wang, K.; Shi, B.; Hai, L., Methylene blue-encapsulated phosphonate-terminated silica nanoparticles for simultaneous in vivo imaging and photodynamic therapy. *Biomaterials* **2009**, 30 (29), 5601-9.
138. McNicholas, K.; MacGregor, M. N.; Gleadle, J. M., In order for the light to shine so brightly, the darkness must be present-why do cancers fluoresce with 5-aminolevulinic acid? *Br J Cancer* **2019**, 121 (8), 631-639.
139. Kofler, B.; Romani, A.; Pritz, C.; Steinbichler, T. B.; Scharfetter, V. H.; Riechelmann, H.; Dudas, J., Photodynamic Effect of Methylene Blue and Low Level Laser Radiation in Head and Neck Squamous Cell Carcinoma Cell Lines. *Int J Mol Sci* **2018**, 19 (4).
140. Dolinski, N. D.; Page, Z. A.; Discekici, E. H.; Meis, D.; Lee, I. H.; Jones, G. R.; Whitfield, R.; Pan, X.; McCarthy, B. G.; Shanmugam, S.; Kottisch, V.; Fors, B. P.; Boyer, C.; Miyake, G. M.; Matyjaszewski, K.; Haddleton, D. M.; de Alaniz, J. R.; Anastasaki, A.; Hawker, C. J., What happens in the dark? Assessing the temporal control of photo-mediated controlled radical polymerizations. *J Polym Sci A Polym Chem* **2019**, 57 (3), 268-273.
141. Zhang, L.; Wu, C.; Jung, K.; Ng, Y. H.; Boyer, C., An Oxygen Paradox: Catalytic Use of Oxygen in Radical Photopolymerization. *Angewandte Chemie* **2019**, 131 (47), 16967-16970.
142. Kabb, C. P.; O'Bryan, C. S.; Deng, C. C.; Angelini, T. E.; Sumerlin, B. S., Photoreversible Covalent Hydrogels for Soft-Matter Additive Manufacturing. *ACS Appl Mater Interfaces* **2018**, 10 (19), 16793-16801.
143. Juodkasis, S., 3D printed micro-optics. *Nature Photonics* **2016**, 10 (8), 499-501.
144. Poelma, J. E.; Fors, B. P.; Meyers, G. F.; Kramer, J. W.; Hawker, C. J., Fabrication of complex three-dimensional polymer brush nanostructures through light-mediated living radical polymerization. *Angew Chem Int Ed Engl* **2013**, 52 (27), 6844-8.

6. Appendix

6.1 Supporting information for publication „Photocontrolled Dopamine Polymerization on DNA Origami with Nanometer Resolution“



Supporting Information

Photocontrolled Dopamine Polymerization on DNA Origami with Nanometer Resolution

Pia Winterwerber, Sean Harvey, David Y. W. Ng, and Tanja Weil**

anie_201911249_sm_miscellaneous_information.pdf

Table of Contents

Experimental Procedures	p. 3
Materials and Instruments	
DNA Origami Structures	
Polydopamine Formation on DNA Origami Structures	
Switch on – Switch off	
Reactive Oxygen Species Assay (ROS Assay)	
Binding Assay	
Template Degradation	
Stability Assay	
Agarose Gel Electrophoresis (AGE)	
Atomic Force Microscopy (AFM)	
Results and Discussion	p. 5
Figure S2. AFM images of DNA origami templates before polymerization.	
Figure S3. Binding assay of protoporphyrin IX to G-quadruplex sequences.	
Figure S4. Binding specificity assay of protoporphyrin IX to different guanine-rich sequences.	
Figure S5. Proposed mechanism of polydopamine formation.	
Figure S6. Reactive oxygen assay (ROS) assay of protoporphyrin IX.	
Figure S7. Polymerization kinetics of dopamine at different pH values.	
Figure S8. Negative control of polydopamine formation in the dark.	
Figure S9. Role of the photosensitizer in the polymerization process.	
Figure S10. Investigation of the reactive oxygen species-mediated polymerization process.	
Figure S11. AFM imaging of the origami tubes after polymerization in the absence of oxygen.	
Figure S12. Agarose gel electrophoresis (AGE) of scaffold DNA, tubes before polymerization, and tubes after polymerization.	
Figure S13. Effects of polydopamine coating on structural behavior of the tubes.	
Figure S14. Degradation of the DNA template.	
Staple DNA Sequences	
References	p. 15

SUPPORTING INFORMATION

Experimental Procedures

Materials and Instruments

All solvents and chemicals were purchased from commercial sources and were used without further purification (Disodium ethylenediaminetetraacetic acid (Na_2EDTA), Sigma; Trizma® Base (TRIS), Sigma; polyethylene glycol 8000 (PEG_{8000}), Roth; protoporphyrin IX (PPIX), Sigma; dopamine hydrochloride, Sigma; Sephacryl S-400 HR, GE Healthcare; *N,N*-dimethyl-4-nitrosoaniline (RNO), Sigma; imidazole, Roth; SYBR gold, Thermo Fisher Scientific; DNA gel loading dye, Thermo Fisher Scientific). DNA staple strands, G-quadruplex extended staple strands, and folding strands were purchased from Sigma. M13mp18 plasmid DNA was synthesized according to the literature.^[1] Annealing of scaffold DNA and the respective staple strands was performed on a Bio-Rad MyCycler™ Thermal Cycler. UV/Vis and fluorescence spectroscopy were conducted on a Spark® Multimode Microplate Reader by Tecan.

DNA Origami Structures

DNA origami tiles were prepared by mixing M13mp18 Scaffold DNA (1 equiv.), staple strands (8 equiv.) and G-quadruplex extended staple strands (8 equiv.) in origami buffer (1 mM Na_2EDTA , 5 mM NaCl, 5 mM TRIS, 12 mM MgCl_2 pH 8). To form tube structures, staple strands located at the long edges of the tile were replaced by folding strands (2 equiv.), respectively. Annealing was performed by running a program from 70 °C to 20 °C over 2 hours (0.5 °C/min to 35 °C, 1 °C/min to 20 °C) and the obtained DNA origami structures were purified by PEG precipitation.^[2] Therefore, the PEG solution (15% PEG_{8000} (w/v), 5 mM TRIS, 1 mM Na_2EDTA , 505 mM NaCl) was added to the reaction solution at a volume ratio of 1:1 and centrifuged for 25 min at 12.5 rpm, room temperature (RT). The supernatant was removed and the resuspended pellet was precipitated by applying the PEG precipitation method for additional 2 times. Sample concentration was determined by Spark® 20M with Nanoquant plate™. DNA origami structures were stored in origami buffer at 4 °C.

Polydopamine Formation on DNA Origami Structures

Standard polydopamine formation on DNA origami structures was carried out in a total reaction volume of 50 μL (or 100 μL , respectively) in a UV-star 384 well plate. Stock solutions of compounds were prepared in reaction buffer (10 mM BIS-TRIS, pH 6.5) at the following concentrations: protoporphyrin IX (PPIX) at 10 μM and dopamine hydrochloride at 0.5 M. A typical reaction was conducted as follows: DNA origami with G4-sequences (10 nM, final concentration) was incubated with PPIX (1.5 equiv., relative to the amount of G4-sequences) in reaction buffer for 30–60 min. Dopamine hydrochloride (10 mM, final concentration) was added and the plate was placed on a shaker (300 rpm), in a distance of approximately 1 cm to the LED array light source (cold white LED, 4600 K–9000 K, 3.0 mW/cm², purchased from Thorlabs, Inc., see Figure S1). After a predetermined irradiation time interval, polymerization was stopped by removing the light source and polydopamine-DNA objects were purified using size exclusion chromatography (200 μL Sephacryl S-400 HR, equilibrated with reaction buffer; centrifuge settings: 2 min, 0.8 g, RT).

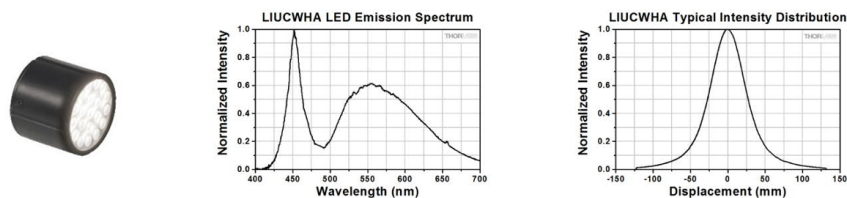


Figure S1. Cold white LED array employed in this study (left). Normalized emission spectrum of the cold white LED array (middle). Intensity distribution of the LED in the plane located 100 mm from the LED along the emission axis (right). Adapted from Manufacturer's specifications Thorlabs, Inc.

Polydopamine Formation in the Absence of Oxygen

In order to allow degassing of the system, the polymerization was conducted in 0.2 mL PCR tubes. The reaction mixture was prepared accordingly to the standard conditions. Imidazole stock solution in reaction buffer (0.5 M; adjusted to approx. pH 6.5) was applied at a final concentration of 100 mM. Oxygen was removed by gently degassing with Argon. To perform UV-Vis spectroscopy, the reaction solution was transferred to a 384 well plate, using the exact wells as the measurement before. The solutions were degassed after each measurement. After a reaction time of 180 min, work-up was conducted as described above.

Switch on – Switch off

Switch on – switch off studies were performed according to standard polydopamine formation protocol either on a shaker with 1 cm distance to the light source (irradiation phase) or in the Tecan plate reader (dark phase) for 1 h, respectively. Absorbance scans were conducted during the dark phase at $t = 0, 15, 30, 45, 60$ min. The reaction mixture was prepared in a 3.1-fold excess and split into 3 wells, whereas well 1, 2, and 3 were exposed to 1, 2, and 3 reaction cycles (1 h dark, 1 h irradiation), respectively. After each cycle, the corresponding reaction mixture was purified as described above for AFM imaging.

Reactive Oxygen Species Assay (ROS Assay)

SUPPORTING INFORMATION

Reactive oxygen species assay of PPIX was conducted in a total reaction volume of 150 μL in a 96 well plate. Wells were charged with PPIX (6.6 μM), *N,N*-dimethyl-4-nitrosoaniline (RNO, 70.7 μM) and imidazole (7.5 mM) in BIS-TRIS buffer (pH 6.5) and either exposed to visible light (cold white LED, 4600 K–9000 K, 3.0 mW/cm^2) or kept in dark. Absorbance scans from 300–500 nm were conducted at $t = 0, 30, 90, 150, 210$ min. The decrease in absorbance of RNO could be followed at 438 nm.

Binding Assay

Binding assay of PPIX and G4-sequences on DNA origami were performed in a total reaction volume of 16.6 μL in a black 384 well plate. PPIX (660 nm) in BIS-TRIS buffer (pH 6.5) was incubated with either DNA origami tile in origami buffer (10 nM) ("bound PPIX") or the same amount of blank origami buffer ("free PPIX"). Excitation wavelength was set at 420 nm and emission scans were recorded from 550–800 nm (bandwidth: 50 nm) every 5 min. Blank values were collected before PPIX addition.

Binding Specificity Assay

Binding specificity assay of PPIX and two different G-rich sequences (G4: 5'-TTTTGGGTAGGGCGGGTTGGG-3' and 12G: 5'-TTTTGAGTGCAGTGCAGTGCAGTGCAGTGC-3') was performed in a total reaction volume of 16.6 μL in a black 384 well plate. PPIX (660 nm) in BIS-TRIS buffer (pH 6.5) was incubated with DNA origami tubes in origami buffer (10 nM), bearing either a ring of G4 sequences ("Origami G4") or 12G sequences ("Origami 12G"). Excitation wavelength was set at 420 nm and emission scans were recorded from 600–800 nm (bandwidth: 20 nm) before and after addition of the origami structures.

Template Degradation

Polydopamine-coated DNA origami was added to a freshly cleaved mica substrate and incubated for 5 min to allow deposition. After selecting a suitable scanning area and taking an image, the scanner head was lifted in the z-direction. Few μL of 1 M HCl were added to the droplet of the origami buffer covering the mica surface, incubated for 5 min and the surface was approached again. Slight manual corrections in x- and y-direction were necessary to reimagine previously observed areas.

Stability Assay

Desalting of samples was achieved by spin filtering with Amicon Ultra-0.5 mL Centrifugal Filters (MWCO 100K). 1 μL of precursor DNA origami (50 nM) or 5 μL of polydopamine-coated DNA origami (approx. 10 nM) were diluted with Milli-Q water to a total volume of 100 μL and centrifuged for 20 min at 12.5 g, RT. The concentrate volume of 15 μL was then refilled up to 100 μL with Milli-Q water, centrifuged, and the procedure was repeated two more times. After 1:1 (v/v) dilution with Milli-Q water, samples were incubated at 37 °C for 4 h and applied to mica substrate for AFM imaging. Final concentration of magnesium ions was calculated as 0.2 μM , based on a dead volume after spin filtering of 15 μL .

Agarose Gel Electrophoresis (AGE)

Agarose gel electrophoresis was performed on 1% agarose gels based on 0.5 \times Tris-Borate-EDTA (TBE, diluted from 10 \times TBE buffer concentrate from Sigma-Aldrich), equipped with 8 wells. The gels were run on ReadySub-Cell GT Cells from Bio-Rad using 0.5 \times TBE buffer as the running buffer. DNA Gel Loading dye (6 \times) was used for sample preparation (approximately 50 fmol origami) with a total volume of 6 μL . Electrophoresis was conducted at 90 V for 90 minutes on ice. Gels were subsequently stained with SYBR Gold in 50 mL 0.5 \times TBE buffer for 30 min and image was taken with G:BOX Chemi Gel Doc System from Syngene.

Atomic Force Microscopy (AFM)

Atomic force microscopy was conducted in liquid state with a Bruker Dimension FastScan BioTM atomic force microscope, which was operated in PeakForce mode. AFM probes with a nominal spring constant of 0.25 Nm^{-1} (FastScan-D, Bruker) were used. Sample solution (30 μL , 1–2 nM in origami buffer) was added onto a freshly cleaved mica substrate (circular, 15 mm) and incubated for 5 min to allow deposition of the origami structures. Remaining solution was removed and 300 μL origami buffer was applied onto the mica surface, forming a droplet for measuring in liquid. Samples were scanned with scan rates between 1 and 2 Hz. Images were processed with NanoScope Analysis 1.8.

SUPPORTING INFORMATION

Results and Discussion

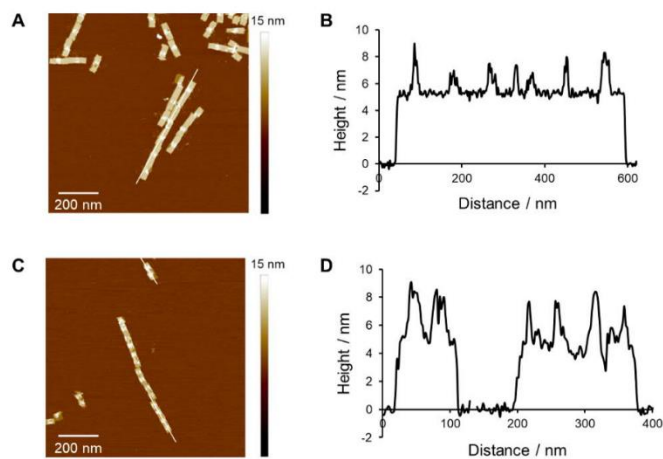


Figure S2. AFM characterization of DNA origami templates before polymerization. AFM topographic images of (A) a tube with 1 centered line of G-quadruplex (G4) sequences (tube I) and the corresponding height profile (B), and (C) a tube with 2 lines of G4 sequences (tube II) and the corresponding height profile (D).

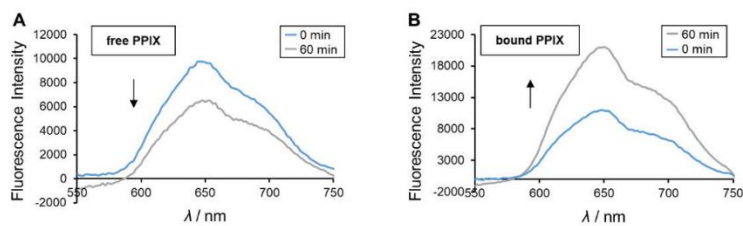


Figure S3. Binding assay of protoporphyrin IX to G-quadruplex sequences. Fluorescence intensity of protoporphyrin IX (PPIX) as (A) "free PPIX" and (B) "PPIX bound" to G-quadruplex sequences within the DNA origami framework. Upon binding, fluorescence significantly increases over time (60 min), whereas fluorescence of free PPIX in solution decreases. Spectra are blank-corrected.

SUPPORTING INFORMATION

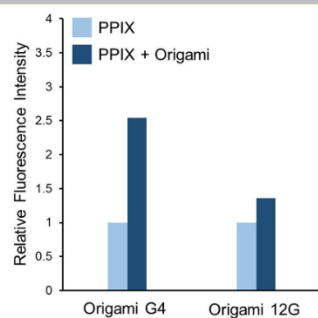


Figure S4. Binding specificity assay of protoporphyrin IX to different guanine-rich sequences. Upon addition of origami tubes bearing either G4 sequences ("Origami G4") or origami tubes with an alternately organized G-rich sequence ("Origami 12G"), only the fluorescence of the Origami G4-treated photosensitizer significantly increases, demonstrating a specific binding event.

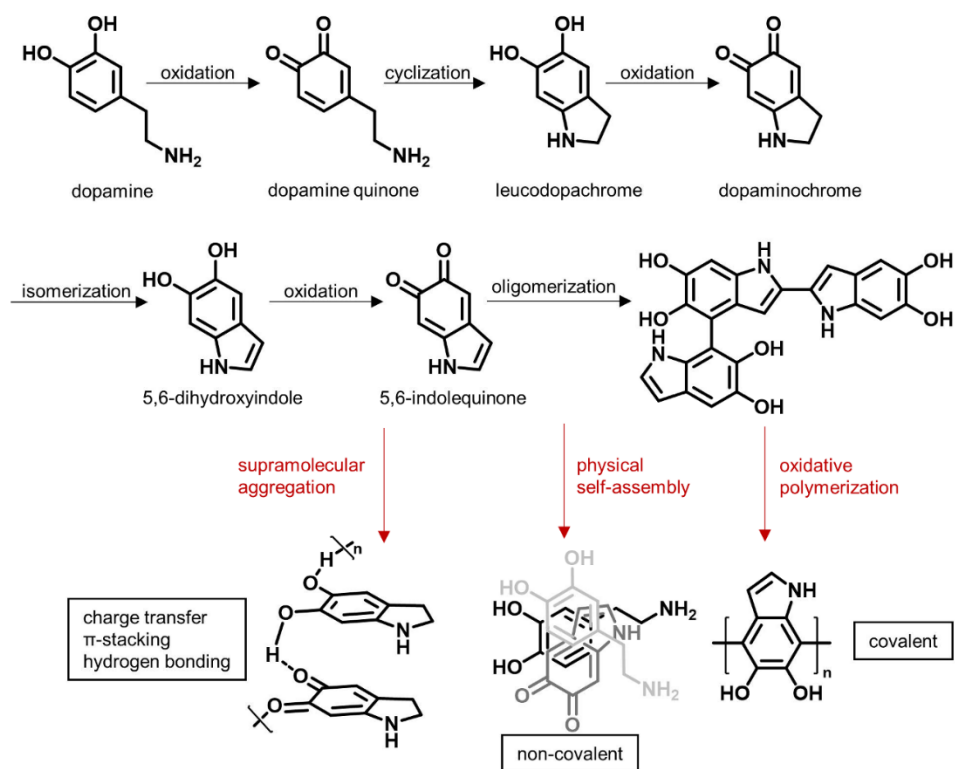


Figure S5. Proposed mechanism of polydopamine formation. After several oxidation steps, cyclization and isomerization, different pathways are suggested to contribute to the complex and many-faceted structure of polydopamine. Apart from covalent interactions generating oligomers and polymers, physical self-assembly and supramolecular aggregation based on charge transfer, π -stacking and hydrogen bonding are determining the polymer's structure. For reason of clarity and simplicity, only the main representative examples are depicted.^[3]

SUPPORTING INFORMATION

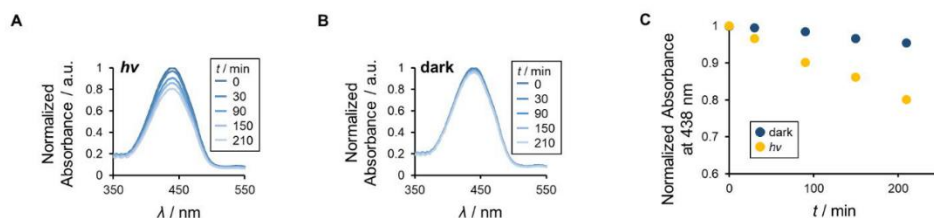


Figure S6. Reactive oxygen species (ROS) assay of protoporphyrin IX (PPIX). Singlet oxygen generated by PPIX upon irradiation with visible light reacts with imidazole and bleaches *N,N*-dimethyl-4-nitrosoaniline (RNO) through oxidation (A), while no reaction occurs in the absence of light (B). Absorbance of RNO was followed at 438 nm (C).

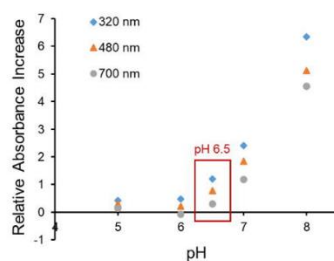


Figure S7. Polymerization kinetics of dopamine at different pH values. For pH studies, the following buffers were employed: pH 5: acetate buffer 10 mM, pH 6 and pH 7: phosphate buffer 10 mM, pH 6.5: BIS-TRIS buffer 10 mM, and pH 8: TRIS buffer 5 mM. Data collected at $t = 120$ min.

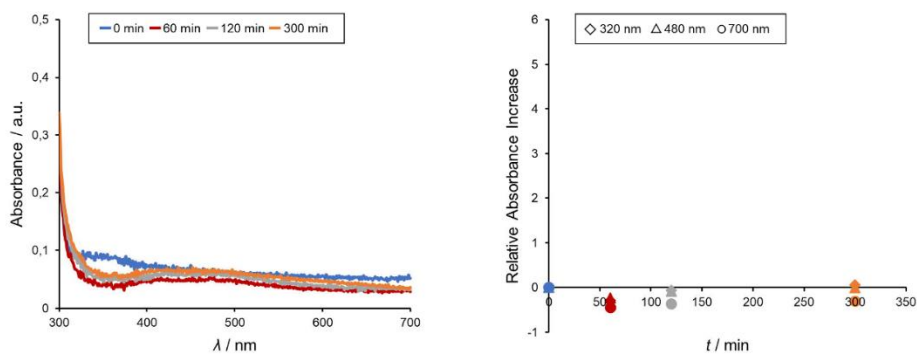


Figure S8. Negative control of polydopamine formation in the dark. UV-Vis spectroscopy of polydopamine formation on DNA origami tiles in BIS-TRIS buffer at pH 6.5 in the absence of light. Neither dopaminochrome, nor oligomer or polymer formation could be detected under these conditions.

SUPPORTING INFORMATION

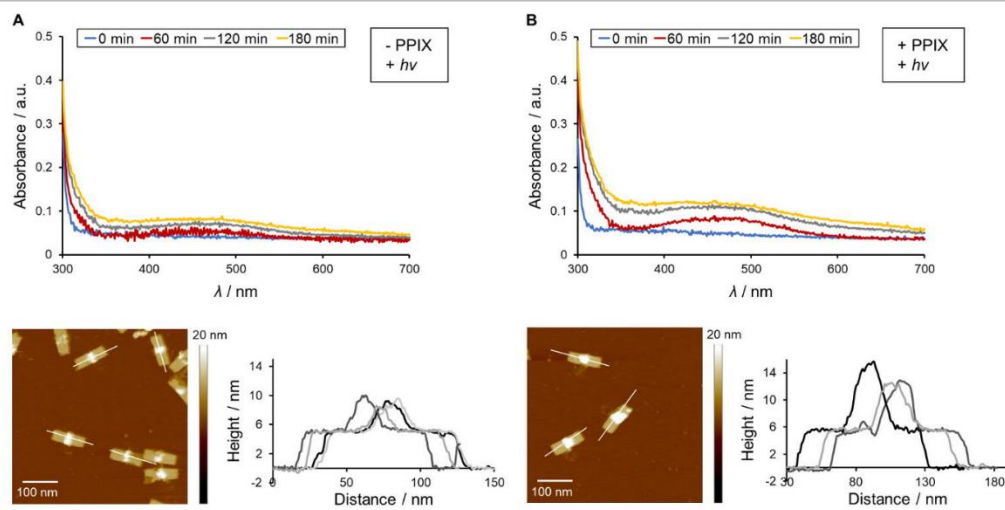


Figure S9 Role of the photosensitizer in the polymerization process. (A) Without protoporphyrin IX (PPIX), no polymerization takes place upon the irradiation with visible light, as visualized by UV/Vis spectroscopy and AFM. (B) Upon the embedding of PPIX and illumination, polydopamine formation is observed.

SUPPORTING INFORMATION

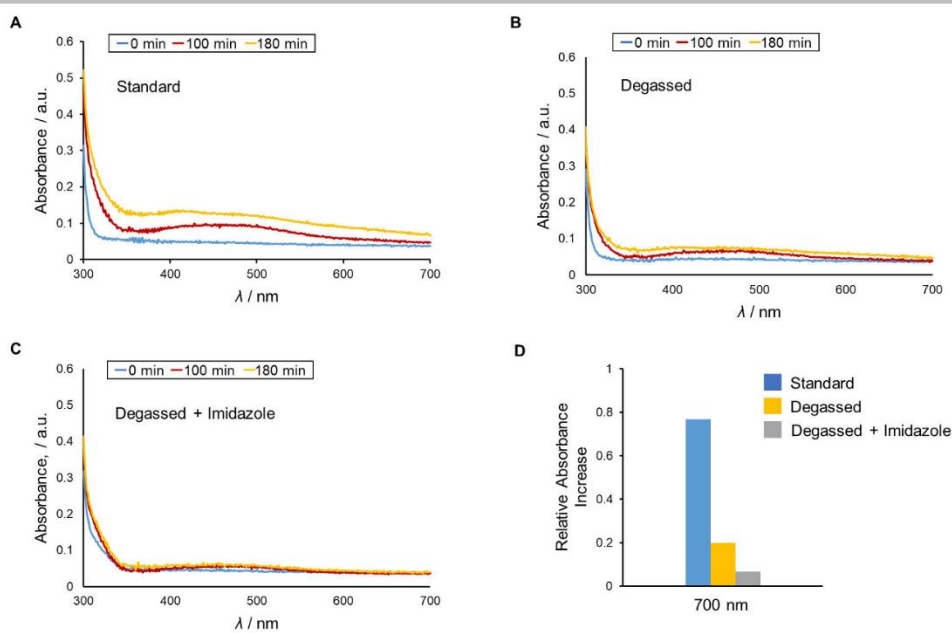


Figure S10. Investigation of the reactive oxygen species-mediated polymerization process under (A) standard conditions, (B) in the absence oxygen and (C) in the absence of oxygen but in the presence of imidazole as a scavenger, visualized by UV-Vis spectroscopy. Thereby, the formation of polydopamine is significantly suppressed (D).

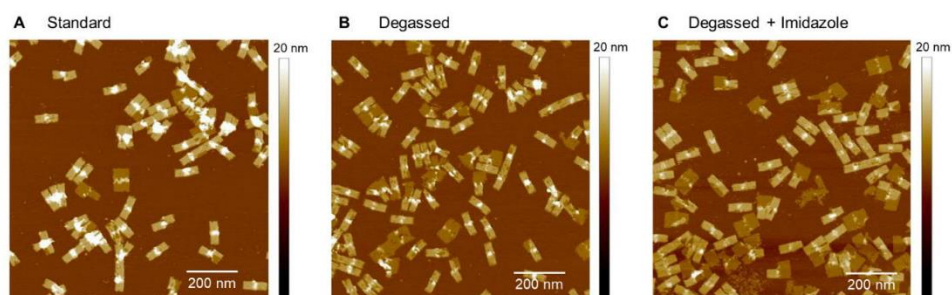


Figure S11. AFM imaging of the origami tubes after reaction under (A) standard, (B) degassed and (C) degassed and imidazole-added conditions also show a suppression of polydopamine formation in the absence of oxygen.

SUPPORTING INFORMATION

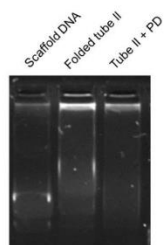


Figure S12. Agarose gel electrophoresis (AGE) of scaffold DNA, tubes before polymerization, and tubes after polymerization. Lanes were charged with scaffold DNA, folded origami tube II before polymerization, and polydopamine-coated tube II after polymerization. A shift in molecular weight upon folding is observed. Upon polydopamine-coating, migration of the polymer-DNA hybrid materials is completely suppressed. For reason of clarity, excess staples in the low molecular weight region are not shown.

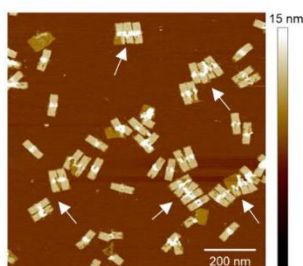


Figure S13. Effects of polydopamine coating on structural behavior of the tubes. Due to the adhesiveness of polydopamine, tubes stick to each other, forming higher-ordered domains.

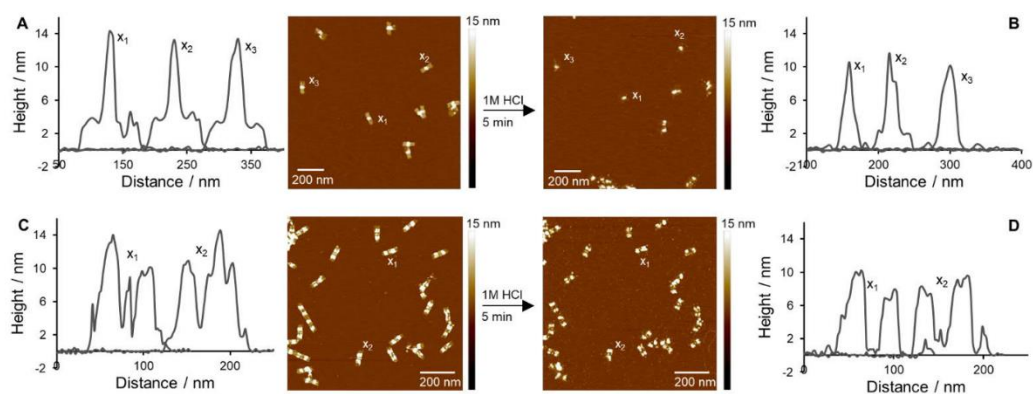


Figure S14. Degradation of the DNA template. Treatment of the polydopamine-coated origami tube I (A) and tube II (C) with hydrochloric acid during AFM measurements. Upon the addition of acid, the DNA template is degraded, liberating the polydopamine structures (B+D).

SUPPORTING INFORMATION

Staple DNA Sequences

DNA origami structures were synthesized together with M13mp18 Scaffold DNA according to the following protocol. For G-quadruplex extended staple strands (G4 staple strands), the sequence of the corresponding staple strand is extended at the 3' end by 5'-TTTTGGGTAGGCGGGTTGGG-3'.

Tile: G4 strands on positions 29, 30, 31–40, 41–50, 53–60, 61–70, 71–74; staple strands on remaining positions

Tube I: G4 strands on positions 2–10, 11–20, 21–24, 26, 112–120, 121–130, 131; folding strands on positions 1, 25, 27, 28, 51, 52, 75, 76, 99, 100, 111, 132, 133, 156, 157, 180, 181, 204, 205, 216; staple strands on remaining positions

Tube II: G4 strands on positions 29, 30, 31–40, 41–50, 53–60, 61–70, 71–74, 134–140, 141–150, 151–155, 158–160, 161–170, 171–179; folding strands on positions 1, 25, 27, 28, 51, 52, 75, 76, 99, 100, 111, 132, 133, 156, 157, 180, 181, 204, 205, 216; staple strands on remaining positions

Table S1. Sequences of staple strands and folding strands.

Position	Sequence 5' → 3'
1	CAAGCCCAATAGGAACCCATGTACAAACAGTT
2	AATGCCCGTAACAGTGCCCGTATCTCCCTCA
3	TGCCTTGACTGCCTATTTTCGGAACAGGGATAG
4	GAGCCGCCACCACCGGAACCGCGACGGAAA
5	AACCAGAGACCCCTCAGAACCGCCAGGGTCTAG
6	TTATTCATAGGGAAGGTAATATTCATTCAGT
7	CATAACCCGAGGCATAGTAAGAGCTTTTTAAG
8	ATTGAGGGTAAAGGTGAATTATCAATCACCGG
9	AAAAGTAATATCTTACCGAAGCCCTCCAGAG
10	GCAATAGCGCAGATAGCCGAACAATCAACCG
11	CCTAATTTACGCTAACGAGCGCTAATCAATA
12	TCTTACCAGCCAGTTACAAAAATAAATGAAATA
13	ATCGGCTGCGAGCATGTAGAAACCTATCATAT
14	CTAATTTATCTTTCCTTATCATTATCCTGAA
15	GCGTTATAGAAAAAGCCTGTTTAGAAGGCCGG
16	GCTCATTTTCGCATTAATTTTTGAGCTTAGA
17	AATTAATAAAATTTTACCAGTAATCCCATC
18	TTAAGACGTTGAAAACATAGCGATAACAGTAC
19	TAGAAATCCCTGAGAAGAGTCAATAGGAATCAT
20	CTTTTACACAGATGAATATACAGTAACAATT
21	TTTAACGTTCCGGGAGAAACAATAATTTCCCT
22	CGACAACCTAAGTATTAGACTTTACAATACCGA
23	GGATTTAGCGTATTAATCCTTTGTTTTTCAGG
24	ACGAACCAAAACATCGCCATTAATGTTGGTT
25	GAACGTGGCGAGAAAGGAAGGAACAACACTAT
26	TAGCCCTACCAGCAGAAGATAAAAACATTTGA
27	CGGCCTGCTGGTAAATCCAGAACGAACCTGA
28	CTCAGAGCCACCACCTCATTTTCTTATTATT
29	CTGAAACAGGTAATAAGTTTTAACCCCTCAGA
30	AGTGTAATGAAAAGTATAAGAGGCCGCCACC
31	GCCACCCTCTTTTCATAATCAAACCGTCACC
32	GTTTGCCACCTCAGAGCCGCCACCGATACAGG
33	GACTTGAGAGACAAAAGGGCGACAAGTTACCA
34	AGCGCAACCATTTGGGAATTAGATTATTAGC
35	GAAGGAAAATAAGAGCAAGAAACAACAGCCAT
36	GCCCAATACCGAGGAAACGCAATAGGTTTACC
37	ATTATTTAACCCAGCTACAATTTTCAAGAACG
38	TATTTTGCTCCCAATCCAAATAAGTGAGTTAA
39	GGTATTAAGAACAAGAAAAATAATTAAGGCCA
40	TAAGTCTTACCAAGTACCGCACTCTTAGTTGC
41	ACGCTCAAAAATAAGAATAAACACCGTGAATTT
42	AGGCGTTACAGTAGGGCTTAATTGACAATAGA
43	ATCAAAATCGTCGCTATTAATTAACGGATTTCG

SUPPORTING INFORMATION

44	CTGTAATCATAGGTCTGAGAGACGATAAATA
45	CCTGATTGAAAGAAATTGCGTAGACCCGAACG
46	ACAGAAATCTTTGAATACCAAGTTCCCTTGCTT
47	TTATTAATGCCGTCAATAGATAATCAGAGGTG
48	AGATTAGATTTAAAAGTTTGAGTACACGTAAT
49	AGGCGGTCAATTAGTCTTTAATGCGCAATATTA
50	GAATGGCTAGTATTAACACCCGCTCAACTAAT
51	CCGCCAGCCATTGCAACAGGAAAAATATTTTT
52	CCCTCAGAACCGCCACCCTCAGAAGTACGACT
53	CCTCAAGAATACATGGCTTTTATAGAACCCAC
54	TAAGCGTCGAAGGATTAGGATTAGTACCGCCA
55	CACCAGAGTTCGGTCATAGCCCCGCGCAGCAA
56	TCGGCATTCCGCCGCGCAGCATTGACGTTCCAG
57	AATCACCAAATAGAAAATTCATATATAACGGA
58	TCACAATCGTAGCACCATTACCATCGTTTTCA
59	ATACCAAGATAACCCACAAGATAAACGATT
60	ATCAGAGAAAGAAGTGGCATGATTTTATTTTG
61	TTTTGTTTAAAGCCTTAAATCAAGAATCGAGAA
62	AGGTTTTGAACGTCAAAAATGAAAGCGCTAAT
63	CAAGCAAGACGCGCCTGTTTATCAAGAATCGC
64	AATGCAGACCGTTTTTATTTTCATCTTGCGGG
65	CATATTTAGAAAATACCGACCGTGTACCTTTT
66	AATGGTTTACAACGCCAACATGTAGTTCAGCT
67	TAACCTCCATATGTGAGTGAATAAACAAAATC
68	AAATCAATGGCTTAGGTTGGGTTACTAAATTT
69	GCGCAGAGATATCAAAAATTTTACATTATC
70	AACCTACCGCAATTAATTCATTCCAGTACAT
71	ATTTTGCCTTTTAGGAGCACTAAGCAACAGT
72	CTAAAATAGAACAAGAACCACCGGGTTAG
73	GCCACGCTATACGTGGCACAGACAACGCTCAT
74	GCGTAAGAGAGAGCCAGCAGCAAAAAGTTAT
75	GGAAATACCTACATTTTACGCTCACCTGAAA
76	TATCACCGTACTCAGGAGGTTTAGCGGGGTTT
77	TGCTCAGTCAGTCTCTGAATTTACCAGGAGGT
78	GGAAAGCGACCAGGCGGATAAGTGAATAGGTG
79	TGAGGCAGGCGTCAGACTGTAGCGTAGCAAGG
80	TGCCTTTAGTCAGACGATTGGCCTGCCAGAAT
81	CCGAAAACACACCACGGAATAAGTAAGACTCC
82	ACGCAAAGGTCACCAATGAAACCAATCAAGTT
83	TTATTACGGTCAGAGGGTAATTGAATAGCAGC
84	TGAACAACAGTATGTTAGCAAATAAAAGAA
85	CTTTACAGTTAGCGAACCTCCCAGCTAGGAA
86	GAGGCGTTAGAGAATAACATAAAAGAACCCC
87	TCATTACCCGACAATAAACAACATATTTAGGC
88	CCAGACGAGCGCCAATAGCAAGCAAGAACGC
89	AGAGGCATAATTTTCATCTTCTGACTATAACTA
90	TTTTAGTTTTTCGAGCCAGTAATAAATCTGT
91	TATGTAACCTTTTTTAAATGGAAAAATACCT
92	TTGAATTATGCTGATGCAAATCCACAATATA
93	GAGCAAAAACCTTCTGAATAATGGAAGAAGGAG
94	TGGATTATGAAGATGATGAAACAAAATTTTCAT
95	CGGAATTATTGAAAGGAATTGAGGTGAAAAAT
96	ATCAACAGTCATCATATTTCTGATTGATTGTT
97	CTAAAGCAAGATAGAACCCTTCTGAATCGTCT
98	GCCAACAGTCACCTTGCTGAACCTGTTGGCAA
99	GAAATGGATTATTTACATTGGCAGACATTCTG
100	TTTTTATAAGTATAGCCCGCCGTCGAG
101	AGGGTTGATTTTATAAATCCTCATTAAATGATATTC
102	ACAAAACAATTTAATCAGTAGCGACAGATCGATAGC

SUPPORTING INFORMATION

103	AGCACCGTTTTTAAAGGTGGCAACATAGTAGAAAA
104	TACATACATTTTGACGGGAGAATTAACACAGGGAA
105	GCGCATTATTTTGCTTATCCGGTATTCTAAATCAGA
106	TATAGAAAGTTTCGACAAAAGGTAAAGTAGAGAATA
107	TAAAGTACTTTTCGCGAGAAAACCTTTTTATCGCAAG
108	ACAAAGAATTTTATTAATTACATTTAACACATCAAG
109	AAAACAATTTTTTCATCAATATAATCCTATCAGAT
110	GATGGCAATTTTAATCAATATCTGGTCACAAATATC
111	AAACCTCTTTTACCAGTAATAAAAGGGATTCCACAGTCACACGTTTT
112	CCGAAATCCGAAATCCTGTTTGAAGCCGGAA
113	CCAGCAGGGGCAAAATCCCTTATAAAGCCGGC
114	GCATAAAGTTCACACAACATACGAAGCGCCA
115	GCTCACAATGTAAGCCTGGGGTGGGTTTGCC
116	TTCGCCATTGCCGAAACCAGGCATTAATCA
117	GCTTCTGGTCAGGCTGCGCAACTGTGTTATCC
118	GTAAAATTTTAAACCAATAGGAACCCGGCACC
119	AGACAGTCATTCAAAAGGGTGAGAAGCTATAT
120	AGGTAAAGAAATCACCATCAATATAATATTTT
121	TTTCATTTGGTCAATAACCTGTTTATATCGCG
122	TCGCAATGGGGCGCGAGCTGAATAATGTGT
123	TTTTAATTGCCGAAAGACTTCAAAACACTAT
124	AAGAGGAACGAGCTTCAAGCGAAGATACATT
125	GGAATTACTCGTTTACCAGACGACAAAAGATT
126	GAATAAGGACGTAACAAAGCTGCTCTAAAACA
127	CCAATCACTTGCCTGACGAGAAGCCTAAAA
128	CTCATCTTGAGGCAAAAGAATACAGTGAATTT
129	AAACGAAATGACCCCGAGGATTATTATTAC
130	CTTAAACATCAGCTTGCTTTCGAGCGTAACAC
131	TCGGTTTAGCTTGATACCGATAGTCCAACCTA
132	TGAGTTTCGTACCAGTACAACTTAATTGTA
133	CCCCGATTTAGAGCTTGACGGGAAATCAAAA
134	GAATAGCCGCAAGCGGTCCACGCTCCTAATGA
135	GAGTTGCACGAGATAGGGTTGAGTAAGGGAGC
136	GTGAGCTAGTTTCTGTGTGAAATTTGGGAAG
137	TCATAGCTACTCACATTAATTGCGCCTGAGA
138	GGCGATCGCACTCCAGCCAGCTTGCATCAAA
139	GAAGATCGGTGCGGGCCTTTCGCAATCATGG
140	AAATAATTTAAATTGTAAACGTTGATATTCA
141	GCAAATATCGCTCTGGCCTTCTGGCCTCAG
142	ACCGTTCTAAATGCAATGCCTGAGAGGTGGCA
143	TATATTTTAGCTGATAAATTAATGTTGTATAA
144	TCAATCTTTTAGTTTGACCATACCAGACCG
145	CGAGTAGAACTAATAGTAGTAGCAAACCTCA
146	GAAGCAAAAAGCGGATTGCATCAGATAAAAA
147	TCAGAAGCCTCCAACAGGTCAGGATCTGCGAA
148	CCAAAATATAATGCAGATACATAAACACCAGA
149	CATTCACGCGAGAGGCTTTTGCATATTATAG
150	ACGAGTAGTGACAAGAACCAGATATACCAAGC
151	AGTAATCTTAAATTGGGCTTGAGAGAATACCA
152	GCGAAACATGCCACTACGAAGGCATGCGCCGA
153	ATACGTAAAAGTACAACGGAGATTTTCATCAAG
154	CAATGACACTCCAAAAGGAGCCTTACAACGCC
155	AAAAAAGGACAACCATCGCCACGCGGGTAAA
156	TGTAGCATTCCACAGACAGCCCTCATCTCCAA
157	GTAAAGCACTAAATCGGAACCTAGTTGTTCC
158	AGTTTGGAGCCCTTACCAGCCTGGTTGCGCTC
159	AGCTGATTACAAGAGTCCACTATTGAGGTGCC
160	ACTGCCCGCGAGCTCGAATTCGTTATTACGC
161	CCCGGTACTTTCCAGTCGGGAAACGGGCAAC

SUPPORTING INFORMATION

162	CAGCTGGCGGACGACGACAGTATCGTAGCCAG
163	GTTTGAGGAAAAGGGGATGTGCTAGAGGATC
164	CTTTCATCCCCAAAAACAGGAAGACCGGAGAG
165	AGAAAAGCAACATTAATGTGAGCATCTGCCA
166	GGTAGCTAGGATAAAAAATTTTAGTTAACATC
167	CAACGCAATTTTTGAGAGATCTACTGATAATC
168	CAATAAATACAGTTGATTCCCAATTTAGAGAG
169	TCCATATACATACAGGCAAGGCAACTTTATTT
170	TACCTTTAAGGCTTTTACCCTGACAAAGAAGT
171	CAAAAATCATTGCTCCTTTTGATAAGTTTCAT
172	TTTGCCAGATCAGTTGAGATTTAGTGGTTTAA
173	AAAGATTCAGGGGTAATAGTAAACCATAAAT
174	TTTCAACTATAGGCTGGCTGACCTTGATCAT
175	CCAGGCGCTTAATCATTGTGAATTACAGGTAG
176	CGCCTGATGGAAGTTCCATTAACATAACCG
177	TTTCATGAAAATTTGTGCGAAATCTGTACAGA
178	ATATATTCCTTTTTCACGTTGAAAATAGTTAG
179	AATAATAAGGTCGCTGAGGCTTGCAAAGACTT
180	CGTAACGATCTAAAGTTTTGTCGTGAATTGCG
181	ACCCAAATCAAGTTTTTGGGGTCAAAGAACG
182	TGGACTCCCTTTTACCAGTGAGACCTGTGCT
183	TGGTTTTAACGTCAAAGGGCGAAGAACCATC
184	GCCAGCTGCCTGCAGGTGACTCTGCAAGGCG
185	CTTGATGCAATTAATGAATCGGCCCGCCAGGG
186	ATTAAGTTCGCATCGTAACCGTGCGAGTAACA
187	TAGATGGGGGTAAACGCCAGGGTTGTCCAAG
188	ACCCGTCGTCATATGTACCCCGGTAAGGCTA
189	CATGTCAAGATTCTCCGTGGGAACCGTTGGTG
190	TCAGGTCACTTTTGCGGGAGAAGCAGAATTAG
191	CTGTAATATTGCCTGAGAGTCTGAAAACTAG
192	CAAAATTAAGTACGGTGTCTGGAAGAGGTCA
193	TGCAACTAAGCAATAAAGCCTCAGTTATGACC
194	TTTTTGCGCAGAAAACGAGAATGAATGTTTAG
195	AAACAGTTGATGGCTTAGAGCTTATTTAAATA
196	ACTGGATAACGGAAACAATATTACCTTATG
197	ACGAACTAGCGTCCAATACTGCGGAATGCTTT
198	CGATTTTAGAGGACAGATGAACGGCGCGACCT
199	CTTTGAAAAGAACTGGCTCATTATTTAATAAA
200	GCTCCATGAGAGGCTTTGAGGACTAGGGAGTT
201	ACGGCTACTTACTTAGCCGGAACGCTGACCAA
202	AAAGGCCGAAAGGAACAATAAGCTTTCCAG
203	GAGAATAGCTTTTGC GGATCGTCGGGTAGCA
204	ACGTTAGTAAATGAATTTCTGTAAGCGGAGT
205	TTTTCGATGGCCCACTACGTAAACCGTC
206	TATCAGGGTTTTCGTTTTGCGTATTGGGAACGCGCG
207	GGGAGAGTTTTTTGTA AACGACGGCCATTTCCAGT
208	CACGACGTTTTTGTAATGGGATAGGTCAAAACGGCG
209	GATTGACCTTTTGATGAACGGTAATCGTAGCAAACA
210	AGAGAATCTTTTGGTTGTACCAAAAACAAGCATAAA
211	GCTAAATCTTTTCTGTAGCTCAACATGTATTGCTGA
212	ATATAATGTTTTTATTGAATCCCCCTCAAATCGTCA
213	TAAATATTTTTTGGGAAGAAAACTACGACCAGTCA
214	GGACGTTGTTTTTATAAGGGAACCGAAAGGCGCAG
215	ACGGTCAATTTTGACAGCATCGGAACGAACCCCTCAG
216	CAGCGAAAATTTTACTTTCAACAGTTTTCTGGGATTTTGCTAAACTTTT
217	AACATCACTTGCCTGAGTAGAAGAACT
218	TGTAGCAATACTTCTTTGATTAGTAAT
219	AGTCTGTCCATCACGCAAAATTAACCGT
220	ATAATCAGTGAGGCCACCGAGTAAAAG

SUPPORTING INFORMATION

221	ACGCCAGAATCCTGAGAAGTGTITTT
222	TTAAAGGGATTTTAGACAGGAACGGT
223	AGAGCGGGAGCTAACAGGAGGCCGA
224	TATAACGTGCTTTCCTCGTTAGAATC
225	GTAATGTTGCTTTGACGAGCACG
226	GCGCTTAATGCGCCGCTACAGGGCGC
F1	CGGCCTTGATAGGAACCCATGTACAAACAGTT
F25	TGAGTTTCCGAGAAAGGAAGGGAACAACTAT
F27	CAAGCCCACTGGTAATATCCAGAACGAACTGA
F28	CCGCCAGCCACCACCCCTCATTTTCTATTATT
F51	CTCAGAGCCATTGCAACAGGAAAAATATTTTT
F52	GGAAATACACCGCCACCCCTCAGAAGTACGACT
F75	CCCTCAGACTACATTTTGACGCTCACCTGAAA
F76	GAAATGGATACTCAGGAGTTTAGCGGGGTTT
F99	TATCACCGTTATTTACATTGGCAGACATTCTG
F132	GAACGTGGGTACCAGTACAACTTAATTGTA
F133	TGTAGCATTAGAGCTTGACGGGAAATCAAAA
F156	CCCCGATTTCCACAGACAGCCCTCATCTCCAA
F157	CGTAACGACTAAATCGGAACCCTAGTTGTCC
F180	GTAAGCATCTAAAGTTTGTGCGTAATTGCG
F181	ACGTTAGTCAAGTTTTTGGGGTCAAAGAACG
F204	ACCCAAATAAATGAATTTCTGTAAGCGGAGT
F100	GTCACACGTTTTTATAAGTATAGCCCGCCGTCGAG
F205	TGCTAAACTTTTTCGATGGCCCACTACGTAACCGTC
N-111	AAACCCTTTTTACCAGTAATAAAAGGATTACCA
N-216	CAGCGAAATTTAACTTTCAACAGTTTCTGGGATT

References

- [1] G. Bellot, M. A. McClintock, J. J. Chou, W. M. Shih, *Nat. Protoc.* **2013**, 8, 755-770.
 [2] E. Stahl, T. G. Martin, F. Praetorius, H. Dietz, *Angew. Chem. Int. Ed.* **2014**, 53, 12735-12740.
 [3] a) H. Lee, S. M. Dellatore, W. M. Miller, P. B. Messersmith, *Science* **2007**, 318, 426-430; b) D. R. Dreyer, D. J. Miller, B. D. Freeman, D. R. Paul, C. W. Bielawski, *Langmuir* **2012**, 28, 6426-6435; c) S. Hong, Y. S. Na, S. Choi, I. T. Song, W. Y. Kim, H. Lee, *Adv. Funct. Mater.* **2012**, 22, 4711-4717.

Author Contributions

P. W. conducted all the experiments and analysis assisted by S. H. on the experimental design. The project was supervised by D.Y.W.N. and T.W. All authors contributed to writing the manuscript.

6.2 Supporting information for publication „Multiple Wavelength Photopolymerization of Stable Poly(Catecholamines)-DNA Origami Nanostructures“



Supporting Information

Multiple Wavelength Photopolymerization of Stable Poly(Catecholamines)-DNA Origami Nanostructures

P. Winterwerber, C. J. Whitfield, D. Y. W. Ng, T. Weil**

SUPPORTING INFORMATION

Table of Contents

Experimental Procedures	p. 2
Materials and Instruments	
DNA origami nanostructures	
Standard photopolymerization on DNA origami tubes	
Two-step photopolymerization on DNA origami tubes	
Reactive Oxygen Species Assay (ROS Assay)	
Cell culture	
Cell experiments	
Cell uptake	
Cell colocalization	
Cell medium stability assay	
DNase I digestion assay	
Confocal laser scanning microscopy	
Atomic Force Microscopy	
Agarose gel electrophoresis	
DNA extraction from agarose gel	
Dynamic light scattering (DLS)	
Results and Discussion	p. 4
SI Figure 1 Photopolymerization of DA with PPIX-G4 at 410 nm and 625 nm.	
SI Figure 2 Proposed mechanism for pDA and pNE formation.	
SI Figure 3 Reactive oxygen assay (ROS) assay of PPIX, MB, and EY.	
SI Figure 4 Photopolymerization of DA with EY-G4 at 525 nm and MB-G4 at 625 nm.	
SI Figure 5 DNA origami tube with a diagonal G4 pattern.	
SI Figure 6 Aggregation of pDA-ringed DNA origami tubes.	
SI Figure 7 Photopolymerization of NE with PPIX-G4 at 410 nm, EY-G4 at 525 nm, and MB-G4 at 625 nm.	
SI Figure 8 Dynamic light scattering analysis of bare and pNE-origami for 3 days.	
SI Figure 9 Agarose gel electrophoresis of DNA origami tubes before and after polymerization.	
SI Figure 10 Stepwise layer-by-layer polymerization of NE and DA.	
SI Figure 11 Control experiments for layer-by-layer polymerization.	
SI Figure 12 Activity and dormancy of EY and MB at opposite wavelengths.	
SI Figure 13 Ring-by-ring polymerization of pDA.	
SI Figure 14 Control experiments for ring-by-ring polymerization.	
SI Figure 15 Cell medium stability assay of bare and polymer-ringed origami tubes.	
SI Figure 16 Fluorescence calibration curve for cell uptake studies.	
SI Figure 17 Cellular uptake of DNA origami structures labelled with Alexa647.	
SI Figure 18 Co-localization cell studies and DNase I assay.	
SI Figure 19 Characterization of dual labelled origami structures for cell uptake studies.	
SI Figure 21 Confocal z-stack analysis of pNE-origami cell uptake studies.	
Appendix	p. 18
DNA sequences and patterns	
References	p. 22

SUPPORTING INFORMATION

Experimental Procedures

Materials and instruments

All solvents and chemicals were purchased from commercial sources and were used without further purification. DNA oligonucleotides (staple strands, sticky strands, G4 staple strands, G4-complementary strands, and folding strands) were purchased from Sigma-Aldrich. M13mp18 plasmid DNA was purchased from tilibit nanosystems. Annealing of DNA origami structures and hybridizing of sticky sequences was performed on a Bio-Rad MyCycler™ Thermal Cycler. UV/Vis and fluorescence spectroscopy were conducted on a Spark® Multimode Microplate Reader by Tecan. Buffers were adjusted on a Mettler Toledo SevenExcellence™ equipped with the InLab Nano pH electrode. Photopolymerizations were conducted in a house-built photobox that is equipped with interchangeable LED-arrays (96 LEDs) of 410 nm, 525 nm, and 625 nm.

DNA origami nanostructures

DNA origami tubes were prepared by mixing M13mp18 Scaffold DNA (1 equiv.), staple strands (8 equiv.), G4 staple strands (8 equiv.), stickyA strands (8 equiv., if necessary), and folding strands (16 equiv.) in origami buffer (1 mM Na₂EDTA, 5 mM NaCl, 5 mM TRIS, 12 mM MgCl₂, pH 8). Annealing was performed by running a program from 70 °C to 20 °C over 2 h (0.5 °C/min to 35 °C, 1 °C/min to 20 °C) and the obtained DNA origami structures were purified by PEG precipitation.^[1] Therefore, the PEG solution (15% PEG₈₀₀₀ (w/v), 5 mM TRIS, 1 mM Na₂EDTA, 505 mM NaCl) was added to the reaction solution at a volume ratio of 1:1 and centrifuged for 25 min at 12.5 rpm, room temperature (RT). The supernatant was removed, and the resuspended pellet was precipitated by applying the PEG precipitation method for additional two times. Sample concentration was determined by Spark® 20M with Nanoquant plate™. DNA origami structures were stored in origami buffer at 4 °C.

Standard photopolymerization on DNA origami tubes

Standard photopolymerization on DNA origami tubes (44x G4 catalytic centers per tube) was carried out in a total reaction volume of 50 µL in a UV-star 384 well plate. Stock solutions of compounds were prepared in reaction buffer (10 mM BIS-TRIS, pH 6.5) at the following concentrations: photosensitizers (PS) at 10 µM; monomers at 0.5 M. A typical reaction was conducted as follows: DNA origami with G4-sequences (10 nM, final concentration) was incubated with PS (1.5 equiv., relative to the amount of G4-sequences) in reaction buffer for 30–60 min. Monomer (10 mM, final concentration) was added and the plate was placed in a house-built photobox. After a predetermined irradiation time interval, polymerization was stopped by switching off the light source and polymer-DNA objects were purified using size exclusion chromatography (200 µL Sephacryl S-400 HR, equilibrated with reaction buffer; centrifuge settings: 2 min, 0.8 g, RT) or 100K spin filtration (5 g, 10 min, 2 times; recovered at 1 g, 2 min). For purification steps, a mixture of origami buffer and reaction buffer ratio (1:4) was utilized.

Two-step photopolymerization on DNA origami tubes

Layer-by-layer polymerization: DNA origami tubes were equipped with one ring of G4 sequences (44 sequences) and incubated with MB under standard conditions (see above) for 30 min. NE was added and the reaction solution was subjected to standard polymerization conditions at 625 nm for 2 h. After 100K spin filtering, DA was added and irradiated for 2 h at 625 nm. Polymer-ringed origami tubes were recovered by 100K spin filtering and stored at 4 °C.

Ring-by-ring polymerizations: DNA origami tubes were equipped with one ring of G4 sequences and one ring of stickyA sequences (44 sequences each). Methylene blue was incubated with G4 sequences on origami tubes in an 1.5 molar excess (related to the amount of G4 sequences) for 30 min. Eosin Y was preloaded into G4 complementary strands in an 1.5 molar excess for 30 min and either annealed with MB-loaded origami tubes before photopolymerization or after the first irradiation phase. Hybridizing of EY-G4 strands (1.5 equiv. compared to stickyA sequences on DNA origami tubes) was performed by a temperature ramp from 35 °C to 20 ° in 5 °C steps (holding each step for 15–30 min). After annealing, excess staple strands were removed by 100K spin filtering. For continuous photopolymerization, MB- and EY-loaded tubes were incubated with DA (standard polymerization conditions, see above) and irradiated at 625 nm and 525 nm for 3 h each. For decoupled photopolymerization, MB-loaded tubes were incubated with NE and subjected to standard photopolymerization at 625 nm for 2 h. After purification (100K spin filtering) and annealing with EY-G4 strands, DA was added, and polymerization continued at 525 nm for 2 h. In both approaches, polymer-ringed origami tubes were purified by 100K spin filtering and stored at 4 °C.

Reactive Oxygen Species Assay (ROS Assay)

Reactive oxygen species assay of photosensitizers (PS) was conducted in a total reaction volume of 150 µL in a 96 well plate. Wells were charged with PS (6.6 µM), *N,N*-dimethyl-4-nitrosoaniline RNO (70.7 µM) and imidazole (7.5 mM) in BIS-TRIS buffer (pH 6.5) and exposed to the respective wavelength or kept in dark. Absorbance scans from 300–500 nm were conducted at several time points within 30 min. The decrease in absorbance of RNO could be followed at 438 nm.

Cell culture

A549 cells were cultured at 37 °C and 5% CO₂ in Dulbecco's Modified Eagle's Medium (DMEM, high glucose), which was supplemented with 10% FBS, 1% penicillin/streptomycin and 1× Minimum Essential Medium (MEM) non-essential amino acids.

Cell experiments

A549 cells were cultured in DMEM medium containing 10% fetal bovine serum and 1% penicillin/streptomycin as well as 1% MEM non-essential amino acids. Cells were seeded into confocal well plates and left for 24h to adhere at 37 °C, 5% CO₂.

Cell uptake

For cell uptake studies, DNA origami tubes with a ring of either pDA or pNE were synthesized (according to standard polymerization protocol, MB, 625 nm, 3 h). Furthermore, origami tubes were equipped with 22 sticky sequences for Alexa-647® oligonucleotide labelling ("sticky C"). Dye-labelling was conducted in a 10-fold molar excess by a 1 hour temperature ramp (from 35 °C to 20 ° in 5 °C steps), followed by 100K spin filter purification. Control samples without polymer coating were labelled in the same way.

Cells were seeded at a density of 5,000 cells/well in a 10-well confocal well plate. After adhering for 24 h, cells were treated with the Alexa647-labeled sample for 24h at 37 °C. Sample solutions were diluted to 20 nM (Alexa647 concentration via a standard curve) in

SUPPORTING INFORMATION

cell media for incubation with the cells. After the incubation time, the media/sample solution was replaced with fresh media. Cells were then imaged by confocal laser scanning microscopy (SI Figure 12).

Cell colocalization

Besides the polymer ring, DNA origami tubes were additionally equipped with 22 sticky sequences each for Alexa-647® and Alexa-488® oligonucleotide labelling (standard protocol, see above; *stickyC for Alexa-647® and stickyA for Alexa-488®). Control samples without polymer coating were labelled in the same way.

Cells were seeded at a density of 5,000 cells/well in a 10-well confocal well plate. After adhering for 24 h, cells were treated with the double-labeled sample for 24 h at 37 °C. Sample solutions were diluted to 10 nM (Alexa647 concentration via a standard curve) in cell media and incubated with the cells. After the incubation time, the sample solution was replaced with fresh media. Cells were then imaged by confocal laser scanning microscopy (Figure 4 and SI Figure 13).

Cell medium stability assay

To test the stability of the employed DNA origami structures under cell medium conditions, samples were incubated with cell medium in an 1:1 ratio (approx. 50 fmol, total volume of 10 or 20 µL) for 24 h at 37 °C in a thermocycler with a heated lid. After incubation time, total sample volume was loaded on gel for AGE. For comparison, an analogue series of samples was mixed with cell medium right before loading onto the gel.

DNase I digestion assay

To digest DNA origami tubes that were only attached to the cell's exterior after overnight incubation, DNase I (20 U) was added to the samples and incubated for 1 hour at 37 °C prior to imaging.

Confocal Laser Scanning Microscopy

Cells were imaged on a Leica TCS SP5 and a Visitron Spinning Disc microscope with an argon laser for excitation at 488 nm for Alexa488 (emission 498-540 nm), and a HeNe laser for excitation at 633 nm for Alexa647 (emission 657-757 nm). Z-stack images were acquired using a Leica Stellaris 8 confocal microscope equipped with a white light laser with tunable excitation wavelengths between 440 – 790 nm. Alexa 488 is excited at 488 nm and emission was collected using the HyD® X detector at 498-540 nm. Alexa 647 is excited at 647 nm and emission was collected using the HyD® R detector at 657-757 nm.

Atomic Force Microscopy (AFM)

Atomic force microscopy was performed in liquid state with a Bruker Dimension FastScan Bio AFM equipped with the ScanAsyst mode. Sample solution (30 µL, 1-2 nM in origami buffer) was added onto a freshly cleaved mica substrate and incubated for 5 min to allow deposition of the origami structures. Remaining solution was removed and 300 µL origami buffer was applied onto the mica surface, forming a droplet for measuring in liquid. Samples were scanned with scan rates between 1 and 2 Hz. Images were processed with NanoScope Analysis 1.8.

Agarose gel electrophoresis (AGE)

Agarose gel electrophoresis was performed on 1% agarose gels (TBE, stained with EtBr, purchased from Bio-Rad or self-casted with 1 × TBE when no staining was desired), equipped with 8 wells. The gels were run on ReadySub-Cell GT Cells from Bio-Rad using 1 × TBE buffer as the running buffer. DNA Gel Loading dye (6 ×) was used for sample preparation (approximately 50 fmol origami) with a total volume of 6, 12, or 18 µL, depending on sample concentration. "GeneRuler DNA Ladder Mix" (100–10000 bp) was used as for the marker. Electrophoresis was conducted at 90 V for 60–100 minutes at 4 °C. Image was taken with G:BOX Chemi Gel Doc System from Syngene or under UV-excitation with a camera.

DNA extraction from agarose gel

For DNA extraction, TBE gels were casted and run as mentioned above. Areas below the wells were defined and cut according to the band pattern found under UV irradiation. The excised gel piece was placed into a Costar® Spin-X® Centrifuge Tube Filter (0.45 µm pore NY membrane), left at –20°C for 1 hour and subsequently centrifuged at 10 g for 10 minutes. 100 µL of the filtrate was placed into a black 384 well plate and subjected to fluorescence measurements.

Dynamic light scattering (DLS)

DLS measurements were performed at 25 °C using a Malvern ZetaSizer Nano S from Malvern Instruments Ltd. with a He/Ne Laser ($\lambda = 633$ nm) at a fixed scattering angle of 173°. All measurements were performed in triplicate. The obtained data was processed by cumulant fitting for Dz and PDI, or by CONTIN fitting for intensity-weighted particle size distribution. For DLS, triple amount of DNA origami (compared to standard polymerization) was photopolymerized (MB, 625 nm), purified and brought to 150 µL with reaction buffer. As a control, 10 µL bare origami tubes (50 nm) were diluted to 150 µL with reaction buffer. Samples were filtered prior to measurement through PFTE (hydrophilic) syringe filters (0.45 µm pore size).

SUPPORTING INFORMATION

Results and Discussion

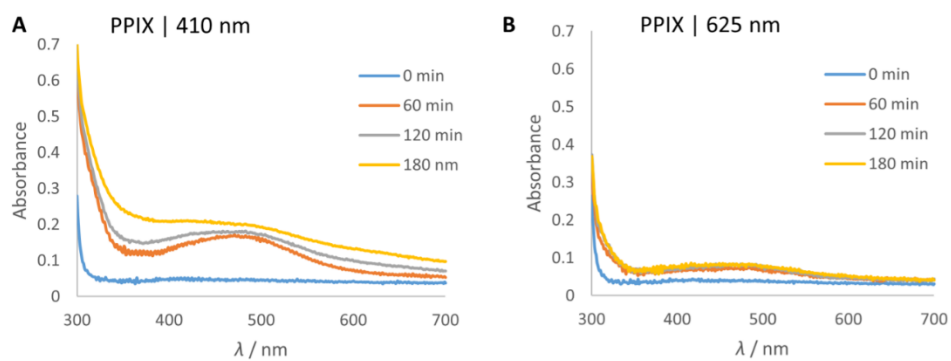


Figure 1 Photopolymerization of dopamine with PPIX-loaded DNA origami tubes under irradiation at 410 nm and 625 nm, respectively. Reaction is followed spectrometrically. (A) Irradiation at 410 nm can successfully induce oxidation and polymerization of dopamine. (B) Irradiation at 625 nm only leads to a reduced generation of oxidized dopamine species.

SUPPORTING INFORMATION

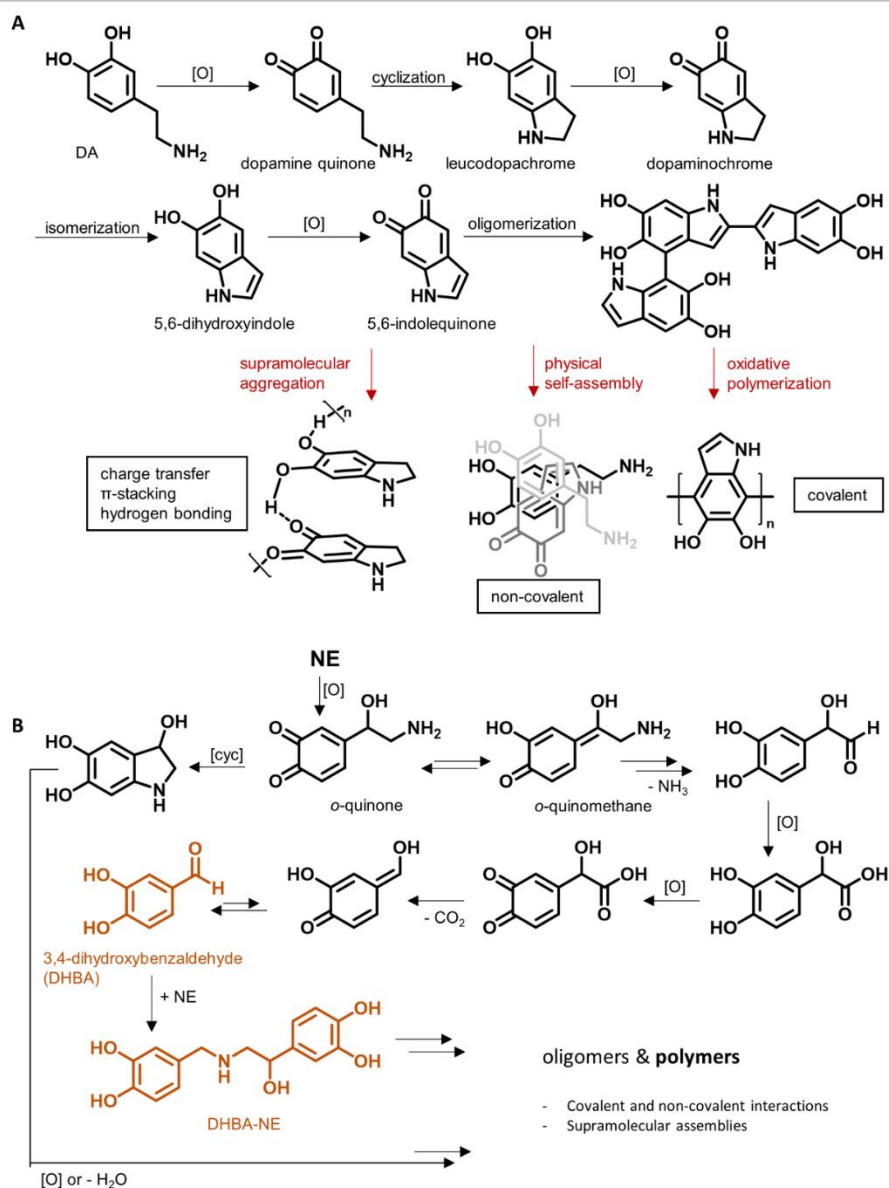


Figure 2 Proposed mechanism for pDA formation^[2] (A) and pNE formation^[3] (B) according to the literature. Both mechanisms are still under ongoing elucidation. Importantly, the polymeric structures are not only built on covalent bonds, but also non-covalent interactions, supramolecular assemblies, charge transfer and (cation-) π -stacking are present. In contrast to pDA, pNE formation is characterized by the occurrence of 3,4-dihydroxybenzaldehyde (DHBA), that can react with the monomer NE again, forming DHBA-NE. This molecule is said to be responsible for the ultrasmooth surface of pNE.

SUPPORTING INFORMATION

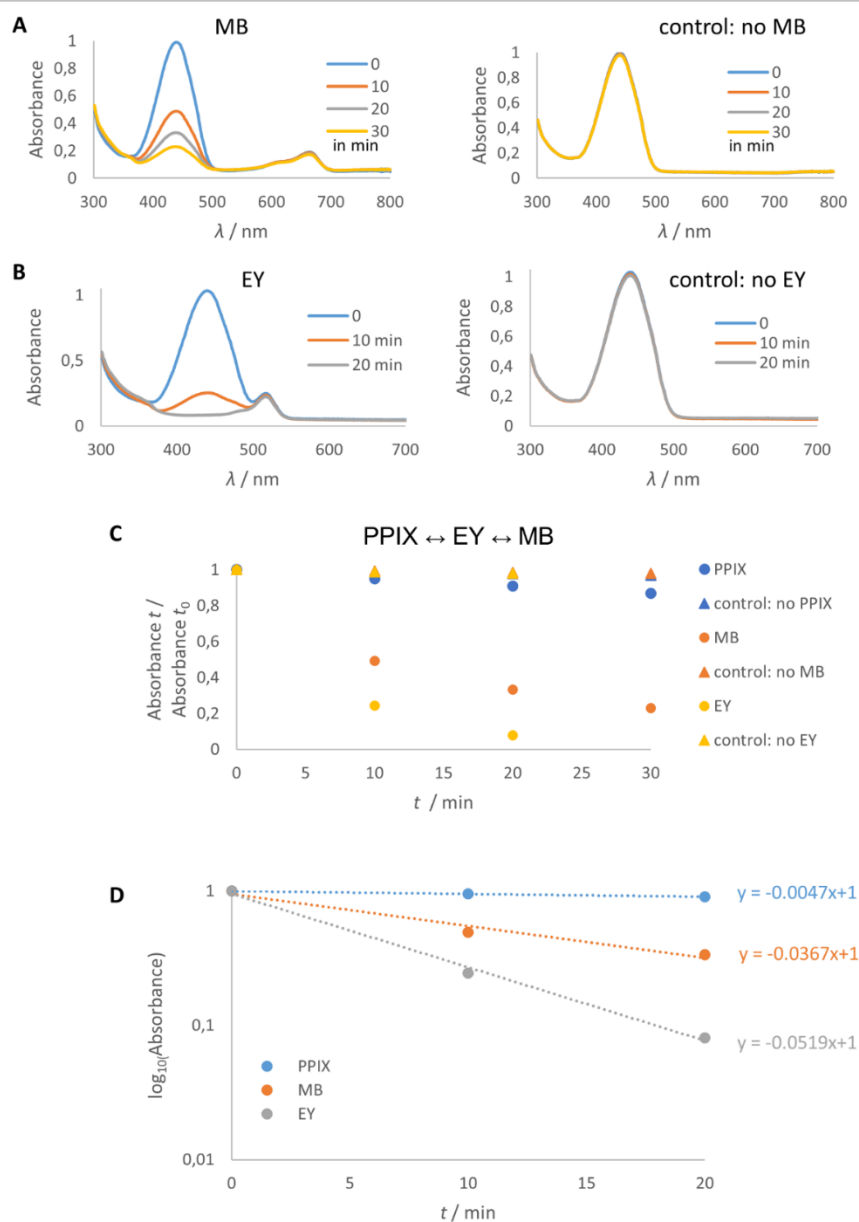


Figure 3 ROS assay of the utilized photosensitizers methylene blue (MB) and eosin y (EY) in the presence of imidazole and p-nitrosodimethylaniline (RNO). Decrease in absorbance of RNO due to singlet oxygen generation can be followed at 438 nm. (A) Methylene blue was irradiated at 625 nm (5 mA), and (B) eosin y was irradiated at 525 nm (5 mA) for the respective timeframes. (C) Relative absorbance decrease at 438 nm shows MB, EY and protoporphyrin IX (PPIX) in comparison. (D)

SUPPORTING INFORMATION

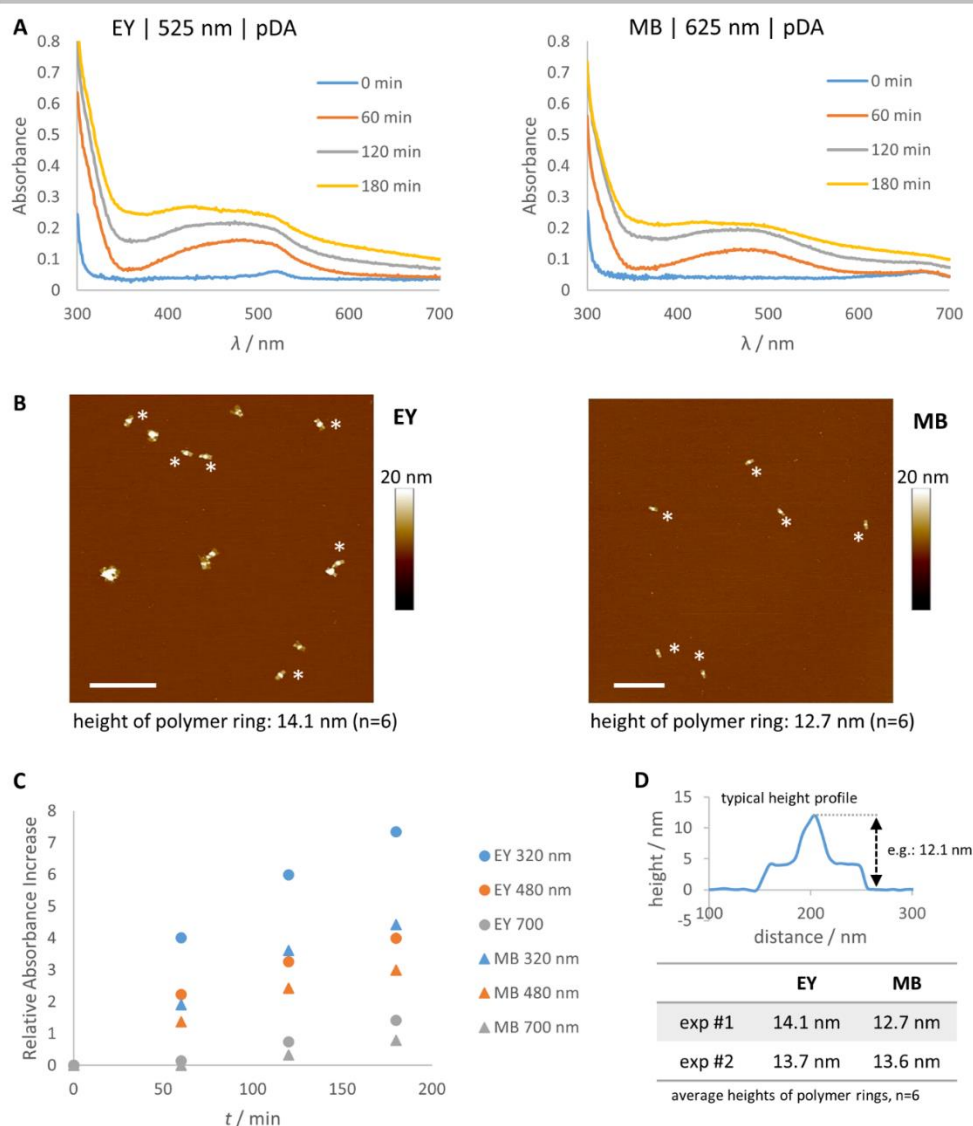


Figure 4 Photopolymerization of dopamine on DNA origami tubes with the photosensitizers eosin Y (EY) and methylene blue (MB) that are irradiated at 525 nm and 625 nm for 3 h, respectively. (A) Successful polymerization in both cases is confirmed by UV/Vis spectroscopy. (B) Topographical AFM images of pDA-ringed origami tubes after photopolymerization with EY (left) and MB (right). The average height of the polymer rings is depicted below the images. Scale bar: 500 nm. (C) Reaction kinetics of EY and MB are compared by plotting relative absorbance increase of the oxidized species dopaminochrome (320 nm), oligomers (480 nm), and polydopamine (700 nm). EY shows higher reaction rates than MB. (D) Statistical overview of the height of the polymer rings when either EY or MB is employed (two experiments each). The typical height image explains how values are taken. Polymer rings are slightly higher when EY is employed but no significant impact on the final product is noted.

SUPPORTING INFORMATION

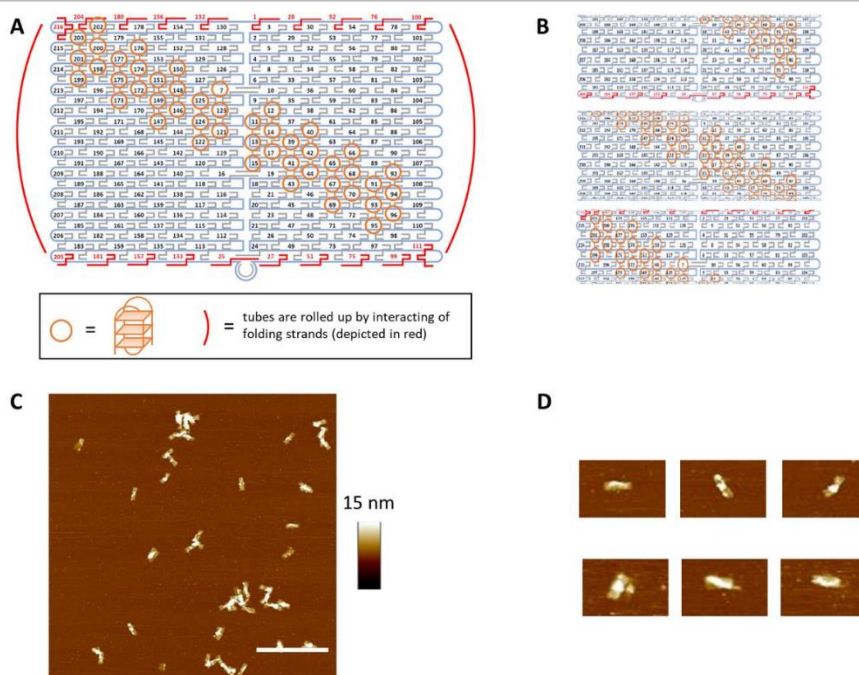


Figure 5 Photopolymerization of dopamine from a DNA origami tube with a diagonal pattern. (A) 48 G4 sequences are arranged in a diagonal pattern on the tube's surface. (B) Here, the top view on the structures deposited on an AFM grid can vary, depending on the orientation. (C) Exemplary overview AFM image of the obtained structures after polymerization. Scale bar: 500 nm. (D) Close-ups of a few representative pDA origamis. The diagonal pattern is only visible in a few cases due to the random orientation of the origami tube. For characterization purposes, ring patterns remain the pattern of choice because of its verticle symmetry and thus removing the orientation factor.

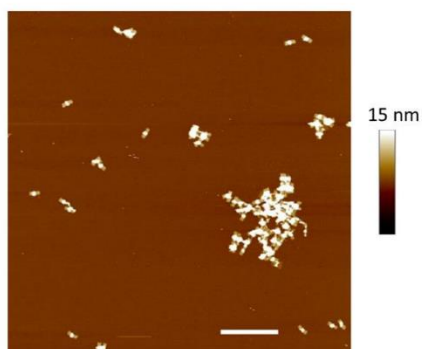


Figure 6 Due to the strong adhesiveness of pDA, polymer-ringed DNA origami tubes tend to aggregate. Scale bar: 500 nm.

SUPPORTING INFORMATION

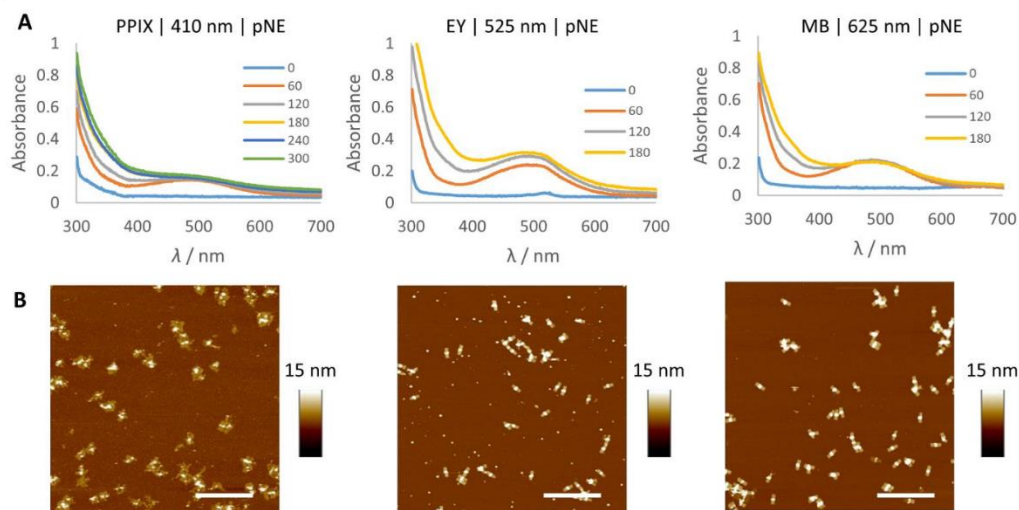


Figure 7 Photopolymerization of norepinephrine (NE) can be stimulated through PPIX, EY, and MB at the respective wavelength. (A) Polymerization can be followed spectrometrically. (B) Topographical AFM images confirm polymer formation at the designated areas. Scale bar: 500 nm.

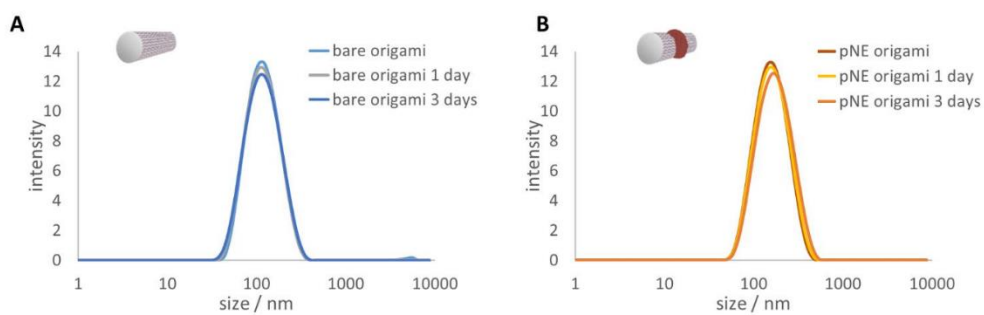


Figure 8 Dynamic light scattering reveals that for both samples, (A) bare origami and (B) pNE-ringed origami tubes, no agglomeration occurs over the course of at least 3 days.

SUPPORTING INFORMATION

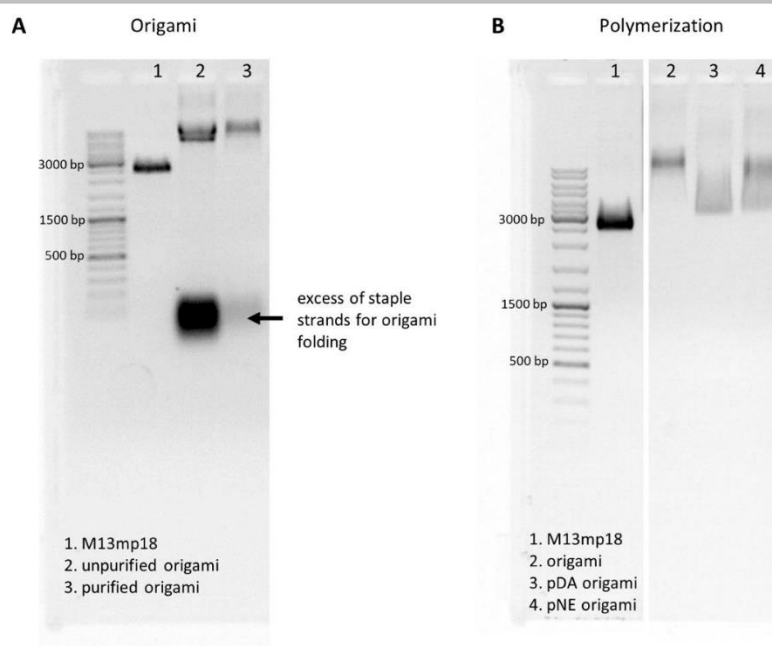


Figure 9 Characterization of (A) DNA origami structures and (B) DNA origami structures before and after pDA and pNE formation by agarose gel electrophoresis. After annealing of scaffold DNA (M13mp18) and an excess of staple strands, the folded DNA origami tubes are apparent as a new band of lower mobility (A2,3); excess of staple strands is removed by purification. Polymer-modification (pDA and pNE) is further visible by a changed running behavior compared to the precursor origami band (Gel B). The polymer bands also show some smearing effect, potentially indicating aggregation of the structures. Especially in the case of pDA-modification, we sometimes also observe the retaining of some material in the well of the gel, also demonstrating the presence of aggregates (gels not shown here). 1 % agarose TBE gels stained with EtBr were used, and run at 90 V for 60 min (Gel A) and 95 min (Gel B) at 4 °C. Please note: Gel (B) is cropped to only show lanes of interest, however, no stretching or shrinking was done, so bands are still comparable.

SUPPORTING INFORMATION

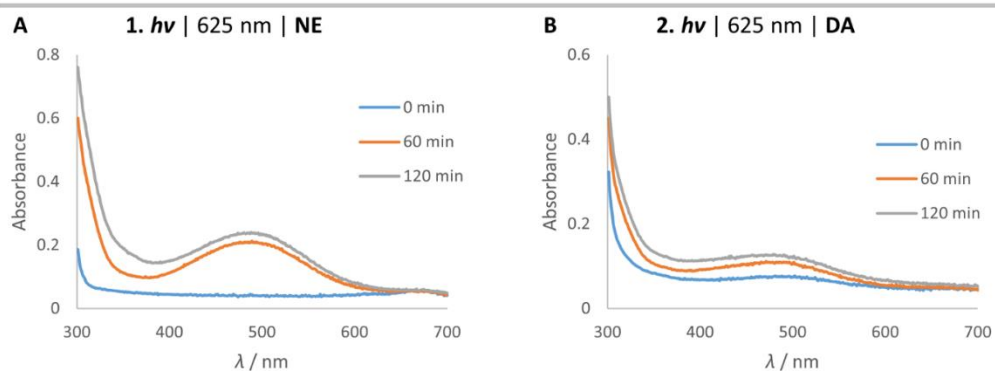


Figure 10 Stepwise layer-by-layer polymerization of the two monomers norepinephrine and dopamine on DNA origami tubes that are activated with MB and irradiated at 625 nm. UV/Vis spectroscopy confirms formation of (A) polynorepinephrine in the first irradiation phase and (B) polydopamine in the second irradiation phase. Spin filtration was performed after step 1 to exchange monomers.

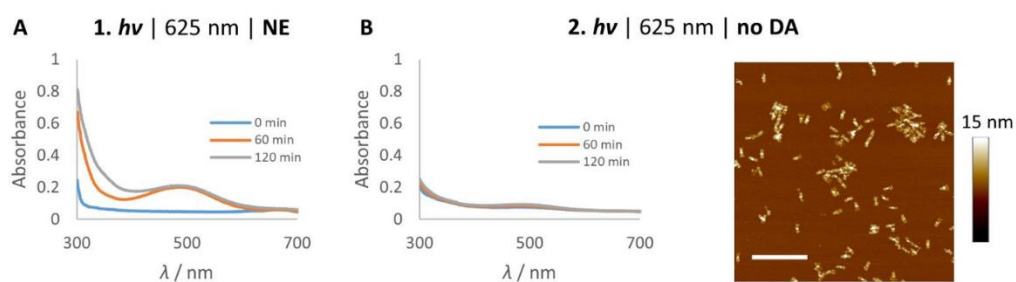


Figure 11 Control experiment for layer-by-layer polymerization, showing that it is in fact pDA that is formed in step 2, not pNE. (A) After pNE is generated in the first irradiation period, NE is removed from the reaction solution and no dopamine is added for the 2nd irradiation phase. (B) UV/Vis spectroscopy shows that no polymer is formed in step 2 and in AFM imaging, only height increase for pNE rings from step 1 is found.

SUPPORTING INFORMATION

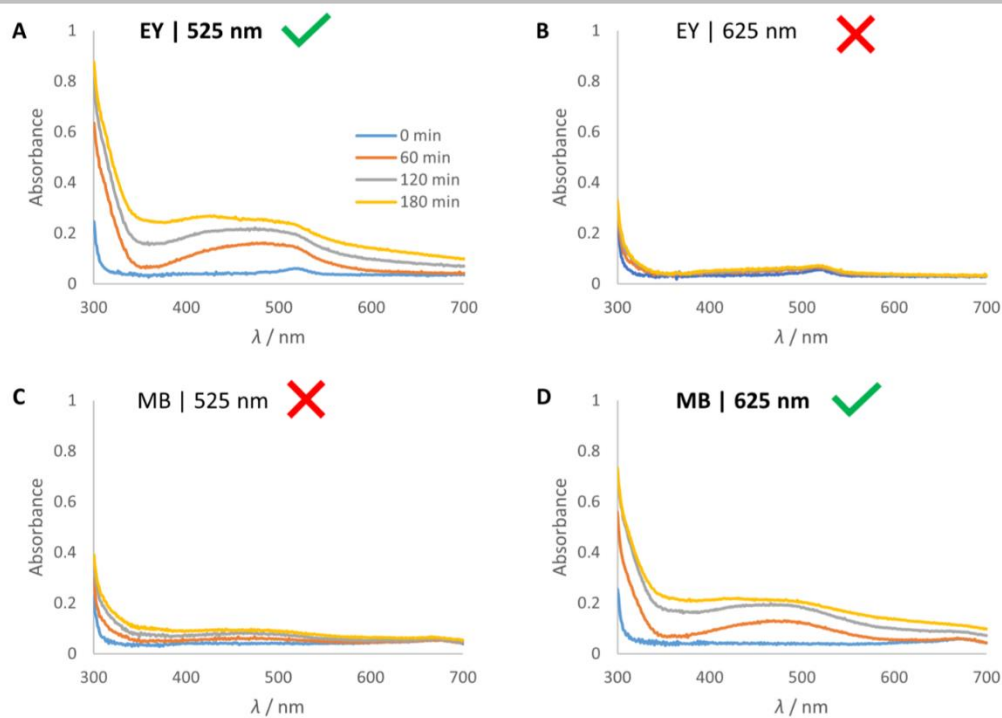


Figure 12 For a two-step polymerization with two photosensitizers, it is important that each photosensitizers only responds to the designated wavelength. This holds true for eosin Y, active at 525 nm (A) and dormant at 625 nm (B), and methylene blue, dormant at 525 nm (C) and active at 625 nm (D), respectively. Polymerization was conducted on standard origami tubes for 3 h with dopamine as the monomer.

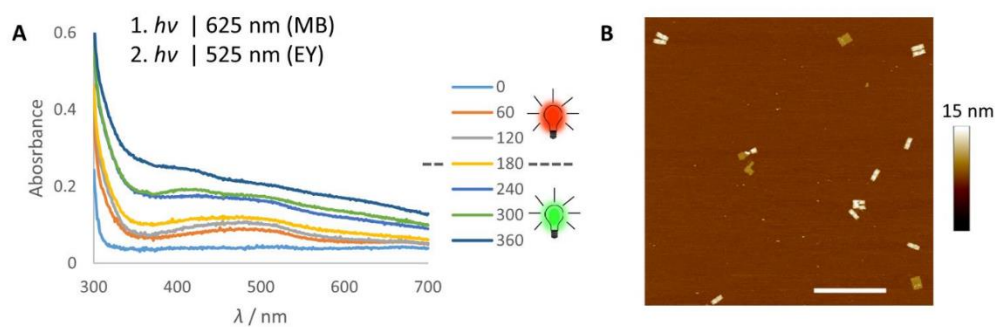


Figure 13 Photopolymerization of dopamine of MB- and EY-loaded origami tubes can be stimulated through irradiation at the respective wavelength (625 nm and 525 nm, respectively). (A) UV/Vis spectroscopy confirms the continuous generation of oxidized species and polymer. (B) AFM images demonstrate the origami's integrity even after irradiation of 6 h in the presence of photosensitizers.

SUPPORTING INFORMATION

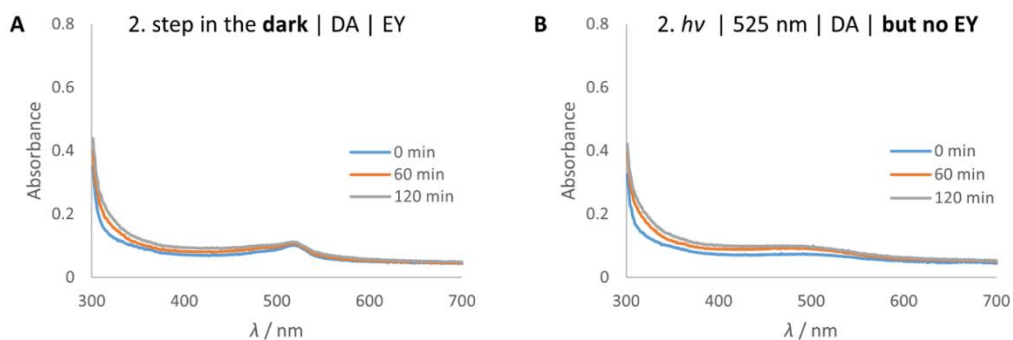


Figure 14 For a sequential two-step polymerization, the presence of all the reactive components is necessary. (A) When photosensitizer (EY) and monomer (DA) are added for step 2, but the reaction is performed in the dark, no polymerization is noted. (B) Same holds true when each component except for the photosensitizer (EY) is applied for the second polymerization step.

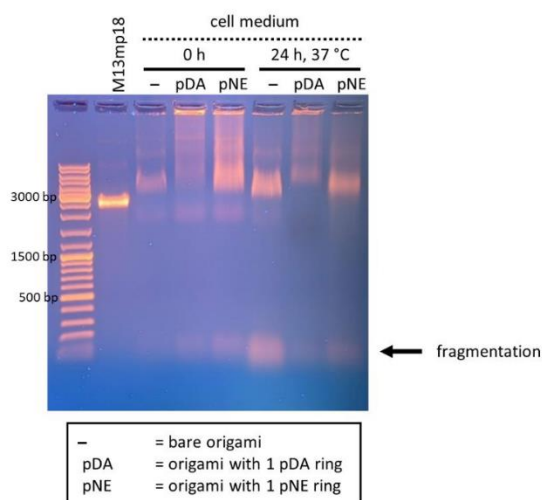


Figure 15 Cell medium stability assay of bare origami tubes as well as polymer-coated ones. Samples were incubated at 37 °C for 24 h and compared to samples that were mixed with cell medium prior to loading the gel. Even the bare origami tubes do show a certain stability under the applied incubation conditions, but also fragmentation. Polymer-ringed origami samples show less fragmentation, especially for pDA, material is stuck in the well, most likely caused by retained aggregates. A 1 % agarose TBE gel stained with EtBr were used, and run at 90 V for 90 min at 4 °C.

SUPPORTING INFORMATION

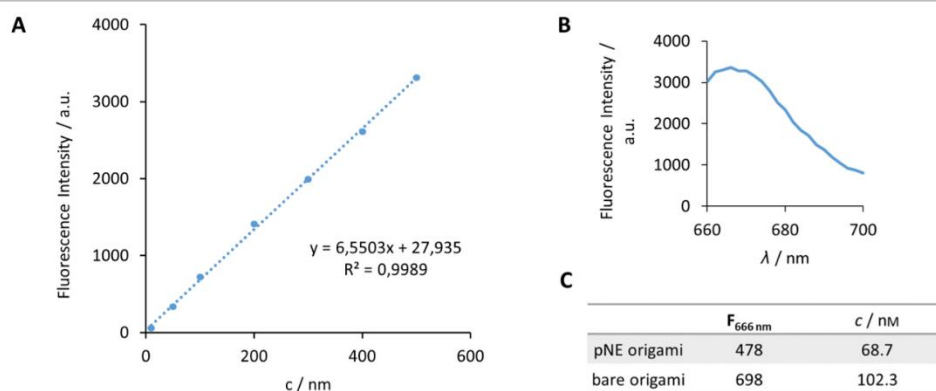


Figure 16 Fluorescence concentration of the origami samples subjected to cell uptake studies was calibrated by an Alexa647 standard curve. (A) A dilution series of Alexa647-oligonucleotide from 500–10 nM was measured in duplets (excitation at 645 nm, emission scan from 660–700 nm, emission maximum at 666 nm). (B) Representative emission scan for Alexa647-oligonucleotide at 500 nM. (C) Fluorescent signal and concentration of DNA samples was calibrated using the Alexa647 standard curve.

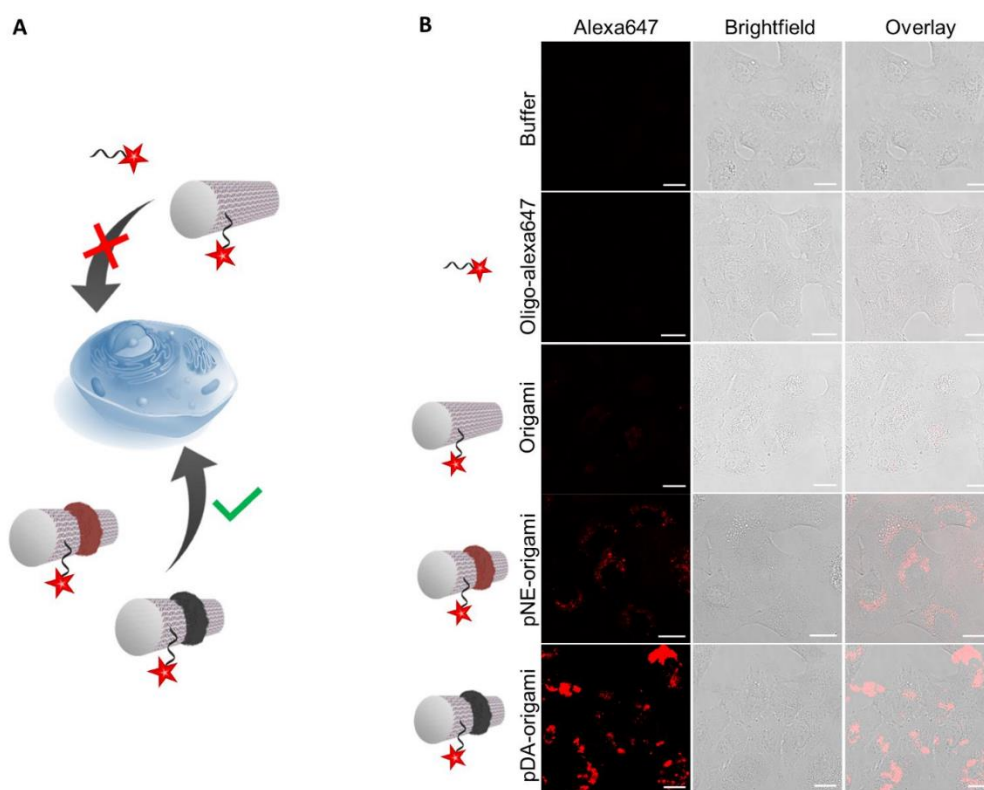


Figure 17 Cellular uptake of origami nanostructures. (A) Free Alexa647-oligonucleotides, bare origami tubes, pNE- and pDA-ringed origami tubes (all origami structures labelled with Alexa647) are incubated with A549 cells. (B) Confocal laser scanning micrographs of A549 cells treated with samples from (A) for 24 h. Scale bar 20 μm .

SUPPORTING INFORMATION

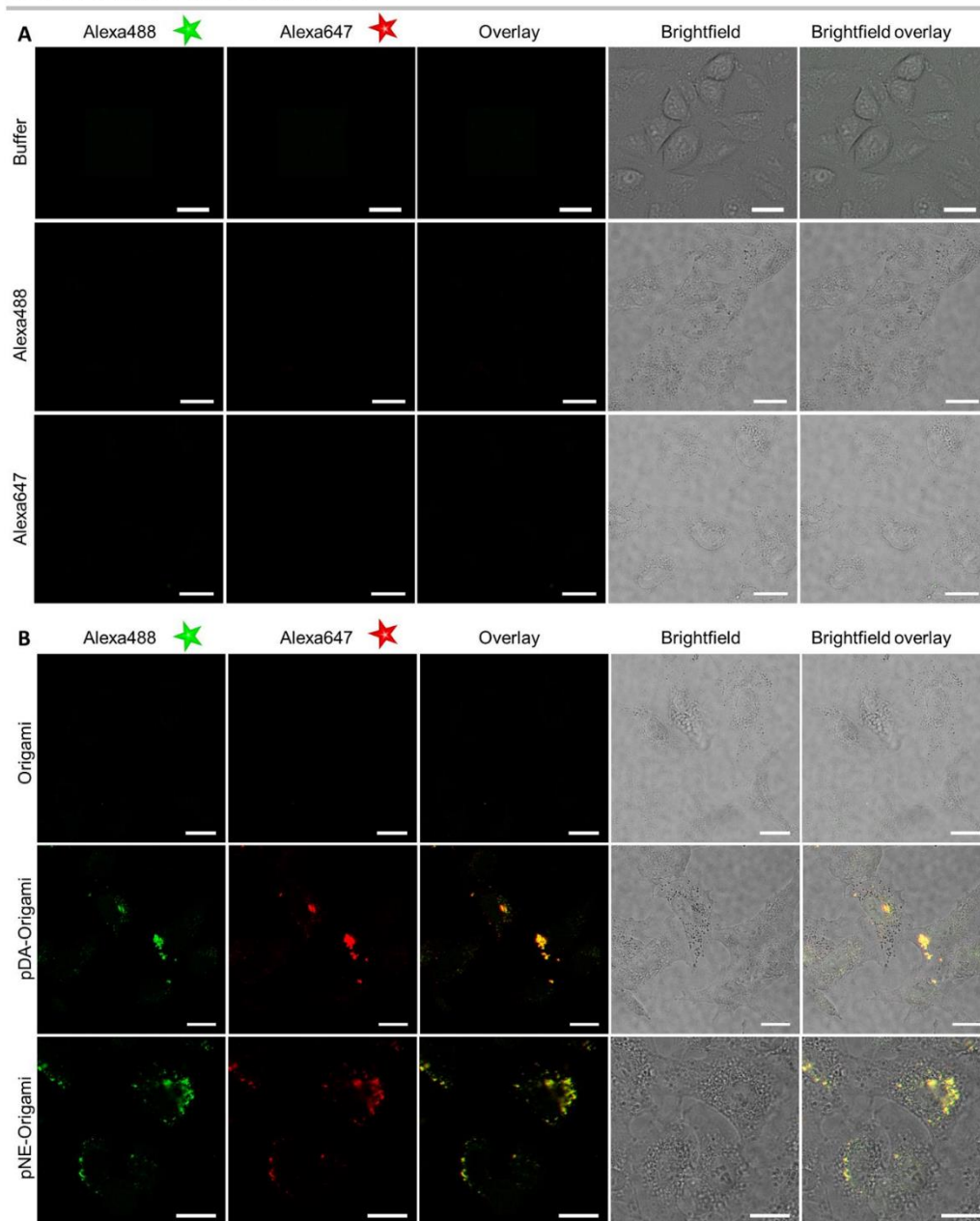


Figure 18 Confocal laser scanning micrographs of A549 cells incubated with (A) buffer only (control), free Alexa488- and Alexa647-oligonucleotides, and (B) double-labeled DNA origami samples (bare origami, pDA-origami, pNE-origami) for 24 h. Scale bars are 20 μm .

SUPPORTING INFORMATION

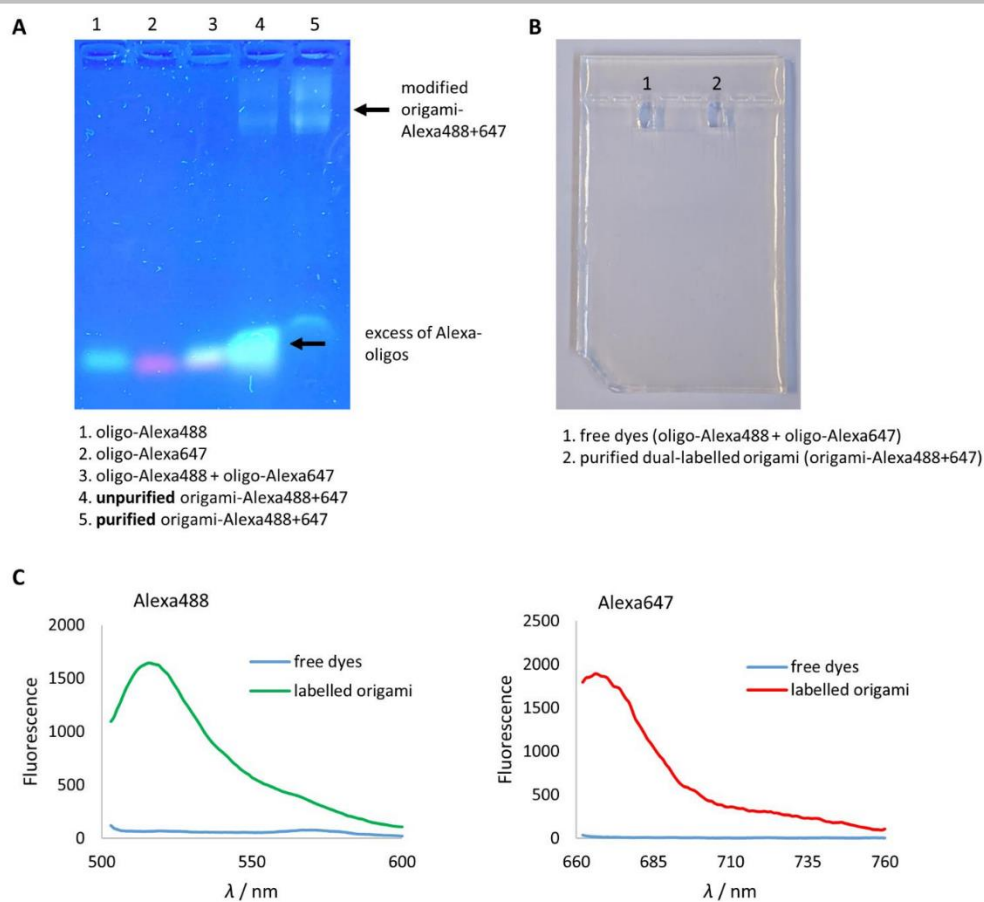
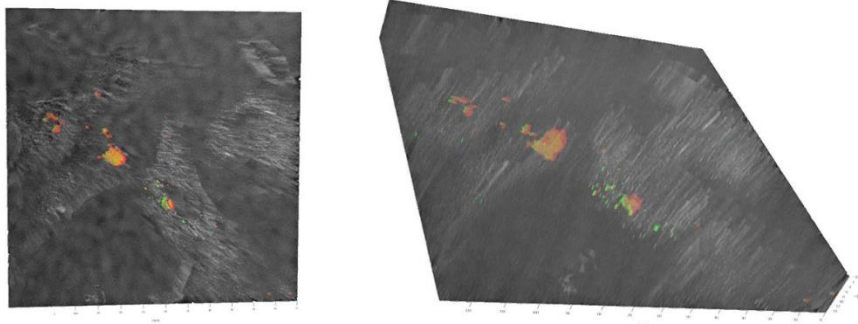


Figure 19 Characterization of dual-labelled origami structures for cell studies by agarose gel electrophoresis and subsequent fluorescence measurements. (A) AGE was performed with the Alexa-oligonucleotides, the unpurified as well as the purified origami sample after modification with both fluorophores. Gels were visualized on a UV plate without further staining. Whereas the free dyes show their respective emission color or a mixture thereof in the lower part of the gel; fluorescent origami structures are visible in the upper part of the gel. Excess of Alexa-oligonucleotides for origami modification was removed by purification. (B) A gel was loaded with both Alexa488- and Alexa647-oligonucleotides (lane 1) and purified, dual-labelled origami sample (lane 2). The areas right below the wells were cut, frozen, centrifuged, and the filtrate was subjected to subsequent fluorescence measurements in a Tecan Plate Reader. (C) Excitation of Alexa488 and Alexa647, respectively, revealed the presence of the Alexa fluorophores in the origami sample but not in the control sample, demonstrating successful labelling with both dyes. Emission spectra of Alexa488 and Alexa647 were recorded from 503–600 nm after excitation at 480 nm and from 662–760 nm after excitation at 640 nm (bandwidths: 10 nm), respectively, and smoothed.

SUPPORTING INFORMATION

A pDA-Origami



B pNE-Origami

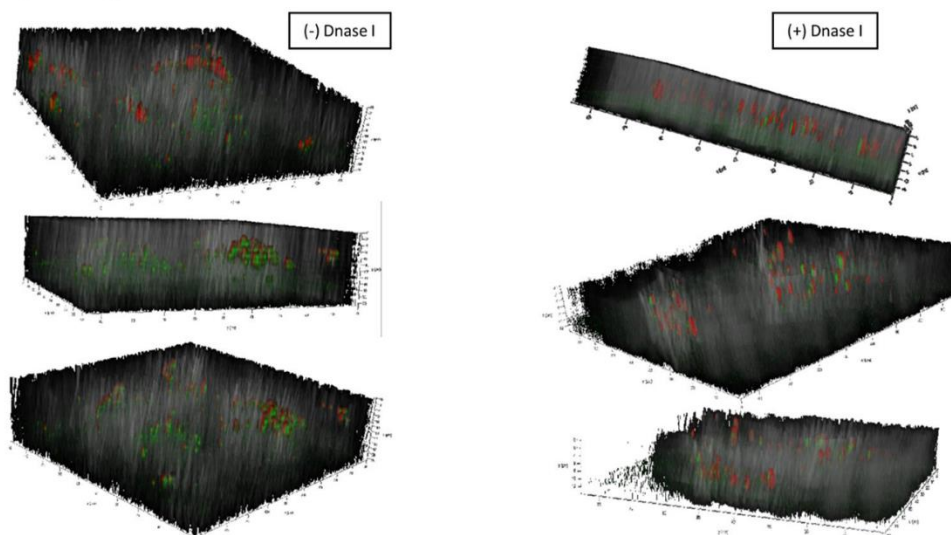


Figure 20 Confocal z-stack analysis followed by 3D reconstruction of pDA- and pNE-origami incubated A549 cells. (A) Z-stacks of the pDA-sample reveal that the observed aggregates are not internalized by the cells (no DNase I treatment). (B) In contrast, pNE-ringed origami tubes are found inside the cells, with and without DNase treatment.

SUPPORTING INFORMATION

Appendix**DNA Sequences**

DNA origami tubes were synthesized together with M13mp18 Scaffold DNA and staple strands according to the above-mentioned protocol. In the following, the sequences of staple strands and additional oligonucleotides are listed.

For G4 staple strands, the sequence of the respective staple strand is extended at the 3' end by 5'-TTTTGGGTAGGGCGGGTTGGG-3'.

For stickyA sequences, the sequence of the respective staple strand is extended at the 3' end by 5'- TTTTATAGTGGTGGTAGAG-3'.

For stickyC sequences, the sequence of the respective staple strand is extended at the 3' end by 5'- TTTTCTCTCCTTCCTTT-3'.

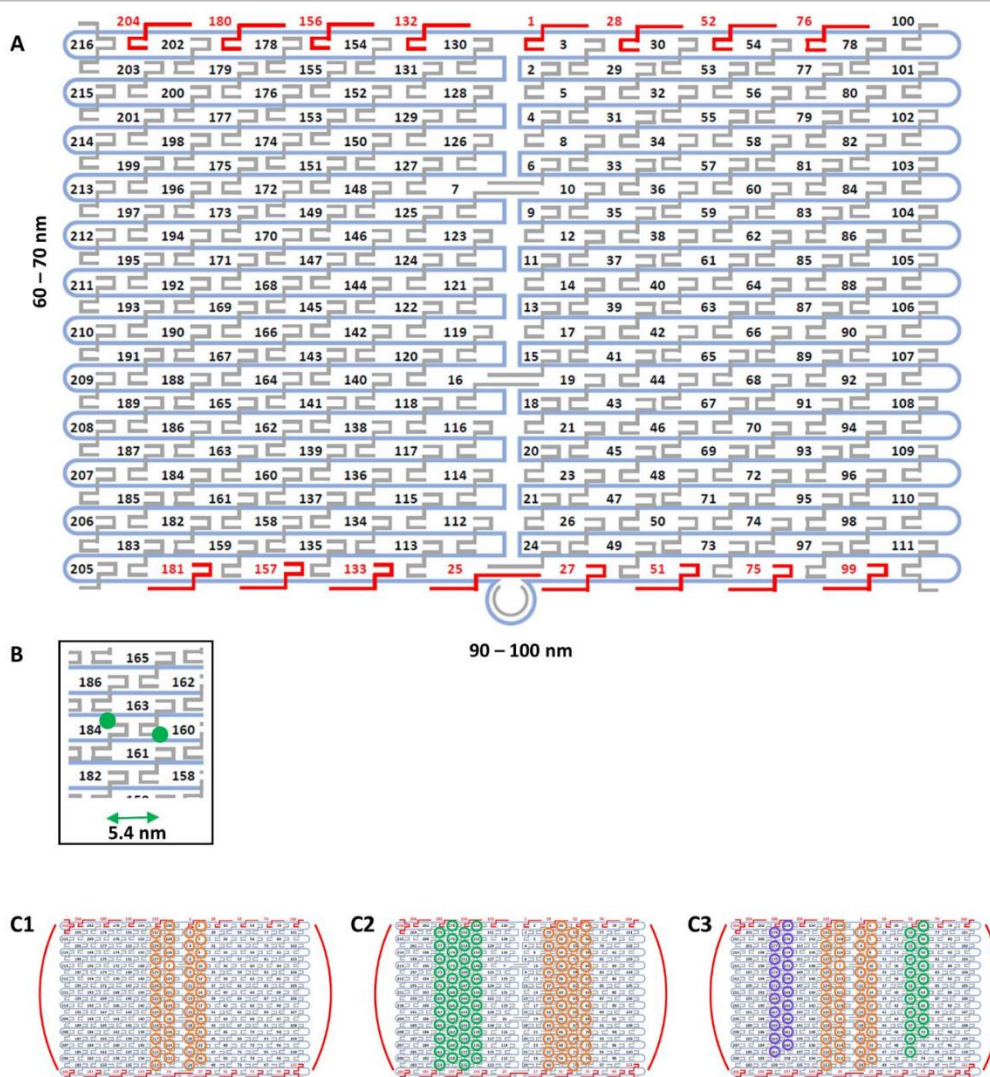
G4 complementary strands: 5'- GGGTTGGGCGGGATGGGTTTTCTCTACCACCTACTA-3'

Alexa-488@ oligonucleotide: Alexa488-5'- TTCTCTACCACCTACTA-3'

Alexa-647@ oligonucleotide: Alexa647-5'-TTAAAGGGAAGGAGAG-3'

To introduce functionalities on the bare DNA origami tube (Scaffold DNA + 206 staple strands + 20 folding strands; Appendix SI Figure 1), respective staple strands were replaced by G4-staple strands or sticky sequences. Staple strands at the long edges of the rectangle were replaced by folding strands.

SUPPORTING INFORMATION



Appendix SI Figure 1 (A) Footprint of a DNA origami rectangle where the position of each staple strand is depicted. By replacing the staple strands at the long edges of the rectangle by folding strands (red), a tube structure is formed. (B) Distance between two attachment points is 5.4 nm. (C) Footprints of the employed structures: (1) tube with 1 central G4 ring (orange), (2) tube with 1 G4 ring and 1 sticky A ring (green), (3) tube for colocalization studies with G4 ring and stickyA and stickyC (purple) for labelling.

Tube with 1 central G4 ring: G4 staple strands on positions 2–10, 11–20, 21–24, 26, 112–120, 121–130, 131; folding strands on positions 1, 25, 27, 28, 51, 52, 75, 76, 99, 100, 111, 132, 133, 156, 157, 180, 181, 204, 205, 216; staple strands on remaining positions.

Tube with 1 G4 ring and 1 stickyA ring at the tubular ends: G4 staple strands on positions 29, 30, 31–40, 41–50, 53–60, 61–70, 71–74; stickyA strands on positions 134–140, 141–150, 151–155, 158–160, 161–170, 171–179; folding strands on positions 1, 25, 27, 28, 51, 52, 75, 76, 99, 100, 111, 132, 133, 156, 157, 180, 181, 204, 205, 216; staple strands on remaining positions.

SUPPORTING INFORMATION

Tube with 1 central G4 ring and stickyC for dye labelling: G4 staple strands on positions 2–10, 11–20, 21–24, 26, 112–120, 121–130, 131; stickyC strands on positions 161–170, 171–179; folding strands on positions 1, 25, 27, 28, 51, 52, 75, 76, 99, 100, 111, 132, 133, 156, 157, 180, 181, 204, 205, 216; staple strands on remaining positions.

Tube with 1 central G4 ring and stickyC+stickyA for two dye labelling: G4 staple strands on positions 2–10, 11–20, 21–24, 26, 112–120, 121–130, 131; stickyC strands on positions 161–170, 171–179; stickyA strands on positions 53–60, 61–70, 71; folding strands on positions 1, 25, 27, 28, 51, 52, 75, 76, 99, 100, 111, 132, 133, 156, 157, 180, 181, 204, 205, 216; staple strands on remaining positions.

Table S1. Sequences of staple strands and folding strands.

#	Sequence 5' → 3'	#	Sequence 5' → 3'
1	CAAGCCCAATAGGAACCATGTACAAACAGTT	124	AAGAGGAACGAGCTTCAAAGCGAAGATACATT
2	AATGCCCGTAAACAGTGCCCGTATCTCCCTCA	125	GGAATTACTCGTTTACCAGACGACAAAAGATT
3	TGCCTTGACTGCCTATTTTCGGAAACAGGGATAG	126	GAATAAGGACGTAACAAAAGCTGCTCTAAAACA
4	GAGCGCCCCACCACCGGAACCGCAGCGGAAA	127	CCAATCACTTGCCTGACGAGAACGCCAAAA
5	AACCAGAGCCCTCAGAACCCGACGGGTGACG	128	CTCATCTTGAGGCAAAAAGTAATCGAATTTT
6	TTATTCATAGGGAAGTAAATATTCATTACAGT	129	AAACGAAATGACCCCGCAGGATTTATTACATC
7	CATAACCCGAGGACATAGTAAAGAGCTTTTTAAG	130	CTTAAACATCAGCTTGCCTTCGAGCGTAAACAC
8	ATTGAGGGTAAAGGTGAATTATCAATCACCGG	131	TCGGTTTTAGCTTGATACCGATAGTCCAACTA
9	AAAAGTAATATCTTACCGAAGCCCTCCAGAG	132	TGAGTTTCGTACCAGTACAACCTAATTTGTA
10	GCAATAGCGCAGATAGCCGAACAATTCACCCG	133	CCCCGATTTAGAGCTTGACGGGGAATCAAAA
11	CCTAATTTACGCTAACGAGCGTCTAATCAATA	134	GAATAGCCGCAAGCGGTCCAGCTCCTAATGA
12	TCTTACCAGCCAGTTACAAAATAAATGAAAAA	135	GAGTTGCACGAGATAGGGTTGAGTAAGGGAGC
13	ATCGGCTGCGAGCATGTAGAAAACCTATCATAT	136	GTGAGTAGTTTTCTGTGTAATTTGGGAAAG
14	CTAATTTATCTTCCCTTATCATTATCTGTAA	137	TCATAGCTACTCACATTAATGCGCCCTGAGA
15	GCGTTATAGAAAAAGCCTGTTTAGAAGGCCGG	138	GCGCATCGCACTCCAGCCAGCTTTGCCATCAA
16	GCTCATTTTCGCATTAATTTTTGAGCTTAGA	139	GAAGATCGGTGCGGGCTCTTCGCAATCATGG
17	AATTAACAATAATCTTACCAAGTATCCCCATC	140	AAATAATTTTAAATTTGAAACGGTTGATATTC
18	TTAAGACGTTGAAAACATAGCCGATAACAGTAC	141	GCAAATATCGCGTCTGGCTTCTGGCCTCAG
19	TAGAATCCCTGAGAAGAGTCAATAGGAATCAT	142	ACCGTTCTAATGCAATGCTGAGAGGTGCA
20	CTTTTACACAGATGAATATACAGTAAACAAT	143	TATATTTAGCTGATAAATTAATGTGTATAA
21	TTTAACGTTTCGGGAGAAAACAATAATTTCCCT	144	TCAATTCITTTAGTTTGACCATACCAGCCG
22	CGACAACCTAAGTATTAGACTTTCAATACCGA	145	CGAGTAGAACATAAGTAGTAGCAAACTTCA
23	GGATTTAGCGTATTAATCCTTTTGTTCAGG	146	GAAGCAAAAAGCGGATGATCAGATAAAAA
24	ACGAACCAAAACATCGCCATTAATGTGGTT	147	TCAGAACCTCCAACAGGTGAGGACTGCGAA
25	GAACGTTGGGAGAAAAGGGAACAACAATAT	148	CCAAAATAATGACAGATACATAAACACCAGA
26	TAGCCCTACCAGCAGAAGATAAAAACATTTGA	149	CATTCAACGCGAGAGGCTTTTGCATATTAG
27	CGGCTTGTGTTAAATCCAGAACGAACTGA	150	ACGAGTAGTGACAAGAACCGGATATACCAAGC
28	CTCAGAGCCACCCCTCATTTCCTATTATT	151	AGTAATCTTAAATTTGGCTTGAGAGAATACCA
29	CTGAACAGGTAAATAGTTTTAACCCCTCAGA	152	GCGAAACATGCCACTCGAAGGCTGCGCCGA
30	AGTGTACTGAAAGTATTAAGAGGCCGCCACC	153	ATACGTAAAAGTACAACGGAGATTTTCAAG
31	GCCCAACTCTTTTTCATAATCAAAACCGTACC	154	CAATGCACTCCAAAAGGAGCTTACAACGCC
32	GTTTGCCACTCAGAGCCGCCACGATACAGG	155	AAAAAAGGCAACCATCGCCACGCGGGTAAA
33	GACTTGAGAGACAAAAGGGCGACAAGTTACCA	156	TGTAGCATTCACAGACAGCCCTCATCTCCAA
34	AGCGCAACCTTTTGGGAATTAGATTATAGC	157	GTAAGCACTAATCGAAACCTAGTTGTCC
35	GAAGGAAAATAAGGAACAAGAAACACAGCCAT	158	AGTTTGGAGCCCTTCCGCTGGTTGCGCTC
36	GCCCAATACCAGGAAACGCAATAGGTTTACC	159	AGCTGATTACAAGAGTCCACTATTGAGGTGCC
37	ATTATTAACCAAGTACAATTTTCAAGAACG	160	ACTGCCCGCAGCTCGAATTCGTTATTACGC
38	TATTTTGTCCCAATCCAATAAGTGAAGTAA	161	CCCGGTACTTTCCAGTCGGGAAACGGCAAC
39	GGTATTAAAGAACAGAAAAATAAAGCCA	162	CAGCTGGCGGACGACGATGATCTGACCGAG
40	TAAGTCTACCAAGTACCGACTCTTAGTTGC	163	GTTTGGGGAAAAGGGGGATGTGTAGAGGATC
41	ACGCTCAAATAAGAATAAACACCGTGAATTT	164	CTTTCACTCCAAAACAGGAAGACCGGAGAG
42	AGGCGTTACAGTAGGGCTTAATTGCAATAGA	165	AGAAAAGCAACATTAATGTGAGCATCTGCCA
43	ATCAAAATCGTCGCTATTAAACAGGATTTCG	166	GGTAGCTAGGATAAAAATTTTAGTTAACATC
44	CTGTAATCATAGTCTGAGAGACGATAAATA	167	CAACGCAATTTTGGAGATCTACTGATAATC
45	CCTGATTGAAAGAAATTCGCTAGACCCGAACG	168	CAATAAATACAGTTGATTTCCAAATTTAGAGAG
46	ACAGAAATCTTGAATACCAAGTTCTTGTCT	169	TCCATATACATACAGGCAAGGCAACTTTATTT
47	TTATTAATGCCGTAATAGATAATCAGAGGTG	170	TACCTTAAGTCTTTACCTTGACAAGGAAGT
48	AGATTAGATTTAAAAGTTTGTAGTACAGTAAA	171	CAAAAATCATTTGCTCCTTTTGTAAAGTTTCAT
49	AGGCGGTATTAGTCTTAAATGCGCAATATTA	172	TTTCCAGATCAGTTGAGATTTAGTGGTTTAA
50	GAATGGCTAGTATAACACCGCTCAACTAAT	173	AAAGATTCAGGGGTAATAGTAAACCATAAAT
51	CCGCCAGCCATTGCAACAGGAAAAATTTTTT	174	TTTCAACTATAGGCTGGCTGACCTTGATCAT
52	CCCTCAGAACCAGCCCTCAGAACTGAGACT	175	CCAGGCGCTTAATCATTGTGAAATACAGGTAG
53	CCTCAAGAATACATGGCTTTGTAGAACCCAC	176	CGCTGATGGGAGTTTCCATTAACATAACCCG
54	TAAGCGTCAAGGATTAGGATTAGTACCGCCA	177	TTTCATGAAAATTTGTCGAAATCTGTACAGA
55	CACCAGAGTTCCGCTATAGCCCCGACGAAA	178	ATATATTTCTTTTACGTTGAAAAATAGTTAG
56	TCGGCATTCCGCGCCAGCATTGACGTTCCAG	179	AATAATAAGGTGCTGAGGCTTGCAAGACTT
57	AATCACCAAAATGAAAATCATATATAACCGGA	180	CGTAACGATCTAAAGTTTTGCTGTAATGGC

SUPPORTING INFORMATION

References

- [1] E. Stahl, T. G. Martin, F. Praetorius, H. Dietz, *Angewandte Chemie* **2014**, *126*, 12949-12954.
- [2] (a) H. Lee, S. M. Dellatore, W. M. Miller, P. B. Messersmith, *Science* **2007**, *318*, 426-430; (b) D. R. Dreyer, D. J. Miller, B. D. Freeman, D. R. Paul, C. W. Bielawski, *Langmuir* **2012**, *28*, 6428-6435; (c) S. Hong, Y. S. Na, S. Choi, I. T. Song, W. Y. Kim, H. Lee, *Advanced Functional Materials* **2012**, *22*, 4711-4717.
- [3] (a) P. Manini, A. Pezzella, L. Panzella, A. Napolitano, M. d'Ischia, *Tetrahedron* **2005**, *61*, 4075-4080; (b) P. Manini, L. Panzella, A. Napolitano, M. d'Ischia, *Chem Res Toxicol* **2007**, *20*, 1549-1555; (c) S. Hong, J. Kim, Y. S. Na, J. Park, S. Kim, K. Singha, G. I. Im, D. K. Han, W. J. Kim, H. Lee, *Angew Chem Int Ed Engl* **2013**, *52*, 9187-9191; (d) X. Tan, P. Gao, Y. Li, P. Qi, J. Liu, R. Shen, L. Wang, N. Huang, K. Xiong, W. Tian, Q. Tu, *Bioact Mater* **2021**, *6*, 285-296.

Author Contributions

P. W. conducted all the DNA origami experiments and analysis. C. J. W. and D.Y.W.N. conducted cell experiments and confocal microscopy analysis. The project was supervised by D.Y.W.N. and T.W. All authors contributed to writing the manuscript.

Functional DNA–Polymer Conjugates

Colette J. Whitfield,[§] Meizhou Zhang,[§] Pia Winterwerber, Yuzhou Wu,^{*} David Y. W. Ng,^{*} and Tanja Weil^{*}Cite This: *Chem. Rev.* 2021, 121, 11030–11084

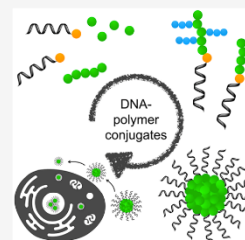
Read Online

ACCESS |

Metrics & More

Article Recommendations

ABSTRACT: DNA nanotechnology has seen large developments over the last 30 years through the combination of solid phase synthesis and the discovery of DNA nanostructures. Solid phase synthesis has facilitated the availability of short DNA sequences and the expansion of the DNA toolbox to increase the chemical functionalities afforded on DNA, which in turn enabled the conception and synthesis of sophisticated and complex 2D and 3D nanostructures. In parallel, polymer science has developed several polymerization approaches to build di- and triblock copolymers bearing hydrophilic, hydrophobic, and amphiphilic properties. By bringing together these two emerging technologies, complementary properties of both materials have been explored; for example, the synthesis of amphiphilic DNA–polymer conjugates has enabled the production of several nanostructures, such as spherical and rod-like micelles. Through both the DNA and polymer parts, stimuli-responsiveness can be instilled. Nanostructures have consequently been developed with responsive structural changes to physical properties, such as pH and temperature, as well as short DNA through competitive complementary binding. These responsive changes have enabled the application of DNA–polymer conjugates in biomedical applications including drug delivery. This review discusses the progress of DNA–polymer conjugates, exploring the synthetic routes and state-of-the-art applications afforded through the combination of nucleic acids and synthetic polymers.



CONTENTS

1. Introduction	11031	4.1. Static Nanostructures	11059
2. Chemistries on DNA	11031	4.1.1. Assemblies Induced by Hydrophobic Interactions through the Polymer Segment	11059
2.1. Solid Phase Synthesis	11031	4.1.2. Assemblies Induced by Sequence Hybridization of the DNA Segments	11061
2.2. In Solution	11033	4.1.3. Nanostructures Involving DNA and Polymer Induced Assembly	11063
2.3. Complexation	11034	4.2. Dynamic Nanostructures	11065
3. DNA–Polymer Synthesis	11037	4.2.1. DNA Programmable Dynamic Nanostructures	11065
3.1. Covalent DNA–Polymer Conjugates	11038	4.2.2. Temperature-Responsive Dynamic Nanostructures	11066
3.1.1. Polymerization Methods	11038	4.2.3. pH-Responsive Dynamic Nanostructures	11069
3.1.2. DNA–Polymer Conjugate Synthesis Limitations	11039	4.2.4. Light-Responsive Dynamic Nanostructures	11069
3.1.3. Solution-Based ODN–Polymer Synthesis	11042	5. Functionality of DNA–Polymer Conjugates	11070
3.1.4. 1D DNA–Polymer Synthesis	11045	5.1. Functionality from the Polymer	11070
3.1.5. 2D and 3D Polymerization Platforms	11046	5.2. Functionality Based on DNA	11072
3.2. Noncovalent DNA–Polymer Interactions	11048		
3.2.1. Templating of Polymers by Single and Double Stranded DNA	11049		
3.2.2. Polymer Decoration of DNA Nanostructures	11053		
3.3. Chemistry of DNA–Polymer Conjugates Postcoupling	11056		
3.3.1. Chemistries on the Polymer	11056		
3.3.2. Chemistries on the DNA	11056		
3.4. Characterization of DNA–Polymer Conjugates	11056		
4. Supramolecular DNA–Polymer Complexes	11058		

Special Issue: Polymeric Biomaterials

Received: October 2, 2020

Published: March 19, 2021



5.3. Synergistic Functionalities	11073
6. Conclusions and Outlook	11076
Author Information	11076
Corresponding Authors	11076
Authors	11076
Author Contributions	11076
Notes	11076
Biographies	11077
Acknowledgments	11077
Abbreviations	11077
References	11078

1. INTRODUCTION

The genetic code, one of the most prominent molecular monuments in nature, is a technological wonder from the perspective of both structural biology and macromolecular chemistry. Within this massive covalent structure twinned supramolecularly by its complementary sequence, the central dogma of biology operates with unrivalled precision that features nature's evolutionary prowess. Chemically speaking, the genetic code is a set of colossal chains of DNA in which the diversity of life is governed through the sequence information stored within the DNA nucleobases (adenine, cytosine, guanine, and thymine).

Although its biological role and impact are clearly unambiguous, DNA has a different facade in the synthetic world—collectively known as DNA nanotechnology. Taking advantage of how the alignment of nucleotides can be woven differently with multiple intersecting chains not present in nature, nanoscale structures can be tailored with near limitless geometric possibilities. From straightforward shapes such as Y-shaped DNA-crossovers and multiarm Holliday junctions to complex folding technologies such as DNA origami, these platforms have made revolutionary advances in biophysics, photonics, nanomedicine, and materials science. This is primarily due to how DNA architectures grant the capability to position two or more (macro)molecules/nanoparticles of interest within a designated 3D space and orientation at nanometer resolution. The level of precision, coupled with the ease of DNA hybridization methods, has resulted in their widespread accessibility across all disciplines.

Nonetheless, while DNA-based technologies receive their deserved accolades within the scientific community, its relatively poor stability and restriction toward aqueous medium containing $\text{Ca}^{2+}/\text{Mg}^{2+}$ has been a glaring limitation to its potential. As such, significant attempts to stabilize DNA structures involving the conjugation of polymers, hydrophobic molecules, nanoparticles, or even higher ordered DNA weaving strategies have been achieved to protect the DNA phosphodiester bonds from hydrolysis. Interestingly, these approaches very often result in the creation of novel materials with unique characteristics and structures due to the differences between the physical properties of the DNA and its attached motif. Naturally, higher ordered architectures resulting from hydrophilic/hydrophobic interactions are among the most abundant, with morphologies including micelles, vesicles, and tubes. The dimensionality of structures from 1D to 3D can be customized by increasing the complexity of the DNA component, i.e. from single stranded DNA (ssDNA) to multiarm double stranded DNA (dsDNA) to space-filling DNA origami. By exploring the influences of synthetic (macro)molecules on a non-natural, yet geometri-

cally precise object, exclusive lessons on self-assembly, patterning, and interactions across 3D space can be learnt.

In this respect, polymer chemistry plays a crucial role in conferring additional properties to the already broad repertoire of capabilities demonstrated by DNA. Here, the near limitless capacity for monomer design coupled with recent advances in radical polymerization methodologies under mild aqueous conditions offers a fertile avenue for the development of novel polymer–DNA conjugates in years to come. Hence, one can easily envision the overwhelming extent of possibilities fusing polymer-based technologies, i.e. block copolymers, sequence defined polymers, and immolative polymers with DNA engineering.

Furthermore, the influence of DNA technology on synthetic chemistry is not solely limited on the nanoscale. By mimicking how nature uses DNA as a template for the proliferation of life, synthetic molecules can be designed to assemble similarly along a chain of ssDNA thereby transferring the sequence information provided by the template DNA onto the newly formed synthetic polymer chain. Beyond the recruitment of small molecules or polymer precursors based on the recognition of the nucleobases, DNA can be used to template polymer synthesis by functioning as a reactive center either as an initiator or a catalyst. In general, each part of the DNA—the nucleobases, the negatively charged phosphate-deoxyribose backbone, the major/minor grooves of the double helix, as well as the 5'/3' termini—is an attractive resource. Exploited differently, these parts of the DNA have expanded the breadth of polymer chemistry and provided alternative routes to fabricate nanoscale architectures.

2. CHEMISTRIES ON DNA

Native DNA is a rather chemically inert structure due to the lack of functional groups and the requirement to largely conserve the base-pairing region to maintain function. Through the motivation of DNA nanotechnology, it can now be functionalized through the incorporation of reactive handles, typically included at the 3'/5' termini as unnatural nucleotides or via unconventional means such as electrostatic complexation or intercalation. Consequently, the plethora of chemistries achievable on DNA has expanded and has been reviewed recently.¹ In this section we will focus on the chemistries relevant to the synthesis of DNA applicable to DNA–polymer conjugation. Specifically, we will discuss the possible techniques to install reactive handles and the challenges to adapt each chemistry for DNA synthesis. These functional handles can be divided into different categories where the target motif can be introduced through covalent modifications or noncovalent interactions with the DNA structure (Figure 1).

2.1. Solid Phase Synthesis

To incorporate covalent handles on DNA, depending on where the desired modification is situated, the attachment of the reactive group can be conducted during or at the end of DNA synthesis. For the synthesis of an oligodeoxynucleotide (ODN) a solid phase approach, employing phosphoramidite chemistry, is typically adopted. Phosphoramidite chemistry was first developed in the 1980s by Caruthers and co-workers and, through the optimization and employment of a solid support, resulted in the high yielding automated system used today.^{2,3} The solid support employed as the accepted standard is the controlled pore glass (CPG) bead. The CPG bead provides a

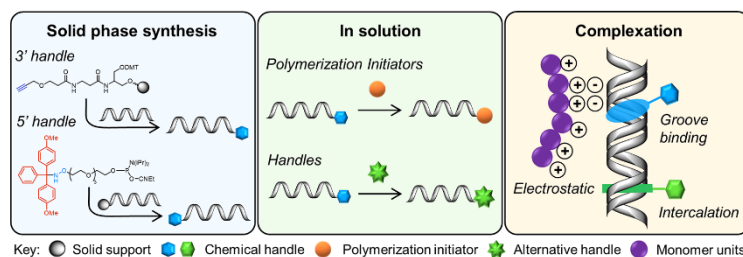


Figure 1. Approaches to synthesize DNA with functional handles applicable for polymer conjugation. Three approaches have been highlighted: solid phase synthesis through phosphoramidite chemistry, the subsequent in solution modifications of solid phase synthesized DNA for additional handles, and the complexation of small molecules and polymers through noncovalent interactions.

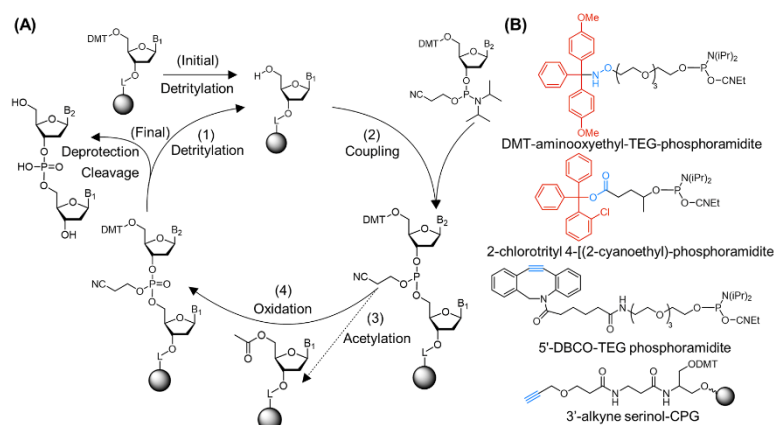


Figure 2. (A) Solid phase synthesis of ODNs through automated phosphoramidite chemistry on a CPG bead. (1) An initial detritylation step is required to activate the primary nucleoside for coupling. (2) Once activated the protected nucleobase phosphoramidite is added for coupling to the 5'-hydroxy of the solid bound nucleoside. (3) Some of the coupling reactions may be unsuccessful; therefore, a capping step is included. Step (4) involves the oxidation of the phosphite to phosphate and completes one cycle. The addition of nucleotides can be continued by repeating step (1) to step (4) until the ODN sequence is complete. Once complete, a final deprotection and cleavage step is performed. (B) Functionalized phosphoramidites bearing chemical handles for column modification or downstream conjugation. Two examples of protecting groups, DMT and 2-chlorotriyl, are shown in red, and each functional group (aminoxy, carboxylic acid, and alkyne groups) is highlighted in blue.

high surface area to offer numerous attachment points in addition to a high stability to chemical environments.^{4,5} Polystyrene (PS) beads can also be adopted for the solid phase approach offering highly efficient synthesis at the nanomole scale.^{6,7} The solid phase synthesis method cycles through coupling, capping, oxidation, and deprotection steps for the addition of each nucleotide (Figure 2A). Once the cycles are complete, the furnished ODNs are deprotected and cleaved from the CPG using a solution of ammonia. In this way, phosphoramidite chemistry provides an approach to synthesize any sequence of DNA up to approximately 200 bases. For DNA-polymer conjugates, ODNs are often shorter than 30 bases; therefore, this method does not pose as a limitation to the length and sequences attainable.

Importantly, phosphoramidite chemistry is not limited to natural nucleotides. Internal modifications can be incorporated through modified phosphoramidites as well as modifications at the 5'-end. The chemical synthesis of ODNs is performed from 3' to 5'; thus, 3'-end modifications are integrated through

functionalized supports which the ODN chain can grow from. Modified phosphoramidites were developed alongside the described method producing varying nucleobase, sugar, and phosphate backbone moieties.⁸ Although modifications can be integrated at several positions on the nucleotide, functional handles at the 3'- and 5'-end are most relevant to DNA-polymer synthesis for the production of diblock copolymers. 5'-terminus-functionalized phosphoramidites include reactive handles such as amines,⁹ carboxylic acids,¹⁰ alkynes,¹¹ and thiols.^{11,12} Each functional moiety must be compatible with phosphoramidite chemistry and may also require protection during the coupling process.

There are several protective groups, including dimethoxytrityl (DMT) for amines and 2-chlorotriyl for carboxylic acids (Figure 2B), which can be employed to incorporate these functional groups. Several moieties can be incorporated without protection and can therefore be readily modified "on column"—an advantageous attribute to grant access toward solid phase polymer coupling. Alkyne moieties, such as

dibenzo-cyclooctyne (DBCO), a strained alkyne capable of copper free click chemistry, are incorporated at the 5'-end, and standard unstrained alkyne groups can be included at the 3'-terminus through bead modifications prior to the solid phase synthesis (Figure 2B). Hydrophobic and hydrophilic linkers are available in the form of alkyl chains and ethylene glycol units, respectively, to link the described functional handles to the phosphoramidite.

The incorporation of the functional groups described above into the DNA makeup provides an avenue to synthesize DNA for conjugation to preformed polymers. Where polymerization directly from DNA is desired, the polymerization initiators, agents or monomers, must be attached prior to polymerization. Atom transfer radical polymerization (ATRP) initiator phosphoramidites are not available commercially; however, several can be synthesized and have been incorporated through solid phase synthesis prior to deprotection and cleavage, demonstrating a feasible method to attach initiator moieties to ODNs.^{13,14} A two-step reaction can conjugate the initiator group to the phosphoramidite moiety, now available for solid phase attachment, followed by cleavage and deprotection in ammonia. This method provides an automated route to synthesize ODNs bearing ATRP initiators. However, the attachment of reversible addition-fragmentation chain transfer (RAFT) agents prior to deprotection and cleavage is not possible due to its instability in ammonia. Similarly, the norbornene-phosphoramidite is also not available commercially; however, its synthesis and consequent incorporation has been established.¹⁵ In this case, two modified nucleoside phosphoramidites as well as the 3'-functionalized column were synthesized demonstrating the versatility and ability to choose the position of the norbornene moiety. Modifications in the base pair region may not be optimal due to conformation dynamics,¹⁶ in addition to sterics and charge repulsion from the overall DNA structure. Thus, to ensure the functional group is positioned externally (i.e., protruding the major or minor groove) on the DNA structure, the 5-position on cytosine and the 4-O-position on thymidine were adopted for the modification. These developments achieved through phosphoramidite chemistry have enabled the initial vision and future realization of covalent DNA-polymer synthesis.

2.2. In Solution

For several functional groups, such as RAFT agents, the corresponding phosphoramidite is either not commercially available or is not compatible with the solid phase synthesis process. However, the chemical handles available through solid phase synthesis can be postmodified after column cleavage to position the unattainable groups. Although the chemistry itself is simpler than the synthesis of a phosphoramidite, unprotected DNA is a polyelectrolyte and requires an aqueous solvent system (e.g., a Tris buffer of pH 8), which can present a new challenge. However, if organic solvents are required for the coupling reaction, surfactants can be employed through complexation to mitigate DNA's incompatibility with hydrophobic compounds.¹⁷ Many coupling reactions have now been demonstrated on functional handles, such as amines, thiols, and alkynes, which were previously incorporated during solid phase synthesis. As native DNA does not bear specific sites for chemoselective reactions, these compatible handles must be incorporated prior to column cleavage through the phosphoramidite chemistry described above. The conjugation of these functional ODNs with small molecules (for example,

fluorophores) has enabled the establishment of common procedures and reagents for coupling in the presence of unprotected DNA.¹ For a more efficient conjugation of DNA to polymers, several moieties are of interest that are not available as phosphoramidites for solid phase synthesis. For instance, norbornene-tetrazine chemistry was established as an efficient self-reporting method for DNA-polymer conjugation; therefore, the modification of a reactive ODN to bear these specialized functions was desired.¹⁸ Both functional groups are not available as a phosphoramidite commercially (although the synthesized ODNs are now available); however, the synthesis in solution has been demonstrated (Figure 3).¹⁸

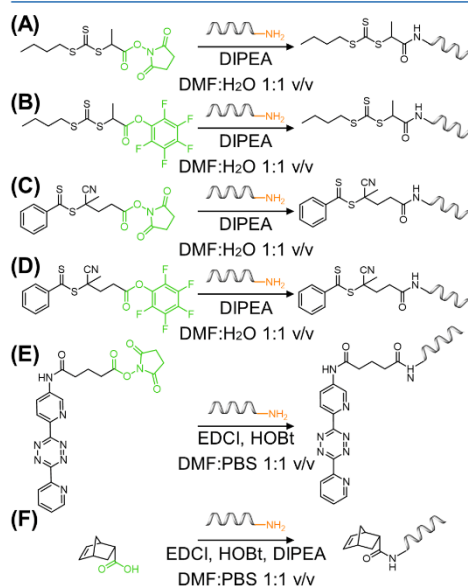


Figure 3. Solution-based modification of ODNs for functional handle attachment. (A)–(D) The attachment of RAFT agents, (((butylthio)carbonothioyl)thio)propanoic acid (BTPA) and 4-cyano-4-(phenylcarbonothioylthio)pentanoic acid (CPADB), to ODNs through amide coupling chemistry with NHS and pentafluorophenol (PFP) activated carboxylic acids. (E) NHS-activated coupling of tetrazine to amine DNA. (F) Amide coupling of norbornene-carboxylic acid with amine DNA. Coupling reagents include diisopropylethylamine (DIPEA), 1-ethyl-3-(3-(dimethylamino)propyl)carbodiimide (EDCI), and 1-hydroxybenzotriazole (HOBT), and solvents include dimethylformamide (DMF) and phosphate buffered saline (PBS).

The reactions were performed in a dimethylformamide (DMF)-phosphate buffered saline (PBS) 1:1 v/v solution to ensure solubility and stability of both the unprotected ODN bearing a carboxylic acid or *N*-hydroxysuccinimide (NHS) functional handle and the small molecules.¹⁸ In this case, the now adapted functional end-groups were available for direct conjugation with a presynthesized polymer.

The examples described so far document the secondary modification of native DNA to bear functional handles for covalent conjugation of DNA with presynthesized polymers.

For polymerization to occur from DNA (*grafting from* approach), the polymerization initiator or agent must be anchored to the DNA structure. Although the synthesis of ODNs bearing ATRP initiators has been realized through phosphoramidite chemistry, in contrast, RAFT agents cannot be conjugated prior to the deprotection and cleavage steps. Postmodification cannot take place on the solid support and must be conducted in solution after cleavage. This synthesis was demonstrated through the postmodification of amine DNA with NHS or pentafluorophenol (PFP) activated-RAFT agents, i.e. ((butylthio)carbonothioyl)thio)propanoic acid (BTPA) and 4-cyano-4-(phenylcarbonothioylthio)pentanoic acid (CPADB) (Figure 3).¹⁹ Such reactions were each performed in a DMF–PBS 1:1 v/v solution and demonstrated efficient yields to position RAFT agents on ODNs. These methods demonstrated the ability to synthesize ODNs bearing a wide range of functional groups for either direct polymer conjugation or growth through RAFT polymerization, aiding the widespread development of DNA–polymer function and application. Nonetheless, the examples described here each adopt an amine-functionalized ODN and therefore do not explore the plethora of coupling chemistries available to position functional groups not available as phosphoramidites. Through the continuous expansion of click chemistry and bioconjugation, the possibilities for ODN functionalization with synthetic macromolecules can be perpetually expanded.

Additionally, in this section we have highlighted the approaches adopted for reported conjugations, which each require a functional handle from solid phase phosphoramidite synthesis. However, the functionalization of DNA is not limited to this method. Chemical handles can also be incorporated through DNA polymerase extension with modified deoxynucleotide triphosphates (dNTPs). The employment of modified dNTPs opens an alternative toolbox to incorporate non-native functional groups through enzymatic synthesis.²⁰ Although this approach has not been employed for DNA–polymer synthesis, efficient incorporation and subsequent coupling has been established,²¹ demonstrating an opportunity for alternative conjugation methods with potentially improved yields and diversity.

2.3. Complexation

In addition to the portfolio of covalent chemistries available to the reactive groups of DNA, noncovalent approaches exploiting the structural elements of DNA offer an alternative route for DNA functionalization. Native dsDNA is a highly charged molecule, formed through many noncovalent interactions which can be exploited for noncovalent complexation. ssDNA forms the duplex through hydrogen bonding and van der Waals forces, π - π stacking, and hydrophobic effects in addition to the entropically favorable disorder of water molecules. These interactions present opportunities for noncovalent dynamic binding of small molecules to the major and minor groove, between base pairs and to the phosphate backbone (Figure 4). Through these binding modes, there is the potential for noncovalent interactions to be used to anchor functional groups as well as to complex whole polymers. In contrast to the covalent conversions described above, noncovalent complexation is a highly dynamic assembly that does not require chemical modifications to the intrinsic DNA makeup.

The capability to employ electrostatic interactions with the charged backbone generates a simple method for cationic

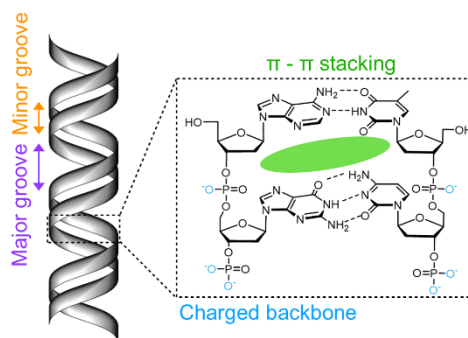
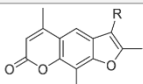
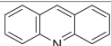
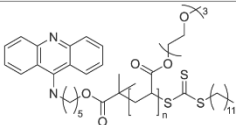
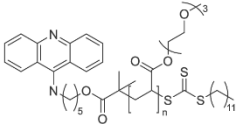
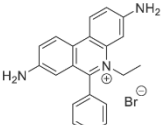
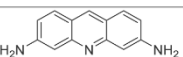
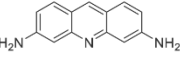
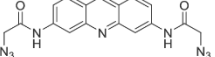
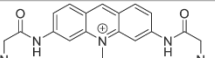


Figure 4. Noncovalent complexation sites of dsDNA. The minor and major groove, base stacking, and charged phosphate backbone have been highlighted.

molecules to bind to the sterically available anionic groups on DNA. The charged backbone plays many important roles in nature, such as guiding proteins and ligands to designated positions,²² for example through the supramolecular assembly of DNA with the positively charged histone protein. These intrinsic interactions inspired the employment of the phosphate backbone for DNA–polymer conjugate synthesis. To afford this interaction, a reduction in ion–ion repulsion is required where stabilization with Group 1 and 2 counterions is commonly used. Thus, equally for the interaction with polymers, ion displacement must occur. A huge charge repulsion must be overcome in comparison to other biological molecules, such as proteins, which are commonly neutral or have low charge counts. This is evidenced by the thermal energy required to bring two DNA molecules into proximity where electronic repulsion is 100× increased without the presence of counterions.²³ Due to the dynamic nature of DNA interactions, it is difficult to study the ion sphere to understand precise interactions;²³ however, the Poisson–Boltzmann equation can be employed to describe the relationship between a charged molecule and the counterions in solution to provide information about the ion–ion interactions.^{24,25} Overall physical properties of the DNA–polymer product, such as zeta potential and morphology, can also be analyzed to predict the complexation interactions. The interaction of polycationic polymers with DNA has gained interest due to the increased ambition to deliver DNA to cells as potential therapeutics. The dissociation of DNA–polycations through the addition of counterions can probe the effect of ionic strength on the polymer interactions.²⁶ Several counterions of varying anion and cation units were added to DNA–polycation complexes, revealing the Group 2 ions, Ca²⁺ followed by Mg²⁺, as the strongest dissociators in comparison to the Group 1 ions. Anion competitors were also studied showing the larger and less electronegative I[−] caused the greatest effect on polymer dissociation followed by Br[−], Cl[−], and F[−].²⁶ Conversely, the study of polymer binding has also been performed exposing an important note—the binding of cationic polymers to DNA reduces the overall charge and thus alters the hydrophobicity.²⁷ Therefore, balancing the concentration of cationic polymer units to DNA's anion charges has crucial implications for solubility and aggregation. Full neutralization of charge leads to DNA condensation, which, depending on the application

Table 1. List of Intercalators and Their Binding Strength

Intercalator	Structure	[Salt] mM	K / M^{-1}	Ref
Trimethylpsoralen		Not declared	1.79×10^4	Maeda (2002) ³⁸
Acridine orange		0.55	2.69×10^4	Tajmir-Riahi (2007) ³⁹
Acridine-polydimethylacrylamide (DMAm)		0.63	4.03×10^3	O'Reilly (2014) ⁴⁰
Acridine-poly(tri(ethylene glycol) methyl ether acrylate)		0.63	1.03×10^3	O'Reilly (2014) ⁴⁰
Ethidium bromide		0.55	6.58×10^4	Tajmir-Riahi (2007) ³⁹
Proflavin		7.5	$\geq 3.8 \times 10^6$	Tuite (2013) ⁴¹
Proflavin		508	1.4×10^5	Tuite (2013) ⁴¹
Proflavin diazide		7.5	5.3×10^5	Tuite (2013) ⁴¹
MeProflavin diazide		7.5	2.0×10^6	Tuite (2013) ⁴¹

desired, can have implications, such as steric hindrance of reactive sites. Similarly, the pH has large consequences on binding strength and, accordingly, the ability to form complexes.²⁸ A lower pH can yield a higher degree of binding as observed by the smaller and more tightly packed morphology in comparison to the larger structures observed at a higher pH—a lower pH yields a higher extent of ionization.²⁸ In addition to the ion displacement, the shape of the polymer also has an effect on DNA complexation.²⁹ The work of Tang and Szoka employed several polymers of similar molecular weight but varying degrees of branching to investigate complexation with DNA.²⁹ Interestingly, the unordered branched polyethyleneimine yielded average complex diameters of 90 nm, which is approximately 5% of the linear polylysine complex average diameter of 2000 nm. Thus, the shape can dictate both the polymer packing and the condensation of DNA. An understanding of the structure and charge effects of cationic polymer binding to DNA can aid the design and choice of the respective polymer to avoid undesired

structure deformation and to ensure applicability for the desired function.

Groove binders have become a major target for small molecule and protein binding for therapeutic action.³⁰ Many natural products have been discovered that offer native antibacterial or anticancer properties through groove binding and grant insight into structural qualities appropriate for association.³⁰ Through the desire to understand the interactive pockets, the precise interactions have been revealed and can therefore be utilized for future therapeutic designs. Groove binders can target either the major or minor groove (Figure 4) through several noncovalent interactions, consisting of hydrogen bonding and van der Waals and electrostatic interactions. Each base pair provides a different environment through the varying electrostatic effects, groove width, and depths. Therefore, selective binding can be employed; for example, small molecule binding tends to prefer AT rich regions due to the increase in van der Waals forces provided through the deeper pocket.³⁰ Additionally, the minor groove offers a tighter

pocket, attracting small molecules or polymer chains bearing small monomer units, such as poly(pyrrole) and polyamides,³¹ that are either cationic or neutral.³² Due to the many interactions possible, binding is afforded through several mechanisms. Specific interactions include H-bonding with the sugar C1, purine N3, and pyrimidine N1 as well as the base pairing moieties.³² Additionally, shape selective binding due to molecular curvature is also apparent, where molecules match that of the native DNA structure.³⁰ All these parameters brought together lead to a high degree of target specificity. Larger molecules, such as proteins and carbohydrates, recognize and bind in the major groove. Although there are more donor and acceptor sites in the major groove providing the platform for stronger overall enthalpic interactions, fewer natural examples of major groove binders are described.³³ Aminoglycosides are nonaromatic molecules which preferentially bind to the major groove of B-DNA due to the dimensions and hydrogen bonding opportunities.³¹ Although initial interactions may be with the phosphate backbone, studies employing a triplex DNA structure demonstrated the competitive release of the third strand on the addition of an aminoglycoside dimer, implying major groove binding of the aminoglycoside structure.^{34,35} A fundamental interaction is the protein–DNA dynamic binding with the major groove. In this case, the noncovalent H-bonds and salt bridges allow a reversible binding and release for processes, such as transcription and gene regulation. The functional groups on the bases and ribose sugar provide several H-bond donor and acceptor sites. A detailed analysis of structure relationships has been reviewed previously by Thornton and co-workers.³⁶ Although current approaches to DNA–polymer conjugation do not directly employ groove binding, understanding the interactions will guide future designs to improve polymer interactions through structure optimization as well as positioning groups for functional anchors along the backbone. Proteins and aminoglycosides both offer many H-bonding sites in addition to positively charged residues to overcome repulsive forces. Through this knowledge, polymer design can be molded to encompass these attributes. However, it is important to also consider the structural distortions groove binding can have on the B-DNA structure. Groove binders that possess a strong overall binding enthalpy that outweighs the conformational changes can induce a fit.³⁷ Depending on the specific application of the DNA, these structural changes may hinder downstream interactions.

While the backbone and grooves offer external interactions with DNA, the structure also offers the conformational flexibility to exploit the base pair stacking to complex small molecules within. π – π stacking interactions between planar aromatic purine and pyrimidine rings and aromatic molecules are possible and have been discovered in many natural products.⁴² Natural product functions have consisted of several inhibitory roles which may act through allosteric interference of protein binding,⁴³ influencing the development of anticancer drugs.⁴⁴ Similar to groove binding, intercalators can cause conformational changes, such as extension. This extension is useful to determine binding through length changes; however, it may also alter recognition and function of DNA as a genetic material.⁴⁵ Intercalators, forming a mono- or bis-intercalation between one or over two base pairs, respectively,⁴⁶ have been developed either for anticancer agents or as fluorescent dyes to visualize or quantify DNA.^{44,47} Several key features aid the association, such as a positive charge as present on ethidium

bromide (Table 1) and three or four conjugated rings. As well as the stacking interactions, complementary dipoles can also increase association strength. The aromatic nature provides a plethora of reaction conditions to perform substitution reactions to anchor reactive handles on the intercalator backbone.⁴⁸ These substitution reactions can yield reactive handles for polymer coupling prior to intercalation allowing the possibility of direct noncovalent conjugation of preformed polymers throughout the DNA duplex.⁴⁰ Prior to polymerization, a two-step synthetic approach was demonstrated employing 9-chloroacridine as the starting material to yield the polymerization-agent bearing acridine intercalator (an example acridine compound is shown in Table 1). Polymerization from the functionalized acridine could then be performed followed by DNA intercalation. Intercalation was noted with each polymer–acridine conjugate; however, there was an effect on the association constant depending on the polymer employed (Table 1). The authors attribute this effect to the molecular weight and structure of the polymer where varying hydrophobicity and side-chain makeup have been explored.⁴⁰ An alternative intercalator is psoralen, a 3-ringed furanocoumarin monointercalator (Table 1), commonly adopted to cause mutagenesis under ultraviolet (UV) light.⁴⁹ Psoralen intercalation occurs preferentially through thymine interactions, although the presence of substituents can shift the precise positioning.⁵⁰ Similarly to acridine, functional handles can be positioned to provide anchors for conjugation of polymers. Specifically, a trimethylpsoralen was functionalized with a terminal amine to afford amide conjugation with an NHS polymer.^{38,39} Once conjugated, the psoralen can intercalate with the dsDNA, yielding a noncovalent DNA–polymer interaction. So far in this section, the two examples have demonstrated the direct assembly of polymers with DNA through covalent polymer conjugation with an intercalator. Although binding was noted in each case, a reduction in association strength was also exhibited.⁴⁰ To ensure efficient binding, an alternative approach where intercalators bearing functional handles are assembled with DNA prior to polymer conjugation can maintain binding strengths. This was demonstrated with proflavin, an acridine derivative, which can undergo modification to produce a diazide, positioning the functional handles in the major groove.⁴¹ The addition of these functional groups reduced the binding by 10-fold (Table 1). However, by a further modification to produce methyl proflavindiazide, the binding strength is returned to the same magnitude as the unmodified proflavin.⁴¹ Once intercalated, the click reaction is then feasible with alkyne-bearing molecules, such as the 5-pentynyl-thienyl-pyrrol monomer.⁵¹ By positioning the polymerizable monomer in the major groove, templated polymerization along the DNA backbone can now be envisaged.

In the complexation interactions described above, each mechanism is explored individually; however, for several DNA binders, multiple interactions are involved. A commonly adopted example is the combination of intercalation and groove binding of antibiotics bearing peptide groups which reside in the minor groove.⁵² Triple interactions have also been noted; for example, the conjugate neomycin–Hoechst 33258 pyrene exhibits a neomycin major groove interaction, a Hoechst 33258 minor groove interaction, and a pyrene-intercalator.⁵³ Importantly, the introduction of conjugate moieties increased the binding constant up to 10-fold in comparison to the individual small molecule (in this case,

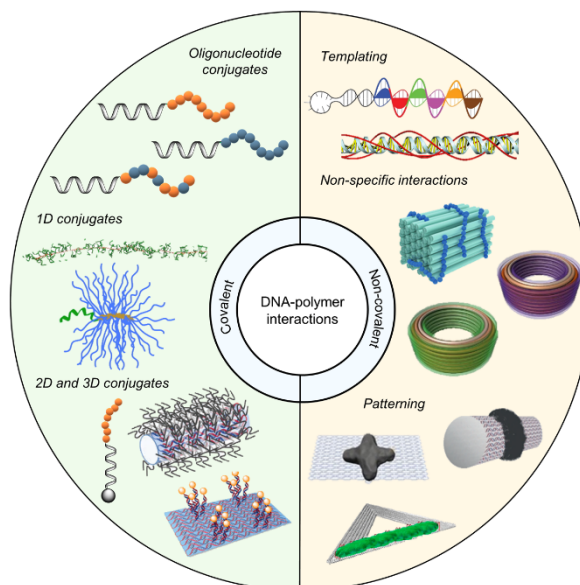


Figure 5. DNA–polymer conjugate synthesis summary. Conjugates are categorized as covalently or noncovalently bound. Covalently bound structures can be conjugated either in solution by combining an oligonucleotide with either a linear polymer or a polymer brush.^{54,55} Reproduced with permission from ref 54. Copyright 2016 American Chemical Society.⁵⁵ Reproduced with permission from ref 55. Copyright 2015 American Chemical Society. Solid supports, such as beads and DNA nanostructures, can also be adopted to provide a platform for the conjugation.^{56,57} Reproduced with permission from ref 56. Copyright 2018 the Royal Society of Chemistry. Reproduced with permission from ref 57. Copyright 2016 John Wiley and Sons. Alternatively, the conjugates can form through noncovalent interactions, such as templating.^{58,59} Reproduced with permission from ref 58. Copyright 2011 the Royal Society of Chemistry. Reproduced with permission from ref 59. Copyright 2013 Springer Nature. Nonspecific interactions through complexation in addition to patterning of polymers on DNA are also possible.^{60–64} Reproduced with permission from ref 60. Copyright 2016 the Royal Society of Chemistry. Reproduced with permission from ref 61. Copyright 2017 Springer Nature. Reproduced with permission from ref 62. Copyright 2018 John Wiley and Sons. Reproduced with permission from ref 63. Copyright 2014 American Chemical Society. Reproduced with permission from ref 64. Copyright 2020 John Wiley and Sons.

Hoechst 33258).⁵³ Therefore, attention to the multifaceted noncovalent design of DNA–polymer conjugates would increase binding strength and thus has potential to prolong complex stability. The interactions noted for intercalator–conjugate assemblies lay the foundation for intercalator–polymer design to guide the synthesis of precise polymeric nanostructures.

3. DNA–POLYMER SYNTHESIS

Polymerization was first noted in the 1800s and has since developed to produce the synthetic polymers commonly used today, such as PS and Nylon (Figure 6). Due to the structural prospects, diblock copolymers have gained growing interest and can be designed to form many nanostructures, such as micelles and vesicles. Through the advancements of living polymerization techniques, polymer length dispersity is now reduced and has enabled the synthesis of copolymers for lithography and many controlled nanostructures. Combining DNA with synthetic polymers enriches functional properties through the combination of the hydrophobic/hydrophilic nature of the polymer and the ease of further functionalization through the complementary DNA sequence. DNA is a highly programmable entity with a plethora of structures, providing

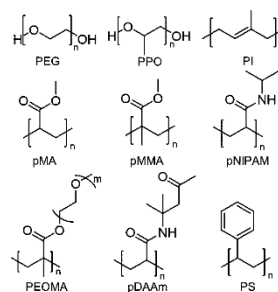


Figure 6. Examples of commonly used polymers for DNA–polymer conjugates: PEG, poly(ethylene glycol); PPO, poly(propylene oxide); PI, poly(isoprene); pMA, poly(methyl acrylate); pMMA, poly(methyl methacrylate); pNIPAM, poly(*N*-isopropylacrylamide); PEOMA, poly(ethylene oxide methyl ether methacrylate); pDAAm, poly(diacetoneacrylamide); PS, polystyrene.

the platform to control the synthesis of polymers as well as their spatial organization. Here, we will discuss the recent advancements, the challenges, and possible solutions to

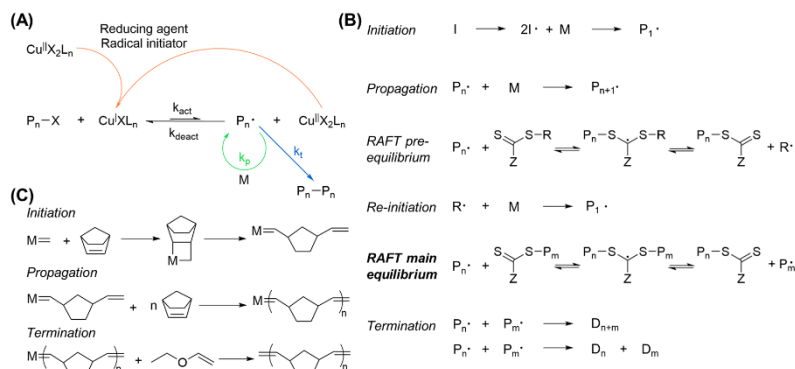


Figure 7. Living polymerization techniques appropriate for DNA–polymer synthesis. (A) Schematic of Cu-catalyzed ATRP. The transition metal catalyst, here Cu, is reduced to activate and initiate the radical. Polymer propagation (K_p) occurs through radical polymerization of reactive monomers. Termination (k_t) proceeds through the combination of reactive polymers. Catalysts are oxidized through the activation step and can deactivate either through the more prominent deactivation or by the reducing agent. The equilibrium between activated (k_{act}) and deactivated (k_{deact}) states is determined by the catalyst used. (B) RAFT polymerization mechanism where I = initiator, M = monomer, P = polymer, Z = radical stabilizing group, and D = dead polymer. (C) ROMP employing a metal catalyst for coordination to a strained alkene for olefin metathesis. Termination can be performed by the addition of ethyl vinyl ether to coordinate to and remove the metal catalyst.

synthesize DNA–polymer conjugates. DNA–polymer conjugates can be categorized through their interaction, either covalent or noncovalent, and through the DNA structure, from ODNs through to nanostructures, such as DNA origami (Figure 5).

3.1. Covalent DNA–Polymer Conjugates

There have been large developments in the synthesis of covalent DNA–polymer conjugates; however, several limitations have hindered progress. We will first introduce the polymerization methods employed for DNA–polymer conjugate synthesis and highlight the limitations of these methods in addition to the challenges of combining synthetic polymers with DNA. Through this discussion, we can build a greater understanding of the progress made in this field through solution- and platform-based conjugation methods which are described in this section.

3.1.1. Polymerization Methods. There are several polymerization methods applicable to DNA–polymer conjugates, including anionic, cationic, ring-opening, and free radical polymerizations. Free radical polymerizations are most commonly adopted for linear polymer synthesis for DNA–polymer conjugates where the equilibrium required to accomplish reduced mass dispersity was first demonstrated through ATRP. ATRP was invented in 1995 and employs an alkyl halide as the initiator along with a redox-active catalyst (Figure 7A).^{65,66} Here, the equilibrium is determined by the rate of activation and deactivation of the propagation reaction, where deactivation must be greater than activation to maintain a low concentration of radical species. The first examples of ATRP required a metal catalyst, which initially led to developments involving reducing agents to reactivate the metal center to reduce the required metal concentration; however, it could not be removed entirely. Metal free ATRP was later developed and employs an organic redox-active catalyst, therefore reducing the biological toxicity of the reaction and increasing the compatibility of ATRP for DNA conjugation.⁶⁷ RAFT polymerization was developed shortly

after ATRP and is also performed metal free. RAFT proceeds by a radical polymerization mechanism in the presence of a chain transfer agent (CTA) to afford the necessary equilibrium for reduced mass distribution (Figure 7B). The added chain transfer step redistributes the radical to allow an equal probability for all chains to grow. Importantly, RAFT polymerization end-group chemistry is readily available through the liberation of the thiol group in the transfer agent. Although ATRP and RAFT are the most prominent, ring-opening polymerizations (ROPs), such as ring-opening metathesis polymerization (ROMP), have also been applied to polymer synthesis for the production of DNA–polymer brush structures. ROMP occurs through olefin metathesis of a strained alkene, which drives the reaction (Figure 7C). Here, a metal catalyst is employed to form an open coordination with the alkene followed by a [2 + 2] cycloaddition. The catalyst, again, provokes challenges for purification and side reactions.

The synthesis of covalently bound DNA–polymer conjugates has seen large developments, now enabling the controlled synthesis of diblock copolymers consisting of many combinations of polymers and DNA nanostructures. The synthesis of DNA–polymer conjugates can be categorized into three methods: *grafting from*, *grafting to*, and *grafting through* (Figure 8). *Grafting from* occurs when the polymerization initiator is covalently bound to the DNA followed by *in situ* polymerization, whereas for *grafting to*, the polymer and DNA parts are presynthesized prior to conjugation. *Grafting through* encompasses the polymerization of macromonomers bearing a polymerizable group to synthesize polymers with defined side chains. Each approach bears advantages—*grafting from* exhibits the greatest attachment chemistry and therefore largest density,⁶⁸ whereas *grafting to* allows thorough polymer characterization prior to conjugation and polymer choice is broader (the polymerization occurs in the absence of DNA—the reaction can occur in larger scales, in many solvents, and using different monomers). *Grafting through* is employed less frequently; however, it can efficiently synthesize many brush

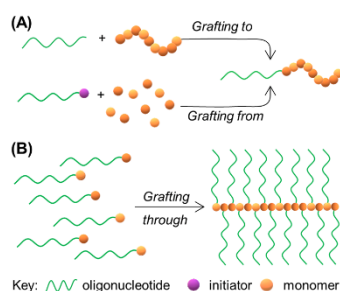


Figure 8. Common approaches to synthesize DNA-polymer conjugates. (A) *Grafting to*, i.e. polymerization in isolation from DNA, prior to covalent attachment and *grafting from*, i.e. polymerizing from an initiator covalently attached to the DNA. (B) *Grafting through*—polymerization of monomers either with the ODN already conjugated or with a functional group for postpolymerization conjugation.

hyperbranched structures. Nonetheless, each approach has drawbacks to either the yield or breadth of polymer conjugates achievable. These drawbacks can be accounted for by both the use of DNA in this system and also the polymerization conditions.

3.1.2. DNA-Polymer Conjugate Synthesis Limitations.

Through the advancement of the polymerization methods described above, polymer synthesis, itself, is a highly established technique, which has been optimized for many monomer and polymer types. In parallel, the expansion of bioorthogonal chemistry has provided a plethora of conjugation reactions between modified DNA and a variety of molecules, providing ample resources for DNA to polymer conjugation reactions. However, for DNA-polymer conjugates, there are several limitations due to the combination of these two materials in one reaction pot because they can each provide contrasting properties. In the approaches discussed here, DNA is present either in the conjugation reaction (*grafting to*) or in the polymerization reaction (*grafting from*). DNA is a highly ionic molecule requiring an aqueous environment which is readily compatible with hydrophilic monomers and polymers; however, hydrophobic monomers and polymers require a solvent mixture to enable solubility. Organic solvents are commonly poor liquids for DNA, altering hydrogen bonding, polarity, and hydrophobicity.⁶⁹ Specifically, solvents consisting of longer or alkyl-substituted chains cause the greatest disruption.⁷⁰ Consequently, initial studies employing the *grafting to* approach reported low yields for the conjugation of hydrophobic polymers to DNA.⁷¹ However, as hydrophobic polymers also pose great interest, several groups have established improved methods such as DNA protection with counterions or sophisticated coupling chemistries.^{17,18} A thorough investigation into possible coupling reactions between DNA and poly(*N*-isopropylacrylamide) (pNIPAM) was performed by O'Reilly and Wilks.¹⁸ They found amine coupling and thiol-ene Michael addition reactions did not synthesize the correct product in organic solvents or were not reproducible. In each case, several solvents were trialed including DMF, dimethyl sulfoxide (DMSO), acetonitrile (ACN), and tetrahydrofuran (THF).

Similarly, the *grafting from* approach also favors hydrophilic monomers. An example employing DMSO as the solvent to polymerize methyl acrylate established a method for successful polymerization.¹⁴ Polymerization induced self-assembly (PISA) can also overcome this challenge by the polymerization of hydrophilic monomers to produce hydrophobic polymers.^{72,73} The use of PISA has been employed to successfully produce DNA-hydrophobic polymer conjugates through the *grafting from* approach.⁷⁴

In addition to solvent compatibility, both blocks of the DNA-polymer conjugate are flexible polymers and can therefore shield the reactive moiety. Steric effects are observed when coupling to all forms of DNA—ss, ds, and nanostructures—although the effects are different for the solution-based (ss and ds) and solid support (nanostructures and DNA origami) forms. Additionally, the sequence of ssDNA requires a fine design to ensure the secondary structures do not hinder the reactive site. This also applies to dsDNA where the duplex may be in equilibrium with higher ordered structures. In both ss- and dsDNA, the sequence can be designed and modeled to ensure that inhibitory secondary structures are avoided. Conjugation to DNA origami presents the greatest hindrance for conjugation. The DNA origami not only burdens the reaction center with steric hindrance, it also, where multiple sites are present on one structure, reduces the distribution of reaction sites in solution and requires a higher local concentration on the origami. This causes drawbacks for both approaches; however, *grafting from* is deemed preferable to synthesize DNA origami-polymer conjugates as the steric hindrance is reduced.⁵⁷ Steric effects are also a large consideration when coupling to a preformed polymer, i.e. *grafting to*. In this case, the larger polymers may shield the reactive handle and therefore reduce the reaction process.

Although the limitations described so far are mainly attained from the *grafting to* approach, the *grafting from* technique performs the polymerization in the presence of DNA, which produces additional challenges. When handling DNA, small volumes are typically employed due to limited resources (reactive group-bearing oligos are commonly produced in microgram quantities); thus, when *grafting from*, small volumes are also adopted for the polymerization process. This limitation is mainly apparent as both RAFT and ATRP techniques are oxygen sensitive and therefore require an anaerobic environment. The approximate length of polymers can be controlled by the monomer to transfer agent or initiator ratio; however, oxygen is a radical scavenger and can therefore quench the initiated or transferred radical, altering the ratio. Radical polymerization in the absence of DNA (i.e., polymerizations performed prior to conjugation and not employing the *grafting from* approach) can be performed in large volumes and is therefore not limited through the available techniques to remove oxygen. The most effective method to remove dissolved oxygen is through N₂ purging.⁷⁵ N₂ purging is possible in large scale synthesis; however, *grafting from* DNA is commonly performed in less than 300 μL, preventing the efficient use of purging. Similarly, the freeze-pump-thaw technique, whereby the solution is frozen before a vacuum is applied to reduce the dissolved oxygen solubility, can take place in larger volumes, i.e. 1 mL. However, this technique is again problematic when performing the polymerization in small volumes, i.e. <300 μL, in the *grafting from* approach where the DNA concentration is limited. Volume loss may compromise reproducibility due to the effects residual oxygen

Table 2. Polymerization Reactions and Conditions in the Presence of DNA⁴⁷

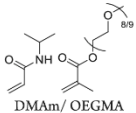
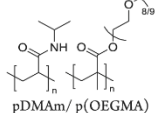
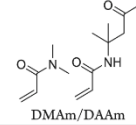
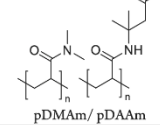
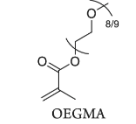
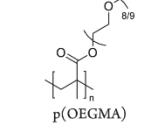
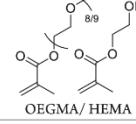
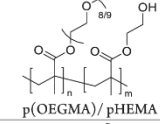
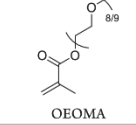
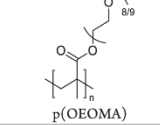
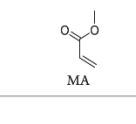
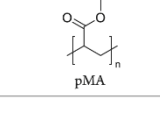
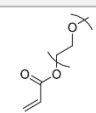
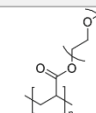
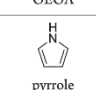
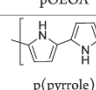
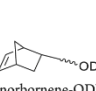
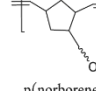
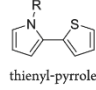
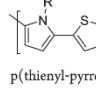
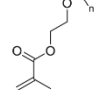
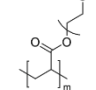
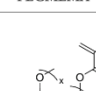
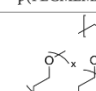
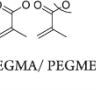
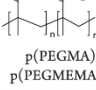
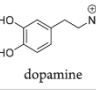
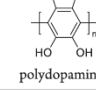
DNA	Monomers	Polymer	Technique	Grafting approach	Catalyst/ radical initiator	Solvent	Volume	Ref.	
ODN			RAFT	from	Eosin Y 470 nm	H ₂ O	400 μL	Ng, Weil (2019) ¹⁹	
			RAFT	from	VA-044	<i>t</i> -butanol/ DPBS, pH 6 (1:5, v/v)	40 μL	Ng, Weil (2020) ⁷⁴	
			ATRP	from	CuCl/CuBr ₂ / bpy 1:0.3:3	H ₂ O	262.5 μL	He (2007) ⁸²	
			RAFT	from	AIBN	H ₂ O	10 mL	He (2009) ⁸³	
			ATRP	from	CuBr ₂ /TPMA Ascorbic acid NaCl	H ₂ O:DMF 1:1 v/v	5 mL	Das (2014) ¹³	
			ATRP	from	CuBr ₂ / Me ₆ TREN UV light	DMSO	400 μL	Matyjaszewski (2017) ¹⁴	
				ATRP	from	CuBr ₂ /TPMA 450 nm light	PBS	5 mL	Matyjaszewski (2018) ⁸⁴
				ATRP	from	CuBr ₂ /TPMA	PBS, pH 6	5 mL	Matyjaszewski (2018) ⁸⁵
				ATRP	from	CuBr ₂ /TPMA Ultrasound	H ₂ O	5 mL	Matyjaszewski (2018) ⁸⁶

Table 2. continued

DNA	Monomers	Polymer	Technique	Grafting approach	Catalyst/radical initiator	Solvent	Volume	Ref.
	 OEOA	 pOEOA	ATRP	from	CuBr ₂ /Me ₆ TREN UV light	DMSO	400 μL	Matyjaszewski (2017) ¹⁴
	 pyrrole	 p(pyrrole)	Oxidation	from	LiClO ₄ Electrical current	H ₂ O	500 μL	Teoule (1994) ⁸⁷
	 norbornene-ODN	 p(norbornene)	ROMP	through	Grubbs catalyst (2nd generation)	THF	3 mL	Herrmann (2014) ¹⁷
Linear DNA	 thienyl-pyrrole	 p(thienyl-pyrrole)	Oxidative	on		H ₂ O/ t-BuOH 1:9 v/v	25 μL	Pike (2015) ⁵¹
	 PEGMEMA	 p(PEGMEMA)	ATRP	from	CuBr ₂ /TPMA ascorbic acid NaCl	H ₂ O:DMF 1:1 v/v	105 μL	Wu, Weil (2016) ⁵⁷
	 PEGMA/PEGMEMA	 p(PEGMA)/ p(PEGMEMA)	ATRP	from	CuBr ₂ /TPMA ascorbic acid NaCl	H ₂ O:DMF 1:1 v/v	105 μL	Wu, Weil (2016) ⁵⁷ (2018) ⁵⁶
DNA origami	 dopamine	 polydopamine*	Oxidation	on	Hemin H ₂ O ₂ TAE/ Mg/ K pH 5.3	H ₂ O	100 μL	Ng, Weil (2018) ^{56,62}
	 dopamine	 polydopamine*	Oxidation	on	Protoporphyrin IX BIS-TRIS, pH 6.5 Visible light	H ₂ O	50 μL	Ng, Weil (2020) ⁶⁴

*Polymerizations are performed either *from*, *on*, or *through* DNA regions. DMAM, dimethylacrylamide; OEGMA, oligoethylene glycol methacrylate; DAAM, diacetoneacrylamide; HEMA, hydroxyethyl methacrylate; OEOMA, oligoethylene oxide methacrylate; MA, methyl acrylate; OEOA, oligoethylene oxide acrylate; PEGMEMA, polyethylene glycol methyl ether methacrylate; TPMA, Tris (2-pyridylmethyl) amine; *, example polydopamine structure.

will have on the polymer length and yield. Additionally, DNA degradation can occur when the sample is subjected to repeated freezing and thawing—tension forces are generated from ice crystals and may lead to strand breakage.⁷⁶ An alternative method is enzyme degassing—a technique that enables oxygen sensitive polymerization in air. Glucose oxidase, an enzyme that converts oxygen to hydrogen peroxide,

can perform successful enzyme degassing for RAFT polymerization in an open, low volume vessel *grafting from* ODNs.⁷⁷ Enzyme degassing provides an avenue to explore a wider range of polymers synthesized through the *grafting from* approach in the presence of DNA and in small volumes. However, purification to remove the enzyme is required after the reaction if downstream processes are desired. There are also

other challenges associated with the reduced concentrations available when working with DNA. Again, polymerization in isolation from DNA can be performed as optimized; however, when reactions with DNA for conjugation or polymerizations from DNA are required, optimal concentrations may not be possible with the limited amount of DNA (Table 2). This is more notable when *grafting from* DNA origami. DNA origami is commonly synthesized in low volumes (less than 100 μL) and in low concentrations (approximately 50 nM). Polymerizations are optimal at mM concentrations; thus, to overcome this, sacrificial initiators are required in solution to ensure the concentration limit is reached.⁵⁷ Although this allows the reaction to proceed, polymerization also takes place in solution, adding competition to the DNA origami surface polymerization leading to downstream purification challenges.

In addition to the challenges described above, which originate from the physical and chemical environment, the absolute control of the polymerization method is still limited. Nature has the ability to demonstrate sequence defined polymerization exhibiting control and self-assembly in a precise and reproducible manner. These characteristics have inspired attempts to replicate controlled self-assembly with DNA–polymer conjugates. Several developments have been noted by the groups of Liu,^{59,78} Sleiman,^{79,80} and O'Reilly,⁸¹ establishing bespoke sequence polymerization. However, the intricacy and length of these polymers is still limited. Although there are several challenges when synthesizing DNA–polymer conjugates, several groups have still accomplished many novel and innovative advancements which will be discussed in the following sections.

3.1.3. Solution-Based ODN–Polymer Synthesis. The development of conjugation chemistry has aided the increased variety of polymers conjugated to ODNs. In this section, we will describe conjugation reactions between free ODNs and polymers to synthesize a diblock product with a 1:1 ratio between each block, i.e. conjugations where the ODNs have been cleaved from the solid support prior to polymer conjugation. By performing the ODN cleavage prior to the conjugation reaction, a wider range of chemistries can be performed as deprotection and side reactions are no longer limiting.




One of the most direct methods of DNA–polymer conjugation employs amine-functionalized ODNs and NHS-activated polymers. Stayton and co-workers demonstrated successful coupling of pNIPAM monofunctionalized with an NHS group to a 7-carbon aliphatic amine-ODN.⁸⁸ Due to the poor solubility of pNIPAM at high temperatures, the reaction was performed at 4 °C to avoid precipitation in aqueous environments. Here, the reaction was performed in 10% DMF with borate pH 9.5, although a successful reaction was also noted in 20% DMF with borate pH 8.2.⁸⁹ In 2001, Park and co-workers employed similar chemistry to conjugate NHS-functionalized poly(D,L-lactic-co-glycolic acid) (PLGA) to amine-ODNs in solution.⁹⁰ In water, PLGA degrades due to its ester linkage; however, by adopting NHS-PEG, reaction in an aqueous system becomes possible.^{71,91,92} The comparison between these approaches highlights the challenge when conjugating DNA with hydrophobic polymers which may require organic solvents to dissolve. Additionally, the hydrophobic nature of the polymer may cause phase-separation from the ODN. In another example, Park and co-workers conjugated PEG to an ODN by amide coupling. In this instance, an acid cleavable linker was incorporated through an

ethylenediamine intermediate attached between the ODN and the tertiary amine group providing a route to DNA release in the acidic environments of cellular compartments.⁹³ This demonstrates the potential for dynamic and changeable structures which will be discussed in section 4.2.3. Alternatively, to overcome DNA solubility restrictions for amphiphilic conjugation, Herrmann and co-workers employed a cationic surfactant to stabilize DNA.¹⁷ In the presence of the surfactant, DNA was soluble in DMF, DMSO, THF, and CHCl_3 and provided the opportunity for higher yielding conjugation reactions toward hydrophobic polymers, such as PPO, PI, and PS. This approach therefore opens great potential for amphiphilic DNA–polymer conjugate synthesis in solution.

Michael addition reactions have also been explored for ODN–polymer conjugation. Kataoka and co-workers synthesized a conjugate through the thiol–ene Michael addition of thiol-ODN to acrylate-PEG in tris-buffer pH 8.0 (aqueous). In each case, either an acetal⁹⁴ or a lactate⁹⁵ group was present at the opposite end of the polymer to the acrylate group but both did not affect the reaction. A similar conjugation was performed by the same group; however, in this instance, the DNA was replaced with RNA and the thiol group was positioned at the 5'-end in contrast to the 3' as in the two previous examples. Here, the reaction was carried out with triphenylphosphine in DMF, which was also compatible and produced the desired product.⁹⁶ Through the reactions with acrylamide described here, the incorporation of the acid labile ester group, β -thiopropionate, is consequently situated between the ODN and polymer blocks to enable a pH-responsive complex for RNA release. Herrmann and co-workers chose to perform Michael addition coupling with a maleimide activated PS to thiol-ODN. The maleimide-PS was dissolved in THF and mixed with thiol-ODN to result in a low yield of 13%.⁷¹

In addition to amine and thiol anchors, azide- and propargyl-ODN can also be exploited through the copper(I)-catalyzed Huisgen [3 + 2] cycloaddition to conjugate free propargyl-DNA to azide-functionalized polymers in solution.⁹⁷ Matyjaszewski and Das employed the polymer poly(oligo(ethylene oxide) methacrylate) (OEOMA), synthesized via ATRP of OEOMA to yield an average molecular weight of 14 700 Da, which was conjugated in high yields to the desired ODNs. Here, ACN was adopted to stabilize Cu(I) in the absence of a ligand while THF was added to dissolve the polymer. Conjugations to PEG have also been demonstrated with moderate yields.⁹⁸ However, to expand the diversity of polymer conjugates, conditions for amphiphilic conjugates are likewise desired. Reaction conditions were investigated by O'Reilly and co-workers for pNIPAM in 100% DMF, with final yields between 70 and 90%.⁹⁹ Hydrophobic polymer conjugation toward DNA was demonstrated using alkyne-modified poly(styrene) (M_n 4.4). In this case, the click reaction between PS and DNA produced high yields of 74% which had not previously been observed for similar approaches, providing an improved avenue for connecting DNA with hydrophobic polymers. Matyjaszewski and Das also demonstrated this click conjugation reaction with three polymers of similar molecular weight (PEG–methacrylate–pOEOMA₄₇₅, pOEOMA₃₀₀-co-MEO₂MA, and pOEOMA₄₇₅-co-DMAEMA) to RNA.¹⁰⁰ Here, the solvent was reduced to 0.6% ACN/H₂O and coupling was again successful. The versatility of DNA–polymer conjugate synthesis was demonstrated by the click

Table 3. Coupling Chemistries to Covalently Bind ODNs to Polymers

Oligo-R	Polymer-R'	Reagent	Solvent	Catalyst	Ref
	PLGA-NHS	-	DMSO	-	Park (2001) ⁹⁰
	PEG-NHS	-	Sodium phosphate buffer (pH 7.0)	-	Park (2003) ^{92, 93} (2005) ⁹¹
	pNIPAM-NHS	-	10% DMF, borate buffer pH 9.5	-	Stayton (1999) ⁸⁸
	pNIPAM-NHS	-	20% DMF, borate buffer pH 8.2	-	Freitag (2003) ⁸⁹
	PS-NHS PPO-NHS PI-NHS	Et ₃ N	DMF DMF THF	-	Herrmann (2014) ¹⁷
	PEG-carboxyl	-	-	-	Herrmann (2007) ⁷¹
	PS-mal	-	THF:H ₂ O	-	Herrmann (2007) ⁷¹
	pNIPAM-mal	-	-	-	Herrmann (2007) ⁷¹
	PEG-acrylate	-	Tris pH 8.0	-	Kataoka (2003), ⁹⁴ (2005) ⁹⁵
ORN-S	PEG-acrylate	PPh ₃	Tris pH 8.0	-	Kataoka (2005) ⁹⁶
	PEG-N ₃	Aminoguanidine Na ascorbate	H ₂ O/ACN	CuSO ₄ :THTA 5:1	Sleiman (2012) ⁹⁸
	pNIPAM-N ₃	-	DMF	CuI-P(OEt) ₃	O'Reilly (2013) ⁹⁹
Norborene-DNA	pNIPAM-tetrazine	-	DMAc, DMF, DMSO, NMP	-	O'Reilly (2016) ¹⁸
Tetrazine-DNA	pNIPAM-norborene	-	DMAc, DMF, NMP	-	O'Reilly (2016) ¹⁸

reaction on both RNA and DNA ODNs with polymers of varying hydrophobicities, which opens opportunities for downstream applications. Additionally, in each example, high yields are reported which exhibit a robust approach for conjugation in solution compared to the thiol–ene Michael addition reaction.

To address the challenge of poor yields often noted for DNA to polymer conjugation reactions in organic solvents, O'Reilly and Wilks conducted a comprehensive investigation of DNA–polymer covalent binding, analyzing amide coupling, thiol–ene Michael addition reactions, and tetrazine–norborene coupling efficiencies to pNIPAM.¹⁸ This work was highlighted in section 3.1.1 and will be expanded here to discuss the limitations and possible solutions. Amine coupling to carboxylic acids was attempted with common coupling agents, such as EDCI and DCC with HOBt as the coreagent in a variety of solvents; however, no product was observed. Coupling with hexafluorophosphate benzotriazole tetramethyl uronium (HBTU) and hexafluorophosphate azabenzotriazole tetramethyl uronium (HATU) agents was successful on the first attempt; however, a lack of reproducibility in both cases was noted. The activated esters, PFP esters, and NHS esters were similarly trialed; however, product formation was also not observed. Under the reported conditions, i.e. <10 μM of DNA in 10 μL, it can be concluded that free carboxylic acids as well as activated acid esters are not efficiently coupled to amines. A similar observation was noted in their studies using thiol–ene Michael addition. Methacrylamide, acrylamide, and maleimide functional groups were investigated for the conjugation with thiol groups which, in all cases, did not provide any conversion. Conversely, tetrazine to norborene coupling appeared most promising with up to 50% yields. The coupling was demonstrated with both tetrazine– and norborene–DNA

to the target polymer, showing the versatility of this approach. The DNA–tetrazine to the pNIPMA–norborene coupling was, however, the most efficient method, improving yields from 10 to 50% and demonstrating its versatility in organic solvents, i.e. DMF, dimethylacetamide (DMAc), and NMP. In this study, low concentrations and a low volume were adopted which highlighted the limit of these reactions for polymer conjugation to DNA. However, these reactions have been successful by other groups where higher volumes, such as 300 μL,⁹⁴ and higher concentrations, such as 25 μM,¹⁰⁰ have been adopted. Therefore, where resources are not limited, successful conjugation via conventional coupling methods can be envisaged.

As with each example so far, the polymers are presynthesized separately from the DNA, and therefore, the polymerization reaction itself is not subjected to the limitations of DNA. Additionally, this *grafting to* approach allows the characterization of both the polymer and DNA blocks to understand the composition and properties prior to conjugation. However, conjugation yields are often low due to either solvent incompatibility, repulsion of charged polymers, or also the steric strain as discussed in section 3.1.1. An alternative method using the *grafting from* approach can reduce the impact of steric strain due to consecutive single monomer attachments as well as increase the ability to access shorter polymers blocks due to the ease of purification of the final conjugate. Matyjaszewski and Das conducted the *grafting from* polymerization from DNA in solution and varied the reaction time, catalyst, monomer, and salt concentration.¹³ Here, they polymerized OEOMA and showed that at a high NaCl concentration of 300 mM, no polymer was produced and that without salt, the higher molecular weight polymer was synthesized. Additionally, the lower Cu% (% compared to

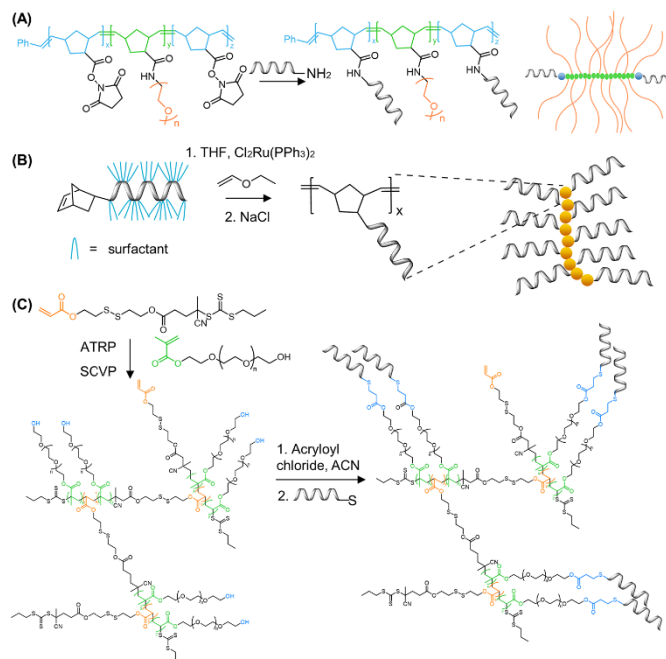


Figure 9. Synthesis of DNA–polymer brushes via *grafting through*. (A) Synthesis of pacDNA through the presynthesis of PEG brush copolymers bearing NHS anchors via a *grafting through* ROMP followed by amide coupling of amine-ODN. The chemical structure of the polymer brush backbone and a 2D schematic are shown as product representatives.^{55,113} Based on figures from refs 55 and 113. (B) DNA side-chain brush polymers synthesized from the norbornene-ODN monomer. Several polymer length scales were synthesized, represented here as a multimer.¹⁷ Based on figures from ref 17. (C) Dual polymerization employing ATRP and SCVP to produce a diblock copolymer consisting of PEG side chains.¹¹⁹ Based on figures from ref 119.

the monomer) yielded the largest molecular weight along with a 120 min reaction time. Of note, Matyjaszewski and Das employed the activators generated by electron transfer technique (AGET) of ATRP, which has been optimized for aqueous and biologically relevant reaction conditions.^{101,102} This advancement has been demonstrated by several groups and provides new avenues for polymerization by *grafting from* ODNs (Table 3).

With the increased interest in synthesizing biologically relevant polymers and, therefore, the incorporation of biological material, methods to reduce the chance of downstream toxicity caused by contaminants from the polymerization were desired. These contaminants typically result from common ATRP methods which require a copper-based catalyst, free radical initiators, and reducing agents. However, through photoinduced ATRP (so-called photo-ATRP), free radical initiators and reducing agents are no longer required and, additionally, the catalyst concentration can be reduced. Several acrylate- and methacrylate-based polymers were synthesized by photoirradiation for 30 min under these mild reaction conditions,¹⁴ demonstrating an important approach to synthesize hydrophobic polymers. This is a key step in polymer synthesis to broaden the scope for DNA–polymer conjugates. Notably, these polymerizations were fully automated on an adapted DNA synthesizer. The

synthesizer was modified to contain a light source in addition to a program that can inject the second monomer to form a diblock copolymer once 100% conversion of the initial monomer has occurred. PhotoATRP is also possible using blue light.⁸⁴ Here, a thorough investigation was performed to determine optimal reagent concentrations for OEOMA₅₀₀ polymerization in aqueous environments. For example, Cu concentrations of at least 100 ppm were required to produce good conversion.⁸⁴ An alternative photoinitiated polymerization from ODNs was demonstrated through photoRAFT using Eosin Y as the photocatalyst.¹⁹ This polymerization was performed in solution which removes the requirement of a DNA synthesizer. Two RAFT agents were trialed, BTPA and CPADB, to synthesize several polymers, DMA, NIPAM, oligo(ethylene glycol) methyl ether acrylate (OEGA), and oligo(ethylene glycol) methacrylate (OEGMA), demonstrating the versatility of this approach. Additionally, the length of the polymer was controlled by the initiator to monomer ratio—at a ratio of 200:1 of monomer to RAFT agent, polymer length was 13.8 kDa in comparison to 31.2 kDa at a ratio of 500:1. One significant challenge of DNA–polymer conjugates is the incompatibility of hydrophobic monomers or polymers with the hydrophilic DNA. However, with the methodology evolved from PISA, this incompatibility was exploited to direct the formation of different DNA–polymer nanostructures.⁷³ This

technique was first demonstrated with ODNs by performing the *grafting from* using DMA, 4-acryloylmorpholine, 2-hydroxyethyl acrylate, and OEGA.⁷⁴ Restrictions imposed by the DNA such as ultralow volumes and its associated problems with degassing were circumvented by using glucose oxidase to ensure an oxygen-free environment for the polymerization.^{77,85} By adopting thermal RAFT polymerization and through the inclusion of enzyme degassing, the monomer to initiator ratio can be controlled precisely and thus can allow the manipulation of architectures.⁷⁴ In addition to thermal and photoinduced polymerization methods, ultrasonication is also a possible stimulus.⁸⁶ Through the use of ultrasonication, room temperature and low levels of Cu catalyst can be adopted to yield polymers with low dispersity and high molecular weight.

Other polymerization methods such as those via oxidative approaches have also been investigated to graft polymers from ODNs. The copolymerization of pyrrole monomers present in solution and those conjugated to ODN was performed *in situ* to yield polypyrrole polymers grown from and attached to DNA.⁸⁷ Here, the polymerization is driven electrochemically and in solution to enable high chemical stability. This technique was also performed in the presence of non-complementary and complementary ODNs demonstrating its capabilities to polymerize from both ss- and ds-ODNs.¹⁰⁵

Beyond conventional homo and block copolymers, the attachment of sequence defined polymers has made several interesting developments. In particular, sequence-specific polymerization of short polymers was demonstrated by employing a cyclic binding and dissociation of complementary ODNs (propagation strands) bearing the desired monomer for sequential polymer growth.^{81,104} On binding, the complementary strands bring the reactive monomers into close proximity for specific polymerization reactions. A Wittig reaction was employed for simultaneous propagation of the polymer and release of the monomer from its original ODN. To afford multiple cycling steps, the initial duplex exhibits a short noncomplementary region (the toehold domain) to enable a fully complementary displacement strand to remove the propagation strand and leave the ss-ODN bearing the polymer chain. Although the local environment from each reaction step is constant, longer lengths are not possible due to each reaction yield reducing cycled material.

3.1.4. 1D DNA–Polymer Synthesis. In this section, the development of 1D structures, such as DNA–polymer brushes will be outlined. The most common method described for DNA–polymer brush synthesis is the ROMP of norbornyl bound to polymer side chains and reactive handles, which can be employed for DNA attachment. Zhang and co-workers applied this approach to synthesize DNA–PEG conjugates consisting of PEG₅₀₀₀ and PEG₁₀₀₀₀ side chains.¹⁰⁵ In their design, branched PEG structures, named pacDNA (polymer assisted compaction DNA), were synthesized via the consequential ROMP of norbornyl-NHS (N-NHS) and norbornyl-PEG (N-PEG), for diblock synthesis, and through chain extension ROMP with N-NHS for triblock copolymer synthesis (Figure 9A).^{55,106–108} The NHS anchors along the backbone were then available to couple amine-ODNs.¹⁰⁹ To further exploit the potential of DNA–polymer conjugates, Zhang and co-workers polymerized norbornyl-paclitaxel (an anticancer drug), again via ROMP prior to DNA conjugation to produce spherical nucleic acids—macromolecular structures to be discussed in section 4.1.1.¹¹⁰ A similar approach was adopted to synthesize DNA–polymer conjugates where

doxorubicin (DOX) was also covalently bound within the structure.¹¹¹ In each case, a diblock copolymer was synthesized by ROMP of norbornyl-DOX and N-PEG, where the carboxyl groups at PEG terminals were activated with EDC and NHS for 5 min prior to amide-coupling with amine-ODN. These two examples demonstrate the potential of DNA–polymer conjugates as drug delivery systems and their ability for high capacity drug loading. Further details of applications will be discussed in sections 5.2 and 5.3. In an example by Mirkin and co-workers, a copolymer consisting of a polycaprolactone (PCL) and PEO block where only the PEO backbone was functionalized with an azide group was synthesized and enabled copper-free click chemistry with a DBCO-ODN for conjugation.¹¹² In this instance, the copper-free click chemistry was performed in a 1:1 DMSO/DMF mixture in the absence of an aqueous buffer. The examples described above demonstrate the employment of diblock copolymer structures synthesized prior to DNA conjugation. However, through the employment of a triblock copolymer, where each block initially consists of non-DNA content, controlled positioning of the ODNs along the polymer backbone can be realized. This was accomplished through a triblock copolymer brush synthesized by the sequential ROMP of N-NHS, followed by N-PEG, and again N-NHS with Grubbs catalyst.¹¹³ Again, the NHS groups were then available to couple amine-ODNs at the terminal polymer blocks of the brush structure. A further development in the design of triblock copolymers enabled the synthesis of an N-NHS-N-PEG-norbornyl maleimide (N-MI) triblock and demonstrated a dual-ODN conjugation approach through the orthogonal reactions of amine-ODN to N-NHS and thiol-ODN to N-MI.¹¹³ This development enabled the incorporation of two distinct and specific ODNs within one nanostructure to open possibilities for dual-functionalization.

In an alternative approach to ROMP, Liu and Li employed the ROP of γ -propargyl-L-glutamate N-carboxyanhydride¹¹⁴ to synthesize a polypeptide capable of click chemistry between azide-functionalized ODNs and the propargyl group after the polymerization was complete.¹¹⁵ This technique enabled the synthesis of a hybrid peptide DNA brush, containing functional possibilities that have high biomedical relevance due to its biocompatibility and postfunctionalization potential. Additionally, it provides a platform for high loading of DNA to target drug delivery entities: 5–6 ssDNA molecules could be conjugated to one polypeptide.

In each case described above, the ODN has been conjugated to the polymer as a postpolymerization strategy. An alternative approach is to incorporate the ODN *in situ* through initial monomer conjugation and proceed with a *grafting through* type polymerization. This was demonstrated by the attachment of norbornyl to the ODN followed by ROMP (Figure 9B).¹⁷ Depending on the ODN length adopted (either a 7- or 14-mer), polymers of short lengths (a tetramer, pentamer, hexamer, and heptamer for the 7-mer and a dimer, trimer, and tetramer for the 14-mer) could be synthesized and purified by polyacrylamide gel electrophoresis (PAGE). Of note, the ROMP here produced the longest polymer products in 100% THF. As described in section 3.1.1, the employment of cationic surfactants is crucial to enable the solubility of DNA in organic solvents for solution-based reactions. Through this approach, postpolymerization functionalization is not required and therefore reduces reaction steps as well as reducing cross-reaction complications. Additionally, using the *grafting through* strategy ensures that every monomer unit contains an ODN

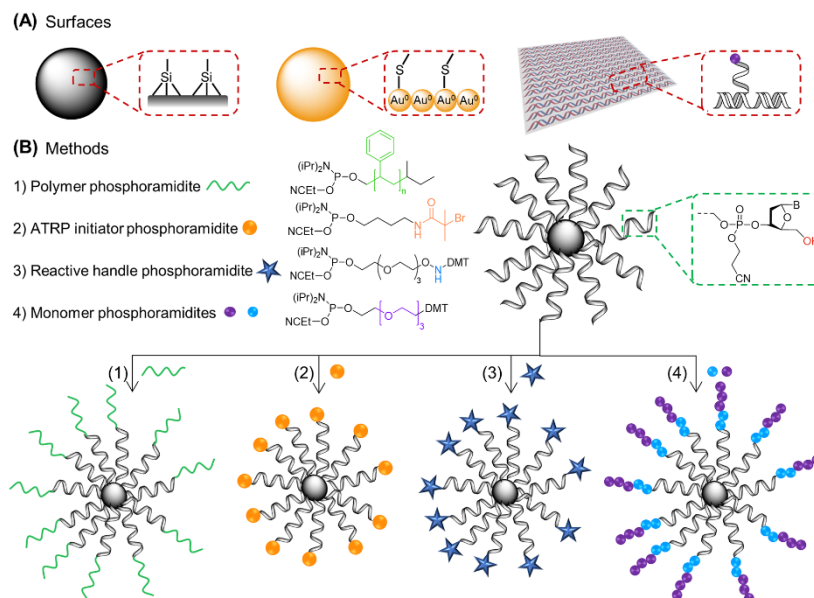


Figure 10. (A) Example surfaces for DNA–polymer conjugation synthesis. Surfaces include whole macro materials in addition to precisely defined nanostructures. (B) Methods for CPG bead surface DNA–polymer synthesis through either the attachment of a (1) polymer phosphoramidite,¹²¹ (2) ATRP initiator phosphoramidite,¹³ (3) reactive handle phosphoramidite,⁹ and (4) monomer phosphoramidite.⁸⁰

whereas a postpolymerization reaction is subjected to a statistically dispersed functionalization of the side chains. This approach has been similarly demonstrated with a peptide nucleic acid (PNA) where the PNA unit was covalently attached to a norbornyl group and subsequently polymerized via ROMP.¹¹⁶

RAFT polymerization can also be employed to synthesize 1D DNA–polymer conjugates. Martyjaszewski, Armitage, and Das adopted the RAFT polymerization of methacrylate groups bearing macroinitiator side chains which can then be polymerized to yield a “bottlebrush” polymer.¹¹⁷ In this instance, each “bristle” contained an azide group to afford click chemistry with an ODN.¹¹⁷

A similar approach to *grafting through*, dual polymerization, can produce highly branched polymer structures. One example combined self-condensing vinyl polymerization (SCVP) and cation ROP to produce a poly(3-ethyl-3-oxetanemethanol)-PEO hyperbranched multiarm copolymer.¹¹⁸ An alternative approach replaced cation ROP with RAFT polymerization to synthesize a hyperbranched polymer structure again bearing PEG side chains but with a RAFT agent core containing a disulfide bond for redox-responsive drug delivery (Figure 9C).¹¹⁹ This method allows the synthesis of both hydrophobic and hydrophilic blocks simultaneously. In both cases described, ODNs were conjugated to the branched polymers by the Michael addition of thiol-ODN to acrylate-functionalized branched polymers through a final *grafting to* step. A hyperbranched polymer network was also demonstrated by the laboratories of Sumerlin and Tan.¹²⁰ SCVP was employed to copolymerize *O*-nitrobenzyl acrylate, PEG-acrylate, and 2-

(2-bromoisobutyryloxy) ethyl acrylate which also served as the iminer to instigate branching. Once synthesized, a two-step substitution was performed to transform the chain end hydroxy groups to azide reactive groups for click chemistry anchors. Copper free click chemistry was then performed utilizing a strained alkyne DBCO-modified DNA to afford high yielding conjugation in 100% DMSO. Through these methods, hyperbranched structures can be readily synthesized and postfunctionalized with the ODN for the required drug loading.

3.1.5. 2D and 3D Polymerization Platforms. The above-mentioned methods each perform the conjugation reaction in solution. In contrast, solid supports and surfaces can also be adopted to synthesize DNA–polymer conjugates through both *grafting to* and *grafting from* methods. Platforms include nanomaterials, such as DNA origami, nanoparticles, and beads which together encompass metal, organic, and biological surfaces consisting of varying 2D and 3D structures and properties (Figure 10A). Several first attempts to conjugate DNA and polymers were performed using solid phase synthesis. In 2004, Mirkin and colleagues synthesized a PS phosphoramidite via solid phase synthesis,¹²¹ demonstrating the ability to synthesize a complex phosphoramidite and carry out an efficient coupling step in the presence of the protecting groups. This technique was further explored by Hermann and co-workers to synthesize PPO conjugates employing polymer phosphoramidites.^{122,123} The polymer-phosphoramidites were synthesized by the reaction of alcohol terminated polymers with chlorophosphoramidite with yields of 41% and 32% for PPO polymers of 1000 and 6800 g/mol,

respectively.¹²² These polymers can then be conjugated to the ODN through standard phosphoramidite chemistry. In addition to PS and PPO, a cholesterol-TEG phosphoramidite was also synthesized to subsequently yield a cholesterol-ODN.¹²⁴ The employment of beads can also grant the selection of shorter polymer brush structures due to the pore size,⁹⁸ which can sometimes be a limitation. However, conjugation employing polymer phosphoramidites on solid supports requires a DNA synthesizer which is a dedicated instrument that requires specialized skills to use. Some commercial companies can offer the delivery of ODNs still attached to the solid support; however, this may not always be possible. Although the reported yields in the above examples are lower than the optimized reactions in solution, by employing phosphoramidite chemistry, the conjugation occurs while nucleotide functional groups are protected and thus conjugation using a solid support offers a more diverse compatibility with coupling reagents and functional groups in comparison to solution-based reactions.

An alternative approach is to synthesize the ODN and polymer with complementary reactive click chemistry handles. Zhang and co-workers synthesized several copolymers using azide-polymers with alkyne-functionalized ODNs on the CPG beads. Polymers consisted of poly(*tert*-butyl acrylate) (PtBA) and PS of molecular weights 3.9, 5.5, 8.5, and 14 kDa.¹²⁵ The yield was determined for each conjugation to three ODN lengths (6-, 19-, and 26-mer) and revealed an increase in yield with decreasing lengths of both polymer and ODN.¹²⁵ This study highlights the limitation of steric hindrance on efficient conjugation where two flexible polymers are required to come into close contact for the reaction to occur. Conjugations with the lowest molecular weight PtBA and PS with the 26-mer produced similar product yields to example click reactions performed in solution (between 70 and 90%);⁹⁹ thus, either method can be adopted. However, on increasing the polymer length to higher molecular weights, the yield decreased; for example, the yield was 56% for the conjugation between the 14 kDa PS and the 26-mer on the CPG bead. Therefore, there is a trade-off between polymer and ODN length and product yield.

A combination of the solid phase synthesis approach with the presynthesized polymer brush was adopted by Gianneschi and co-workers to produce a polymer brush with multiple ODNs attached to solid supports, followed by the deprotection and cleavage steps.¹²⁶ The polymer brush was synthesized via ROMP of a benzene-norbornyl followed by norbornyl-N-acetyloxy-succinimide. After polymerization, the acetyl group was available for conjugation to the amine-ODN with DIPEA and HBTU to activate the carboxylic acid. Conjugations with ODNs capable of forming defined secondary structures (aptamers) were similarly performed.¹²⁷ However, alterations to relative equivalents were noted, 3× higher DIPEA and 4× less HBTU in comparison to the previous solid support reaction, demonstrating that optimization is required for different reacting partners. Gianneschi and co-workers also synthesized an RNA-polymer conjugated following the same procedure for the aptamer DNA,¹²⁸ demonstrating the robustness of this approach. Inspired from the development of conjugating polymers from the surface of CPG, presynthesized polymer nanoparticles, which bear chemical handles, became a natural expansion of the technology. A copolymer consisting of MA and azide-modified MMA units self-assembled into a nanoparticle, exhibiting the azide on the

surface.¹²⁹ Cu-free click reaction is then possible with DBCO-ODNs to yield 3D DNA-polymer nanoparticles.

Similar to the *grafting to* approach, *grafting from* has been demonstrated on solid supports. Matyjaszewski and Das explored polymerization from initiators bound to ODNs through both solid phase and solution phase ATRP by performing the polymerization either pre- or post-CPG bead cleavage.¹³ Performing the polymerization on the solid support provides easier purification from the unreacted monomers and catalyst; however, the initiator phosphoramidite must be compatible with deprotection and cleavage reactions. After the polymerization of OEOMA for 4 h, a molecular weight of 205 kDa was noted after cleavage from the CPG beads. On solid support, it is challenging to accurately quantify the concentration of initiators and thus the initiator/monomer ratios. Conversely, in solution, concentrations can be determined and, therefore, optimizations involving reagent ratios can be performed more accurately.

Solid phase synthesis *grafting from* the ODN was also performed on a gold surface through the complementary binding of a thiol-modified ODN (attached to the surface) to an ATRP initiator-modified ODN.¹³⁰ This approach produced poly(hydroxyethyl methacrylate) (PHEMA) from a gold surface, only when the complementary initiator sequence was bound. Further exploration employed a dual-functionalized ODN bearing a thiol group at the 3'-end and an ATRP initiator at the 5'-end and demonstrated ATRP growth from a purely ssDNA sequence on the gold surface.¹³¹ Here, faster growth kinetics were observed when the initiator was present on the ssDNA rather than directly on the surface. This effect can be noted due to the localization of the Cu catalysts on DNA, increasing proximity to the initiator site. Several RAFT conditions were also investigated to optimize pOEGMA and PHEMA synthesis via RAFT polymerization. Temperature, time, CTA% surface density, and AIBN concentration were each explored and showed a temperature of 30 to 40 °C (although higher temperatures were not investigated) is required for polymerization to occur, a reduction in growth as AIBN concentration increases from 0.4 mM, as well as a linear growth trend on increasing time for pOEGMA.⁸³ Through the employment of a conductive 2D surface, the development of chips for applications requiring sensitive surfaces can be envisaged. To further establish the *grafting from* approach on a solid support, He and co-workers adopted a gold nanoparticle employing the thiol-gold interaction.⁸² ATRP was performed through the initial coupling of an ATRP initiator, bromoisobutryl, to the thiol-ODN, followed by Au nanoparticle (NP) attachment and incubation in polymerization reagents. Here, pOEGMA was synthesized from the ODN-modified AuNP, and through the presence of DNA, these reactions could be performed in an aqueous environment without aggregation or solvent exchange requirements. In each case described here, surface attachment is utilized; thus, characterization of the polymer is limited and requires cleavage prior to analysis.

In the examples described so far in this section, the polymer sequence is either a repetitive monomer or a copolymer of random arrangement. Nature consists of several polymers, such as DNA and proteins, which contain a complex but controlled sequence of monomer units. These biological and precise polymers inspired the group of Sleiman to develop a method for sequence defined synthetic polymers.⁸⁰ Through the employment of phosphoramidite chemistry, the sequential

addition of defined monomers via stepwise coupling and washing was realized. In this instance, two phosphoramidite oligomers consisting of either a hexaethylene glycol or hexaethylene (HE) unit were adopted as hydrophilic and hydrophobic monomers and ordered in a controlled manner (Figure 10B). In their first work, polymer lengths of up to 12 units were explored and shown to have high control over the sequence. They next explored polymer lengths up to 24 units with varying content demonstrating the ability to increase polymer length through this approach.⁷⁹ This method highlighted the potential for DNA–polymer conjugation where both the DNA and polymer content are sequence defined, although polymer length is still limited and may require further exploration to improve the solid phase monomer conjugation scope.

The examples so far have produced a conjugate containing DNA as a polymer block; however, they have not exploited the capabilities of DNA to guide the polymerization to precise assemblies through its sequence-specific interactions. DNA sequences can be programmed through their specific base pairing to form folded nanostructures. DNA nanostructures were first envisaged by Seeman in 1980, beginning as lattice structures up to more recent examples of sophisticated DNA origami structures as reviewed previously.¹³² DNA origami was proposed by Rothemund¹³³ and has provided a powerful approach to engineer nanoscale functional structures.^{134,135} Structural DNA nanotechnology was first employed in covalent conjugation with polymers by O'Reilly's group, demonstrating the use of a DNA tetrahedron as a structural anchor for polymer attachment.⁹⁹ The polymer-decorated DNA nanostructure was realized through Cu-catalyzed click chemistry between the alkyne bearing DNA tetrahedron and azido-functionalized pNIPAM (Figure 11A). A 100-fold decrease in reagent concentrations was stipulated in comparison to their ODN equivalent solution-based click reactions. Additionally, $\text{CuSO}_4/\text{tris}(\text{hydroxypropyltriazolylmethyl})\text{amine}$ (THPTA) was adopted rather than $\text{CuI}\cdot\text{P}(\text{OEt})_3$. However, as with the attempts using polymer brushes, steric effects are deterministic on the efficiency and can result in low coupling yields. By *grafting from* the nanostructure, steric restraints are reduced for the monomer polymerization processes. The added advantage of employing a 3D DNA nanostructure backbone afforded polymer patterning through the site specific attachment.

In the previous example, the functionalized DNA strand was part of the folded nanostructure. However, in another instance, site specific control was employed through complementary base pairing an ODN bearing the radical initiators.⁵⁷ The origami was designed to exhibit “sticky” ssDNA at precise locations to guide the initiator-ODN to the pre-designated sites (Figure 11B). To perform the polymerizations from DNA origami, ATRP was employed to achieve reactions in aqueous conditions and at room temperature—a requirement when handling DNA origami. Due to the low concentrations of DNA origami available, sacrificial ATRP initiators were required in solution to maintain the radical equilibrium. Under these conditions, polymerization of PEGMA successfully generated a polymer brush. By adopting copolymerization with the cross-linker PEG dimethacrylate (PEGDMA), a dense polymer network can also be created. The DNA origami tile structure can also fold to form a tube shape, converting the 2D patterned surface to a 3D dual-surface containing specific internal and external contours (Figure 11C).⁵⁶ Here, ATRP initiators were

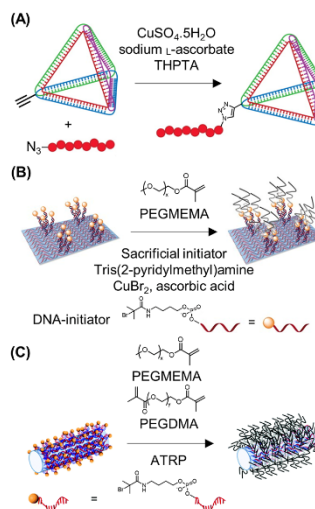


Figure 11. 2D and 3D DNA polymer conjugates on “solid” DNA nanostructures. (A) *Grafting to* DNA tetrahedron through click chemistry of pNIPAM to the alkynyl-DNA nanostructure.⁹⁹ Adapted with permission from ref 99. Copyright 2013 American Chemical Society. (B) *Grafting from* DNA origami tiles through Cu-catalyzed ATRP. Initiators are initially bound to the origami structure through complementary sticky sequences followed by the ATRP reaction.⁵⁷ Adapted with permission from ref 57. Copyright 2016 John Wiley and Sons. (C) *Grafting from* a DNA origami tube through ODN bound initiators.⁵⁶ Adapted with permission from ref 56. Copyright 2018 the Royal Society of Chemistry.

similarly placed in precise patterns to decorate the outer surface of the tube. The polymerization conditions remained unchanged between the tile and tube configuration, therefore demonstrating the versatility of ATRP on DNA origami for nanoscale precision of DNA–polymer hybrid nanostructures.

3.2. Noncovalent DNA–Polymer Interactions

Apart from the covalent DNA–polymer conjugates reviewed above, there is also the emerging class of supramolecular assemblies of DNA and polymers which is driven by noncovalent interactions. Here, intermolecular communication is enabled through the close proximity and attraction of both materials, which lead to systems of dynamic nature. While covalent conjugation requires chemical manipulation of the DNA strands to equip them with reactive handles, noncovalent approaches do not face these constraints and can typically be realized with nonmodified and readily available nucleic acids. The highly programmable primary structure of DNA as well as the ability to shape secondary and tertiary structures can be exploited to control the sequence of polymers that are structurally unrelated to nucleic acids. This strategy takes inspiration from one of the essential processes found in living nature, where the DNA-encoded information on life is replicated, transcribed, and translated through RNA into proteins. Noncovalent assemblies can be classified by their mode of interaction as well as by the designated purpose. DNA provides multifaceted interaction modes that arise from its unique structure in all three dimensions as discussed in section

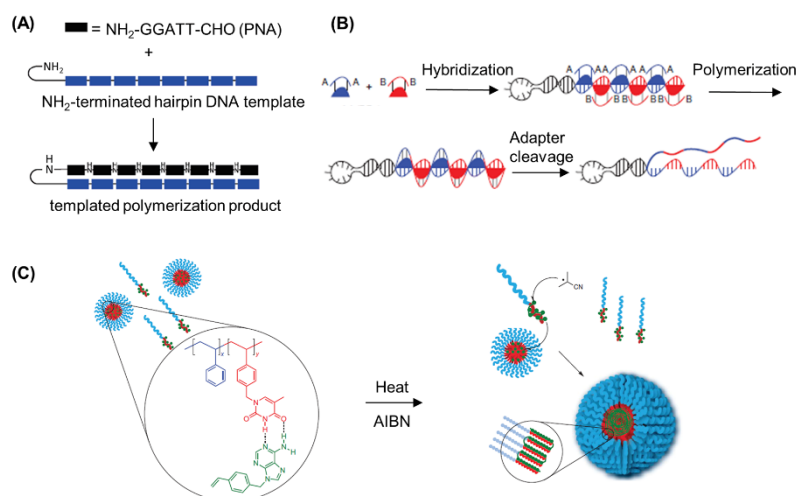


Figure 12. Various strategies to sequence-controlled polymer growth with ssDNA. (A) DNA-templated polymerization of PNA pentamer aldehydes on an amine-terminated hairpin DNA template.⁷⁸ Reproduced with permission from ref 78. Copyright 2008 American Chemical Society. (B) Codon-mediated linkage of AA/BB-substrates yields polymers that can be released from the templating DNA by cleavage of the disulfide linkers.⁵⁹ Reproduced with permission from ref 59. Copyright 2013 Springer Nature. (C) The combination of segregation and templating techniques ensures confined chain growth along a template in discrete micelle cores that affords polymers of high molecular weights.¹³⁸ Reproduced with permission from ref 138. Copyright 2012 Springer Nature.

2. ssDNA is accessible via Watson–Crick base pairing whereas the negatively charged phosphate backbone is prone to electrostatic interaction with polycations. dsDNA expands the toolkit by enabling hydrophobic groove binding and intercalation of planar molecules into the stacking bases along the DNA backbone. In comparison to covalent conjugation strategies, the herein described noncovalent interactions are *per se* not specific, yet several studies aim to circumvent these intrinsic restrictions and seek for spatially controlled attachments. Since DNA is a multifaceted platform, one can utilize its exceptional customizability to design tailor-made polymers by either templating or patterning approaches. On the one hand, ssDNA and dsDNA allow sequence transfer onto growing polymers and the templating of supramolecular 1D and 2D structures, respectively. On the other hand, DNA can be arranged in complex nanostructures which can be covered with polymers, rendering new features to the synthetic building block and yielding three-dimensional constructs. Furthermore, the extraordinary fidelity of certain DNA arrays, e.g., DNA origami, permits the patterning of polymers in distinct shapes and with a precision that outcompetes other techniques, such as lithography or conventional self-assembly. However, independent of the applied technique, the DNA template can be either removed after polymer synthesis or become part of the reaction product. In line with the focus of this review, we survey promising strategies to develop DNA–polymer conjugates via noncovalent interactions.

3.2.1. Templating of Polymers by Single and Double Stranded DNA. One of the greatest advantages of DNA over synthetic polymers is the unprecedented level of sequence-control as well as the consequential precision in molecular weight and distribution. It therefore is attractive to exploit this unique characteristic and potentially transfer the molecular

information onto polymers. In this way, ODNs can function as molecular matrices that recognize and interact with guest molecules and, thus, organize them according to their sequence and guide subsequent polymerization. An early example of how the sequence of nucleic acids might be harnessed was demonstrated by Liu and co-workers¹³⁶ wherein short PNA sequences were arranged in a sequence-specific fashion along an amine-end-modified ODN template via complementary base pairing. Aldehyde moieties on the tetrameric PNA monomers allowed for distance-dependent reductive amination coupling, ligating the monomeric units, which consequently generated polymers with molecular weights of 10 kDa. Introduction of mismatches afforded no or only truncated polymers, depending on the position at which the error was placed. Furthermore, the presence of additional building blocks with closely related sequences did not disturb the formation of the desired product. Thus, efficient and sequence-specific conjugation of nucleic acid templates and non-natural polymers steered by hydrogen bonding of base pairs could be established. In a follow-up study, the group expanded their monomer scope through a side-chain-functionalized PNA tetramer and pentamer aldehydes⁷⁸ (Figure 12A). Thereby, they could fabricate densely functionalized polymers, involving a PNA 40-mer with more than half the nucleotides bearing side chains. Interestingly, the polymerization efficiency mainly depended on the position and stereochemistry of the side chains rather than on size, hydrophobicity, or charge. As briefly mentioned above, Nature has the capability to translate the genetic information stored in nucleic acids into amino acid-based peptides and proteins. Based on their previous work, Liu's group aimed to mimic the last step of Nature's protein machinery where the sequence of a nucleic acid template allows a codon-mediated conversion into an amino acid

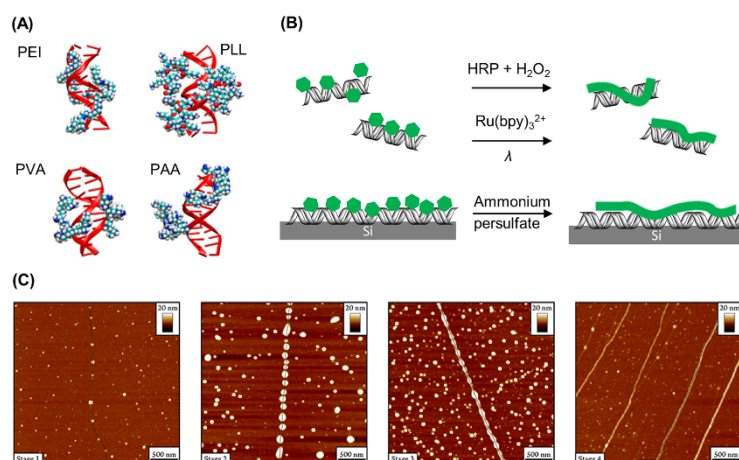


Figure 13. Electrostatic interactions allow the alignment of positively charged monomers and polymers along the DNA backbone. (A) Complexes of DNA with two polycation chains for DNA–PEI, DNA–PLL, DNA–PVA, and DNA–PAA systems.¹⁴¹ Reproduced with permission from ref 141. Copyright 2018 Elsevier Ltd. (B) The electrostatic alignment of aniline monomers on DNA, either in solution or on Si substrates, and subsequent oxidation leads to the formation of poly(aniline) structures along the DNA template. Oxidation can be induced enzymatically (HRP), via photo-oxidation of Ru complexes or by using oxidants (APS). (C) AFM images of the polymerization process could reveal four distinct stages in the formation and growth of poly(pyrrole).¹⁴⁹ Reproduced with permission from ref 149. Copyright 2014 American Chemical Society.

sequence and, in the end, a protein is released (Figure 12B).⁵⁹ These codons bear a template recognition site as well as the corresponding amino acid. In order to exploit this strategy and likewise introduce sequence-specificity to non-natural polymers, the group designed a codon comprising a PNA pentamer for template recognition and a synthetic polymer building block. Through the employment of PEG as the initial polymer model and by achieving molecular weights of up to 10 kDa, they could further incorporate α -(D)- and β -peptide backbones with various side-chain functionalities to accomplish longer and structurally more diverse polymers (26 kDa). Among several investigated conjugation strategies, copper-catalyzed alkyne–azide cycloaddition of AA-/BB-substrates proved to be most efficient. Moreover, by equipping the codon with a disulfide bridge between the polymer building block and the PNA adapter as a cleavable linker, the polymeric product could be liberated afterward. Though the approach described here utilizes Watson–Crick base pairing to produce sequence-controlled polymers without the need for Nature’s enzymatic toolbox, the structural diversity of the substrates is still limited to macrocycles for entropic reasons. However, the codon design theoretically supports the incorporation of several building blocks without the need to readjust the template recognition site.

Another seminal approach to adopt from Nature’s capability to make exact copies of nucleic acid strands was investigated by the Sleiman group.¹³⁷ Step-growth polymerization techniques typically suffer from poor control over molecular weight which inevitably leads to broad molecular weight distributions. They therefore employed nucleobase recognition to surpass these barriers and to synthesize conducting polymers of low dispersities. Instead of using pure ODNs as a template, a thymine-decorated polymer was manufactured via living ring-opening metathesis polymerization (ROMP). Alignment of

adenine-containing monomers by complementary base pairing along the template strand and subsequent Sonogashira coupling afforded well-defined daughter strands of conducting polymers. Whereas nontemplated polymerization or polymerization with an incorrect template only produced low polymerization degrees and high dispersities ($PDI > 2$), the presence of the correct template significantly narrowed the molecular weight distribution ($PDI = 1.2$) and yielded similar polymerization degrees compared to the parent strands. Thus, the all-synthetic strategy proved to be capable of programming the structure, length, and dispersity of commonly poorly-defined polymers by hydrogen bonding interactions. Following this, O’Reilly and co-workers furthered nucleobase-promoted polymer templating by combining the methodology with a segregation strategy that makes use of block copolymer self-assembly (Figure 12C).¹³⁸ Their bioinspired dual templating/segregation approach relies on the isolation of propagating radicals in discrete micelle cores, thus enabling confined chain growth along a template. Briefly, a block copolymer of styrene (St) and the thymine analogue 1-(vinylbenzyl)thymine (VBT), $PSt_{11.5}\text{-}b\text{-}PVBT_{18}$, was synthesized that forms stable micelles in chloroform. The hydrogen bond interaction of the thymine template with a vinyl derivative of adenine (VBA) ensured the solubility of the adenine monomer in the solvent. Furthermore, the addition of the complementary adenine monomer led to a dynamic exchange of adenine-loaded templates into the micelle where the ensuing polymerization was taking place. A so-called “hopping” mechanism of propagating radicals along adjacent templates in the micelle core can theoretically explain the remarkably high molecular weights of the daughter polymers of up to 400 kDa, even though the template only counts 18 thymine residues. Hence, nucleobase templating enriched the free radical polymerization to yield narrowly distributed

daughter strands ($PDI \leq 1.08$) by suppressing bimolecular termination in a confined environment.

The examples discussed so far mainly report on nucleobase-modified polymers or closely related structures such as peptide nucleic acids. To further develop the field, Zhou et al. studied the triplex hybridization of a polymer with a full carbon backbone alongside DNA and RNA ODNs to produce conjugates that might be suitable for DNA loading onto nanoparticles or delivery of siRNA in biomedical applications.¹³⁹ Here, RAFT polymerization of various acrylates yielded polyacrylates with tunable side chains. As a key step, these copolymers were equipped with triaminotriazine (so-called melamine) handles by amidation of NHS moieties along the backbone. Melamine can recognize thymine and uracil hydrogen bonding patterns in various media and, therefore, ensured the hybridization with ODNs comprising two blocks of the respective amino acid that are bridged by a cytosine linker ($dT_{10}C_{10}T_{10}$). Notably, the RAFT copolymers are intrinsically characterized by stereoregio backbone heterogeneity and still engage T/U rich ODNs with nanomolar affinity upon mixing in a 1:1 ratio. The supposed triplex hairpin binding model of the compounds was further affirmed by FRET studies.

The work described here represents a rare example of DNA–polymer conjugates that are solely based on hydrogen bonding between a fully synthetic polymer and complementary nucleic acids without the support of electrostatic interaction. However, substantially more studies address the negatively charged phosphate backbone of DNA with respective polyanilines due to the convenient and spontaneous mode of interaction. For instance, electrostatic complexation can be exploited to condense siRNA onto a positively charged supramolecular polymer for drug delivery purposes.¹⁴⁰ The cationic polymer can enter cellular membranes via charged-mediated endocytosis and successfully deliver its cargo, thus inducing gene silencing. Supramolecular complexes of nucleic acids with cationic polymers have emerged prominently in the area of gene delivery in order to circumvent viral delivery vectors. In this respect, several positively charged polymers such as polyethylenimine (PEI), poly L-lysine (PLL), polyvinylamine (PVA), and polyallylamine (PAA) are subjects of current research (Figure 13A).¹⁴¹

Electrostatic interactions also play a key role in the studies of the Herrmann group where they fabricated light harvesting DNA complexes and described the salt-free hybridization of PEGylated ODNs in water.^{142,143} In a two-step process, a water-soluble surfactant is employed to transfer the DNA into an organic phase where it is substituted by an amine-containing molecule, for instance, amine-PEG. Hereby, ODNs can be noncovalently encapsulated with a PEG shell that allows for the formation of metal-free dsDNA with remarkably high thermostability.

Likewise, electrostatic interactions can be further utilized to template polymerization along DNA, enabling these interactions to dictate bond formation processes. There are a high number of studies demonstrating the use of DNA templates to exert control over the respective sequence and structure as an appealing strategy in the field of conducting nanowires. In particular, polyaniline, polypyrrole, and polythiophene are well investigated.¹⁴⁴ Polyaniline (PANI) is commonly synthesized in a strongly acidic environment through chemically or electrochemically induced oxidation of aniline monomers. However, these harsh conditions prevent the use of biological

templates as they are highly sensitive materials. Oxidative polymerization of aniline therefore necessitates the adjustment of reaction conditions toward mild pH ranges and tolerable oxidation agents (Figure 13B). In an initial attempt, Simmel and co-workers employed three different stimuli to trigger the polymerization of aniline along a λ -DNA template in solution as well as on a chip surface.¹⁴⁵ Prior to polymerization, DNA and monomers were simply incubated in phosphate buffer at pH 4.3, without the need for any chemical modification. Positively charged anilinium ions act as counterions for the negatively charged phosphate backbone and are organized accordingly. Enzyme-mediated oxidation through horseradish peroxidase (HRP) and hydrogen peroxide, photo-oxidation using a ruthenium complex, and ammonium persulfate as an oxidant all proved to be capable of yielding PANI-decorated DNA conjugates. In a similar approach, the group of He aimed to fabricate conducting polyaniline nanowires along pre-oriented DNA templates which were aligned on a Si substrate.¹⁴⁶ Oxidation of aniline was also induced enzymatically by HRP and hydrogen peroxide. Adjusting the pH value to pH 4.0 turned out to be crucial with regard to wire quality: at a pH of 5, the continuous formation of wires was interrupted by polyaniline particles; however, lowering the pH to 3.2 yielded only incomplete polymerization. Thus, the optimal pH range to ensure continuous and regular polymerization was on the one hand determined by the optimized electrostatic alignment of aniline monomers along the template and on the other hand helped to retain sufficient enzyme activity. By incorporating AuNPs into polyaniline nanowires derived from DNA templates, Wang et al. showed the novel construction of hybrid nanowires with expanded electrical properties.¹⁴⁷ Therefore, a sequential assembly process was applied: positively charged AuNPs were aligned on surface-immobilized DNA templates, affording narrow AuNP chains. The gaps between neighboring particles were then bridged by Ru-mediated photopolymerization of aniline derivatives in acidic media. The alternating AuNP–polyaniline hybrid nanowire could then be visualized by atomic force microscopy (AFM).

As with many other aromatic heterocycles, pyrrole can also be polymerized in oxidative environments. Thus, double helical DNA permits the construction of 1D nanostructures through the organization of the pyrrole precursors and subsequent oxidation and polymerization. In order to generate pure polypyrrole–DNA conjugates with alkynyl side groups, Horrocks and co-workers implemented chemical modifications into a thienyl-pyrrole monomer (TP).¹⁴⁸ It could be shown that monomer functionalization had no negative impact on the oxidative polymerization that was mediated through ferric chloride ($FeCl_3$). Treatment of the conjugates with Tollen's reagent led to the binding of silver cations to alkynyl residues which facilitated nucleation and growth of Ag clusters along the backbone. Compared to unmodified poly(thienyl-pyrrole), many small nanocrystals are formed closely to each other, attaining uniform distribution and enhanced conductive properties. In an ensuing study by Hannant et al., the same monomer was employed to further investigate click chemistry for postmodifications which might be of interest for sensing applications.¹⁵⁰ Importantly, the pentynyl-substituted pyrrole derived nanowires retained structural integrity and remained active, i.e., conductive, after addition of azido molecules via the succeeding click reaction. To broaden the monomer scope and to demonstrate the generality of the electrostatically driven templating approach, Houlton and co-workers polymerized

dithienyl pyrrole monomers (TPT) along DNA templates.¹⁵¹ Though this monomer only comprises 1/3 of the number of hydrogen donor sites compared to pyrrole and therefore reduced bonding capabilities, successful DNA recognition and interaction was still possible. The higher structural regularity of the polymer justifies the use of a less active monomer, since simply mixing thiophene and pyrrole monomers only yields randomly alternating sequences.

Investigation of the growth mechanism of pyrrole monomers along DNA templates by AFM imaging unveiled a stepwise polymerization process. First, low densities of conducting polymer bind to DNA as apparently spherical particles, followed by denser particle packing in a beads-on-a-string fashion, which then resulted in subsequent dynamic reconfiguration, finally elongating and merging the particles in highly regular nanowires with smooth morphology (Figure 13C).¹⁴⁹

The controllable interplay of not only electrostatic but also hydrophobic interactions between DNA and polymers opens up a completely different possibility to define the morphology of resulting conjugates. Once more, nature was used as a role model with respect to its outstanding ability to store genomic DNA with the help of histones. Chen and co-workers tread new pathways for the noncovalent interaction of block copolymers and DNA by establishing a two-step self-assembly process.¹⁵² Notably, the micelle formation of amphiphiles is not only determined by their concentration (critical micelle concentration, CMC) but also significantly relies on the ratio of water phase to organic phase, which is known as the critical water content (CWC). Based on the latter phenomenon, the group designed a self-assembling system of polymers and DNA which is first guided by weak electrostatic interactions that are subsequently caught up by hydrophobic driving forces. They therefore utilized a copolymer that comprises two blocks, a hydrophilic PEG and a hydrophobic poly(4-vinylpyridine) (P4VP). Below the CWC for micellization, the positively charged P4VP interacts with DNA, forming linear complexes in which the DNA is encapsulated by the polymer. Gradual increase of the water content allows for hydrophobic aggregation of the P4VP blocks between polymer chains in solution and polymer chains on the DNA. The hydrophobic interaction then forces rearrangement of the complex and finally leads to core-shell nanofibers in which DNA wraps around the hydrophobic polymer aggregate. When employing monodisperse and relatively short DNA templates, these properties were transferred into the DNA-polymer conjugates which are monodisperse in both length and width. The necessity of the DNA template is clearly evident since the copolymer alone only accumulated in spherical micelles under identical conditions.

Besides the binding modes discussed here, the Watson-Crick base pairing and resultant double helix structure further render DNA attractive for the intercalation of planar molecules. In duplex DNA, the environment of nucleobases leads to π - π -stacking of adjacent aromatic systems, a structural motif that has a greater impact on helix stability than hydrogen bonds of complementary bases. Compounds that recognize DNA via interaction within the stacking bases are therefore potential handles for attaching or growing polymers along the DNA template. Hence, respective initiators, monomers, or the *a priori* synthesized polymer have to be equipped with suitable intercalators. Although ethidium bromide is a very strong DNA binder, utilization of weaker intercalating molecules such as acridine can add the potential for reversibility to the complex.

O'Reilly and co-workers employed RAFT polymerization to synthesize a series of acridine end-terminated polymers, including pNIPAM and pDMAm and investigated the effect of polymer structure on the nature and strength of the interaction with DNA.⁴⁰ Indeed, differences in complexation behavior were observed, which were potentially caused by the relative tendencies of the different polymers to self-assemble when brought into close proximity. For instance, a high load of pNIPAM onto calf thymus DNA and full occupancy of intercalation sites induced irreversible aggregation. The DNA-guided vicinity of polymer chains quasi-imitates the process when hydrogen bonds between the amide groups of pNIPAM are formed, normally giving rise to its temperature-responsive character. On the other hand, the compact structure of pDMAm tolerated higher densities of polymer intercalation without aggregation occurring. Thus, the combination of pDMAm and a significantly shorter and well-defined DNA sequence (63 base pairs) yielded discrete and possibly brush-like nanoparticles with sizes of 10 nm. Importantly, DNA or polymer alone as well as acridine-lacking polymer does not form comparable assemblies. In a different approach, Pike and co-workers instead used monomers with π -stacking anchoring groups to arrange the monomers within the DNA helix and conducted polymerization after intercalation.⁵¹ Based on the intercalation of diazido derivatives of proflavine into the double helix, the azido groups exposed themselves into the major grooves of the DNA. Here, copper-catalyzed click reaction with thienyl-pyrrole monomers was performed. Crucially, proflavine intercalation was not hampered by the ensuing click reaction of the functional groups nor was intercalation of a presynthesized unit of intercalator and monomer successful, due to hydrophobic and steric impediments. Polymerization of the spatially organized pyrrole units was initiated by residual oxygen species in the solvent, without the need for a chemical oxidant.

While this strategy relies both on intercalation within the stacking nucleobases and on chemical reactions taking place in the major groove of DNA, DNA grooves alone also provide the opportunity for noncovalent attachment of polymers. Furthermore, the impact of adjacent base pairs on the groove environment adds a certain level of sequence-specificity to the system which is less prominent among intercalators. To ensure an ideal interaction, groove binding compounds typically comprise at least two aromatic rings while still being flexible in contrast to rigid polycyclic planar molecules that are suitable for intercalation. Deiana et al. investigated the binding mode of an anthracenyl polymer with dsDNA as well as the binding strength and mechanism.¹⁵³ The polymer was synthesized by ATRP from an anthracene macroinitiator with 4 initiator sites, and DNA interaction was induced by simple mixing of the compounds. Association constants in the 10^5 M⁻¹ range are higher than those found for intercalating molecules or electrostatic interactions, thus indicating successful groove binding. Furthermore, the association stoichiometry was ascertained to be 1 polymer-adduct for every 5 base pairs, showing that most sites of DNA participate in the association process. Although groove binding is mainly attributed to hydrophobic forces, van der Waals forces and hydrogen bonding may also be involved in the process, promoted by the hydrophilic polymeric arms.

As already emphasized in the previous section (3.1), the synthesis of covalent amphiphilic conjugates of ODNs and polymers is problematic, especially due to solvent incompat-

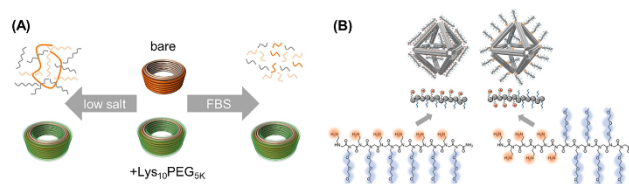


Figure 14. Intrinsic instability of DNA nanostructures under low salt conditions or in the presence of nucleases and fetal bovine serum (FBS) is addressed by many groups. (A) Shih and co-workers could increase the stability of DNA origami by electrostatic coating with PEG–polylysine copolymers.⁶¹ Reproduced with permission from ref 61. Copyright 2017 Springer Nature. (B) Block- and brush-type copolymers of PEG and peptide mimetics (so-called peptoids) were found to also reduce the susceptibility of DNA nanostructures.¹⁶¹ Reproduced with permission from ref 161. Copyright 2020 National Academy of Sciences.

ibility, low conjugation yields, and phase-separation. Host–guest interactions can potentially alleviate some of these concerns by constructing a special hydrophobic molecular environment to compensate for the difference between hydrophilic and hydrophobic components in solution. This environment exists as hydrophobic cavities within a general hydrophilic exterior thus allowing the encapsulation of molecules that would otherwise phase-separate. Varghese and co-workers exploited this interaction mode by equipping DNA with a prominent host molecule (β -cyclodextrin) which can trap adamantane-modified hydrophobic guests.¹⁵⁴ Supramolecular chemistry widely explores this class of host–guests due to their efficient and highly specific molecular recognition, low price, and simplistic modification. The spontaneously formed self-assemblies from the generated DNA-amphiphiles were found to be thermally stable which is attributed to extremely strong hydrophobic interactions. However, this technique is predominantly exploited to attach small molecules or oligomers rather than polymers.¹⁵⁵ At this point it is important to note that this observation applies to almost all approaches relying on noncovalent interactions. A rare example for a polymer-based strategy is reported by Thelu et al. in a follow-up study to their work described above.¹⁵⁶ Herein, adamantyl-terminated 8-arm PEG polymer is encapsulated by X- or Y-shaped DNA carrying β -cyclodextrin at the end of all ODN arms. The combination of a multivalent host with a star-like guest led to nanogel formation, and the gelation was concentration dependent. Moreover, the applicability of these nanoparticles in a biomedical context was accomplished by demonstrating successful drug loading, good cell permeability, and delivery into cells. Thus, due to the universal and modular nature of the host–guest interaction, the approach holds the potential to be further developed.

3.2.2. Polymer Decoration of DNA Nanostructures.

While ss- and dsDNA are extensively leveraged to tailor the polymer sequence and nanostructure and to provide integrative functions, polymers themselves can also benefit DNA in several ways. Higher ordered DNA arrays such as DNA origami are exceedingly versatile building platforms, but they face intrinsic stability drawbacks. Due to their nature, DNA objects are prone to enzymatic degradation through nucleases when encountering physiological environments, thus limiting their progress in biomedicine. Even though degradation might be delayed by packing DNA structures of high density or by having multiple interstrand crossings, it cannot be completely impeded.^{157,158} In addition, DNA origami's integrity is highly dependent on sufficient levels of divalent cations that allow close proximity of DNA strands by

compensating charge repulsion of the phosphate backbones. Hence, several studies seek to diminish DNA susceptibility through polymer-based approaches. Despite the drastically reduced accessibility of 2D and 3D DNA objects in contrast to nonfolded DNA sequences, electrostatic interaction can still be exploited in order to achieve an efficient polymer coating. Divalent cations are hereby substituted by polymeric polycations, either naturally derived or of artificial origin. However, without the possibility of confining the electrostatic interactions in a designated area, coverage will occur nonspecifically which might hamper additional postmodifications.

Various polymers were investigated to determine their structure-binding relationship and their impact on origami stability. For instance, ATRP-generated block copolymers of PEG (to improve biocompatibility and protection efficiency) and methacrylate derivatives (to serve as cationic blocks) were attached to a 60-helix bundled DNA structure.⁶⁰ Notably, for successful binding, the ratio of amines within the polymer to phosphate groups within the DNA backbone (N/P ratio) was found to be pivotal. The number of cationic blocks of the copolymer; however, only had a minor impact on binding affinities. Ahmadi et al. followed suit and studied the effect of polymerization degree, charge density, and N/P ratio of linear PEI and chitosan on coating efficiency.¹⁵⁹ In line with other studies, the N/P ratio significantly determines the extent of interaction with DNA. However, LPEI performed better than chitosan in protecting DNA from salt-depletion and nucleases, even at lower ratios which the authors attributed to its higher charge density. Moreover, the study reveals how challenging the characterization of polymer-decorated DNA nanostructures might be. While bare origamis could be imaged by negative stain TEM, LPEI-coated origamis were only visible after removing the polymer shell. The indirect proof of polymer coverage described here is often the only way to analyze the conjugate (more examples to follow within this section). In 2017, electrostatic coating of DNA origami structures by copolymers from PEG- and polylysine-building blocks were reported by two different groups.^{61,160} The polylysine block interacts with DNA while the corresponding PEG block builds a protective layer and shields the sensitive DNA backbone. The Schmidt lab synthesized PEG_{12 kDa}PLys₁₈ by ring-opening polymerization induced by an amino-terminated PEG macroinitiator while the Shih group utilized commercially available PEG_{5 kDa}PLys₁₀ polymers (Figure 14A). Both coatings proved to enable DNA nanostructures to withstand low salt and high nuclease conditions. However, it is important to note that the coating produced with the in-

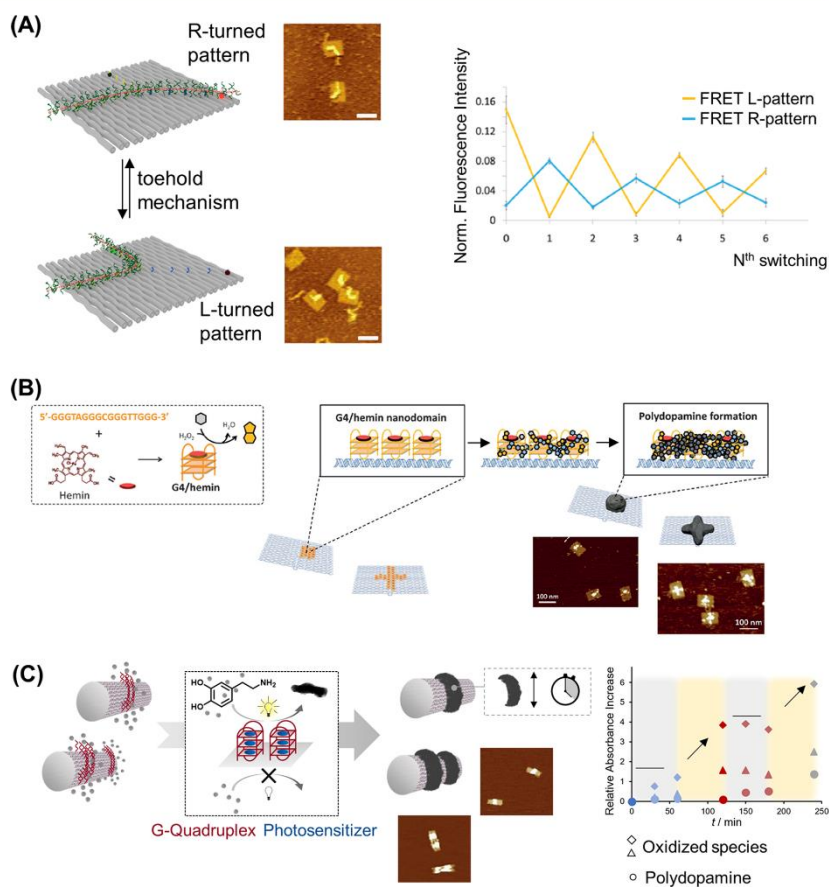


Figure 15. By exploiting the unique addressability of DNA origami, polymer patterning on the nanoscale can be realized. (A) The Gothelf lab developed various strategies to synthesize sophisticated polymers that can be routed on DNA origami platforms on a single-chain level. Furthermore, repetitive switching of the polymer chains was achieved. Switching of the polymer conformation could be monitored by FRET pairs.⁵⁴ Reproduced with permission from ref 54. Copyright 2016 American Chemical Society. (B) The spatially controlled formation of polydopamine in designated patterns was demonstrated by the Weil group by installing enzyme mimicking reaction centers on DNA origami that guided the polymer growth.⁶² Reproduced with permission from ref 62. Copyright 2018 John Wiley and Sons. (C) Further temporal control over polymer formation was implemented by trapping a photosensitizer at distinct positions on 3D origami tubes.⁶⁴ Reproduced with permission from ref 64. Copyright 2020 John Wiley and Sons.

house synthesized copolymer did not allow for further surface functionalization due to the shielding effect by the polymers. Schmidt and co-workers circumvented these restrictions by applying the shorter polymer as it was utilized in the Shih lab, and thus, modifications using AuNP were no longer hampered by the polyplex formation. An important consideration for an electrostatic-based polymer coating is its suitability in a physiological context where charged interactions are subjected to the influences of complex fluids. Interestingly, Shih and co-workers could not only reach a 1000-fold increased stability under cell culture conditions but also confirm the integrity of protected DNA origamis after cell uptake. Remarkably, these

results were achieved with dendritic cells that are known for highly efficient DNA degradation, which therefore represent a challenging scenario for the DNA nanostructures. Recently, Gang and co-workers expanded the polymer scope for electrostatic protection by presenting peptoids as valuable candidates.¹⁶¹ (Figure 14B) Peptoids are peptide mimetics in which side chains are anchored to the nitrogen atom of the backbone instead of the α -carbon, so that secondary structures and proteolysis are suppressed. Positively charged motifs and PEG monomers were used to construct block-type and brush-type copolymers via solid phase synthesis. The latter architectures were advantageous in stabilizing DNA in

biomimetic fluids due to multivalent interactions along the backbone.

In summary, electrostatic polymer coatings provide appealing simplicity when aiming for increased stability of DNA nanostructures. Additionally, polyamines are even more competent in their stabilizing effect than commonly utilized magnesium ions during origami synthesis.¹⁶² Nevertheless, the polymer–DNA conjugates derived are of rather low specificity, which is adequate in only addressing stability issues. For more sophisticated objectives, polymer deposition with spatial and temporal control is more ideal. Additionally, unspecific coating inadvertently wraps reactive handles within the polymer shell thus jeopardizing the key aspect of DNA origami structures. In order to conserve the fidelity of DNA origami, some researchers designed individual strategies to orchestrate polymer alignment. Among the spectrum of suitable non-covalent interactions, complementary base pairing can enable highly precise attachment of polymers, even on a single polymer chain level. Therefore, it is necessary to furnish both DNA origami and polymers prior to conjugation: complementary ODNs have to be mounted on the DNA origami scaffold at designated positions as well as on the polymer chains, guiding the interaction of both building blocks. Gothelf and co-workers developed a method to equip several side groups of a polymer with ODN handles allowing a polymer to interact with a DNA origami template on multiple sites, not only via, e.g., end-group modification. Thus, the alignment of single polymer chains along a predestined path on DNA origami was envisioned.¹⁶³ In detail, solid phase DNA synthesis was employed to graft ODNs from several side chains of a poly(phenylenevinylene) polymer while additional PEG side chains ensured water solubility of the construct which is required for successful DNA conjugation later on. The sophisticated nature of the polymer led to a rather broad size distribution as characterized by GPC (340–3300 kDa) and AFM (length range of 20 to 200 nm), presumably due to partial degradation during purification. However, binding yields of polymers to various DNA origami tiles were still very high according to AFM images. It should be noted that more complex alignments, for instance, a staircase path instead of a U-shape, lower the assembly efficiency. While the visualization of these 2D origami structures was accessible by AFM, the same analysis was highly difficult for 3D objects. 3D characterization was only possible when applying the DNA PAINT technique, again highlighting the challenges in investigating polymer–DNA origami conjugates. In a follow-up study, the Gothelf lab further developed their strategy by installing a programmable switch within the polymer configuration on DNA origami (Figure 15A).⁵⁴ Since complementary base pairing is always of a reversible nature, a so-called toehold mechanism can be applied to trap and release the ODN-modified polymers through different anchors on the DNA origami platform, thus guiding the polymer along various routes. Despite the elaborated efforts, the approach is hampered by synthetic and analytical issues, arising from the very low dimensions on the nanometer scale. Notably, only half of the origami structures exhibited well-aligned polymers, demonstrating challenges during conjugation. Furthermore, repeated switching of the polymer conformation and subsequent AFM imaging was not possible due to very strong background noise resulting from added displacement strands. Subsequently, each cycle of conformation switch was performed in solution, which enabled purification after each

step. Moreover, simultaneous alignment of two different conductive polymers and the ensuing interpolymer energy transfer was not successful, indicating the limits for conjugation of intricate polymers.¹⁶⁴

Despite the rather low number of reports on distinct polymer patterning on DNA origami, there are some studies that do not involve base pairing but electrostatic interactions. In contrast to the studies discussed above, here, electrostatic coating is restricted to only occur within distinct boundaries. This is enabled by pursuing a fundamentally different strategy compared to the aforementioned interactions of polycations with the DNA origami. Here, polymers are grown directly from the DNA surface while simultaneously forming stabilizing electrostatic interactions. As mentioned earlier, the aniline monomer responds to oxidative polymerization as it can be activated by oxidants, photoreactive metal complexes, or enzymes, such as horseradish peroxidase (HRP). Ding and co-workers took inspiration from the latter mechanism and established a HRP-mimicking system to polymerize aniline on DNA.¹⁶⁵ Therefore, they equipped a DNA template with guanine-rich sequences that are known to build so-called G-quadruplexes, representing DNAzymes. Upon incorporation of hemin as a cofactor and the addition of hydrogen peroxide, oxidation of aniline is induced. Due to electrostatic interactions, generated aniline radicals adhere to the negatively charged phosphate backbone in close proximity, thus attaining local polyaniline formation close to the DNAzymes. The group then transferred the regioselective polymer growth to 2D DNA origami triangles.⁶³ They could demonstrate that polyaniline was only fabricated around the catalytic sites whereas DNAzyme-free regions did not form any polymer. However, polymerization directly on DNA origami templates required specific adjustment to the ionic strength of the system to balance reaction kinetics and DNA stability. Weil and co-workers adapted the HRP-mimicking polymerization system for the shape-controlled formation of polydopamine (Figure 15B).⁶² Normally, dopamine tends to self-polymerize in neutral and basic pH, yielding a highly adhesive polymer comprising a multifaceted structure of covalent and non-covalent interactions that is not yet fully understood. By conducting the polymerization in acidic milieu with the help of DNAzymes, the group could implement significant control over dopamine formation. Various polymer patterns on a DNA nanosheet were accomplished, and furthermore, polydopamine acted as a “supramolecular glue”, shaping the origami conformation as the polymerization progressed. It is important to recognize that a slightly acidic pH was crucial for successfully controlling polymer formation as well as the ionic strength of the reaction. High ionic concentration disfavored the electrostatic interaction of dopamine and subsequent reaction intermediates with the DNA template, giving rise to polymerization in solution instead of the origami surface. Nevertheless, DNA stability has to be monitored closely when operating in ion-deficient environments. Recently, the Weil group further developed the method by switching from a chemically induced polymerization to a photo triggered variant allowing the control of the reaction over time (Figure 15C).⁶⁴ G-quadruplexes were employed to trap the photosensitizer protoporphyrin IX at distinct positions on 3D DNA origami tubes, and upon irradiation with visible light, polydopamine formation was induced without the need for further reagents. Not only was the process locally confined, temporal control was dictated by simply switching off and on

the light. Despite the noncovalent nature of the polydopamine–DNA hybrid structure, electrostatic interaction between polydopamine and the DNA survived the total depletion of ions in aqueous medium, confirming its high binding capabilities. Additionally, it was shown that just the presence of one or two polymer rings was sufficient to confer stabilization of the DNA origami in pure water.

In the studies reviewed here, the patterning of polymeric structures on a DNA template via noncovalent interactions remains relatively scarce due to several aforementioned challenges. Complementary base pairing appears to be the most intuitive approach to arrange polymers along several ODN anchors on a DNA template; however, it necessitates a modification of both building blocks. Electrostatic coating leads to nonspecific coverage in general, yet various groups designed DNazyme-based systems to locally restrict polymer growth from the DNA surface. The nanopatterning achieved using this method has allowed the customization of structures in nanoscale resolutions that are yet unachievable by other technologies.

3.3. Chemistry of DNA–Polymer Conjugates Postcoupling

3.3.1. Chemistries on the Polymer. In the synthetic approaches reviewed above, we describe the conjugation of polymers to DNA where reactions are often compromised by the combined limitations of the polymer and the DNA. However, postfunctionalization of the DNA–polymer conjugate offers further access to manipulate nanostructure behavior and function. To realize these postfunctionalization prospects, functional groups need to be embedded in the polymer backbone or at the antipodal terminus. Depending on the polymer employed, modifications can be implemented at points along the backbone; however, functional groups must be compatible with or protected from the coupling chemistry employed for DNA conjugation. In doing so, there are several avenues for secondary polymer functionalization, such as cross-linking or small molecule attachment. Postconjugation polymer cross-linking of an amphiphilic polymer was demonstrated to create a nanoparticle bearing six ODNs.¹⁶⁶ Here, a DNA nanocage was synthesized bearing 8 ssDNA–amphiphile conjugates at the cube corners. The amphiphiles were found to self-assemble in the hollow cube core, demonstrating the guided self-assembly through DNA structures. The polymer consisted of HE and amino groups (Am) in the sequence 5'-Am-(HE)3-Am-(HE)3-Am-DNA-3' and was cross-linked with sebacic acid bis(*N*-succinimidyl) ester to produce the nanoparticle. Cross-linking the polymer chains provides the opportunity to alter the physical properties as well as structure and function, which will be considered in section 4.2.1.

Small molecular attachment is also possible through secondary coupling reactions. In one example, a PEG chain was functionalized by a NHS group at one terminal and a maleimide at the other.¹⁶⁷ DNA coupling was performed through amine-NHS coupling, leaving the maleimide group available and unchanged. A thiol-modified folic acid could then be coupled through a thiol Michael addition to yield a doubly conjugated polymer chain. Although there are a few examples in the literature, the development of biorthogonal reactions directly fuels the available prospects of postconjugation functionalization of DNA–polymer conjugates. In doing so, this strategy can potentially enable an increase in functional diversity as well as the capability to program complex solution behavior.

3.3.2. Chemistries on the DNA. Likewise, postconjugation modification can be achieved through the DNA block, offering several additional strategies unique to the DNA such as chain extension with PCR or hybridization of a complementary ssDNA. One drawback of DNA–polymer synthesis with a user-defined DNA sequence is the length limitation of solid phase synthesis. The polymerase chain reaction (PCR) is a well-established technique employed to replicate short (50 bp) to long (30 kb) lengths of DNA using specific primers to amplify the region of interest. In the case of DNA–polymer conjugates, PCR was employed to synthesize di- and triblock copolymer conjugates of defined DNA length and content bearing polymer termini.⁷¹ This PCR method employs presynthesized ODN–polymer conjugates as the primers, where the conjugation was produced via *grafting to*, to amplify a specific length of DNA. The amplification occurs through the binding of each primer to the long ssDNA sequence, followed by extension from the 3'-ODN-end by the DNA polymerase. This results in a long length of DNA bearing a polymer at the 5'-end. Monodispersity of the central block is therefore achieved and yields either a single or double terminal polymer conjugate determined by the primers used. Additionally, as the primers are independent of each other, the conjugated polymer can be varied and therefore can bear two alternative polymers as part of the triblock, for example, PEG–DNA–PPO or NIPAM–DNA–PEG. In this example, amplification was employed to reshape the conjugate structure. Amplification can also pose benefits for downstream binding or signal enhancement. Rolling circle amplification is an alternative DNA replication technique where DNA sequences are copied from circular DNA. In the case of DNA–polymer conjugates, ssDNA penetrating from the conjugate is available to perform primer functions for DNA polymerase extension from the 3-end. Specifically, ssDNA was bound to polymers at the 5'-end and could bind to the circular DNA at designated positions through complementary base pairing.¹⁶⁸ Once bound, the DNA polymerase can perform the extension and displacement for continued amplification resulting in long ssDNA protruding from the polymer conjugate. Through the employment of postmodification, the long DNA chain is not present during the conjugation reaction, thus avoiding steric challenges. Therefore, the use of postcoupling extension to the DNA block through PCR and RCA demonstrates a synthetic approach to long DNA–polymer conjugates. Chemistries could also be envisaged on DNA postcoupling. As with the polymer reactions, the compatibility with the DNA–polymer coupling reaction is required.

3.4. Characterization of DNA–Polymer Conjugates

The characterization of DNA–polymer conjugates requires a range of techniques due to the variety of approaches and products synthesized. In particular, the production scale of DNA–polymer conjugates has been a primary concern, which is often the bottleneck for analytical tools with poor limit of detection. For conventional polymer synthesis, there are two key techniques: gel permeation chromatography (GPC) and dynamic light scattering (DLS), which are the benchmark characterization techniques to determine polymer quality. For both techniques, approximately 10–50 nmoles of conjugate is required to provide an adequate signal for analysis. This often restricts the number of experimental variables one is able to explore due to the limited amount of material available. GPC and DLS analysis can be applied to all conjugates formed

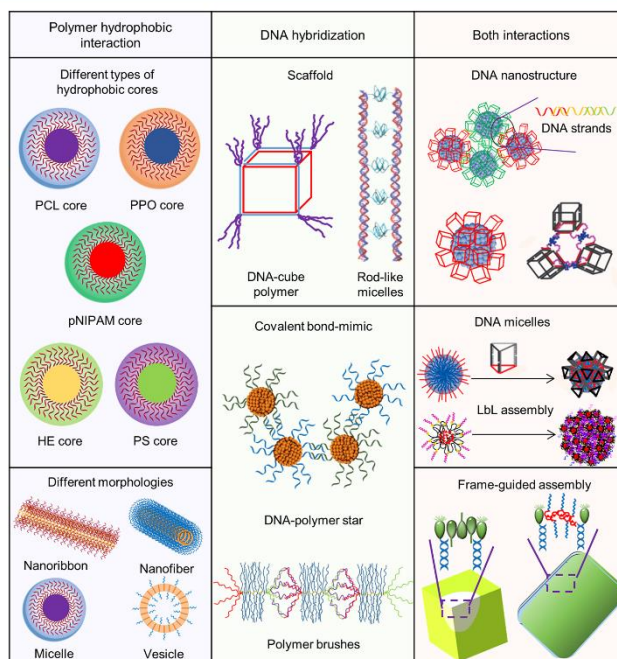









Figure 16. Summary of DNA–polymer static nanostructures. The assembly methods are categorized as a hydrophobic polymer interaction, DNA hybridization, and both interactions. Through polymer hydrophobic interactions amphiphilic DNA–polymer can self-assemble into DNA nanostructures with various morphologies.¹⁷² Reproduced with permission from ref 172. Copyright 2014 American Chemical Society. When the long DNA templates are regarded as the rigid scaffolds, rodlike micelles can be formed by DNA hybridization.¹⁸⁷ Reproduced with permission from ref 187. Copyright 2007 John Wiley and Sons. The assemblies of static DNA–polymer superstructures can form through both DNA hybridization and the polymer hydrophobic interactions to guide the assembly of DNA nanostructures–polymer hybrids.^{79,171} Reproduced with permission from ref 79. Copyright 2016 American Chemical Society. Reproduced with permission from ref 171. Copyright 2014 American Chemical Society.

through the *grafting to* approach as polymers can be fully characterized prior to attachment. For the *grafting from* approach, DLS and GPC^{19,74,85,86} are still applicable to determine the polymer length of 1D DNA–polymer conjugates; however, polymer characterization can pose greater challenges when 2D or 3D nanostructure conjugates are fabricated. Hence, for 2D and 3D conjugates, AFM and high resolution transmission electron microscopy (TEM) can be used to determine the presence of the polymer conjugate on the DNA nanostructures. Spatial information in 2D/3D architectures of the polymer remains a challenge as it is often difficult to determine the orientation of the attached molecules. The overall structure, such as a rodlike or spherical micelle, however, can be determined.⁷⁴ Alterations to the DNA-block can also be analyzed by AFM.^{169,170} In one instance, the height increase of the micelle due to dT incorporation by a terminal deoxynucleotidyl transferase (TdT) polymerase could be monitored to assess DNA chain extension.¹⁷⁰ Agarose and PAGE are also useful techniques to confirm successful attachment or polymerization through band shifts. PAGE is often the preferred method of electrophoresis due to the increased resolution and can be employed to analyze covalent and noncovalent attachment. Using PAGE, *grafting from* can be monitored by the appearance of a new

band at a higher molecular weight depicting successful polymerization,^{19,74,85} as can *grafting to*—the higher molecular weight band depicts efficient conjugation.^{17,18,88,96,98,99} A band shift can also be noted on noncovalent attachment due to the increase in size or also due to the change in overall charge—DNA coated in positively charged polymers is either retarded or can even migrate toward the negative electrode. In addition, the formation of more complex nanostructures can also be analyzed by PAGE, where increasing molecular weight leads to a band shift of lower migration.¹⁷¹ Both electrophoresis methods can be employed for all DNA structures and preparation techniques; however, they do not show specifics, such as orientation or precise polymer length. Matrix assisted laser desorption/ionization spectroscopy (MALDI) can also be employed to demonstrate that the correct molecular weight has been achieved after conjugate synthesis via *grafting to*;⁹¹ however, conjugate flight can be challenging and not always achievable. The increase in experimental analysis techniques has enabled the analysis and therefore development of highly sophisticated DNA–polymer conjugates, although further developments would enable absolute visualization or precision of the DNA–polymer conjugates to assist this field of research.

Table 4. Construction of DNA–Polymer Micelles Containing Different Hydrophobic Cores Driven by the Hydrophobicity of the Polymer

DNA–polymer micelle	Hydrophobic core	Formation	Property of the hydrophobic core	Ref.
	PS	a. Preparation of amphiphilic DNA-PS conjugates by employing copper catalyzed azide-alkyne cycloaddition b. Self-assembly of amphiphilic DNA-PS conjugates	High hydrophobicity and high glass transition temperature	O'Reilly (2013) ⁹⁹
	PPO	a. Formation of DNA- <i>b</i> -PPO copolymers by the conjugation of PPOs to the 5' end of the ODN b. Self-assembly of DNA- <i>b</i> -PPO copolymers	Higher accumulation of hydrophobic reactants in the micelle core and excellent biocompatibility toward different cell types	Herrmann (2006) ¹²²
	PCL	a. Construction of the brush DNA- <i>g</i> -PCL- <i>b</i> -PCL block copolymer by grafting multiple DNA strands onto the end of a diblock copolymer b. Self-assembly of the brush DNA- <i>g</i> -PCL- <i>b</i> -PCL block copolymer	A biodegradable polymer core under physiological conditions	Mirkin (2015) ¹¹²
	pNIPAM	a. Formation of micelle-like nanoparticles by the assembly of pNIPAM b. Modification of micelle-like nanoparticles by amine-modified polyA ₃₀	Temperature responsiveness	Caruso (2009) ¹⁷⁶
	Polyethylene	a. Fabrication of sequence-defined DNA-HE conjugates through a stepwise solid-phase approach b. Self-assembly of DNA-HE conjugates through the addition of Mg ²⁺ buffer	A sequence defined polymer core	Sleiman (2014) ⁸⁰
	PTX ₁₀ polymer	a. Formation of DNA-PTX ₁₀ amphiphile. The ratio between the number of PTX and DNA molecules could be controlled by ring-opening metathesis polymerization b. Self-assembly of DNA-PTX ₁₀ amphiphile	An anticancer drug core	Zhang (2016) ¹⁷⁷
	BODIPY-dUTP	a. Formation of ssDNA amphiphiles by a two-step enzymatic polymerization reaction b. Self-assembly of ssDNA amphiphile	A hydrophobic fluorescent nucleotide was designed as the core to drive the self-assembly of ssDNA amphiphiles	Zauscher (2014) ¹⁷⁸

4. SUPRAMOLECULAR DNA–POLYMER COMPLEXES

Supramolecular interactions between biology and synthetic materials have attracted more attention in recent years. Historically, the development of polymer and block copolymer assemblies has been widely regarded as the first entry of synthetic macromolecular objects in the understanding of the chain dynamics involved in complex solution processes. Biohybrid systems, in particular DNA–polymer conjugates, provide an intrinsic bridge to investigate supramolecular interactions promoted by the respective synthetic and biological entities. As expanded by previous sections, the chemical and physical orthogonality of both blocks allows them to be tailored largely independently, hence the potential

for nanostructural design and supramolecular behavior to be studied in greater detail.

DNA–polymer conjugates behave like block copolymers, thus assembling into nanostructures due to hydrophobic and electrostatic interactions. Moreover, the sequence-specific interactions between DNA strands allow programmed assembly of exquisite nanostructures with stimuli-responsiveness, which is unique for block copolymers with DNA components. Meanwhile, the polymer segments display diverse chemical and physical properties, thus rendering more possibilities to tune the assembling behavior. Therefore, DNA–polymer conjugates can result in large diverse self-assembled nanostructures, which is one of the most attractive features of such hybrids. In this section, we classify the DNA–

polymer assembled nanostructures into static and dynamic structures. The strategies to induce self-assembly, either by hydrophobic interactions through the polymer segment or by sequence hybridization by the DNA segments, are discussed for static structures, whereas the dynamic structures section mainly focuses on the stimuli that can trigger structural or behavioral changes.

4.1. Static Nanostructures

There has been much progress on the solution assembly of amphiphilic copolymers; however, the assembly of DNA–polymer conjugates has become a promising new field due to significant breakthroughs in DNA conjugation chemistry. When DNA is attached to the polymer to obtain a DNA–polymer conjugate, the properties of the conjugate are dictated by both the DNA and polymer component. One of the most common approaches to synthesize DNA–polymer nanostructures employs the hydrophobic interaction of polymers in combination with DNA sequence–specific recognition. Figure 16 shows the summary of DNA–polymer static nanostructures and their self-assembly principles. According to the properties of DNA and the polymer, the assembly methods of static DNA–polymer nanostructures can be classified into three types: assemblies induced by hydrophobic interactions through the polymer segment, assemblies induced by sequence hybridization via the DNA segments, and nanostructures involving DNA and polymer induced assembly.

4.1.1. Assemblies Induced by Hydrophobic Interactions through the Polymer Segment. Due to the wide range of hydrophilic and hydrophobic properties that can be customized by synthetic polymers, DNA–polymer conjugates consist of two categories: hydrophilic and amphiphilic DNA–polymer conjugates. Amphiphilic DNA–polymer conjugates can self-assemble into nanoconstructions with various morphologies and are therefore attractive as unique nanomaterials. Amphiphilic DNA–polymer conjugates self-assemble into spherical micelles through the hydrophobic interactions with the aqueous solvent, exhibiting a hydrophilic DNA shell and a hydrophobic polymer core. The first DNA–polymer micelles, formed from DNA–PLGA polymers, were introduced by Park's group.⁹⁰ The formed micelles would continuously release ODNs by controlling the degradation of PLGA chains and exhibited enhanced cellular uptake by endocytosis thus leading to a new strategy for gene delivery. Since then, with the development of block copolymer self-assembly, DNA nanotechnology and DNA–polymer micelles with different hydrophobic polymer cores have been reported in succession.^{110,112,121,122,173,174} Table 4 summarizes the construction of DNA–polymer micelles containing various hydrophobic cores with different properties.

Mirkin and co-workers prepared spherical DNA block copolymer micelles containing a PS core through self-assembly of PS-*b*-DNA conjugates.¹²¹ The PS-*b*-DNA block copolymers were fabricated through CPG solid phase synthesis. The micelles subsequently formed by hydrophobic interactions of PS-*b*-DNA copolymers, and the resultant hydrophilic DNA exterior of the micelles exhibited unique sequence-specific recognition properties. Furthermore, the average diameters of the micelle structures could be controlled by varying the DNA sequence length and PS molecular weight. Conversely, O'Reilly's group employed copper-catalyzed azide–alkyne cycloaddition to synthesize the amphiphilic PS–DNA block copolymer.⁹⁹ The resulting amphiphilic PS–DNA conjugate

could then form micellar structures in aqueous solution. Whereas the conjugation efficiency achieved by Mirkin's group was low, the copper-catalyzed azide–alkyne cycloaddition adopted by O'Reilly's group resulted in PS–DNA conjugates in a 74% yield. The well-defined micelles were approximately 20 nm in diameter in O'Reilly's work, which confirmed the amphiphilic properties of the PS–DNA block copolymer. Inspired by the synthetic strategy of Mirkin's group, Herrmann and co-workers¹²² constructed a new class of DNA–PPO micelles. Phosphoramidite-PPO derivatives were obtained by the reaction of hydroxyl-group-terminated PPOs with phosphoramidite chloride. The corresponding derivatives were attached to the 5'-end of ODN on a solid support to obtain the DNA–PPO conjugates. The DNA–PPO conjugates self-assembled to form DNA–PPO micelles. Then, on the surface of the micelles several chemical reactions could be produced in a perfectly programmed and controlled manner. In addition to DNA amphiphiles, DNA triblock copolymers can also be developed to assemble DNA–polymer micelles. Gauffre and Mirkin both prepared DNA–polymer micelles containing PCL hydrophobic cores by using triblock copolymers.^{112,174} The PCL hydrophobic cores could then be gradually degraded under physiological conditions by cleavage of ester bonds with acid-promotion or esterase-catalysis.¹⁷⁵ Gauffre et al. focused on micelle preparation and DNA-based recognition ability,¹⁷⁴ whereas Mirkin's group¹¹² aimed to graft many more DNA strands onto the end of a diblock copolymer. Thereby they synthesized a micelle structure consisting of a DNA-brush block copolymer. The micelle exhibited a higher nucleic acids surface density, a higher melting temperature, and more effective cellular uptake without transfection agent. In contrast, Caruso's group¹⁷⁶ prepared pNIPAM-cored DNA micelles in an alternative two-step approach. First, at a temperature lower than its lower critical solution temperature (LCST), the pNIPAM terpolymer formed micelle-like nanoparticles. Second, an amino-modified polyA₃₀ or polyT₃₀ was conjugated to the micelle-like nanoparticles to obtain DNA–pNIPAM micelles. Although there have been some reports on the construction of DNA–polymer micelles using DNA triblock copolymers, with the development of DNA amphiphilic preparation technology in recent years, more work has been done to prepare DNA–polymer micelles using DNA amphiphiles. Sleiman and co-workers constructed HE–DNA micelles containing a polyethylene core by the self-assembly of either HE₆–DNA or HE₁₂–DNA conjugates.⁸⁰ A stepwise solid phase approach was performed to sequence-specifically conjugate synthetic HE oligomers on DNA, which would form monodisperse DNA–polymer conjugates with a defined sequence. The formed DNA–polymer conjugates displayed self-assembly behavior, which could be tuned by the polymer length employed. Specifically, in a buffer with 10 mM Mg²⁺, HE–DNA conjugates containing five or fewer HE units existed as discrete molecules. In contrast, HE–DNA conjugates containing more than six monomer units could self-assemble to form DNA–polymer micelles. Furthermore, the successful preparation of the micelles was verified by encapsulating a guest molecule, Nile Red, within the hydrophobic core of the micelles. Zhang's group also constructed a DNA–polymer micelle through the self-assembly of DNA–drug conjugates.¹⁷⁷ By covalently binding nucleic acids and paclitaxel (PTX, an anticancer drug), the amphiphilic nucleic acid–drug conjugates could form micellar nanoparticles, which were

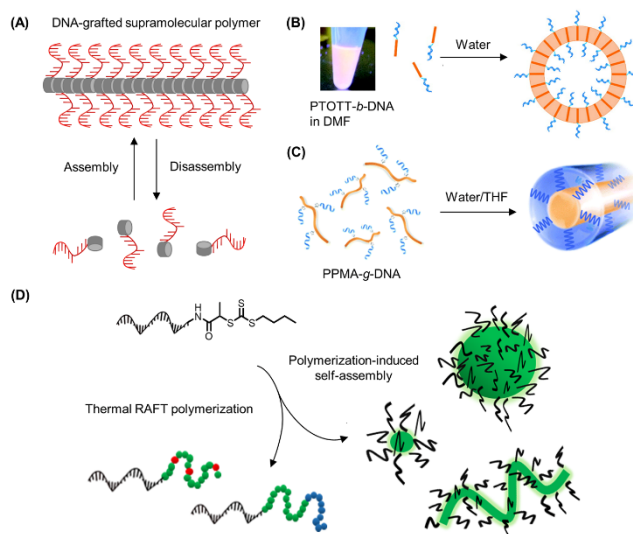


Figure 17. Construction of DNA–polymer static nanostructures with different morphologies assembly driven by hydrophobicity. (A) Schematic representation of 1D DNA–polymer ribbon structures via the self-assembly of chimeric pyrene–ODNs.¹⁷⁹ Reproduced with permission from ref 179. Copyright 2015 John Wiley and Sons. (B) DNA-*b*-PTOTT conjugates were used to construct vesicles.¹⁷² Adapted with permission from ref 172. Copyright 2014 American Chemical Society. (C) Construction of PPMA-*g*-DNA nanofibers.¹⁸¹ Reproduced with permission from ref 181. Copyright 2015 the Royal Society of Chemistry. (D) Fabrication of DNA–polymer nanostructures of various shapes by targeted chain length synthesis of the polymer block.⁷⁴ Reproduced with permission from ref 74. Copyright 2020 John Wiley and Sons.

structurally analogous to spherical nucleic acids (SNAs). This example treated the anticancer drug PTX as the hydrophobic core, which is discussed in more detail in section 5.3.

In addition to the series of methods reported above for preparing DNA–polymer micelles, Zauscher’s group used an enzyme-catalyzed polymerization reaction to construct starlike micelles.¹⁷⁸ dNTPs were sequentially introduced to the oligonucleotide primer through the polymerase TdT. Thereby, ssDNA amphiphiles with high molecular weight and low polydispersity could be prepared by the enzyme-catalyzed polymerization reaction in solution. Through the incorporation of multiple hydrophobic unnatural BODIPY fluorophore-modified dUTP (B-dUTP) nucleotides at the terminus, ssDNA amphiphiles could self-assemble into the starlike micelles. In this work, the successful preparation of micelles was verified by agarose gel electrophoresis and AFM and well predicted by the dissipative particle dynamics simulations. The enzyme polymerization method has great potential in the field of drug carrier development as the DNA building blocks can also be adapted as the drug.

In addition to spherical micelles, DNA–polymer conjugates have also been used to assemble into other morphologies. So far, DNA–polymer-based self-assembly has made the successful preparation of micelles, nanofibers, nanoribbons, and vesicles possible. In addition to these structures, via the self-assembly of chimeric pyrene–DNA oligomers, Haner’s group^{179,180} fabricated helical ribbon structures (Figure 17A). Here, the pyrene–ODNs were prepared through the conjugation of a pyrene segment with various lengths (0, 1, 4, or 7 units) to an ODN (10 nucleotides) at the 5′-end.

Ultimately 1D ribbon-like DNA-grafted supramolecular polymers were formed due to stacking and hydrophobic interactions between pyrene chains. Unlike Haner’s approach, Park and co-workers prepared DNA-modified 1D polythiophene nanoribbons via a simultaneous assembly of DNA-*b*-poly[3-(2,5,8,11-tetraoxatridecanyl)-thiophene] (PTOTT) with PEG-*b*-PTOTT.¹⁷² PEG-*b*-PTOTT drove the self-assembly which offered an approach to attach the DNA’s molecular recognition properties to several self-assembling structures. In this work, not only DNA–polymer nanoribbons were prepared, but also size-controllable DNA–polymer vesicles by the assembly of DNA-*b*-PTOTT (Figure 17B). When only DNA-*b*-PTOTT was present, vesicle assembly was observed. The formation of vesicles was favorable due to the rigid polythiophene structure in combination with the high negative charge of DNA. In general, simple spherical micelles could form by the self-assembly of DNA–polymer conjugates due to the highly negatively charged DNA backbone. However, the π – π interaction of the rigid PTOTT block induced the self-assembly of DNA-*b*-PTOTT to form an unusual vesicle. In the self-assembly process of rod–coil copolymers, the trade-off between interface energy, coil stretching, and rod filling could affect the assembly structure. Vesicles are thermodynamically more advantageous than simple micelles—simple micelles formed through assembling rod–coil block copolymers possessed a high curvature and can create rod packing defects. Furthermore, the experiment verified that the increase in vesicle size was mainly dependent on increasing the polymer concentration. Subsequently poly(propargyl methacrylate) (PPMA)-*g*-DNA nanofibers were fabricated by Nardin’s

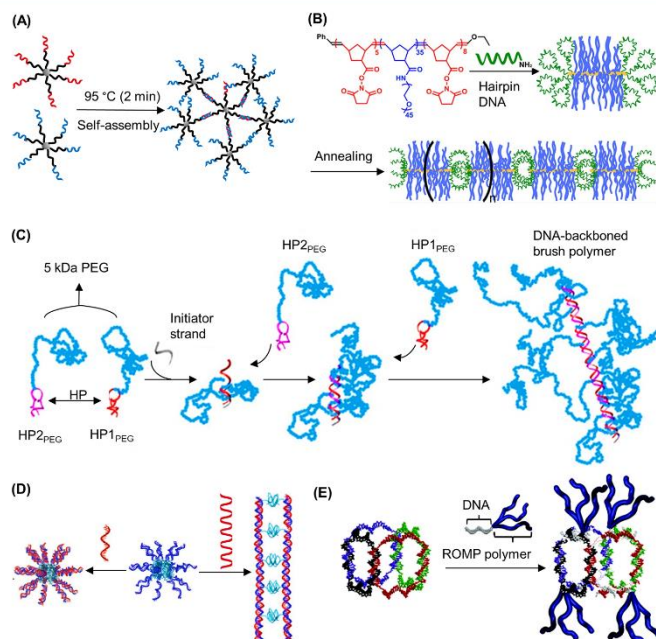


Figure 18. Static DNA–polymer nanostructure assemblies mediated by DNA hybridization. (A) Construction of star-polymer conjugates.⁹⁷ Reproduced with permission from ref 97. Copyright 2011 American Chemical Society. (B) The formation of wormlike nanostructures by the self-assembly of a hairpin DNA–polymer conjugate via DNA hybridization.¹¹³ Adapted with permission from ref 113. Copyright 2014 American Chemical Society. (C) Schematic illustrations of forming a DNA-backed bottlebrush polymer through DNA hybridization.¹⁸⁶ Adapted with permission from ref 186. Copyright 2016 American Chemical Society. (D) Construction of ss-DNA-*b*-PPO micelles and rod by using short and long DNA templates, respectively.¹⁸⁷ Adapted with permission from ref 187. Copyright 2007 John Wiley and Sons. (E) Formation of DNA cubes. DNA–polymer conjugates are organized onto a 3D DNA scaffold.¹⁰⁹ Adapted with permission from ref 109. Copyright 2012 American Chemical Society.

group through the assembly of an amphiphilic poly(2-alkyl-2-oxazoline) (POX)-*graft*-DNA copolymer.¹⁸² Since POX is similar to a polypeptide in structure, it could be considered as a pseudo polypeptide. This was the first report of a DNA sequence and an assembly composed of a pseudo peptide through a nucleation polymerization mechanism. The nanofibrils were formed by inter- and intramolecular hydrogen bonding. Jiang et al. also successfully prepared a primary nanofiber structure using the PPMA-*g*-DNA brush. The nanofiber structure possessed a hydrophilic DNA shell and a hydrophobic PPMA core formed by DNA strands covalently grafted to a PPMA backbone via “click” chemistry (Figure 17C).¹⁸¹ Herein, PPMA selective solvents, such as THF, could influence the morphology of the PPMA-*g*-DNA nanofibers; for example, when 20 vol % THF was added to the aqueous system randomly interwound nanofibers were observed. Conversely, the introduction of 40 vol % THF drastically increased the tendency to form multistrand helices. The methods used in the examples described above provide DNA–polymer nanostructures with a single shape by altering a single factor. Wei’s group developed a new platform technology to construct DNA–polymer nanostructures with multiple shapes. This technology mainly leveraged PISA for polymerization from ssDNA to fabricate nanostructures.⁷⁴ The solution-based

thermal RAFT polymerization from DNA was achieved by enzymatic degassing of glucose, glucose oxidase, and sodium pyruvate under ambient conditions. Furthermore, this was the first time PISA was performed with RAFT polymerization from DNA and it provided a convenient path to construct complex DNA–polymer worm architectures. This technology was successfully used to prepare DNA–polymer conjugates with narrow molecular weight and variable lengths. The assemblies could reassemble into the thermodynamically most favored state with increasing degrees of polymerization. Subsequently, DNA–polymer nanostructures of various shapes were manufactured by targeting the chain length of the polymer block, which established a new platform technology toward functional DNA–polymer nanostructures (Figure 17D).

4.1.2. Assemblies Induced by Sequence Hybridization of the DNA Segments. Amphiphilic block copolymers consist of a hydrophilic block and a hydrophobic segment that can self-assemble into various predictable morphologies fueled by the phase separating constituents.¹⁸³ Although the chemistry of block copolymers is diverse and offers varying optimization approaches to tune stability and biocompatibility, it lacks sequence selectivity, monodispersity, programmability, and the fine structural control provided by DNA. With the advances in DNA nanotechnology, flexible

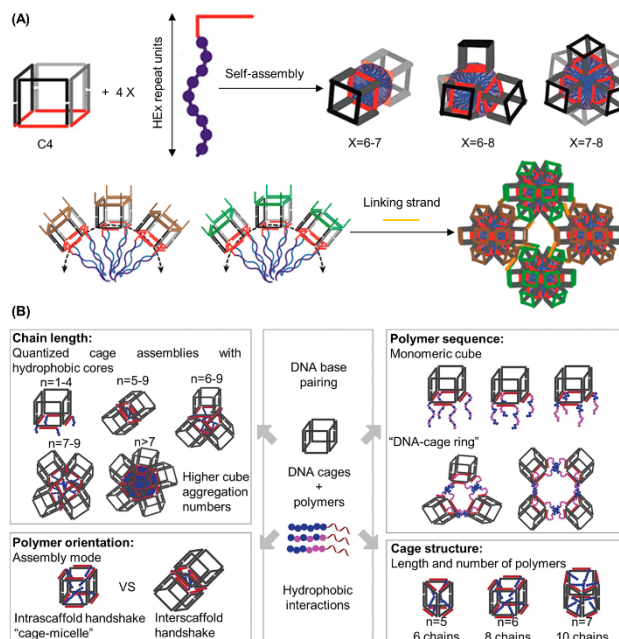


Figure 19. Static DNA–polymer nanostructure assemblies mediated by the hydrophobicity of the polymer and DNA hybridization. (A) Construction of micelle-of-cubes by HE-DNA strands with different polymer lengths attached to C4.¹⁷¹ Adapted with permission from ref 171. Copyright 2014 American Chemical Society. (B) Schematic illustrations of the self-assembly of sequence-defined hydrophobic polymers on DNA cages.⁷⁹ The magenta circles represent hydrophilic monomers, and blue denotes hydrophobic monomers. “N” presents the number of hydrophobic repeats. Adapted with permission from ref 79. Copyright 2016 American Chemical Society.

structural manipulation of DNA has provided an intelligent tool to program the self-assembly of DNA block copolymer materials. In the previous section, static DNA–polymer nanostructures were discussed based on how polymer design can motivate self-assembly by hydrophobic interactions. This section reviews the static DNA–polymer nanostructure induced by sequence hybridization of the DNA segments and associated technologies.

In one assembly approach, the DNA component mediated the static DNA–polymer supramolecular complexes through complementary strand hybridization.¹⁸⁴ Here, Das and co-workers prepared star-polymer–DNA conjugates via the click reaction, where subsequent higher-order nanoassemblies could be achieved by complementary DNA hybridization, where DNA was treated as a covalent bond-mimic (Figure 18A).⁹⁷ Zhang and co-workers reported a series of examples to assemble polymer–DNA conjugates via DNA cross-linking. In one study, nucleic acids were covalently conjugated to the termini of triblock copolymer brushes to yield interactive handles which could then form head-to-tail ordered wormlike supramolecular nanostructures (Figure 18B).¹¹³ In this assembly process, intermolecular DNA hybridization was prevented by the triblock copolymer brushes, inducing the multivalent conjugate to mimic a divalent structure. The DNA moieties were designed to attach complementary brushes, thus forming well-defined 1D nanostructures. This elegant design was ensured by two key parameters. First, the directionality of

assembly needs to be controlled by a sufficiently rigid polymer backbone so that the monomer cyclization is energy-unfriendly. Second, the number of DNA strands at one termini is critical to avoid multiple connections on one block. Their further studies also investigated the self-assembly kinetics and provided a model to accurately predict the degree of polymerization and size distribution of the assembled products.¹⁸⁵ Moreover, in order to improve the biopharmaceutical properties of ODN therapeutics, in another example, they developed a DNA-backboned bottlebrush structure with PEG side chains (Figure 18C).¹⁸⁶ Here, the PEGylated ODN hairpins were constructed to realize a hybridization chain reaction, which lead to a living polymerization using two hairpins as monomers. Thereby, a “bottom-up” synthetic approach was devised to obtain the uniformly PEGylated DNA nanostructures. The position and number of the PEG chains could be accurately controlled throughout the nanostructure surface.

Another assembly model used for DNA-mediated static DNA–polymer supramolecular complexes is to regard DNA as a rigid scaffold for organizing polymer molecules at specific locations with particular direction and number.¹⁸⁴ Herrmann and co-workers achieved the preparation of rodlike micelles by using long DNA templates as scaffolds.¹⁸⁷ This work clearly reflected how DNA hybridization altered the structural properties of DNA block copolymer micelles, transforming the ssDNA shell of the micelles into dsDNA through base

complementation. When the short complementary sequences were introduced to spherical DNA block copolymer micelles through base pairing, a spherical DNA-*b*-PPO micelle with a double stranded corona could be fabricated and the overall shape of micelles was conserved. However, when hybridized with long DNA templates, the morphology of the spherical micelles was transformed from spheres to uniform rods (Figure 18D). Four and five DNA-*b*-PPO polymers were annealed on two long DNA templates, T88 and T110, respectively. Upon hybridization, the spherical ssDNA-polymer micelles were disintegrated and DNA-*b*-PPOs were arranged linearly along the long DNA strand. Eventually, nucleic acid segments participated in the formation of a double helix structure with the template, and hydrophobic blocks protruded from dsDNA, resulting in spherical micelles transformed into a rodlike structure. Using a different form of DNA nanotechnology, Sleiman's group built a new type of biohybrid material in which the positions of polymer chains were programmed in 3D treating DNA cages as scaffolds (Figure 18E).¹⁰⁹ DNA cubes composed of four 80-nucleotide strands were fabricated by a new method that could be quantitatively assembled from a minimal number of DNA strands. In this instance, the polymer component, hexanediol, aided the nanostructure formation by increasing the flexibility and reducing strain. Hence, four hexanediol insertions were introduced into these DNA cubes at the junctions where the square faces were formed. The DNA-polymer conjugates were synthesized by combining a block copolymer with a short DNA strand and were subsequently introduced into the cubes by DNA hybridization, allowing the arrangement of a precise number of polymers on a specific surface of the cube. In this study, DNA was treated as a rigid scaffold, which could be used to sequence polymers remotely, as well as to control quantity, density, and direction.

4.1.3. Nanostructures Involving DNA and Polymer Induced Assembly. In this part, we will discuss static DNA-polymer nanostructures that were assembled through both DNA hybridization and the polymer hydrophobic interactions. From the previous section, the regulation of polymer hydrophobicity can promote the assembly of ssDNA-conjugated polymers into ribbons, micelles, or other forms in water. The DNA strands of these self-assembled systems could present the thermodynamically favored radial arrangement around the core. However, polymers can also be exploited to mediate DNA superstructure formation by guiding the assembly of DNA nanostructure-polymer hybrids. These polymers are mainly attached to the surface of DNA nanostructures by DNA hybridization. To date, only a small amount of DNA superstructure formation induced by hydrophobic polymer has been published. The first polymer-mediated DNA superstructure was reported by O'Reilly's group by the assembly of a tetrahedron-pNIPAM conjugate.⁹⁹ Herein, DNA-pNIPAM conjugates were attached to a DNA tetrahedron by DNA hybridization and, in the presence of excess polymer, formed polymer-decorated DNA tetrahedrons, which self-assembled into tetrahedron-pNIPAM composite nanoparticles. Due to the thermal-responsiveness of pNIPAM, the formed superstructures are of dynamic nature, which is described in detail in the next section. Similarly, Sleiman and co-workers constructed a series of new nanostructures through the self-assembly of DNA cages and sequenced polymers,^{79,171} as presented in Figure 19A. In this instance higher order nanostructures could be created through orthogonal applications of DNA nanotechnology and precision polymers, which

exhibited an unprecedented level of control over the number of polymers.¹⁷¹ The work first varied the multiplicity position and multiplicity of hydrophobic polymers on DNA cages and found that C4 (four binding regions on a single face), a geometric structure that promoted the aggregation of proximal polymers and thus superamphiphiles, was hence selected for self-assembly of a micelle containing the cubes. The number of aggregated DNA cages was programmed by changing the number of hydrophobic polymer repeating units on the cages. With increasing length of the polymer, the monomeric (polymer chains potentially aggregated on one face) structures gave way to a higher-order dispersed assembly of the dimer and an increase in the finite number of aggregates, followed by a monodisperse oligomer micelle. Moreover, higher-order micelle assemblies were also possible by recognition of the external DNA nanostructures to create functional macroscopic materials. A network of micelles were formed by attaching different chains to the micelles of two different populations and then adding a connecting chain (Figure 19A, bottom). This constituted the first reported example which used quantified polymer to mediate self-assembly.¹⁷¹

The same group further investigated the limits of their self-assembly method and its value for application by adding hydrophilic monomers to the hydrophobic polymer.⁷⁹ In this system, Sleiman and co-workers focused on the investigation of systematic change in cage size and structure as well as the orientation of individual polymer chains on the DNA scaffold. Importantly, this study elucidated the assembly behavior of precision polymers attached to DNA cages by changing the length of the polymers, by adjusting the polymer sequence and direction of individual polymer chains on the DNA cage, and by varying the shapes of the DNA cages. When the hydrophobic polymer was attached to one face of the DNA cage by DNA hybridization, "quantified cage assemblies" with a hydrophobic core were obtained. The number of hydrophobic repeats directly affected the aggregation number of the cage (Figure 19B, top left). In this work, the polymers were sequence-controlled by precisely changing the number of hydrophilic and hydrophobic repeats. By introducing hydrophilic segments into the polymer, polymers could guide conjugates to form monomeric cages or donut-shaped "cage-rings" (Figure 19B, top right). Furthermore, the diameter and density of DNA cage-rings could be adjusted by controlling the length of the polymer blocks. By studying the orientation of polymer chains on the cages, a DNA cage intrascaffold "handshake" to form DNA-micelle cages was demonstrated. When both sides of the DNA cage were decorated with hydrophobic polymers, it was more stable than the cage that was unsubstituted (Figure 19B, bottom left). Additionally, the successful formation of the hydrophobic core in the fabricated DNA-micelle cages was verified by the encapsulation of the hydrophobic Nile Red. Finally, in order to probe whether the geometry of the cage can change the number of cages per aggregate, cages with different sizes and geometries were efficiently constructed (Figure 19B, bottom right). According to the experimental results, the different cage geometries resulted in an intrascaffold "handshake" within the scaffold with different capacities for small molecules and with various hydrophobic repeats. The loading capacity of hydrophobic guests could be increased when the larger cages were used to assemble the cage-micelles.

Furthermore, DNA-polymer micelles could also be used to assemble static DNA-polymer supramolecular complexes. As

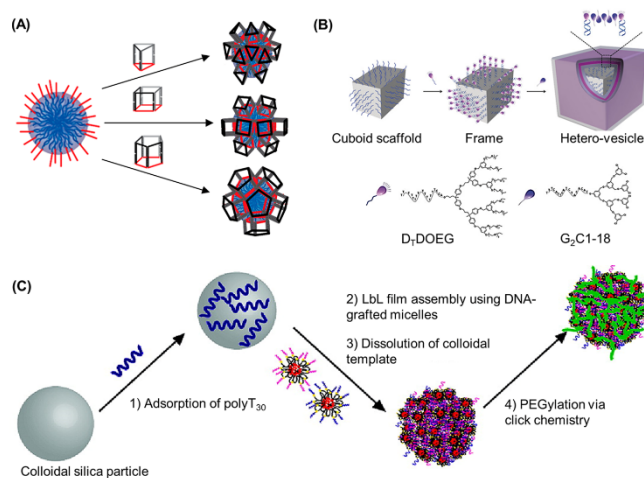


Figure 20. (A) Construction of micelle-of-cubes by incubating preassembled micelles with preassembled DNA nanostructures. Adapted with permission from ref 171. Copyright 2014 American Chemical Society. (B) Formation of cuboid vesicles by the FGA method on DNA origami scaffolds.¹⁸⁸ Adapted with permission from ref 188. Copyright 2017 John Wiley and Sons. (C) Construction of PEGylated DNA-pNIPAM capsules through multilayer assembly of pNIPAM-T₃₀ and pNIPAM-A₃₀ micelles.¹⁷⁶ Adapted with permission from ref 176. Copyright 2009 American Chemical Society.

shown in Sleiman's work, they constructed a micelle-of-cubes by polymer hydrophobic interactions and DNA hybridization.¹⁷¹ Here, HE₁₂-DNA micelles were fabricated by the assembly of polymer-DNA conjugates which has been discussed in section 4.1.1. Subsequently prisms with various geometry and size were adsorbed onto the surface of the HE₁₂-DNA micelles to form micelle-of-cubes by DNA hybridization (Figure 20A). This assembly method was used to assess the integrity of DNA nanostructures attached to micelles. Conversely, Caruso and co-workers constructed DNA-polymer microcapsules employing a layer-by-layer assembly approach of DNA grafted polymer micelles.¹⁷⁶ Here, amine-modified ssDNA was conjugated to pNIPAM to synthesize pNIPAM-T₃₀ and pNIPAM-A₃₀ micelles. Colloidal silica particles were used as templates to assemble pNIPAM-T₃₀ and pNIPAM-A₃₀ micelles layer-by-layer. The silica particles were then dissolved to obtain the DNA-polymer microcapsules, which possessed lower permeability than single-component DNA capsules due to the presence of pNIPAM (Figure 20B).

In general, vesicles, spherical micelles, or other symmetric forms can be assembled by amphiphilic molecules in water. However, obtaining amphiphilic assemblies with concrete sizes and shapes is still a significant challenge in this area.¹⁸⁹ Liu's group developed frame-guided assembly (FGA), an approach to prepare a series of shape-controlled DNA-polymer amphiphilic assemblies.^{188,190,191} This method could be employed to assist the assembly of polymers driven by the hydrophobic polymer outside the frame, which offered greater control over self-assembly. First, they employed DNA-functionalized AuNPs as the frame to fabricate customized heterovesicles.¹⁹⁰ Prepositioned, discontinuous leading hydrophobic groups (LHG) were introduced by DNA hybridization to the corresponding positions of the frame, outlining the

edges of the designed structures. Other amphiphilic molecules could be guided to fill the gaps between LHGs and ultimately produce monodispersed vesicles. This work improved the understanding of the fundamental mechanism of self-assembly through the FGA method. Subsequently, a similar method was employed to fabricate a 2D nanosheet and 3D heterovesicle assemblies by constructing DNA origami nanostructures.^{188,191} A variety of DNA origami shapes could be prepared through the folding of a long scaffold DNA sequence by a series of carefully designed short DNA strands. The ssDNA-modified amphiphilic molecule named DDOEG was positioned reasonably on the DNA origami platform through sequential specific DNA hybridization to form a 2D hydrophobic framework domain on the DNA origami. Consequently, a homogeneous or heterogeneous 2D nanosheet could be gradually formed on the DNA origami by absorbing additional amphiphilic molecules into this hydrophobic frame domain through the hydrophobic interactions.¹⁹¹ Through this study it was finally demonstrated that the FGA strategy can overcome the obstacle of 2D amphiphile assembly in aqueous solution. Importantly, the size and shape of the 2D amphiphilic assemblies could be readily controlled by the shape of the DNA origami. Additionally, by varying the design of the DNA origami scaffolds, cuboid and dumbbell-shaped heterovesicles could be constructed.¹⁸⁸ As shown in Figure 20C, once the DNA origami nanostructure was formed, 115 copies of polyA strands were positioned on the surface. Subsequently, the polyT-modified D₇-DOEG (selected as the LHG) could be introduced to the surface of the DNA origami through DNA hybridization. The added amphiphilic molecules, G₂C1-18 (see Figure 20C for the specific structure), were assembled along the frame under the guidance of LHG, filling the gap between LHG and forming the heterovesicle. Altogether, the results in these articles demonstrated the flexibility of the FGA strategies

to guide specific geometrically challenging amphiphilic assemblies by using the geometric programmability of DNA origami nanostructures.

In summary, this section systematically studied the formation of static nanostructures according to the properties of the polymer and DNA segment. As a traditional direction, the assembly behavior of DNA–polymer conjugates has been widely studied. Currently, different shapes of static nanostructures such as micelles, nanoribbons, nanorods, and microcapsules have been successfully prepared by the corresponding DNA–polymer conjugates. Among them, DNA–polymer micelles were studied the most. However, although the structures are now expansive, only a few types of polymers have been explored in conjugation with ssDNA. We believe that in the future, as the conjugation chemistry develops, more synthetic polymers with distinct structures and properties could be conjugated to DNA terminals and, therefore, the variety of DNA–polymer micelles would be further expanded.

4.2. Dynamic Nanostructures

Unlike static DNA–polymer assembly, smart dynamic DNA–polymer nanostructures can alter their shape and size in response to external stimuli,¹⁹² which has been greatly investigated by several groups.^{98,192,193} As shown in Figure 21, these structures can respond to chemical stimuli (e.g., pH),

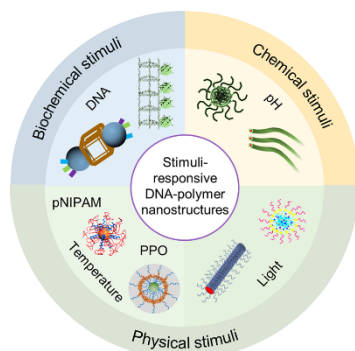


Figure 21. Schematic illustrations of different types of stimuli-responsive DNA–polymer dynamic nanostructures.^{93,200} Adapted with permission from ref 93. Copyright 2003 American Chemical Society. Adapted with permission from ref 200. Copyright 2013 American Chemical Society.

biochemical stimuli (e.g., ssDNA), and physical stimuli (e.g., light and temperature). They are widely used in biomedical fields, such as intracellular delivery of genes via a pH-mediated mechanism and light-guided delivery of small molecule drugs. In this section, we discuss the dynamic nanostructures formed by DNA–polymer conjugates under each stimuli category.

4.2.1. DNA Programmable Dynamic Nanostructures.

Due to stimuli-responsiveness, the precise sequence-control, desirable molecular properties through base pairing, and ease of modification, DNA could also be used to mediate the programmed assemblies of dynamic DNA–polymer supramolecular nanostructures. The dynamics of these types of materials are mainly reflected by the strand displacement

strategy and the reversible transformation of complementary base pairing (RTCBP).

Sleiman and co-workers fabricated a series of dynamic DNA–polymer supramolecular nanostructures by the strand displacement strategy. In their first work, a long DNA strand containing a repeating sequence was created by the use of rolling circle amplification and then employed as a guide strand to construct robust nanotubes with a non-nicked backbone (Figure 22A).⁹⁸ Subsequent block copolymer assemblies were sequence-specifically and longitudinally positioned on robust DNA nanotubes. These materials were dynamic, and the block copolymer structures could also be cleanly removed from the DNA nanotubes when a specific competitor DNA sequence was added (shown in Figure 22A). The second work employed the strand displacement strategy, providing an economic approach to build DNA nanotubes functionalized with lipid-like polymers.¹⁹³ A spacer was used to link polymers to the nanotube, and polymers folded inside to create a hydrophobic environment within the nanotube. The spacer was vital to the morphology of the dynamic DNA–polymer nanostructures. A network of DNA bundles was formed when the polymers were directly linked to the nanostructure without spacers. However, in the presence of 8T spacers on the amphiphilic strands, the micellar microenvironments were generated along the repeating units of the nanotubes due to the DNA amphiphiles accumulating in the nanotube (Figure 22B). These micellar microenvironments were constructed mainly to encapsulate the small molecule Nile Red. Subsequently, a series of specific DNA strands were designed to interact with the 8T spacer, and the amphiphilic strands LS 1–3 were removed by strand displacement, which illustrated the dynamics of this nanostructure. Small molecules encapsulated in the nanotube would ultimately be released from the nanostructures when specific DNA strands were added. Another type of dynamic DNA–polymer nanostructure was also developed to demonstrate that not only small molecules but also nucleic acid therapeutics could be delivered by DNA–polymer dynamic nanostructures. Sleiman and co-workers designed a stimuli-responsive spherical nucleic acid, which could be used to load and release nucleic acid therapeutics.¹⁹⁴

This spherical nucleic acid vehicle was assembled from only four strands, and nucleic acid therapeutics could be delivered upon recognition of specific ODN triggers via strand displacement. This work led to a new class of responsive drug delivery vehicles that were stimuli-responsive and more accessible than previous examples.

Besides strand displacement, DNA hybridization is also thermally responsive; thus, it could be reversible depending on the temperature, and therefore, it is possible to exploit to induce dynamics to the nanostructures. For instance, as shown in Figure 22C, Sleiman's group constructed dynamic supramolecular DNA–polymer nanostructures through the RTCBP.¹⁶⁶ Here, the hexavalent printed particle was formed inside the DNA cage. Under thermal denaturing conditions the hexavalent particles with different DNA strands could be obtained and hence precisely controlled in terms of the number of DNA strands and their directionality, while preserving sequence anisotropy. These hexavalent printed polymeric particles could reassemble into well-defined structures by scaffold rebinding and then again be released from the DNA scaffold via strand displacement. In this work, the dynamics of DNA nanostructures were reflected in both strand replacement and reversible DNA hybridization. In

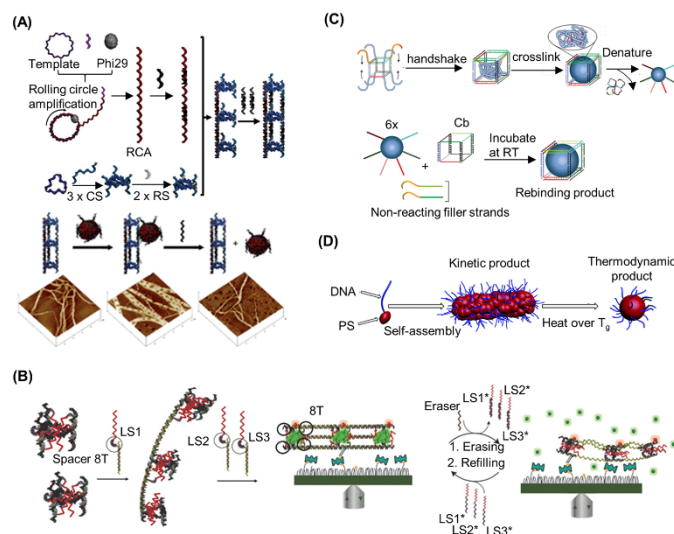


Figure 22. Use of DNA for reversible structural control of dynamic supramolecular DNA–polymer nanostructures. (A) Construction of DNA programmed nanotubes through a rolling circle amplification process.⁹⁸ Reproduced with permission from ref 98. Copyright 2012 the Royal Society of Chemistry. (B) Schematic illustration of the assembly of dynamic nanotubes with hydrophobic pockets.¹⁹³ Adapted with permission from ref 193. Copyright 2018 John Wiley and Sons. (C) The construction and denaturation of the cube with eight amphiphiles after cross-linking.¹⁶⁶ Adapted with permission from ref 166. Copyright 2018 Springer Nature. (D) Schematic presentation for the kinetic micellization of DNA_{6-mer}-b-PS_{8,SLD3} and subsequent reversible micelle morphological changes.¹²⁵ Adapted with permission from ref 125. Copyright 2015 the Royal Society of Chemistry.

addition, Zhang and co-workers assembled dynamic DNA-PS supramolecular nanostructures through the RTCBP (Figure 22D).¹²⁵ In this example, the DNA–polymer micelles were prepared first and then used to form higher-order assemblies. Here, the kinetic and thermodynamic self-assemblies of several DNA-*b*-PS amphiphiles were investigated via DNA hybridization. The kinetic products were obtained through a pair of complementary DNA-PS micelles, and the thermodynamic DNA–polymer micelles formed again when heated to 99.5 °C for 10 min.

4.2.2. Temperature-Responsive Dynamic Nanostructures. In recent years, temperature-responsive polymers, as “intelligent” materials sensitive to temperature, have been widely studied. These polymers show mainly hydrophobicity changes in response to altered temperature and can therefore be used in the preparation of “dynamic polymer” materials. Among them, pNIPAM and PPO are the two most widely studied thermoresponsive polymers, which can be coupled to DNA to form DNA–polymer conjugates.^{99,192,195,196} When the temperature changes, the hydrophobicity of the polymers increases, leading to the formation of the DNA–polymer conjugates into temperature-responsive DNA–polymer dynamic nanostructures. In the following sections recent work in this area is discussed.

DNA–pNIPAM. pNIPAM has been widely studied as a thermoresponsive polymer, and as a linear form, at room temperature it is water-soluble. However, when the LCST is exceeded, pNIPAM transforms from hydrophilic to hydrophobic as the chains collapse with the entropic release of water. Therefore, pNIPAM can be used to prepare temperature-

responsive materials. The first example of a DNA–pNIPAM conjugate was reported by Maeda’s group.¹⁹⁷ In this work, a DNA–pNIPAM conjugate was used to capture a DNA-binding genotoxin, ethidium. Subsequently, DNA–pNIPAM conjugates could be widely used to assemble dynamic DNA–pNIPAM nanostructures due to the reversible phase-transition properties of pNIPAM. Furthermore, according to the type of DNA–pNIPAM conjugate adopted, the formed dynamic DNA–pNIPAM nanostructures could be divided into two categories: assemblies driven by ssDNA–polymer conjugates and DNA nanostructure–polymer conjugates, respectively.

The first class of dynamic ssDNA–polymer conjugates were formed by the well-established hydrophilic–hydrophobic transition of ssDNA–pNIPAM nanostructures. Maeda and co-workers connected pNIPAM-SH to 5′-maleimide-modified DNA to form the DNA–pNIPAM conjugates by using the Michael addition reaction.¹⁹⁸ When the solution temperature rose above the LCST of the DNA–pNIPAM conjugates, micelles were produced via the self-assembly of the conjugates. The subsequent experimental results demonstrated that the large size polymer micelles could produce non-cross-linking aggregation and exhibited colloidal stabilization induced by terminal mismatch. The dynamics of the temperature-responsive supramolecular assemblies was also demonstrated by morphological changes. Park’s group assembled dual-responsive DNA triblock copolymer dynamic nanostructures (molecular recognition of DNA and temperature-responsiveness of PNIPAM) through constructing a thermally switchable triblock copolymer, DNA-*b*-pNIPAM-*b*-pMA (Figure 23A).¹⁹² Both DNA and pNIPAM were hydrophilic at temperatures

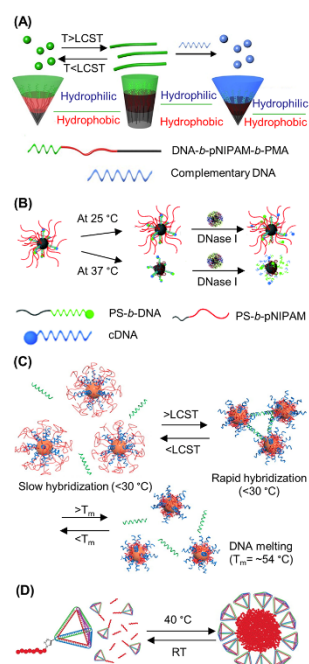


Figure 23. Fabrication of thermoresponsive dynamic DNA–pNIPAM nanostructures. (A) Schematic illustration of the dual-responsive DNA triblock copolymer dynamic nanostructures. The dual-responses were reflected in the temperature change and DNA’s molecular recognition properties.¹⁹² Adapted with permission from ref 192. Copyright 2016 American Chemical Society. (B) Nuclease-catalyzed degradation of hybrid temperature-responsive DNA micelles.¹⁹⁹ Reproduced with permission from ref 199. Copyright 2019 the Royal Society of Chemistry. (C) Construction of DNA-functionalized AuNPs and verification of the recognition characteristics of DNA molecules on the surface of AuNPs.²⁰⁰ Adapted with permission from ref 200. Copyright 2013 American Chemical Society. (D) Temperature-induced formation of “surfactant”-stabilized nanoparticles by the self-assembly of the DNA tetrahedron–pNIPAM conjugate.⁹⁹ Adapted with permission from ref 99. Copyright 2013 American Chemical Society.

below the LCST of pNIPAM, and hence, the overall hydrophilic/hydrophobic volume ratio favored the formation of spherical micelles.

However, when the solution temperature exceeded the LCST, pNIPAM became hydrophobic which induced the increased volume fraction of the hydrophobic part, reducing the micellar interfacial curvature and transforming the spheres into cylinders. This shape transformation was reversible. The cylinder could be transformed into a spherical shape when the temperature dropped below the LCST. In addition to the temperature response, the system was also designed to respond to DNA. The binding of “stimulus” DNA induced cylinder-to-sphere morphological changes due to the increase of the hydrophilic block volume (Figure 23A, right). The same group modified ssDNA with PS and then used ssDNA-PS and PS-pNIPAM to successfully prepare other dynamic DNA–

polymer micelles which contained a DNA/pNIPAM corona and a PS hydrophobic core (Figure 23B).¹⁹⁹ Through experimental design it was found that pNIPAM strands present a significant steric hindrance to bind to DNA immobilized on nanoparticles. However, by increasing the temperature above the LCST, the steric hindrance could be minimized as the conformation of pNIPAM would change from the extended form to the collapsed form, demonstrating the switching behavior of the resulting DNA–polymer micelles. The dynamics of the structures could also be reflected by the nuclease-catalyzed degradation. As shown in Figure 23B, when the temperature was above 37 °C, pNIPAM assumed the collapsed state and DNA sequences were degraded by DNase I. Conversely, when the temperature was lower than 25 °C, the dynamic DNA–polymer micelles were stable and DNA sequences could not be degraded by DNase I. The above work used PS as the hydrophobic core and described the response of reversible hidden or exposed DNA sequences to temperature cues. Mirkin and co-workers used a similar concept to fabricate a dynamic DNA–polymer micelle, with the hydrophobic core being replaced by AuNPs. As shown in Figure 23C, the DNA and pNIPAM were cossembled onto Au NPs.²⁰⁰ By increasing the temperature higher than LCST, pNIPAM shrank and the DNA sequences were exposed from the polymer surface, which induced the assembly of DNA–AuNPs by DNA hybridization, whereas, at a lower temperature, the formed complex assembly would be disassembled.

Another class of dynamic DNA–pNIPAM nanostructures was formed by using DNA nanostructure–polymer conjugates. pNIPAM could be conjugated to DNA nanostructures, followed by dynamic DNA nanostructures formation through the hydrophilic–hydrophobic transition of pNIPAM. Baumberg and colleagues designed a temperature-responsive DNA origami flexor by introducing a hydrophobic pNIPAM switch that reversibly regulates the DNA structure.²⁰¹ The work paved the way for the intelligent design of preprogrammed nanomachines. O’Reilly’s group fabricated the dynamic tetrahedron–pNIPAM composite nanoparticles by adding an excess of pNIPAM homopolymer (Figure 23D).⁹⁹ The DNA block copolymers could be used to assemble a DNA tetrahedron due to the DNA segment remaining sequence-specific during hybridization. Subsequently, due to the elevation of temperature above the polymer LCST, temperature-responsive dynamic structures with surface DNA tetrahedra would be formed when an excess of free pNIPAM was used.

DNA–PPO. PPO is another temperature-responsive polymer, with many groups focusing on the assembly behavior of DNA block poly(propylene oxide) (DNA–b-PPO) copolymers currently.^{122,173,202} PPO displays hydrophobic characteristics at room temperature and is hydrophilic at lower temperatures (below 20 °C). As a result, dynamic spherical micelles in aqueous solution can be formed by the self-assembly of ODN–b-PPO. Liu’s group has made outstanding contributions to the development of the thermally responsive DNA–PPO dynamic structures,^{195,196} in which they first fabricated DNA–PPO dynamic nanostructures by the self-assembly of PPO–dsDNA–PPO triblock copolymers.¹⁹⁵ The unimer of the inverse coil–rod–coil triblock copolymer PPO–dsDNA–PPO was formed via specific DNA hybridization below the LCST of PPO, which resulted in two thermally responsive PPO segments at the ends and a rigid dsDNA segment in the middle (Figure 24A).

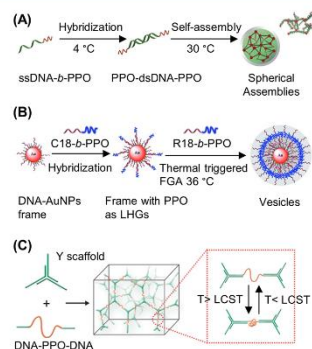


Figure 24. Dynamic DNA–polymer nanostructures formed by the self-assembly of DNA–PPO conjugates. (A) Construction of a supramolecular spherical DNA–PPO nanostructure.¹⁹⁵ Adapted with permission from ref 195. Copyright 2015 American Chemical Society. (B) Illustration of the construction of temperature-responsive heterovesicles by the FGA strategy.¹⁹⁶ Reproduced with permission from ref 196. Copyright 2014 John Wiley and Sons. (C) Construction of a 3D DNA network through the inset of temperature-responsive polymer PPO.²⁰³ Reproduced with permission from ref 203. Copyright 2018 John Wiley and Sons.

Subsequently, the spherical assemblies were self-assembled via hydrophobic interactions of PPO above the LCST by using the

prepared triblock copolymer. Usually, DNA diblock copolymers self-assembled randomly without forming an ordered compact structure. However, the self-assembly process in this work was different from the DNA diblock copolymers commonly used. Subsequently, they employed the FGA strategy to fabricate heterovesicles with controlled size and shape.¹⁹⁶ DNA-modified AuNPs were adopted as the frame (Figure 24B) to prepare the vesicles, and PPO was employed to make the LHGs thermally responsive. By DNA hybridization, the frame could attach DNA-*b*-PPO conjugates and the LHGs. After heating, the temperature-responsive heterovesicles were obtained due to hydrophobic transformation of the PPO segment and further induction of random DNA-*b*-PPOs around the AuNP frame. This work provided further information to understand the principles FGA and offered the chance to manipulate the FGA process by a thermal trigger. Moreover, the development of FGA enabled the construction of more complex and functional nanostructures.

To expand on the structures responsive to temperature, the triblock copolymer DNA–PPO–DNA was utilized to insert the thermally responsive polymer PPO into a 3D DNA network.²⁰³ This work verified the feasibility of the in situ study of the collapse of hydrophobic polymers in solution. By base pairing recognition, a DNA Y-shaped nanostructure could be connected by using DNA–PPO–DNA as the linker (Figure 24C). At a low temperature PPO was hydrophilic and could be uniformly distributed in the 3D DNA network, whereas increasing the temperature induced a hydrophobic change to PPO, which self-collapsed in the network. As the self-collapsing

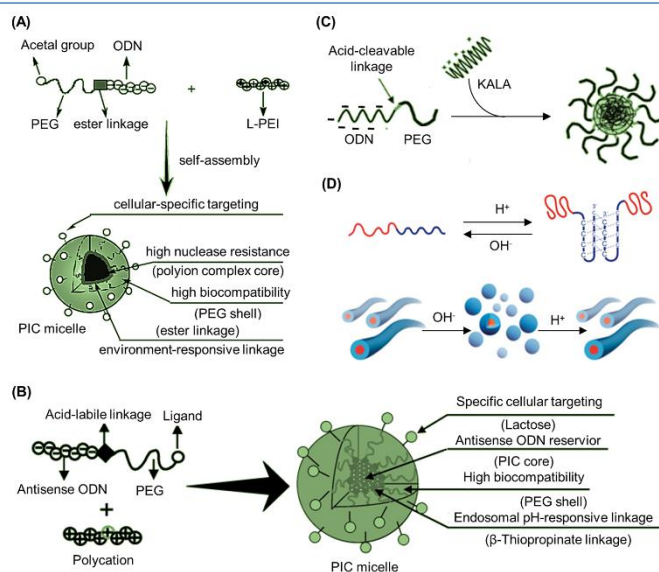


Figure 25. Construction of several pH-responsive DNA–polymer dynamic nanostructures. (A) Conceptual schematic illustrations of a pH-responsive PIC micelle formation.⁹⁴ Adapted with permission from ref 94. Copyright 2003 American Chemical Society. (B) Construction of a new delivery system that is pH-sensitive and can target antisense ODN.⁹³ Reproduced with permission from ref 93. Copyright 2003 American Chemical Society. (C) Construction of polyelectrolyte complex micelles by the self-assembly of ODN–PEG conjugates and peptide KALA.²⁰⁷ Reproduced with permission from ref 207. Copyright 2012 the Royal Society of Chemistry. (D) Reversible shape transformation of the pH-responsive DNA-*b*-PPO copolymer micelles.⁹⁵ Adapted with permission from ref 95. Copyright 2005 John Wiley and Sons.

process was reversible, this strategy offered a good method to explore the nucleation-growing process of block copolymers. At the same time, this strategy also provided a good opportunity to study the molecular mechanism of mechanical properties of responsive materials.

4.2.3. pH-Responsive Dynamic Nanostructures. Based on the unique properties of DNA and polymers, some supramolecular DNA–polymer complexes can exhibit pH-responsiveness. The DNA backbone is negatively charged and can be used to assemble pH-responsive DNA–polymer dynamic nanostructures through electrostatic interactions of DNA and cationic polymers. Numerous examples have shown that cationic polymers can form a nanocomplex by absorbing negatively charged DNA. The pH environment greatly affected the surface charge of the polymerized nanoparticles, and the loaded DNA could be intracellularly released by a pH-mediated mechanism.^{204–206} Such pH-responsive systems are highly valuable for gene delivery, which has been intensively discussed in a previous review.²⁰⁴ Herein, we focus our discussion on pH-responsive dynamic nanostructures where at least one composition is a covalent DNA–polymer conjugate.

Other than the facile adsorption to DNA via electrostatic interactions to form pH-responsive DNA–polymer nanoparticles, DNA delivery could also be achieved by conjugating DNA with polymers via a pH-responsive linker. For instance, Kataoka and co-workers constructed pH-responsive polyion complex (PIC) micelles,⁹⁴ which was the first report describing the design and synthesis of pH-responsive DNA–polymer dynamic nanostructures. The PIC micelle was formed through the association of a PEG–ODN conjugate and linear-PEI. A pH-responsive ester linkage (β -thiopropionate linkage) was introduced into the micelles to achieve the pH-responsiveness (Figure 25A). Subsequently, they developed a novel targetable antisense ODN delivery system, employing a PIC micelle. The system was intracellular environment-responsive and was composed of poly(L-lysine) (PLL) and a lactosylated PEG-antisense ODN (Lac-PEG–ODN) conjugate. An acid-labile linkage (b-propionate) was introduced into the micelle between PEG and ODN segments to realize the pH-response (Figure 25B).⁹⁵ The experiment demonstrated that the lactosylated PIC micelles exhibited an antisense effect (65% inhibition). However, the lactosylated PIC micelles without any acid-labile linkage exhibited a decrease in antisense effect (65 \rightarrow 27% inhibition). This suggested the endosomal compartment contained a possible cleavage of the acid-labile linkage which was in response to the lower pH. In a similar approach, Park's group prepared pH-responsive polyelectrolyte complex micelles by the combination of the peptide KALA and the ODN–PEG conjugates (Figure 25C).⁹⁵ The ODN–PEG conjugates were prepared by covalently conjugating the ODN, c-myc, to PEG, and an acid-cleavable phosphoramidate linkage was introduced into the conjugates. The phosphoramidate linkage could be cleaved completely within 5 h when the micelle was in an endosomal acidic condition (pH 4.7). This experiment mainly illustrated that the micelles were more efficiently transported into cells than the c-myc ODN and the polyelectrolyte complex micelles were a good carrier to deliver antisense ODN.

In addition to obtaining pH-responsiveness with a polycationic polymer or chemical linker, specially designed DNA sequences could also be used to impart similar responsiveness to the assembled structures. For example, Liu's group reported a dynamic nanostructure with pH and

temperature dual-responsiveness due to the combination of a thermoresponsive PPO and sequence-specific DNA strands.²⁰⁷ As shown in Figure 25D, a bimolecular “i-motif” could be formed through the folding of two DNA molecules of sequence, 5'-TTTCCCCTAACCCC-3'. Through the “i-motif” interaction two DNA-*b*-PPO conjugates were brought together and thus resulted in a triblock PPO–DNA–PPO copolymer. In addition, by adjusting the pH to slightly basic conditions the “i-motif” structure could be decomposed into random coils. Meanwhile, DNA-*b*-PPO copolymers could embody the characteristics of diblock copolymer under high pH. In this case, the assembly behavior of DNA-*b*-PPO was influenced by this stimuli-responsive nature. Hence, the morphologies of DNA-*b*-PPO dynamic nanostructures in an aqueous solution could eventually be transformed by adjusting the pH and temperature stimuli reversibly. DNA-*b*-PPO copolymers were assembled to form nanofibers at pH 5.0, and at pH 8.0 the morphologies would be transformed into spherical micelles (Figure 25D).

4.2.4. Light-Responsive Dynamic Nanostructures. In addition to temperature and pH, light-responsive dynamic nanostructures were also constructed through supramolecular DNA–polymer complexes. Among the different stimuli, light is a cheap and easily manipulated clean resource, which can be precisely controlled in space and time and thus is unique in its administration. The wavelength of light is often the main design consideration that affects light-responsive materials. UV light is able to provide high energy, thus resulting in efficient light-responsive structural changes; however it is harmful for cells and tissues which is unfavorable for biomedical applications. The UV light may also lead to DNA damage, which must be considered when designing such systems. As such, visible light and even near-infrared light sources are more preferred. However, they have been rarely explored due to the lack of efficient photochemical reactions with low energy light. In general, only a few studies have investigated light-responsive DNA–polymer assemblies; therefore, there are several areas to explore to improve irradiation wavelengths and structural variety.

Tan and Sleiman's groups both provided seminal studies to the progress of UV-irradiation light-responsive dynamic nanostructures.^{120,208} Through the self-assembly of HBP–DNA conjugates, Tan's group constructed a light-responsive drug delivery system (Figure 26A).¹²⁰ *O*-Nitrobenzyl derivatives were introduced to the delivery system to form the UV-responsive hydrophobic core. Under UV irradiation, the cleavage of *o*-nitrobenzyl moieties occurred, which reduced the hydrophobicity of the core and caused drug release through the disintegration of the nanoparticles. Conversely, Sleiman and co-workers fabricated 1D light-responsive DNA nanofibers by introducing a photocleavable linker to DNA–polymer conjugates (Figure 26B).²⁰⁸ As mentioned in section 4.1.1, assemblies induced by hydrophobic interactions through the polymer segment highlighted that the position of a cyanine (Cy3) dye played a crucial role in the shape-shifting of DNA nanostructures. The presence of Cy3 and its position in DNA–polymer hybridization were important for the formation of DNA nanofibers. The introduction of a photocleavable linker between the HE₁₂ and Cy3Cy3 units would induce the formation of light-responsive DNA nanofibers. Furthermore, the morphology of DNA nanostructures was transformed from nanofibers to spherical nanoparticles through the cleavage of

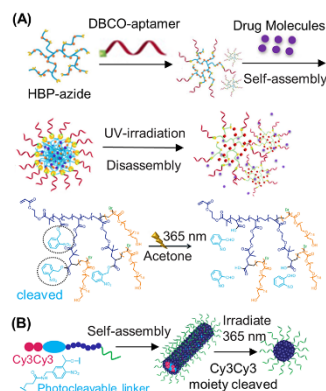


Figure 26. Different types of light-responsive DNA–polymer dynamic nanostructures. (A) Schematic of UV-promoted degradation of hyperbranched polymer (HBP)–OH. *O*-Nitrobenzyl moieties were introduced to the HBP side chains and would be cleaved under UV irradiation.¹²⁰ Adapted with permission from ref 120. Copyright 2018 John Wiley and Sons. (B) Light-responsive shape-shifting of photocleavable Cy3Cy3-DNA nanofibers. The morphology of DNA nanostructures would be transformed from nanofibers to spherical nanoparticle due to the cleavage of Cy3Cy3 units from the structure under UV irradiation at 365 nm.³⁰⁸ Adapted with permission from ref 208. Copyright 2018 American Chemical Society.

Cy3Cy3 units from the structure under UV irradiation at 365 nm.

In summary, this section mainly reviewed DNA–polymer dynamic nanostructures. From the above description, we can see that these dynamic DNA nanostructures are mainly generated by DNA regulation, temperature response, pH response, and light response. By the strand displacement strategy and the reversible transformation of complementary base pairing, DNA could be used to mediate the programmed assemblies of dynamic DNA–polymer supramolecular nanostructures. The introduction of temperature-responsive polymers such as pNIPAM and PPO and the addition of a pH-responsive linker or a photocleavable linker to polymers could also bring in stimuli-responsive dynamics to the system. Even though the examples of dynamic DNA–polymer conjugated nanostructures reported so far are still very limited, especially for the ones with clear application potentials, DNA-based dynamic nanostructures which did not incorporate polymers have been quickly developed in recent years. A series of temperature-actuated DNA nanopores, pH-actuated DNA-only devices utilizing Hoogsteen base pairing, and salt-actuated devices utilizing salt to mediate sticky end interactions between DNA pieces were fabricated.²⁰⁹ Even the electric field-actuated and magnetic field-actuated DNA nanodevices were also invented.^{210,211} Combining these dynamic DNA structures with polymers would pave the way to more smart and dynamic DNA–polymer systems with advantages of both DNA design and polymer properties.

5. FUNCTIONALITY OF DNA–POLYMER CONJUGATES

In recent years, the functions and applications of DNA–polymer conjugates have attracted more and more attention

from scientists. Polymers are a class of widely studied materials, which consist of a range of types, functions, and applications. When polymers are conjugated to DNA, the functionality of DNA–polymer conjugates will be affected by polymer properties. Therefore, hydrophobic polymers attached to DNA induce the self-assembly of DNA–polymer conjugates to form DNA–polymer micelles with a hydrophobic core and a hydrophilic DNA corona. These structures have great potential applications in medicine and biology. Some types of hydrophobic polymers conjugated to DNA, due to their good biocompatibility, can be used to develop drug carriers to deliver small molecule drugs and nucleic acid therapeutics. Several hydrophilic polymers can also be attached to DNA and are often used to enhance the stability of DNA nanostructures. However, the functionality of DNA–polymer micelles is influenced not only by the polymer but also by the DNA. Several specific sequences of DNA can manifest different functions, such as targeting, catalyzing, and therapeutic action. These specific sequences of DNA can be introduced to DNA–polymer micelles, which will give new functionalities to DNA–polymer nanostructures. Therefore, as shown in Figure 27, this

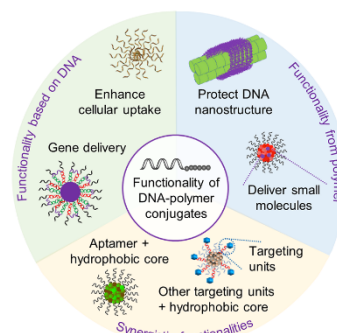


Figure 27. Functionalities of DNA–polymer conjugates. According to the hydrophobicity of polymers and DNA-based recognition ability, the functionalities of these DNA–polymer conjugates are mainly reflected in the protection of DNA nanostructures and used as drug carriers.

section can be divided into three categories according to the source of functionalities: (1) functionality from the polymer, (2) functionality based on DNA, and (3) synergistic functionalities.

5.1. Functionality from the Polymer

To date, many types of polymers such as PPO, pNIPAM, PS, and PCL have been conjugated to DNA to form DNA–polymer conjugates. Due to the different chemical and physical properties of the polymer, the polymer can vary the functionality of the corresponding conjugate. Based on the progress reported so far, these functionalities from the polymer are mainly reflected by the following two aspects: (1) small molecule drugs can be delivered by DNA–polymer conjugates due to the hydrophobic core of DNA–polymer micelles, and (2) polymers can be conjugated to DNA for stability enhancement of DNA–polymer conjugates.

The amphiphilic block copolymers based on DNA–polymer conjugates can phase-separate into micelles containing a

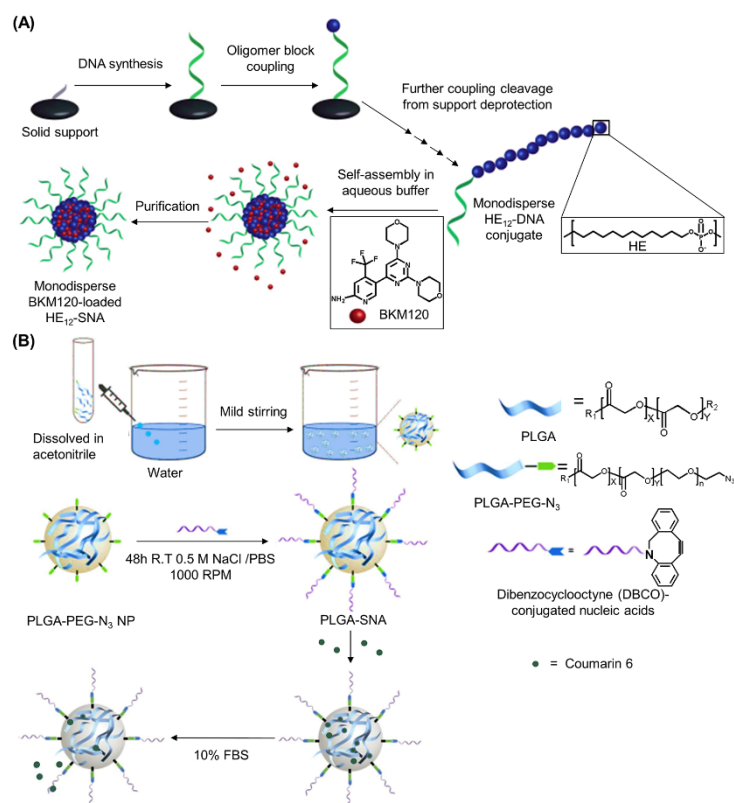


Figure 28. Construction of a spherical nucleic acid (SNA) system to deliver small molecule drugs. (A) Schematic representation of the self-assembly of the monodisperse BKM120-loaded HE₁₂-SNAs.²¹² Adapted with permission from ref 212. Copyright 2017 the Royal Society of Chemistry. (B) Synthesis of PLGA-SNAs utilizing nanoprecipitation and coumarin encapsulation. Coumarin 6 encapsulated inside the PLGA hydrophobic core was utilized as a fluorescent model drug to evaluate drug-release kinetics.²¹³ Adapted with permission from ref 213. Copyright 2018 John Wiley and Sons.

hydrophobic core and a hydrophilic DNA corona. Due to the hydrophobic interactions, several small molecule hydrophobic drugs can be complexed to the core of the micelle and delivered to the cells. As shown in Figure 28A, a novel delivery platform was constructed by Sleiman and co-workers to deliver small-molecule chemotherapeutics through the self-assembly of sequence-defined polymer–DNA conjugates.²¹² In this study, an SNA system was constructed to deliver the anticancer drug BKM120 (a small molecule drug with low water solubility) for the treatment of chronic lymphocytic leukemia. The DNA–polymer conjugates (HE₁₂–DNA conjugates) were prepared via solid phase synthesis and subsequently used to form spherical micellar DNA nanoparticles in aqueous solution. The hydrophobic HE₁₂ core of the formed DNA nanoparticles provided a favorable environment to encapsulate the hydrophobic drug BKM120. Meanwhile, this work also showed that HeLa cells had enhanced uptake of these structures, as well as their cargo internalization. Moreover, in vitro studies illustrated that BKM120-loaded HE₁₂-SNAs induced cellular death and

apoptosis. In addition, Mirkin's group used an extremely facile strategy to construct another new types of polymer SNA conjugates which were comprised of PLGA NP cores that could be used to deliver small molecules (Figure 28B).²¹³ PLGA–PEG–N₃ nanoparticles were prepared under mild stirring followed by ODN conjugation to these nanoparticles to form the PLGA-SNAs. A hydrophobic model drug, coumarin 6, was encapsulated into the PLGA-SNAs and then released in a tunable manner depending on the polymer composition.

The work described above highlights that DNA–polymer carriers have great potential for biomedical applications. However, as discussed in section 3.2.2, the in vivo nuclease activity could result in rapid degradation, which has strongly hindered their application. Therefore, the desire to enhance the stability of DNA–polymer carriers has attracted more attention. Zhang's group explored the stability of ODN hairpins and demonstrated that the introduction of PEG side chains increased the resistance of DNA-backboned bottlebrush

polymers against nucleolytic degradation and improved the thermal stabilities.¹⁶⁶ Importantly, the PEGylation did not affect the hybridization of ODN hairpins. The stability of DNA nanostructures was also enhanced by coating polymers at the exterior. As shown by Schmid's group,¹⁶⁰ coating with a cationic PEG–polylysine (p(lys)) block copolymer by electrostatic adsorption successfully enhanced the stability of DNA origami structures (Figure 29A).

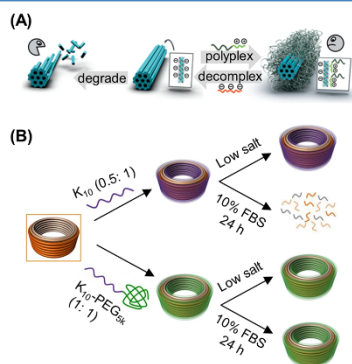


Figure 29. Protection of DNA nanostructures from nuclease digestion and denaturation through polymer coating strategies. (A) Cationic polymer was coated on DNA origami to form the polyplex micelles by electrostatic interaction.¹⁶⁰ Native DNA nanostructures could be degraded easily by nucleases, but the formed polyplex micelles were resistant to nuclease digestion. Reproduced with permission from ref 160. Copyright 2017 John Wiley and Sons. (B) Schematic representing the differences in stability of native and coated DNA nanostructures in physiological buffers at 37 °C containing low salt and/or 10% FBS.⁶¹ Reproduced with permission from ref 61. Copyright 2017 Springer Nature.

The nuclease digestion of DNase I and FBS and denaturation under low salt concentration are the main factors affecting the stability of DNA structures. The formed robust shell, via PEG-p(lys) block copolymers coating around the DNA origami nanostructures, could protect the DNA structures from nuclease digestion and denaturation. As a direct, economical, and reliable approach, this protection strategy could be used to protect various types of DNA origami nanostructures. Moreover, it was demonstrated that the DNA origami template directly determined the shape of the prepared DNA origami polyplex micelles after coating with PEG-p(lys) block copolymers. Shih and co-workers adopted a similar approach to enhance the stability of DNA nanostructures. Through an oligolysine coating the major challenges which limited the effective use of DNA nanostructures in vivo were overcome.⁶¹ They found that DNA nanostructures coated with oligolysines were significantly more stable and were 10 times more resistant to DNase I in low-salt environments than in uncoated environments at 0.5:1 N:P (ratio of nitrogen in lysine to phosphorus in DNA) (Figure 29B). However, it is of important note that when N:P ratios increased, DNA nanostructures coated by oligolysines aggregated. Oligolysine-PEG copolymers could also be used instead of oligolysines to coat DNA nanostructures to avoid aggregation,

which resulted in up to 1,000-fold resistance to digestion by serum nucleases.

5.2. Functionality Based on DNA

In this section, we discuss functionalities of DNA–polymer conjugates, which are based on DNA. These functionalities are mainly embodied in the delivery of genes and small-molecule cargos through the complementary pairing of DNA bases and more effective cellular uptake of DNA–polymer supramolecular nanostructures caused by nucleic acid shells. As shown by Haner's group, functional DNA-grafted supramolecular polymers were designed and synthesized from monodisperse diblock oligophosphates.¹⁸⁰ Through complementary base pairing, ssDNA chains arranged along the edges of the formed ribbons were available to load DNA-modified AuNPs, which served as a model cargo. Subsequently, Zhang and co-workers successfully realized the delivery of siRNA via nucleic acid hybridization.²¹⁴ DNA-g-PCL brushes with complete water solubility were synthesized by grafting DNA onto a PCL trunk followed by the self-assembly of spherical and nanosized hydrogels by functional siRNAs cross-linking (Figure 30A). The nanogels delivered siRNA to different cells, generating effective gene silencing in vitro and in vivo to enable the development of a novel siRNA delivery system. In addition to delivering siRNA, antisense nucleic acid therapeutics could also be delivered by DNA–polymer supramolecular nanostructures as Sleiman's group demonstrated (Figure 30B). They developed a novel responsive drug delivery vehicle to deliver nucleic acid therapeutics.¹⁹⁴ This yielded a stimuli-responsive SNA which was assembled by monodisperse DNA–polymer conjugate interactions. Nucleic acid therapeutics were incorporated to the SNA via partial base complementation and could only be released through chain replacement in the presence of cytoplasmic genetic markers.

The nucleic acid shell of SNAs not only enables cargo loading and delivery of nucleic acid therapeutics but also facilitates the effective cellular uptake of SNAs. Mirkin and co-workers designed a strategy to construct micelle–SNAs with a biodegradable core and ODNs (Figure 30C)¹¹² and demonstrated that the density of DNA affected its SNA-like properties. When the terminal segment of a diblock copolymer was connected with multiple DNA strands, the formed SNA would be induced with a higher DNA surface density. The DNA-brush block copolymer-based micelle–SNAs exhibited more effective cellular uptake than linear DNA block copolymer-based micelle–SNAs due to the higher surface density of nucleic acids. It was demonstrated that the cellular uptake would be enhanced due to the interaction of the ODN with class A scavenger receptors presented on the cell surface.^{215,216} In accordance with Mirkin's theory, Nguyen's group modified DOX-loaded polymeric nanoparticles with a dense ODN shell which greatly increased the cellular uptake of doxorubicin-loaded polymeric SNA (Figure 30D).¹¹¹ Furthermore, the dense shell of ODNs could increase the colloidal stability of DOX-loaded SNA structures in biological media under physiological conditions. Not only does the density of DNA on the surface of a DNA nanostructure affect its cellular uptake efficiency, but the different shapes also have an effect. As shown in Figure 18D, the different lengths of DNA template introduced by DNA hybridization affect the morphology of DNA nanostructures. The introduction of long DNA templates induced the morphology of the spherical micelles transforming from spheres to uniform rods. The cell

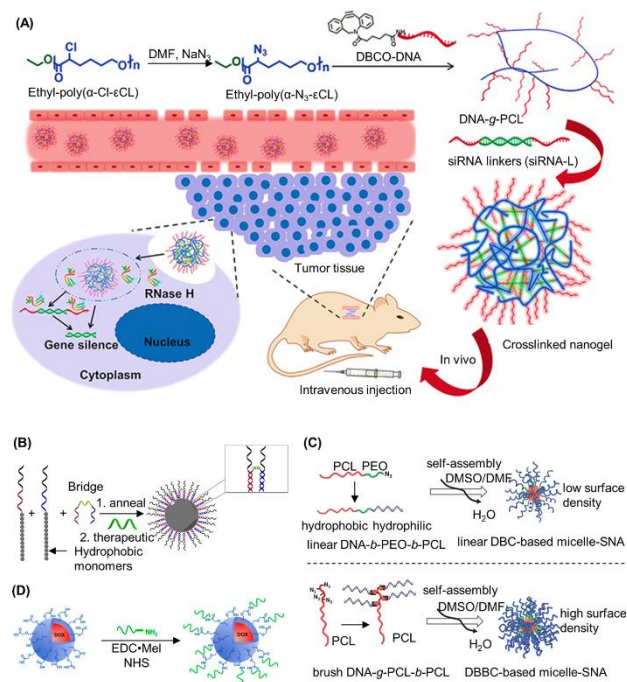


Figure 30. Example functionalities of DNA–polymer supramolecular nanostructures based on DNA. (A) siRNA was effectively delivered by a cross-linked nanogel through the complementation of bases between RNA and DNA.²¹⁴ Reproduced with permission from ref 214. Copyright 2018 John Wiley and Sons. (B) The ODN therapeutic (green) was introduced to the responsive spherical nucleic acid (SNA) by DNA hybridization.¹⁹⁴ Adapted with permission from ref 194. Copyright 2019 American Chemical Society. (C) Formation of micelle–SNA with different surface densities by using different DNA–polymer block copolymers, respectively.¹¹² Adapted with permission from ref 112. Copyright 2015 John Wiley and Sons. (D) Amine-terminated ODNs were introduced into polymeric nanoparticles via amide-coupling chemistry to form the doxorubicin (DOX)-loaded polymeric SNAs.¹¹¹ Adapted with permission from ref 111. Copyright 2017 American Chemical Society.

uptake experimental study illustrated that even though the components of the DNA nanostructures were the same, the cellular uptake efficiency of the rod-shaped polymer particles was 12 times more efficient than their spherical counterparts.²¹⁷

5.3. Synergistic Functionalities

The reports above describe functionalities of DNA–polymer conjugates from the polymer and DNA, respectively. The following section focuses on the synergistic functionalities from the polymer and DNA which are mainly reflected in the design and development of targeted drug delivery systems. Generally, the polymer fragment can form a hydrophobic core to carry hydrophobic drug molecules and the DNA shell can enhance cellular uptake and introduce selectivity to targeted cells.

The first targeted drug delivery system designed through DNA–polymer micelles was published by Herrmann and his colleagues in 2008.¹⁷³ In this work, due to the proven biocompatibility toward different cell types, PPO was used as the hydrophobic component of the micelles to load the anticancer drug DOX efficiently.²¹⁸ Subsequently folate targeting units were introduced to the micelle corona through base complementation (Figure 31A). It was demonstrated by

subsequent experiments that the density of targeting units had a strong effect on cellular uptake and that the combined action of targeting units and chemotherapy drugs within the micelles resulted in cancer cells being effectively killed. Since then, there has been an influx of designs for targeted drugs based on DNA–polymer micelles.

Several special short ssDNA sequences known as aptamers have been shown to recognize cellular surface receptors and thus can be used to import the desired DNA–polymer micelles into targeted cells. Zhu and co-workers fabricated a targeted drug delivery carrier by modifying a polymer with the DNA aptamer AS1411.¹¹⁹ A new kind of hyperbranched poly(2-((2-(acryloyloxy)ethyl) disulfanyl)ethyl 4-cyano-4-((propylthio)carbonothioyl)-thio)-pentanoate-co-poly(ethylene glycol) methacrylate) (HPAEG) polymer with a backbone possessing a redox-responsive property was first successfully prepared through combining RAFT polymerization and SCVP. Then HPAEG was functionalized with AS1411 to form the drug delivery carrier (HPAEG-AS1411). Subsequently, the formed HPAEG-AS1411 nanoparticles were loaded with the anticancer drug DOX (Figure 31B). HPAEG-AS1411 nanoparticles could exhibit ascending tumor cell uptake when compared with pure HPAEG nanoparticles due to the high

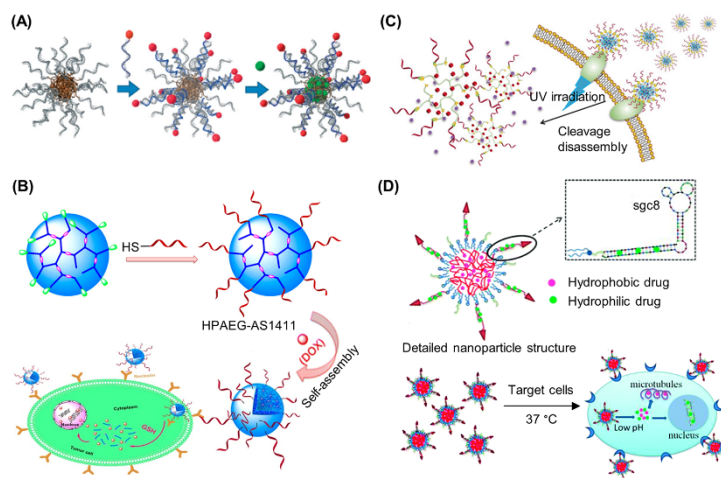


Figure 31. Design and development of various DNA–polymer targeted drugs based on the synergistic functionalities from polymer and DNA. (A) Schematic illustration of DNA–PPO drug delivery system.¹⁷³ The red targeting units were introduced to the micelles by DNA hybridization, and the green anticancer drug was encapsulated into the core of the micelles. Reproduced with permission from ref 173. Copyright 2008 John Wiley and Sons. (B) DNA aptamer AS1411 was conjugated to HPAEG via the Michael addition reaction and then self-assembled to form the targeting drug delivery carrier.¹¹⁹ Adapted with permission from ref 119. Copyright 2016 American Chemical Society. (C) On-demand and controlled release of a targeted and photoresponsive drug delivery system could be achieved when UV irradiation is applied.¹²⁰ Reproduced with permission from ref 120. Copyright 2018 John Wiley and Sons. (D) Construction of a hybrid nanoparticle-based drug delivery system. Two different drugs were codelivered into cancer cells with the targeted drug delivery system.²²¹ Reproduced with permission from ref 221. Copyright 2014 the Royal Society of Chemistry.

affinity of AS1411 to the overexpressed nucleolin on the cancer cells.^{219,220} This work confirmed that DOX-loaded HPAEG-AS1411 nanoparticles could exhibit a higher tumor cellular proliferation inhibition rate and lower cytotoxicity to normal cells, providing a new pathway for the development of targeted drug delivery for tumor therapy. Tan's group also designed a targeted drug delivery carrier by conjugating the DNA aptamer AS1411 to the polymer.¹²⁰ This work was the first attempt to develop a new photoresponse-based drug delivery system. The drug release system could realize controlled drug release by light mediation and be used for aptamer-targeted tumor therapy. In addition to targeting, aptamer sgc8 was used to functionalize the hyperbranched polymer (HBP) to form the assemblies and increase colloidal stability of this nanostructure. The model drug Nile Red was encapsulated into the core of the drug delivery system which could undergo cleavage under UV irradiation by employing *o*-nitrobenzyl moieties.

Once cleavage had occurred, the hydrophobicity of the drug delivery system core was rapidly reduced, causing the breakdown of the system and the resulting release of drugs (Figure 31C).

The two examples above mainly focused on directly modifying the polymer with aptamers to achieve the targeting effect. An alternative approach could introduce the aptamers to the surface of DNA–polymer micelles by DNA hybridization. As demonstrated by Tan's group in 2013, the sgc8 aptamers could be introduced to the drug delivery system through hybridization of a diacylipid-modified DNA strand.²²¹ dsDNA on the hydrophilic shell formed through the hybridization of the sgc8 aptamers were used to load DOX via intercalation, while the hydrophobic PLGA core was designed to encapsulate

the PTX through hydrophobic interactions (Figure 31D). The drug delivery system was successfully constructed by the assembly of PLGA and the lipid-functionalized DNA aptamer. DOX and PTX were codelivered by the constructed carriers to cancer cells in antitumor therapy. By crossing the blood–brain barrier (BBB) to deliver a second near-infrared (NIR-II, 1000–1700 nm) dye to the brain with a tumor-targeted aptamer, Tian and colleagues achieved brain-tumor imaging using DNA nanotechnology.²²² For many years, the obstacle of the BBB limited the exploration of NIR-II nanofluorophore in the brain tumor's imaging and diagnosis.^{223,224} In this work, the brain-tumor targeting aptamer was attached to the surface of SNA by hybridization with the DNA shell to cross the BBB (Figure 32A).²²² NIR-II dyes could be encapsulated into the hydrophobic core of the SNA structure to be used for brain-tumor imaging. In addition, the brain-tumor targeting aptamer attached to the surface of the SNA structure could be used to increase the accumulation of the NIR-II dye in brain tumors to realize better brain-tumor imaging.

In addition to DNA aptamers, short hairpin RNA (shRNA) was used to design a targeted drug delivery carrier. Chen and co-workers constructed a new kind of nucleic acid–polymer nanodrug formulation which could be used to codeliver nucleic acid therapeutics (shRNA) and DOX (Figure 32B).²²⁵ ShRNA on amphiphilic DNA–poly(lactide) (PLA) micelles was synthesized through in situ rolling circle transcription (RCT), which promoted the generation of PLA poly shRNA microflowers. This was the first time to employ in situ RCT to produce a layer of multidrug resistance protein 1 (MDR1)-silencing poly shRNA concatemers on the DNA–polymer micelle. Hydrophobic DOX was concurrently loaded into the

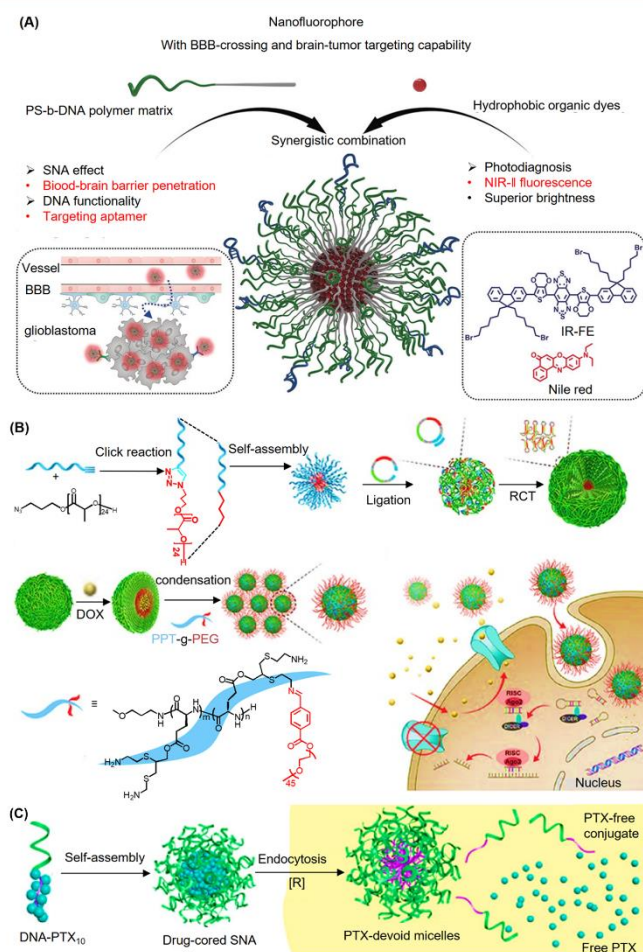


Figure 32. (A) Schematic illustration of spherical nucleic acids consisting of PS-*b*-DNA and NIR-II dyes.²²² Reproduced with permission from ref 222. Copyright 2020 John Wiley and Sons. (B) Construction of drug-loaded DNA-PLA micelles and the corresponding synergistic treatment of drug resistant BC cells.²²⁵ Reproduced with permission from ref 225. Copyright 2018 John Wiley and Sons. (C) Schematic illustration of DNA-PTX₁₀ micelles and the corresponding application.¹⁷⁷ Adapted with permission from ref 177. Copyright 2016 American Chemical Society.

PLA cores, and then biocompatible and multifunctional PEG-grafted polypeptides (PPT-*g*-PEG) were designed to induce microflowers electrostatically condensing into PLA-poly shRNA-PPT-*g*-PEG nanoparticles. The *in vivo* and *in vitro* experiments finally revealed the great potential of this vector in the combination of nucleic acid therapeutics and chemotherapeutics in tumor therapy.

The above work summarized that the DNA corona of DNA-polymer micelles could be functional aptamers to increase the efficiency of cell uptake. In addition, the DNA on the surface of the micelles can also be used for gene therapy. As shown in Figure 32C, Zhang's group developed an SNA-like drug delivery system with the small-molecule drug

PTX treated as the hydrophobic core of the micelle.¹⁷⁷ In this work, the DNA corona of the SNA performed two functions: first as a gene therapeutic and second as a delivery vehicle for small-molecule drugs. A self-immolative disulfide linker could be introduced to this system to control the release of free drug. Multiple PTX molecules were combined to ssDNA to provide the sufficient driving force for DNA-PTX micelle formation through screening of the repulsive interactions between DNA strands.²²⁶ These self-assembled DNA-PTX nanostructures bypassed the need for a complex carrier system and allowed one to access a gene target and a drug target using only the payloads themselves. Additionally, as these nanostructures enable gene therapy and chemotherapy using the payloads

themselves, cytotoxicity and immunogenicity challenges associated with complex vector systems are potentially avoided.

Although substantial studies have been reported on DNA–polymer conjugates as drug carriers, their application is still limited by many challenges. For instance, the stability of DNA nanostructures needs to be further improved to adapt to the complicated bioenvironment. To solve this challenge, scientists have attempted to use cationic polymers to coat DNA nanostructures to improve their stability, as described in section 5.1. However, there has been little research to confirm whether the function of DNA–polymer conjugates would be affected by polymer coating. Moreover, the poor understanding of the cytotoxicity, immunogenicity, and pharmacokinetics of DNA–polymer conjugates has also limited the development of their applications. Additionally, beyond the application as drug delivery carriers, DNA nanostructures have shown broad application prospects in fields such as in sensing, nanorobotics, and diagnostics. Hence, we can reasonably envision that DNA–polymer conjugates will also present promising future applications in these fields.

6. CONCLUSIONS AND OUTLOOK

The development of DNA technology, from chemical functionalization to nanoscale strategies, has seen significant refinement and breakthrough in recent years. Given the ease of access toward these methodologies, the possibilities for which DNA can be exploited have expanded far beyond conventional biology related disciplines. In particular, this review has summarized the impact of DNA on the construction of precision macromolecular conjugates and on programming supramolecular assemblies.

On the molecular scale, DNA offers a high level of customization provided by both solid phase synthesis and state-of-the-art biorthogonal chemistry thereby granting general accessibility to the community. These chemical approaches subsequently inspired the development of other reactions that can be conducted on the DNA such as polymerizations and assembly driven chemistry. Nonetheless, the technical challenge of DNA stability, its polyelectrolytic nature, and nucleophilic functional groups are still prevalent issues. These considerations become more complex at the macromolecular level as conjugation toward hydrophobic polymers/materials relies heavily on the exposure of reactive groups that are often masked by chain dynamics in solution. Nonetheless, the greater accessibility of DNA materials will ensure increasing efforts in method development.

At the nanostructure level, supramolecular interactions dictated by both the polymer and the DNA component take the central role in determining their eventual morphology. As such, polymer physics of DNA–polymer materials has overwhelming room for future innovation. In this respect, DNA offers new insights in phase transitional behavior, packing of polymer chains, and crystallinity by using precise chain conformational switches such as *i*-motifs and hairpins. Additionally, the balance between the ordered and mono-disperse sequences of DNA against the intrinsically disordered polymer chain is a unique relationship that can foster novel nanoscience frontiers. Customization at this size regime involves polymer design and the effect of different monomers (i.e., hydrophobicity, charge interactions) in directing structure formation. Hence, most technical challenges involve irreversible aggregation of the conjugates due to incompatibility between the two blocks and the solvent system.

Structures of higher complexity rely on DNA playing a larger role in directing structure formation and hence are limited to aqueous systems. This includes highly polygonal 3D objects created by the DNA origami technology where polymer chains can be attached at any position by both *grafting to* and *grafting from* methods. Here, transference of the shape profile and information from the precise DNA scaffold to control polymerization become a powerful technique to guide polymer synthesis and orientation. However, additional restrictions with regard to stabilizing ions are imposed as polygonal DNA structures are much more fragile. Increasing efforts by exploring DNA-crossover techniques have shown optimistic outcomes, and its broader application can be envisioned. While this review covered the aspect of polymer stabilization of these polygonal objects, it still lacks breakthrough strategies that allow broad implementations.

At each length scale, it is unambiguous how the synergy between DNA and macromolecular chemistry can bring about new horizons in multiple disciplines. However, at the same time, multiple challenges in each facet need to be overcome by the scientific community to access this knowledge. As such, every success will bring forth new technologies and features that will stimulate the collective understanding of precise nanoscopic 3D architectures in materials science and nanomedicine.

AUTHOR INFORMATION

Corresponding Authors

Yuzhou Wu – Hubei Key Laboratory of Bioinorganic Chemistry and Materia Medica, School of Chemistry and Chemical Engineering, Huazhong University of Science and Technology, Hongshan, Wuhan 430074, People's Republic of China; orcid.org/0000-0003-3229-4982; Email: wuyuzhou@hust.edu.cn

David Y. W. Ng – Max Planck Institute for Polymer Research, 55128 Mainz, Germany; orcid.org/0000-0002-0302-0678; Email: david.ng@mpip-mainz.mpg.de

Tanja Weil – Max Planck Institute for Polymer Research, 55128 Mainz, Germany; orcid.org/0000-0002-5906-7205; Email: weil@mpip-mainz.mpg.de

Authors

Colette J. Whitfield – Max Planck Institute for Polymer Research, 55128 Mainz, Germany

Meizhou Zhang – Hubei Key Laboratory of Bioinorganic Chemistry and Materia Medica, School of Chemistry and Chemical Engineering, Huazhong University of Science and Technology, Hongshan, Wuhan 430074, People's Republic of China

Pia Winterwerber – Max Planck Institute for Polymer Research, 55128 Mainz, Germany

Complete contact information is available at: <https://pubs.acs.org/10.1021/acs.chemrev.0c01074>

Author Contributions

[§]Colette J. Whitfield and Meizhou Zhang contributed equally to this work.

Notes

The authors declare no competing financial interest.

Biographies

Colette Whitfield completed her Ph.D. in the Pike group at Newcastle University (U.K.) establishing protocols for the synthesis of chemically modified long DNA. She then conducted a research visit at Hokkaido University where she continued her interest in DNA nanotechnology, focusing on 3D DNA patterning with Professor Ijiro. On returning to the U.K., Colette joined the Howard group at Newcastle University and established cell-free protein synthesis in hydrogels to develop stimuli-responsive materials. Colette joined the Weil group in 2019 where she utilizes DNA origami to afford specific attachment chemistry for cellular targeting and function.

Meizhou Zhang is a student at the School of Chemistry and Chemical Engineering, Huazhong University of Science and Technology (HUST). He graduated from Hubei Minzu University and obtained a Master's degree from Sichuan University. He started his Ph.D. studies at Huazhong University in Wuhan (China) under the supervision of Professor Yuzhou Wu. He is currently continuing his graduate studies on topics relating to the synthesis and application of DNA-polymer nanomaterials.

Pia Winterwerber studied Biomedical Chemistry at the Johannes Gutenberg University, Mainz (Germany), and received her master's degree in 2018. During her studies she focused on the synthesis of hyperbranched star polymers as well as amphiphilic biomacromolecule conjugates. She joined the group of Prof. Dr. Tanja Weil in 2018 as a Ph.D. student and is now working on the development of DNA origami hybrid nanostructures.

Yuzhou Wu is a Professor at the School of Chemistry and Chemical Engineering, Huazhong University of Science and Technology (HUST). She graduated from Zhejiang University and obtained a Master's degree from the National University of Singapore and a Ph.D. degree from Ulm University in Germany. Before joining HUST, she worked as a project leader at Ulm University and at the Max Planck Institute for Polymer Research from 2013 to 2016. Her research interests include nanobio interface engineering, novel chemical methods for functionalization of protein and DNA nanostructures, and nature-inspired nanofabrication techniques for precision nanomedicine.

David Ng leads the Synthetic Life-like Systems Group within the Department for Synthesis of Macromolecules and is concurrently the Head of the BioCore Facility at the Max Planck Institute for Polymer Research (MPIP). He received his B.Sc. Hons (National University of Singapore) and Ph.D. (MPIP/Ulm University) in 2009 and 2014, respectively. In 2019, he was featured as an emerging investigator by the ChemBioTalents initiative by Wiley-VCH. His research interests include DNA-guided polymer architectures and the *in situ* assembly of synthetic functional nanostructures in living systems.

Tanja Weil received her Ph.D. from Mainz University in 2002. She held several leading positions at Merz Pharmaceuticals GmbH (Frankfurt, 2002–2008). She was an Associate Professor at the National University of Singapore (NUS, 2008–2010) and, since 2010, director at the Institute of Organic Chemistry III (OC III) at Ulm University (Ulm). In 2016, she was appointed as director of the Department of Synthesis of Macromolecules at the Max Planck Institute for Polymer Research (MPIP) in Mainz, Germany. She has received an ERC Synergy Grant. Her scientific interests focus on innovative synthesis concepts to achieve functional macromolecules, hybrid materials, and life-like systems to solve current challenges in biomedicine and material science.

ACKNOWLEDGMENTS

The authors are grateful to the Max Planck-Bristol Center for Minimal Biology, Deutsche Forschungsgemeinschaft (DFG, German Research Foundation)—Project number 407426226—TRR 234, the National Key R&D Program of China (2018YFA0903500) and the National Natural Science Foundation of China (grant number 51703073, 22077042) for financial support.

ABBREVIATIONS

A	adenine
ACN	acetonitrile
AFM	atomic force microscopy
AGET	activators generated by electron transfer
Am	amino groups
ATRP	atom transfer radical polymerization
BBB	blood-brain barrier
B-dUTP	BODIPY-dUTP
BTPA	(((butylthio)carbonothioyl)thio) propanoic acid
C	cytosine
CMC	critical micelle concentration
CPADB	4-cyano-4-(phenylcarbonothioylthio) pentanoic acid
CPG	controlled pore glass
CROP	cationic ring-opening polymerizations
CTA	chain transfer agent
CWC	critical water content
DBCO	dibenzo-cyclooctyne
DLS	dynamic light scattering
DMA	dimethacrylate
DMAc	dimethylacetamide
DMAm	<i>N,N</i> -dimethylacrylamide
DMF	dimethylformamide
DMSO	dimethyl sulfoxide
DMT	dimethoxytrityl
DNA	deoxyribonucleic acid
dNTP	deoxynucleotide triphosphate
DOX	doxorubicin
dsDNA	double stranded DNA
FBS	fetal bovine serum
FGA	frame-guided assembly
FRET	Förster resonance energy transfer
HATU	hexafluorophosphate azabenzotriazole tetramethyl uranium
HBP	hyperbranched polymer
HBTU	hexafluorophosphate benzotriazole tetramethyl uranium
HE	hexa-ethylene
HPAEG	hyperbranched poly(2-(2-(acryloyloxy)ethyl) disulfanyl)ethyl 4-cyano-4-((propylthio)-carbonothioyl)-thio)-pentanoate-co-poly(ethylene glycol) methacrylate)
HPLC	high performance liquid chromatography
HRP	horseradish peroxidase
LCST	lower critical solution temperature
LHGs	leading hydrophobic groups
MALDI	matrix assisted laser desorption ionization
MDRI	multidrug resistance protein 1
NHS	<i>N</i> -hydroxysuccinimide
NIPAM	<i>N</i> -isopropylacrylamide
N-NHS	norbornenyl- <i>N</i> -hydroxysuccinimide
N-MI	norbornenyl-maleimide

N-PEG	norborenyl-PEG
NP	nanoparticles
ODN	oligodeoxyribonucleotide
ORN	oligoribonucleotide
P4VP	poly(4-vinylpyridine)
PAGE	polyacrylamide gel electrophoresis
PANI	polyaniline
PBS	phosphate buffered saline
PCL	polycaprolactone
PCR	polymerase chain reaction
pDAAm	poly(diacetone acrylamide)
PDI	polydispersity index
PEG	poly(ethylene glycol)
PEGDMA	PEG dimethacrylate
PEI	polyethylenimine
PIC	polyion complex
PPF	perfluorophenol
PHEMA	poly(hydroxyethyl methacrylate)
PISA	polymerization induced self-assembly
PLA	polylactide
PLGA	poly(D,L-lactic-co-glycolic acid)
p(lys)	polylysine
pMA	poly(methyl acrylate)
pMMA	poly(methyl methacrylate)
PNA	peptide nucleic acid
pNIPAM	poly(N-isopropylacrylamide)
pOEGMA	poly(oligoethylene glycol methacrylate)
pOEOMA	poly(oligoethylene oxide methacrylate)
PPMA	poly(propargyl methacrylate)
PPO	poly(propylene oxide)
PPT	polypeptides
PS	polystyrene
PtBA	poly(<i>tert</i> -butyl acrylate)
PTOTT	poly[3-(2,5,8,11-tetraoxatridecanyl)-thiophene]
PTX	paclitaxel
RAFT	reversible addition-fragmentation chain transfer polymerization
RCT	rolling circle transcription
RNA	ribonucleic acid
ROP	ring-opening polymerization
RTCBP	reversible transformation of complementary base pairing
SCVP	self-condensing vinyl polymerization
shRNA	short hairpin RNA
SNAs	spherical nucleic acids
ssDNA	single stranded DNA
St	styrene
T	thymine
TdT	terminal deoxynucleotidyl transferase
TEM	transmission electron microscopy
THF	tetrahydrofuran
TPMA	tris(2-pyridylmethyl) amine
U	uracil
UV	ultraviolet

REFERENCES

- (1) Madsen, M.; Gothelf, K. V. Chemistries for DNA Nanotechnology. *Chem. Rev.* **2019**, *119*, 6384–6458.
- (2) Beaucage, S. L.; Caruthers, M. H. Deoxynucleoside Phosphoramidites - a New Class of Key Intermediates for Deoxypolynucleotide Synthesis. *Tetrahedron Lett.* **1981**, *22*, 1859–1862.
- (3) Caruthers, M. H.; Barone, A. D.; Beaucage, S. L.; Dodds, D. R.; Fisher, E. F.; McBride, L. J.; Matteucci, M.; Stabinsky, Z.; Tang, J. Y.

Chemical Synthesis of Deoxyoligonucleotides by the Phosphoramidite Method. *Methods Enzymol.* **1987**, *154*, 287–313.

(4) Koster, H.; Biernat, J.; Mcmanus, J.; Wolter, A.; Stumpe, A.; Narang, C. K.; Sinha, N. D. Polymer Support Oligonucleotide Synthesis.15. Synthesis of Oligodeoxynucleotides on Controlled Pore Glass (Cpg) Using Phosphate and a New Phosphite Triester Approach. *Tetrahedron* **1984**, *40*, 103–112.

(5) Koster, H.; Stumpe, A.; Wolter, A. Polymer Support Oligonucleotide Synthesis.13. Rapid and Efficient Synthesis of Oligodeoxynucleotides on Porous-Glass Support Using Triester Approach. *Tetrahedron Lett.* **1983**, *24*, 747–750.

(6) Pon, R. T. Solid-phase supports for oligonucleotide synthesis. *Methods Mol. Biol.* **1993**, *20*, 465–96.

(7) Mccollum, C.; Andrus, A. An Optimized Polystyrene Support for Rapid, Efficient Oligonucleotide Synthesis. *Tetrahedron Lett.* **1991**, *32*, 4069–4072.

(8) Goodchild, J. Conjugates of Oligonucleotides and Modified Oligonucleotides: A Review of Their Synthesis and Properties. *Bioconjugate Chem.* **1990**, *1*, 165–187.

(9) Telsner, J.; Cruickshank, K. A.; Morrison, L. E.; Netzel, T. L. Synthesis and Characterization of DNA Oligomers and Duplexes Containing Covalently Attached Molecular Labels - Comparison of Biotin, Fluorescein, and Pyrene Labels by Thermodynamic and Optical Spectroscopic Measurements. *J. Am. Chem. Soc.* **1989**, *111*, 6966–6976.

(10) Kachalova, A.; Zubin, E.; Stetsenko, D.; Gait, M.; Oretskaya, T. Oligonucleotides with 2'-O-carboxymethyl group: synthesis and 2'-conjugation via amide bond formation on solid phase. *Org. Biomol. Chem.* **2004**, *2*, 2793–2797.

(11) Stetsenko, D. A.; Gait, M. J. New Phosphoramidite Reagents for the Synthesis of Oligonucleotides Containing a Cysteine Residue Useful in Peptide Conjugation. *Nucleosides, Nucleotides Nucleic Acids* **2000**, *19*, 1751–1764.

(12) Soukchareun, S.; Haralambidis, J.; Tregear, G. Use of N-alpha-Fmoc-cysteine(S-thiobutyl) Derivatized Oligodeoxynucleotides for the Preparation of Oligodeoxynucleotide-Peptide Hybrid Molecules. *Bioconjugate Chem.* **1998**, *9*, 466–475.

(13) Averick, S. E.; Dey, S. K.; Grahacharya, D.; Matyjaszewski, K.; Das, S. R. Solid-Phase Incorporation of an ATRP Initiator for Polymer-DNA Biohybrids. *Angew. Chem., Int. Ed.* **2014**, *53*, 2739–2744.

(14) Pan, X.; Lathwal, S.; Mack, S.; Yan, J.; Das, S. R.; Matyjaszewski, K. Automated Synthesis of Well-Defined Polymers and Biohybrids by Atom Transfer Radical Polymerization Using a DNA Synthesizer. *Angew. Chem., Int. Ed.* **2017**, *56*, 2740–2743.

(15) Schoch, J.; Wiessler, M.; Jaschke, A. Post-Synthetic Modification of DNA by Inverse-Electron-Demand Diels-Alder Reaction. *J. Am. Chem. Soc.* **2010**, *132*, 8846–8847.

(16) Hirao, I. Unnatural Base Pair Systems for DNA/RNA-Based Biotechnology. *Curr. Opin. Chem. Biol.* **2006**, *10*, 622–627.

(17) Liu, K.; Zheng, L. F.; Liu, Q.; de Vries, J. W.; Gerasimov, J. Y.; Herrmann, A. Nucleic Acid Chemistry in the Organic Phase: From Functionalized Oligonucleotides to DNA Side Chain Polymers. *J. Am. Chem. Soc.* **2014**, *136*, 14255–14262.

(18) Wilks, T. R.; O'Reilly, R. K. Efficient DNA-Polymer Coupling in Organic Solvents: A Survey of Amide Coupling, Thiol-Ene and Tetrazine-Norbornene Chemistries Applied to Conjugation of Poly(N-Isopropylacrylamide). *Sci. Rep.* **2016**, *6*, 39192.

(19) Lueckerath, T.; Strauch, T.; Koynov, K.; Barner-Kowollik, C.; Ng, D. Y. W.; Weil, T. DNA-Polymer Conjugates by Photoinduced RAFT Polymerization. *Biomacromolecules* **2019**, *20*, 212–221.

(20) Whitfield, C. J.; Little, R. C.; Khan, K.; Ijiro, K.; Connolly, B. A.; Tuite, E. M.; Pike, A. R. Self-Priming Enzymatic Fabrication of Multiply Modified DNA. *Chem. - Eur. J.* **2018**, *24*, 15267–15274.

(21) Gramlich, P. M. E.; Warncke, S.; Gierlich, J.; Carell, T. Click-Click-Click: Single to Triple Modification of DNA. *Angew. Chem., Int. Ed.* **2008**, *47*, 3442–3444.

(22) Cherstvy, A. G. Electrostatic Interactions in Biological DNA-Related Systems. *Phys. Chem. Chem. Phys.* **2011**, *13*, 9942–9968.

- (23) Lipfert, J.; Doniach, S.; Das, R.; Herschlag, D. Understanding Nucleic Acid-Ion Interactions. *Annu. Rev. Biochem.* **2014**, *83*, 813–841.
- (24) Chu, V. B.; Bai, Y.; Lipfert, J.; Herschlag, D.; Doniach, S. Evaluation of Ion Binding to DNA Duplexes Using a Size-Modified Poisson-Boltzmann Theory. *Biophys. J.* **2007**, *93*, 3202–3209.
- (25) Gray, C. G.; Stiles, P. J. Nonlinear Electrostatics: the Poisson-Boltzmann Equation. *Eur. J. Phys.* **2018**, *39*, 053002.
- (26) Izumrudov, V. A.; Zhiryakova, M. V. Stability of DNA-Containing Interpolyelectrolyte Complexes in Water-Salt Solutions. *Macromol. Chem. Phys.* **1999**, *200*, 2533–2540.
- (27) Kabanov, A. V.; Kabanov, V. A. Interpolyelectrolyte and Block Ionomer Complexes for Gene Delivery: Physicochemical Aspects. *Adv. Drug Delivery Rev.* **1998**, *30*, 49–60.
- (28) Rungsardthong, U.; Eltezazi, T.; Bailey, L.; Armes, S. P.; Garnett, M. C.; Stolnik, S. Effect of Polymer Ionization on the Interaction with DNA in Nonviral Gene Delivery Systems. *Biomacromolecules* **2003**, *4*, 683–690.
- (29) Tang, M. X.; Szoka, F. C. The Influence of Polymer Structure on the Interactions of Cationic Polymers with DNA and Morphology of the Resulting Complexes. *Gene Ther.* **1997**, *4*, 823–832.
- (30) Tse, W. C.; Boger, D. L. Sequence-selective DNA Recognition: Natural Products and Nature's Lessons. *Chem. Biol.* **2004**, *11* (12), 1607–1617.
- (31) Bhaduri, S.; Ranjan, N.; Arya, D. P. An Overview of Recent Advances in Duplex DNA Recognition by Small Molecules. *Beilstein J. Org. Chem.* **2018**, *14*, 1051–1086.
- (32) Reddy, B. S. P.; Sondhi, S. M.; Lown, J. W. Synthetic DNA Minor Groove-Binding Drugs. *Pharmacol. Ther.* **1999**, *84*, 1–111.
- (33) Hamilton, P. L.; Arya, D. P. Natural Product DNA Major Groove Binders. *Nat. Prod. Rep.* **2012**, *29*, 134–143.
- (34) Arya, D. P.; Coffee, R. L.; Xue, L. From Triplex to B-form Duplex Stabilization: Reversal of Target Selectivity by Aminoglycoside Dimers. *Bioorg. Med. Chem. Lett.* **2004**, *14*, 4643–4646.
- (35) Kumar, S.; Xue, L.; Arya, D. P. Neomycin-Neomycin Dimer: An All-Carbohydrate Scaffold with High Affinity for AT-Rich DNA Duplexes. *J. Am. Chem. Soc.* **2011**, *133*, 7361–7375.
- (36) Luscombe, N. M.; Austin, S. E.; Berman, H. M.; Thornton, J. M. An overview of the structures of protein-DNA complexes. *Genome Biol.* **2000**, *1* (reviews001.1).
- (37) Miao, Y.; Lee, M. P. H.; Parkinson, G. N.; Batista-Parra, A.; Ismail, M. A.; Neidle, S.; Boykin, D. W.; Wilson, W. D. Out-of-Shape DNA Minor Groove Binders: Induced Fit Interactions of Heterocyclic Dications with the DNA Minor Groove. *Biochemistry* **2005**, *44*, 14701–14708.
- (38) Soh, N.; Umeno, D.; Tang, Z. L.; Murata, M.; Maeda, M. Affinity Precipitation Separation of DNA Binding Protein using Block Conjugate Composed of poly(N-isopropylacrylamide) Grafted Double-Stranded DNA and Double-Stranded DNA Containing a Target Sequence. *Anal. Sci.* **2002**, *18*, 1295–1299.
- (39) Nafisi, S.; Saboury, A. A.; Keramat, N.; Neault, J. F.; Tajmir-Riahi, H. A. Stability and Structural Features of DNA Intercalation with Ethidium Bromide, Acridine Orange and Methylene Blue. *J. Mol. Struct.* **2007**, *827*, 35–43.
- (40) Wilks, T. R.; Pitto-Barry, A.; Kirby, N.; Stulz, E.; O'Reilly, R. K. Construction of DNA-Polymer Hybrids using Intercalation Interactions. *Chem. Commun.* **2014**, *50*, 1338–1340.
- (41) Moradpour-Hafshejani, S.; Hedley, J. H.; Haigh, A. O.; Pike, A. R.; Tuite, E. M. Synthesis and Binding of Proflavine Diazides as Functional Intercalators for Directed Assembly on DNA. *RSC Adv.* **2013**, *3*, 18164–18172.
- (42) Godziewa, M.; Ciesielski, S. Natural DNA Intercalators as Promising Therapeutics for Cancer and Infectious Diseases. *Curr. Cancer Drug Targets* **2020**, *20*, 19–32.
- (43) Tan, G. T.; Lee, S. K.; Lee, I. S.; Chen, J. W.; Leitner, P.; Besterman, J. M.; Kinghorn, A. D.; Pezzuto, J. M. Natural-Product Inhibitors of Human DNA ligase I. *Biochem. J.* **1996**, *314*, 993–1000.
- (44) Brana, M. F.; Cacho, M.; Gradillas, A.; de Pascual-Teresa, B.; Ramos, A. Intercalators as Anticancer Drugs. *Curr. Pharm. Design* **2001**, *7*, 1745–1780.
- (45) Biebricher, A. S.; Heller, I.; Roijmans, R. F. H.; Hoekstra, T. P.; Peterman, E. J. G.; Wuite, G. J. L. The Impact of DNA Intercalators on DNA and DNA-Processing Enzymes Elucidated through Force-Dependent Binding Kinetics. *Nat. Commun.* **2015**, *6*, 7304.
- (46) Gago, F. Stacking Interactions and Intercalative DNA Binding. *Methods* **1998**, *14*, 277–292.
- (47) Barbas, C. F., 3rd; Burton, D. R.; Scott, J. K.; Silverman, G. J. Quantitation of DNA and RNA. *CSH Protoc.* **2007**, 47.
- (48) Carey, F. A.; Sundberg, R. J. Aromatic Substitution Reactions. In *Advanced Organic Chemistry*; Springer: Boston, MA, 1983.
- (49) Derheimer, F. A.; Hicks, J. K.; Paulsen, M. T.; Canman, C. E.; Ljungman, M. Psoralen-Induced DNA Interstrand Cross-Links Block Transcription and Induce p53 in an Ataxia-Telangiectasia and Rad3-Related-Dependent Manner. *Mol. Pharmacol.* **2009**, *75*, 599–607.
- (50) Demaret, J. P.; Brunie, S.; Ballini, J. P.; Vigny, P. Geometry of Intercalation of Psoralens in DNA Approached by Molecular Mechanics. *Photochem. Photobiol.* **1989**, *50*, 7–21.
- (51) Hafshejani, S. M.; Watson, S. M. D.; Tuite, E. M.; Pike, A. R. Click Modification of Diazido Acridine Intercalators: A Versatile Route towards Decorated DNA Nanostructures. *Chem. - Eur. J.* **2015**, *21*, 12611–12615.
- (52) Geisterstanger, B. H.; Wemmer, D. E. Complexes of the Minor-Groove of DNA. *Annu. Rev. Biophys. Biomol. Struct.* **1995**, *24*, 463–493.
- (53) Willis, B.; Arya, D. P. Triple Recognition of B-DNA by a Neomycin-Hoechst 33258-Pyrene Conjugate. *Biochemistry* **2010**, *49*, 452–469.
- (54) Krissanaprasit, A.; Madsen, M.; Knudsen, J. B.; Gudnason, D.; Surareungchai, W.; Birkedal, V.; Gothelf, K. V. Programmed Switching of Single Polymer Conformation on DNA Origami. *ACS Nano* **2016**, *10*, 2243–2250.
- (55) Lu, X.; Tran, T. H.; Jia, F.; Tan, X.; Davis, S.; Krishnan, S.; Amiji, M. M.; Zhang, K. Providing Oligonucleotides with Steric Selectivity by Brush-Polymer-Assisted Compaction. *J. Am. Chem. Soc.* **2015**, *137*, 12466–12469.
- (56) Tokura, Y.; Harvey, S.; Xu, X. M.; Chen, C. J.; Morsbach, S.; Wunderlich, K.; Fytas, G.; Wu, Y. Z.; Ng, D. Y. W.; Weil, T. Polymer tube Nanoreactors via DNA-Origami Templated Synthesis. *Chem. Commun.* **2018**, *54*, 2808–2811.
- (57) Tokura, Y.; Jiang, Y. Y.; Welle, A.; Stenzel, M. H.; Krzemien, K. M.; Michaelis, J.; Berger, R.; Barner-Kowollik, C.; Wu, Y. Z.; Weil, T. Bottom-Up Fabrication of Nanopatterned Polymers on DNA Origami by In Situ Atom-Transfer Radical Polymerization. *Angew. Chem., Int. Ed.* **2016**, *55*, 5692–5697.
- (58) Galindo, M. A.; Hannant, J.; Harrington, R. W.; Clegg, W.; Horrocks, B. R.; Pike, A. R.; Houlton, A. Pyrrolyl-, 2-(2-thienyl)pyrrolyl- and 2,5-bis(2-thienyl)pyrrolyl-Nucleosides: Synthesis, Molecular and Electronic Structure, and Redox Behaviour of C5-Thymidine Derivatives. *Org. Biomol. Chem.* **2011**, *9*, 1555–1564.
- (59) Niu, J.; Hili, R.; Liu, D. R. Enzyme-Free Translation of DNA into Sequence-Defined Synthetic Polymers Structurally Unrelated to Nucleic Acids. *Nat. Chem.* **2013**, *5*, 282–92.
- (60) Kiviahio, J. K.; Linko, V.; Ora, A.; Tiainen, T.; Jarvihaavisto, E.; Mikkila, J.; Tenhu, H.; Nonappa Kostianen, M. A. Cationic Polymers for DNA Origami Coating - Examining their Binding Efficiency and Tuning the Enzymatic Reaction Rates. *Nanoscale* **2016**, *8*, 11674–11680.
- (61) Ponnuswamy, N.; Bastings, M. M. C.; Nathwani, B.; Ryu, J. H.; Chou, L. Y. T.; Vinther, M.; Li, W. A.; Anastassacos, F. M.; Mooney, D. J.; Shih, W. M. Oligolysine-Based Coating Protects DNA Nanostructures from Low-Salt Denaturation and Nuclease Degradation. *Nat. Commun.* **2017**, *8*, 15654.
- (62) Tokura, Y.; Harvey, S.; Chen, C.; Wu, Y.; Ng, D. Y. W.; Weil, T. Fabrication of Defined Polydopamine Nanostructures by DNA Origami-Templated Polymerization. *Angew. Chem., Int. Ed.* **2018**, *57*, 1587–1591.

- (63) Wang, Z.-G.; Liu, Q.; Ding, B. Shape-Controlled Nanofabrication of Conducting Polymer on Planar DNA Templates. *Chem. Mater.* **2014**, *26*, 3364–3367.
- (64) Winterwerber, P.; Harvey, S.; Ng, D. Y. W.; Weil, T. Photocontrolled Dopamine Polymerization on DNA Origami with Nanometer Resolution. *Angew. Chem., Int. Ed.* **2020**, *59*, 6144–6149.
- (65) Kato, M.; Kamigaito, M.; Sawamoto, M.; Higashimura, T. Polymerization of Methyl-Methacrylate with the Carbon-Tetrachloride Dichlorotris(Triphenylphosphine)Ruthenium(II) Methylaluminum Bis(2,6-Di-Tert-Butylphenoxide) Initiating System - Possibility of Living Radical Polymerization. *Macromolecules* **1995**, *28*, 1721–1723.
- (66) Wang, J. S.; Matyjaszewski, K. Controlled Living Radical Polymerization - Halogen Atom-Transfer Radical Polymerization Promoted by a Cu(I)/Cu(II) Redox Process. *Macromolecules* **1995**, *28*, 7901–7910.
- (67) Treat, N. J.; Sprafke, H.; Kramer, J. W.; Clark, P. G.; Barton, B. E.; de Alaniz, J. R.; Fors, B. P.; Hawker, C. J. Metal-Free Atom Transfer Radical Polymerization. *J. Am. Chem. Soc.* **2014**, *136*, 16096–16101.
- (68) Hansson, S.; Trouillet, V.; Tischer, T.; Goldmann, A. S.; Carlmark, A.; Barner-Kowollik, C.; Malmstrom, E. Grafting Efficiency of Synthetic Polymers onto Biomaterials: a Comparative Study of Grafting-versus Grafting-to. *Biomacromolecules* **2013**, *14*, 64–74.
- (69) Nakano, S. I.; Sugimoto, N. The Structural Stability and Catalytic Activity of DNA and RNA Oligonucleotides in the Presence of Organic Solvents. *Biophys. Rev.* **2016**, *8*, 11–23.
- (70) Herskovits, T. T. Nonaqueous Solutions of DNA - Factors Determining Stability of Helical Configuration in Solution. *Arch. Biochem. Biophys.* **1962**, *97*, 474–484.
- (71) Safak, M.; Alemdaroglu, F. E.; Li, Y.; Ergen, E.; Herrmann, A. Polymerase Chain Reaction as an Efficient Tool for the Preparation of Block Copolymers. *Adv. Mater.* **2007**, *19*, 1499–1505.
- (72) Charleux, B.; Delaitre, G.; Rieger, J.; D'Agosto, F. Polymerization-Induced Self-Assembly: From Soluble Macromolecules to Block Copolymer Nano-Objects in One Step. *Macromolecules* **2012**, *45*, 6753–6765.
- (73) Warren, N. J.; Armes, S. P. Polymerization-Induced Self-Assembly of Block Copolymer Nano-objects via RAFT Aqueous Dispersion Polymerization. *J. Am. Chem. Soc.* **2014**, *136* (29), 10174–10185.
- (74) Luckerath, T.; Koynov, K.; Loescher, S.; Whitfield, C. J.; Nuhn, L.; Walther, A.; Barner-Kowollik, C.; Ng, D. Y. W.; Weil, T. DNA-Polymer Nanostructures by RAFT Polymerization and Polymerization-Induced Self-Assembly. *Angew. Chem., Int. Ed.* **2020**, *59*, 15474–15479.
- (75) Butler, I. B.; Schoonen, M. A. A.; Rickard, D. T. Removal of Dissolved-Oxygen from Water - a Comparison of 4 Common Techniques. *Talanta* **1994**, *41*, 211–215.
- (76) Shao, W.; Khin, S.; Kopp, W. C. Characterization of Effect of Repeated Freeze and Thaw Cycles on Stability of Genomic DNA Using Pulsed Field Gel Electrophoresis. *Biopreserv. Biobanking* **2012**, *10*, 4–11.
- (77) Sun, Y.; Lathwal, S.; Wang, Y.; Fu, L. Y.; Olszewski, M.; Fantin, M.; Enciso, A. E.; Szczepaniak, G.; Das, S.; Matyjaszewski, K. Preparation of Well-Defined Polymers and DNA-Polymer Bioconjugates via Small-Volume eATRP in the Presence of Air. *ACS Macro Lett.* **2019**, *8*, 603–609.
- (78) Kleiner, R. E.; Brudno, Y.; Birnbaum, M. E.; Liu, D. R. DNA-Templated Polymerization of Side-Chain-Functionalized Peptide Nucleic Acid Aldehydes. *J. Am. Chem. Soc.* **2008**, *130*, 4646–4659.
- (79) Chidchob, P.; Edwardson, T. G.; Serpell, C. J.; Sleiman, H. F. Synergy of Two Assembly Languages in DNA Nanostructures: Self-Assembly of Sequence-Defined Polymers on DNA Cages. *J. Am. Chem. Soc.* **2016**, *138*, 4416–4425.
- (80) Edwardson, T. G. W.; Carneiro, K. M. M.; Serpell, C. J.; Sleiman, H. F. An Efficient and Modular Route to Sequence-Defined Polymers Appended to DNA. *Angew. Chem., Int. Ed.* **2014**, *53*, 4567–4571.
- (81) Milnes, P. J.; McKee, M. L.; Bath, J.; Song, L.; Stulz, E.; Turberfield, A. J.; O'Reilly, R. K. Sequence-Specific Synthesis of Macromolecules using DNA-Templated Chemistry. *Chem. Commun.* **2012**, *48*, 5614–5616.
- (82) Lou, X.; Wang, C.; He, L. Core-shell Au Nanoparticle Formation with DNA-Polymer Hybrid Coatings using Aqueous ATRP. *Biomacromolecules* **2007**, *8*, 1385–1390.
- (83) He, P.; He, L. Synthesis of Surface-Anchored DNA-Polymer Bioconjugates using Reversible Addition-Fragmentation Chain Transfer Polymerization. *Biomacromolecules* **2009**, *10*, 1804–1809.
- (84) Fu, L. Y.; Wang, Z. H.; Lathwal, S.; Enciso, A. E.; Simakova, A.; Das, S. R.; Russell, A. J.; Matyjaszewski, K. Synthesis of Polymer Bioconjugates via Photoinduced Atom Transfer Radical Polymerization under Blue Light Irradiation. *ACS Macro Lett.* **2018**, *7* (10), 1248–1253.
- (85) Enciso, A. E.; Fu, L. Y.; Lathwal, S.; Olszewski, M.; Wang, Z. H.; Das, S. R.; Russell, A. J.; Matyjaszewski, K. Biocatalytic "Oxygen-Fueled" Atom Transfer Radical Polymerization. *Angew. Chem., Int. Ed.* **2018**, *57* (49), 16157–16161.
- (86) Wang, Z. H.; Wang, Z. H.; Pan, X. C.; Fu, L. Y.; Lathwal, S.; Olszewski, M.; Yan, J. J.; Enciso, A. E.; Wang, Z. Y.; Xia, H. S.; et al. Ultrasonication-Induced Aqueous Atom Transfer Radical Polymerization. *ACS Macro Lett.* **2018**, *7*, 275–280.
- (87) Livache, T.; Roget, A.; Dejean, E.; Barthet, C.; Bidan, G.; Teoule, R. Preparation of a DNA Matrix Via an Electrochemically Directed Copolymerization of Pyrrole and Oligonucleotides Bearing a Pyrrole Group. *Nucleic Acids Res.* **1994**, *22*, 2915–2921.
- (88) Fong, R. B.; Ding, Z. L.; Long, C. J.; Hoffman, A. S.; Stayton, P. S. Thermoprecipitation of Streptavidin via Oligonucleotide-Mediated Self-Assembly with poly (N-isopropylacrylamide). *Bioconjugate Chem.* **1999**, *10*, 720–725.
- (89) Costioli, M. D.; Fisch, L.; Garret-Flaudy, F.; Hilbrig, F.; Freitag, R. DNA Purification by Triple-Helix Affinity Precipitation. *Biotechnol. Bioeng.* **2003**, *81*, 535–545.
- (90) Jeong, J. H.; Park, T. G. Novel Polymer-DNA Hybrid Polymeric Micelles Composed of Hydrophobic Poly(D,L-lactic-co-glycolic acid) and Hydrophilic Oligonucleotides. *Bioconjugate Chem.* **2001**, *12*, 917–923.
- (91) Jeong, J. H.; Kim, S. H.; Kim, S. W.; Park, T. G. Polyelectrolyte Complex Micelles Composed of c-raf Antisense Oligodeoxynucleotide-Poly(ethylene glycol) Conjugate and Poly(ethylenimine): Effect of Systemic Administration on Tumor Growth. *Bioconjugate Chem.* **2005**, *16*, 1034–1037.
- (92) Jeong, J. H.; Kim, S. W.; Park, T. G. A New Antisense Oligonucleotide Delivery System Based on Self-Assembled ODN-PEG Hybrid Conjugate Micelles. *J. Controlled Release* **2003**, *93*, 183–191.
- (93) Jeong, J. H.; Kim, S. W.; Park, T. G. Novel Intracellular Delivery System of Antisense Oligonucleotide by Self-Assembled Hybrid Micelles composed of DNA/PEG Conjugate and Cationic Fusogenic Peptide. *Bioconjugate Chem.* **2003**, *14*, 473–479.
- (94) Oishi, M.; Sasaki, S.; Nagasaki, Y.; Kataoka, K. pH-Responsive Oligodeoxynucleotide (ODN)-Poly(Ethylene Glycol) Conjugate through Acid-Labile *i*-Thiopropionate Linkage: Preparation and Polyion Complex Micelle Formation. *Biomacromolecules* **2003**, *4*, 1426–1432.
- (95) Oishi, M.; Nagatsugi, F.; Sasaki, S.; Nagasaki, Y.; Kataoka, K. Smart Polyion Complex Micelles for Targeted Intracellular Delivery of PEGylated Antisense Oligonucleotides Containing Acid-Labile Linkages. *ChemBioChem* **2005**, *6*, 718–725.
- (96) Oishi, M.; Nagasaki, Y.; Itaka, K.; Nishiyama, N.; Kataoka, K. Lactosylated Poly(ethylene glycol)-siRNA Conjugate through Acid-Labile *ss*-Thiopropionate Linkage to Construct pH-Sensitive Polyion Complex Micelles Achieving Enhanced Gene Silencing in Hepatoma Cells. *J. Am. Chem. Soc.* **2005**, *127*, 1624–1625.
- (97) Averick, S.; Paredes, E.; Li, W.; Matyjaszewski, K.; Das, S. R. Direct DNA Conjugation to Star Polymers for Controlled Reversible Assemblies. *Bioconjugate Chem.* **2011**, *22*, 2030–2037.

- (98) Carneiro, K. M. M.; Hamblin, G. D.; Hänni, K. D.; Fakhoury, J.; Nayak, M. K.; Rizis, G.; McLaughlin, C. K.; Bazzi, H. S.; Sleiman, H. F. Stimuli-Responsive Organization of Block Copolymers on DNA Nanotubes. *Chem. Sci.* **2012**, *3*, 1980.
- (99) Wilks, T. R.; Bath, J.; de Vries, J. W.; Raymond, J. E.; Herrmann, A.; Turberfield, A. J.; O'Reilly, R. K. Giant Surfactants Created by the Fast and Efficient Functionalization of a DNA Tetrahedron with a Temperature-Responsive Polymer. *ACS Nano* **2013**, *7*, 8561–8572.
- (100) Averick, S. E.; Paredes, E.; Dey, S. K.; Snyder, K. M.; Tapinos, N.; Matyjaszewski, K.; Das, S. R. Autotransfecting Short Interfering RNA through Facile Covalent Polymer Escorts. *J. Am. Chem. Soc.* **2013**, *135*, 12508–12511.
- (101) Matyjaszewski, K. Atom Transfer Radical Polymerization (ATRP): Current Status and Future Perspectives. *Macromolecules* **2012**, *45*, 4015–4039.
- (102) Sumerlin, B. S. Proteins as Initiators of Controlled Radical Polymerization: Grafting-from via ATRP and RAFT. *ACS Macro Lett.* **2012**, *1*, 141–145.
- (103) Lassalle, N.; Vieil, E.; Correia, J. P.; Abrantes, L. M. Study of DNA Hybridization on Polypyrrole Grafted with Oligonucleotides by Photocurrent Spectroscopy. *Biosens. Bioelectron.* **2001**, *16*, 295–303.
- (104) McKee, M. L.; Milnes, P. J.; Bath, J.; Stulz, E.; Turberfield, A. J.; O'Reilly, R. K. Multistep DNA-Templated Reactions for the Synthesis of Functional Sequence Controlled Oligomers. *Angew. Chem., Int. Ed.* **2010**, *49*, 7948–7951.
- (105) Cao, X. Y.; Lu, X. G.; Wang, D. L.; Jia, F.; Tan, X. Y.; Corley, M.; Chen, X. Y.; Zhang, K. Modulating the Cellular Immune Response of Oligonucleotides by Brush Polymer-Assisted Compaction. *Small* **2017**, *13*, 1701432.
- (106) Jia, F.; Lu, X.; Tan, X.; Wang, D.; Cao, X.; Zhang, K. Effect of PEG Architecture on the Hybridization Thermodynamics and Protein Accessibility of PEGylated Oligonucleotides. *Angew. Chem., Int. Ed.* **2017**, *56*, 1239–1243.
- (107) Jia, F.; Lu, X.; Wang, D.; Cao, X.; Tan, X.; Lu, H.; Zhang, K. Depth-Profiling the Nuclease Stability and the Gene Silencing Efficacy of Brush-Architected Poly(ethylene glycol)-DNA Conjugates. *J. Am. Chem. Soc.* **2017**, *139*, 10605–10608.
- (108) Lu, X.; Jia, F.; Tan, X.; Wang, D.; Cao, X.; Zheng, J.; Zhang, K. Effective Antisense Gene Regulation via Noncationic, Polyethylene Glycol Brushes. *J. Am. Chem. Soc.* **2016**, *138*, 9097–9100.
- (109) McLaughlin, C. K.; Hamblin, G. D.; Hänni, K. D.; Conway, J. W.; Nayak, M. K.; Carneiro, K. M.; Bazzi, H. S.; Sleiman, H. F. Three-Dimensional Organization of Block Copolymers on "DNA-Minimal" Scaffolds. *J. Am. Chem. Soc.* **2012**, *134*, 4280–4286.
- (110) Tan, X. Y.; Lu, X. G.; Jia, F.; Liu, X. F.; Sun, Y. H.; Logan, J. K.; Zhang, K. Blurring the Role of Oligonucleotides: Spherical Nucleic Acids as a Drug Delivery Vehicle. *J. Am. Chem. Soc.* **2016**, *138*, 10834–10837.
- (111) Banga, R. J.; Krovci, S. A.; Narayan, S. P.; Sprangers, A. J.; Liu, G.; Mirkin, C. A.; Nguyen, S. T. Drug-Loaded Polymeric Spherical Nucleic Acids: Enhancing Colloidal Stability and Cellular Uptake of Polymeric Nanoparticles through DNA Surface-Functionalization. *Biomacromolecules* **2017**, *18*, 483–489.
- (112) Zhang, C.; Hao, L.; Calabrese, C. M.; Zhou, Y.; Choi, C. H.; Xing, H.; Mirkin, C. A. Biodegradable DNA-Brush Block Copolymer Spherical Nucleic Acids Enable Transfection Agent-Free Intracellular Gene Regulation. *Small* **2015**, *11*, 5360–5368.
- (113) Lu, X.; Watts, E.; Jia, F.; Tan, X.; Zhang, K. Polycondensation of Polymer Brushes via DNA Hybridization. *J. Am. Chem. Soc.* **2014**, *136*, 10214–10217.
- (114) Liu, Y.; Chen, P.; Li, Z. B. Molecular Bottlebrushes with Polypeptide Backbone Prepared via Ring-Opening Polymerization of NCA and ATRP. *Macromol. Rapid Commun.* **2012**, *33*, 287–295.
- (115) Chen, P.; Li, C.; Liu, D. S.; Li, Z. B. DNA-Grafted Polypeptide Molecular Bottlebrush Prepared via Ring-Opening Polymerization and Click Chemistry. *Macromolecules* **2012**, *45*, 9579–9584.
- (116) James, C. R.; Rush, A. M.; Insley, T.; Vukovic, L.; Adamiak, L.; Kral, P.; Gianneschi, N. C. Poly(oligonucleotide). *J. Am. Chem. Soc.* **2014**, *136*, 11216–11219.
- (117) Fouz, M. F.; Mukumoto, K.; Averick, S.; Molinar, O.; McCartney, B. M.; Matyjaszewski, K.; Armitage, B. A.; Das, S. R. Bright Fluorescent Nanotags from Bottlebrush Polymers with DNA-Tipped Bristles. *ACS Cent. Sci.* **2015**, *1*, 431–438.
- (118) Yu, S. R.; Dong, R. J.; Chen, J. X.; Chen, F.; Jiang, W. F.; Zhou, Y. F.; Zhu, X. Y.; Yan, D. Y. Synthesis and Self-Assembly of Amphiphilic Aptamer-Functionalized Hyperbranched Multiarm Copolymers for Targeted Cancer Imaging. *Biomacromolecules* **2014**, *15*, 1828–1836.
- (119) Zhuang, Y.; Deng, H.; Su, Y.; He, L.; Wang, R.; Tong, G.; He, D.; Zhu, X. Aptamer-Functionalized and Backbone Redox-Responsive Hyperbranched Polymer for Targeted Drug Delivery in Cancer Therapy. *Biomacromolecules* **2016**, *17*, 2050–2062.
- (120) Yang, L.; Sun, H.; Liu, Y.; Hou, W.; Yang, Y.; Cai, R.; Cui, C.; Zhang, P.; Pan, X.; Li, X.; et al. Self-Assembled Aptamer-Grafted Hyperbranched Polymer Nanocarrier for Targeted and Photo-responsive Drug Delivery. *Angew. Chem., Int. Ed.* **2018**, *57*, 17048–17052.
- (121) Li, Z.; Zhang, Y.; Fullhart, P.; Mirkin, C. A. Reversible and Chemically Programmable Micelle Assembly with DNA Block-Copolymer Amphiphiles. *Nano Lett.* **2004**, *4*, 1055–1058.
- (122) Alemdaroglu, F. E.; Ding, K.; Berger, R.; Herrmann, A. DNA-Templated Synthesis in Three Dimensions: Introducing a Micellar Scaffold for Organic Reactions. *Angew. Chem., Int. Ed.* **2006**, *45*, 4206–4210.
- (123) Rodriguez-Pulido, A.; Kondrachuk, A. I.; Prusty, D. K.; Gao, J.; Loi, M. A.; Herrmann, A. Light-Triggered Sequence-Specific Cargo Release from DNA Block Copolymer-Lipid Vesicles. *Angew. Chem., Int. Ed.* **2013**, *52*, 1008–1012.
- (124) Yernen, S. S.; Lathwall, S.; Shrestha, P.; Shirwan, H.; Matyjaszewski, K.; Weiss, L.; Yolcu, E. S.; Campbell, P. G.; Das, S. R. Rapid On-Demand Extracellular Vesicle Augmentation with Versatile Oligonucleotide Tethers. *ACS Nano* **2019**, *13*, 10555–10565.
- (125) Jia, F.; Lu, X.; Tan, X.; Zhang, K. Facile Synthesis of Nucleic Acid-Polymer Amphiphiles and Their Self-assembly. *Chem. Commun.* **2015**, *51*, 7843–7846.
- (126) Chien, M. P.; Rush, A. M.; Thompson, M. P.; Gianneschi, N. C. Programmable Shape-Shifting Micelles. *Angew. Chem., Int. Ed.* **2010**, *49*, 5076–5080.
- (127) Roloff, A.; Carlini, A. S.; Callmann, C. E.; Gianneschi, N. C. Micellar Thrombin-Binding Aptamers: Reversible Nanoscale Anticoagulants. *J. Am. Chem. Soc.* **2017**, *139*, 16442–16445.
- (128) Roloff, A.; Nelles, D. A.; Thompson, M. P.; Yeo, G. W.; Gianneschi, N. C. Self-Transfecting Micellar RNA: Modulating Nanoparticle Cell Interactions via High Density Display of Small Molecule Ligands on Micelle Coronas. *Bioconjugate Chem.* **2018**, *29*, 126–135.
- (129) Melnychuk, N.; Klymchenko, A. S. DNA-Functionalized Dye-Loaded Polymeric Nanoparticles: Ultrabright FRET Platform for Amplified Detection of Nucleic Acids. *J. Am. Chem. Soc.* **2018**, *140*, 10856–10865.
- (130) Lou, X. H.; Lewis, M. S.; Gorman, C. B.; He, L. Detection of DNA Point Mutation by Atom Transfer Radical Polymerization. *Anal. Chem.* **2005**, *77*, 4698–4705.
- (131) Lou, X. H.; He, L. DNA-Accelerated Atom Transfer Radical Polymerization on a Gold Surface. *Langmuir* **2006**, *22*, 2640–2646.
- (132) Seeman, N. C.; Sleiman, H. F. DNA Nanotechnology. *Nat. Rev. Mater.* **2018**, *3*, 17068.
- (133) Rothmund, P. W. K. Folding DNA to Create Nanoscale Shapes and Patterns. *Nature* **2006**, *440*, 297–302.
- (134) Hong, F.; Zhang, F.; Liu, Y.; Yan, H. DNA Origami: Scaffolds for Creating Higher Order Structures. *Chem. Rev.* **2017**, *117*, 12584–12640.
- (135) Topping, T.; Voigt, N. V.; Nangreave, J.; Yan, H.; Gothelf, K. V. DNA Origami: a Quantum Leap for Self-Assembly of Complex Structures. *Chem. Soc. Rev.* **2011**, *40*, 5636–5646.

- (136) Rosenbaum, D. M.; Liu, D. R. Efficient and Sequence-Specific DNA-Templated Polymerization of Peptide Nucleic Acid Aldehydes. *J. Am. Chem. Soc.* **2003**, *125*, 13924–13925.
- (137) Lo, P. K.; Sleiman, H. F. Nucleobase-Templated Polymerization: Copying the Chain Length and Polydispersity of Living Polymers into Conjugated Polymers. *J. Am. Chem. Soc.* **2009**, *131*, 4182–4183.
- (138) McHale, R.; Patterson, J. P.; Zetterlund, P. B.; O'Reilly, R. K. Biomimetic Radical Polymerization via Cooperative Assembly of Segregating Templates. *Nat. Chem.* **2012**, *4*, 491–497.
- (139) Zhou, Z.; Xia, X.; Bong, D. Synthetic Polymer Hybridization with DNA and RNA Directs Nanoparticle Loading, Silencing Delivery, and Aptamer Function. *J. Am. Chem. Soc.* **2015**, *137*, 8920–8923.
- (140) Bakker, M. H.; Lee, C. C.; Meijer, E. W.; Dankers, P. Y.; Albertazzi, L. Multicomponent Supramolecular Polymers as a Modular Platform for Intracellular Delivery. *ACS Nano* **2016**, *10*, 1845–1852.
- (141) Kondinskaia, D. A.; Gurtovenko, A. A. Supramolecular Complexes of DNA with Cationic Polymers: The Effect of Polymer Concentration. *Polymer* **2018**, *142*, 277–284.
- (142) Chakraborty, G.; Balinin, K.; Portale, G.; Loznik, M.; Polushkin, E.; Weil, T.; Herrmann, A. Electrostatically PEGylated DNA Enables Salt-Free hybridization in Water. *Chem. Sci.* **2019**, *10*, 10097–10105.
- (143) Chen, W.; Gerasimov, J. Y.; Zhao, P.; Liu, K.; Herrmann, A. High-Density Noncovalent Functionalization of DNA by Electrostatic Interactions. *J. Am. Chem. Soc.* **2015**, *137*, 12884–12889.
- (144) Tang, H.; Chen, L.; Xing, C.; Guo, Y. G.; Wang, S. DNA-Templated Synthesis of Cationic Poly(3,4-ethylenedioxythiophene) Derivative for Supercapacitor Electrodes. *Macromol. Rapid Commun.* **2010**, *31*, 1892–1896.
- (145) Nickels, P.; Dittmer, W. U.; Beyer, S.; Kotthaus, J. P.; Simmel, F. C. Polyaniline Nanowire Synthesis Templated by DNA. *Nanotechnology* **2004**, *15*, 1524–1529.
- (146) Ma, Y.; Zhang, J.; Zhang, G.; He, H. Polyaniline Nanowires on Si Surfaces Fabricated with DNA Templates. *J. Am. Chem. Soc.* **2004**, *126*, 7097–7101.
- (147) Wang, G.; Tanaka, H.; Hong, L.; Matsuo, Y.; Niikura, K.; Abe, M.; Matsumoto, K.; Ogawa, T.; Ijiro, K. Novel Charge Transport in DNA-Templated Nanowires. *J. Mater. Chem.* **2012**, *22*, 13691–13697.
- (148) Farha Al-Said, S. A.; Hassanien, R.; Hannant, J.; Galindo, M. A.; Pruneanu, S.; Pike, A. R.; Houlton, A.; Horrocks, B. R. Templating Ag on DNA/Polymer Hybrid Nanowires: Control of the Metal Growth Morphology using Functional Monomers. *Electrochem. Commun.* **2009**, *11*, 550–553.
- (149) Watson, S. M.; Galindo, M. A.; Horrocks, B. R.; Houlton, A. Mechanism of Formation of Supramolecular DNA-Templated Polymer Nanowires. *J. Am. Chem. Soc.* **2014**, *136*, 6649–6655.
- (150) Hannant, J.; Hedley, J. H.; Pate, J.; Walli, A.; Farha Al-Said, S. A.; Galindo, M. A.; Connolly, B. A.; Horrocks, B. R.; Houlton, A.; Pike, A. R. Modification of DNA-Templated Conductive Polymer Nanowires via Click Chemistry. *Chem. Commun.* **2010**, *46*, 5870–5872.
- (151) Watson, S. M.; Hedley, J. H.; Galindo, M. A.; Al-Said, S. A.; Wright, N. G.; Connolly, B. A.; Horrocks, B. R.; Houlton, A. Synthesis, Characterisation and Electrical Properties of Supramolecular DNA-Templated Polymer Nanowires of 2,5-(bis-2-thienyl)-pyrrole. *Chem. - Eur. J.* **2012**, *18*, 12008–12019.
- (152) Wang, W.; Zhang, K.; Chen, D. From Tunable DNA/Polymer Self-Assembly to Tailorable and Morphologically Pure Core-Shell Nanofibers. *Langmuir* **2018**, *34*, 15350–15359.
- (153) Deiana, M.; Mettra, B.; Matczyszyn, K.; Piela, K.; Pitrat, D.; Olesiak-Banska, J.; Monnereau, C.; Andraud, C.; Samoc, M. Interactions of a Biocompatible Water-Soluble Anthracenyl Polymer Derivative with Double-Stranded DNA. *Phys. Chem. Chem. Phys.* **2015**, *17*, 318–327.
- (154) Albert, S. K.; Thelu, H. V. P.; Golla, M.; Krishnan, N.; Varghese, R. Modular Synthesis of Supramolecular DNA Amphiphiles Through Host-Guest Interactions and Their Self-Assembly into DNA-Decorated Nanovesicles. *Nanoscale* **2017**, *9*, 5425–5432.
- (155) Zhou, X.; Pathak, P.; Jayawickramarajah, J. Design, Synthesis, and Applications of DNA-Macrocyclic Host Conjugates. *Chem. Commun.* **2018**, *54*, 11668–11680.
- (156) Thelu, H. V. P.; Albert, S. K.; Golla, M.; Krishnan, N.; Ram, D.; Srinivasula, S. M.; Varghese, R. Size Controllable DNA Nanogels from the Self-Assembly of DNA Nanostructures through Multivalent Host-Guest Interactions. *Nanoscale* **2018**, *10*, 222–230.
- (157) Rajendran, A.; Endo, M.; Katsuda, Y.; Hidaka, K.; Sugiyama, H. Photo-Cross-Linking-Assisted Thermal Stability of DNA Origami Structures and its Application for Higher-Temperature Self-Assembly. *J. Am. Chem. Soc.* **2011**, *133*, 14488–14491.
- (158) Ramakrishnan, S.; Ijas, H.; Linko, V.; Keller, A. Structural Stability of DNA Origami Nanostructures Under Application-Specific Conditions. *Comput. Struct. Biotechnol. J.* **2018**, *16*, 342–349.
- (159) Ahmadi, Y.; De Llano, E.; Barisic, I. (Poly)cation-Induced Protection of Conventional and Wireframe DNA Origami Nanostructures. *Nanoscale* **2018**, *10*, 7494–7504.
- (160) Agarwal, N. P.; Matthies, M.; Gur, F. N.; Osada, K.; Schmidt, T. L. Block Copolymer Micellization as a Protection Strategy for DNA Origami. *Angew. Chem., Int. Ed.* **2017**, *56*, 5460–5464.
- (161) Wang, S. T.; Gray, M. A.; Xuan, S.; Lin, Y.; Byrnes, J.; Nguyen, A. L.; Todorova, N.; Stevens, M. M.; Bertozzi, C. R.; Zuckermann, et al. DNA Origami Protection and Molecular Interfacing through Engineered Sequence-Defined Peptoids. *Proc. Natl. Acad. Sci. U. S. A.* **2020**, *117*, 6339–6348.
- (162) Chopra, A.; Krishnan, S.; Simmel, F. C. Electrotransfection of Polyamine Folded DNA Origami Structures. *Nano Lett.* **2016**, *16*, 6683–6690.
- (163) Knudsen, J. B.; Liu, L.; Bank Kodal, A. L.; Madsen, M.; Li, Q.; Song, J.; Woehrstein, J. B.; Wickham, S. F.; Strauss, M. T.; Schueder, F.; et al. Routing of Individual Polymers in Designed Patterns. *Nat. Nanotechnol.* **2015**, *10*, 892–898.
- (164) Madsen, M.; Christensen, R. S.; Krissanaprasit, A.; Bakke, M. R.; Riber, C. F.; Nielsen, K. S.; Zelikin, A. N.; Gothelf, K. V. Preparation, Single-Molecule Manipulation, and Energy Transfer Investigation of a Polyfluorene-graft-DNA polymer. *Chem. - Eur. J.* **2017**, *23*, 10511–10515.
- (165) Wang, Z. G.; Zhan, P.; Ding, B. Self-Assembled Catalytic DNA Nanostructures for Synthesis of Para-Directed Polyaniline. *ACS Nano* **2013**, *7*, 1591–1598.
- (166) Trinh, T.; Liao, C.; Toader, V.; Barlog, M.; Bazzi, H. S.; Li, J.; Sleiman, H. F. DNA-Imprinted Polymer Nanoparticles with Monodispersity and Prescribed DNA-Strand Patterns. *Nat. Chem.* **2018**, *10*, 184–192.
- (167) Jeong, J. H.; Kim, S. H.; Kim, S. W.; Park, T. G. In vivo Tumor Targeting of ODN-PEG-folic acid/PEI Polyelectrolyte Complex Micelles. *J. Biomater. Sci., Polym. Ed.* **2005**, *16*, 1409–1419.
- (168) Lee, J.; Lee, B. J.; Lee, Y. M.; Park, H.; Kim, J. H.; Kim, W. Self-Assembled Nanoconstructs Modified with Amplified Aptamers Inhibited Tumor Growth and Retinal Vascular Hyperpermeability via Vascular Endothelial Growth Factor Capturing. *Mol. Pharmaceutics* **2017**, *14*, 1460–1468.
- (169) Alemdaroglu, F. E.; Zhuang, W.; Zophel, L.; Wang, J.; Berger, R.; Rabe, J. P.; Herrmann, A. Generation of Multiblock Copolymers by PCR: Synthesis, Visualization and Nanomechanical Properties. *Nano Lett.* **2009**, *9*, 3658–3662.
- (170) Wang, J.; Alemdaroglu, F. E.; Prusty, D. K.; Herrmann, A.; Berger, R. In-situ Visualization of the Enzymatic Growth of Surface-Immobilized DNA block Copolymer Micelles by Scanning Force Microscopy. *Macromolecules* **2008**, *41*, 2914–2919.
- (171) Serpell, C. J.; Edwardson, T. G.; Chidchob, P.; Carneiro, K. M.; Sleiman, H. F. Precision Polymers and 3D DNA Nanostructures: Emergent Assemblies from new Parameter Space. *J. Am. Chem. Soc.* **2014**, *136*, 15767–15774.
- (172) Kamps, A. C.; Cativo, M. H. M.; Chen, X.-J.; Park, S.-J. Self-Assembly of DNA-Coupled Semiconducting Block Copolymers. *Macromolecules* **2014**, *47*, 3720–3726.

- (173) Alemdaroglu, F. E.; Alemdaroglu, N. C.; Langguth, P.; Herrmann, A. DNA Block Copolymer Micelles - A Combinatorial Tool for Cancer Nanotechnology. *Adv. Mater.* **2008**, *20*, 899–902.
- (174) Talom, R. M.; Fuks, G.; Kaps, L.; Oberdisse, J.; Clercier, C.; Gaillard, C.; Mingotaud, C.; Gauffre, F. DNA-polymer Micelles as Nanoparticles with Recognition Ability. *Chem. - Eur. J.* **2011**, *17*, 13495–13501.
- (175) Lassalle, V.; Ferreira, M. L. PLA Nano- and Microparticles for Drug Delivery: an Overview of the Methods of Preparation. *Macromol. Biosci.* **2007**, *7*, 767–783.
- (176) Cavalieri, F.; Postma, A.; Lee, L.; Caruso, F. Assembly and Functionalization of DNA-Polymer Microcapsules. *ACS Nano* **2009**, *3*, 234–240.
- (177) Tan, X.; Lu, X.; Jia, F.; Liu, X.; Sun, Y.; Logan, J. K.; Zhang, K. Blurring the Role of Oligonucleotides: Spherical Nucleic Acids as a Drug Delivery Vehicle. *J. Am. Chem. Soc.* **2016**, *138*, 10834–10837.
- (178) Tang, L.; Tjong, V.; Li, N.; Yingling, Y. G.; Chilkoti, A.; Zauscher, S. Enzymatic Polymerization of High Molecular Weight DNA Amphiphiles That Self-Assemble into Star-Like Micelles. *Adv. Mater.* **2014**, *26*, 3050–3054.
- (179) Vyborna, Y.; Vybornyi, M.; Rudnev, A. V.; Haner, R. DNA-Grafted Supramolecular Polymers: Helical Ribbon Structures Formed by Self-Assembly of Pyrene-DNA Chimeric Oligomers. *Angew. Chem., Int. Ed.* **2015**, *54*, 7934–8.
- (180) Vyborna, Y.; Vybornyi, M.; Haner, R. Functional DNA-Grafted Supramolecular Polymers - Chirality, Cargo Binding and Hierarchical Organization. *Chem. Commun.* **2017**, *53*, S179–S181.
- (181) Meng, Y. F.; Wei, J.; Gao, P. C.; Jiang, Y. Self-Assembling Amphiphilic poly(propargyl methacrylate) Grafted DNA Copolymers into Multi-Strand Helices. *Soft Matter* **2015**, *11*, 5610–5613.
- (182) Kedracki, D.; Filippov, S. K.; Gour, N.; Schlaad, H.; Nardin, C. Formation of DNA-Copolymer Fibrils Through an Amyloid-Like Nucleation Polymerization Mechanism. *Macromol. Rapid Commun.* **2015**, *36*, 768–773.
- (183) Mai, Y.; Eisenberg, A. Self-Assembly of Block Copolymers. *Chem. Soc. Rev.* **2012**, *41*, 5969–5985.
- (184) Jia, F.; Li, H.; Chen, R.; Zhang, K. Self-Assembly of DNA-Containing Copolymers. *Bioconjugate Chem.* **2019**, *30*, 1880–1888.
- (185) Lu, X.; Fu, H.; Shih, K. C.; Jia, F.; Sun, Y.; Wang, D.; Wang, Y.; Ekatan, S.; Nieh, M. P.; Lin, Y.; et al. DNA-Mediated Step-Growth Polymerization of Bottlebrush Macromonomers. *J. Am. Chem. Soc.* **2020**, *142*, 10297–10301.
- (186) Jia, F.; Wang, D.; Lu, X.; Tan, X.; Wang, Y.; Lu, H.; Zhang, K. Improving the Enzymatic Stability and the Pharmacokinetics of Oligonucleotides via DNA-Backboned Bottlebrush Polymers. *Nano Lett.* **2018**, *18*, 7378–7382.
- (187) Ding, K.; Alemdaroglu, F. E.; Borsch, M.; Berger, R.; Herrmann, A. Engineering the Structural Properties of DNA Block Copolymer Micelles by Molecular Recognition. *Angew. Chem., Int. Ed.* **2007**, *46*, 1172–1175.
- (188) Dong, Y.; Yang, Y. R.; Zhang, Y.; Wang, D.; Wei, X.; Banerjee, S.; Liu, Y.; Yang, Z.; Yan, H.; Liu, D. Cuboid Vesicles Formed by Frame-Guided Assembly on DNA Origami Scaffolds. *Angew. Chem., Int. Ed.* **2017**, *56*, 1586–1589.
- (189) Service, R. F. How Far can we Push Chemical Self-Assembly? *Science* **2005**, *309*, 95.
- (190) Dong, Y.; Sun, Y.; Wang, L.; Wang, D.; Zhou, T.; Yang, Z.; Chen, Z.; Wang, Q.; Fan, Q.; Liu, D. Frame-Guided Assembly of Vesicles with Programmed Geometry and Dimensions. *Angew. Chem., Int. Ed.* **2014**, *53*, 2607–2610.
- (191) Zhou, C.; Zhang, Y.; Dong, Y.; Wu, F.; Wang, D.; Xin, L.; Liu, D. Precisely Controlled 2D Free-Floating Nanosheets of Amphiphilic Molecules through Frame-Guided Assembly. *Adv. Mater.* **2016**, *28*, 9819–9823.
- (192) Kim, C. J.; Hu, X.; Park, S. J. Multimodal Shape Transformation of Dual-Responsive DNA Block Copolymers. *J. Am. Chem. Soc.* **2016**, *138*, 14941–14947.
- (193) Rahbani, J. F.; Vengut-Climent, E.; Chidchob, P.; Gidi, Y.; Trinh, T.; Cosa, G.; Sleiman, H. F. DNA Nanotubes with Hydrophobic Environments: Toward New Platforms for Guest Encapsulation and Cellular Delivery. *Adv. Healthcare Mater.* **2018**, *7*, 1701049.
- (194) Fakhri, H. H.; Fakhoury, J. J.; Bousmail, D.; Sleiman, H. F. Minimalist Design of a Stimuli-Responsive Spherical Nucleic Acid for Conditional Delivery of Oligonucleotide Therapeutics. *ACS Appl. Mater. Interfaces* **2019**, *11*, 13912–13920.
- (195) Wu, F.; Song, Y.; Zhao, Z.; Zhang, S.; Yang, Z.; Li, Z.; Li, M.; Fan, Q.-H.; Liu, D. Preparation and Self-Assembly of Supramolecular Coil-Rod-Coil Triblock Copolymer PPO-dsDNA-PPO. *Macromolecules* **2015**, *48*, 7550–7556.
- (196) Zhao, Z.; Chen, C.; Dong, Y.; Yang, Z.; Fan, Q. H.; Liu, D. Thermally Triggered Frame-Guided Assembly. *Angew. Chem., Int. Ed.* **2014**, *53*, 13468–13470.
- (197) Umeno, D.; Maeda, M. Poly(N-isopropylacrylamide) Carrying Double-Stranded DNA for Affinity Separation of Genotoxins. *Anal. Sci.* **1997**, *13*, 553–556.
- (198) Isoda, K.; Kanayama, N.; Fujita, M.; Takarada, T.; Maeda, M. DNA Terminal Mismatch-Induced Stabilization of Polymer Micelles from RAFT-Generated poly(N-isopropylacrylamide)-DNA Block Copolymers. *Chem. - Asian J.* **2013**, *8*, 3079–3084.
- (199) Kim, C. J.; Jeong, E. H.; Lee, H.; Park, S. J. A Dynamic DNA Nanostructure with Switchable and Size-Selective Molecular Recognition Properties. *Nanoscale* **2019**, *11*, 2501–2509.
- (200) Zhang, K.; Zhu, X.; Jia, F.; Auyeung, E.; Mirkin, C. A. Temperature-Activated Nucleic Acid Nanostructures. *J. Am. Chem. Soc.* **2013**, *135*, 14102–14105.
- (201) Turek, V. A.; Chikkaraddy, R.; Cormier, S.; Stockham, B.; Ding, T.; Keyser, U. F.; Baumberg, J. J. Thermo-Responsive Actuation of a DNA Origami Flexor. *Adv. Funct. Mater.* **2018**, *28*, 1706410.
- (202) Alemdaroglu, F. E.; Wang, J.; Borsch, M.; Berger, R.; Herrmann, A. Enzymatic Control of the Size of DNA Block Copolymer Nanoparticles. *Angew. Chem., Int. Ed.* **2008**, *47*, 974–976.
- (203) Wu, F.; Zhao, Z.; Chen, C.; Cao, T.; Li, C.; Shao, Y.; Zhang, Y.; Qiu, D.; Shi, Q.; Fan, Q.-H.; et al. Self-Collapsing of Single Molecular Poly-Propylene Oxide (PPO) in a 3D DNA Network. *Small* **2018**, *14*, 1703426.
- (204) Lee, P. W.; Hsu, S. H.; Tsai, J. S.; Chen, F. R.; Huang, P. J.; Ke, C. J.; Liao, Z. X.; Hsiao, C. W.; Lin, H. J.; Sung, H. W. Multifunctional Core-Shell Polymeric Nanoparticles for Transdermal DNA Delivery and Epidermal Langerhans Cells Tracking. *Biomaterials* **2010**, *31*, 2425–2434.
- (205) Guo, A.; Wang, Y.; Xu, S.; Zhang, X.; Li, M.; Liu, Q.; Shen, Y.; Cui, D.; Guo, S. Preparation and Evaluation of pH-Responsive Charge-Convertible Ternary Complex FA-PEI-CCA/PEI/DNA with Low Cytotoxicity and Efficient Gene Delivery. *Colloids Surf., B* **2017**, *152*, 58–67.
- (206) Yuan, Y.; Zhang, C.-J.; Liu, B. A Photoactivatable AIE Polymer for Light-Controlled Gene Delivery: Concurrent Endo/Lysosomal Escape and DNA Unpacking. *Angew. Chem., Int. Ed.* **2015**, *54*, 11419–11423.
- (207) Zhao, Z.; Wang, L.; Liu, Y.; Yang, Z.; He, Y. M.; Li, Z.; Fan, Q. H.; Liu, D. pH-Induced Morphology-Shifting of DNA-b-poly(propylene oxide) Assemblies. *Chem. Commun.* **2012**, *48*, 9753–9755.
- (208) Bousmail, D.; Chidchob, P.; Sleiman, H. F. Cyanine-Mediated DNA Nanofiber Growth with Controlled Dimensionality. *J. Am. Chem. Soc.* **2018**, *140*, 9518–9530.
- (209) DeLuca, M.; Shi, Z.; Castro, C. E.; Arya, G. Dynamic DNA Nanotechnology: Toward Functional Nanoscale Devices. *Nanoscale Horiz.* **2020**, *5*, 182–201.
- (210) Kopperger, E.; List, J.; Madhira, S.; Rothfischer, F.; Lamb, D. C.; Simmel, F. C. A Self-Assembled Nanoscale Robotic Arm Controlled by Electric Fields. *Science* **2018**, *359*, 296–300.
- (211) Lauback, S.; Mattioli, K. R.; Marras, A. E.; Armstrong, M.; Rudibaugh, T. P.; Sooryakumar, R.; Castro, C. E. Real-Time Magnetic Actuation of DNA Nanodevices via Modular Integration with Stiff Micro-Levers. *Nat. Commun.* **2018**, *9*, 1446.

- (212) Bousmail, D.; Amrein, L.; Fakhoury, J. J.; Fakh, H. H.; Hsu, J. C. C.; Panasci, L.; Sleiman, H. F. Precision Spherical Nucleic Acids for Delivery of Anticancer Drugs. *Chem. Sci.* **2017**, *8*, 6218–6229.
- (213) Zhu, S.; Xing, H.; Gordlichuk, P.; Park, J.; Mirkin, C. A. PLGA Spherical Nucleic Acids. *Adv. Mater.* **2018**, *30*, No. e1707113.
- (214) Ding, F.; Mou, Q.; Ma, Y.; Pan, G.; Guo, Y.; Tong, G.; Choi, C. H. J.; Zhu, X.; Zhang, C. A Crosslinked Nucleic Acid Nanogel for Effective siRNA Delivery and Antitumor Therapy. *Angew. Chem., Int. Ed.* **2018**, *57*, 3064–3068.
- (215) Choi, C. H.; Hao, L.; Narayan, S. P.; Auyeung, E.; Mirkin, C. A. Mechanism for the Endocytosis of Spherical Nucleic Acid Nanoparticle Conjugates. *Proc. Natl. Acad. Sci. U. S. A.* **2013**, *110*, 7625–7630.
- (216) Giljohann, D. A.; Seferos, D. S.; Patel, P. C.; Millstone, J. E.; Rosi, N. L.; Mirkin, C. A. Oligonucleotide Loading Determines Cellular Uptake of DNA-Modified Gold Nanoparticles. *Nano Lett.* **2007**, *7*, 3818–3821.
- (217) Alemdaroglu, F. E.; Alemdaroglu, N. C.; Langguth, P.; Herrmann, A. Cellular Uptake of DNA Block Copolymer Micelles with Different Shapes. *Macromol. Rapid Commun.* **2008**, *29*, 326–329.
- (218) Miller, D. W.; Batrakova, E. V.; Waltner, T. O.; Alakhov, V. Y.; Kabanov, A. V. Interactions of Pluronic Block Copolymers with Brain Microvessel Endothelial Cells: Evidence of Two Potential Pathways for Drug Absorption. *Bioconjugate Chem.* **1997**, *8*, 649–657.
- (219) Bates, P. J.; Laber, D. A.; Miller, D. M.; Thomas, S. D.; Trent, J. O. Discovery and Development of the G-rich Oligonucleotide AS1411 as a Novel Treatment for Cancer. *Exp. Mol. Pathol.* **2009**, *86*, 151–164.
- (220) Reyes-Reyes, E. M.; Teng, Y.; Bates, P. J. A New Paradigm for Aptamer Therapeutic AS1411 Action: Uptake by Macropinocytosis and its Stimulation by a Nucleolin-Dependent Mechanism. *Cancer Res.* **2010**, *70*, 8617–8629.
- (221) Huang, F.; You, M.; Chen, T.; Zhu, G.; Liang, H.; Tan, W. Self-Assembled Hybrid Nanoparticles for Targeted Co-Delivery of Two Drugs into Cancer Cells. *Chem. Commun.* **2014**, *50*, 3103–3105.
- (222) Xiao, F.; Lin, L.; Chao, Z.; Shao, C.; Chen, Z.; Wei, Z.; Lu, J.; Huang, Y.; Li, L.; Liu, et al. Organic Spherical Nucleic Acids for the Transport of a NIR-II-Emitting Dye Across the Blood-Brain Barrier. *Angew. Chem., Int. Ed.* **2020**, *59*, 9702–9710.
- (223) Xue, J.; Zhao, Z.; Zhang, L.; Xue, L.; Shen, S.; Wen, Y.; Wei, Z.; Wang, L.; Kong, L.; Sun, H.; et al. Neutrophil-Mediated Anticancer Drug Delivery for Suppression of Postoperative Malignant Glioma Recurrence. *Nat. Nanotechnol.* **2017**, *12*, 692–700.
- (224) Tang, W.; Fan, W.; Lau, J.; Deng, L.; Shen, Z.; Chen, X. Emerging Blood-Brain-Barrier-Crossing Nanotechnology for Brain Cancer Theranostics. *Chem. Soc. Rev.* **2019**, *48*, 2967–3014.
- (225) Ni, Q.; Zhang, F.; Zhang, Y.; Zhu, G.; Wang, Z.; Teng, Z.; Wang, C.; Yung, B. C.; Niu, G.; Lu, G.; et al. In Situ shRNA Synthesis on DNA-Polylactide Nanoparticles to Treat Multidrug Resistant Breast Cancer. *Adv. Mater.* **2018**, *30*, 1705737.
- (226) Tan, X.; Li, B. B.; Lu, X.; Jia, F.; Santori, C.; Menon, P.; Li, H.; Zhang, B.; Zhao, J. J.; Zhang, K. Light-Triggered, Self-Immolative Nucleic Acid-Drug Nanostructures. *J. Am. Chem. Soc.* **2015**, *137*, 6112–6115.

6.4 Publication „Squaric Ester-Based, pH-Degradable Nanogels: Modular Nanocarriers for Safe, Systemic Administration of Toll-like Receptor 7/8 Agonistic Immune Modulators“

Squaric Ester-Based, pH-Degradable Nanogels: Modular Nanocarriers for Safe, Systemic Administration of Toll-like Receptor 7/8 Agonistic Immune Modulators

Anne Huppertsberg, Leonard Kaps, Zifu Zhong, Sascha Schmitt, Judith Stickdorn, Kim Deswarte, Francis Combes, Christian Czysch, Jana De Vrieze, Sabah Kasmi, Niklas Choteschovsky, Adrian Klefenz, Carolina Medina-Montano, Pia Winterwerber, Chaojian Chen, Matthias Bros, Stefan Lienenklaus, Niek N. Sanders, Kaloian Koynov, Detlef Schuppan, Bart N. Lambrecht, Sunil A. David, Bruno G. De Geest, and Lutz Nuhn*

Cite This: *J. Am. Chem. Soc.* 2021, 143, 9872–9883

Read Online

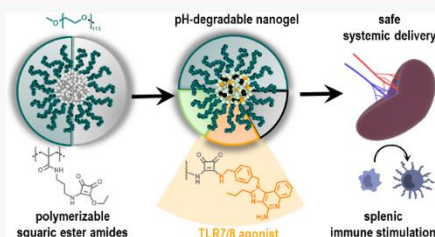
ACCESS |

Metrics & More

Article Recommendations

Supporting Information

ABSTRACT: Small-molecular Toll-like receptor 7/8 (TLR7/8) agonists hold promise as immune modulators for a variety of immune therapeutic purposes including cancer therapy or vaccination. However, due to their rapid systemic distribution causing difficult-to-control inflammatory off-target effects, their application is still problematic, in particular systemically. To address this problem, we designed and robustly fabricated pH-responsive nanogels serving as versatile immunodrug nanocarriers for safe delivery of TLR7/8-stimulating imidazoquinolines after intravenous administration. To this aim, a primary amine-reactive methacrylamide monomer bearing a pendant squaric ester amide is introduced, which is polymerized under controlled RAFT polymerization conditions. Corresponding PEG-derived squaric ester amide block copolymers self-assemble into precursor micelles in polar protic solvents. Their cores are amine-reactive and can sequentially be transformed by acid-sensitive cross-linkers, dyes, and imidazoquinolines. Remaining squaric ester amides are hydrophilized affording fully hydrophilic nanogels with profound stability in human plasma but stimuli-responsive degradation upon exposure to endolysosomal pH conditions. The immunomodulatory behavior of the imidazoquinolines alone or conjugated to the nanogels was demonstrated by macrophages *in vitro*. *In vivo*, however, we observed a remarkable impact of the nanogel: After intravenous injection, a spatially controlled immunostimulatory activity was evident in the spleen, whereas systemic off-target inflammatory responses triggered by the small-molecular imidazoquinoline analogue were absent. These findings underline the potential of squaric ester-based, pH-degradable nanogels as a promising platform to permit intravenous administration routes of small-molecular TLR7/8 agonists and, thus, the opportunity to explore their adjuvant potency for systemic vaccination or cancer immunotherapy purposes.



INTRODUCTION

Nanosized drug carriers can improve the pharmacokinetics of potent but systemically toxic small-molecular drugs; however, key challenges remain to establish robust fabrication processes, prevent premature drug release, and guarantee sufficient carrier integrity under physiological conditions. Moreover, opportunities toward on-demand drug release and carrier degradation would be desired.^{1–4} Polymer-based nanocarriers can be designed to address these challenges chemically, especially for applications in immunotherapy.^{5,6} A spatiotemporal control over recently identified, highly potent immunomodulators is crucial, since their drug leakage can cause uncontrolled systemic immune responses combined with immense off-target toxicity.^{7,8} Covalent conjugation of immunomodulators to polymer-based nanocarriers that control the drug's pharmaco-

kinetic profile can pave the way to safer systemic applications in cancer immunotherapy or as adjuvants during vaccination.^{9–11}

One promising class of immunomodulators are agonists of Toll-like receptor 7/8 (TLR7/8) that usually sense viral single-stranded RNA and raise an immediate cellular innate immune response.¹² Imidazoquinolines, a class of synthetic TLR7/8 agonists, are particularly powerful in stimulating these receptors.

Received: April 9, 2021
Published: June 24, 2021



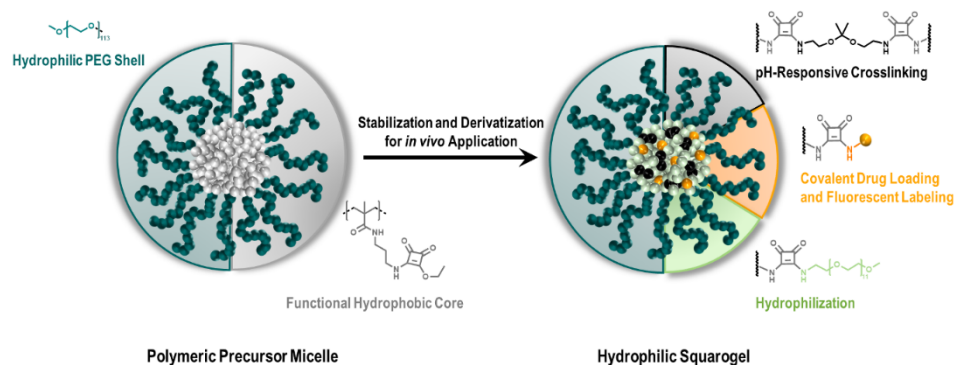


Figure 1. Squaric ester-based nanogels derived from polymeric precursor micelles formed by self-assembly of squaric ester amide-containing amphiphilic block copolymers. Subsequent transformation for *in vivo* application is achieved by amidation of pendant squaric ester amide groups inside the amine-reactive, hydrophobic core including pH-responsive cross-linking, covalent drug or dye loading, and hydrophilization, affording fully hydrophilic drug-loaded nanogels.

They can induce the maturation of antigen-presenting cells and the release of cytokines that promote cellular immune responses, especially via activation of T helper 1 (Th1) and cytotoxic T cells.^{13,14} The latter play a key role in combating cancer and intracellular pathogens.^{15,16} As TLR7/8 are located at the endosomal membrane of phagocytosing innate immune cells, they can be preferentially targeted by nanocarriers equipped with imidazoquinoline-derived TLR7/8 agonists.¹⁷

Previous studies demonstrated that undesired systemic inflammation by the highly potent small-molecular TLR7/8 agonist 1-(4-(aminomethyl)benzyl)-2-butyl-1*H*-imidazo[4,5-*c*]quinolin-4-amine (IMDQ)¹⁸ can be circumvented through its covalent conjugation to different types of nanocarriers. Thereby, its activity upon subcutaneous administration can be restricted to the site of injection and the draining lymph nodes. A variety of nanocarriers has been investigated for this objective including lipids,^{19,20} polysaccharides,²¹ synthetic polymers,²² micelles,²³ and nanogels.^{24,25} These nanocarrier formulations have generally been injected subcutaneously and provided a local TLR7/8 activation by lymph node trafficking. However, a few findings revealed that intravenous injections would result in even improved immune responses.^{26–29} Especially during intravenous nanoparticle vaccination, more stem-like antigen-specific CD8⁺ T cells are generated that lead to superior antitumor responses, especially during immune checkpoint inhibition therapy.³⁰ Yet, systemic treatments set new requirements for safety and allow for new targeting strategies as compared to local administration. Thus, new efforts have to be made in the design of novel blood-stable nanocarriers enabling intravenous and organ-targeted TLR7/8 agonist administration.

A straightforward way to covalently load IMDQ into nanocarriers is self-assembled reactive ester block copolymers that are converted by amidation reactions into pH-degradable nanogels.^{24,25,31} Via controlled radical polymerization processes we have previously generated poly(triethylene glycol monomethyl ether methacrylate)-*block*-poly(pentafluorophenyl methacrylate) as precursor polymers for which the pentafluorophenyl esters trigger both micellar self-assembly in polar aprotic solvents such as DMSO and selective reactivity toward primary amines.^{32,33} This could also be applied for conjugation of IMDQ and subsequent transformation into fully hydrophilic

nanogels. However, for this approach the hydrophilic triethylene glycol monomethyl ether methacrylate block renders a lower critical solution temperature in water,³⁴ which can impair the required shielding properties after exposure to biological media. Additionally, the applied pentafluorophenyl ester exhibits only limited hydrolytic resistance. Already slight traces of water can risk its hydrolysis into methacrylic acid³⁵ and, thus, impede access to the nanogel formation process. In addition, during amidation toxic pentafluorophenol is released,³⁶ which requires careful purification prior to applications *in vitro* or *in vivo*.

Consequently, alternative amine-reactive groups with higher hydrolytic stability and nontoxic byproducts are needed. Tietze et al. reported on squaric alkyl esters for selective amine coupling reactions with high functional group tolerance as well as excellent yields, even under mild conditions in aqueous media.³⁷ Due to their homo-bifunctionality squaric alkyl esters can consecutively be aminolyzed by two different amines, whereby an enhanced aromatic stability after first amidation is obtained, providing reduced reactivity for another amidation. Thus, it assures a controlled sequential squaric bisamide formation.³⁸ Compared to other reactive esters (including pentafluorophenyl) this alternative linking chemistry allows conjugation in biocompatible solvents (e.g., water, ethanol) while releasing alcohols as nontoxic byproducts.³⁹

In this study, we therefore introduce polymerizable squaric ester amides for a more robust and hydrolysis-resistant postpolymerization modification of pH-degradable, immunodrug-loaded nanogels. Methacrylamides with pendant squaric ester amides are grafted under controlled radical polymerization conditions onto linear hydrophilic PEG chains and serve as solvophobic groups for spontaneous micellar self-assembly now also in polar protic solvents (Figure 1).

By sequential functionalization with primary amines, they can be converted into a modular pH-responsive nanogel platform. This process supports covalent conjugation of both hydrophobic and hydrophilic drugs into the core of these nanogels, e.g., the amine-functionalized TLR7/8 agonist IMDQ. Due to its high degree of PEGylation, this system features excellent stability in blood that permits intravenous administration and local maturation of antigen-presenting immune cells inside the spleen, while circumventing systemic inflammatory responses

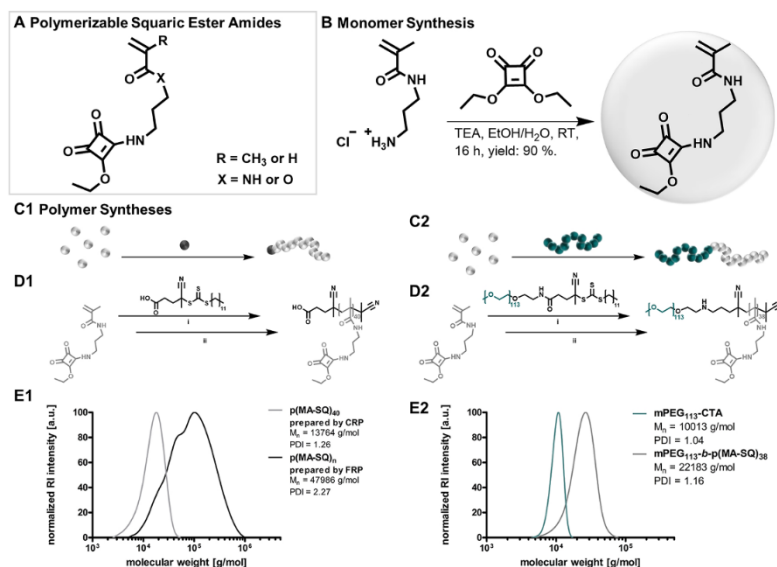


Figure 2. Synthesis of polymerizable squaric ester amides. (A) General chemical structure of synthesized monomers with a pendant squaric ester amide group. (B) Synthesis route toward the most suitable monomer squaric ester amide methacrylamide (MA-SQ). (C) Schematic illustrations and (D) synthesis schemes of RAFT homopolymerization of MA-SQ with a small molecular trithiocarbonate chain transfer agent (TTC-CTA) (C1 and D1) and block copolymerization with macro-chain-transfer agent PEG-TTC-CTA (C2 and D2) (reaction conditions: (i) DMF, 70 °C, 0.2 equiv AIBN per 1.0 equiv TTC-CTA, and (ii) DMF, 70 °C, 50 equiv AIBN (to remove the TTC end group)). (E) Molecular weight distributions of polymers obtained by radical polymerization: (E1) RAFT-derived homopolymer compared to the homopolymer obtained by FRP; (E2) RAFT-derived block copolymer compared to PEG-TTC-CTA as macro-chain-transfer agent.

caused by the unbound TLR7/8 agonist. Altogether, these observations demonstrate the broad versatility of amine-reactive squaric ester-based precursor polymers and how they provide access to a modular pH-degradable nanogel platform for safe systemic administration of immune modulators.

RESULTS AND DISCUSSION

We first aimed to synthesize a polymerizable squaric ester amide monomer that can be polymerized under controlled conditions into well-defined homo- and block copolymers using reversible addition–fragmentation chain transfer (RAFT) agents. While squaric ester amides have already been studied as amine-reactive groups for atom transfer radical polymerization (ATRP)⁴⁰ or RAFT⁴¹ chain transfer agents, to the best of our knowledge, the use of squaric esters as functional side groups of monomers and corresponding polymers has not been introduced before. They provide access to a new class of hydrolysis-resistant, amine-reactive precursor polymers for multiple postpolymerization purposes.³⁹ We investigated the polymer's reactivity toward different types of amines and observed a self-assembly behavior of corresponding block copolymers in water or ethanol. The core of the resulting micelles can be used to ligate fluorescent dyes or IMDQ followed by core-cross-linking and hydrophilization affording pH-degradable nanogels. Subsequent *in vitro* and *in vivo* characterization revealed long blood circulation and maturation of antigen-presenting cells in the spleen while omitting inflammatory off-target effects.

Monomer and Polymer Syntheses. Initially, polymerizable squaric ester amide monomers with acrylate, acrylamide, or methacrylamide groups were synthesized (Figure 2A). Direct (meth-)acryloylation of 2-aminoethanol-functionalized squaric ester amides failed due to occurring bisacryloyl derivatives and autopolymerization. For instance, we carefully treated 3-ethoxy-4-((2-hydroxyethyl)amino)cyclobut-3-ene-1,2-dione with acryloyl chloride but obtained besides the desired squaric ester amide acrylate product 2-((2-ethoxy-3,4-dioxocyclobut-1-en-1-yl)amino) ethyl acrylate (At-SQ) also a bisacrylated species (At-SQ-At) at similar yields, as documented in the Supporting Information (Figures S14–S23). We therefore opted for (meth-)acrylamides by controlled monoamidation of squaric acid diethyl ester with amine-functionalized (meth-) acrylamides. Unfortunately, due to their aza-Michael reactivity, amino-functionalized (meth-)acrylamides are only stable as protonated salt species. While the corresponding methacrylamide-based monomer was commercially available, we synthesized the TFA salt of *N*-(3-aminopropyl)acrylamide as corresponding acrylamide derivative (Supporting Information Figure S7). It was converted with squaric acid diethyl ester catalyzed by triethylamine in ethanol and water and provided the desired acrylamide monomer at acceptable yields (64%, A-SQ, NMR characterization in Supporting Information Figures S10–S13). However, several attempts to polymerize it, even under free radical polymerization (FRP) conditions, failed or yielded only conversions below 30%. Fortunately, synthesis and polymerization of the methacrylamide analogue was more promising.

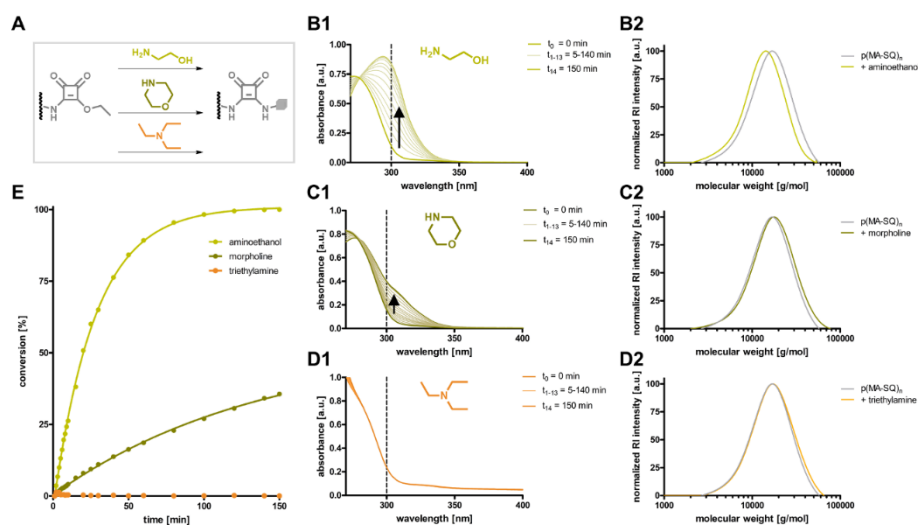


Figure 3. Amine selectivity of pendant squaric amide groups of $p(\text{MA-SQ})_{40}$. (A) Scheme for the conversion of polymeric squaric ester amides to squaric bisamides by amidation with aminoethanol, morpholine, or triethylamine. UV/vis spectra during conversion with (B1) aminoethanol, (C1) morpholine, or (D1) triethylamine and the corresponding molecular weight distributions of $p(\text{MA-SQ})_{40}$ before and after conversion with (B2) aminoethanol, (C2) morpholine, or (D2) triethylamine. (E) Corresponding conversions estimated by UV absorbance over time.

Monoamidation of squaric acid diethyl ester with the commercially available *N*-(3-aminopropyl)methacrylamide hydrochloride was again conducted in ethanol and water catalyzed by triethylamine. It afforded a squaric ester amide methacrylamide monomer (MA-SQ) with a high yield of 90% (Figure 2B, NMR and MS characterization in Supporting Information, Figures S1–S6).

MA-SQ could afterward be polymerized under FRP conditions at 70 °C using AIBN as radical source with quantitative conversion. Consequently, it was an ideal candidate for RAFT polymerization. We chose a trithiocarbonate as chain transfer agent (TTC-CTA) and polymerized MA-SQ with either a small-molecular TTC-CTA or a PEG-functionalized macro-TTC-CTA (Supporting Information Figure S24–S26; note that instead of commercially available macro-TTC-CTAs bearing an ester group between PEG and the CTA group, we preferred to apply an amide derivative to avoid possible ester aminolysis and cleavage during amidation). At a monomer to CTA ratio of 50:1, conversions of 75–80% were found affording $p(\text{MA-SQ})_{40}$ as homopolymer and $\text{PEG}_{113}\text{-}b\text{-}p(\text{MA-SQ})_{38}$ as block copolymer (Figure 2C/D).

Consistent with earlier reports, NMR analysis validated that squaric ester amide moieties withstood radical polymerization conditions and remained intact (Figures S28 and S32).^{40,41} Molecular weight distributions of $p(\text{MA-SQ})_{40}$ obtained by size-exclusion chromatography (SEC) revealed well-defined homopolymers with a number-average molar mass (M_n) of 13 800 g/mol and polydispersity index (PDI) of 1.26 (Figure 2E1). In stark contrast to the FRP, the RAFT homopolymers of MA-SQ confirmed controlled polymerization conditions. Via NMR spectroscopy, monomer conversion over time demonstrated first-order kinetics for the polymer formation (Figures S34 and S35). Similar conditions were applied during block copoly-

merization and provided polymers with a narrow PDI of 1.16 and M_n of 22 200 g/mol (Figure 2E2). The molecular weight shift of the block copolymer ($\text{PEG}_{113}\text{-}b\text{-}p(\text{MA-SQ})_{38}$) compared to PEG-TTC-CTA clearly attested full MA-SQ monomer grafting onto the macro-CTA. Additionally, DOSY NMR analysis confirmed successful block copolymer formation by providing identical diffusion coefficients of both blocks (Figure S29). To avoid interference with the trithiocarbonate (TTC) end group during subsequent amidation of the squaric ester amides, both homo- and block copolymer were further treated with an excess of AIBN for end group removal. This additional step did not impair the composition or distribution of the polymers (compare Supporting Information Figures S30 and S33).

Amine-Selective Conversion. In order to verify amine reactivity, the homopolymer $p(\text{MA-SQ})_{40}$ was first reacted with an excess of primary, secondary, or tertiary amine. As model compounds aminoethanol, morpholine, and triethylamine were selected (Figure 3A, note that these reactions were conducted in DMSO to ensure complete solubility of the homopolymer). Interestingly, the formed squaric bisamides provide an absorption maximum around 300 nm compared to the squaric ester amide educts. Therefore, their aminolysis can easily be monitored over time by UV/vis absorbance spectroscopy.⁵⁹ A strong and fast increase in absorbance at 300 nm revealed rapid and quantitative conversion of the squaric ester amides by the primary amine aminoethanol. The secondary amine morpholine could only convert about 25% after 2 h, while no conversion was observed with triethylamine as tertiary amine (Figure 3B1–D1, Figure 3E, and Supporting Information Figure S37). The respective homopolymers were isolated by precipitation in diethyl ether. Recorded molecular weight distributions by SEC demonstrated no significant change in M_n and PDI for $p(\text{MA-SQ})_{40}$.

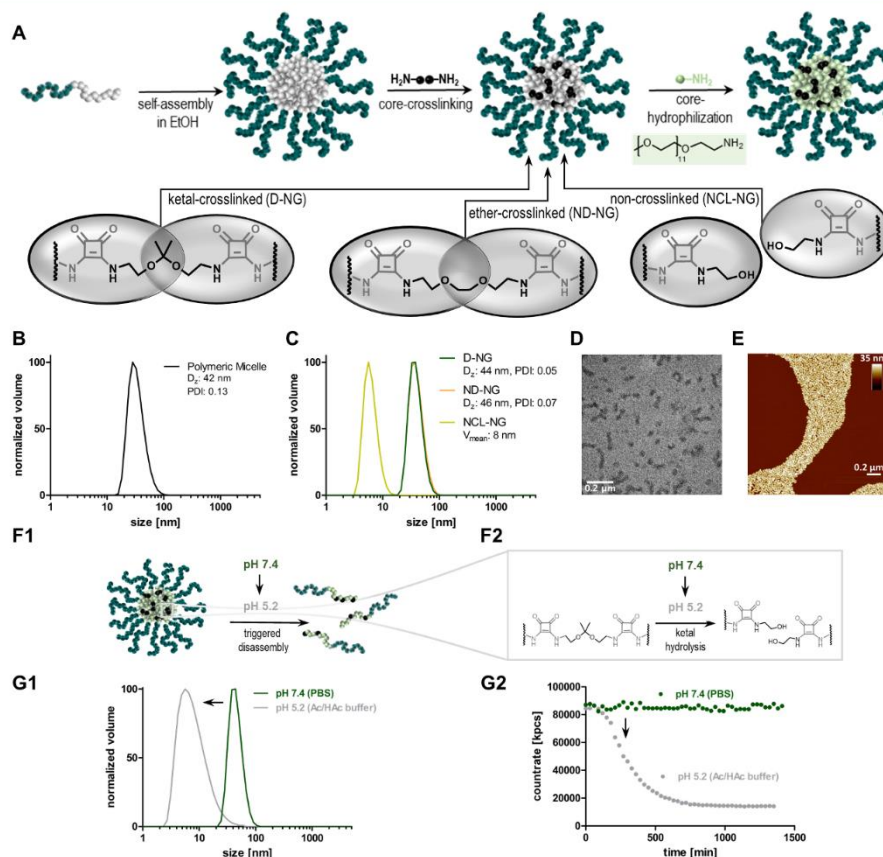


Figure 4. Nanogel fabrication process. (A) Scheme of sequential nanogel formation from squaric ester amide-derived, self-assembling precursor polymers. Based on the cross-linking strategy, degradable nanogels (D-NG) as well as nondegradable or non-cross-linked control samples (ND-NG, NCL-NG) can be obtained. (B) DLS size distribution of self-assembled micelles in ethanol and (C) fully fabricated nanogels D-NG, ND-NG, and NCL-NG in PBS. (D) TEM image of D-NG. (E) AFM image of D-NG. (F1 and F2) Scheme of ketal-hydrolysis in acidic media resulting in D-NG's disassembly into soluble unimers (NCL-NG). (G) DLS study of D-NG at neutral pH in PBS compared to mildly acidic pH in HAc/Ac buffer by (G1) size distribution and (G2) DLS count rate over time.

SQ₄₀ treated with triethylamine, while a complete peak shift to smaller molecular weights was found after conversion with aminoethanol (Figure 3B2–D2). The squaric ester amide polymers treated with morpholine showed only a minimal peak shift reflecting their incomplete conversion. These observations were confirmed by NMR analysis (Figures S38 and S39). Further studies indicated that full conversion by secondary amine morpholine can still be achieved at elevated temperature and extended reaction time (Figure S40, e.g., after 22 h at 70 °C complete squaric ester amide aminolysis was demonstrated; compare Figures S41 and S42). These results highlight the suitability of squaric ester amides as reactive polymer side groups for quantitative postpolymerization modification with preferentially fast conversion of primary amines.

Nanogel Fabrication and Characterization. Polymeric squaric ester amides can be used as precursors to introduce new

functionalities by amidation reactions. Following the design concept of Figure 4A, we were interested in whether this postpolymerization modification can also be combined with self-assembly to sequentially access nanogels (by micelle formation, covalent core-cross-linking, and transformation of the core from hydrophobic to hydrophilic). The well-defined amphiphilic block copolymer PEG₁₁₃-*b*-p(MA-SQ)₃₈ was suspended in ethanol and treated with ultrasound, yielding narrowly dispersed micelles. By dynamic light scattering (DLS) their sizes were analyzed, revealing a *z*-average diameter (D_z) of 44 nm and a narrow PDI of 0.13 (Figure 4B). Next, the polarity of the core was switched chemically by exploiting its reactivity toward hydrophilic amines. After addition of 5.0 equiv of PEG₁₁-amine the micelles disassembled within 30 min and provided fully soluble polymers (Supporting Information Figures S43 and S44; note that amines like aminoethanol did not increase the polarity

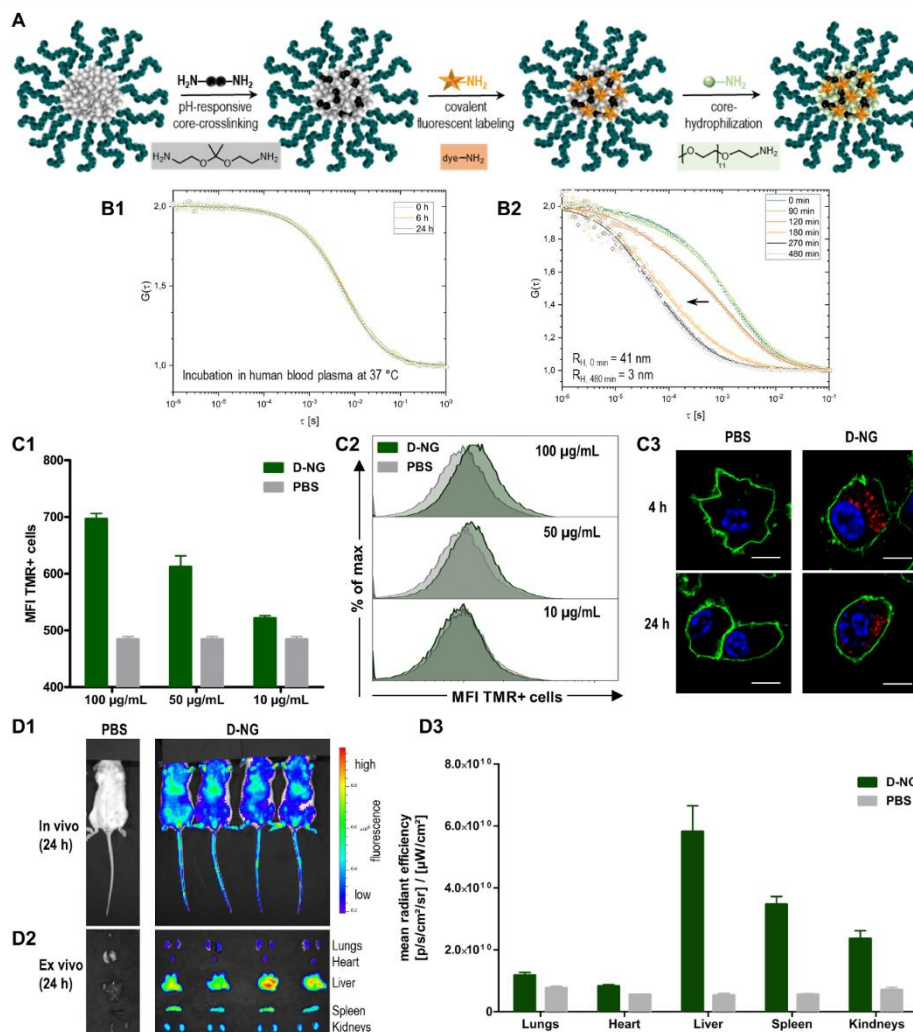


Figure 5. Fluorescently labeled nanogels provide sufficient particle integrity for safe *in vivo* administration. (A) Scheme of sequential nanogel fabrication with *in situ* installed fluorescent dye-labeling. (B) Oregon Green cadaverine (OG)-labeled nanogels (D-NG) investigated by fluorescence correlation spectroscopy toward stability in plasma and the ability to disassemble upon exposure to endolysosomal pH values: (B1) normalized autocorrelation curves (dots) and corresponding fits (solid line) of OG-labeled D-NG incubated in human blood plasma for 0, 6, and 24 h; (B2) normalized autocorrelation curves (dots) and corresponding fits (solid line) of OG-labeled D-NG incubated in acidic buffer (pH 5.2) over time. (C) Tetramethylrhodamine cadaverine (TMR)-labeled nanogels (D-NG) investigated for the *in vitro* uptake behavior in RAW murine macrophages using flow cytometry and confocal microscopy imaging ($n = 3$): (C1) cellular mean fluorescence intensities (MFI) of RAW macrophages incubated with TMR-labeled D-NG at 100, 50, and 10 $\mu\text{g/mL}$ for 24 h; (C2) corresponding histograms of RAW macrophages incubated with TMR-labeled D-NG at 100, 50, and 10 $\mu\text{g/mL}$ for 24 h ($n = 3$) or PBS (control). (C3) Confocal microscopy images of RAW macrophages incubated with TMR-labeled D-NG at 100 $\mu\text{g/mL}$ for 4 and 24 h (blue: nuclei stained with Hoechst 33258; green: cell membrane stained with cholera toxin B (CTB)-AF488; red: TMR-labeled D-NG, scale bar 10 μm). (D) Near infrared dye 800RS cadaverine (NIR)-labeled nanogels (NIR-labeled D-NG) investigated for their biodistribution after systemic application to BALB/c mice via tail vein injection using an *in vivo* NIR-imaging system (IVIS): (D1) whole body fluorescence imaging 24 h after intravenous injection of 100 μL of NIR-labeled D-NG dispersion (2 mg/mL); (D2) *ex vivo* organ distribution imaging and (D3) semiquantitative analysis ($n = 4$).

9877

<https://doi.org/10.1021/jacs.1c03772>
J. Am. Chem. Soc. 2021, 143, 9872–9883

to unfold the micelles). Thus, core hydrophilization is possible to fabricate fully hydrophilic nanogels.

Next, polymeric micelles were modified by pH-responsive cross-links prior to hydrophilization (note that the following process is possible in both pure ethanol and buffered water; compare Supporting Information Figure S50). In relation to 1.0 equiv of pendant squaric ester amide moieties, 0.15 equiv of the ketal-containing bisamine 2,2'-bis(aminoethoxy)propane was added. Its ketal unit renders the nanocarriers' sensitivity to endosomal acidic pH. As shown in previous reports, it can effectively hydrolyze at pH 5, resulting in a disassembly of nanogels into soluble polymer chains.^{33,42,43} In order to provide a nondegradable nanogel version, the core of the micelles was conjugated with 0.15 equiv of an ether-containing bisamine (1,2-bis(aminoethoxy)ethane). Additionally, a non-cross-linked soluble polymer representing the ketal-cross-linked nanogel after hydrolysis was obtained by aminolysis with 0.3 equiv of 2-aminoethanol. For each species, all remaining squaric ester amide moieties were finally converted with 3.0 equiv of PEG₁₁-amine, resulting in fully hydrophilic nanogel or soluble polymer species (Figure 4A). All samples were purified by dialysis against water containing 0.1 wt % ammonia to prevent premature ketal-hydrolysis. Subsequent lyophilization afforded the nanogels as dry powders, which could be easily redispersed in PBS buffer.

UV/vis absorbance spectroscopy could again be used to monitor the conversion of the squaric esters inside the self-assembled micelles/core-cross-linked nanogels by following the increase of the absorption maximum around 300 nm related to the formed squaric bisamides (compare Supporting Information Figures S46–S48). Sequential addition of primary amines for functionalization, cross-linking, and final conversion of the remaining squaric ester amide moieties with PEG₁₁-amine yielded a stepwise increase of the absorbance. Note that no difference between the absorption after addition of 3.0 equiv of PEG₁₁-amine and the purified nanogel after extensive dialysis against water with 0.1 wt % ammonia could be found, confirming quantitative squaric ester conversion inside the nanogels during the fabrication process (compare Supporting Information Figures S46–S48).

As shown by DLS analysis, the ketal-cross-linked, degradable nanogel (D-NG) showed a very narrow monomodal distribution and a D_z of 44 nm, which was similar to the size of the precursor micelle. The same was found for the nondegradable nanogel (ND-NG, $D_z = 46$ nm), while for the non-cross-linked version (NCL-NG) a significantly lower count rate was detected indicating the absence of particular scattering. The average volume diameter of the NCL-NG was 8 nm (Figure 4C). The ketal-cross-linked nanogels were imaged by transmission electron microscopy (TEM) and atomic force microscopy (AFM). The dried particles could be recorded as spherical and some slightly elongated morphologies with narrow dispersities (Figure 4D and E; Supporting Information Figure S49). To prove that the ketal-cross-linked nanogels fully disassemble into soluble unimers under endolysosomal pH conditions (Figure 4F1,F2), several DLS stability studies at pH 7.4 or 5.2 were performed. D-NG was exposed to acidic pH in acetate buffer at 10 mg/mL and subsequently monitored over time by DLS. A gradual decline in count rate within 600 min was observed, while a decrease of the particles' size distribution demonstrated complete nanogel disassembly into single polymer chains (Figure 4G1,G2). In contrast, no change in count rate or size was observed at neutral pH for D-NG in PBS (Figure 4G1,G2).

This was also the case for ND-NG and NCL-NG at both pH levels over time (Supporting Information Figure S54). Thus, ketal-cross-linked nanogels represent ideal candidates for drug delivery due to their transient supramolecular architecture that unfolds into secretable smaller entities upon exposure to endolysosomal pH values.

Nanogel Functionalization. To further investigate the nanogels' covalent drug delivery function, their squaric ester amides were first used to introduce fluorescent labels. Prior to the described cross-linking and core-hydrophilization, 0.01 equiv of amine-bearing fluorescent dyes (e.g., Oregon Green cadaverine (OG), tetramethylrhodamine cadaverine (TMR), or the near-infrared dye 800RS cadaverine (NIR)) was conjugated to the core (Figure 5A). Covalent dye conjugation did not affect the nanogel fabrication process. To ensure the absence of free dye, nanogels were extensively spin-filtrated (MWCO: 10 000 g/mol) using a mixture of 0.1 wt % ammonia in water/EtOH (v/v, 1:2) in addition to the described purification methods. Dye labeling enables analyses of the nanocarriers' behavior in complex biological environment and, thus, provides key features to evaluate their applicability for immunomodulating drug delivery.

We first investigated the dye-labeled nanogel's stability in human blood plasma as complex biological medium relevant for *in vitro* and *in vivo* application. Selective monitoring of nanogel integrity over time was facilitated by fluorescence correlation spectroscopy (FCS). It provides information about the nanocarrier's size in solution by autocorrelation analysis of fluorescence intensity fluctuations that result from diffusional motions of fluorescent species (e.g., labeled nanocarriers) through a confocal volume.⁴⁴ After incubation of pH-degradable nanogels (OG-labeled D-NG) in human blood plasma for 0, 6, and 24 h at 37 °C, FCS analysis confirmed that the nanogel's autocorrelation curve and the corresponding hydrodynamic radius remained identical (Figure 5B1). Consequently, the carriers are profoundly stable under these biologically relevant conditions: Neither an increase of the nanogel's size, which would reflect aggregation with serum components nor its decrease was observed, which would imply nanogel degradation. The latter could only be observed by FCS when the ketal-cross-linked OG-labeled D-NG was again exposed to pH 5.2 using acetate buffer. As evident from the shift of the autocorrelation curves, one can perfectly observe a sequential disassembly of the nanogels into single unimers (Figure 5B2).

Next, cellular nanogel interaction was studied for TMR-labeled D-NG using flow cytometry as well as confocal microscopy. RAW macrophages were selected as model for phagocytosing cells of the reticuloendothelial system that usually rapidly engulf nanocarriers after systemic administration. However, only a minor uptake of D-NG was observed after dosing from 10 to 100 $\mu\text{g/mL}$. A weak increase in mean fluorescence intensity from 500 (basal autofluorescence) to 700 could be recorded by flow cytometry (Figure 5C1), and the resulting histogram provided only a minor but homogeneous shift of all cells to increased fluorescence (Figure 5C2). These observations were independent from the type of nanogel, as similar low mean fluorescence intensities and low TMR-positive cells were found for all species (D-NG, ND-NG, and NCL-NG; compare Supporting Information Figure S56). These results were further supported by confocal microscopy images of RAW macrophages incubated at 100 $\mu\text{g/mL}$ for both 4 and 24 h (Figure 5C3 and Supporting Information Figure S55). All cells provided a homogeneous intracellular localization of some

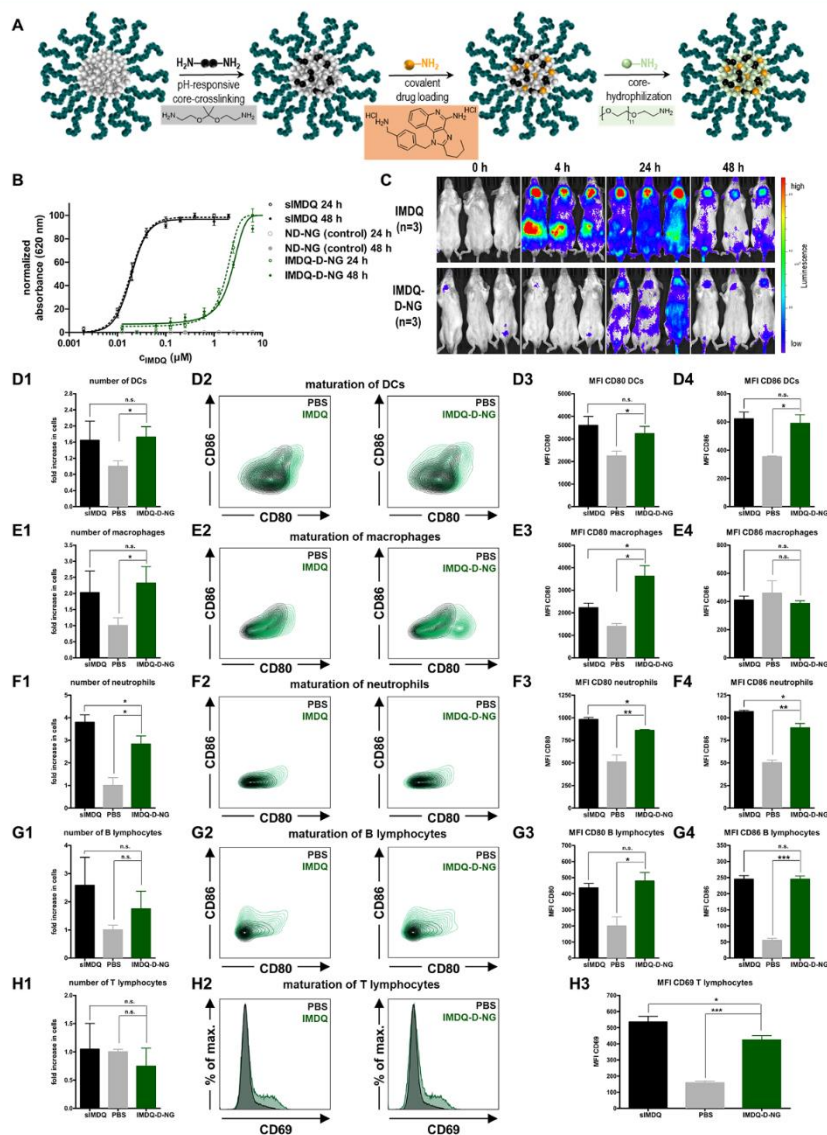


Figure 6. Squaric ester amide-based nanogels with covalently attached TLR7/8 agonist IMDQ. (A) Scheme of sequential nanogel fabrication with integral *in situ* conjugation of IMDQ. (B) TLR agonistic activity of soluble IMDQ (sIMDQ) and covalently attached IMDQ to degradable nanogels (IMDQ-D-NG) measured by NF- κ B activation of RAW Blue cells after 24 and 48 h via a Quanti-Blue reporter assay ($n = 4$). (C) Bioluminescence images of heterozygous IFN- β (IFN- $\beta^{\Delta\beta/lacZ}$) reporter mice intravenously injected with sIMDQ and covalently attached IMDQ-D-NG ($5 \mu\text{g}$ of IMDQ soluble or bound to nanogel in $100 \mu\text{L}$ of PBS); images were recorded before (0 h) as well as 4, 24, and 48 h after tail vein injection ($n = 3$). (D–H) Results of flow cytometric analysis of isolated splenocytes (compare Figure S60 for the applied gating procedure) after systemic administration of soluble IMDQ vs nanogel-conjugated IMDQ (1: fold increase of cells in the spleen in relation to PBS treated mice; 2: maturation plots by CD86 and CD80 or CD69 for T cells; 3: corresponding MFI values). (D) Dendritic cells (DCs), (E) macrophages, (F) neutrophils, (G) B lymphocytes, and (H) T lymphocytes.

9879

<https://doi.org/10.1021/jacs.1c03772>
J. Am. Chem. Soc. 2021, 143, 9872–9883

nanogels presumably inside vesicular compartments. Due to the fact that particle uptake was only observed upon high particle dosing at 100 $\mu\text{g}/\text{mL}$, these *in vitro* studies suggested the potentially useful property of these nanogel carriers to withstand rapid phagocytosis, making them applicable for systemic *in vivo* applications.

We therefore intravenously injected NIR-labeled D-NG into mice's tail veins and observed after 24 h still a strong fluorescent signal distributed all over the body by the *in vivo* NIR imaging system (IVIS) (Figure S51). These findings confirmed that the nanogels remained in the blood circulation long enough to address multiple organs. Subsequently, major organs were harvested and imaged *ex vivo* to better quantitate the NIR signals (Figure S52). Semiquantitative analysis confirmed that nanogels were sequestered not only in the liver, a typical nonspecific sink for systemically administered nanocarriers, and kidneys (probably due to the renal clearance properties of the soluble polymers after hydrolysis of ketal-cross-linked nanogels), but also in the spleen. The spleen is a central organ of the lymphatic system, being highly relevant for immunodrug delivery because it harbors many antigen-presenting cells (Figure S53). We, therefore, opted for a strategy to systemically deliver a TLR7/8 agonist into this organ and induce a local immune modulation.

Effective and Safe TLR7/8 Agonist Delivery for Intravenous Routes of Administration. The highly potent small-molecular TLR7/8 agonist IMDQ¹⁸ was selected as an immune modulatory compound to trigger maturation of splenic antigen-presenting cells. This compound has been demonstrated to activate TLR7/8 even when it is bound to macromolecular nanocarriers.^{24,45,46} Due to its primary benzylic amine, IMDQ can straightforwardly be conjugated to pendant squaric ester amide groups and, therefore, directly be incorporated into the nanogel fabrication process (Figure 6A). IMDQ conjugation did not affect the nanogel fabrication, as cross-linked nanogels (IMDQ-D-NG and IMDQ-ND-NG) were of similar size and the non-cross-linked species (IMDQ-NCL-NG) was again completely soluble (compare Supporting Information Figure S51). Quantification of the covalently attached IMDQ was conducted by ¹H NMR spectroscopy. For the soluble NCL-NG species, a drug load of 2.7 wt % was found (compare Supporting Information Figure S52) being covalently attached to the polymer (confirmed by DOSY NMR, Figure S53).

For demonstrating TLR7/8 stimulation activity, we used a RAW-Blue macrophage reporter cell line that is genetically engineered to secrete embryonic alkaline phosphatase (SEAP) in response to TLR activation and downstream signaling via the NF- κ B pathway. SEAP expression itself can readily be detected from the cell culture supernatant via UV/vis spectrophotometry after addition of a coloring substrate (Quanti-Blue assay). RAW Blue macrophages were pulsed with increasing doses of either soluble IMDQ (sIMDQ) or IMDQ-D-NG (empty nanogel D-NG served as a control). A strong TLR activation was found for sIMDQ already at sub-micromolar concentrations, while nonligated control nanogels did not induce any significant activation (Figure 6B). IMDQ-D-NG led to a dose-dependent activation, albeit less potent than sIMDQ but still active in the micromolar concentration range. Similar activities were found after 24 h as well as 48 h and could be confirmed for both IMDQ-ND-NG and IMDQ-NCL-NG (Figure S58), which may corroborate the weak cellular internalization. In parallel, RAW Blue cellular viability was monitored by an MTT assay. No significant influence on metabolic activity was found for all

nanogel samples in the tested experimental window (Figure S57).

We then investigated the nanogel's *in vivo* immune stimulatory activity with a special focus on the activation of antigen-presenting cells in the spleen while avoiding systemic off-target effects. The latter can be visualized by bioluminescence imaging of heterozygous BALB/c IFN- β (IFN- $\beta^{+/\Delta\beta-luc}$) reporter mice,⁴⁷ in which luciferase as reporter gene is genetically linked to the expression of type I interferon IFN- β , a cytokine that is induced upon TLR7/8 stimulation. Mice were intravenously injected into the tail vein, and bioluminescence was monitored after 4, 24, and 48 h (Figure 6C and Supporting Information Figure S59). For sIMDQ, a strong signal was observed all over the body, reflecting a systemic inflammatory response in those mice. A prominent IFN- β expression occurred in the neck and abdomen and remained high up to 48 h postinjection. The nanogel-conjugated IMDQ, however, did not cause such a severe global immune activation all over the body. After 4 h no severe systemic inflammation was recorded. Only after 24 h a mild activity was observed with some expression in the abdomen and neck region, but with reduced gain compared to sIMDQ (Figure 6C and Supporting Information Figure S59). These observations clearly underline that severe systemic inflammatory responses are absent for the nanogel carrier system.

To further corroborate the absence of soluble IMDQ's acute toxicity, we also monitored the systemic inflammatory cytokines in sera of mice treated with soluble IMDQ vs nanogel-conjugated IMDQ. The results are provided in the Supporting Information Figure S62–S64 and confirm the observations of the IFN- β reporter mice: After 4 h, increasing serum cytokine levels of TNF- α , IL-6, and INF- γ are found in mice treated with soluble IMDQ. They are significantly elevated compared to mice treated with PBS, while mice treated with nanogel-bound IMDQ only provide slightly increased but not significant TNF- α , IL-6, and INF- γ levels (Supporting Information Figure S62).

After 24 h, those cytokines are again decreased to levels of PBS-treated mice. The elevated cytokine levels for soluble IMDQ-treated mice caused further liver toxicities by increased ALT, AST, and GLDH enzyme serum activities (Supporting Information Figure S63). Additionally, further influence on pancreas toxicity by high lipase serum activity as well as kidney toxicity by elevated blood urea nitrogen (BUN) can be observed (Supporting Information Figure S64). These data underline again the improved safety profile for the IMDQ-loaded nanogels to circumvent these acute toxicities but focus the immune stimulatory potential of the TLR7/8 agonist to the spleen.

One may speculate that such reduced systemic off-target effects for the nanogel-conjugated IMDQ might simply be caused by the minor receptor activation potency or reduced bioavailability. However, when it comes to immune intervention strategies (e.g., vaccination or cancer immunotherapy), site-specific immune activation (i.e., spleen specific, rather than systemic) is of important relevance and the major goal of this study.

Previous biodistribution analysis confirmed that a sufficient amount of nanogels was found inside the spleen after systemic activation (Figure 5D). To further validate that IMDQ-loaded nanogels still activate spleen-resident immune cells, we isolated splenocytes from the mice 48 h after injection and performed quantitative flow cytometric analyses (for further details on the gating procedure compare Supporting Information Figure S60). Both sIMDQ and IMDQ-D-NG comparably increased the

number of myeloid cells with no influence on B and T lymphocytes (Figure 6D–H1). Dendritic cells (DCs), macrophages, and neutrophils are known to express and respond to TLR7/8 activation effectively. Their numbers are therefore increased to a similar extent for both sIMDQ and IMDQ-D-NG (Figure 6D1–F1).

We then checked for maturation markers on those cells and found again that IMDQ-D-NG triggered their expression to a similar level as sIMDQ while omitting systemic inflammations (Figure 6D2–H2 and Supporting Information Figure S61). For DCs and neutrophils (Figure 6D3/4 and F3/4) the expression levels of CD80 and CD86 were significantly enhanced by IMDQ-D-NG as well as sIMDQ. They were also upregulated on B lymphocytes that in contrast to T lymphocytes have antigen presenting ability (Figure 6G3/4). Also, the T lymphocyte activation marker CD69 was induced, again comparably, by IMDQ-D-NG and sIMDQ treatment, indicating further downstream T lymphocyte activation (Figure 6H3).

Most interestingly, for macrophages no difference in the expression of CD86 was observed (Figure 6E4), as CD86 upregulation is more typical for DCs. However, CD80 expression was more significantly triggered by IMDQ-D-NG and even exceeded the expression levels of sIMDQ (Figure 6E3). Apparently, nanogel-bound IMDQ seems to have a preferential stimulation potential in those highly phagocytotic immune cells inside the spleen. These properties outperform the treatment with sIMDQ and make the nanogels highly interesting for further therapeutic immune interventions.

Altogether, these observations confirm the hypothesis that our nanocarrier can deliver the TLR7/8 agonist into the spleen and maintain its immune stimulatory activity inside that organ. It prevents massive systemic immune activations and subsequent severe inflammatory off-target effects but conserves organ-specific immune stimulation inside the spleen, especially to resident macrophages. Since this organ is highly relevant for further immune intervention strategies including cancer immunotherapy or vaccination,^{48,49} we consider squaric ester-based, pH-degradable nanogels as a relevant platform to exploit further systemic immunologic adjuvant strategies.

CONCLUSIONS

In this study, we have introduced polymerizable squaric ester amides as novel functional tool to robustly fabricate pH-responsive nanogels serving as a versatile nanocarrier platform for safe delivery of the highly potent immunomodulator IMDQ after intravenous administration. To the best of our knowledge, the synthesis of methacrylamide monomers with a functional pendant squaric ester amide moiety has not been reported before. Its subsequent controlled RAFT block copolymerization as well as its self-assembling behavior in polar protic solvents provides access to precursor micelles with amine-reactive cores. Through their sequential amidation, covalent dye or drug loading, acid-sensitive cross-linking, and core-transformation from hydrophobic to hydrophilic polarity can be performed, affording fully hydrophilic nanogels with profound stability in plasma and the bloodstream, with modest uptake by phagocytic cells and with an inherently triggered degradation upon exposure to mildly endolysosomal pH conditions. The carriers' potential to covalently conjugate IMDQ as a highly potent immunomodulator enables the drug's safe and efficient delivery by preventing systemic off-target inflammation but retaining its spatial activity in the spleen. These findings underline the potential of this carrier platform to access intravenous

administrations routes for small-molecular TLR7/8 agonists (and other relevant immune modulators) and, thus, provide novel opportunities to explore their superior adjuvant potency for systemic vaccination or cancer immunotherapy purposes.

ASSOCIATED CONTENT

Supporting Information

The Supporting Information is available free of charge at <https://pubs.acs.org/doi/10.1021/jacs.1c03772>.

Experimental details including materials, instrumentation, monomer and polymer syntheses, and characterization, nanogel fabrication and characterization, IMDQ ligation and quantification, *in vitro* and *in vivo* evaluation (PDF)

AUTHOR INFORMATION

Corresponding Author

Lutz Nuhn – Max Planck Institute for Polymer Research, 55128 Mainz, Germany; orcid.org/0000-0003-0761-1106; Phone: +49 (0) 6131-379-311; Email: lutz.nuhn@mpip-mainz.mpg.de

Authors

Anne Huppertsberg – Max Planck Institute for Polymer Research, 55128 Mainz, Germany

Leonard Kaps – Institute for Translational Immunology and Research Center for Immune Therapy, University Medical Center, Johannes Gutenberg-University Mainz, 55131 Mainz, Germany; Department of Internal Medicine I, University Medical Center of the Johannes Gutenberg-University Mainz, 55131 Mainz, Germany

Zifu Zhong – Department of Pharmaceutics and Cancer Research Institute Ghent (CRIG), Ghent University, Ghent 9000, Belgium

Sascha Schmitt – Max Planck Institute for Polymer Research, 55128 Mainz, Germany

Judith Stickdorn – Max Planck Institute for Polymer Research, 55128 Mainz, Germany

Kim Deswarte – Department of Internal Medicine and Pediatrics, Ghent University, VIB Center for Inflammation Research, Ghent 9002, Belgium

Francis Combes – Laboratory of Gene Therapy, Department of Nutrition, Genetics and Ethology, Ghent University, Merelbeke 9820, Belgium

Christian Czysch – Max Planck Institute for Polymer Research, 55128 Mainz, Germany

Jana De Vrieze – Department of Pharmaceutics and Cancer Research Institute Ghent (CRIG), Ghent University, Ghent 9000, Belgium

Sabah Kasmi – Department of Pharmaceutics and Cancer Research Institute Ghent (CRIG), Ghent University, Ghent 9000, Belgium

Niklas Choteschovsky – Institute for Translational Immunology and Research Center for Immune Therapy, University Medical Center, Johannes Gutenberg-University Mainz, 55131 Mainz, Germany

Adrian Klefenz – Institute for Translational Immunology and Research Center for Immune Therapy, University Medical Center, Johannes Gutenberg-University Mainz, 55131 Mainz, Germany

Carolina Medina-Montano – Department of Dermatology, University Medical Center of Johannes Gutenberg-University Mainz, 55131 Mainz, Germany

Pia Winterwerber – Max Planck Institute for Polymer Research, 55128 Mainz, Germany

Chaojian Chen – Max Planck Institute for Polymer Research, 55128 Mainz, Germany; orcid.org/0000-0002-2588-2447

Matthias Bros – Department of Dermatology, University Medical Center of Johannes Gutenberg-University Mainz, 55131 Mainz, Germany

Stefan Lienenklaus – Institute for Laboratory Animal Science and Institute of Immunology, Hannover Medical School, 30625 Hannover, Germany

Niek N. Sanders – Laboratory of Gene Therapy, Department of Nutrition, Genetics and Ethology, Ghent University, Merelbeke 9820, Belgium; orcid.org/0000-0003-4585-0343

Kaloian Koynov – Max Planck Institute for Polymer Research, 55128 Mainz, Germany; orcid.org/0000-0002-4062-8834

Detlef Schuppan – Institute for Translational Immunology and Research Center for Immune Therapy, University Medical Center, Johannes Gutenberg-University Mainz, 55131 Mainz, Germany; Division of Gastroenterology, Beth Israel Deaconess Medical Center, Harvard Medical School, Boston, Massachusetts 02215, United States

Bart N. Lambrecht – Department of Internal Medicine and Pediatrics, Ghent University, VIB Center for Inflammation Research, Ghent 9052, Belgium; Department of Pulmonary Medicine, Erasmus University Medical Center, Rotterdam 3015, Netherlands

Sunil A. David – ViroVax, LLC, Lawrence, Kansas 66047, United States; orcid.org/0000-0003-1655-4641

Bruno G. De Geest – Department of Pharmaceutics and Cancer Research Institute Ghent (CRIG), Ghent University, Ghent 9000, Belgium; orcid.org/0000-0001-9826-6170

Complete contact information is available at:
<https://pubs.acs.org/10.1021/jacs.1c03772>

Author Contributions

The manuscript was written through contributions of all authors. All authors have given approval to the final version of the manuscript.

Notes

The authors declare no competing financial interest.

ACKNOWLEDGMENTS

A.H. and L.N. acknowledge support by the Max Planck Graduate Center with the Johannes Gutenberg-Universität Mainz (MPGC). Moreover, L.N. kindly acknowledges financial support by the DFG through the Emmy Noether program as well as the SFB 1066 projects Q02, B03, and B04. Both A.H. and L.N. would also like to thank Tanja Weil for providing access to excellent laboratory facilities.

REFERENCES

- (1) Singh, R.; Lillard, J. W. Nanoparticle-Based Targeted Drug Delivery. *Exp. Mol. Pathol.* **2009**, *86* (3), 215–223.
- (2) Mitchell, M. J.; Billingsley, M. M.; Haley, R. M.; Wechsler, M. E.; Peppas, N. A.; Langer, R. Engineering Precision Nanoparticles for Drug Delivery. *Nat. Rev. Drug Discovery* **2021**, *20* (2), 101–124.
- (3) Talelli, M.; Barz, M.; Rijcken, C. J. F.; Kiessling, F.; Hennink, W. E.; Lammers, T. Core-Crosslinked Polymeric Micelles: Principles, Preparation, Biomedical Applications and Clinical Translation. *Nano Today* **2015**, *10* (1), 93–117.

- (4) Crommelin, D. J. A.; Florence, A. T. Towards More Effective Advanced Drug Delivery Systems. *Int. J. Pharm.* **2013**, *454* (1), 496–511.

- (5) Banik, B. L.; Fattahi, P.; Brown, J. L. Polymeric Nanoparticles: The Future of Nanomedicine. *Wiley Interdiscip. Rev. Nanomedicine Nanobiotechnology* **2016**, *8* (2), 271–299.

- (6) Tong, R.; Tang, L.; Ma, L.; Tu, C.; Baumgartner, R.; Cheng, J. Smart Chemistry in Polymeric Nanomedicine. *Chem. Soc. Rev.* **2014**, *43* (20), 6982–7012.

- (7) Harrison, L. L.; Astry, C.; Kumar, S.; Yunis, C. Pharmacokinetics of 852A, an Imidazoquinoline Toll-Like Receptor 7-Specific Agonist, Following Intravenous, Subcutaneous, and Oral Administrations in Humans. *J. Clin. Pharmacol.* **2007**, *47* (8), 962–969.

- (8) Gunzer, M.; Riemann, H.; Basoglu, Y.; Hillmer, A.; Weishaupt, C.; Balkow, S.; Benninghoff, B.; Ernst, B.; Steinert, M.; Scholzen, T.; Sunderkötter, C.; Grabbe, S. Systemic Administration of a TLR7 Ligand Leads to Transient Immune Incompetence Due to Peripheral-Blood Leukocyte Depletion. *Blood* **2005**, *106* (7), 2424–2432.

- (9) Stäckdorn, J.; Nuhn, L. Reactive-Ester Derived Polymer Nanogels for Cancer Immunotherapy. *Eur. Polym. J.* **2020**, *124*, 109481.

- (10) Lybaert, L.; Vermaelen, K.; De Geest, B. G.; Nuhn, L. Immunoengineering through Cancer Vaccines – A Personalized and Multi-Step Vaccine Approach towards Precise Cancer Immunity. *J. Controlled Release* **2018**, *289*, 125–145.

- (11) Milling, L.; Zhang, Y.; Irvine, D. J. Delivering Safer Immunotherapies for Cancer. *Adv. Drug Delivery Rev.* **2017**, *114*, 79–101.

- (12) O'Neill, L. A. J.; Golenbock, D.; Bowie, A. G. The History of Toll-like Receptors-Redefining Innate Immunity. *Nat. Rev. Immunol.* **2013**, *13* (6), 453–460.

- (13) Mancini, R. J.; Stutts, L.; Ryu, K. A.; Tom, J. K.; Esser-Kahn, A. P. Directing the Immune System with Chemical Compounds. *ACS Chem. Biol.* **2014**, *9* (5), 1075–1085.

- (14) Iwasaki, A.; Medzhitov, R. Control of Adaptive Immunity by the Innate Immune System. *Nat. Immunol.* **2015**, *16* (4), 343–353.

- (15) Schön, M. P.; Schön, M. TLR7 and TLR8 as Targets in Cancer Therapy. *Oncogene* **2008**, *27* (2), 190–199.

- (16) Baldrige, J. R.; McGowan, P.; Evans, J. T.; Cluff, C.; Mossman, S.; Johnson, D.; Persing, D. Taking a Toll on Human Disease: Toll-like Receptor 4 Agonists as Vaccine Adjuvants and Monotherapeutic Agents. *Expert Opin. Biol. Ther.* **2004**, *4* (7), 1129–1138.

- (17) Kawai, T.; Akira, S. The Role of Pattern-Recognition Receptors in Innate Immunity: Update on Toll-like Receptors. *Nat. Immunol.* **2010**, *11* (5), 373–384.

- (18) Beesu, M.; Salyer, A. C. D.; Brush, M. J. H.; Trautman, K. L.; Hill, J. K.; David, S. A. Identification of High-Potency Human TLR8 and Dual TLR7/TLR8 Agonists in Pyrimidine-2,4-Diamines. *J. Med. Chem.* **2017**, *60* (5), 2084–2098.

- (19) Van Hoven, N.; Fox, C. B.; Granger, B.; Evers, T.; Joshi, S. W.; Nana, G. I.; Evans, S. C.; Lin, S.; Liang, H.; Liang, L.; Nakajima, R.; Felgner, P. L.; Bowen, R. A.; Marlenee, N.; Hartwig, A.; Baldwin, S. L.; Coler, R. N.; Tomai, M.; Elvecrog, J.; Reed, S. G.; Carter, D. A Formulated TLR7/8 Agonist Is a Flexible, Highly Potent and Effective Adjuvant for Pandemic Influenza Vaccines. *Sci. Rep.* **2017**, *7* (1), 1–15.

- (20) De Vrieze, J.; Louage, B.; Deswarte, K.; Zhong, Z.; De Coen, R.; Van Herck, S.; Nuhn, L.; Kaas Frich, C.; Zelikin, A. N.; Lienenklaus, S.; Sanders, N. N.; Lambrecht, B. N.; David, S. A.; De Geest, B. G. Potent Lymphatic Translocation and Spatial Control Over Innate Immune Activation by Polymer–Lipid Amphiphile Conjugates of Small-Molecule TLR7/8 Agonists. *Angew. Chem., Int. Ed.* **2019**, *58* (43), 15390–15395.

- (21) Yoo, E.; Salyer, A. C. D.; Brush, M. J. H.; Li, Y.; Trautman, K. L.; Shukla, N. M.; De Beuckelaer, A.; Lienenklaus, S.; Deswarte, K.; Lambrecht, B. N.; De Geest, B. G.; David, S. A. Hyaluronic Acid Conjugates of TLR7/8 Agonists for Targeted Delivery to Secondary Lymphoid Tissue. *Bioconjugate Chem.* **2018**, *29* (8), 2741–2754.

- (22) Lynn, G. M.; Chytil, P.; Francica, J. R.; Lagová, A.; Kueberuwa, G.; Ishizuka, A. S.; Zaidi, N.; Ramirez-Valdez, R. A.; Blobel, N. J.; Baharom, F.; Leal, J.; Wang, A. Q.; Gerner, M. Y.; Etrych, T.; Ulbrich,

- K.; Seymour, L. W.; Seder, R. A.; Laga, R. Impact of Polymer-TLR-7/8 Agonist (Adjuvant) Morphology on the Potency and Mechanism of CD8 T Cell Induction. *Biomacromolecules* **2019**, *20* (2), 854–870.
- (23) Van Herck, S.; Deswarte, K.; Nuhn, L.; Zhong, Z.; Portela Catani, J. P.; Li, Y.; Sanders, N. N.; Lienenklaus, S.; De Koker, S.; Lambrecht, B. N.; David, S. A.; De Geest, B. G. Lymph-Node-Targeted Immune Activation by Engineered Block Copolymer Amphiphiles-TLR7/8 Agonist Conjugates. *J. Am. Chem. Soc.* **2018**, *140*, 14300–14307.
- (24) Nuhn, L.; De Koker, S.; Van Lint, S.; Zhong, Z.; Catani, J. P.; Combes, F.; Deswarte, K.; Li, Y.; Lambrecht, B. N.; Lienenklaus, S.; Sanders, N. N.; David, S. A.; Tavernier, J.; De Geest, B. G. Nanoparticle-Conjugate TLR7/8 Agonist Localized Immunotherapy Provokes Safe Antitumoral Responses. *Adv. Mater.* **2018**, *30* (45), 1–9.
- (25) Nuhn, L.; Van Hoecke, L.; Deswarte, K.; Schepens, B.; Li, Y.; Lambrecht, B. N.; De Koker, S.; David, S. A.; Saelens, X.; De Geest, B. G. Potent Anti-Viral Vaccine Adjuvant Based on PH-Degradable Nanogels with Covalently Linked Small Molecule Imidazoquinoline TLR7/8 Agonist. *Biomaterials* **2018**, *178*, 643–651.
- (26) Lynn, G. M.; Sedlik, C.; Baharom, F.; Zhu, Y.; Ramirez-Valdez, R. A.; Coble, V. L.; Tobin, K.; Nichols, S. R.; Itzkowitz, Y.; Zaidi, N.; Gammon, J. M.; Blobel, N. J.; Denizeau, J.; de la Roche, P.; Francica, B. J.; Decker, B.; Maciejewski, M.; Cheung, J.; Yamane, H.; Smelkinson, M. G.; Francica, J. R.; Laga, R.; Bernstock, J. D.; Seymour, L. W.; Drake, C. G.; Jewell, C. M.; Lantz, O.; Piaggio, E.; Ishizuka, A. S.; Seder, R. A. Peptide–TLR-7/8a Conjugate Vaccines Chemically Programmed for Nanoparticle Self-Assembly Enhance CD8 T-Cell Immunity to Tumor Antigens. *Nat. Biotechnol.* **2020**, *38* (3), 320–332.
- (27) Van Lysebetten, D.; Malfanti, A.; Deswarte, K.; Koynov, K.; Golba, B.; Ye, T.; Zhong, Z.; Kasmi, S.; Lamoot, A.; Chen, Y.; Van Herck, S.; Lambrecht, B. N.; Sanders, N. N.; Lienenklaus, S.; David, S. A.; Vicent, M. J.; De Koker, S.; De Geest, B. G. Lipid-Polyglutamate Nanoparticle Vaccine Platform. *ACS Appl. Mater. Interfaces* **2021**, *13* (5), 6011–6022.
- (28) Cho, H.; Il; Barrios, K.; Lee, Y. R.; Linowski, A. K.; Celis, E. BiVax: A Peptide/Poly-IC Subunit Vaccine That Mimics an Acute Infection Elicits Vast and Effective Anti-Tumor CD8 T-Cell Responses. *Cancer Immunol. Immunother.* **2013**, *62* (4), 787–799.
- (29) Seder, R. A.; Chang, L. J.; Enama, M. E.; Zephir, K. L.; Sarwar, U. N.; Gordon, I. J.; Holman, L. S. A.; James, E. R.; Billingsley, P. F.; Gunasekera, A.; Richman, A.; Chakravarty, S.; Manoj, A.; Velmurugan, S.; Li, M. L.; Ruben, A. J.; Li, T.; Eappen, A. G.; Stafford, R. E.; Plummer, S. H.; Hendl, C. S.; Novik, L.; Costner, P. J. M.; Mendoza, F. H.; Saunders, J. G.; Nason, M. C.; Richardson, J. H.; Murphy, J.; Davidson, S. A.; Richie, T. L.; Sedegah, M.; Sutaniharidja, A.; Fahle, G. A.; Lyke, K. E.; Laurens, M. B.; Roederer, M.; Tewari, K.; Epstein, J. E.; Sim, B. K. L.; Ledgerwood, J. E.; Graham, B. S.; Hoffman, S. L. Protection against Malaria by Intravenous Immunization with a Nonreplicating Sporozoite Vaccine. *Science (Washington, DC, U. S.)* **2013**, *341* (6152), 1359–1365.
- (30) Baharom, F.; Ramirez-Valdez, R. A.; Tobin, K. K. S.; Yamane, H.; Dutertre, C. A.; Khalilnezhad, A.; Reynoso, G. V.; Coble, V. L.; Lynn, G. M.; Mule, M. P.; Martins, A. J.; Finnigan, J. P.; Zhang, X. M.; Hamerman, J. A.; Bhardwaj, N.; Tsang, J. S.; Hickman, H. D.; Ginhoux, F.; Ishizuka, A. S.; Seder, R. A. Intravenous Nanoparticle Vaccination Generates Stem-like TCF1+ Neoaantigen-Specific CD8+ T Cells. *Nat. Immunol.* **2021**, *22* (1), 41–52.
- (31) Nuhn, L.; Vanparijs, N.; De Beuckelaer, A.; Lybaert, L.; Verstraete, G.; Deswarte, K.; Lienenklaus, S.; Shukla, N. M.; Salyer, A. C. D.; Lambrecht, B. N.; Grooten, J.; David, S. A.; De Koker, S.; De Geest, B. G. PH-Degradable Imidazoquinoline-Ligated Nanogels for Lymph Node-Focused Immune Activation. *Proc. Natl. Acad. Sci. U. S. A.* **2016**, *113* (29), 8098–8103.
- (32) Nuhn, L.; Hirsch, M.; Krieg, B.; Koynov, K.; Fischer, K.; Schmidt, M.; Helm, M.; Zentel, R. Cationic Nanohydrogel Particles as Potential siRNA Carriers for Cellular Delivery. *ACS Nano* **2012**, *6* (3), 2198–2214.
- (33) Nuhn, L.; Van Herck, S.; Best, A.; Deswarte, K.; Kokkinopoulou, M.; Lieberwirth, I.; Koynov, K.; Lambrecht, B. N.; De Geest, B. G. FRET Monitoring of Intracellular Ketal Hydrolysis in Synthetic Nanoparticles. *Angew. Chem., Int. Ed.* **2018**, *57* (33), 10760–10764.
- (34) Bebis, K.; Jones, M. W.; Haddleton, D. M.; Gibson, M. I. Thermoresponsive Behaviour of Poly[(Oligo(Ethylene glycol Methacrylate)]s and Their Protein Conjugates: Importance of Concentration and Solvent System. *Polym. Chem.* **2011**, *2* (4), 975–982.
- (35) Mohr, N.; Barz, M.; Forst, R.; Zentel, R. A Deeper Insight into the Postpolymerization Modification of Polypenta Fluorophenyl Methacrylates to Poly(N-(2-Hydroxypropyl) Methacrylamide). *Macromol. Rapid Commun.* **2014**, *35* (17), 1522–1527.
- (36) Jones, K. Pentafluorophenol. In *Encyclopedia of Reagents for Organic Synthesis*; American Cancer Society, 2001.
- (37) Tietze, L. F.; Arlt, M.; Beller, M.; Glienskamp, K.-H.; Jahdeb, E.; Rajewsky, M. F. Squaric Acid Diethyl Ester: A New Coupling Reagent for the Formation of Drug Biopolymer Conjugates. Synthesis of Squaric Acid Ester Amides and Diamides. *Chem. Ber.* **1991**, *124*, 1215–1221.
- (38) Quiñero, D.; Frontera, A.; Ballester, P.; Deyá, P. M. A Theoretical Study of Aromaticity in Squaric Acid and Oxocarbons. *Tetrahedron Lett.* **2000**, *41* (12), 2001–2005.
- (39) Wurm, F. R.; Klok, H. A. Be Squared: Expanding the Horizon of Squaric Acid-Mediated Conjugations. *Chem. Soc. Rev.* **2013**, *42* (21), 8220–8236.
- (40) Steinbach, T.; Wurm, F.; Klok, H. A. Squaric Acid Mediated Bioconjugation Expanded to Polymers Prepared by ATRP. *Polym. Chem.* **2014**, *5* (13), 4039–4047.
- (41) Zhang, Z.; Vanparijs, N.; Vandewalle, S.; Du Prez, F. E.; Nuhn, L.; De Geest, B. G. Squaric Ester Amides as Hydrolysis-Resistant Functional Groups for Protein-Conjugation of RAFT-Derived Polymers. *Polym. Chem.* **2016**, *7* (47), 7242–7248.
- (42) Kockelmann, J.; Stickdorn, J.; Kasmi, S.; De Vrieze, J.; Pieszka, M.; Ng, D. Y. W.; David, S. A.; De Geest, B. G.; Nuhn, L. Control over Imidazoquinoline Immune Stimulation by PH-Degradable Poly-(Norbornene) Nanogels. *Biomacromolecules* **2020**, *21* (6), 2246–2257.
- (43) Leber, N.; Kaps, L.; Aslam, M.; Schupp, J.; Brose, A.; Schäffel, D.; Fischer, K.; Diken, M.; Strand, D.; Koynov, K.; Tuettnerberg, A.; Nuhn, L.; Zentel, R.; Schuppan, D. siRNA-Mediated in Vivo Gene Knockdown by Acid-Degradable Cationic Nanohydrogel Particles. *J. Controlled Release* **2017**, *248*, 10–23.
- (44) Koynov, K.; Butt, H. J. Fluorescence Correlation Spectroscopy in Colloid and Interface Science. *Curr. Opin. Colloid Interface Sci.* **2012**, *17* (6), 377–387.
- (45) Shukla, N. M.; Malladi, S. S.; Mutz, C. A.; Balakrishna, R.; David, S. A. Structure-Activity Relationships in Human Toll-like Receptor 7-Active Imidazoquinoline Analogues. *J. Med. Chem.* **2010**, *53* (11), 4450–4465.
- (46) Kim, W. G.; Choi, B.; Yang, H. J.; Han, J. A.; Jung, H.; Cho, H.; Kang, S.; Hong, S. Y. Covalent Conjugation of Small-Molecule Adjuvants to Nanoparticles Induces Robust Cytotoxic T Cell Responses via DC Activation. *Bioconjugate Chem.* **2016**, *27* (9), 2007–2013.
- (47) Lienenklaus, S.; Cornitescu, M.; Ziętara, N.; Lyszczewicz, M.; Gekara, N.; Jabłońska, J.; Edenhofer, F.; Rajewsky, K.; Bruder, D.; Hafner, M.; Staeheli, P.; Weiss, S. Novel Reporter Mouse Reveals Constitutive and Inflammatory Expression of IFN- β In Vivo. *J. Immunol.* **2009**, *183* (5), 3229–3236.
- (48) Steenbrugge, J.; De Jaeghere, E. A.; Meyer, E.; Denys, H.; De Wever, O. Splenic Hematopoietic and Stromal Cells in Cancer Progression. *Cancer Res.* **2020**, *81*, 27–34.
- (49) Bronte, V.; Pittet, M. J. The Spleen in Local and Systemic Regulation of Immunity. *Immunity* **2013**, *39* (5), 806–818.

Fluorescent Nanodiamond–Nanogels for Nanoscale Sensing and Photodynamic Applications

Yingke Wu, Md Noor A Alam, Priyadharshini Balasubramanian, Pia Winterwerber, Anna Ermakova, Michael Müller, Manfred Wagner, Fedor Jelezko,* Marco Raabe,* and Tanja Weil*

Fluorescent nanodiamonds (NDs) are carbon-based nanoparticles with various outstanding magneto–optical properties. After preparation, NDs have a variety of different surface groups that determine their physicochemical properties. For biological applications, surface modifications are crucial to impart a new interface for controlled interactions with biomolecules or cells. Herein, a straightforward synthesis concept denoted “adsorption–crosslinking” is applied for the efficient modification of NDs, which sequentially combines fast noncovalent adsorption based on electrostatic interactions and subsequent covalent crosslinking. As a result, a very thin and uniform nanogel (NG) coating surrounding the NDs is obtained, which imparts reactive groups as well as high colloidal stability. The impact of the reaction time, monomer concentration, molecular weight, structure of the crosslinker on the resulting NG shell, the availability of reactive chemical surface functions, and the quantum sensing properties of the coated NDs are assessed and optimized. Postmodification of the NG-coated NDs is achieved with phototoxic ruthenium complexes yielding ND-based probes suitable for photodynamic applications. The adsorption–crosslinking ND functionalization reported herein provides new avenues toward functional probes and traceable nanocarriers for high-resolution bioimaging, nanoscale sensing, and photodynamic applications.

1. Introduction


Among many carbon-based nanoscale materials, fluorescent nanodiamonds (NDs) have emerged for diverse applications in nanomedicine and bioimaging, because of their unique magneto–optical properties as well as their high biocompatibility.^[1] The optically active atom defects in the lattice of NDs, such as the nitrogen vacancy (NV) center, provide stable fluorescence without photobleaching or photoblinking.^[2] Due to their stable fluorescence, NDs with NV centers have been applied widely in bioimaging,^[3] as well as real-time reporters for drug delivery.^[4–6] In addition, the emission wavelength of NDs is size independent but tunable from the visible to the near-infrared region based on the color center (e.g., Si, Ge, etc.).^[7] Furthermore, NDs containing negatively charged NV (NV⁻) centers can serve as single-spin sensors to detect critical physical parameters in a biological microenvironment, such as temperature,^[8] magnetic fields,^[9] electron spins,^[10] and mechanical strain.^[11]

However, for most of these applications, an appropriate surface functionalization of the NDs is essential, because the colloidal stability of unmodified nanosized NDs in physiological buffer systems is extremely poor due to aggregation.^[12] Moreover, the shell provides further reactive groups to attach the desired functionalities, such as drug molecules, dyes, cell- or tissue-targeting groups, or various proteins like antibodies.^[13] The surface coating shields the inner ND surface and creates a new interface, which is particularly attractive for *in vitro* or *in vivo* applications, i.e., to prevent foreign body interactions^[14] or increase their circulation times^[12] or their accumulation at the target site.^[15] In the past, various different ND surface coating materials and strategies have been reported. The covalent attachment of functionalities such as a silica shell,^[16] hyperbranched polyglycerols (HPG),^[17] poly(*t*-DOPA),^[5] and antibodies^[18] has been explored as well as noncovalent adsorption of biomolecules or polymers like polyethyleneimine,^[19] insulin,^[20] and albumin-based copolymers.^[4] Nevertheless, uncontrolled aggregation as well as precipitation still represents a challenge and each reported functionalization strategy has its benefits but also inherent limitations. Covalent conjugation approaches are typically challenged by the low number of

Y. Wu, M. N. A. Alam, P. Winterwerber, Dr. A. Ermakova, M. Müller, Dr. M. Wagner, Dr. M. Raabe, Prof. T. Weil
Department of Synthesis of Macromolecules
Max Planck Institute for Polymer Research
Ackermannweg 10, Mainz 55128, Germany
E-mail: raabe@mpip-mainz.mpg.de; weil@mpip-mainz.mpg.de

M. N. A. Alam, Dr. M. Raabe, Prof. T. Weil
Institute of Inorganic Chemistry I
Ulm University
Albert-Einstein-Allee 11, Ulm 89081, Germany

P. Balasubramanian, Prof. F. Jelezko
Institute for Quantum Optics and IQST
Ulm University
Albert-Einstein-Allee 11, Ulm 89081, Germany
E-mail: fedor.jelezko@uni-ulm.de

 The ORCID identification number(s) for the author(s) of this article can be found under <https://doi.org/10.1002/anbr.202000101>.

© 2021 The Authors. Advanced NanoBiomed Research published by Wiley-VCH GmbH. This is an open access article under the terms of the Creative Commons Attribution License, which permits use, distribution and reproduction in any medium, provided the original work is properly cited.

DOI: 10.1002/anbr.202000101

functionalities intrinsically present at the ND surface.^[21] Therefore, often only few surface groups could be attached and batch-to-batch variations of the NDs can cause reproducibility problems. ND coating by physical adsorption is a straightforward procedure, which is less influenced by changes of the ND surface groups. However, ligand loss often occurs in biological media, thus limiting the stability of the nanoparticle, i.e., during cell studies.^[22] We propose that the combination of both covalent and non-covalent coating approaches offers efficient functionalization and stabilization of NDs.

Herein, we report a straightforward procedure based on the noncovalent adsorption and covalent crosslinking method that imparts a nanogel (NG) shell at the ND surface. First, the adsorption of multifunctional and positively charged ligands pre-coats the NDs based on electrostatic interactions followed by a cross-linking step to afford a stable and soft NG shell. Hyperbranched polyethyleneimine (PEI) is a highly branched, cationic polymer with multiple primary amino groups that allow cellular uptake by endocytosis, which has been widely used in biomedical applications, such as cell transfection^[23] and gene therapy.^[24] In addition, to avoid aggregation of NDs during the adsorption of PEI, polyvinylpyrrolidone (PVP) has been applied as a commonly used stabilizer^[25] with proven biocompatibility, as demonstrated in biomedical applications such as in tissue engineering.^[26] PEI has been crosslinked with poly(ethylene glycol) to generate the soft and homogeneous ND–NG shell, providing high colloidal stability, reactive primary amino groups for postmodifications, and low cellular toxicity. We accomplished a ND–NG platform for the design of ND-based photosensitizers for photodynamic applications. Photodynamic therapy (PDT) is widely applied in skin cancer and here, light energy is converted locally at the tumor site into reactive oxygen species that affect cancer cell viability.^[27] In the future, real-time monitoring of the local changes in ion concentration of certain protein markers, i.e., upon drug treatment, could give new insights into cellular processes during therapy. In this way, a traceable ND-based photodynamic agent combining sensing, imaging, and drug delivery offers great prospects for nanomedicine.

2. Results and Discussion

The adsorption and crosslinking procedure to generate a NG shell around NDs is shown in **Figure 1A**. First, the NDs are mixed with hyperbranched polyethyleneimine (PEI, MW: 25 kDa) in the presence of polyvinylpyrrolidone (PVP, MW: 10 kDa) in Milli-Q water. At slightly alkaline (pH 7.4) conditions in the presence of phosphate-buffered saline (PBS), the 4-arm PEG-NHS ester was applied to crosslink the surface-adsorbed PEI for about 90 min. Purification was accomplished by several washing steps to remove unreacted precursors and smaller NGs without the embedded ND to obtain the pure ND–NGs, as shown in Table S1, Supporting Information.

The ND and ND–NGs were characterized with regard to their distribution, shape, and morphology by transmission electron microscopy (TEM; **Figure 1B,C**). As shown in **Figure 1B**, TEM images revealed that bare NDs were prone to significant aggregation and displayed a heterogeneous distribution, whereas nonaggregating, homogeneous single particles

could be observed for ND–NGs (**Figure 1C**). High-resolution transmission electron microscopy (HRTEM) imaging showed a uniform ring of 2 nm surrounding the NDs, indicating the presence of a dry NG coating (**Figure S1**, Supporting Information). Because the shell was low in contrast and measured under dry conditions by TEM, we further assessed the core–shell structure of the ND–NGs by liquid-mode atomic force microscopy (AFM; **Figure 1D,E**), in which the NG could swell compared with the dry TEM conditions. In **Figure 1D**, the topographic image of ND–NGs and deformation images showed good distribution with no obvious aggregation. NanoScope Analysis 1.8 software was used to process the data and visualize the NG coating.^[28] Apart from the height profile images, further nanomechanical properties were simultaneously recorded. In particular, the deformation of the sample caused by the probe was analyzed to receive in-depth information on the structure of the coated NDs. As the ND core is much harder than the NG shell, the deformation of the NG shell could be detected with greater intensity under the same stress conditions. The deformation image revealed clearly that all NDs were uniformly surrounded by a soft shell (**Figure 1D**, right). Furthermore, the deformation image was studied at higher magnification (**Figure 1E**), and ≈ 10 nm thickness of the NG was determined in liquid, which is sufficiently thin for nanoscale sensing applications.

The ND–NGs were characterized by dynamic light scattering (DLS) to measure the shell thickness of dispersed ND–NGs in aqueous solution. The average hydrodynamic diameters in Milli-Q water of NDs and ND–NGs were 36.2 ± 2.4 and 57.0 ± 1.2 nm, respectively, resulting in a shell thickness of 10.4 ± 3.6 nm of the ND–NGs ($n = 3$, **Figure 2A**, Table S2 and **Figure S3A**, Supporting Information). The ND–NGs were also characterized by multiangle light scattering, which is more sensitive to detect aggregation. No aggregate formation was observed and a shell thickness of about 9 nm (**Figure S2**, Supporting Information) was determined, which are in agreement with the results from the AFM measurements (10 nm). Variation of the reaction conditions on the hydrodynamic diameters of the ND–NGs was investigated by DLS. As shown in **Figure S3B**, Supporting Information, their sizes increased with the reaction time from 45.7 ± 5.6 to 52.2 ± 4.0 nm. However, the increments slowed down gradually and stabilized after 90 min, suggesting that the reaction reached saturation or completion. When the concentration of the crosslinker was increased from 0.125 to 8 mg mL⁻¹, ND–NGs of 57.0 ± 1.2 nm were obtained with 2 mg mL⁻¹ but the sizes subsequently increased to 74.9 ± 9.9 nm for 8 mg mL⁻¹ crosslinker. In addition, the PEI concentrations also varied from 0.01 to 10 mg mL⁻¹ to assess the influence on the resulting colloidal stability (**Figure 2B**). Aggregation was detected at a concentration, for ND–NGs, of 0.01 mg mL⁻¹, most likely because the low amount of PEI around single ND was insufficient to impart sufficient colloidal stability. At 1 mg mL⁻¹, ND–NGs with dimensions of about 50.2 ± 6.0 nm were detected, indicating that a sufficient amount of PEI covered the surface of the NDs, thus forming a thin shell. Further increase in PEI to 10 mg mL⁻¹ resulted in a significantly thicker shell (160.9 ± 22.6 nm). The influence of the molecular weight (MW) of PEI and a regularly branched polyamidoamine (PAMAM) dendrimer with a globular sphere-like structure

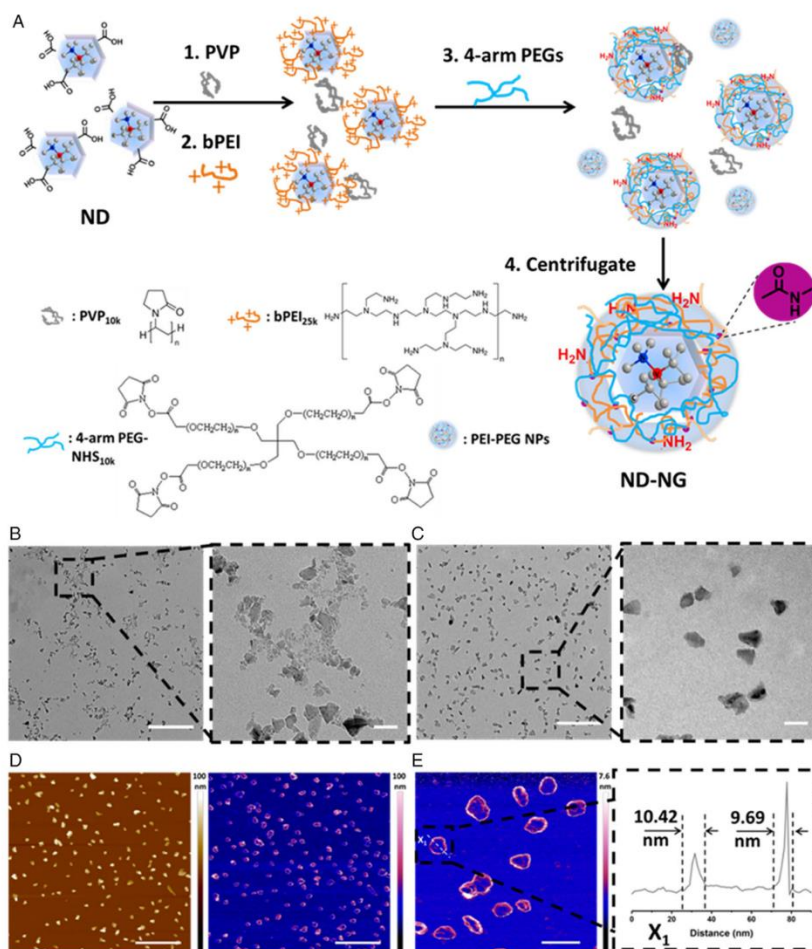


Figure 1. A) Schematic illustration of the preparation of ND–NGs. B) TEM images of NDs (left: scale bar = 500 nm; right: scale bar = 50 nm). C) TEM images of ND–NGs (left: scale bar = 500 nm; right: scale bar = 50 nm). D) AFM images of ND–NGs at liquid state (left: height sensor; right: deformation; scale bar = 500 nm). E) AFM images of ND–NGs (left: scale bar = 100 nm; right: deformation distance curve of ND–NGs).

(PAMAM-G3) as well as the buffer, which was used to prepare ND–NGs, was investigated (Figure S4, Supporting Information). NDs aggregated and precipitated when PEIs with lower MW were used (PEI 600 Da and PEI 2000 Da). Alternatives, such as the positively charged dendrimer PAMAM-G3, did not improve colloidal stability, and precipitation was likewise observed, implying that only the positively charged branched polymer with appropriate MW (PEI 25 000 Da) and molecular structure allowed the preparation of stable ND–NGs. The ionic strengths of the buffer affected the preparation of ND–NGs as well (Figure 2A, Table S2, Supporting Information), yielding ND–NGs with various sizes in

Milli-Q water (83.3 ± 11.0 nm), PBS (57.0 ± 1.2 nm), and HEPES (59.6 ± 6.7 nm).

Postfunctionalization allows controlling the chemical, physical, and physiological properties of ND essential for further applications.^[12] PEI possesses many amine groups, which are positively charged at physiological pH. Bare NDs have a zeta potential of -37.2 ± 0.6 mV, which increased to about 18.8 ± 0.78 mV (Table S1, Supporting Information) after coating, due to many free primary amino groups located at the ND–NG surface. Fluorescamine is a commonly used fluorogenic reagent for the detection and quantification of amino groups. An excess

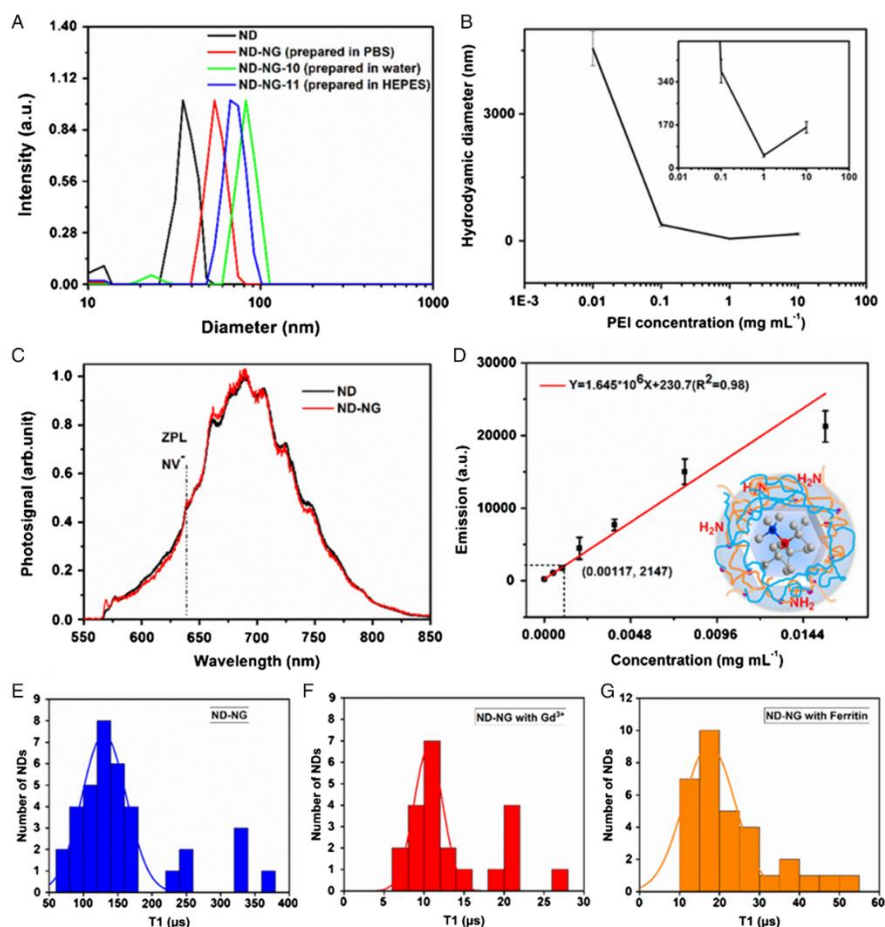


Figure 2. A) Hydrodynamic diameter of NDs and ND–NGs measured by DLS. B) Influence of the PEI concentration on the size of ND–NGs. Data presented as mean \pm SD, $n = 3$. C) Normalized emission spectra (e.g., 532 nm) of NDs and ND–NGs. NV^- zero-phonon lines are visible in both spectra. D) Standard curve of fluorescence intensity using ethylenediamine concentration. Data presented as mean \pm SD, $n = 3$. E) T_1 time of ND–NG ($129.47 \pm 32.5 \mu\text{s}$). Data presented as mean \pm SD, $n = 37$. F) T_1 time of ND–NG with Cd^{3+} ($10.53 \pm 1.82 \mu\text{s}$). Data presented as mean \pm SD, $n = 22$. G) T_1 time of ND–NG with ferritin ($17.43 \pm 6.45 \mu\text{s}$). Data presented as mean \pm SD, $n = 34$.

of fluorescamine was added to the ND–NG solution and the fluorescence intensity was measured using an excitation and emission wavelength of 365 and 470 nm (Figure S6, Supporting Information), respectively. In comparison with the control samples, ND–NG, fluorescamine, and water, only the ND–NGs incubated with fluorescamine showed significant fluorescence, proving the accessibility of amino groups present on the surface of ND–NGs. Using ethylenediamine to achieve a calibration plot (Figure 2D), the content of the amine groups on ND–NGs was calculated, suggesting about 3.90×10^{-5} mol primary amino groups ($-\text{NH}_2$) per gram ND–NGs. Assuming that

the NDs consist only of C atoms and that all ND–NGs particles have a spherical shape of about 40 nm diameter,^[17] this results in an estimated number of about 2769 amino groups per ND–NG that could be used for postmodifications.

The effect of the NG shell on the photophysical properties of NDs containing NV centers was investigated (Figure 2C, Figure S5, Supporting Information). For optical measurements, ND–NGs with a diameter of 57.0 ± 1.2 nm were used. The fluorescence intensity of ND–NGs in water was measured using a laser beam ($\lambda_{\text{ex}} = 560$ nm and $\lambda_{\text{em}} = 680$ nm, Figure S5, Supporting Information). No significant reduction in the

fluorescence intensity was observed for ND–NGs compared with bare NDs. In addition, no change in the spectral shape was detected. Furthermore, the effect of the NG shell on the charge state of NV centers in NDs was studied at the single nanoparticle level (Figure 2C). The spectra were measured on a custom-built confocal microscope with an excitation laser at 532 nm and 100 μ W power in front of the objective (oil, NA = 1.35). Obviously, the NG shell did not affect the emission properties, and the zero-phonon lines of NV⁻ centers were still well visible without any shift or background noise. NV centers in NDs are very sensitive to the surface states and at some conditions, they can switch to the dark state (neutral NV center; NV⁰ and positively charged NV center; NV⁺). These results demonstrate that the NG coating did not affect the charge properties of the NV centers, which remained in the optically active states (NV⁻) and which is important for the future application in bioimaging and nanoscale sensing. To prove the nanoscale sensing ability of ND–NG, Gd³⁺ salt and the iron-storage protein ferritin containing iron in ferric state were selected exemplarily as paramagnetic species. ND–NG was incubated with GdCl₃ or ferritin overnight and purified by centrifugation. While the adsorption of ferritin was revealed by TEM (Figure S8A, Supporting Information), Gd³⁺ ions probably penetrated into the NG and were not visible in TEM (Figure S8B + C, Supporting Information). To evaluate the influence of the Gd³⁺ and ferritin adsorbed to ND–NG on the NV spin longitudinal T_1 relaxation time, we used a confocal microscope equipped to conduct T_1 spin relaxometry. A pulsed T_1 sequence was chosen, consisting of repetitive laser pulses in the absence of a microwave. The spin relaxation from the $m_s = 0$ spin state to the thermally mixed state was probed and the relaxometry measurements were carried out on randomly selected single particles (Figure S9, Supporting Information). For each sample, the resulting T_1 constants were averaged. The T_1 time decreased from 129.47 \pm 32.5 μ s of ND–NG to 10.53 \pm 1.82 μ s of ND–NG with complexed Gd³⁺ and 17.43 \pm 6.45 μ s of ND–NG with ferritin, indicating that the ND–NGs are in principle able to sense magnetic fields in their direct surrounding (Figure 2E–G).

Next, the biocompatibility of ND–NGs was investigated using A549 human lung adenocarcinoma cell line (Figure 3). As shown in Figure 3B,C, and Figure S7A, Supporting Information, ND–NGs were efficiently taken up into A549 cells after 4 h of incubation. We found many homogeneously distributed spherical structures, indicating that ND–NGs were located in intracellular vesicles. The uptake was dependent on the ND–NG concentration and incubation time. When we increased the incubation time from 6 to 24 h and the concentration of ND–NGs from 100 to 200 μ g mL⁻¹, the uptake became even more prominent. In addition, cells proliferated well and the cell morphology was not altered. Low cytotoxicity of ND–NGs was observed after the treatment of the cells with a concentration up to 800 μ g mL⁻¹ (Figure 3A).

To further evaluate the biocompatibility of ND–NG, the Hen's Egg Test on the Chorioallantoic Membrane (HET-CAM) method^[29] was chosen, a potential alternative of animal experiments. The wide availability of fertile eggs and easily achievable hatching temperature (37–38 °C) made the HET-CAM a desirable experiment platform. CAM has an ample vascular network, which is suitable for studying tissue xenograft, tumor growth,

drug delivery, wound healing, and toxicologic study.^[30] CAM is not innervated, and the chick embryo develops a functional brain only on day 13 of incubation.^[31] Therefore HET-CAM model can be considered as an animal-friendly and humane alternative of in vivo testing. In our HET-CAM test, we observed hemorrhage from blood vessels within 2–4 s after applying the positive control (1% sodium dodecyl sulfate; SDS). Lysis occurred after 25–27 s, and we observed coagulation within 24 h. For the negative control (phosphate-buffered saline) and various concentrations of NG–NG (100, 400, 800 μ g mL⁻¹), no instance of irritation was detected from 5 min to 24 h of application (Figure 3D and Figure S7B, Supporting Information). A summary of the results is shown in Table S3, Supporting Information. These in ovo results support the biocompatibility of ND–NG.

To underline the potential of ND–NGs as a theranostic platform, a PDT agent, [4-(1*H*-imidazo[4,5-*f*][1,10]phenanthrolin-2-yl- κ N7, κ N8)benzoato]-bis(2,2'-bipyridine- κ N1, κ N1')ruthenium(II+) chloride (Ru–COOH), was conjugated with the ND–NGs by the reaction of its carboxylic acid with the amine groups of ND–NGs in the presence of EDC to afford ND–NG–Ru (Figure 4A). PDT is a treatment using photosensitizing agents, whose bioactivity is activated by light.^[32] The photosensitizer produces reactive oxygen species, i.e., singlet oxygen (¹O₂) for therapeutic purposes. Singlet oxygen is cytotoxic, which strongly decreases, i.e., viability of tumor cells.^[33] PDT is minimally invasive compared with other treatment procedures (e.g., surgery) and can be used together with other therapeutic techniques. Due to the low invasiveness of this approach, small or no scarring at the application site after healing represents an additional benefit for the patient's quality of life. However, there are some drawbacks including low tumor specificity, inefficient cellular uptake, and higher activation energies (if required), leading to prolonged illumination times. To overcome these challenges, ND–NG was used as a carrier system. After modification with Ru–COOH, the attenuated total reflection Fourier-transform infrared (ATR-FTIR) spectrum of ND–NG–Ru was measured (Figure S10, Supporting Information) and this showed that the peak intensity of the stretching vibration of N–H decreased as the amine group reacted with the carboxylic acid groups of Ru–COOH. To quantify the number of Ru complexes on ND–NG–Ru, the fluorescence intensity was measured using an excitation and emission wavelength of 460 and 610 nm, respectively. In comparison with the control samples (ND–NG), only ND–NG–Ru showed emission properties in the characteristic range (Figure S11, Supporting Information). Using a series of Ru–COOH solutions, a calibration plot was generated (Figure 4B) and the content of the Ru complexes on the ND–NG–Ru was calculated to be 3.78 μ g mg⁻¹ of ND–NGs. The DLS and TEM measurements of ND–NG–Ru revealed a high colloidal stability with good dispersion and stability in aqueous media (Figure S12 and S13, Supporting Information). Compared with the hydrodynamic size of ND–NG, the dimension of ND–NG–Ru increased from 57.0 \pm 1.2 to 73.7 \pm 4.9 nm, respectively. In addition, no significant aggregation was observed in TEM images. PDT relies on the efficient production of singlet oxygen in cellular environments. To monitor the generation of ¹O₂ in a quantitative fashion, we conducted ¹O₂ production efficiency tests as reported previously.^[34] The singlet oxygen sensor 9,10-anthracenediyl-bi(methylene)dimalonic acid (ABDA) was used, which forms an

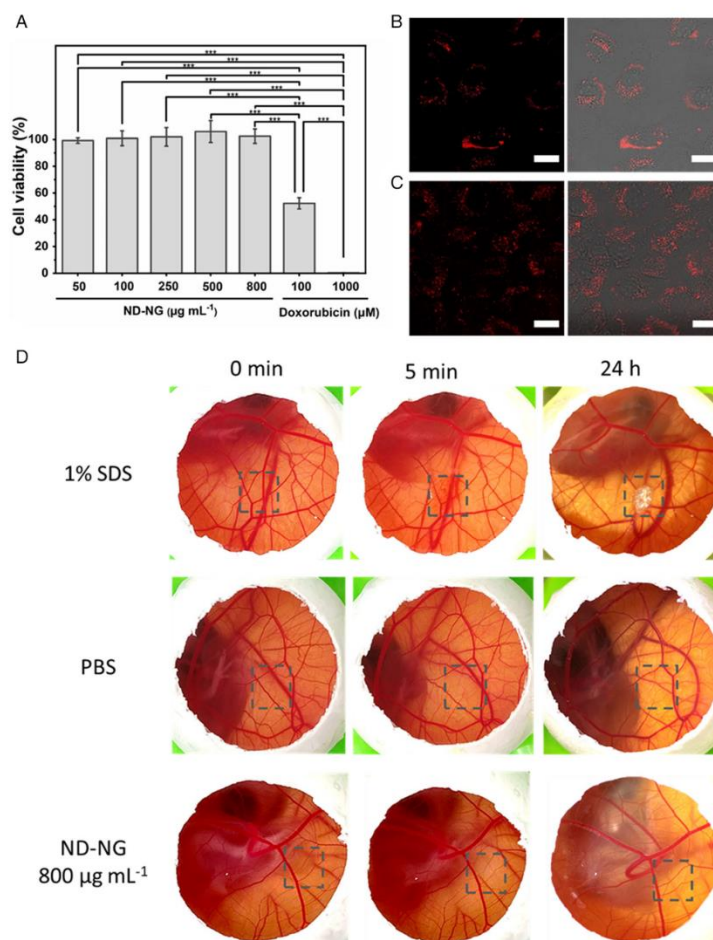


Figure 3. A) Cell viability in A549 cells with various concentrations of ND–NG, $n = 5$, one-way ANOVA with Tukey's posthoc test, $***p < 0.001$. All ND–NG concentrations are statistically nonsignificant. B,C) Confocal microscopy images of ND–NGs taken up into A549 cells (scale bar = $20 \mu\text{m}$) (B) at $100 \mu\text{g mL}^{-1}$ for 6 h and (C) at $200 \mu\text{g mL}^{-1}$ for 24 h. D) Photographs of HET-CAM test results for 1% SDS (positive control), PBS (negative control), and ND–NG at $800 \mu\text{g mL}^{-1}$.

endoperoxide of ABDA in the presence of $^1\text{O}_2$ that alters its absorbance spectrum. Therefore, the production of $^1\text{O}_2$ was monitored by measuring this particular change in absorbance of ABDA (Figure 4C, Figure S14, Supporting Information). ND–NG–Ru, ND–NGs, and bare NDs as control were mixed with $100 \mu\text{M}$ of ABDA and were irradiated with a 470 nm light-emitting diode (LED) array (20 mW cm^{-2}) for 15 min. Relative changes in absorbance confirmed the successful generation of $^1\text{O}_2$. We also examined the intracellular localization of ND–NG–Ru in a human cervical cancer cell line (HeLa cells) by laser scanning confocal microscopy. These cells were

incubated with ND–NG–Ru ($100 \mu\text{g mL}^{-1}$) for about 4 h before images were recorded (Figure 4E). ND–NG–Ru were efficiently taken up and many homogeneously distributed spherical structures were observed, suggesting that ND–NGs were mainly located in intracellular vesicles. To evaluate light-induced cellular toxicity, HeLa cells were incubated with $0\text{--}200 \mu\text{g mL}^{-1}$ ND–NG–Ru for 4 h before irradiation with 470 nm LED light for 15 min (50 mW cm^{-2}). The applied power is comparable with the reported photosensitizing drugs.^[35] We found a very low IC_{50} of around $23 \mu\text{g mL}^{-1}$ for the ND–NG–Ru (Figure 4D), which is similar to the reported IC_{50}

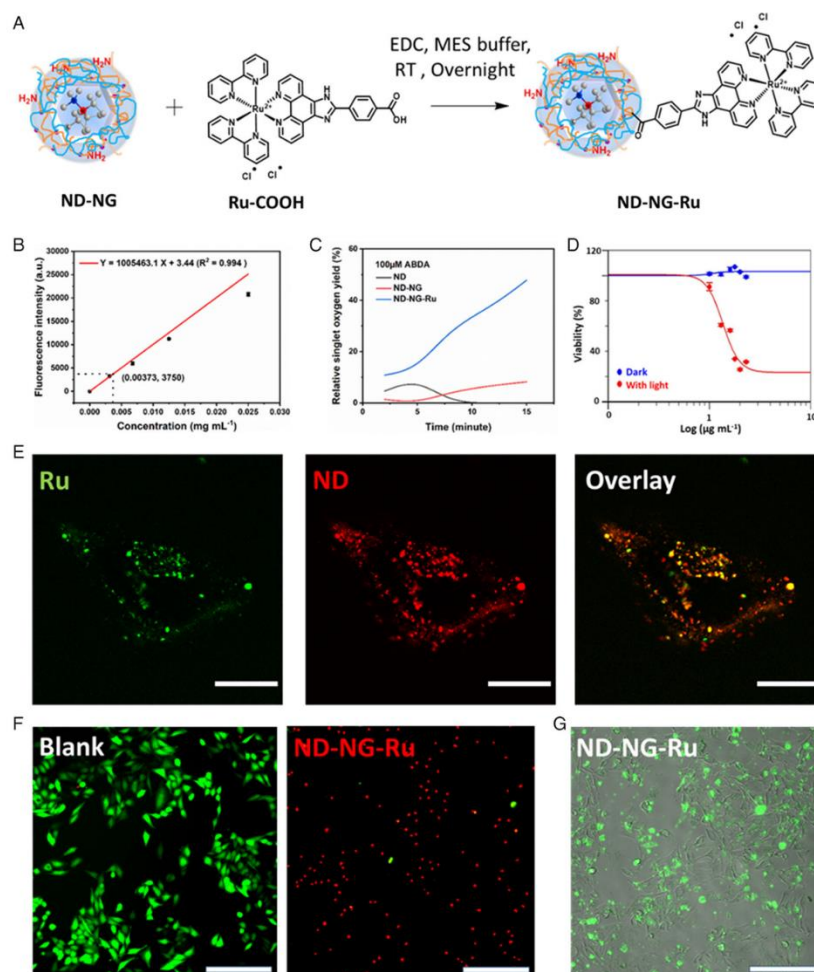


Figure 4. A) Schematic illustration of the preparation of ND-NG-Ru. B) Standard curve of fluorescence intensity using different concentrations of Ru-COOH. Data presented as mean \pm SD, $n = 3$. C) Singlet oxygen yield of ND-NG-Ru. D) Logarithmic fitting curve for cell viability of ND-NG-Ru. Data presented as mean \pm SD, $n = 3$. E) Confocal microscopy images in HeLa cells after 4 h incubation with $100 \mu\text{g mL}^{-1}$ ND-NG-Ru (15 min of irradiation, scale bar = $20 \mu\text{m}$). Green and red colors represent Ru and ND signal, respectively. F) Live/dead staining of HeLa cells incubated without or with $100 \mu\text{g mL}^{-1}$ ND-NG-Ru after 15 min of irradiation (scale bar = $200 \mu\text{m}$). G) Early apoptosis detection by Annexin V, FITC. Green color represents apoptotic cells (scale bar = $200 \mu\text{m}$).

of $15 \mu\text{g mL}^{-1}$ of the Ru-tetrazole-coordinated nanoparticles.^[36] Live/dead staining of the cells using fluorescein diacetate/propidium iodide further demonstrated that ND-NG-Ru-induced cell death upon irradiation could be spatially controlled (Figure 4F). Furthermore, we confirmed induced cell death using Annexin-V, a protein that binds to phosphatidylserine, which is only present during apoptosis (Figure 4G).

3. Conclusion

In summary, we established the adsorption-crosslinking method as a novel synthesis concept for the surface modification of NDs. This approach combines both noncovalent adsorption and covalent stabilization, thus integrating the advantages of both coating strategies within one system, while overcoming

their respective drawbacks. Using this method, we successfully prepared ND–NG samples with a thin and uniform NG shell, as well as a narrow size distribution, while elucidating the chemical tools to control its formation. Critically, the photophysical properties of the NV centers in ND were not affected by surface modification, thus facilitating the nanoscale sensing applications. Quantification of the number of amine groups, which are present on the surface of ND–NGs, was achieved. Furthermore, the ND–NGs were well tolerated in cell experiments and in vivo testing. Introduction of a PDT agent, Ru–COOH, was achieved in a postmodification approach. ND–NG–Ru showed successful photodynamic activity in vitro. By demonstrating the capability to combine multiple functions, i.e., the nanoscale sensing and photodynamic ability, the versatility of the platform was proven. Importantly, the adsorption–crosslinking method can be expanded to other chemical motifs, as reactive groups are still available within the NGs for further modification. We believe that our studies pave the way to customized ND-based nanotheranostics for precise diagnosis and therapy at the subcellular level.

Supporting Information

Supporting Information is available from the Wiley Online Library or from the author.

Acknowledgements

Y.W. and M.N.A.A. contributed equally to this work. The authors thank the Polymer Analytics for multiangle DLS measurements, Dr. David Yuen Wah Ng for the fruitful discussion and suggestions, Dr. Gönül Kizilsavas for her support, and Adriana Sobota for her suggestions regarding the HET-CAM assay. The authors are grateful for the financial support from the European Union's Horizon 2020 Research and Innovation Program under FETOPEN grant agreement no. 858149 (AlternativeToGd) and from the Deutsche Forschungsgemeinschaft (DFG, German Research Foundation)—project number 316249678—SFB 1279 (C04). Y.W. thanks the China Scholarship Council for a fellowship.

Conflict of Interest

The authors declare no conflict of interest.

Data Availability Statement

The data that supports the findings of this study are available in the supplementary material of this article.

Keywords

adsorption–crosslinking, nanodiamonds, nanogels, nanoscale sensing, photodynamic applications

Received: December 3, 2020

Revised: March 24, 2021

Published online: May 13, 2021

- a) M. Ibrahim, Y. Xue, M. Ostermann, A. Sauter, D. Steinmueller-Nethl, S. Schweeberg, A. Krueger, M. R. Cimpan, K. Mustafa, *J. Biomed. Mater. Res., Part A* **2018**, *106*, 1697; b) K. Adach, M. Fijalkowski, G. Gajek, J. Skolimowski, R. Kontek, A. Blaszczyk, *Chem.-Biol. Interact.* **2016**, *254*, 156; c) V. Vaijayanthimala, P.-Y. Cheng, S.-H. Yeh, K.-K. Liu, C.-H. Hsiao, J.-I. Chao, H.-C. Chang, *Biomaterials* **2012**, *33*, 7794.
- G. Balasubramanian, I. Chan, R. Kolesov, M. Al-Hmoud, J. Tisler, C. Shin, C. Kim, A. Wojcik, P. R. Hemmer, A. Krueger, *Nature* **2008**, *455*, 648.
- a) S. Han, M. Raabe, L. Hodgson, J. Mantell, P. Verkade, T. Lasser, K. Landfester, T. Weil, I. Lieberwirth, *Nano Lett.* **2019**, *19*, 2178; b) M. D. Torelli, N. A. Nunn, O. A. Shenderova, *Small* **2019**, *15*, 1902151; c) H. S. Jung, K. J. Cho, Y. Seol, Y. Takagi, A. Dittmore, P. A. Roche, K. C. Neuman, *Adv. Funct. Mater.* **2018**, *28*, 1801252.
- Y. Wu, A. Ermakova, W. Liu, G. Pramanik, T. M. Vu, A. Kurz, L. McGuinness, B. Naydenov, S. Hafner, R. Reuter, *Adv. Funct. Mater.* **2015**, *25*, 6576.
- S. Harvey, M. Raabe, A. Ermakova, Y. Wu, T. Zapata, C. Chen, H. Lu, F. Jelezko, D. Y. Ng, T. Weil, *Adv. Ther.* **2019**, *2*, 1900067.
- a) Y. Zhang, Z. Cui, H. Kong, K. Xia, L. Pan, J. Li, Y. Sun, J. Shi, L. Wang, Y. Zhu, *Adv. Mater.* **2016**, *28*, 2699; b) Z. Cui, Y. Zhang, K. Xia, Q. Yan, H. Kong, J. Zhang, X. Zuo, J. Shi, L. Wang, Y. Zhu, *Nat. Commun.* **2018**, *9*, 1; c) T. K. Ryu, S. W. Baek, R. H. Kang, S. W. Choi, *Adv. Funct. Mater.* **2016**, *26*, 6428.
- M. H. Alkahtani, F. Alghannam, L. Jiang, A. Almethen, A. A. Rampersaud, R. Brick, C. L. Gomes, M. O. Scully, P. R. Hemmer, *Nanophotonics* **2018**, *7*, 1423.
- a) P. Neumann, I. Jakobi, F. Dolde, C. Burk, R. Reuter, G. Waldherr, J. Honert, T. Wolf, A. Brunner, J. H. Shim, *Nano Lett.* **2013**, *13*, 2738; b) D. A. Simpson, E. Morrisroe, J. M. McCoe, A. H. Lombard, D. C. Mendis, F. Treussart, L. T. Hall, S. Petrou, L. C. Hollenberg, *ACS Nano* **2017**, *11*, 12077; c) T. Sekiguchi, S. Sotoma, Y. Harada, *Biophys. Physicobiol.* **2018**, *15*, 229.
- a) A. Ermakova, G. Pramanik, J.-M. Cai, G. Algara-Siller, U. Kaiser, T. Weil, Y.-K. Tzeng, H.-C. Chang, L. McGuinness, M. B. Plenio, *Nano Lett.* **2013**, *13*, 3305; b) T. Zhang, G.-Q. Liu, W.-H. Leong, C.-F. Liu, M.-H. Kwok, T. Ngai, R.-B. Liu, Q. Li, *Nat. Commun.* **2018**, *9*, 1.
- a) V. R. Horowitz, B. J. Alemán, D. J. Christle, A. N. Cleland, D. D. Awschalom, *Proc. Natl. Acad. Sci.* **2012**, *109*, 13493; b) R. D. Akiel, X. Zhang, C. Abeywardana, V. Stepanov, P. Z. Qin, S. Takahashi, *J. Phys. Chem. B* **2016**, *120*, 4003.
- K. Xia, C.-F. Liu, W.-H. Leong, M.-H. Kwok, Z.-Y. Yang, X. Feng, R.-B. Liu, Q. Li, *Nat. Commun.* **2019**, *10*, 1.
- K. van der Laan, M. Hasani, T. Zheng, R. Schirrhagl, *Small* **2018**, *14*, 1703838.
- J. J. Virgen-Ortiz, J. C. dos Santos, Á. Berenguer-Murcia, O. Barbosa, R. C. Rodrigues, R. Fernandez-Lafuente, *J. Mater. Chem. B* **2017**, *5*, 7461.
- L. Zhao, Y.-H. Xu, T. Akasaka, S. Abe, N. Komatsu, F. Watari, X. Chen, *Biomaterials* **2014**, *35*, 5393.
- L.-W. Tsai, Y.-C. Lin, E. Perevedentseva, A. Lugovtsov, A. Priezhev, C.-L. Cheng, *Int. J. Mol. Sci.* **2016**, *17*, 1111.
- A. Bumb, S. K. Sarkar, N. Billington, M. W. Brechbiel, K. C. Neuman, *J. Am. Chem. Soc.* **2013**, *135*, 7815.
- L. Zhao, T. Takimoto, M. Ito, N. Kitagawa, T. Kimura, N. Komatsu, *Angew. Chem., Int. Ed.* **2011**, *50*, 1388.
- X. Q. Zhang, R. Lam, X. Xu, E. K. Chow, H. J. Kim, D. Ho, *Adv. Mater.* **2011**, *23*, 4770.
- X.-Q. Zhang, M. Chen, R. Lam, X. Xu, E. Osawa, D. Ho, *ACS Nano* **2009**, *3*, 2609.

- [20] R. A. Shimkunas, E. Robinson, R. Lam, S. Lu, X. Xu, X.-Q. Zhang, H. Huang, E. Osawa, D. Ho, *Biomaterials* **2009**, *30*, 5720.
- [21] J. Ackermann, A. Krueger, *Carbon* **2020**, *163*, 56.
- [22] S. R. Hemelaar, A. Nagl, F. Bigot, M. M. Rodríguez-García, M. P. de Vries, M. Chipaux, R. Schirhagl, *Microchim. Acta* **2017**, *184*, 1001.
- [23] a) P. A. Longo, J. M. Kavan, M.-S. Kim, D. J. Leahy, in *Methods in Enzymology*, Vol. 529, Elsevier, Amsterdam/New York **2013**, 227; b) H. Wang, Q. Li, J. Yang, J. Guo, X. Ren, Y. Feng, W. Zhang, *J. Mater. Chem. B* **2017**, *5*, 1408.
- [24] a) Y. H. Kim, J. H. Park, M. Lee, Y.-H. Kim, T. G. Park, S. W. Kim, J. Yang, M. Shen, L. Wang, X. Shi, *Biomater. Sci.* **2017**, *5*, 258; c) W. Sun, Y. Wang, M. Cai, L. Lin, X. Chen, Z. Cao, K. Zhu, X. Shuai, *Biomater. Sci.* **2017**, *5*, 2468.
- [25] a) C. Graf, D. L. Vossen, A. Imhof, A. van Blaaderen, *Langmuir: ACS J. Surf. Colloids* **2003**, *19*, 6693; K. M. Koczkur, S. Mourdikoudis, L. Polavarapu, S. E. Skrabalak, *Dalton Trans.* **2015**, *44*, 17883; b) M. Farahmandjou, S. Honarbakhsh, S. Behrouzinia, *Phys. Chem. Res.* **2016**, *4*, 655.
- [26] a) R. Mishra, R. Varshney, N. Das, D. Sircar, P. Roy, *Eur. Polym. J.* **2019**, *119*, 155; b) E. Doğan, P. Tokcan, M. Diken, B. Yılmaz, B. Kizilduman, P. Sabaz, *Adv. Mater. Sci.* **2019**, *19*, 32; c) Y. Guo, Z. Hao, C. Wan, *Tribol. Int.* **2016**, *93*, 214.
- [27] F. Heinemann, J. Karges, G. Gasser, *Acc. Chem. Res.* **2017**, *50*, 2727.
- [28] R. Garcia, R. Proksch, *Eur. Polym. J.* **2013**, *49*, 1897.
- [29] G. Winter, A. B. Koch, J. Löffler, M. Lindén, C. Solbach, A. Abaei, H. Li, G. Glatting, A. J. Beer, V. Rasche, *Cancers* **2020**, *12*, 1248.
- [30] A. Vargas, M. Zeisser-Labouèbe, N. Lange, R. Gurny, F. Delie, *Adv. Drug Delivery Rev.* **2007**, *59*, 1162.
- [31] E. Aleksandrowicz, I. Herr, *ALTEX-Altern. Animal Exp.* **2015**, *32*, 143.
- [32] M. C. DeRosa, R. J. Crutchley, *Coord. Chem. Rev.* **2002**, *233*, 351.
- [33] T. J. Dougherty, C. J. Gomer, B. W. Henderson, G. Jori, D. Kessel, M. Korbelik, J. Moan, Q. Peng, *JNCI, J. Natl. Cancer Inst.* **1998**, *90*, 889.
- [34] T. Wang, N. Zabarska, Y. Wu, M. Lamla, S. Fischer, K. Monczak, D. Y. Ng, S. Rau, T. Weil, *Chem. Commun.* **2015**, *51*, 12552.
- [35] S. Chakraborty, B. K. Agrawalla, A. Stumper, N. M. Vegi, S. Fischer, C. Reichardt, M. Kögler, B. Dietzek, M. Feuring-Buske, C. Buske, *J. Am. Chem. Soc.* **2017**, *139*, 2512.
- [36] B. Wei, M. Y. Guo, Y. M. Lu, P. P. Sun, G. W. Yang, Q. Y. Li, *Anorg. Allg. Chem.* **2018**, *644*, 6.

FULL PAPER

Targeted Protein Delivery



ADVANCED
HEALTHCARE
MATERIALS

www.advhealthmat.de

Supramolecular Toxin Complexes for Targeted Pharmacological Modulation of Polymorphonuclear Leukocyte Functions

Astrid Johanna Heck, Theresa Ostertag, Leonie Schnell, Stephan Fischer, Bikram Keshari Agrawalla, Pia Winterwerber, Eva Wirsching, Michael Fauler, Manfred Frick, Seah Ling Kuan,* Tanja Weil,* and Holger Barth*

The targeted pharmacological modulation of polymorphonuclear leukocytes (PMNs) is of major medical interest. These innate immune cells play a central role in the defense against pathogenic microorganisms. However, their excessive chemotactic recruitment into tissues after traumatic injury is detrimental due to local and systemic inflammation. Rho-GTPases, being the master regulators of the actin cytoskeleton, regulate migration and chemotaxis of PMNs, are attractive pharmacological targets. Herein, supramolecular protein complexes are assembled in a “mix-and-match” approach containing the specific Rho-inhibiting clostridial C3 enzyme and three PMN-binding peptides using an avidin platform. Selective delivery of the C3 Rho-inhibitor with these complexes into the cytosol of human neutrophil-like NB-4 cells and primary human PMNs *ex vivo* is demonstrated, where they catalyze the adenosine diphosphate (ADP) ribosylation of Rho and induce a characteristic change in cell morphology. Notably, the complexes do not deliver C3 enzyme into human lung epithelial cells, A549 lung cancer cells, and immortalized human alveolar epithelial cells (hAELVi), demonstrating their cell type-selectivity. The supramolecular complexes represent attractive molecular tools to decipher the role of PMNs in infection and inflammation or for the development of novel therapeutic approaches for diseases that are associated with hyperactivity and reactivity of PMNs such as post-traumatic injury.

1. Introduction

Polymorphonuclear leukocytes, also termed PMNs or neutrophils, are the most abundant leukocytes in human blood and a major component of the innate immune system. In the human

body, molecules derived from microbial pathogens and/or the host, recruit PMNs via chemotactic mechanisms from the blood stream to sites of infection. PMNs evade from the blood vessels into the tissue to ingest the pathogenic microorganisms by phagocytosis and to eliminate bacteria and fungi via their arsenal of cytotoxic substances. However, besides the beneficial role of PMN activity with infections, hyperactivity of PMNs can be detrimental for patients, if PMNs are excessively recruited into injured tissues.^[1] Such conditions are, for example, reported for multiple injured patients suffering from blunt thorax trauma, where the enhanced chemotactic recruitment of PMNs and monocytic cells into the lungs and the subsequent release of their toxic mediators enhance the alveolar barrier breakdown resulting in local and systemic inflammation and contributing to the poor outcome of such patients.^[1–6]

Therefore, the targeted, cell type-selective, pharmacological inhibition of excessive chemotactic recruitment of PMNs

will enhance our understanding of their role in the first-line defense against microbes and their contribution to the excessive inflammatory responses after traumatic tissue injury. Since migration, chemotaxis, and phagocytosis of PMNs depend on the remodeling of the actin cytoskeleton, which is regulated by

A. J. Heck, Dr. B. K. Agrawalla, P. Winterwerber, Dr. S. L. Kuan, Prof. T. Weil
Max Planck Institute for Polymer Research
Ackermannweg 10, 55128 Mainz, Germany
E-mail: kuan@mpip-mainz.mpg.de; weil@mpip-mainz.mpg.de

The ORCID identification number(s) for the author(s) of this article can be found under <https://doi.org/10.1002/adhm.201900665>.

© 2019 The Authors. Published by WILEY-VCH Verlag GmbH & Co. KGaA, Weinheim. This is an open access article under the terms of the Creative Commons Attribution License, which permits use, distribution and reproduction in any medium, provided the original work is properly cited.

The copyright line for this article was changed on 16 August 2019 after original online publication.

DOI: 10.1002/adhm.201900665

Adv. Healthcare Mater. 2019, 8, 1900665

1900665 (1 of 12)

T. Ostertag, Dr. L. Schnell, Dr. S. Fischer, Prof. H. Barth
Institute of Pharmacology and Toxicology – Ulm University Medical Center
Albert-Einstein-Allee 11, 89081 Ulm, Germany
E-mail: holger.barth@uni-ulm.de

E. Wirsching, M. Fauler, Prof. M. Frick
Institute of General Physiology – Ulm University
Albert-Einstein-Allee 11, 89081 Ulm, Germany

Dr. S. L. Kuan, Prof. T. Weil
Institute of Inorganic Chemistry I
Ulm University
Albert-Einstein-Allee 11, 89081 Ulm, Germany

© 2019 The Authors. Published by WILEY-VCH Verlag GmbH & Co. KGaA, Weinheim

Rho-GTPases,^[7–12] PMN-selective Rho inhibition represents an attractive strategy to downmodulate excessive PMN recruitment from blood into tissues after traumatic injury.^[13] Moreover, PMN-selective molecules modulating Rho-signaling and actin dynamics of these immune cells certainly offer great potential as molecular tools in cell biology and experimental pharmacology to decipher the role of PMN activity in both infection and inflammation. In this context, the C3 enzymes from *Clostridium (C.) botulinum* (C3bot1) and *C. limosum* (C3lim) are of major interest as they represent the only known specific Rho inhibitors.^[6,10,14–16] C3 proteins are taken up into the cytosol of monocytic cells where they catalyze the specific mono-ribosylation of Rho A and Rho B. This inhibits Rho-signaling resulting in the reorganization of actin filaments accompanied by a characteristic change in cell morphology.^[11,17–21] Recently, it has been demonstrated by our groups that the targeted pharmacological inhibition of Rho activity by C3 enzyme inhibits the migration and chemotaxis of primary human monocytes *ex vivo*.^[11] Moreover, the local intra-tracheal application of this Rho-inhibitor prevented the excessive recruitment of monocytic cells from the blood into the lungs of mice after blunt thorax trauma.^[11] However, the C3 Rho-inhibitor has no effect on PMNs *ex vivo* and does not reduce the amount of PMNs in the lungs of mice after blunt thorax trauma.^[11] Therefore, the selective introduction of C3 Rho-inhibitor into PMNs would be highly desirable for such applications.

Herein, we developed PMN-selective Rho-inhibitors based on the supramolecular assembly of C3 Rho-inhibitor and specific PMN-targeting peptides on an avidin (Avi) platform to provide cell-type selectivity. The PMN-targeting peptide sequences have previously been identified using random peptide phage display that addresses the neutrophils specifically.^[22–24] For instance, the Ac-GGPNLTGRWGPPVESALAK-NH₂ (GGP) sequence reveals neutrophil and monocyte selective binding, which has been applied to liposomes for targeted delivery.^[25] In addition, the peptide cinnamoyl-F(D)LF(D)LFK-NH₂ (FK), an antagonist of the formyl peptide receptor 1 (FPR-1) of neutrophils, has been conjugated to imaging agents or nanoparticles for *in vivo* imaging.^[26,27]

Although peptide sequences such as GGP could be recombinantly fused to C3 Rho-inhibitor, the expression of C3 enzyme with cyclic or chemically modified peptides, such as FK cannot be achieved by molecular biology techniques. Furthermore, the fusion of multiple peptide sequences to a single enzyme is challenging by genetic means and would require tedious optimization.^[28,29] Release characteristics are controlled by chemical linker design to impart a variety of stimulus-responsive groups for, e.g., pH-controlled release in acidic endosomal vesicles or inside the cytoplasm of cancer cells, which is also challenging to achieve by genetic engineering.^[30] Hence, there is a great interest in novel “chemistry” methods to design and produce customized protein drugs.^[31,32] In particular, supramolecular assembly of protein complexes provides convenient access to sophisticated multiprotein architectures that cannot be achieved by molecular biology methods.^[31]

The assembly of multiprotein complexes that contained functional subunits of bacterial protein toxins and dendrimers^[33,34] or multiple copies of the cancer-cell targeting peptide somatostatin at an avidin platform has been established by our groups before. Recently, we have reported the

selective delivery of a supramolecular complex that contains the Rho-inhibitor C3bot1 (henceforth C3) and somatostatin as cell-targeting peptide into the cytosol of human cancer cells overexpressing the somatostatin receptor, resulting in reduced growth of a human xenograft lung tumor.^[35] The best effect was achieved when three somatostatin peptides and one C3 enzyme were bound to the avidin platform presumably via the multivalency effect.^[35] We further expand on this versatile strategy and report herein for the first time the stoichiometric-controlled assembly of 1) multiple copies of different PMN-targeting peptides and 2) C3 Rho-inhibitor via 3) a pH-cleavable hydrazone linker for controlled intracellular release of the C3 enzyme into the cytosol of PMNs (Figure 1). Our platform allows rapid generation of different supramolecular toxin combinations, e.g., by varying the PMN-targeting peptides, which is highly desirable for throughput synthesis and screening to evaluate the efficacy of the different combinations of the C3 Rho-inhibitor and different PMN targeting peptide sequences. We believe that our approach offers great potential for the development of cell type-selective biotherapeutics for the targeted treatment of local and systemic inflammation, e.g., after traumatic injury of multiple injured patients in a convenient “mix-and-match” assembly.

2. Results and Discussion

2.1. “Mix-and-Match” Assembly and Characterization of the Supramolecular Complexes (GGP)₃-Avi-C3 and (FK)₃-Avi-C3

The supramolecular complexes (GGP)₃-Avi-C3 and (FK)₃-Avi-C3 containing the PMN-targeting peptides GGP and FK as well as C3 (Figure 1) were both designed based on avidin-biotin technology. Avidin (Avi), the central platform for assembly, is a tetrameric protein (pI > 9) that forms strong noncovalent interactions ($K_d = 10^{-15}$ M) with its natural binding partner biotin at four binding sites. Here, Avi is selected as a monodisperse supramolecular “glue” to combine the PMN-targeting peptides and C3 Rho-inhibitor at spatially distinct locations. To incorporate biotin into the Ac-GGPNLTGRWGPPVESALAK-NH₂ (GGP) sequence, GGP was functionalized using a bifunctional maleimide-biotin with a short ethylene glycol linker (compound 1, Figure 2A) that improves water solubility. The biotinylated GGP (B-GGP) peptide was obtained in 40% yield after high-performance liquid chromatography (HPLC) purification with >95% purity (Figure S4, Supporting Information). The PMN-targeting peptide cinnamoyl-F(D)LF(D)LFK-NH₂ (FK) with a biotin at the C-terminus (Figure 2B) was purchased commercially (PhtdPeptides Co., Ltd. with 95% purity). To control the stoichiometry of peptides with terminal biotin bound to Avi, a competitive binding assay with 2-(4-hydroxyphenylazo)benzoic acid (HABA) was performed. HABA binds to Avi with lower affinity compared to biotin and shows absorbance at 500 nm in the complexed form (Figure 2C). Thus, disappearance of the absorption peak indicates displacement of HABA by biotin. A stepwise reduction in absorbance was observed upon addition of 1–4 equivalents of biotin indicating the controlled binding of the respective biotinylated neutrophil targeting peptide to Avi (Figure 2C).

It was determined that 1.25 mole equiv of B-GGP and 1.0 mole equiv of B-FK are required per binding pocket in Avi,

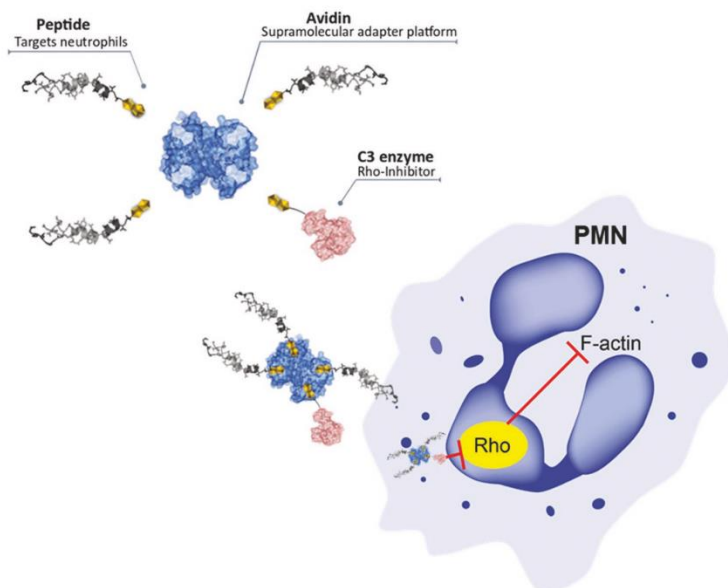


Figure 1. Design and potential mode of action of supramolecular complexes containing specific PMN-targeting peptides and C3-Rho-inhibitor assembled on a central avidin (Avi) platform. The resultant protein complex is designed to selectively internalize into PMNs where the C3-catalyzed Rho-inhibition down-modulates Rho-signaling in order to modulate PMN functions such as migration and chemotaxis.

respectively, most likely for steric reasons. Subsequently, the transporters with three biotinylated peptides per Avi were prepared by mixing the corresponding mole equiv of B-GGP or B-FK with Avi (Figure 2D). These (GGP)₃-Avi or (FK)₃-Avi conjugates offer a free available binding site for conjugation to mono-biotinylated C3.

Next, mono-biotinylation of a cysteine mutant of C3 was accomplished. The enzyme activity and substrate specificity as well as the biological activity of this recombinant C3 variant has been confirmed earlier in J774A.1 macrophages and osteoclast-like RAW 264.7 cells.^[21] A biotin-maleimide conjugation with a pH-sensitive hydrazone linkage (4) that allows cleavage at acidic pH was synthesized with modification from a procedure published previously (Figure 3A and Scheme S1, Supporting information).^[35] The pH-sensitive hydrazone triggers controlled toxin release in acidic endosomal compartments of the cells.^[35] Compound 4 was conjugated to C3 to afford mono-biotinylated C3 (B-C3, Figure 3B) in 78% yield, determined by bicinchoninic acid (BCA) assay and Quant[®]Tag biotin quantification assay (Figure S3, Supporting Information). The successful biotinylation was determined using Western blot analysis (Figure 5), and the degree of biotinylation was quantified to be 91% using the Quant[®]Tag Biotin Kit (Figure S3, Supporting Information).

The controlled assembly of (GGP)₃-Avi-C3 and (FK)₃-Avi-C3 was accomplished through stoichiometric control according to the optimized ratio of 1.25 equiv of B-GGP and 1.0 equiv of B-FK per binding pocket (GGP-B:Avi:B-C3 = 3.75:1:1); (B-FK:Avi:B-C3 = 3:1:1, Figure 4A). Sodium dodecyl sulfate polyacrylamide gel electrophoresis (SDS-PAGE) analysis of

(GGP)₃-Avi-C3 and (FK)₃-Avi-C3 with and without heating against a known concentration of B-C3bot1 (Figure 4B) further revealed that nearly all of the C3 protein reacted during the conjugation reaction, confirming the formation of the supramolecular complexes. The height profile of the constructs (3–6 nm) was determined by using atomic force microscopy (AFM) and no larger aggregates were detected indicating sample homogeneity (Figure 4C). Furthermore, no aggregates were detected by dynamic light scattering in solution (Table S1, Supporting Information). The zeta-potential of (FK)₃-Avi-C3 and (GGP)₃-Avi-C3 was determined to be –4.56 and –2.39 mV, respectively, which is consistent with the theoretical isoelectric point (pI) of FK (pI = 6) and GGP (pI = 9) peptides (Table S2, Supporting Information).

Next, the stoichiometry of the complexes was assessed using absorption spectroscopy of dye-labeled constructs. First, (GGP)₃-Avi-C3 was triply labeled with dyes in a controlled fashion: First, Avi was labeled with Alexa-594 dye, B-C3 was functionalized with Alexa-647 dye and GGP with Alexa-488 (details are given in the Supporting Information). The ratio of GGP:Avi:C3 was determined from the absorption envelopes using a multiplate reader and a ratio of 3.2:1:0.7 was calculated (Figure 4B). Similarly, absorbance measurement of a dual-labeled (FK)₃-Avi-C3 construct was determined to give a ratio of Avi:C3 of 1:0.8 (Figure S7, Supplementary Information).

The assembly and pH-induced release was further demonstrated with the construct, (FK)₃-Avi-C3, through fluorescence resonance energy transfer (FRET) study (Figure 5A). The labeled proteins and peptides were prepared as outlined in

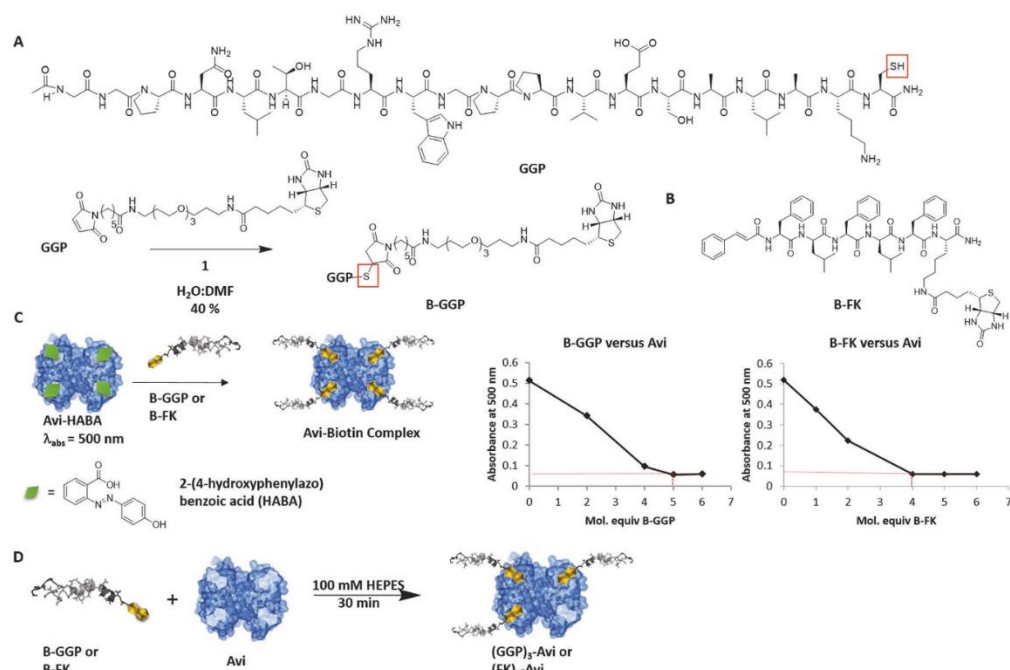


Figure 2. A) Synthesis of biotinylated GGP (B-GGP, H₂O:DMF, 1:0.5, 7.5 mL), room temperature, overnight, 40% isolated yield. B) Chemical structure of B-FK peptide. C) Competitive binding of 2-(4-hydroxyphenylazo)benzoic acid (HABA) and biotin to avidin (Avi). The amount of B-GGP or B-FK required to saturate a tetrameric Avi was determined using the HABA assay. In the case of B-FK 4 mole equiv saturated the binding sites of Avi, while 5 mole equiv of B-GGP are required to saturate the binding sites of Avi. D) Assembly of neutrophil targeting transporters (GGP)₃-Avi and (FK)₃-Avi.

Figure 4A. Only when the donor–acceptor dye pairs are in close proximity (<10 nm), an energy transfer is observed in the fluorescence spectrum,^[36] which confirms the assembly. Upon excitation at 550 nm in the absorption maximum of Alexa-594 dye (purple star), an emission band was observed at 680 nm, indicating energy transfer from the Avi to B-C3 (Figure 5A, left). No energy transfer was observed for the negative controls (FK)₃-Avi alone or (FK)₃-Avi mixed with nonbiotinylated C3 (Figure 5A, left), thereby corroborating the successful assembly. Upon incubation of the construct at pH 4.5 for 4 h, the FRET is no longer observed (Figure 5A, right), confirming the pH-induced release of C3 in acidic environment. To ensure that the construct can be successfully applied in biological media, the stability of (FK)₃-Avi-C3 was investigated in fetal calf serum (FCS). (FK)₃-Avi-C3 was incubated for up to 24 h in 10% FCS in phosphate buffer saline (PBS) and Western blot analysis was applied to monitor its stability. Notably, no increase in free C3 was observed up to 24 h (Figure 5B), which would have indicated disintegration of the construct. To eliminate false positive due to absorption of C3 by serum proteins, FRET measurements were performed, indicating the presence of molecular and nondegraded (FK)₃-Avi-C3 in 10% FCS (Figure S10, Supporting Information). Taken together, our results show the successful assembly of the (FK)₃-Avi-C3 and (GGP)₃-Avi-C3 constructs with about one C3 per conjugate, thus supporting the postulated formulation.

Furthermore, the release of C3 was induced under acidic conditions in vitro and the constructs remained stable in biological media such as FCS.

2.2. The Supramolecular Complexes (GGP)₃-Avi-C3 and (FK)₃-Avi-C3 are Selectively Internalized into Neutrophil-Like NB-4 Cells and C3 is Released into Their Cytosol

The selective delivery of the Rho-inhibitor C3 into the cytosol of neutrophils by either (GGP)₃-Avi or (FK)₃-Avi was investigated as proof-of-concept for these novel transporter molecules. First, human NB-4 cells, a neutrophil-like cell line, were used to test the ability of (GGP)₃-Avi and (FK)₃-Avi to deliver the C3 Rho-inhibitor into the cytosol of these cells. Therefore, differentiated NB-4 cells were incubated at 37 °C with either (GGP)₃-Avi-C3 or (FK)₃-Avi-C3. For negative controls, the Avi alone and the C3 protein alone were applied. Moreover, cells remained untreated as a further control. The recombinant fusion toxin C2IN-C3lim is a specific Rho inhibitor based on the C3lim enzyme. In combination with the C2IIa transport component of the binary C2 toxin from *C. botulinum* served as positive control.^[37] C2IN-C3lim alone is specifically taken up into monocytic cells, but essentially requires C2IIa for its uptake into the cytosol of other cell types such as epithelial cells. Therefore, in

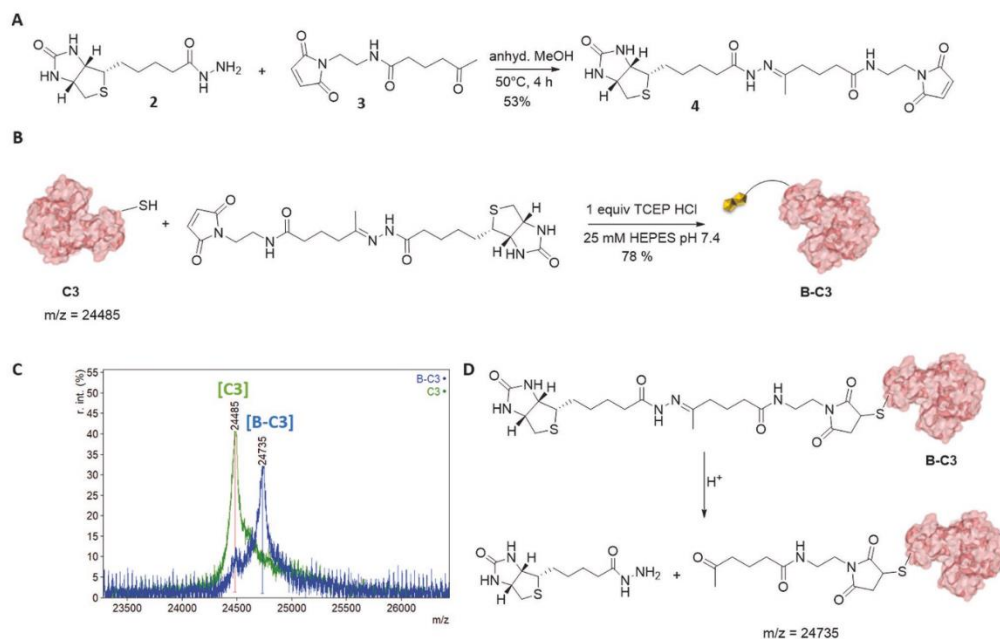


Figure 3. A) Synthesis of compound 4 B) Mono-biotinylation of C3 C) Matrix-assisted laser desorption/ionization (MALDI)-time of flight (ToF) mass spectrometry (MS) spectra of C3 (green) $m/z = 24485$ and biotinylated C3 (B-C3) $m/z = 24735$ using CHCA as matrix. D) Acidic cleavage of B-C3.

combination with C2IIa, the uptake of C2IN-C3lim is not cell-type selective.^[10,37]

In the next step, we determined the characteristic C3-induced changes in cell morphology (Figure 6A) after release of C3 into the cytosol of NB-4 cells. Images of the cells were recorded after different incubation periods and the number of these intoxicated cells was determined based on the morphological changes (Figure 6B). This is a well-established,^[15,17,18,21,35,37,38] highly sensitive and specific endpoint to monitor the uptake of C3 Rho-inhibitor into the host cell cytosol. The changes in cell morphology essentially depend on the C3-catalyzed ADP-ribosylation of Rho in the cytosol.^[15,17,18,21,35,37] As expected, the combination of C2IN-C3lim and C2IIa exhibited the strongest effect while C3 alone and the platform (Avi) alone had almost no effect on cell morphology. Importantly, treatment of NB-4 with (GGP)₃-Avi-C3 as well as (FK)₃-Avi-C3 resulted in a significantly increased number of cells showing the characteristic C3-induced morphology when compared to untreated control cells (Figure 6A,B). This indicates that C3 enzyme activity reached the cytosol of NB-4 cells after their treatment with either (GGP)₃-Avi-C3 or (FK)₃-Avi-C3 ex vivo.

The ability of both transporters to deliver the Rho-inhibitor C3 into the cytosol of NB-4 cells was also confirmed by the biochemical analysis of the ADP-ribosylation status of Rho from these cells and exemplarily shown for (FK)₃-Avi-C3 (Figure 6C). In this assay, the ADP-ribosylation status of Rho was analyzed in cell lysates by sequential ADP-ribosylation with biotin-labeled NAD⁺.^[37,38] A strong signal in the Western blot indicated that

no Rho ADP-ribosylation took place in the intact cells. In contrast, a weak signal in the blot indicated that all/most of the Rho protein have already undergone ADP ribosylation in the intact cells during the incubation with the C3-containing compounds or fusion toxins and therefore is proofed unsuitable as a substrate for the subsequent in vitro ADP-ribosylation with biotin NAD⁺. The observation that C3 alone had no comparable effect as (GGP)₃-Avi-C3 or (FK)₃-Avi-C3 regarding the morphology change and the ADP-ribosylation of Rho in the cells indicated that (GGP)₃-Avi or (FK)₃-Avi are essential for the transport of C3 into the cytosol of the neutrophils. Moreover, it excluded the possibility that C3 was separated from the transporters (GGP)₃-Avi or (FK)₃-Avi already in the medium during the incubation with the cells and that some resulting free C3 might have caused the observed effects in the neutrophils independently from the supramolecular transporters.

2.3. Effect of (GGP)₃-Avi-C3 and (FK)₃-Avi-C3 on Primary PMNs Isolated from the Human Blood

After successful demonstration of the transport of the Rho inhibitor C3 into the cytosol of a human neutrophil-like cell line by both supramolecular C3-containing complexes, the effect of (GGP)₃-Avi-C3 and (FK)₃-Avi-C3 on biologically and medically more relevant primary human PMNs was investigated. PMNs were isolated from the blood of healthy human volunteers and incubated at 37 °C with either (GGP)₃-Avi-C3 or

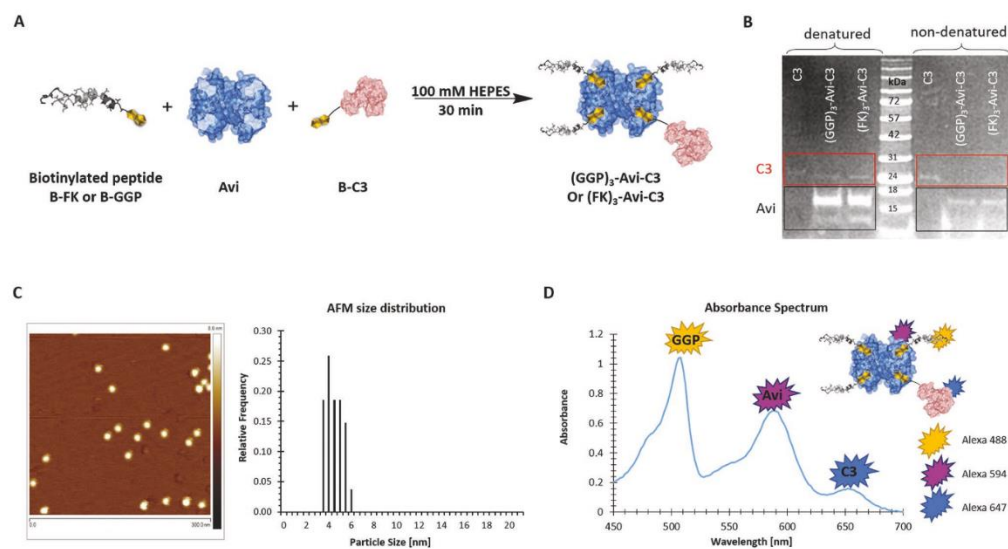


Figure 4. Assembly of the supramolecular complexes $(FK)_3$ -Avi-C3 and $(GGP)_3$ -Avi-C3 and their characterization. A) The controlled assembly of $(GGP)_3$ -Avi-C3 and $(FK)_3$ -Avi-C3 was accomplished through stoichiometric control according to the optimized ratio of 1.25 equiv of B-GGP and 1.0 equiv of B-FK per binding pocket. B) SDS-PAGE characterization of the protein complexes under denaturing and non-denaturing conditions indicate the successful assembly by the disappearance of C3 band under non-denaturing conditions. C) AFM image of $(FK)_3$ -Avi-C3 with height profile analysis of protein particles. D) Absorbance spectrum of $(GGP)_3$ -Avi-C3. Avi was labeled with Alexa-594 dye (purple star), B-C3 was labeled with Alexa-647 dye (blue star) and GGP with Alexa-488 (orange star). The ratio of GGP:Avi:C3 was determined from the absorption envelopes and a ratio of 3.2:1:0.7 was calculated.

$(FK)_3$ -Avi-C3. Images of the cells were taken and the changes in cell morphology were compared with cells left untreated or treated with either Avi alone or C3 alone. The fusion toxin, C2IN-C3lim+ C2IIa, where C2IIa delivers the Rho-inhibitor C2IN-C3lim into the cytosol of all cell types, served as positive control. Like the NB-4 cells, the human PMNs responded with significant changes in cell morphology to the treatment with either $(GGP)_3$ -Avi-C3 or $(FK)_3$ -Avi-C3 and C2IN-C3lim + C2IIa (Figure 7A–C). These results clearly indicated that $(GGP)_3$ -Avi-C3 and $(FK)_3$ -Avi-C3 were able to deliver C3 into the cytosol of primary human PMNs. Moreover, $(GGP)_3$ -Avi as well as $(FK)_3$ -Avi, but not Avi alone, bound to the surface of PMNs at 4 °C as analyzed by flow cytometry, confirming the specific function of the PMN targeting peptides (Figure 7D).

In contrast, neither $(GGP)_3$ -Avi-C3 nor $(FK)_3$ -Avi-C3 showed similar effects on the morphology of human lung epithelial cells A549 (Figure 8A and Figure S11A, Supporting Information) or the recently established human alveolar epithelial cell line hAELVi (Figure 8C and Figure S11B, Supporting Information), a model for the air–blood barrier of the peripheral lung,^[39] implicating that in these cells, the Rho-inhibitor C3 was not delivered into the cytosol by the supramolecular complexes. These findings were confirmed by the biochemical evaluation of the ADP-ribosylation status of Rho of these cells (Figure 8B,D). Our results clearly indicate that C3 enzyme activity was not present in the cytosol of these epithelial cells. On the other hand, treatment of the A549 cells with C2IN-C3lim + C2IIa resulted in the expected C3-induced change

in cell morphology (Figure 8A and Figure S11A, Supporting Information) and the strong ADP-ribosylation of Rho in the cytosol of the living cells by C3 (Figure 8B,D).

3. Conclusion

In conclusion, PMN-targeting supramolecular multiprotein complexes consisting of the specific Rho-inhibitor C3, Avi as molecular glue and three PMN-targeting peptides were prepared by convenient “mix-and-match” assembly using Avi/biotin technology to inhibit Rho-mediated signal transduction in PMNs. $(GGP)_3$ -Avi-C3 or $(FK)_3$ -Avi-C3 were generated, characterized and their biological mode of action was evaluated in vitro and ex vivo. A set of cell-based experiments clearly underlined the efficient and cell type-selective transport of the Rho-inhibitor C3 into the cytosol of primary human PMNs ex vivo and into the cytosol of human neutrophil-like NB-4 cells but not into human lung epithelial cells, which provides strong evidence for cell type-selectivity of $(GGP)_3$ -Avi and $(FK)_3$ -Avi. We envision that our strategy provides new therapeutic avenue for diseases such as post-traumatic injury of multiple injured patients, which are associated with hyperactivity and reactivity of PMNs.

Based on these seminal proof-of-concept investigations, future studies will focus on the application of the novel supramolecular complexes containing C3 Rho-inhibitor to elucidate whether inhibition of Rho-mediated signal transduction interferes with migration and chemotaxis of human PMNs in trans-well and human “lung-on-a-chip” approaches ex vivo.

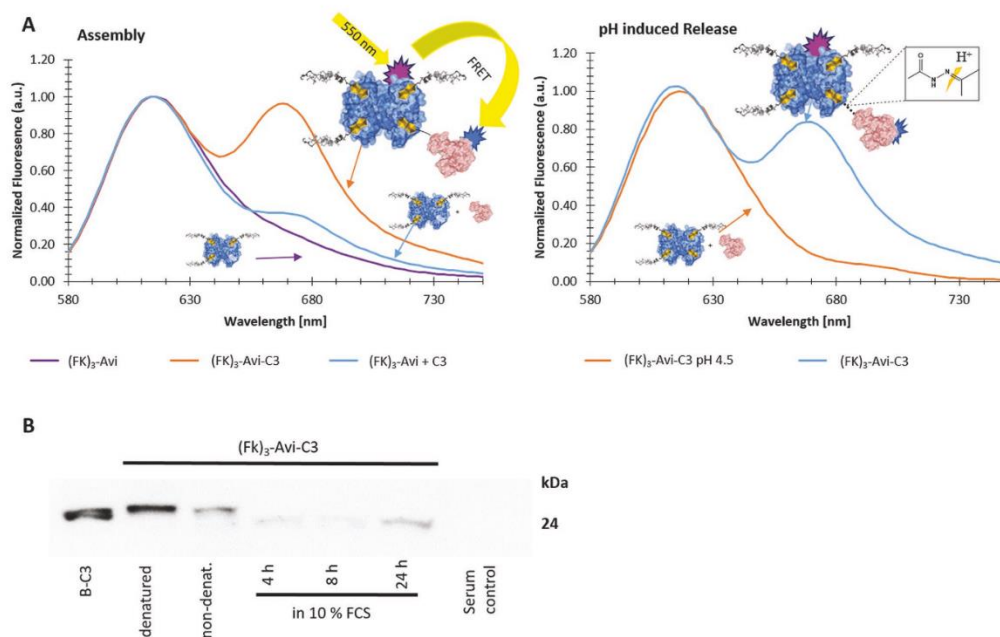


Figure 5. A) Left: Emission spectrum of dual-labeled assembled construct (FK)₃-Avi-C3 (blue), showing FRET and Avi (purple), (FK)₃-Avi + C3, mixed (orange) as control. right: pH induced release, showing no FRET after 4 h incubation time at pH 4.5. B) Stability of (FK)₃-Avi-C3 protein complex in fetal calf serum (FCS). Western blot analysis showed no significant increase up to 24 h. B-C3 and (FK)₃-Avi-C3 in PBS as well as 10% FCS were applied as control.

Moreover, it will be tested by our established animal model whether the local intratracheal application of the novel supra-molecular C3-containing complexes decreases the enhanced invasion of PMNs from the blood into the lungs of mice after blunt thorax trauma. This approach is inspired by earlier proof-of-concept studies which indicate that the intratracheal application of the recombinant Rho-inhibiting C3IN-C3lim fusion toxin significantly reduced the amount of monocytic cells in the lungs of mice after blunt thorax trauma, but had no effect on PMNs because of its cell type-selectivity.^[11] Besides, the stability of the complexes *in vivo*, e.g., in human blood will also be investigated. Ultimately, we envision the application of supra-molecular toxin complexes to downmodulate excessive PMN recruitment and migration across the disturbed alveolar barrier of patients after trauma—a hallmark event in the progression of Acute Lung Injury and Acute Respiratory Distress Syndrome.^[40,41]

4. Experimental Section

General information, methods for AFM, dynamic light scattering (DLS), Zeta-potential, SDS-PAGE and Western blot analysis are provided in the Supporting Information.

Materials: Unless otherwise stated, all chemicals were obtained from commercial sources (Merck, Sigma Aldrich, Fluka and Thermo Scientific, Fisher Scientific) and used without further purification. All organic

solvents (acetonitrile (CH₃CN), chloroform (CHCl₃), dichloromethane (DCM), dimethylformamide (DMF), dimethyl sulfoxide (DMSO), methanol (MeOH)) were obtained from Fisher Scientific and used without further purification (HPLC or analytical grades). The peptides Ac-GGPNLTGRWGPPVESALAK-NH₂ (GGP) and cFLFLFK-Biotin (B-FK) were purchased from PhtdPeptides Co., Ltd. (Zhengzhou City, China) with 95% purity. Water used for the reactions was obtained from the Merck Millipore purification system.

Cell culture media (Dulbecco's modified Eagle's medium (DMEM), Roswell Park Memorial Institute (RPMI) 1640 Medium) and fetal calf serum were from Gibco Life Technologies (Karlsruhe, Germany), cell culture materials from TPP (Trasadingen, Switzerland) and Sarstedt (Nümbrecht, Germany). Monovettes were from Sarstedt (Nümbrecht, Germany) and Biocoll Separating Solution from Biochrom GmbH (Berlin, Germany). Penicillin–streptomycin and Page Ruler prestained protein ladder were purchased from Thermo Fisher Scientific (Ulm, Germany). Page Ruler unstained protein ladder was purchased from GE Healthcare Life Sciences (Uppsala, Sweden). Complete protease inhibitor and streptavidin–peroxidase were from Roche (Mannheim, Germany) and biotinylated NAD⁺ from R&D Systems GmbH (Wiesbaden-Nordenstadt, Germany). The antibody against GAPDH and the peroxidase-coupled antimouse binding protein were from Santa Cruz Biotechnology (Heidelberg, Germany). Thrombin was purchased from Sigma-Aldrich Chemie GmbH (Steinheim, Germany), the nitrocellulose blotting membrane from GE Healthcare Life Sciences (Uppsala, Sweden), and the enhanced chemiluminescence (ECL) system from Millipore (Schwalbach, Germany). All-trans-retinoic acid (ATRA) and *N,N'*-hexamethylene bis(acetamide) (HMBAA) were from Sigma-Aldrich (Steinheim, Germany). G-CSF was purchased from Sino Biological Inc. (Wayne, PA, USA). The expression, purification and biochemical

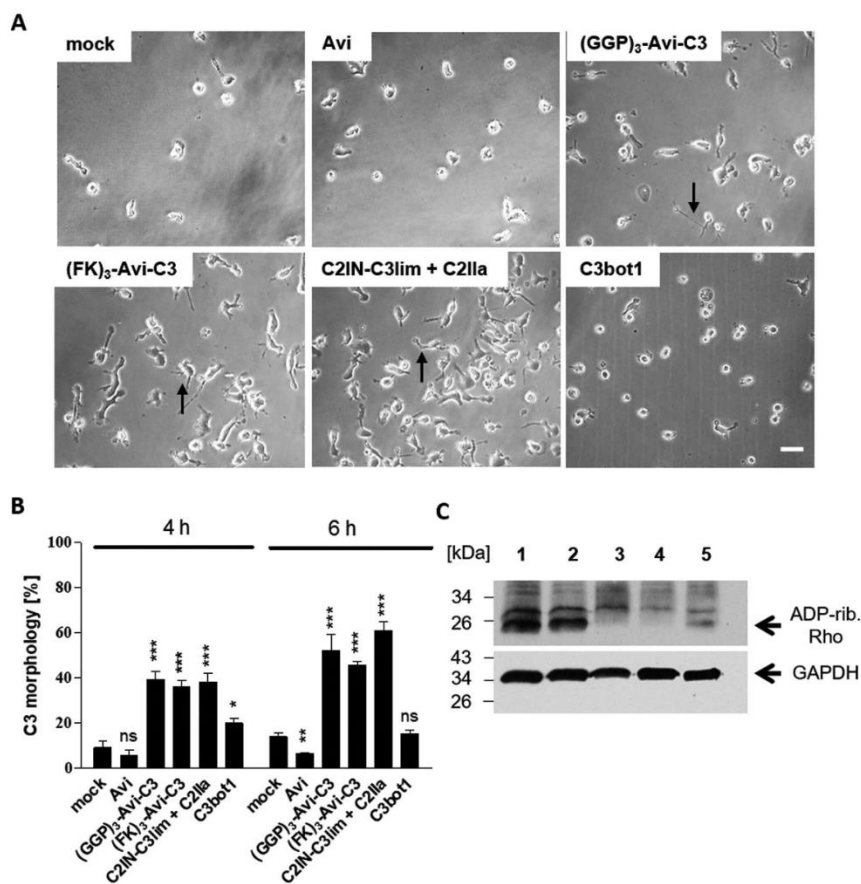


Figure 6. Effect of (GGP)₃-Avi-C3 and (FK)₃-Avi-C3 on human neutrophil-like NB-4 cells. A) Differentiated NB-4 cells were incubated with 320×10^{-9} M Avi, 320 nM (GGP)₃-Avi-C3, 320×10^{-9} M (FK)₃-Avi-C3, $1 \mu\text{g mL}^{-1}$ C2IN-C3lim + $2 \mu\text{g mL}^{-1}$ C2IIa, 320×10^{-9} M C3bot1 or left untreated for control (mock). The cells were incubated at 37°C and cell morphology was observed by phase contrast microscopy and documented over 6 h. The arrows indicate cells showing characteristic changes in cell morphology induced by the C3 Rho-inhibitor. The scale bar represents $50 \mu\text{m}$. B) Quantitative analysis of NB-4 cells showing the C3-induced morphology from pictures after 4 and 6 h. Values are given as mean \pm SEM ($n = 6$). Significance was tested using Student's *t*-test (ns, not significant, $*p < 0.05$, $**p < 0.01$, $***p < 0.001$). C) Analysis of the ADP-ribosylation status of these cells. The cells were treated as described in (A) and subsequently lysed. Equal amount of lysate protein of each sample was subjected to in vitro ADP-ribosylation with C3 enzyme and biotin-NAD⁺. The biotinylated, i.e., ADP-ribosylation of Rho was detected by Western blotting (upper panel). Note: A strong signal in the blot indicates that no ADP-ribosylation of Rho took place in the living cells, demonstrating that the C3 Rho-inhibitor was not present in their cytosol. A weak signal indicates that most ADP-ribosylation of the Rho protein took already place in the cytosol of the living cells by C3 Rho-inhibitor during the incubation period, indicating that active C3 enzyme reached the cytosol of these cells. Lower panel: GAPDH-staining to demonstrate comparable protein loading and blotting. 1) mock, 2) Avi, 3) (FK)₃-Avi-C3, 4) C2IN-C3lim + C2IIa, 5) C3.

characterization of the recombinant proteins C2IIa, C2IN-C3lim, and cysteine mutant of C3 was performed as described earlier.^[16,20,21]

Synthesis of (E)-N-(2-(2,5-dioxo-2,5-dihydro-1H-pyrrol-1-yl)ethyl)-5-(2-(5-(3aS,4S,6aR)-2-oxohexahydro-1H-thieno[3,4-d]imidazol-4-yl)pentanoyl)hydrazinylidene)hexanamide 4: N-(2-(2,5-dioxo-2,5-dihydro-1H-pyrrol-1-yl)ethyl)-5-oxohexamide (63 mg, 0.25 mmol, 1 equiv) and 5-(3aS,4S,6aR)-2-oxohexahydro-1H-thieno[3,4-d]imidazol-4-yl)pentanohydrazide (78 mg, 0.3 mmol, 1.2 equiv) were dissolved in 10 mL anhydrous MeOH under argon atmosphere. The resulting reaction

mixture was heated to 50°C and was continuously stirred for 4 h. The solvent was removed under high vacuum, and the residue was purified by column chromatography using eluting solvents 10% MeOH in DCM to afford 63 mg (0.12 mmol, 53%) of the final product; ¹H-NMR (300 MHz, MeOD δ) 6.83 (s, 2H) 4.51 (m, 1H) 4.33 (m, 1H), 3.63 (m, 2H), 3.36 (m, 2H), 3.22 (m, 1H) 2.94 (d, 1H, $J = 12.7$ Hz), 2.71 (d, 1H, $J = 12.7$ Hz), 2.11–2.44 (m, 6H), 1.98 (1H), 3.36 (m, 2H), 3.63 (m, 2H), 4.33 (m, 1H), 4.51 (m, 1H), 6.83 (s, 2H). ¹³C-NMR (100 MHz, MeOD, δ) 176.20, 172.56, 165.93, 162.15, 135.45, 127.34, 63.41, 61.63, 56.96,

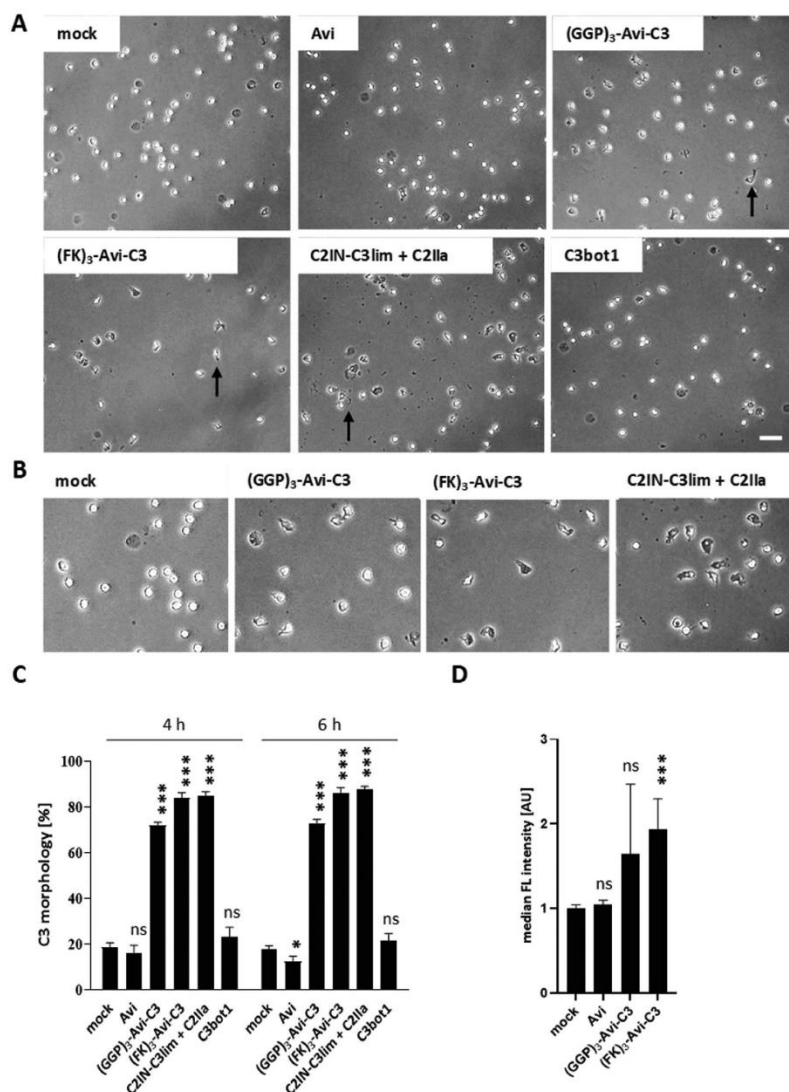


Figure 7. Effect of (GGP)₃-Avi-C3 and (FK)₃-Avi-C3 on primary human PMNs ex vivo. A) PMNs were isolated from blood of healthy donors and then treated ex vivo with 320×10^{-9} M Avi, 320×10^{-9} M (GGP)₃-Avi-C3, 320×10^{-9} M (FK)₃-Avi-C3, $1 \mu\text{g mL}^{-1}$ C2IN-C3lim + $2 \mu\text{g mL}^{-1}$ C2IIa, 320×10^{-9} M C3 or left untreated for control (mock). Cells were incubated at 37°C and cell morphology was observed over a period of 6 h. Arrows indicate cells showing the characteristic changes in cell morphology induced by C3 Rho-inhibitor. The scale bar represents $50 \mu\text{m}$. B) Cells of the same experiment with typical C3-induced morphology were enlarged for better visualization. C) Quantitative analysis of cells showing the C3-induced morphology from pictures after 4 and 6 h. Values are given as mean \pm SEM ($n = 9$). Significance was tested using Student's *t*-test (ns, not significant, $*p < 0.05$, $***p < 0.001$). D) Analysis of the binding of (GGP)₃-Avi-C3 and (FK)₃-Avi-C3 to PMNs by flow cytometry. PMNs ($200\,000$ cells in $200 \mu\text{L}$ complete medium) were incubated for 10 min at 4°C with either Avi, (GGP)₃-Avi-C3, or (FK)₃-Avi-C3 (all labeled with bodipy-fl (BDP)) or left untreated for control (mock). Subsequently, the cells were washed and analyzed by flow cytometry for the cell-bound BDP-proteins. The median fluorescence (FL) intensity of the respective histogram peaks was calculated, normalized to untreated control (mock) and is shown as arbitrary units (AU). Values are given as mean \pm SEM ($n = 5$). Significance was tested using Student's *t*-test (ns, not significant, $***p < 0.001$).

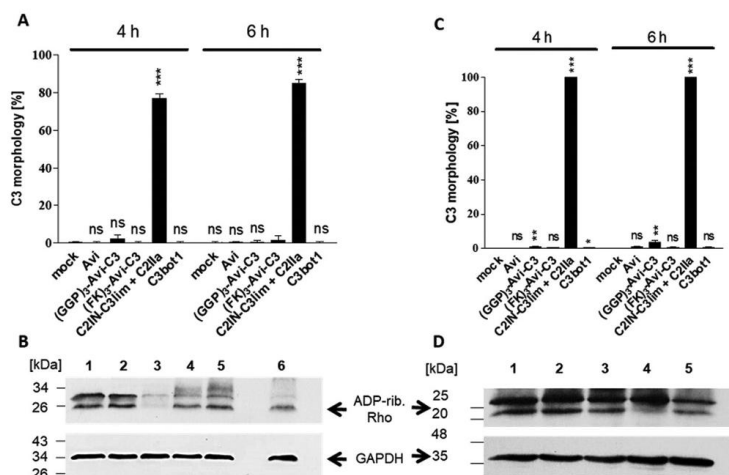


Figure 8. Effect of (GGP)₃-Avi-C3 and (FK)₃-Avi-C3 on human A549 lung cancer epithelial cells and on the human alveolar epithelial cell line hAELVi. A) A549 cells were treated with 320×10^{-9} M Avi, 320×10^{-9} M (GGP)₃-Avi-C3, 320×10^{-9} M (FK)₃-Avi-C3, $1 \mu\text{g mL}^{-1}$ C2IN-C3lim + $2 \mu\text{g mL}^{-1}$ C2IIa, 320×10^{-9} M C3 or left untreated for control (mock). Cells were incubated at 37°C and cell morphology was analyzed after a period of 4 and 6 h. Values are given as mean \pm SD ($n = 3$). Significance was tested using Student's *t*-test (ns, not significant, $***p < 0.001$). B) Analysis of the ADP-ribosylation status of these cells. The cells were treated as described in (A) and then lysed. Equal amount of lysate protein of each sample was subjected to *in vitro* ADP-ribosylation with C3 enzyme and biotin-NAD⁺. The biotinylated, i.e., ADP-ribosylation of Rho was detected by Western blotting (upper panel). A strong signal in the blot indicates that no ADP ribosylation of Rho took place in the living cells, demonstrating that no C3 Rho-inhibitor was present in their cytosol. A weak signal indicates that most ADP-ribosylation of the Rho took already place in the cytosol, of the living cells during the incubation period. Lower panel: GAPDH-staining to demonstrate comparable protein loading and blotting. 1) mock, 2) Avi, 3) (FK)₃-Avi-C3, 4) C2IN-C3lim + C2IIa, 5) C3, 6) (GGP)₃-Avi-C3. C) hAELVi cells were treated with 320×10^{-9} M Avi, 320×10^{-9} M (GGP)₃-Avi-C3, 320×10^{-9} M (FK)₃-Avi-C3, $3 \mu\text{g mL}^{-1}$ C2IN-C3lim + $6 \mu\text{g mL}^{-1}$ C2IIa, 320×10^{-9} M C3 or left untreated for control (mock). Cells were incubated at 37°C and cell morphology was analyzed after a period of 4 and 6 h. Values are given as mean \pm SEM ($n = 9$). Significance was tested using Student's *t*-test (ns, not significant, $*p < 0.05$, $**p < 0.01$, $***p < 0.001$). D) Analysis of the ADP-ribosylation status of these cells. The cells were treated as described in (C) and then lysed. Equal amount of lysate protein of each sample was subjected to *in vitro* ADP-ribosylation with C3 enzyme and biotin-NAD⁺. The biotinylated, i.e., ADP-ribosylation of Rho was detected as described in (B) 1) mock, 2) Avi, 3) (FK)₃-Avi-C3, 4) C2IN-C3lim + C2IIa, 5) C3.

41.03, 38.89, 38.41, 38.26, 35.68, 34.59, 29.80, 29.53, 26.62, 23.53, 16.54. Liquid chromatography-mass spectrometry (LC-MS): T_R : 3.51 min, m/z : 493 [M+H]⁺, 515 [M+Na]⁺, 253 [2+Na]⁺ (calcd. mass: 492.22, formula: C₂₂H₃₂N₆O₅S).

Biotinylation of Ac-GGPNLTGRWGPPVESALAK-NH₂ (B-GGP): A 2 mg mL^{-1} solution of GGP-peptide (5 mg, 2.5 μmol) in DMF and a 1 mg mL^{-1} solution of biotin-(PEO)₃-maleimide in phosphate buffer (50×10^{-3} M, pH 7.4) were mixed and incubated overnight at RT under shaking. The respective solution was lyophilized and washed with DCM to remove unreacted biotin reagent. The crude product was further purified by HPLC using a XDB-C18 column with the mobile phase starting from 100% solvent A (0.1% TFA in water) and 0% solvent B (0.1% TFA in acetonitrile) (0–5 min) with a flow rate of 4 mL min^{-1} , raising to 5% solvent B in 5 min, 15% solvent B in 10 min, and then reaching 100% solvent B after 29 min. It remained in this state for 1 min. Solvent B concentration was then finally lowered to 5% over five minutes. Absorbance was monitored at 280 and 254 nm. The retention time for GGP-B was 17.5 min, and 2.75 mg (1.02 μmol , 40%) of the product was obtained after lyophilization; LC-MS: T_R : 4.51, m/z : 898 [M+3H]³⁺. MALDI-ToF-MS (CHCA): m/z : 2691 [M+H]⁺, 2713 [M+Na]⁺ (calcd. mass: 2689 formula: C₁₂₀H₁₉₂N₃₂O₃₄S₂).

Biotinylation of C3 (B-C3): The recombinant cysteine mutant of C3 was expressed and purified in *Escherichia coli* BL21 as described in the literature.^[35]

$60 \mu\text{L}$ of 4-(2-hydroxyethyl)-1-piperazine-ethanesulfonic acid (HEPES) buffer (100×10^{-3} M, pH 7.4) and tris(2-carboxyethyl)phosphine (TCEP) HCl were sequentially added to the C3 solution ($200 \mu\text{g}$,

8 nmol , 1 equiv) and were incubated for 30 min at RT under shaking. Subsequently, $30 \mu\text{L}$ of compound **3** (5 mg mL^{-1} in DMF, 30 equiv) were added to the reaction mixture and the resulting mixture was shaken for 3 h at 4°C . Thereafter, rigorous ultrafiltration with $3 \times 500 \mu\text{L}$ buffer (molecular weight cut off (MWCO) = 10 kDa, 25×10^{-3} M HEPES buffer, pH 7.4) was used to remove excess of compound **3** to yield $208 \mu\text{L}$ B-C3 (0.7 mg mL^{-1} , 73% yield). The concentration of B-C3 was determined using a bicinchoninic acid (BCA) assay (A562 nm) with BSA as reference. Successful biotinylation was confirmed by MALDI-ToF-MS (Figure 3C) and degree of labeling was quantified by Quant[®]Tag Biotin Kit at A535 nm.

Assembly of Transport Proteins (GGP)₃-Avi and (FK)₃-Avi: (GGP)₃-Avi was assembled by dissolving 2 mg (31.7 nmol, 1 equiv) of Avi-BDP in 1 mL phosphate buffer (50×10^{-3} M, pH 7.4) and subsequent adding $383 \mu\text{L}$ GGP-B ($383 \mu\text{g}$ in MilliQ water, 143 nmol, 4.5 equiv). The mixture was incubated for 1 h at RT under shaking and purified by rigorous ultracentrifugation (MWCO = 20 kDa, using $3 \times 500 \mu\text{L}$ 50×10^{-3} M phosphate buffer pH 7.4). (FK)₃-Avi was assembled by dissolving 1 mg (15.9 nmol, 1 equiv) Avi-BDP in 1 mL phosphate buffer (50×10^{-3} M, pH 7.4) and 5.57 μL FK-B ($56 \mu\text{g}$ in DMSO, 47.7 nmol, 3 equiv) were subsequently added. The mixture was incubated for 1 h at RT under shaking and purified by ultracentrifugation (MWCO = 20 kDa, using $3 \times 800 \mu\text{L}$ 50×10^{-3} M phosphate buffer pH 7.4).

Assembly of (GGP)₃-Avi-C3 and (FK)₃-Avi-C3: (FK)₃-Avi-C3 was assembled by using $66 \mu\text{L}$ Avi-BDP (2 mg mL⁻¹ in HEPES buffer 25×10^{-3} M, pH 7.4) dissolved in $100 \mu\text{L}$ of HEPES buffer (50×10^{-3} M, pH 7.4). Then, $62 \mu\text{L}$ (0.8 mg mL^{-1} in 25×10^{-3} M HEPES buffer pH 7.4,

50 µg, 2.0 nmol, 1 equiv) of B-C3 and 0.7 µL of B-FK (1 mg mL⁻¹ in DMSO, 6.0 nmol, 3 equiv) were added.

(GGP)₃-Avi-C3 was assembled by using 66 µL (2 mg mL⁻¹ in HEPES buffer 25 × 10⁻³ M, pH 7.4) of Avi-BDP dissolved in 100 µL of HEPES buffer (50 × 10⁻³ M, pH 7.4) and adding 62 µL (0.8 mg mL⁻¹ in 25 × 10⁻³ M HEPES buffer pH 7.4, 50 µg, 2.0 nmol, 1 equiv) of B-C3 and 24 µL of B-GGP (1 mg mL⁻¹ in MilliQ water, 9.0 nmol, 4.5 equiv).

Analysis of the ADP-Ribosylation Status of Rho in Cells: To analyze the ADP-ribosylation of Rho in the cytosol of cells, *in vitro* ADP-ribosylation with biotin-labeled NAD⁺ as cosubstrate and C3 enzyme was performed as described earlier.^[11,17,37] In brief, cells were incubated at 37 °C with the respective transporters and toxins or left untreated for control as described in the previous section. Then, the cells were lysed and equal amount of lysate protein was incubated with 10 × 10⁻³ M biotin-labeled NAD⁺ and 300 ng C3 for 30 min at 37 °C. The enzyme reaction was terminated by adding SDS sample buffer and boiling the samples at 95 °C for 10 min. The biotinylated, i.e., ADP-ribosylation of Rho was detected by Western blotting with streptavidin-peroxidase using the ECL system. To confirm comparable amount of blotted protein, GAPDH was detected in addition.

Flow Cytometry: PMNs were isolated as described before. For flow cytometry analysis 2 × 10⁵ cells in 100 µL RPMI + 1% FCS were incubated with Avi (320 × 10⁻⁹ M), (GGP)₃-Avi-C3 (320 × 10⁻⁹ M), or (FK)₃-Avi-C3 (320 × 10⁻⁹ M) for 10 min on ice to prevent an endocytic uptake. Cells were washed with ice-cold PBS, resuspended in 200 µL complete medium and analyzed by flow cytometry using BD FACSCelesta flow cytometer and the BD FACSDiva software. BDP was excited with a blue laser (488 nm), emitted fluorescence was detected with a 530 nm (530/30) bandpass filter. Analysis and creation of fluorescence histograms from gated cell populations was performed using Flowing Software v2.5.1 (Perttu Terho, Turku Centre for Biotechnology, Finland).

Statistical Analysis: Preprocessing of data was performed as described in each experimental section. The results were presented as mean ± SD or mean ± SEM as described in each figure description. Sample sizes are given in figure legends or as described in this section. Analyses comparing means of different treatment groups were performed using Student's *t* test (GraphPad Prism 5; GraphPad Software, Inc.) and *p* values less than 0.05 were considered significant.

Supporting Information

Supporting Information is available from the Wiley Online Library or from the author.

Acknowledgements

A.J.H. and T.O. contributed equally to this work. The authors are grateful to the Max Planck Society and the Deutsche Forschungsgemeinschaft (DFG, German Research Foundation) project number 251293561-SFB 1149, Projects A04, A05; project number 316249678-SFB 1279, Projects C01, C02. T.W. acknowledges the support of the ERC Synergy Grant under grant agreement no. 319130 (BioQ).

Conflict of Interest

The authors declare no conflict of interest.

Keywords

C3 Rho inhibitor, polymorphonuclear leukocytes (PMNs), supramolecular toxin complex, targeted protein delivery

Received: May 24, 2019

Revised: July 4, 2019

Published online: July 18, 2019

- [1] A. Kovtun, D. A. C. Messerer, K. Scharffetter-Kochanek, M. Huber-Lang, A. Ignatius, *J. Immunol. Res.* **2018**, 2018, 1.
- [2] M. W. Knoferl, U. C. Liener, D. H. Seitz, M. Perl, U. B. Bruckner, L. Kinzl, F. Gebhard, *Shock* **2003**, 19, 519.
- [3] K. Raghavendran, B. A. Davidson, J. A. Woytash, J. D. Helinski, C. J. Marschke, P. A. Manderscheid, R. H. Notter, P. R. Knight, *Shock* **2005**, 24, 132.
- [4] D. H. Seitz, U. Niesler, A. Palmer, M. Sulger, S. T. Braumuller, M. Perl, F. Gebhard, M. W. Knoferl, *Crit. Care Med.* **2010**, 38, 1852.
- [5] U. Niesler, A. Palmer, J. S. Froba, S. T. Braumuller, S. Zhou, F. Gebhard, M. W. Knoferl, D. H. Seitz, *J. Trauma Acute Care Surgery* **2014**, 76, 386.
- [6] C. D. Nobes, A. Hall, in *Bacterial Toxins: Tools in Cell Biology and Pharmacology* (Ed: K. Aktories), Wiley-Blackwell, Hoboken, NJ **1993**, Ch. 6.
- [7] C. Laudanna, J. J. Campbell, E. C. Butcher, *Science* **1996**, 271, 981.
- [8] L. Liu, B. R. Schwartz, N. Lin, R. K. Winn, J. M. Harlan, *J. Immunol.* **2002**, 169, 2330.
- [9] A. P. Wheeler, A. J. Ridley, *Exp. Cell Res.* **2007**, 313, 3505.
- [10] H. Barth, S. Fischer, A. Moglich, C. Fortsch, *Front. Immunol.* **2015**, 6, 6.
- [11] T. Martin, A. Moglich, I. Felix, C. Fortsch, A. Rittlinger, A. Palmer, S. Denk, J. Schneider, L. Notbohm, M. Vogel, H. Geiger, S. Paschke, M. Huber-Lang, H. Barth, *Arch. Toxicol.* **2018**, 92, 323.
- [12] R. T. Jennings, M. Strengert, P. Hayes, J. El-Benna, C. Brakebusch, M. Kubica, U. G. Knaus, *Blood* **2014**, 123, 3635.
- [13] R. A. Worthylyake, S. Lemoine, J. M. Watson, K. Burridge, *J. Cell Biol.* **2001**, 154, 147.
- [14] K. Aktories, J. Frevert, *Biochem. J.* **1987**, 247, 363.
- [15] P. Chardin, P. Boquet, P. Madaule, M. R. Popoff, E. J. Rubin, D. M. Gill, *EMBO J.* **1989**, 8, 1087.
- [16] M. Vogelsgesang, A. Pautsch, K. Aktories, *Naunyn-Schmiedeberg's Arch. Pharmacol.* **2007**, 374, 347.
- [17] J. Fahrner, J. Kuban, K. Heine, G. Rupps, E. Kaiser, E. Felder, R. Benz, H. Barth, *Cell. Microbiol.* **2010**, 12, 233.
- [18] A. Tautzenberger, C. Fortsch, C. Zwerger, L. Dmochewicz, L. Kreja, A. Ignatius, H. Barth, *PLoS One* **2013**, 8, e85695.
- [19] J. Rotsch, A. Rohrbeck, M. May, T. Kolbe, S. Hagemann, I. Schelle, I. Just, H. Genth, S. C. Huelsenbeck, *Naunyn-Schmiedeberg's Arch. Pharmacol.* **2012**, 385, 883.
- [20] A. Rohrbeck, L. von Elsner, S. Hagemann, I. Just, *Toxins* **2015**, 7, 380.
- [21] J. Gacanin, A. Kovtun, S. Fischer, V. Schwager, J. Quambusch, S. L. Kuan, W. N. Liu, F. Boldt, C. Li, Z. Q. Yang, D. S. Liu, Y. Z. Wu, T. Weil, H. Barth, A. Ignatius, *Adv. Healthcare Mater.* **2017**, 6, 1700392.
- [22] D. L. Jaye, F. S. Nolte, L. Mazzucchelli, C. Geigerman, A. Akyildiz, C. A. Parkos, *Am. J. Pathol.* **2003**, 162, 1419.
- [23] D. L. Jaye, H. A. Edens, L. Mazzucchelli, C. A. Parkos, *J. Immunol.* **2001**, 166, 7250.
- [24] L. Mazzucchelli, J. B. Burritt, A. J. Jesaitis, A. Nusrat, T. W. Liang, A. T. Gewirtz, F. J. Schnell, C. A. Parkos, *Blood* **1999**, 93, 1738.
- [25] E. Karathanasis, C. M. Geigerman, C. A. Parkos, L. Chan, R. V. Bellamkonda, D. L. Jaye, *Ann. Biomed. Eng.* **2009**, 37, 1984.
- [26] L. W. Locke, M. D. Chordia, Y. Zhang, B. Kundu, D. Kennedy, J. Landseadel, L. Xiao, K. D. Fairchild, S. S. Berr, J. Linden, D. Pan, *J. Nucl. Med.* **2009**, 50, 790.
- [27] J. Pellico, A. V. Lechuga-Vieco, E. Almarza, A. Hidalgo, C. Mesa-Nunez, I. Fernandez-Barahona, J. A. Quintana, J. Bueren, J. A. Enriquez, J. Ruiz-Cabello, F. Herranz, *Sci. Rep.* **2017**, 7, 13242.
- [28] A. S. Wayne, D. J. FitzGerald, R. J. Kreitman, I. Pastan, *Blood* **2014**, 123, 2470.
- [29] T. Kohl, C. Schmidt, S. Wiemann, A. Poustka, U. Korf, *Proteome Sci.* **2008**, 6, 4.
- [30] S. L. Kuan, D. Y. W. Ng, Y. Z. Wu, C. Fortsch, H. Barth, M. Doroshenko, K. Koynov, C. Meier, T. Weil, *J. Am. Chem. Soc.* **2013**, 135, 17254.

- [31] S. L. Kuan, F. R. G. Bergamini, T. Weil, *Chem. Soc. Rev.* **2018**, *47*, 9069.
- [32] Y. Z. Wu, D. Y. W. Ng, S. L. Kuan, T. Weil, *Biomater. Sci.* **2015**, *3*, 214.
- [33] S. L. Kuan, C. Fortsch, D. Y. W. Ng, S. Fischer, Y. Tokura, W. N. Liu, Y. Z. Wu, K. Koynov, H. Barth, T. Weil, *Macromol. Biosci.* **2016**, *16*, 803.
- [34] P. Moscariello, D. Y. W. Ng, M. Jansen, T. Weil, H. J. Luhmann, J. Hedrich, *Adv. Sci.* **2018**, *5*, 1700897.
- [35] S. L. Kuan, S. Fischer, S. Hafner, T. Wang, T. Syrovets, W. Liu, Y. Tokura, D. Y. W. Ng, A. Riegger, C. Förtsch, D. Jäger, T. F. E. Barth, T. Simmet, H. Barth, T. Weil, *Adv. Sci.* **2018**, *5*, 1701036.
- [36] A. K. Kenworthy, *Methods* **2001**, *24*, 289.
- [37] H. Barth, F. Hofmann, C. Olenik, I. Just, K. Aktories, *Infect. Immun.* **1998**, *66*, 1364.
- [38] I. Just, C. Mohr, G. Schallehn, L. Menard, J. R. Didsbury, J. Vandekerckhove, J. van Damme, K. Aktories, *J. Biol. Chem.* **1992**, *267*, 10274.
- [39] A. Kuehn, S. Kletting, C. de Souza Carvalho-Wodarz, U. Repnik, G. Griffiths, U. Fischer, E. Meese, H. Huwer, D. Wirth, T. May, N. Schneider-Daum, C. M. Lehr, *Altex* **2016**, *33*, 251.
- [40] C. Sharp, A. B. Millar, A. R. Medford, *Respiration* **2015**, *89*, 420.
- [41] M. A. Matthay, R. L. Zemans, *Annu. Rev. Pathol.: Mech. Dis.* **2011**, *6*, 147.